Opening Session

(Chair: F.L. Fabbri)

Frascati Physics Series Vol. XXXVI (2004), pp. 3–14
DAΦNE 2004: Physics at meson factories – Frascati, June 7-11, 2004

VIEWS ON FLAVOUR PHYSICS

Luciano Maiani
Universitá di Roma "La Sapienza", Roma, Italy
I.N.F.N. Roma, Italy

Abstract

1 Introduction

The plot of energy vs. time for particle colliders (the Wilkinson plot) features a line which departs from the general, almost exponential, energy increase. This is the line of quark factories: charm (IHEP, Beijing, 1989), strange (DAΦNE, Frascati, 1997), and beauty (PEPII, Stanford, 1999; KEK-b, Tsukuba, 1999), machines specifically addressing the properties of quarks with different flavours:

flavour physics in brief. Results in the same area have also been steadily coming from more general-purpose accelerators, such as the AGS at Brookhaven National Lab and the SPS at CERN, the Tevatron in Fermi Lab and LEP at CERN.

Given the nature of this meeting and the time at my disposal, I shall restrict to a brief review of the most exciting developments in flavour physics at low energy, leaving out e.g. all the new developments coming from the b-factories. Fortunately, it seems to me that low energy flavour physics is quite representative of the main lines in this field: pushing the precision to the limits of the Standard Theory and exploring the dynamics of QCD forces in the making of hadrons out of quarks and antiquarks.

Of course, I shall present a view biased by my personal opinions and I apologize from the start for the many contributions I shall have no time to review.

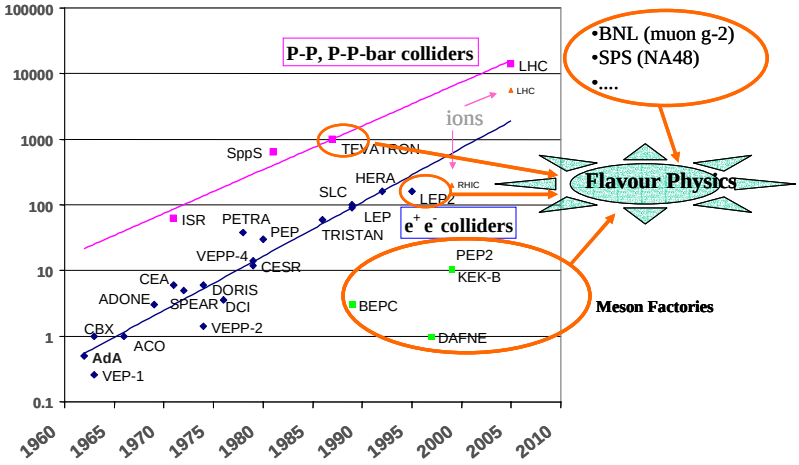

Figure 1: *Contributions to flavour physics.*

2 The muon $g-2$

The most recent results from the Muon $g-2$ Collaboration at BNL (2004 data, positive and negative muons combined) give:

$$a_\mu(\text{exp}) = 11\,659\,208\,(6)\;10^{-10}\;(\text{Muon g}-2\,\text{Coll.},\,2004\,\text{data}) \qquad (1)$$

Table 1: *The different contributions to the muon anomaly in the Standard Theory* [1].

SM contributions to the muon anomaly		
Pure QED	11 658 470.35 (0.28) 10^{-10}	
Hadronic (Vac. Pol.)	682.6 (6.4) 10^{-10}	CMD2+KLOE
Electroweak correction	15.4 (0.2) 10^{-10}	two loops included
Hadr. light-by-light scatt.	8 (4) 10^{-10}	
Total: SM prediction	**11 659 176.3 (7.5)** 10^{-10}	
Discrepacy: expt-th	(32 $\pm$ 10) 10^{-10}	

The prediction of the Standard Theory is shown in Table 1, with a break-up of the different contributions [1].

Speaking of the muon anomaly, it is customary to praise the level of precision attained by the experiment. It is so, indeed, to the point that while being a property of a lepton, its present experimental value is sensitive to the details of the strong interactions, via the vacuum polarization diagram (a self-energy correction in the photon line exchanged by the lepton external lines) and the light-by-light scattering (four-photon amplitude, one from the external magnetic field and the others attached to the lepton line). Vacuum-polarization gives the most important hadronic contribution and, happily, it can be expressed rigorously in terms of the cross section of $e^+e^- \to hadrons$. Most important is the low energy region, from the $\pi\pi$ threshold to the $\rho(770)$. If one accepts isotopic spin symmetry, a substitute for this cross section is the exclusive semileptonic τ decay rate, where hadrons are excited from the vacuum by the $I = 1$, $I_3 = \pm 1$ components of the vector current, rather than by the $I = 1$, $I_3 = 0$ (the isoscalar component of the e.m. current gives a negligible contribution). This has been tried in the past years and it gave a hadronic vacuum-polarization correction in better agreement with the experimental muon anomaly. High-precision measurements of the $e^+e^- \to hadrons$ cross section have been now perfomed at Novosibirsk [2], CMD2, and Frascati [3], KLOE. The two results are quite consistent among themselves:

$$\begin{aligned} a_\mu^{had-\pi\pi}(0.37\ \mathrm{GeV}^2 < (M_{\pi\pi})^2 < 0.93\ \mathrm{GeV}^2) = \\ (376.5 \pm 0.8_{stat} \pm 5.9_{sys.+th})10^{-10}\ \text{(KLOE)}; \\ (378.6 \pm 2.7_{stat} \pm 2.3_{sys.+th})\,10^{-10}\ \text{(CMD2)}. \end{aligned} \tag{2}$$

Unfortunately (or fortunately?) it so happens that the vacuum polar-

ization correction computed from the hadron cross section is about $24 \cdot 10^{-10}$ lower than the one computed from tau decay. Isospin breaking cannot be neglected at this level of precision. In fact, the difference accounts for most part of the discrepancy shown in Table 1. A comparison of the vacuum-polarization correction from $e^+e^- \to$ *hadrons* and from τ-decay is shown in Fig. 2, taken from a recent talk by Juliet Lee-Franzini [4].

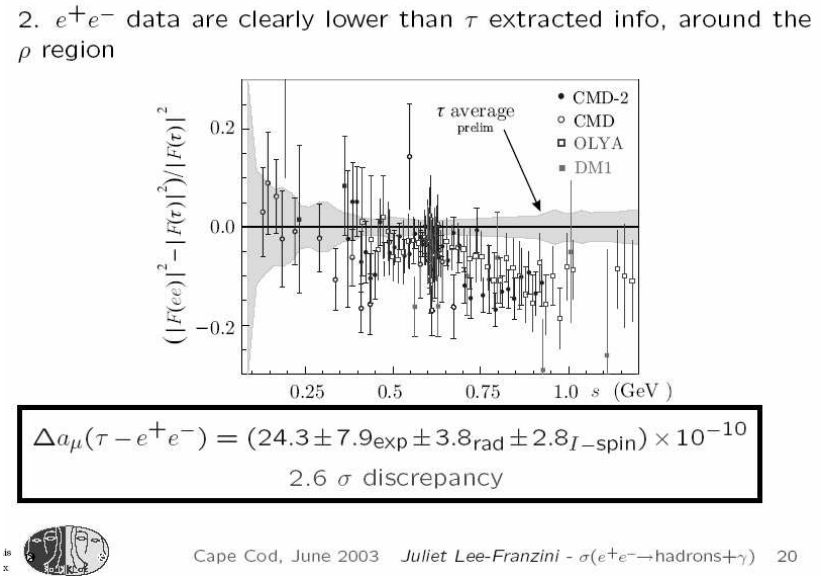

Figure 2: *Comparison of the vacuum-polarization correction from* $e^+e^- \to$ *hadrons and from* τ*-decay.*

The light-by-light scattering contribution is the bad guy. It has been estimated on the basis of a simple π-exchange model [5] and there are no perspectives to get a more rigorous estimate, at least for the moment. Nonetheless, the 50% error quoted in the table is most likely conservative and it should give a reasonable estimate of how far can we go in predicting the muon anomaly in the Standard Theory.

The discrepancy shown in Table 1 is 3σ only, still it is 2 times the electroweak corrections [6] and it could very well signal new physics in the energy region of electroweak unification, for example the contributions of light supersymmetric particles. Improving on the error is therefore crucial.

The approximate knowledge of light-by-light scattering leaves a margin for improvement of, say, a factor of 2-3 with respect to the present error. More

effort on the measurement of $e^+e^- \to hadrons$ (in particular at higher energy) is justified as well as another round of the $g-2$ experiment. The experiments are clearly worth the effort since the result may have fundamental implications on the planning of the next HEP machine, beyond the LHC.

3 Unitarity of the weak mixing matrix

Very accurate measurements have been recently performed on the neutron beta decay and on the superallowed beta transitions of $I = 1, J^P = 0^+$ nuclei. They have produced a very precise value of the $u \to d$ weak coupling:

$$|V_{ud}| = 0.9739 \pm 0.0005 \tag{3}$$

Since the contribution of V_{ub} is negligible, the unitarity of the weak mixing (CKM) matrix implies then:

$$\sqrt{1-(V_{ud})^2} = 0.2269 \pm 0.0021 = |V_{us}|_{unit.} \tag{4}$$

In turn, the value of $|V_{us}|$ can be quite accurately measured in Kl3 decays, where the Gatto-Ademollo theorem guarantees the vanishing of first order $SU(3)$ symmetry breaking effects, thus affording a very sensitive test of the Standard Theory.

The PDG 2002 value of $|V_{us}|$ disagreed with the prediction given above. The discrepancy has been there for some time, but the new data from E865 [7] at BNL (for K^+) and KLOE [8] at Frascati (for K_S) seem to have resolved it.

An analysis of the previous Kl3 results has been made by Cirigliano et al. [9] (see Isidori [10] for details)).To give a flavour of the technicalities involved, I recall that the experimental rate gives the product: $f_+^{K\pi}(0)|V_{us}|$ where f_+ is one of the two form factors for the K to π vector transition. Parallel to the progress in the experimental determination of the rates, a great theoretical effort has gone in the calculation of the form factor at zero momentum transfer. The CKM Working group agrees with the earlier determination [11]: $f_+^{K\pi}(0) = 0.961 \pm 0.008$. The result is:

$$|V_{us}|_{(old)} = 0.2201 \pm 0.0024 \tag{5}$$

corresponding to a 2.2σ discrepancy. The most recent progress is summarized in Fig. 3 (taken from the talk of S. Miscetti at Moriond 04 [12]), which shows a comparison of the BNL and Frascati results with the PDG 02 values. The results look now quite consistent with the prediction from unitarity (grey band). Two other measurements have confirmed the picture, from the KTeV collaboration at FermiLab [13] and from a recent analysis [14] of the hyperon decays data obtained by the NA48 Collaboraton at CERN:

$$|V_{us}|_{KTeV-K_L} = 0.2252 \pm 0.0008_{KTeV} \pm 0.0021_{ext} \quad (6)$$

$$|V_{us}|_{hyp.dec.} = 0.2250 \pm 0.0027 \quad (7)$$

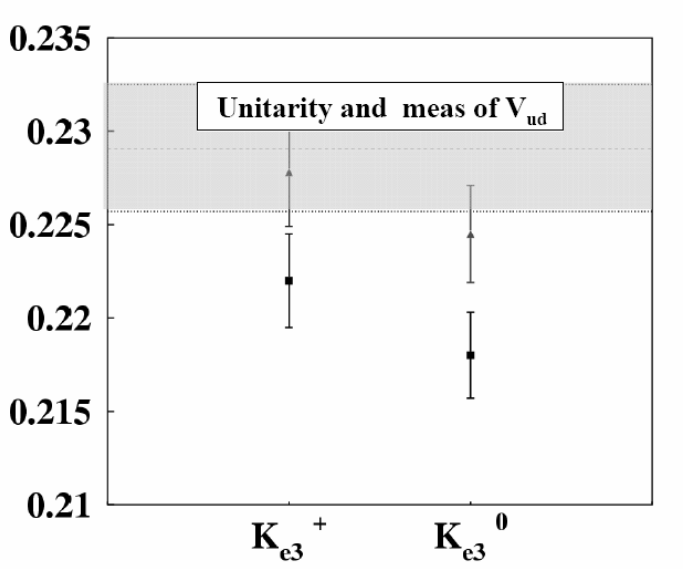

Figure 3: $|V_{us}|$ *measurements from* K^+_{e3} *at* E865 *and from* K^0_{e3} *at* KLOE *(triangles) compared to corresponding* PDG 02 *data (squares). The grey band represents the prediction from Unitarity and* V_{ud} *measurements.*

The accuracy of the present results is about 1%, a remarkable achievement indeed. There seems to be some margin to improve the experimental errors on Kℓ3 decays and, in addition, to increase the precision on the $\Delta S = 0$, $\pi^+ \to \pi^0$ β-decay [15], thereby reinforcing the determination of the $u \to d$ transition from nuclear decays.

On the theoretical side, isospin and $SU(3)$ breaking, the largest sources of errors, could be kept under control with Chiral Perturbation Theory. A test of the Standard Theory to 0.1% errors seems (perhaps!) possible (but, do not forget the failure of ChpTh in predicting the $\eta \to 3\pi$ decay rate!).

4 A fresh look at the scalar mesons

It's an old concept that two quarks may form a particularly tight state inside a hadronic system (for a recent review see e.g. [16]). The most attractive channel for light quarks is the fully antisymmetric state, $[q_1 q_2]$:

$$[q_1 q_2] = (\bar{3}_{colour}, \bar{3}_{flavour}, spin = 0) \tag{8}$$

The bound-diquark idea has been recently revisited by Jaffe and Wilczeck to explain the observed (but still controversial) exotic baryon states as pentaquark states of the form [17]:

$$[qq] \oplus [qq] \oplus \bar{q} = (0_{colour}, (\bar{10} \oplus 8)_{flavour}, J^P = 1/2^+) \tag{9}$$

A related scheme has been proposed by Lipkin and Karliner [18]. The fully antisymmetric diquark is a boson. However at short distances its fermionic composition should reveal itself and it is unlikely that two diquarks can be in relative S-wave. For this reason, the two diquarks in the pentaquark are assumed to be in P-wave, giving a peculiar overall positive parity, notwithstanding the negative parity that the antiquark brings in.

Jaffe and Wilczeck recalled also the old suggestion that the lowest energy scalar mesons are diquark-antidiquark states. Motivated by the recent observation by KLOE [19] of a low-lying $\pi\pi$ enhancement in $\phi \to \gamma + \pi^0 + \pi^0$, we have re-examined spectrum and decay modes of the lowest scalars as four-quark states [20]:

$$[qq][\bar{q}\bar{q}] = (8 \oplus 1)_{flavour} \tag{10}$$

The $a(980)$, $I = 1$, and the $f(980)$, $I = 0$, fit very well in the picture. For example:

$$a^+ = [su]\,[\bar{s}\bar{d}], \ldots; \; f = \frac{1}{\sqrt{2}}([su]\,[\bar{s}\bar{u}] + [sd]\,[\bar{s}\bar{d}]) \tag{11}$$

Indeed, these particles are almost degenerate ($\Delta m = 10 - 20$ MeV) and $a(980)$ likes to decay in states with a strange quark pair ($\eta\pi, K\bar{K}$), unlike any well-behaved $I = 0$, $q\bar{q}$ state.

To complete the nonet we need:

$$\sigma = [ud]\,[\bar{u}\bar{d}]; \; \kappa^{+,0} = [ud][\bar{s}\bar{d}(\bar{u})] \tag{12}$$

The first particle is the $\sigma(480)$, claimed in the past by many groups and seen more recently by the E791 Collaboration in D decays [22] as well as by KLOE [19]. With $\sigma(480)$ and $a(980)$ and quadratic mass formula we find [20]

(for earlier work see [23]): $m_\kappa \sim 770$ MeV, fitting very well with the $\kappa(800)$, a resonance that appeared intermittently in the PDG tables and is also seen by E791 [24].

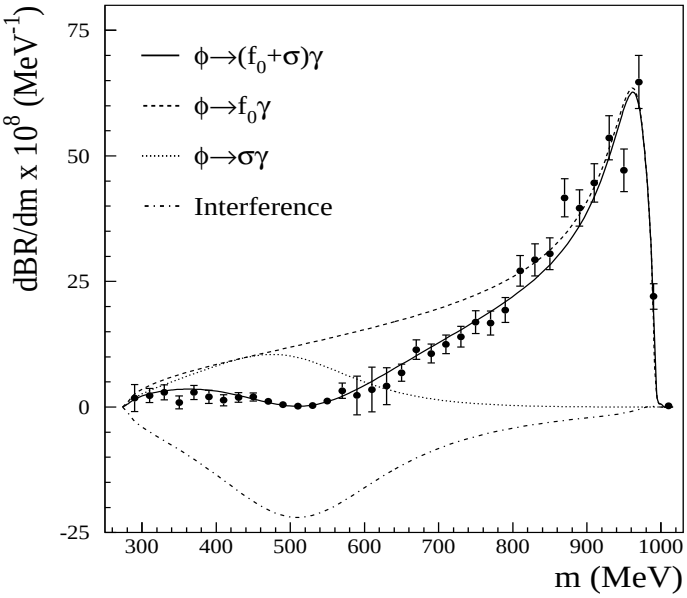

Figure 4: *The $\pi\pi$ mass spectrum in $\phi \to \gamma + \pi^0 + \pi^0$ from* [19]. *Mass and width of σ are taken from* E791 [22]*: $M_\sigma = (478 \pm 24 \pm 17)$ MeV, $\Gamma_\sigma = (324 \pm 40 \pm 21)$ MeV.*

Antisymmetric diquarks explain neatly the opposite properties of the scalar with respect to the vector nonet: the isolated $I = 0$ is the lightest state and it likes to decays in $\pi\pi$.

Diquarks are coloured objects, if we try to separate a diquark from its antidiquark, a quark pair pops out of the vacuum and the state becomes a baryon-antibaryon pair. This is the essence of the baryonium scheme, proposed time ago by Rossi and Veneziano [25] in a different context. However, light scalars are below threshold for baryon-antibaryon decay and a different mechanism has to be envisaged. We can describe the meson-meson decay by assuming that there is a non vanishing amplitude for switching one quark-antiquark pair between the two diquarks thus creating a pair of $q\bar{q}$ colour singlets:

$$[su]\,[\bar{s}\bar{d}] \to (s\bar{s})_{col.singlet}(u\bar{d})_{col.singlet} \tag{13}$$

Table 2: *Fit with a single parameter* $A = 2.6$ GeV. *Theoretical predictions on the left of each column,* $g_{\pi,K} = \Gamma_{\pi,K}/p$ *where* p *is the decay momentum. For* g_π *we have reported the upper limit obtained from the* $f - \sigma$ *mixing allowed by the masses.*

	$\pi\pi$		KK	
σ	345 MeV	$324 \pm 50 MeV$	-	
f	$g_\pi < 0.02$	$g_\pi = 0.19 \pm 0.05$	$g_K = 0.28$	$g_K = 0.40 \pm 0.6$
	$\eta\pi$			
a	43 MeV	60± 13 MeV	23 MeV	12± 3 MeV
	$K\pi$			
κ	138 MeV	410 ± 100 MeV	-	

The potential barrier provided by the attraction of color singlets is finite (if it exists at all!) and the singlets may proceed into a pair of outgoing mesons. The process is described by a single amplitude, A.

The switch amplitude makes contact with the model describing the scalar mesons $a(980)$ and $f(980)$ as $K\bar{K}$ molecules, but the physics is different. Here, the meson-meson pair results after tunnelling under the barrier which binds the diquark-antidiquark pair and it describes the unbound, final state, particles.

The decay rates into two pseudo scalar mesons thus obtained, with $A =$ 2.6 GeV, are given in Table 2.

The full $SU(3)$ invariant couplings are also considered in ref. [20].

The agreement is quite reasonable, considering the large disparity between the widths of $\sigma(480)$ and of $a(980)$ or $f(980)$. We do not use derivative couplings for the pseudo scalar mesons as in ref. [23]. We are far from the soft-pion, Goldstone, regime and derivative couplings would unduly weight the decays of the heaviest particles. The decay $f \to \pi\pi$ is forbidden by the OZI rule and is not well accounted for. One possibility is that it occurs via one-loop diagrams, with a $K\bar{K}$ intermediate state (as in the $K\bar{K}$ molecule picture) or via a $B\bar{B}$ state (as in the baryonium scheme).

If there are diquark-antidiquark bound states, we should see states of this kind with one or more heavy quarks [20, 21]. Consider the case of charm.

– **Hidden charm**: we expect the $SU(3)$ flavor composition:

$$[cq]\,[\bar{c}\bar{q}] = 8 \oplus 1 \tag{14}$$

corresponding to a charmonium nonet with possible decays:

$$a_c(I = 1) \to (D\bar{D}), \eta_c + \pi, \Psi + \rho \tag{15}$$

$$f_c(I=0) \rightarrow (D\bar{D}), \Psi + \omega \tag{16}$$

- Open charm [21]:

$$[cq]\,[\bar{q}\bar{q}] = \bar{3} \oplus 6 \rightarrow D + ps - meson \tag{17}$$

Unlike the light quark case, we expect exotic states and spectacular signatures. In particular, the representation 6 of $SU(3)$ contains very conspicuous doubly charged states.

Extrapolating boldly from the light scalar decays with the same switch amplitude A=2.6 GeV, one would predict small widths, of the order of ten MeV. Narrow states of this kind are seen in the hadronic final states of B non-leptonic decays, by Belle and PEPII. Some of them are explained by conventional $c - \bar{q}$ bound states, but there may be a wholly new spectroscopy waiting for us there, which we are only now beginning to discover.

In conclusion, there are still many open questions on scalar mesons at low energy, like getting a fully consistent picture of the hadronic widths or of the $\phi(1020) \rightarrow \gamma + S$ decays. But, all in all, the diquark-antidiquark picture seems solid. The study of $\gamma\gamma \rightarrow$ hadrons may be very useful to clarify the nature of the σ. Narrow states are seen by BABAR, CLEO and BELLE in charm containing hadrons: can they receive a similar explanation?

Other kinds of exotic states have been considered in the past, in addition to $qq - \bar{q}\bar{q}$: glue balls and hybrid (i.e. gluons+quarks) states. A rich spectroscopy is waiting for us at intermediate and low energy, to be tested in heavy flavour systems.

5 Flavour physics: why continue?

Flavour Physics is alive and well. This is true at low energy, as I tried to show with few examples, and at higher energies, where an exciting, new hadron spectroscopy is coming from the observation of D and B decays with high statistics. Here, in Frascati, time is ripe to decide how to continue the DAΦNE line: higher luminosity at $\phi(1020)$, higher energies in the intermediate region up to charm? In this respect, DAΦNE 04 is timely and important: we need to know options and perspectives, more and better. This is indeed one of the goals of this week.

My personal view. The LHC will be coming soon, but the next HEP machine may not be exactly behind the corner. It is important to keep going the intermediate scale projects, to fill the time gap.

Flavour and neutrino physics projects have just the right size and a very, very rich physics.

6 Acknowledgements

I would like to thank Cesare Bini, Paolo Franzini and Gino Isidori for very informative discussions.

References

1. For a recent review see: E. De Raphael in XVI Recontres de Physique de La Vallee d'Aoste, August 2002, hep-ph/0208251.
2. R.R. Akhmetshin et al. (CMD-2 Collaboration), Phys. Lett. **B527** (2002) 161.
3. See Juliet Lee-Franzini, Measurement of $\sigma e^+e^{|\rightarrow}$ Colliders, Hep-ex/0403006.
4. Juliet Lee Franzini, Lepton Moments International Symposium 2003, Cape Cod, June 2003 [http: //www.lnf.infn.it juliet].
5. M. Hayakawa, T. Kinoshita, Phys. Rev. **D57** (1998) 465; J. Bijnens, E.Pallante and J. Prades, Nucl. Phys. **B474** (1996) 379; M.Knecht and A.Nyffeler, Phys. Rev. **D65** 073034 (2002).
6. W.A. Bardeen, R. Gastmans and B.E. Lautrup, Nucl. Phys. **B46** (1972) 315; G. Altarelli, N. Cabibbo and L. Maiani Phys. Lett. **40B** (1972) 415; R. Jackiw and S. Weinberg, Phys. Rev. **D5** (1972) 2473; I. Bars and M. Yoshimura, Phys. Rev. **D6** (1972) 374; M. Fujikawa, B.W. Lee and A.I. Sanda, Phys. Rev. **D6** (1972) 2923.
7. A. Sher et al. [BNL-E865] Phys. Rev. Lett. **91** (2003) [hep-ex/0305042].
8. C. Gatti [KLOE] these proceedings.
9. V. Cirigliano in "Workshop on the CKM Unitarity Triangle, IPPP Durham, April 2003 [hep-ph/0305154].
10. G.Isidori in "Workshop on the CKM Unitarity Triangle, IPPP Durham, April 2003 [hep-ph/0311044].
11. H. Leutwyler and M. Roos, Z. Phys. C **25** (1984) 91.
12. S. Miscetti in Rencontres de Moriond, March 2004.
13. T. Alexopoulos et al. [KteV], hep-ex/0406001, hep-ex/0406002, hep-ex/0406003.

14. N. Cabibbo, E. C. Swallow and R. Winston, hep-ph/0307214, hep-ph/0307298.

15. PIBETA Collaboration, M. Bychkov et al., PSI Scientific Report 2001, Vol. 1, p. 8 , eds. J. Gobrecht et al., Villigen PSI (2002); http://pibeta.web.psi.ch.

16. R. L. Jaffe, "Exotica", hep-ph/0409065.

17. R. L. Jaffe and F. Wilczek, Phys. Rev. Lett. **91** (2003) 232003.

18. M. Karliner, H. J. Lipkin, hep-ph/0307243 and Phys. Lett. **B** 575: 249-255, 2003 [hep-ph/0402260].

19. A. Aloisio et al., Phys. Lett. **B** 537: 21-27, 2002 [hep-ex/0204013].

20. L. Maiani, F. Piccinini, A. Polosa, V. Riquer, hep-ph/0407017, to appear in Phys. Rev. Letters.

21. L. Maiani, F. Piccinini, A. Polosa, V. Riquer, hep-ph/0407025, to appear in Phys. Rev. D.

22. E. M. Aitala et al., Phys. Rev. Lett. **86** 270, (2001).

23. D. Black A. H. Fariborz, F. Sannino and J. Schechter, Phys. Rev. **D59**, 074026 (1999), 507.

24. E. M. Aitala et al., Phys. Rev. Lett **89** 121801-1 (2002).

25. G. C. Rossi and G. Veneziano, Nucl. Phys. B123 (1977) 507; Phys. Lett. B70, 255 (1977); for a recent update see hep-th/0404262.

Session I — CP Violation

(Chairpersons: J. Lee Franzini, W. Kluge, M. Curatolo)

Frascati Physics Series Vol. XXXVI (2004), pp. 17–24
DAΦNE 2004: Physics at meson factories – Frascati, June 7-11, 2004
Invited Review Talk in Plenary Session

THE THEORY OF CP-VIOLATION – IN AS MUCH OF A NUTSHELL AS WILL FIT ON 8 PAGES

Patricia Ball
IPPP, University of Durham, Durham DH1 3LE, UK

Abstract

Did you know that CP violation is intrinsically linked to the scalar sector of the Standard Model and its extensions? If yes, you need read no further — if no, you may turn over the title page and start reading now.

It is difficult to do justice to a topic as vast and complex as CP-violation in a 30-minutes conference talk — and even more so in a 8-pages contribution to the proceedings. Well, practitioners in teaching & learning do know that nothing is impossible, and so I shall try to stand up to the challenge and concentrate on a less common viewpoint on the subject than is to be found in most textbooks[1], in the hope the reader may find it as entertaining as enlightening.

[1]Everything you ever wanted to know about CP-violation (and more) can be found in Ref. [1)].

It is actually very surprising that CP should be violated at all. Many gauge-theories preserve C(harge conjugation symmetry) and P(arity) naturally & separately, the probably most prominent ones being (massless) QED and QCD. Even more contrived theories, especially designed to violate parity, like the chiral gauge-theory

$$\mathcal{L} = -\frac{1}{4} F_{\mu\nu} F^{\mu\nu} + \bar{\psi}_L i\sigma D \psi_L, \tag{1}$$

where only the left-handed (Weyl) fermions ψ_L interact with gauge-bosons[2], are still invariant under CP transformations, which implies that *CP is a natural symmetry of massless gauge theories*. So where does CP-violation come in? The catch is that, as the mass term

$$m\bar{\psi}\psi \equiv m(\bar{\psi}_L \psi_R + \bar{\psi}_R \psi_L) \tag{2}$$

violates gauge-symmetry, it is forbidden in $\mathcal{L}$ and hence left-handed fermions must be massless — at obvious variance with experiment. If the theory (1) is to serve as model for parity-violating interactions, it has to be amended in some ingenious way as to give mass to the fermions (and gauge-bosons), but at the same time preserve gauge-invariance.

In the Standard Model (SM), this objective is being achieved by adding a scalar (Higgs) sector which generates a nontrivial ground-state (vacuum) of the theory. In general, this vacuum-state is less symmetric than the full theory — a phenomenon usually referred to as spontaneous symmetry breaking (SSB), which in the case of gauge-theories is dubbed Higgs mechanism and allows gauge-bosons (and chiral fermions) to become massive. The Lagrangian of the SM can be written as

$$\mathcal{L}_{\mathrm{SM}} = \mathcal{L}_{\mathrm{gauge}}(\psi_L, \psi_R, W, \phi) + \mathcal{L}_{\mathrm{Higgs}}(\phi) + \mathcal{L}_{\mathrm{Yukawa}}(\psi_L, \psi_R, \phi), \tag{3}$$

where the first term on the right-hand side, the equivalent of (1), contains the kinetic terms of the fields involved, i.e. left- and right-handed fermions ψ_L and ψ_R, gauge-bosons W and scalar (Higgs) fields ϕ, as well as their gauge-interactions. The second term is the potential felt by the scalar fields and is responsible for some of them to acquire a nonzero vacuum expectation value

[2]Whereas their right-handed counterparts are "sterile" and hence omitted from the theory.

(VEV) which gives rise to SSB. The third term describes interactions between fermionic and scalar fields, which after SSB induce fermion mass terms. In the SM, $\mathcal{L}_{\rm Higgs}$ is automatically CP-invariant[3], which leaves us with $\mathcal{L}_{\rm Yukawa}$ as the only possible source of CP-violation in the SM[4]. It is given by

$$\mathcal{L}_{\rm Yukawa} = -\lambda^d_{ij}\bar{Q}^i_L \cdot \Phi d^j_R - (\lambda^d_{ij})^* \bar{d}^j_R \Phi^\dagger \cdot Q^i_L + \ldots, \tag{4}$$

where the indices i, j run over the three generations and the dots denote terms with up-type quarks. Q^i_L denotes the $\mathrm{SU_L}(2)$ quark doublet (u^i_L, d^i_L) and Φ the $\mathrm{SU_L}(2)$ Higgs doublet (ϕ^+, ϕ^0). The second term on the right-hand side of (4) is the complex conjugate of the first one — as required by the condition that the Lagrangian be a Hermitian operator.

So how does $\mathcal{L}_{\rm Yukawa}$ transform under CP? The P-transformation exchanges L (left) and R (right) indices, the C-transformation exchanges particles (d etc.) and antiparticles ($\bar{d}$ etc.), so that

$$CP: \quad \bar{Q}^i_L \cdot \Phi d^j_R \to \bar{d}^j_R \Phi^\dagger \cdot Q^i_L. \tag{5}$$

Comparing with (4), we see that $\mathcal{L}_{\rm Yukawa}$ is CP-invariant if $\lambda \equiv \lambda^*$. Hence, a necessary (but not sufficient) condition for CP-violation is that the Yukawa couplings $\lambda^{u,d}$ are complex.

What does all that actually mean? Well, one conclusion is that *CP-violation happens in the scalar sector* — at least in the SM. What about extensions? The statement stays evidently true for "simple" extensions of the SM with just an enlarged gauge- and scalar-field content (e.g. two Higgs-doublet model), and it also applies to theories where CP is not violated explicitly by complex couplings, but by spontaneous symmetry breaking — which by definition is related to the scalar sector. What about supersymmetry? Again, CP is conserved in theories with unbroken SUSY, for the same reasons as above, but complex couplings occur after SUSY-breaking. Another conclusion is that studying CP-violation means probing the scalar sector — which is also one of the main objectives of the Tevatron and the LHC. In this sense the measurement of CP-asymmetries in K and B decays is complementary to the direct searches for Higgs *et al.* at high-energy colliders.

[3]The reason being that there is only one Higgs-doublet; CP-violation in $\mathcal{L}_{\rm Higgs}$ can occur, however, in models with more than one Higgs-doublet.

[4]Note that the QCD θ-term $\theta_{\rm QCD} g_s^2/(64\pi^2)\epsilon^{\mu\nu\rho\sigma} G^a_{\mu\nu} G^a_{\rho\sigma}$ can be set to 0 if all quarks are massless.

What about CP-violation in the SM? Well, after SSB the Yukawa couplings $\lambda^{u,d}$ induce 3×3 mass matrices for u and d-type quarks which are eigenstates under weak interactions. If the theory is to be expressed in terms of states with definite mass, these matrices have to be diagonalized. The resulting transformation from the basis of weak eigenstates to that of mass eigenstates,

$$u_i^{(\text{weak})} = U_{ij}^{(u)} u_j^{(\text{mass})}, \qquad d_i^{(\text{weak})} = U_{ij}^{(d)} d_j^{(\text{mass})}, \tag{6}$$

has no effect on neutral interactions[5], $\bar{u}_i^{(\text{weak})} u_i^{(\text{weak})} \equiv \bar{u}_i^{(\text{mass})} u_i^{(\text{mass})}$, but profoundly changes charged interactions:

$$\bar{u}_i^{(\text{weak})} d_i^{(\text{weak})} \to \bar{u}_i^{(\text{mass})} (U^{(u)})^\dagger U^{(d)} d_i^{(\text{mass})}. \tag{7}$$

The matrix $V \equiv (U^{(u)})^\dagger U^{(d)}$ describes the strength of d-type quarks decaying into u-type quarks and is nothing else but the well-known CKM matrix. As $U^{(u,d)}$ just rotate the quark basis, they are unitary, and so is V. Any 3×3 unitary matrix can be parametrised in terms of three angles (the familiar Euler angles of three-dimensional rotations) and six complex phases. In the present case, however, not all six phases are physical: five of them can be "rotated away" by redefining the phases of the quark fields — which leaves three angles and one phase to describe the CKM matrix V. It is this complex phase that is the *one and only source of CP-violation in the SM.*

The fact that V is unitary allows one to express the conditions for CP-violation in the SM in an intuitively appealing form: unitarity means

$$\sum_j V_{ij} V_{kj}^* = \delta_{ik}, \tag{8}$$

which, for $i \neq k$, implies three complex numbers to add up to zero. This relation can be represented by a triangle in the complex plane, as shown in the left half of Fig. 1. For three generations, there are six of these triangles in total. This statement is true for arbitrary unitary matrices; the CKM matrix with only one complex phase (instead of six in the general case) is distinguished by the fact that all these six triangles have the same area, which consequently is a measure of the strength of CP-violation in the SM. From an experimental point of view, four of the triangles are rather difficult to explore: one side is much

[5]That is: there are no tree-level flavour-changing neutral interactions in the SM. Such interactions (e.g. $b \to s$) show up only at loop-level.

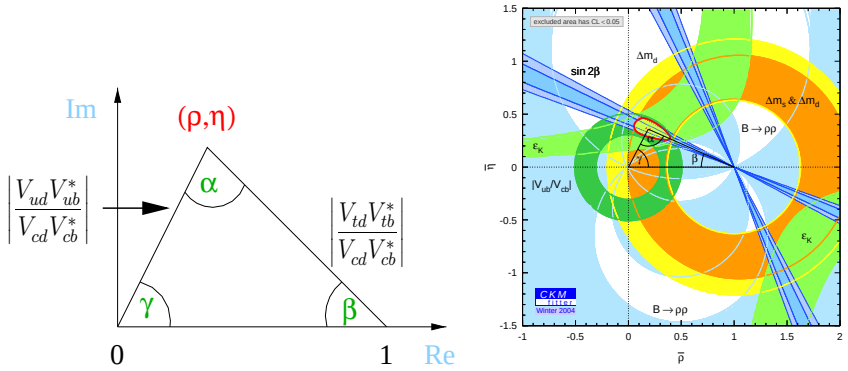

Figure 1: *Left: the B_d unitarity triangle (UT). The apex is labelled (ρ, η), which refers to the Wolfenstein parametrisation of the CKM-matrix. Right: the present (early 2004) experimental status of the UT* [2].

smaller than the others, which makes it difficult to measure the area (or angles) of these triangles with sufficient precision. The two remaining triangles, with $i \in \{d, s\}$ and $k = b$, have sides of comparable length, so that all their sides and angles are, in principle, accessible in experiment: the *bd* triangle is presently being studied at the B factories Babar and Belle and its current experimental status is shown in Fig. 1, right. The various constraints depicted in this figure are discussed in other contributions to these proceedings. The *bs* triangle will be the subject of experimental scrutiny at the LHC. The objective of all these studies is to overconstrain the triangles by measuring their sides and angles from various channels and possibly refute the SM picture of CP-violation. Figure 1 shows that significant discrepancies have yet to be found.

The experimental determination of the sides and angles of the UT is nothing less than trivial and will be the subject of other contributions to these proceedings. Rather than embarking on a discussion of the respective merits and shortcomings of various methods aiming to master the all-important (and, in general, yet unmastered) nonperturbative QCD effects in K and B decays, I would like to spend the remaining three pages of this note on a discussion of the bigger picture in which to embed any non-standard results on CP-violation.

So what are the alternatives to the SM picture of CP-violation? I men-

tioned a few of them already; a more complete list includes

- complex couplings in the Higgs potential (e.g. multi Higgs-doublet models);
- complex couplings in the effective low-energy Lagrangian obtained from a fundamental theory by SSB (e.g. soft SUSY-breaking terms);
- CP-violation from spontaneous symmetry breaking.

The latter scenario is rather attractive from the theorists' point of view as it relieves us from the task of coming up with clever explanations for where the complex couplings come from — other than the standard excuse that they are there because there is nothing to forbid them. If CP-violation is the result of SSB, the underlying fundamental theory must be manifestly CP-invariant, which requires the addition of (at least) an $\mathrm{SU_R}(2)$ gauge-group to the SM. This type of theories goes by the name of left-right symmetric models [3] and has been studied rather extensively. CP-violation occurs as consequence of the SSB $SU_\mathrm{L}(2) \times SU_\mathrm{R}(2) \times U(1) \to SU_\mathrm{L}(2) \times U(1)$. Like in the SM, fermion masses are generated from Yukawa interactions, but $\mathcal{L}_\mathrm{Yukawa}$ is now a bit more involved and includes a Higgs-bidoublet Φ, that is a doublet under both $\mathrm{SU_L}(2)$ and $\mathrm{SU_R}(2)$. CP-violation occurs as the VEV of Φ can carry a complex phase:

$$\langle \Phi \rangle = \begin{pmatrix} v & 0 \\ 0 & w\, e^{i\alpha} \end{pmatrix}. \tag{9}$$

The phenomenology of this model has been recently studied in Ref. [4], for the quark sector; the main prediction, a small value of $\sin 2\beta$, one of the angles of the *bd* UT, has not been confirmed by experiment. The other main prediction is large CP-violation in B_s decays, which will be tested at the LHC. One major problem of left-right symmetric models is the generically large value of the electric dipole moment of the neutron, which is a two-loop electroweak effect in the SM and hence exceedingly small, but occurs at one-loop level and is dangerously large in left-right symmetric models (and other models with additional sources of flavour-violation, including SUSY). At present public opinion is rather in disfavour of left-right models, but it is to be hoped that their more attractive features, in particular the possibility of spontaneous CP-violation, will eventually lead to their revival in an up-to-date form.

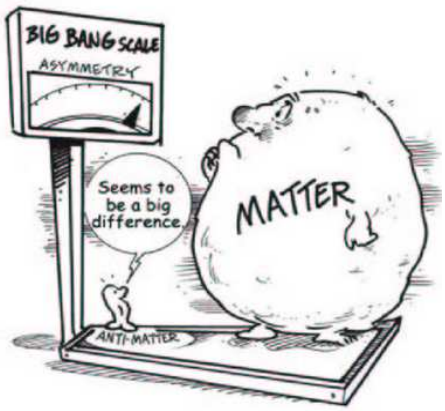

Figure 2: *One rather weighty consequence of CP-violation.*

The last point I would like to stress in this note is the truly cosmic implication of CP-violation: as Sakharov has shown in 1967 [5], the fact that the Universe is dominated by matter, and antimatter suspiciously absent, can only be explained if

1. fundamental interactions violate baryon number conservation;
2. the Universe has undergone non-equilibrium processes (phase-transitions) in its youth;
3. there is CP-violation, which allows Nature to distinguish baryons from antibaryons.

Do we understand the origin of the cosmic matter-antimatter asymmetry? Well, not *really*. Sakharov's conditions give us the minimum ingredients, but don't tell us the recipe to use for cooking up the asymmetry. Ever since 1967 creative *maîtres d'* have come up with ingenious compositions (e.g. GUT baryogenesis, leptogenesis, electroweak baryogenesis), but none of them seems to get it quite right. One result, however, does have emerged: CP-violation as observed in weak interactions is not strong enough to explain the scale of the observed asymmetry — which leaves us with the exciting certainty that new physics must be out there, longing to be discovered.

Let me conclude this *tour de force* by summarizing the messages I want to convey to you:

- CP-violation occurs in the scalar sector of the SM and its extensions;
- in the SM, all CP-violation is related to one single complex phase in the CKM-matrix V;
- the fact that V is unitary and complex allows a simple visualisation of CP-violation in the SM: the unitarity triangle;
- CP-violation is a phenomenon that does not only occur in the subatomic regime, but has profound consequences on the world we live in and is at the heart of the matter-antimatter asymmetry of the Universe.

Acknowledgments

I would like to thank the organisers of the workshop for providing a pleasant and stimulating atmosphere. I also thank J.M. Frère who first introduced me to the marvels of CP-violation.

References

1. G.C. Branco, L. Lavoura and J.P. Silva, International Series of Monographs on Physics, No. 103, Oxford University Press (1999); I. Bigi and A.I. Sanda, Cambridge Monogr. Part. Phys. Nucl. Phys. Cosmol. **9** (2000) 1.
2. Cf. the CKMfitter homepage `http://ckmfitter.in2p3.fr/`.
3. R. N. Mohapatra and J. C. Pati, Phys. Rev. D **11** (1975) 566; Phys. Rev. D **11** (1975) 2558; G. Senjanovic and R. N. Mohapatra, Phys. Rev. D **12** (1975) 1502.
4. It is difficult to withstand the temptation of self-citations, so here they are: P. Ball, J.M. Frere and J. Matias, Nucl. Phys. B **572** (2000) 3 [arXiv:hep-ph/9910211]; P. Ball and R. Fleischer, Phys. Lett. B **475** (2000) 111 [arXiv:hep-ph/9912319]; P. Ball, arXiv:hep-ph/0004245.
5. A. D. Sakharov, Pisma Zh. Eksp. Teor. Fiz. **5** (1967) 32 [JETP Lett. **5** (1967) 24].

Frascati Physics Series Vol. XXXVI (2004), pp. 25–34
DAΦNE 2004: Physics at meson factories – Frascati, June 7-11, 2004
Invited Review Talk in Plenary Session

CP VIOLATION AT B-FACTORIES

A. Bondar
Budker Institute of Nuclear Physics,
Lavrentieva 11, Novosibirsk 630090, Russia

Abstract

Recent results on CP violation from the *BaBar* and *BELLE* experiments at asymmetric e^+e^- B-Factories are summarized. The results of two groups on the time dependent CP asymmetry in $b \to sc\bar{c}$ are in good agreement. The similar measurements for penguin dominated B meson decays may indicate a contribution from physics beyond Standard Model. The first meaningful measurements of ϕ_2 and ϕ_3 angles of the CKM unitarity triangle are presented.

Introduction

Nature of CP violation is important for understanding of the origin of the matter in the Universe. Numerous experimental studies aim to constrain the parameters of the Cabibbo-Kobayashi-Maskawa (CKM) quark-mixing matrix [1)] as a unique source of CP violation in the Standard Model (SM). The key to test

the SM is to do many overconstrained measurements, *i.e.*, compare them by putting constraints on three angles of the unitary triangle (UT). These angles can be extracted from the measured time-dependent CP asymmetry in different neutral B decay channels. Independent measurements of ϕ_1, ϕ_2 and ϕ_3 allow us to verify the unitarity relation, and perform a search for New Physics (NP) comparing magnitudes of the same angle measured with modes dominated by either tree or penguin amplitudes [1].

1 B-Factories

Last few years most of the CP violation measurements in B meson decays are coming from e^+e^- asymmetric colliders (B-Factories). Due to multibunch operation, efficient suppression of the electron cloud beam instability and day-by-day tremendous efforts in understanding of the machine, two B-Factories, PEP-II at SLAC (USA) and KEKB at KEK (Japan) achieved luminosities of about $10^{34}cm^{-2}s^{-1}$. Detectors, *BaBar* [2] and *Belle* [3], operating at PEP-II and KEKB by summer 2004 recorded integrated luminosity $244fb^{-1}$ and $287fb^{-1}$, respectively.

2 Measurement of the time dependent CP asymmetry

At the B-Factories $B\bar{B}$ pairs are produced in Υ(4S) decays almost at rest in the center-of-mass frame. Due to the different energy of colliding e^+e^- beams the B mesons are boosted with a parameter $\beta\gamma = 0.56(0.43)$ for *BaBar* (*Belle*) enabling a measurement of the time-dependent CP asymmetry in B^0 decays [1].

This CP asymmetry is obtained by measuring the proper time difference Δt between a fully reconstructed B^0 meson (B_{cp}) decaying into a given final state f, and the partially reconstructed recoil B^0 meson (B_{tag}). The asymmetry in the decay rate is

$$a_{f_{CP}} = \frac{\Gamma[\bar{B^0}(t) \to f] - \Gamma[B^0(t) \to f]}{\Gamma[\bar{B^0}(t) \to f] + \Gamma[B^0(t) \to f]} = S \sin(\Delta m_d \Delta t) - C \cos(\Delta m_d \Delta t), \quad (1)$$

where Δm_d is the B^0–$\bar{B^0}$ mixing frequency. The parameters C and S describe the magnitude of CP violation in the decay and in the interference between decay and mixing (mixing-induced), respectively. We expect $C = 0$ in the case of a single dominant decay amplitude, because direct CP violation requires at

Table 1: The CP asymmetry ($\sin 2\phi_1$) from different charmonium modes.

Mode	*BaBar*	*Belle*
$J\psi K_S(K_S \to \pi^+\pi^-)$	0.82 ± 0.08	0.67 ± 0.08
All with $\eta_f = -1$	0.76 ± 0.07	0.73 ± 0.06
$J\psi K_L$	0.72 ± 0.16	0.80 ± 0.13
All charmonium modes	$0.74 \pm 0.07 \pm 0.03$	$0.73 \pm 0.06 \pm 0.03$

least two comparable amplitudes with different CP violating phases, while S is linked to the CKM phases, e.g. S=$sin2\phi_1$ for $B^0 \to J/\psi K_S$.

3 CKM phase $\phi_1(\beta)$

3.1 $b \to c\bar{c}s$ modes

The first observation of CP violation in the B^0 system was announced in 2001 by *BaBar* and *Belle* [4]. New and most precise measurements of ϕ_1 were reported in [5, 6]. The data sample of 88 (152) millions $B\bar{B}$ pairs has been used by *BaBar* (*Belle*) to fully reconstruct the B^0 mesons decaying into CP eigenstates such as $J/\psi K_S$, $\psi(2S)K_S$, $\chi_{c1}K_S$, $\eta_c K_S$ (CP-odd) and $J/\psi K_L$ (CP-even) as well as $J/\psi K^*$ final state. The obtained results are listed in Table 1, where two experiments are in good agreement. The average of the two experiments [7] $\sin 2\phi_1 = 0.739 \pm 0.049$ is consistent with SM predictions.

The interference of the vector-vector final state $J/\psi K^*$ and vector-scalar $J/\psi K_0^*(1430)$ can be used to measure the sign and magnitude of $\cos 2\phi_1$. Knowledge of the $\cos 2\phi_1$ sign partially resolves the four-fold ambiguity in the ϕ_1 angle. The simultaneous time-dependent and angular analysis of *BaBar* in $J/\psi K_S\pi^0$ decay favors a positive sign for $\cos 2\phi_1$ [8]:

$$\cos 2\phi_1 = +2.72^{+0.50}_{-0.79}(stat) \pm 0.27(syst).$$

3.2 CP Violation in the Penguin dominated modes

In the SM, decays to the charmless final states with odd strange mesons like $B^0 \to \phi K_S$ are dominated by the $b \to s\bar{s}s$ gluonic penguin diagrams. We expect $C = 0$ in the SM because there is only one dominant decay mechanism. Since

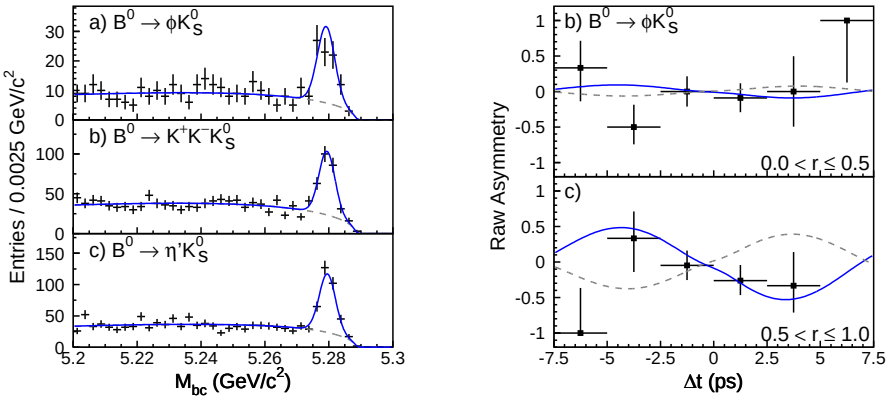

Figure 1: *The beam-energy constrained mass distributions for three penguin dominated modes: $\phi K_S, K^+K^-K_S, \eta' K_S$ (left) and the raw asymmetry for ϕK_S decay (right) mode measured by Belle.*

ϕK_S decays proceed through a CP odd final state, we expect $S = \sin 2\phi_1$. Other contributions in the SM which can deviate the measured asymmetry from $\sin 2\phi_1$ are rather small [9]. Figure 1 shows the beam-energy constrained mass distributions for three modes: $\phi K_S, K^+K^-K_S$, $\eta' K_S$, obtained by *Belle*. The CP violation result indicates a deviation from the value obtained with charmonium modes of about 3.5σ:

$$S_{\phi K^0} = -0.96 \pm 0.50(stat)^{+0.09}_{-0.11}(syst)$$

Figure 1 shows the raw asymmetry for such a mode with the SM expectation overlaid. On the other hand, the *BaBar* result [10]

$$S_{\phi K^0} = +0.47 \pm 0.34(stat)^{+0.08}_{-0.06}(syst),$$

is consistent with $\sin 2\phi_1$.

A more statistically accurate CP violation study can be made using all decays to KKK_S. This sample is a few times larger than in ϕK_S decay. The CP content of the three-body final state can be determined from isospin symmetry assumptions and measured branching fractions of KKK_S and KK_SK_S decays, as suggested by *Belle* [11]. One then observes [12] that the CP-even

state is strongly dominating the decay channel ($f_{even} = 0.98 \pm 0.15 \pm 0.04$). It is fortunate because it increases the experimental sensitivity to CP violation. Two results reported in [13, 14]

$$\begin{aligned} -S_{KKK_S} &= +0.51 \pm 0.26(stat) \pm 0.05(syst)^{+0.18}_{-0.00}(CP_+cont.)\ (Belle) \\ -S_{KKK_S} &= +0.57 \pm 0.26(stat) \pm 0.04(syst)^{+0.17}_{-0.00}(CP_+cont.)\ (BaBar) \end{aligned}$$

are in a good agreement with the SM expectation.

HFAG-group summarized the measured CP asymmetry relevant to $\sin 2\phi_1$ for the charmonium and penguin dominated modes [7]. The 2.4σ difference in average between the two types of decays is not enough to state whether it is a NP effect. Much more data are necessary for a conclusive result.

4 The measurements of time-dependent CP asymmetry related to CKM phase $\phi_2(\alpha)$

The extraction of $\sin 2\phi_2$ from time-dependent asymmetry is complicated by the presence of both tree and gluonic penguin amplitudes in $B \to hh(h = \pi, \rho)$ like decays. Neutral B transitions to the CP eigenstate $\pi^+\pi^-$ can exhibit mixing-induced CP violation through interference between decays with and without B^0–$\bar{B}^0$ mixing, and direct CP violation through interference between the $b \to u$ tree and $b \to d$ penguin decay processes. The significant tree-penguin interference leads to $C_{\pi\pi} \neq 0$ and introduces additional phase which can shift the experimentally measurable parameter $\phi_{2\text{eff}}$ away from the value of ϕ_2. The difference between $\phi_{2\text{eff}}$ and ϕ_2 can be determined from an isospin analysis of the related decays $B^\pm \to \pi^\pm\pi^0$ and $B^0, \bar{B}^0 \to \pi^0\pi^0$ [15]. The observation of the last decay with a relatively large branching fraction [16], [17] demonstrates the essential gluonic penguin contribution in this mode. However, this leads to additional difficulties for ϕ_2 extraction from $B \to \pi^+\pi^-$ decays.

Results on CP violation in the $B^0, \bar{B}^0 \to \pi^+\pi^-$ decay are summarized in Table 2, see Ref. [18, 19]. The *Belle* group rules out the CP-conserving case, $S_{\pi\pi} = C_{\pi\pi} = 0$ at the 5.2σ level. It also finds evidence of direct CP violation with a 3.2σ significance. *BaBar* does not confirm the observation of large CP violation in this decay channel reported by *Belle*. However, two results agree within errors.

The first measurement of the $B^\pm \to \rho^\pm\rho^0$ branching fraction by *Belle* [20] and the upper limit for $B^0 \to \rho^0\rho^0$ [21] by *BaBar* indicate a small penguin con-

Table 2: Results on CP violation measurements in $B \to \pi^+\pi^-$ and $B \to \rho^+\rho^-$.

Parameter	*BaBar* (123 M $B\bar{B}$)	*Belle* (152 M $B\bar{B}$)
$S_{\pi\pi}$	$-0.40 \pm 0.22(stat) \pm 0.03(syst)$	$-1.00 \pm 0.21(stat) \pm 0.07(syst)$
$C_{\pi\pi}$	$-0.19 \pm 0.19(stat) \pm 0.05(syst)$	$-0.58 \pm 0.15(stat) \pm 0.07(syst)$
$S_{\rho\rho}$	$-0.19 \pm 0.33(stat) \pm 0.11(syst)$	
$C_{\rho\rho}$	$-0.23 \pm 0.24(stat) \pm 0.14(syst)$	

tribution to the $B \to \rho\rho$ decay. Higher branching fraction and smaller shift of the measured $\phi_{2\text{eff}}$ from ϕ_2 compared to $B^0, \bar{B}^0 \to \pi^+\pi^-$ make $B^0, \bar{B}^0 \to \rho^+\rho^-$ decays more attractive for the extraction of the CKM angle ϕ_2. Measurements of the longitudinal polarization in the $B^+ \to \rho^+\rho^0$ decay [20] provide evidence that the CP-even component dominates in $B \to \rho\rho$ decays.

This fortunate situation for measuring ϕ_2 in the $\rho^+\rho^-$ final state was confirmed by *BaBar* in [22] with an angular analysis. The first attempt to observe the time-dependent CP-violation in $B^0 \to \rho^+\rho^-$ had been done by *BaBar* in a pioneering work [23]. Fig. 2 shows the Δt distribution for the reconstructed $\rho^+\rho^-$ events. The time-dependent CP asymmetry is shown in Figure 2 (c), where the curve represents the fit of the asymmetry. The new *BaBar* result [24] for $B^0, \bar{B}^0 \to \rho^+\rho^-$ decay, obtained with 123 million $B\bar{B}$ is presented in Table 2. Ignoring possible non-resonant contributions, interference, I=1 amplitudes and assuming isospin symmetry, by using the data on $BR(B^0 \to \rho^0\rho^0)$, one can relate the CP parameters $S_{\rho\rho}$ and $C_{\rho\rho}$ to the CKM angle ϕ_2 up to a four-fold ambiguity. Selecting the solution closest to the CKM best fit average [25], this corresponds to

$$\phi_2 = 96^\circ \pm 10^\circ(stat) \pm 4^\circ(syst) \pm 13^\circ(peng),$$

where the last error is the additional contribution from penguins that is bounded at $< 13^\circ$ (68.3% C.L.)

Figure 2 (right) shows the constraint on ϕ_2 from the $\pi\pi$ and the $\rho\rho$ systems. *BaBar* and *Belle* average branching fractions, polarization in $\rho\rho$ and asymmetry C and S measurements are used to perform the Gronau-London isospin analysis. One can conclude that $\rho\rho$ system provides the most precise constraint on α, where the knowledge of penguin pollution is dominant.

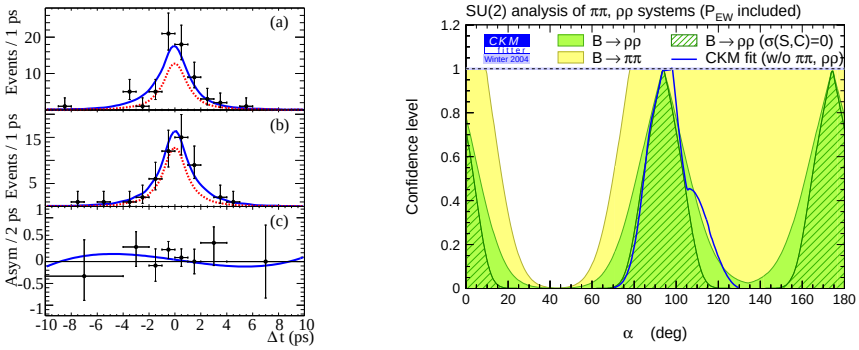

Figure 2: *The Δt distribution for signal enriched (a) B^0 and (b) $\bar{B}^0$ tagged events. The dashed line represents the sum of backgrounds and the solid line is the sum of signal and backgrounds. The time-dependent CP asymmetry is shown in (c), where the curve represents the asymmetry (left). Constraints on ϕ_2 obtained from the $\pi\pi$ and the $\rho\rho$ systems (right).*

5 CKM phase $\phi_3(\gamma)$

Various methods using $B \to DK$ decays have been introduced [26] to measure the unitarity triangle angle ϕ_3 but the statistics accumulated by current experiments is not yet sufficient to reasonably constrain ϕ_3. A novel technique based on the analysis of the three-body D^0 decay [27] has a higher statistical precision compared to branching fraction based methods.

This method is based on two key observations: D^0 and $\bar{D}^0$ mesons can decay to a common final state such as $K_s\pi^+\pi^-$, and the decay $B^+ \to D^{(*)}K^+$ can produce D^0 mesons of both flavors via $\bar{b} \to \bar{c}u\bar{s}$ and $\bar{b} \to \bar{u}c\bar{s}$ transitions, where the relative phase θ_+ between the two interfering amplitudes is the sum, $\delta + \phi_3$, of strong and weak interaction phases. In the charge conjugate mode, the relative phase $\theta_- = \delta - \phi_3$, so both phases can be extracted from the measurements of such B decays and their charge conjugate modes. The phase measurement is based on the analysis of the Dalitz distribution of the D^0 three-body final state. The two amplitudes interfere if D^0 and $\bar{D}^0$ mesons decay into the same final state $K_s\pi^+\pi^-$. Assuming no CP asymmetry in D decays, the

amplitude of the $B^{\pm}$ decay is written as

$$M_{\pm} = f(m^2_{\pm}, m^2_{\mp}) + re^{i\phi_3 \pm i\delta} f(m^2_{\mp}, m^2_{\pm}), \quad (2)$$

where m^2_+ and m^2_- are the squared invariant masses of the $K_s\pi^+$ and $K_s\pi^-$ combinations, respectively, and $f(m_+, m_-)$ is the complex amplitude of the decay $D^0 \to K_s\pi^+\pi^-$. Once the functional form of f is fixed by choosing a model for $D \to K_S\pi^+\pi^-$ decays, the D Dalitz distributions for B^+ and B^- decays can be fitted simultaneously by the above expressions for M_+ and M_-, with r, ϕ_3, and δ as free parameters. Thus the method is directly sensitive to the value of ϕ_3 and does not require additional assumptions on the values of r and δ.

The first measurement of ϕ_3 using this technique was performed by *Belle* based on 140 fb^{-1} [28]. From the combined fit of the $D \to K_S\pi^+\pi^-$ Dalitz plot distributions in the $B \to D^0K$ and $B \to D^{0*}K$ decays, *Belle* obtained the value of $\phi_3 = 81^\circ \pm 19^\circ(stat) \pm 13^\circ(syst) \pm 11^\circ(mod)$. The 95% confidence interval is $35^\circ < \phi_3 < 127^\circ$.

Conclusion

Two B-factories have established CP violation in B^0 decays, its magnitude is in agreement with the CKM interpretation of this phenomenon in the SM. The similar measurements for penguin dominated B meson decays may indicate a contribution from physics beyond SM. The first meaningful measurements of ϕ_2 and ϕ_3 angles of the CKM unitarity triangle were done. More data which will provide definitive results regarding these measurements are coming.

Acknowledgments

I am grateful to my colleagues from *Belle* and *BaBar* who kindly provided necessary materials for preparation of this contribution.

References

1. For a review of CP violation phenomenology, see D. Kirkby and Y. Nir in S. Eidelman *et al.*, Phys. Rev. Lett. **592**, 1 (2004). We use the (ϕ_1, ϕ_2, ϕ_3) notation for the angles of the Unitarity Triangle.

2. BaBar, B. Aubert *et al.*, Nucl. Instrum. Methods **A479** 1 (2002).

3. Belle, A. Abashian *et al.*, Nucl. Instrum. Methods **A479** 117 (2002).

4. BaBar, B. Aubert *et al.*, Phys. Rev. Lett. **87**, 091801; Belle, K. Abe *et al.*, Phys. Rev. Lett. **87**, 091802 (2001).

5. BaBar, B. Aubert *et al.*, Phys. Rev. Lett. **89**, 201802 (2002).

6. Belle, K. Abe *et al.*, BELLE-CONF-0353, (2003), presented at LP'03, hep-ex/0308036.

7. Havy Flavour Averaging Group: http://www.slac.stanford.edu/xorg/hfag

8. M.Verderi, hep-ex/0406082, Contributed to the Proceedings Recontres de Moriond, EW session, 21-28 March, 2004, La Thuile, Italy.

9. D.London and A.Soni, Phys. Lett. B **407**, 61 (1997); Y.Grossman, Z.Ligeti, Y.Nir and H.Quinn, Phys. Rev. D **68**, 015004 (2003); M.Gronau, Y.Grossman and J.Rosner, Phys. Lett. B **579**, 331 (2004).

10. BaBar, B. Aubert *et al.*, hep-ex/0403026, submitted to PRL.

11. Belle, K. Abe *et al.*, hep-ex/0208030. Contributed to 31st International Conference on High Energy Physics (ICHEP 2002), Amsterdam, The Netherlands, 24-31 Jul 2002.

12. Belle, A.Garmash *et al.*, Phys. Rev. D **69**, 012001 (2004).

13. Belle, K.Abe *et al.*, Phys. Rev. Lett. **91**, 261801 (2003).

14. BaBar, B. Aubert *et al.*, hep-ex/0406005, submitted to PRL.

15. M. Gronau and D. London Phys. Rev. Lett. **65**, 3381 (1990).

16. BaBar, B. Aubert *et al.*, hep-ex/0303028.

17. Belle, K. Abe *et al.*, Phys. Rev. Lett. **91**, 261801 (2003).

18. BaBar, B. Aubert *et al.*, hep-ex/0408089, 32^{nd} International Conference on High-Energy Physics, ICHEP 04, 16-22 August, 2004, Beijing, China.

19. Belle, K. Abe *et al.*, Phys. Rev. Lett. **93**, 021601 (2004).

20. Belle, J. Zhang *et al.*, Phys. Rev. Lett. **91**, 221801 (2003), hep-ex/0306007.

21. BaBar, B. Aubert *et al.*, Phys. Rev. Lett. **91**, 171802 (2003), hep-ex/0307026.

22. BaBar, B. Aubert *et al.*, Phys. Rev. D **69**, 031102 (2004).

23. BaBar, B. Aubert *et al.*, hep-ex/0404029, submitted to PRL.

24. L.Roos, hep-ex/0407051, Contributed to the Proceedings Recontres de Moriond, EW session, 21-28 March, 2004, La Thuile, Italy.

25. A. Höcker *et al.*, Eur. Phys. Jour. **21**, 225 (2001).

26. M. Gronau and D. Wyler, Phys. Lett. **B265**, 172 (1991); I. Dunietz, Phys. Lett. **B270**, 75 (1991); D. Atwood, I. Dunietz and A. Soni, Phys. Rev. Lett. **78**, 3257 (1997).

27. A. Giri, Yu. Grossman, A. Soffer, J. Zupan, Phys. Rev. D **68**, 054018 (2003); This technique was proposed independently in Belle Collaboration, and the analysis of experimental data was under way before the A.Giri *et al.* publication appeared (Proceedings of BINP Special Analysis Meeting on Dalitz Analysis, 24-26 Sep. 2002, unpublished).

28. Belle, A.Poluektov, *et al.*, hep-ex/0406067, submitted to PRD.

Frascati Physics Series Vol. XXXVI (2004), pp. 35–42
DAΦNE 2004: Physics at meson factories – Frascati, June 7-11, 2004
Invited Review Talk in Plenary Session

STATUS OF THE CKM MATRIX

Paolo Gambino
INFN, sez. di Torino and Dip. di Fisica Teorica, Univ. di Torino,
Via P. Giuria 1, 10125 Torino, Italy

Abstract

I briefly review recent progress in the the determination of the CKM matrix.

1 Introduction

The only source of flavor and CP violation in the SM is the CKM matrix, but most models of new physics naturally involve new sources of flavor and CP violation. The precise verification of the CKM mechanism is therefore central in the search for new physics and represents the modern equivalent of the tests of the universality of the charged currents. CKM studies are made difficult by the ubiquitous presence of strong interactions. In most cases, theoretical errors have become the dominant source of uncertainty: we are learning slowly but steadily how to minimize them. Significant recent progress in this direction is

due to a synergy with experiment [1]. The selection of topics presented below is incomplete, but I hope it reflects the main directions of progress in the field.

The CKM matrix has a highly hierarchical structure, that is best exposed in the Wolfenstein parameterization,

$$\begin{pmatrix} V_{ud} & V_{us} & V_{ub} \\ V_{cd} & V_{cs} & V_{cb} \\ V_{td} & V_{ts} & V_{tb} \end{pmatrix} = \begin{pmatrix} 1-\frac{\lambda^2}{2} & \lambda & A\lambda^3(\varrho - i\eta) \\ -\lambda & 1-\frac{\lambda^2}{2} & A\lambda^2 \\ A\lambda^3(1-\varrho-i\eta) & -A\lambda^2 & 1 \end{pmatrix} + \mathcal{O}(\lambda^4), \tag{1}$$

where $\lambda \approx 0.22$ is the sine of the Cabibbo angle. There are only four independent parameters: λ, A, ρ and η.

2 The Cabibbo angle

We see from (1) that, up to higher orders in λ, the upper left 2×2 submatrix is nothing but the Cabibbo matrix. Indeed, because of the smallness of $|V_{ub}| \approx 0.004$, the unitarity of the first row of the CKM matrix can be verified by a comparison of λ extracted from V_{ud} and V_{us}. Of course, λ can also be extracted from the second row, using DIS and W decay data, but with much lower precision [2].

The most precise determination of $|V_{ud}|$ comes from superallowed Fermi transitions (SFT), i.e. $0^+ \to 0^+$ nuclear β decays. Nine different such decays give consistent results and the error of the final value, $|V_{ud}| = 0.9740(5)$ [3] or $\lambda \equiv |V_{us}| = 0.2265(22)$, is dominated by the theoretical uncertainty in radiative corrections and nuclear effects. Neutron β decay provides a valuable alternative and starts being competitive, $\delta V_{ud} \sim 0.0015$, with further improvements expected at PERKEO. Theoretically, however, the cleanest channel is $\pi^+ \to \pi^0 e\nu$, which is penalized by a 10^{-8} BR. The present uncertainty based on preliminary PIBETA results, $\delta V_{ud} \sim 0.006$, is still far from being competitive, but the goal of PIBETA is to reduce it by a factor 3.

So far, the extraction of $|V_{us}|$ has been dominated by old data on semileptonic $K \to \pi l \nu$ decays (K_{l3}). For several years, K_{l3} data have preferred a value of λ lower than that coming from SFT, leading to a $\sim 2.3\sigma$ violation of unitarity. Last year, however, the BNL experiment E865 has published a new K^+ result implying a much higher λ than the old ones, in good agreement with unitarity. A new, thorough analysis of K_L semileptonic decays by the KTeV Collaboration [4], as well as new K_{Se3} and K_L results by KLOE [5] and

K_L, K^+ data from NA48 have confirmed the E865 result, improving significantly the experimental accuracy. The new results' average is $\lambda = 0.2259(22)$. The dominant source of error here is the theoretical error in the determination of the form factor at zero momentum $f_+(0)$. The form factor can be chirally expanded

$$f_+(0) = 1 + f_2 + f_4 + ... \tag{2}$$

where f_n are SU(3) breaking correction of $\mathcal{O}(M^n_{K,\pi}/(4\pi f_\pi)^n)$. While f_2, thanks to the Ademollo-Gatto theorem, can be precisely calculated, the real challenge is the estimate of f_4. It has recently be computed for the first time in quenched lattice QCD [6]. This exploratory analysis agrees with the reference quark model value by Leutwyler and Roos, and can be hopefully improved in several ways. It has also recently been realized that f_4 can be constrained by data on the slope and curvature of the form factor [7], but that requires higher experimental accuracy, an interesting challenge for present experiments. A 0.5% determination of $|V_{us}|$ in the next few years is conceivable.

The apparent violation of unitarity and the unclear experimental situation for K_{l3} of the last years have stimulated fresh ideas and a revisitation of older ones. A first example is the extraction of $|V_{us}|$ from hadronic τ decays [1, 8]. This requires a precise value of the strange quark mass, that can be obtained from lattice QCD or from sum rules. The value of λ obtained in [8] is compatible with unitarity and the present uncertainty, $\delta V_{us} \sim 0.035$, is dominated by the experimental errors on the τ BRs, expected to decrease significantly with B-factories data. A second possibility is to use hyperon decays [9], fitting the ratio of axial over vector current from data. While the experimental error on $|V_{us}|$ is close to 1%, SU(3) breaking effects require a dedicated lattice study (the convergence of the chiral expansion is slower) and have not yet been included. A third recent proposal [3] is to extract $|V_{us}/V_{ud}|$ from the experimental ratio

$$\frac{\Gamma(K \to \mu\bar{\nu}_\mu(\gamma))}{\Gamma(\pi \to \mu\bar{\nu}_\mu(\gamma))} = \left|\frac{V_{us}}{V_{ud}}\right|^2 \frac{f_K^2 m_K (1 - m_\mu^2/m_K^2)^2}{f_\pi^2 m_\pi (1 - m_\mu^2/m_\pi^2)^2} R_{rc} \tag{3}$$

using the radiative corrections factor $R_{rc} = 0.9930(35)$ and the new, partially unquenched lattice result $f_K/f_\pi = 1.210(4)(13)$ by the MILC collaboration [10]. The resulting $\lambda = 0.2221(27)$ has an uncertainty dominated by the lattice and, in principle, great potential for improvement. On the other hand, unquenched calculations have not yet reached maturity and the MILC error estimate is presently debated.

3 V_{cb}

The parameter A can be best determined from V_{cb}, see (1). The exclusive determination of $|V_{cb}|$ uses the extrapolation of the $B \to D^* l\nu$ rate to the kinematic endpoint where the D^* is produced at rest (zero-recoil). In this limit, the form factor $F(1)$ is known, up to corrections suppressed by at least two powers of $m_{c,b}$ that have to be computed, e.g. on the lattice. Since one needs to estimate only the $\mathcal{O}(10\%)$ correction to the heavy quark limit, an interesting accuracy can be reached even with present methods. In fact, current lattice QCD and sum rule results are both consistent with $F(1) = 0.91 \pm 0.04$ [1)]. The overall uncertainty is therefore close to 5%: $|V_{cb}^{excl}| = 41.5(1.0)_{ex}(1.8)_{th} \times 10^{-3}$, but the two most precise experimental results, by Babar and Cleo, differ by almost 3σ [11, 12)]. Semileptonic decays to D mesons give consistent but less precise results. Progress is expected especially from unquenched lattice calculations.

While the non-perturbative unknowns in the exclusive determination of $|V_{cb}|$ have to be calculated, those entering the inclusive semileptonic decays, $B \to X_c l\nu$, can be measured in a self-consistent way. Indeed, the inclusive decay rate depends only on the hadronic structure of the decaying B meson, but the sensitivity is actually suppressed by two powers of Λ_{QCD}/m_b, as the highly energetic decay products are (generally) unable to probe the long wavelengths characteristic of the B meson. The differential rate for $B \to X_c l\nu$ can therefore be expressed as a double expansion in α_s and Λ_{QCD}/m_b (Heavy Quark Expansion), whose leading term is nothing but the parton model result. However, the HQE results for the spectra can be compared to experiment only after smearing over a range of energies $\gg \Lambda_{QCD}$ and away from the endpoints. This is evident in the case of the hadronic mass spectrum, is dominated by resonance peaks that have no counterpart in the HQE: the HQE results have no *local* meaning.

The moments (weighted integrals) of the lepton energy and hadronic mass spectra, as well as the photon spectrum in radiative decays, are therefore employed, often with a lower cut on the charged lepton energy. Their HQE is analogous to that of the integrated rate,

$$\Gamma_{cl\nu} = \frac{G_F^2 m_b^5 \eta^{ew}}{192\pi^3} |V_{cb}|^2 z(r) \left[1 + a_1(r)\frac{\mu_\pi^2}{m_b^2} + a_2(r)\frac{\mu_G^2}{m_b^2} + b_1(r)\frac{\rho_D^3}{m_b^3} + b_2(r)\frac{\rho_{LS}^3}{m_b^3}\right], \tag{4}$$

where $r = (m_c/m_b)^2$, the Wilson coefficients a_i, b_i are series in α_s, and power corrections up to $1/m_b^3$ have been kept. Theoretical predictions are therefore given in terms of α_s, of properly defined *quark* masses $m_{c,b}$ and of the B meson matrix elements of four *local* operators, $\mu^2_{\pi,G}$, $\rho^3_{D,LS}$. Because they depend on the various parameters in different ways, the moments serve a double purpose: they allow to constrain the non-perturbative parameters and they test the overall consistency of the HQE framework. Effects that cannot be described by the HQE (and so violate *parton-hadron duality*) and higher order power corrections can be severely constrained.

In this sense, the new Babar analysis [13], based on [14], represents a real step forward, both in completeness and accuracy. It shows a remarkable consistency of a variety of leptonic and hadronic moments, leading to an excellent fit, values of the quark masses in agreement with lattice and spectral sum rule determinations, important bounds on the other non-perturbative parameters in agreement with other independent constraints, and $|V_{cb}^{incl}| = 41.4(0.4)_{ex}(0.4)_{hqe}(0.6)_{th} \times 10^{-3}$. The main results have been recently confirmed [15]. Semileptonic and radiative moments from Belle, Cleo, Delphi, and CDF can be included as well, without deteriorating the quality of the fit. A 1% determination of $|V_{cb}|$ might be possible, but requires some theoretical effort.

4 The unitarity triangle

As illustrated in Fig. 1, various measurements constrain differently $\bar{\rho} = \rho(1 - \lambda^2/2)$ and $\bar{\eta} = \eta(1 - \lambda^2/2)$. The triangle in the $(\bar{\rho}, \bar{\eta})$ plane with vertices in (0,0), (1,0), and $(\bar{\rho}, \bar{\eta})$ represents the unitarity relation $\sum_i V_{ib}^* V_{id} = 0$ and is usually called *unitarity triangle*.

The ratio $|V_{ub}/V_{cb}|$ measures the left side of the unitarity triangle, identifying a circle in the $(\bar{\rho}, \bar{\eta})$ plane. The determination of $|V_{ub}|$ from $b \to u$ semileptonic decays parallels that of $|V_{cb}|$, but the exclusive determination ($B \to \pi l\nu, B \to \rho l\nu$, etc.) is penalized by the absence of a heavy quark normalization for the form factors at a certain kinematical point, while the inclusive determination is affected by the kinematic cuts necessary to isolate $b \to u$ transitions from the dominant $b \to c$ background. Moreover, if theoretical precision is lower, so is statistics, by two orders of magnitude. In the exclusive case, lattice QCD and light cone sum rules complement each other, but as the first unquenched calculations appear the accuracy does not exceed

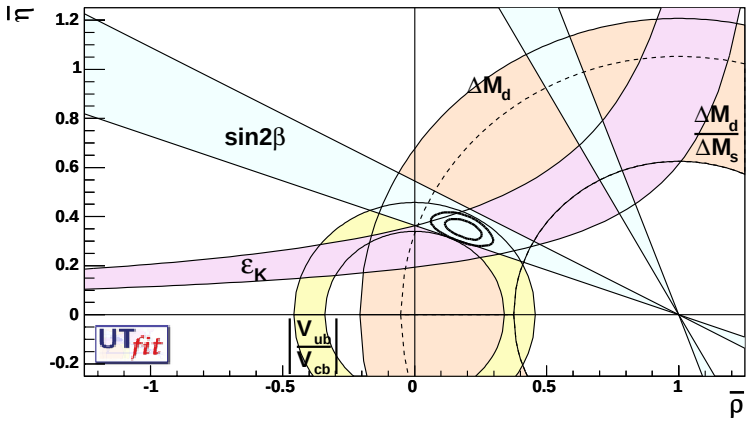

Figure 1: *Determination of the Unitarity Triangle using various constraints.*

15-20%, with central values for $|V_{ub}|$ around 0.0035. In the inclusive case, the cuts destroy the convergence of the HQE and introduce a sensitivity to local b-quark wave function properties like the Fermi motion, not suppressed by powers of $1/m_b$. Different strategies have been proposed (cuts on the hadronic invariant mass $M_X < M_D$, on the electron energy, on the q^2 of the lepton pair, and combinations thereof), each of them with peculiar experimental and theoretical systematics [16]. Recently, an intense theoretical activity has concerned the optimization of the cuts, subleading non-perturbative effects, the resummation of Sudakov logs, the role of the radiative decay spectrum in constraining the shape function, etc. As witnessed by the latest HFAG average of inclusive determinations, $|V_{ub}| = 4.70(44)\ 10^{-3}$, the present error is close to 10% and dominated, again, by theory. Improvements will come from high statistics experimental data, in particular from a precise determination of the radiative spectrum, from a careful application of the constraints on the shape function coming from spectral moments, and from the $b \to u$ differential rate itself. Eventually, the variety of complementary approaches that have been developed will be extremely useful.

The other interesting side of the unitarity triangle is proportional to $|V_{td}/V_{cb}|$, which can be accessed only via loop induced FCNC transitions, more sensitive to new physics. The useful observables are ε_K, ΔM_d, and $\Delta M_s/\Delta M_d$, from K^0, B_d^0, and B_s^0 mixing. Their theoretical interpretation depends crucially on input from lattice QCD, whose accuracy generally does not exceed 10-15% accuracy at present. B physics lattice simulations are multiscale, and present

lattices can resolve neither the b quark (too heavy if one wants to minimize discretization errors), nor the light quarks: various extrapolations are therefore needed. In addition, most calculations are performed without dynamical sea quarks (*quenched QCD*). Although error bars have not shrunk much, there has been significant progress in the last few years and more will come. The next frontier are unquenched simulations, that might reduce the lattice error by a factor three but are still in their infancy. It is easy to realize the dramatic impact this could have in Fig. 1. A measurement of ΔM_s at Tevatron would also have an important impact, even if it agrees with the SM. Alternative and promising routes to access V_{td} are the rare decays $K \to \pi\nu\bar{\nu}$ and $B \to \rho\gamma$.

Finally, various CP asymmetries measure directly some of the angles of the unitarity triangle. The measurement of $\sin 2\beta$ from the CP asymmetry in $B \to J/\Psi K_S$, in particular, has become a clean and very precise input (see Fig. 1). The measurement of the other angles is more difficult and is affected by various theoretical systematics, but is becoming the focus of the B-factories [17].

Global fits to the unitarity triangle give $\bar{\rho} = 0.172(47)$ and $\bar{\eta} = 0.348(28)$ [18] or $\bar{\rho} = 0.189(78)$ and $\bar{\eta} = 0.358(44)$ [19], according to the two main methodologies on the market. They mostly differ in the treatment of theoretical errors, but have been shown to be practically equivalent at the 95% CL [1]. The agreement between the various constraints is impressive. For instance, one can compare the direct and indirect determinations of $\sin 2\beta$, $0.707^{+0.043}_{-0.053}$ and 0.739 ± 0.048, respectively. The prediction for the angle γ is $62^\circ \pm 7^\circ$, while Belle analysis gives $81(19)(13)(11)^\circ$. The expected value for ΔM_s is $18.3(1.6)\, ps^{-1}$, to be compared with the direct lower bound $\Delta M_s > 14.5\, ps^{-1}$: in the absence of new physics Tevatron should be able to measure it soon.

In summary, the CKM mechanism describes successfully a host of data. Present errors are dominantly theoretical: lattice QCD still represents the best hope, but theory control can be very often improved by new data, a lesson never to forget.

5 Acknowledgements

I am grateful to the organizers for the invitation to this interesting and pleasant conference. I am indebted to M. Bona, G. Isidori, V. Lubicz, M. Pierini, A. Stocchi, N. Uraltsev for useful discussions and communications.

References

1. M. Battaglia *et al.*, hep-ph/0304132 and refs. therein; see also eConf C0304052 (2003) and `http://ckm-workshop.web.cern.ch`.
2. S. Eidelman *et al.* [Particle Data Group], Phys. Lett. B **592** (2004) 1.
3. A. Czarnecki, W. J. Marciano and A. Sirlin, hep-ph/0406324; W. J. Marciano, hep-ph/0402299.
4. E. Blucher, these proceedings.
5. C. Gatti, these proceedings; P. Franzini, hep-ex/0408150.
6. D. Becirevic *et al.*, hep-ph/0403217; V. Lubicz, these proceedings.
7. Bijnens and Talavera, Nucl. Phys. B **669** (2003) 341; Cirigliano *et al.*, Eur. Phys. J. C **35** (2004) 53.
8. E. Gamiz, *et al.* arXiv:hep-ph/0408044.
9. N. Cabibbo, E. C. Swallow and R. Winston, Ann. Rev. Nucl. Part. Sci. **53**, 39 (2003), Phys. Rev. Lett. **92**, 251803 (2004).
10. The MILC Coll., hep-lat/0407028.
11. Heavy Flavor Averaging Group, `http://www.slac.stanford.edu/xorg/hfag/`.
12. E. Barberio, these proceedings.
13. D. Cote, these proceedings; B. Aubert *et al.* [BABAR Coll.], Phys. Rev. Lett. **93** (2004) 011803.
14. P. Gambino and N. Uraltsev, Eur. Phys. J. C **34** (2004) 181.
15. C. W. Bauer, *et al.* hep-ph/0408002.
16. M. Luke, hep-ph/0307378 and refs. therein.
17. A. Bondar, A. Mihalyi, M. Legendre, T. Gershon, these proceedings.
18. M. Bona *et al.* [UTfit Coll.], hep-ph/0408079, `http://www.utfit.org`.
19. CKMfitter Coll., `http://ckmfitter.in2p3.fr`.

Frascati Physics Series Vol. XXXVI (2004), pp. 43–48
DAΦNE 2004: Physics at meson factories – Frascati, June 7-11, 2004
Selected Contribution in Plenary Session

RECENT RESULTS ON THE CKM ANGLE α

Attila Mihalyi *
University of Wisconsin-Madison
Madison, Wisconsin 53706 USA

Abstract

The method to measure the CKM angle α and the modes sensitive to it are discussed. It is shown that the $B \to \rho\rho$ decays provide the most stringent constraint on α, which is found to be $\alpha = 96^o \pm 10^o(stat) \pm 4^o(syst) \pm 13^o(penguin)$

1 Introduction

In the Standard Model, CP-violation arises from an irreducible phase in the Cabibbo-Kobayashi-Maskawa (CKM) matrix that describes weak interaction quark mixing [1]. This matrix is unitary, which leads to several relations among its elements, one being $V_{ud}V_{ub}^* + V_{cd}V_{cb}^* + V_{td}V_{tb}^* = 0$, where V_{ij} gives the coupling of the W-boson to the ij quark pair. This relationship can be

* On behalf of the BaBar collaboration

presented geometrically as a rescaled triangle in the complex plane. The angles of this triangle (α, β, γ) are related to CP-violation, in the sense that no CP-violation would imply a flat triangle. This report focuses on recent measurements that probe the angle $\alpha = arg[-(V_{td}V_{tb}^*)/(V_{ud}V_{ub}^*)]$. Three $b \to u\bar{u}d$ modes, $B \to \pi\pi$, $B \to \rho\pi$ and $B \to \rho\rho$ are directly sensitive to α. The time dependent asymmetry rates (for the $\pi\pi$ and $\rho\rho$ systems) when either the B^0 or the $\bar{B}^0$ from the $\Upsilon(4S)$ decay into a CP eigenstate, f_{CP} and the other into a state, f_{tag} that allows one to distinguish between B^0 and $\bar{B}^0$, is written as

$$f_{\pm}(\Delta t) = \frac{e^{-|\Delta t|/\tau}}{4\tau}[1 \pm S_f sin(\Delta m_d \Delta t) \mp C_f cos(\Delta m_d \Delta t)] \quad (1)$$

where $f_+(f_-)$ is the decay rate distribution when B_{tag} is a $B^0(\bar{B}^0)$, τ is the B-meson lifetime, Δm_d is the mass difference between the two B^0 mass eigenstates and $\Delta t = \Delta t_{CP} - \Delta t_{tag}$. The CP-parameters of interest are

$$S_f = \frac{2Im\lambda}{1+|\lambda|^2}, C_f = \frac{1-|\lambda|^2}{1+|\lambda|^2}, \quad (2)$$

The parameter λ describes all the interference effects that give rise to CP-violation, $\lambda = (q/p)(\bar{A}_{\bar{f}}/A_f)$. The first part q/p is the mixing phase $\pm e^{-2i\beta}$, where the sign depends on the CP final state. The experimentally favored assumption that there is no CP violation in mixing, $|q/p| = 1$ is implicit. The information about the decay is contained in the decay amplitudes $\bar{A}_{\bar{f}}$ and A_f. The decays can proceed through both so called tree and penguin amplitudes and what makes the extraction of α complicated is that the trees and the penguins carry different weak phases. This scenario is different from $b \to c\bar{c}s$ transitions, where both amplitudes carry the same weak phase. In the presence of penguins one obtains for $\pi\pi$ (and also for $\rho\rho$),

$$\lambda = e^{2i\alpha}\frac{1-re^{i(\delta-\alpha)}}{1-re^{i(\delta+\alpha)}} = |\lambda|e^{2i\alpha_{eff}} \quad (3)$$

where r is the ratio of the penguin and tree amplitudes. In the absence of penguin contributions one would obtain $S = sin2\alpha$. However as long as there is a penguin contribution to the process, the shift on α, $\theta = \alpha_{eff} - \alpha$, can be significant and can also lead to direct CP-violation, $C \neq 0$. Performing a time-dependent analysis and measuring S is the first step. To extract alpha one needs to perform an SU(2) isospin analysis [2]. In an isospin analysis

one constructs two triangular relations from the decay amplitudes, and their complex conjugates, to the charged and neutral final states. The closure of the triangles is required by SU(2) symmetry and if electroweak penguins are neglected the two triangles can be given a common base. All observables, CP-asymmetries and branching ratios, can be related to the sides of the triangles.

Alternatively one could use a general bound on the penguin induced shift, θ [3]. One such bound is the Grossman-Quinn bound and is obtained from the ratio of branching fractions for $B^0 \to \pi^0\pi^0$ and $B^+ \to \pi^+\pi^0$ (or the corresponding ones for $B \to \rho\rho$). This bound provides a good initial estimate of the maximum shift on α from penguins.

2 $B \to \pi\pi$

The $B \to \pi\pi$ system has been studied extensively at both BaBar and Belle experiments [4]. The current HFAG [5] average values of the CP-asymmetries are, $C_{\pi\pi} = -0.46 \pm 0.13$, $S_{\pi\pi} = -0.73 \pm 0.16$ and $A_{CP}(\pi^+\pi^0) = -0.07 \pm 0.14$ and corresponding average branching ratios are, $BR(B \to \pi^+\pi^-) = (4.55 \pm 0.44) \times 10^{-6}$ and $BR(B^+ \to \pi^+\pi^0) = (5.18^{+0.77}_{-0.76}) \times 10^{-6}$.

The last side of the isospin triangle, the $B^0 \to \pi^0\pi^0$ branching ratio, is considerably more difficult to measure. Measurements were only recently provided by Babar and Belle and the average value is $BR(B^0 \to \pi^0\pi^0) = (1.90 \pm 0.47) \times 10^{-6}$ [5]. Penguin processes are expected to contribute significantly to this decay, although a large branching ratio does not necessarily imply large penguin contributions. However a small $B^0 \to \pi^0\pi^0$ branching ratio would imply small penguin contributions and consequently a small shift on alpha, $\theta = \alpha_{eff} - \alpha$. With the current measurements, the general Grossman-Quinn bound on θ is not very constraining as it implies $\theta < 48^o$ at $90\%CL$. If the $\pi^0\pi^0$ decay rate were larger one could in addition measure $C_{\pi^0\pi^0}$ and do the full isospin analysis. Thus there are currently no meaningful constraints on α from the $B \to \pi\pi$ system.

3 $B \to \rho\pi$

The $B \to \rho\pi$ decay is also sensitive to α but its extraction is complicated by the fact that $\rho^+\pi^-$ is not a CP-eigenstate and therefore two more decay amplitudes are introduced. This yields a new relative unknown strong phase that needs to

be considered in addition to the shift from penguins.

A quasi-two body time dependent analysis of $B^0 \to \rho^+\pi^-$ has been carried out at BaBar [7] but unfortunately the results do not provide a constraint on α. With the current measurements, even in the absence of penguins, one would have an eightfold ambiguity on the solution.

A full SU(2) isospin analysis for the $\rho\pi$ system has been proposed [8], and instead of triangular relations, pentagon relations need to be constructed. The branching ratio of $B^0 \to \rho^0\pi^0$ is important for the full isospin analysis, since a small value would indicate a small penguin contribution. BaBar has set an upper limit, $BR(B^0 \to \rho^0\pi^0) < 2.5 \times 10^{-6}$, while Belle finds a large but not statistically significant value [9]: $BR(B^0 \to \rho^0\pi^0) = (5.1 \pm 1.6 \pm 0.9) \times 10^{-6}$. Studies indicate that only a small branching ratio for this mode would allow a determination of α from a full isospin analysis of the $B \to \rho\pi$ system [10]. However even such a favorable scenario is beyond the reach of first generation B-factories, as data on the order of $1ab^{-1}$ are required.

4 $B \to \rho\rho$

This process is a vector-vector decay and three partial waves (S, P, D) contribute to it. The P wave corresponds to a CP-odd eigenstate while S and D are CP-even. Three helicity states, $h = \pm 1$ and $h = 0$, need to be considered. The zero helicity state, $h = 0$, is longitudinally polarized while the other two are transversely polarized. Only the S and D partial waves contribute to the longitudinal polarization, which makes this a CP-even final state. Recently BaBar measured the $B^0 \to \rho^+\rho^-$ branching ratio and polarization [11]. The decay was found to have a relatively large branching ratio,$(30 \pm 4 \pm 5) \times 10^{-6}$, and to be 99% longitudinally polarized, implying that nearly all events are decays into a state with a definite CP value. The state with transverse polarization is a mixture of CP-even and odd eigenstates.

Applying the Grossmann-Quinn bound, one finds the upper limit on the penguin pollution to be less than $13^o(16^o)$ at $67(90)\% C.L.$ Such a good constraint is achievable due to the small branching ratio of $B^0 \to \rho^0\rho^0$ relative to that of $B^+ \to \rho^+\rho^0$.

The $B^0 \to \rho^+\rho^-$ time dependent analysis has been performed at Babar with a simultaneous measurement of the polarization and branching fraction [11]. The CP-parameters from the initial measurement have been updated with more

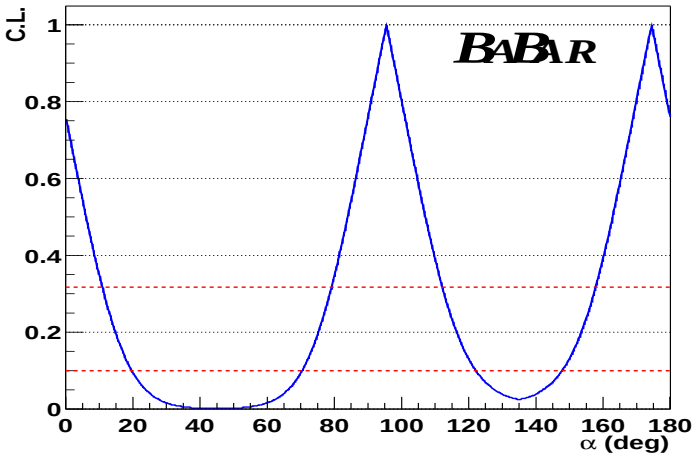

Figure 1: *Confidence level scan in α from $B \to \rho\rho$.*

statistics and the new results are [12], $C_{\rho^+\rho^-} = -0.23 \pm 0.24 \pm 0.14$ and $S_{\rho^+\rho^-} = -0.19 \pm 0.33 \pm 0.11$.

An SU(2) isospin analysis, to determine the angle α was also performed. This analysis neglects $I = 1$ transition amplitudes, electroweak penguins and interference with other modes that decay to the same final state. This isospin analysis uses the $\rho^+\rho^-$ CP-parameters, the averaged branching fractions and polarizations for the neutral and charged $\rho\rho$ decay modes [5]. In the case of $B^0 \to \rho^0\rho^0$ no polarization measurement is available, thus the longitudinal polarization fraction was conservatively assumed to be 1.0. The isospin analysis confidence level scan in α is plotted in Figure 1. Selecting the solution closest to the global CKM best fit [10], we find $\alpha = 96^o \pm 10^o(stat) \pm 4^o(syst) \pm 13^o(penguin)$.

The limiting factor in the measurement is the theoretical uncertainty of the amount of penguin pollution. Of great importance is the $B^0 \to \rho^0\rho^0$ branching ratio, which if truly small ($< 1 \times 10^{-6}$) can be used to set a stringent limit on the shift on α. If the branching ratio is however large ($> 2 \times 10^{-6}$), a time dependent analysis on this mode can be done. The new additional observables $S_{\rho^0\rho^0}, C_{\rho^0\rho^0}$, would make a full isospin analysis possible, giving a better measurement of α.

In summary, the best constraint on the CKM angle α is currently pro-

vided by the $B \to \rho\rho$ system. The measurement still remains limited by the uncertainty about the precise amount of penguin pollution.

References

1. N. Cabibbo, Phys. Rev. Lett **10**, 531 (1963); M. Kobayashi, T. Maskawa, Prog. Th. Phys. **49**, 652 (1973).
2. M. Gronau, D. London, Phys. Rev. Lett. **65**, 3381 (1990).
3. Y. Grossman, H.R. Quinn, Phys. Rev. **D58**, 017504 (1998).
4. *BABAR* Collaboration, B. Aubert *et al.*, Phys. Rev. Lett. **89**, 281802 (2002); *BELLE* Collaboration, K. Abe *et al.*, Phys. Rev. Lett. **93**, 021601 (2004).
5. The Heavy Flavor Averaging Group, http://www.slac.stanford.edu/xorg/hfag (Summer 2003 and Winter 2004 averages).
6. *BABAR* Collaboration, B. Aubert *et al.*, Phys. Rev. Lett. **91**, 241801 (2003); *BELLE* Collaboration, K. Abe *et al.*, Phys. Rev. Lett. **91**, 261801 (2003).
7. *BABAR* Collaboration, B. Aubert *et al.*, Phys. Rev. Lett. **91**, 201802 (2003).
8. H.J. Lipkin, Y. Nir, H.R. Quinn and A. Snyder, Phys. Rev. **D44**, 1454 (1991).
9. *BABAR* Collaboration, B. Aubert *et al.*, Phys. Rev. Lett. **93**, 051802 (2004); *BELLE* Collaboration, hep-ex/0405068, submitted to Phys. Rev. Lett.
10. J Charles *et al.* hep-ph/0406184, see also http://ckmfitter.in2p3.fr/ .
11. *BABAR* Collaboration, B. Aubert *et al.*, Phys. Rev. **D69**, 031102 (2004); *BABAR* Collaboration, B. Aubert *et al.*, hep-ex/0404029, submitted to Phys. Rev. Lett.
12. L. Roos (for the *BABAR* collaboration), Talk given at 39th Rencontres de Moriond:Electroweak Interactions and and Unified Theories, La Thuile, Italy, 21-28 Mar 2004.

Frascati Physics Series Vol. XXXVI (2004), pp. 49–54
DAΦNE 2004: Physics at meson factories – Frascati, June 7-11, 2004
Selected Contribution in Plenary Session

STATUS AND PROSPECTS FOR THE MEASUREMENT OF ANGLE γ

Marie Legendre*
CEA Saclay - DAPNIA/SPP

Abstract

We present results on B decays to modes sensitive to the CKM angle γ. These include the time-dependant CP analysis of the mode $B^0 \to D^*\pi$, using both full reconstruction and a powerful method in which the D^{*+} is partially reconstructed using only the soft pion. This process provides a measurement of $\sin(2\beta + \gamma)$. We also present the decay rate asymmetry for $B^+/B^- \to D_{CP^+}K^+/K^-$, where the neutral D meson is reconstructed in the CP even final states $\pi^+\pi^-$ and K^+K^-. Finally we present results from a search for the decay $B^- \to D_{K\pi}K^-$ where the "wrong-sign" $K^+\pi^-$ final sates results either from the usual $b \to c$ transition together with a doubly-Cabibbo-suppressed D decay or a $b \to u$ transition that produces a $\bar{D}^0$, with a favored decay $\bar{D}^0 \to K^+\pi^-$. The interference between these channels means that the mode is sensitive to γ.

* On behalf of BaBar Collaboration

1 Introduction

One of the main purpose of BaBar is to study CP violation in the B mesons system, and to test the Standard model, in particular by the measurement of the angles of the unitarity triangle. CP violation is now well established in B mesons by the precise measurement of $\sin(2\beta)$. The next step is now to overconstrain the unitarity triangle by studying other channels and by the measurements of the other angles α and γ. Several ways to measure γ will be presented here. $\sin(2\beta+\gamma)$ has been measured using the decay channels $B^0 \to D^{(*)}\pi$, with full and partial reconstruction methods. γ can also be measured in the decays $B^\pm \to D^0 K^{(*)\pm}$ by two methods (GLW and ADS).

2 Measurement of $\sin(2\beta+\gamma)$ with $B^0 \to D^{(*)}\pi$ decays

2.1 CP violation in $B^0 \to D^{(*)}\pi$

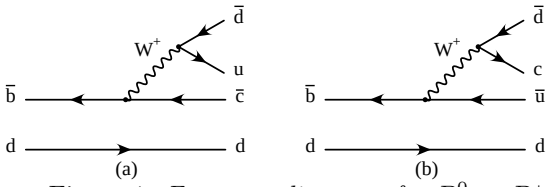

Figure 1: *Feynman diagrams for* $B^0 \to D^{*-}\pi^+$

In that channel, interferences between $b \to c$ and $b \to u$ transitions can occur. The relative weak phase between these diagrams is $2\beta+\gamma$ and we also have to consider a relative strong phase $\delta^{(*)}$.We define $r^{(*)}$ as the ratio between the amplitudes of these two diagrams : $r^{(*)} = \left|A(B^0 \to D^{(*)-}\pi^+)/A(\bar{B}^0 \to D^{(*)-}\pi^+)\right|$. $r^{(*)}$ is estimated using the branching fraction $\mathcal{B}(B^0 \to D_s^{(*)+}\pi^-)$ and assuming $SU(3)$: $r = 0.021^{+0.004}_{-0.005}$ and $r^* = 0.017^{+0.005}_{-0.007}$. We are expecting very small asymmetries, of the order of $2r^{(*)}$. This mode is interesting because only tree decays are involved. The main uncertainty is about the value of $r^{(*)}$.
The CP asymmetries are time-dependant. The B mesons are produced by pairs of correlated B in BaBar : B_{rec}, which decays in $D^{(*)}\pi$ and B_{tag}, which is used to tag the flavor of the B_{rec}, using the time-evolution of the B and the correlation between the 2 B mesons. One need to measure $\Delta t = (z_{rec} - z_{tag})/(\gamma\beta c)$, where z_{rec} (z_{tag}) is the decay position of the B_{rec} (B_{tag}) along the beam axis (z) in the laboratory frame. The decay probabilities for $B^0/\bar{B}^0 \to D^{(*)\mp}\pi^\pm$ are : $P(B^0 \to D^{(*)\mp}\pi^\pm, \Delta t) \propto [1 \pm \cos(\Delta m_d \Delta t) + (a \mp c \pm b)\sin(\Delta m_d \Delta t)]$ and

$P(\bar{B}^0 \to D^{(*)\mp}\pi^{\pm}, \Delta t) \propto [1 \mp \cos(\Delta m_d \Delta t) - (a \pm c \mp b)\sin(\Delta m_d \Delta t)]$ where a, b, c are the CP parameters. One have to take into account possible $(b \to u)$ interference effects in the tag side. They are parameterized by the effective parameters r' and δ'. The CP parameters are then : $a^{(*)} = 2r^{(*)}\sin(2\beta+\gamma)\cos(\delta^{(*)})$, $b^{(*)} = 2r'\sin(2\beta+\gamma)\cos(\delta')$, $c^{(*)} = 2\cos(2\beta+\gamma)(r^{(*)}\sin(\delta^{(*)}) - r'\sin(\delta'))$.

2.2 Full reconstruction of $B^0 \to D^{(*)}\pi$ [1)]

This method provides a large sample with few background. Signal and background are discriminated by two kinematic variables : the beam-energy substituted mass, $m_{ES} \equiv \sqrt{(\sqrt{s}/2)^2 - p_B^{*\,2}}$, and the difference between the B candidate's measured energy and the beam energy, $\Delta E \equiv E_B^* - (\sqrt{s}/2)$, where E_B^* (p_B^*) is the energy (momentum) of the B candidate in the e^+e^- center-of-mass frame, and $\sqrt{s}$ is the total center-of-mass energy. With $82 fb^{-1}$, we

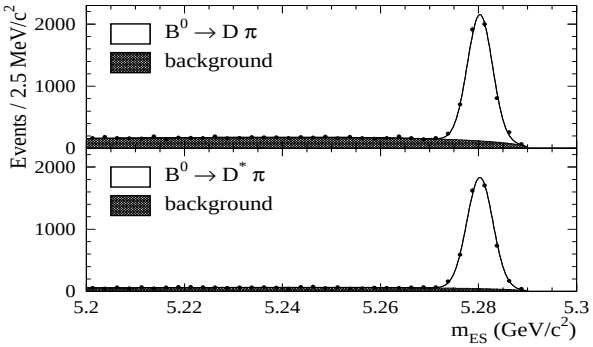

Figure 2: *Distributions of m_{ES} in the ΔE signal region for events in the $B^0 \to D^{\pm}\pi^{\mp}$ (upper plot) and the $B^0 \to D^{*\pm}\pi^{\mp}$ sample (lower plot).*

have 5207 ± 87 and 4746 ± 78 events for the $B^0 \to D^{\pm}\pi^{\mp}$ and $B^0 \to D^{*\pm}\pi^{\mp}$ sample respectively. We measure : $a = -0.022 \pm 0.038 \pm 0.020$ and $a^* = -0.068 \pm 0.038 \pm 0.020$.

2.3 Partial reconstruction of $B^0 \to D^*\pi$ [2)]

In the partial reconstruction method, only the hard pion track π_h from the B decay and the soft pion track π_s from the decay $D^{*-} \to \bar{D}^0\pi_s^-$ are used. Applying kinematic constraints, we calculate the four-momentum of the non-reconstructed D, obtaining its invariant mass M_{miss} [3)]. Signal events peak in the M_{miss} distribution at the nominal D^0 mass (Fig. 3).

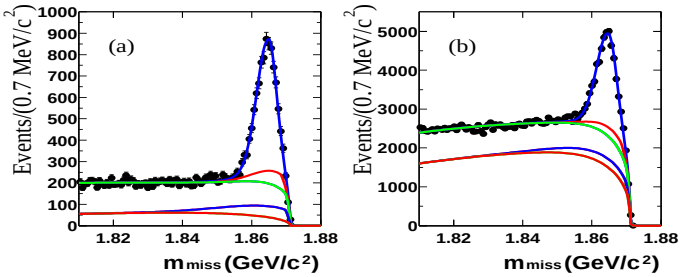

Figure 3: *The M_{miss} distributions for on-resonance lepton-tagged (left) and kaon-tagged (right) data.*

This method allows to select more events but there is also more background. With $76 fb^{-1}$, we have 6400 ± 130 (25160 ± 320) signal events for the lepton- (kaon-) tagged sample. The CP asymmetry is then $a^* = -0.063 \pm 0.024 \pm 0.014$. It deviates from zero by 2.3σ.

2.4 Combining the two results to put limits on $\sin(2\beta+\gamma)$

The measured CP-parameters are used to minimize a χ^2, in which we fit $|\sin(2\beta+\gamma)|$, δ, δ^*, r and r^*, applying the method of Ref. [4]. In this method, we assume SU(3) for the value of $r^{(*)}$ and we add a 30% flat theoretical error for $r^{(*)}$. It allows to put constrains in the (ρ, η) plane and the limits $|\sin(2\beta+\gamma)| > 0.74$ (0.58) at 90% (95%) of confidence level. Another method has been used only with the measurements related to $B^0 \to D^*\pi$ decays. In this method, no assumption are made on r^*, which is scanned. It allows to put a 95% confidence level lower limit on $|\sin(2\beta+\gamma)|$ as a function of r^*.

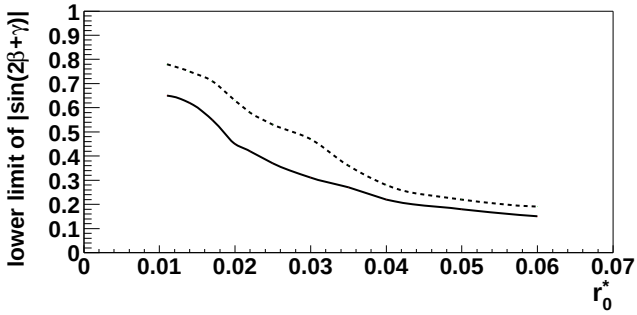

Figure 4: *95% CL lower limit on $|\sin(2\beta+\gamma)|$ as a function of r^*. The solid (dashed) curve corresponds to partial (partial and full) reconstruction*

3 Measuring γ with $B \to DK$ decays

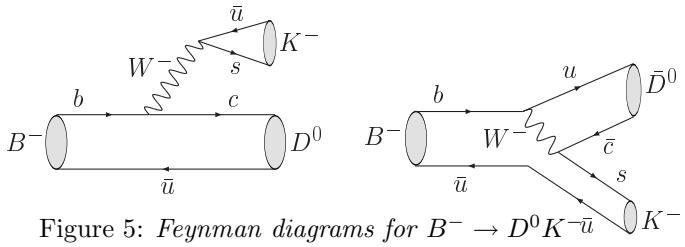

Figure 5: *Feynman diagrams for* $B^- \to D^0 K^- \bar{u}$

The phase γ is due to the interferences between $b \to u$ and $b \to c$ decay amplitudes. These interferences are possible if D^0 and $\bar{D}^0$ decay in the same final state f. Two methods are presented here to extract γ in that decays: GLW, if f is a CP-eigenstate ($\pi^+\pi^-$, K^+K^-) and ADS if f is a non CP eigenstate ($K^+\pi^-$).

3.1 Gronau-London-Wyler method : $B^\pm \to D^0_{CP} K^\pm$ [5)]

The angle γ is related to the ratios of Cabibbo-suppressed to Cabibbo-favored decays $R_{(CP)} = [\mathcal{B}(B^- \to D^0(D^0_{CP})K^-) + \mathcal{B}(B^+ \to \bar{D}^0(D^0_{CP})K^+)]/[\mathcal{B}(B^- \to D^0(D^0_{CP})\pi^-) + \mathcal{B}(B^+ \to \bar{D}^0(D^0_{CP})\pi^+)]$ with D^0 reconstructed in Cabibbo-allowed or CP-even (D^0_{CP}) channels. The direct CP asymmetry is : $A_{CP} = [\mathcal{B}(B^- \to D^0_{CP}K^-) - \mathcal{B}(B^+ \to D^0_{CP}K^+)]/[\mathcal{B}(B^- \to D^0_{CP}K^-) + \mathcal{B}(B^+ \to D^0_{CP}K^+)]$. We measure $R = (8.31 \pm 0.35$ (stat) ± 0.20 (syst) $) \times 10^{-2}$, $R_{CP} = (8.8 \pm 1.6$ (stat) ± 0.5 (syst) $) \times 10^{-2}$ and the CP asymmetry $A_{CP} = 0.07 \pm 0.17$ (stat) ± 0.06 (syst). The measured ratio R is consistent with Standard Model expectation ($\approx 7.5\%$) assuming factorization [8)]. In the Standard Model $R_{CP}/R = 1 + r^2 + 2r\cos\delta\cos\gamma$ and $A_{CP} = 2r\sin\delta\sin\gamma/(1 + r^2 + 2r\cos\delta\cos\gamma)$, where $r \approx 0.1 - 0.2$ is the magnitude of the ratio of the amplitudes for the processes $B^- \to D^0 K^-$ and $B^- \to D^0 K^-$, and δ is the (unknown) relative strong phase between these two amplitudes [9)]. The measured values of R and R_{CP} are equal within errors, and A_{CP} is consistent with zero.

3.2 Atwood-Dunietz-Soni method : $B^\pm \to D^0 K^\pm$, $D^0 \to K^+\pi^-/K^-\pi^+$ [6)]

We measure the branching ratios of the decay chains $B^- \to D^0 K^-$ ($b \to c$ transition) followed by the doubly Cabibbo-suppressed $D^0 \to K^+\pi^-$ and $B^- \to \bar{D}^0 K^-$ ($b \to u$ transition) followed by the Cabibbo-favored $\bar{D}^0 \to K^+\pi^-$.

The interferences between these two decay chains is sensitive to γ. We measure $R = [\mathcal{B}(B^- \to D_{K^+\pi^-} K^-) + \mathcal{B}(B^+ \to D_{K^-\pi^+} K^+)]/[\mathcal{B}(B^- \to D_{K^-\pi^+} K^-) + \mathcal{B}(B^+ \to D_{K^+\pi^-} K^+)]$, which corresponds to the ratio of branching fractions for suppressed and favored decays. We measure no events for the suppressed decays ($N_{suppressed} = 1.1 \pm 3.0$ and $N_{favored} = 261 \pm 32$). This leads to $R = 0.004 \pm 0.012$. We can put the limit $R < 0.026$ at 90 % C.L. We don't have enough statistics to conclude for that mode but it seems difficult to measure γ in that way.

4 Conclusion and prospects

The first steps to extract γ are promising. $D^{(*)}\pi$ analysis are well established ($|\sin(2\beta+\gamma)| > 0.74$ (0.58) at 90% (95%)) and will be updated with more data. GLW and ADS methods are actually limited by the statistics, but the analysis will also be updated and interesting results are expected. There are several other channels to explore in order to extract γ : $D^{(*)}\rho$, by the measurement of $\sin(2\beta+\gamma)$, GLW and ADS method with other final states and using D^*K^* and D^*K decays.

References

1. BABAR Collaboration, B. Aubert *et al*, Phys. Rev. Lett. **92** 251801 (2004).
2. BABAR Collaboration, B. Aubert *et al*, Phys. Rev. Lett. **92** 251802 (2004).
3. BABAR Collaboration, B. Aubert *et al*, Phys. Rev. D **67** 091101 (2003).
4. G. Feldman and R. Cousins, Phys. Rev. D **57**, 3873 (1998).
5. BABAR Collaboration, B. Aubert *et al*, hep-ex/0311032.
6. BABAR Collaboration, B. Aubert *et al*, hep-ex/0408028.
7. J.H. Christenson *et al*, Phys. Rev. Lett. **13**, 138 (1964).
8. M Gronau *et al.*, Phys. Rev. **D52** 6356-6373 (1995).
9. M. Gronau and D. Wyler, Phys. Lett. **B265**, 172 (1991); M. Gronau and D. London, Phys. Lett. **B253** 483 (1991); D. Atwood, I. Dunietz and A. Soni, Phys. Rev. Lett. **78**, 3257 (1997); M. Gronau, Phys. Lett. **B557** 198-206 (2003).

Frascati Physics Series Vol. XXXVI (2004), pp. 55–60
DAΦNE 2004: Physics at meson factories – Frascati, June 7-11, 2004
Selected Contribution in Plenary Session

MEASUREMENT OF ϕ_3 IN $B^\pm \to D^{(*)}K^\pm$ DECAYS AT BELLE

T. Gershon*
IPNS, KEK, 1-1 Oho, Tsukuba-shi, Ibaraki-ken, 305-0801, Japan

Abstract

We present a measurement of the unitarity triangle angle ϕ_3 using a Dalitz plot analysis of $D \to K_S\pi^+\pi^-$, using neutral D mesons produced in $B^\pm \to D^{(*)}K^\pm$ decay. Using 140 fb^{-1} of data collected by the Belle experiment we obtain $\phi_3 = 81^\circ \pm 19^\circ \pm 13^\circ$(syst) $\pm 11^\circ$(model). The 95% confidence interval is $35^\circ < \phi_3 < 127^\circ$. Note that the results presented here have been superseded. [1)]

1 Introduction

The determination of the Cabibbo-Kobayashi-Maskawa (CKM) matrix elements [2)] is important to check the consistency of the Standard Model and search for new physics. Various methods using $B \to DK$ decays have been

* On behalf of Belle Collaboration

introduced [3] to measure the unitarity triangle angle ϕ_3. Here we use a novel technique based on the analysis of the three-body decay of the D^0 meson. [4] This method is based on two key observations: neutral D^0 and $\bar{D}^0$ mesons can decay to a common final state $K_s\pi^+\pi^-$, and the decay $B^+ \to D^{(*)}K^+$ can produce neutral D mesons of both flavors via $\bar{b} \to \bar{c}u\bar{s}$ and $\bar{b} \to \bar{u}c\bar{s}$ transitions, where the relative phase θ_+ between the two interfering amplitudes is the sum, $\delta + \phi_3$, of strong and weak interaction phases. In the charge conjugate mode, the relative phase $\theta_- = \delta - \phi_3$, so both phases can be extracted from measurements of such B decays. The phase measurement is based on the analysis of the Dalitz distribution of the three body final state.

If the amplitude at each point in the Dalitz plot of $\bar{D^0} \to K_s\pi^+\pi^-$ is defined as $f(m_+^2, m_-^2)$, where m_+^2 and m_-^2 are the squared invariant masses of the $K_s\pi^+$ and $K_s\pi^-$ combinations, respectively, then assuming no CP asymmetry in D decays, the amplitude of the B^+ decay is written as

$$M_+ = f(m_+^2, m_-^2) + re^{i(\delta+\phi_3)} f(m_-^2, m_+^2), \tag{1}$$

where r is the absolute value of the ratio between the two interfering amplitudes. Similarly, the amplitude of the charge conjugate B^- decay is

$$M_- = f(m_-^2, m_+^2) + re^{i(\delta-\phi_3)} f(m_+^2, m_-^2). \tag{2}$$

Once the functional form of f is fixed, the Dalitz distributions for B^+ and B^- decays can be fitted simultaneously using the above expressions with r, ϕ_3, and δ as free parameters. The method is therefore directly sensitive to the value of ϕ_3; moreover, the obtained value of r can be used in other ϕ_3 measurements. The method has only a single ambiguity ($\phi_3 \to \phi_3 + \pi$, $\delta \to \delta + \pi$).

To fit the $\tilde{D} \to K_s\pi^+\pi^-$ Dalitz plot distributions corresponding to B^+ and B^- decays, we use an unbinned maximum likelihood technique with a neutral D decay model determined from a flavor-tagged D sample. The drawback of this approach is that while the absolute value of the $\bar{D}^0$ decay amplitude f is determined directly, its complex form can be obtained only with certain assumptions, leading to substantial model uncertainties in the determination of ϕ_3. These uncertainties can be controlled in future using data from $c\tau$-factories. A sample of CP tagged neutral D mesons, which can be produced in the decay of the $\psi(3770)$ resonance, will provide information about the complex phase of f, allowing a model-independent measurement of ϕ_3.

2 Event selection

The analysis uses 140 fb^{-1} of data collected by the Belle detector. [5] From this data sample we select 146 $B^\pm \to DK^\pm$ candidates, with a background fraction of $25 \pm 4\%$, and 39 $B^\pm \to D^*K^\pm$ candidates, with a background fraction of

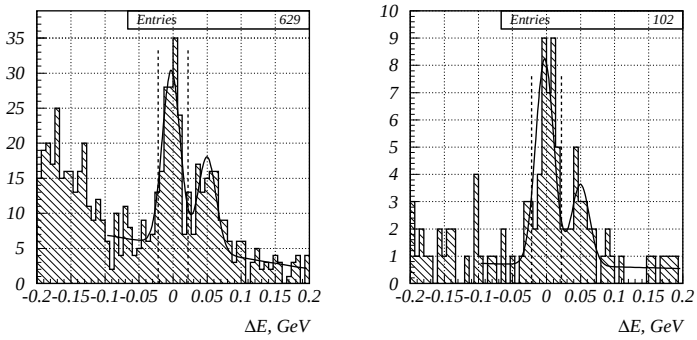

Figure 1: *ΔE distributions for (left) $B^{\pm} \to DK^{\pm}$ and (right) $B^{\pm} \to D^{*}K^{\pm}$ candidates. The signal region is shown by dotted lines.*

$12 \pm 4\%$. The ΔE distributions (the difference between the reconstructed and expected B candidate energies) are shown in Fig. 1. We also select 104204 $D^{*\pm} \to D\pi_s^{\pm}$ candidates, with a background fraction of 3.09±0.05%, which are used in the determination of the $\bar{D}^0$ decay model.

3 Determination of $\bar{D}^0 \to K_s\pi^+\pi^-$ decay model

The amplitude f of the $\bar{D}^0 \to K_s\pi^+\pi^-$decay is represented by a coherent sum of two-body decay matrix elements, each having its own amplitude and phase, plus one non-resonant decay amplitude. To be consistent with the CLEO analysis, [6] we have chosen the $K_s\rho$ mode to have unit amplitude and zero relative phase, and use an established description of the matrix elements. [7]

We use a set of 15 two-body amplitudes, as shown in Table 1. These include four Cabibbo-allowed $K^*\pi$ amplitudes, their doubly Cabibbo-suppressed partners, and seven channels with K_s and a $\pi\pi$ resonance. The masses and Breit-Wigner widths of scalars σ_1 and σ_2 are left unconstrained, while the parameters of other resonances are the same as in the CLEO analysis. [6] The parameters of the σ resonances obtained in the fit are as follows: $M_{\sigma_1} = 539 \pm 9$ MeV/c^2, $\Gamma_{\sigma_1} = 453 \pm 16$ MeV/c^2, $M_{\sigma_2} = 1048 \pm 7$ MeV/c^2, $\Gamma_{\sigma_2} = 109 \pm 11$ MeV/c^2.

We perform an unbinned maximum likelihood fit to the Dalitz plot distribution. The fit function is represented by the sum of the squared absolute value of the decay amplitude $|f(m_+^2, m_-^2)|^2$ and the background distribution, with momentum resolution and detector efficiency taken into account. The amplitudes and phases obtained from the fit are presented in Table 1.

Table 1: *Fit results for $\bar{D}^0 \to K_s\pi^+\pi^-$ decay. Errors are statistical only.*

Resonance	Amplitude	Phase (°)
$K^*(892)^-\pi^+$	1.656 ± 0.012	137.6 ± 0.6
$K^*(892)^+\pi^-$	$(14.9 \pm 0.7) \times 10^{-2}$	325.2 ± 2.2
$K_0^*(1430)^-\pi^+$	1.96 ± 0.04	357.3 ± 1.5
$K_0^*(1430)^+\pi^-$	0.30 ± 0.05	128 ± 8
$K_2^*(1430)^-\pi^+$	1.32 ± 0.03	313.5 ± 1.8
$K_2^*(1430)^+\pi^-$	0.21 ± 0.03	281 ± 9
$K^*(1680)^-\pi^+$	2.56 ± 0.22	70 ± 6
$K^*(1680)^+\pi^-$	1.02 ± 0.2	103 ± 11
$K_s\rho^0$	1.0(fixed)	0(fixed)
$K_s\omega$	$(33.0 \pm 1.3) \times 10^{-3}$	114.3 ± 2.3
$K_sf_0(980)$	0.405 ± 0.008	212.9 ± 2.3
$K_sf_0(1370)$	0.82 ± 0.10	308 ± 8
$K_sf_2(1270)$	1.35 ± 0.06	352 ± 3
$K_s\sigma_1$	1.66 ± 0.11	218 ± 4
$K_s\sigma_2$	0.31 ± 0.05	236 ± 11
non-resonant	6.1 ± 0.3	146 ± 3

4 Dalitz plot analysis of $B^\pm \to D^{(*)}K^\pm$ decay

The Dalitz plots (shown for $B^\pm \to DK^\pm$ candidates in Fig. 2) are fitted by minimizing the combined logarithmic likelihood function for B^- and B^+ data sets. The corresponding Dalitz plot densities are based on decay amplitudes $M_\pm$ described by Eqs. 1 (B^+) and 2 (B^-). The $\bar{D}^0$ decay model f is fixed, and the free parameters of the fit are the amplitude ratio r and phases ϕ_3 and δ. Contributions from several background sources are taken into account; the largest background source is of combinatoric origin.

To test the consistency of the fit, we use $B^\pm \to D^{(*)}\pi^\pm$ and $\bar{B}^0(B^0) \to D^{*\pm}\pi^\mp$ control samples. For the control sample fits, we consider B^+ and B^- data separately, to check for the absence of CP violation. In the fit of $B^\pm \to D\pi^\pm$ data, we obtain $r \sim 0.06$, more than two standard deviations from zero; however, no CP asymmetry is found. (Note that a non-zero amplitude ratio is expected - $r \sim |V_{ub}V_{cd}^*|/|V_{cb}V_{ud}^*| \sim 0.02$). This bias is considered as a systematic effect. The other control samples do not show any significant deviation from $r = 0$.

The combined unbinned maximum likelihood fit of B^+ and B^- samples with free parameters r, ϕ_3 and δ yields the following values: $r = 0.31 \pm 0.11$, $\phi_3 = 86° \pm 17°$, $\delta = 168° \pm 17°$ for $B^\pm \to DK^\pm$ and $r = 0.34 \pm 0.14$, $\phi_3 = 51° \pm 25°$, $\delta = 302° \pm 25°$ for $B^\pm \to D^*K^\pm$.

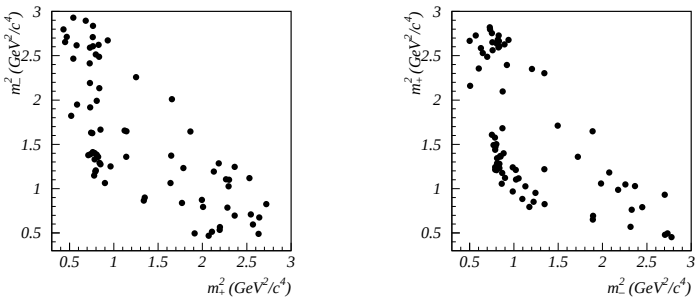

Figure 2: *Dalitz plots for (left) $B^+ \to DK^+$ and (right) $B^- \to DK^-$ candidates. CP violation would appear as a difference between these two plots.*

To estimate the statistical errors we do not use the values obtained from the likelihood fit given above, but follow a Bayesian approach in which a large number of MC pseudo-experiments are used to obtain a probability density function (PDF) of the fitted parameters for any set of true parameters.

The results for ϕ_3 from the "toy" MC are: $\phi_3 = 86 \pm 20°(49°)$ for $B^\pm \to DK^\pm$ and $\phi_3 = 51 \pm 47°(82°)$ for $B^\pm \to D^*K^\pm$; where the errors are 68% (95%) confidence limits. We obtain a combined result from $B^\pm \to DK^\pm$ and $B^\pm \to D^*K^\pm$ by multiplying the ϕ_3 PDFs; the result is $\phi_3 = 81 \pm 19°(46°)$.

The model used for the $\bar{D}^0 \to K_s\pi^+\pi^-$ decay is one of the main sources of uncertainty in our analysis. To estimate the model uncertainties, a MC simulation is performed. Event samples are generated according to the amplitude described by Eqs. 1 and 2 with resonance parameters as in Table. 1, and then fit these samples with different models for $f(m_+, m_-)$. Since the Breit-Wigner amplitude only describes narrow resonances well, we scan for the maximum deviation of the fit parameters using a fit model containing only narrow resonances, with wide ones approximated by a constant complex term. The estimated value of the systematic uncertainty on ϕ_3 is 11°.

Other sources of systematic errors include the uncertainties of the knowledge of the detector response, background estimation and possible fit biases. The non-zero amplitude ratio observed in the $B^\pm \to D\pi^\pm$ control sample may be due to a statistical fluctuation or may indicate some systematic effect such as background structure or a deficiency of the decay model; we conservatively treat it as an additional systematic effect. The corresponding bias of the weak and strong phases is 11°; this contribution dominates the systematic error.

5 Conclusion

We have studied a new method to measure the unitarity triangle angle ϕ_3 using Dalitz plot analysis of the three-body D^0 decay in the process $B^\pm \to$

$D^{(*)}K^{\pm}$. The first measurement of ϕ_3 using this technique was performed based on 140 fb^{-1} statistics collected by the Belle detector. From the combined fit of $B^{\pm} \to DK^{\pm}$ and $B^{\pm} \to D^*K^{\pm}$ modes, we obtain the value of $\phi_3 = 81^\circ \pm 19^\circ \pm 13^\circ \pm 11^\circ$. The first error is statistical, the second is experimental systematics and the third is model uncertainty. The 95% confidence interval is $35^\circ < \phi_3 < 127^\circ$ The statistical significance of the CP violation is 94% for $B^{\pm} \to DK^{\pm}$ mode and 38% for $B^{\pm} \to D^*K^{\pm}$ mode.

The method has a number of advantages over other methods to measure ϕ_3. [3] It is directly sensitive to the value of ϕ_3 and has only one discrete ambiguity. Note that the results presented here have been superseded. [1]

6 Acknowledgments

I would like to thank the organizers for an enjoyable conference. I am grateful to A. Poluektov for his help in preparing these proceedings. The author is supported by the Japan Society for the Promotion of Science.

References

1. A. Poluektov, *et al.* (Belle Collaboration), `hep-ex/0406067`, submitted to Phys. Rev. D.

2. M. Kobayashi and T. Maskawa, Prog. Theor. Phys. **49**, 652 (1973); N. Cabibbo, Phys. Rev. Lett. 10, 531 (1963).

3. M. Gronau and D. Wyler, Phys. Lett. **B265**, 172 (1991); I. Dunietz, Phys. Lett. **B270**, 75 (1991); D. Atwood, G. Eilam, M. Gronau and A. Soni, Phys. Lett. **B341**, 372 (1995); D. Atwood, I. Dunietz and A. Soni, Phys. Rev. Lett. **78**, 3257 (1997).

4. A. Giri, Yu. Grossman, A. Soffer and J. Zupan, Phys. Rev. D **68**, 054018 (2003); this technique was proposed independently in the Belle Collaboration, (Proceedings of BINP Special Analysis Meeting on Dalitz Analysis, 24-26 Sep. 2002, unpublished).

5. A. Abashian *et al.* (Belle Collaboration), Nucl. Instr. and Meth. **A479**, 117 (2002).

6. H. Muramatsu *et al.* (CLEO Collaboration), Phys. Rev. Lett.**89**, 251802 (2002), Erratum-ibid: **90**, 059901 (2003).

7. S. Kopp *et al.* (CLEO Collaboration), Phys. Rev. **D63**, 092001 (2001).

Frascati Physics Series Vol. XXXVI (2004), pp. 61–66
DAΦNE 2004: Physics at meson factories – Frascati, June 7-11, 2004
Selected Contribution in Plenary Session

SEARCH FOR CP VIOLATION IN HYPERON DECAYS WITH THE HYPERCP SPECTROMETER AT FERMILAB

E. Craig Dukes*
University of Virginia, Charlottesville, VA 22901, USA

Abstract

Searches for *CP* violation in hyperon decays are sensitive to beyond-the-standard-model sources that are not probed in other systems. We report on a new result from the Fermilab *HyperCP* experiment, which is searching for *CP* violation by comparing the proton and antiproton angular distributions in $\Xi^- \to \Lambda\pi^- \to p\pi^-\pi^-$ and $\overline{\Xi}^+ \to \overline{\Lambda}\pi^+ \to \overline{p}\pi^+\pi^+$ decays. This result represents a greatly increased sensitivity over previous measurements and is confronting some beyond-the-standard-model theory predictions.

1 Introduction

Although *CP* violation is accommodated quite nicely in the standard model — in the complex phase of the CKM matrix — its origin remains a mystery. And

* On behalf of the *HyperCP* collaboration.

although *CP* violation is expected to be ubiquitous in weak interactions, albeit often vanishingly small, the experimental evidence is still meager. In addition, many beyond-the-standard-model theories can produce relatively large *CP*-violating effects, none of which have yet been seen. It behooves us then to search for other manifestations of this phenomenon. Hyperon decays offer a promising venue for such searches as hyperons are particularly sensitive to certain exotic sources of *CP* violation.

2 Theoretical Expectations

The most accessible signature for *CP* violation in spin-1/2 hyperons is the comparison of the angular decay distribution of the daughter baryon with that of the conjugate antibaryon in their two-body nonleptonic weak decays. These distributions are not isotropic because of parity violation, but are given by:

$$\frac{dN}{d\cos\theta} = \frac{N_0}{2}(1 + \alpha P_p \cos\theta), \tag{1}$$

where P_p is the parent hyperon polarization, $\cos\theta$ is the daughter baryon direction in the rest frame of the parent, and $\alpha = 2\mathrm{Re}(S^*P)/(|S|^2 + |P|^2)$, where S and P are the usual angular momentum amplitudes. If *CP* is good $\overline{\alpha} = -\alpha$; hence a difference in the magnitudes of the hyperon and antihyperon alpha parameters is evidence of *CP* violation. To extract α, hyperons whose polarizations are exactly known are needed.

To leading order the differences in alpha parameters for $\Lambda \to p\pi^-$ and $\Xi^- \to \Lambda\pi^-$ decays are [1]:

$$A \equiv \frac{\alpha + \overline{\alpha}}{\alpha - \overline{\alpha}} \cong -\tan(\delta_P - \delta_S)\sin(\phi_P - \phi_S), \tag{2}$$

where the δ are the strong phase shifts and the ϕ are the weak phases. The strong final-state phase-shift differences are small: $7^\circ \pm 1^\circ$ for $p\pi$ [2] and $4.6^\circ \pm 1.8^\circ$ for $\Lambda\pi$ [3]. A recent standard model calculation of the *CP* asymmetries has values that range from $-0.3\times10^{-4} \leq A_\Lambda \leq 0.4\times10^{-4}$ and $-0.2\times10^{-4} \leq A_\Xi \leq 0.1\times10^{-4}$ [4]. These magnitudes are too small to be experimentally observable at the present time. However, beyond-the-standard-model theories can produce larger asymmetries that *are not well constrained by kaon CP measurements* because hyperon *CP* violation probes both parity-conserving and parity-violating amplitudes whereas ϵ and ϵ' probe only parity-violating amplitudes. For example, a recent paper shows that the upper bound on the combined asymmetry

$A_{\Xi\Lambda} \equiv A_\Xi + A_\Lambda$ from ϵ and ϵ' measurements is $\sim 100\times10^{-4}$ [5]. The supersymmetric calculation of Ref. [6], which does not contribute to ϵ', can produce a value of A_Λ of $\mathcal{O}(10^{-3})$. Other beyond-the-standard-model theories also have enhanced *CP* asymmetries. Therefore, any observed effect will almost certainly be due to new physics.

3 The *HyperCP* Search for *CP* Violation

The *HyperCP* experiment produced Λ's and $\overline{\Lambda}$'s with *almost* precisely known polarizations by requiring that they come from $\Xi^- \to \Lambda\pi^-$ and $\overline{\Xi}^+ \to \overline{\Lambda}\pi^+$ decays. The Ξ^- and $\overline{\Xi}^+$ hyperons were forced by parity conservation in the strong interaction to have *zero* polarization by producing them with an average angle of 0°. A Λ from the weak decay of an unpolarized Ξ is found in a pure helicity state with a polarization magnitude given by the parent Ξ alpha parameter. The decay distributions of the proton and antiproton in the frame in which the Λ polarization defines the polar axis — the Lambda Helicity Frame — are given by:

$$\frac{dN}{d\cos\theta} = \frac{N_0}{2}(1 + \alpha_\Lambda P_\Lambda \cos\theta) = \frac{N_0}{2}(1 + \alpha_\Lambda \alpha_\Xi \cos\theta). \tag{3}$$

If *CP* symmetry is good then $\overline{\alpha}_\Xi = -\alpha_\Xi$ and $\overline{\alpha}_\Lambda = -\alpha_\Lambda$ and any difference in the proton and antiproton decay distributions is evidence of *CP* violation. The experiment is sensitive to *CP* violation in both Ξ and Λ decays:

$$A_{\Xi\Lambda} \equiv A_\Lambda + A_\Xi \cong \frac{\alpha_\Lambda\alpha_\Xi - \overline{\alpha}_\Lambda\overline{\alpha}_\Xi}{\alpha_\Lambda\alpha_\Xi + \overline{\alpha}_\Lambda\overline{\alpha}_\Xi}. \tag{4}$$

The *HyperCP* spectrometer (Fig. 1) was designed to be simple, fast, and to have considerable redundancy [7]. A charged secondary beam with a mean momentum of about 160 GeV/c was produced by steering the Tevatron 800 GeV/c primary proton beam onto a $2\times2\,\mathrm{mm}^2$ Cu target which was immediately followed by a collimator embedded in a 6.1 m long dipole magnet (Hyperon Magnet). The central orbit of the beam exited the collimator upward at 19.51 mrad. Following an evacuated decay region was a magnetic spectrometer employing nine high-rate, narrow-pitch wire chambers. The spectrometer magnets (Analyzing Magnets) had sufficient field integrals to insure that the protons from $\Xi \to \Lambda\pi \to p\pi\pi$ decays were always deflected to one side of the spectrometer, with the two pions deflected to the opposite side,

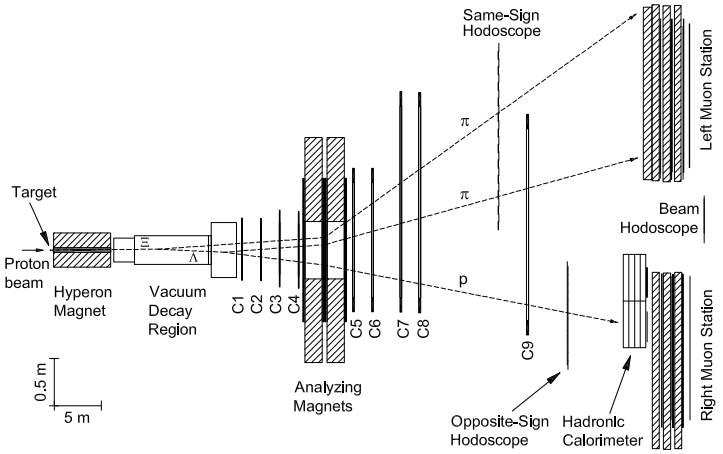

Figure 1: *Plan view of the HyperCP apparatus.*

and that both were well separated from the intense ($\sim 13\times10^6\,\mathrm{s}^{-1}$) secondary beam. A simple trigger was formed by requiring the coincidence at the rear of the spectrometer of charged particles in two hodoscopes (Same-Sign and Opposite-Sign Hodoscopes) situated on either side of the spectrometer, as well as a minimum amount of energy in a hadronic calorimeter on the proton side of the spectrometer. The Ξ^- and $\overline{\Xi}^+$ hyperons were produced alternately by periodically switching the polarities of the Hyperon and Analyzing Magnets.

In two running periods (1997 and 1999) of about 12 months duration one of the largest data samples ever was recorded, at 231 billion events, and by far the largest number of hyperons. The final dataset was approximately 2.5 billion $\Xi^- \to \Lambda\pi^- \to p\pi^-\pi^-$ and $\overline{\Xi}^+ \to \overline{\Lambda}\pi^+ \to \overline{p}\pi^+\pi^+$ decays, *four orders of magnitude more than that of all other hyperon CP violation searches combined.*

The analysis method was simple: compare the proton and antiproton $\cos\theta$ distributions directly, without acceptance corrections. Before this could be done the momentum and spatial distributions of the Ξ^- and $\overline{\Xi}^+$ events at the collimator exit (their effective production point) had to be made identical, since different production dynamics give different momentum spectra for the two. This was done by weighting the Ξ^- and $\overline{\Xi}^+$ events in each of the three momentum-dependent parameters at the collimator exit: the magnitude of the momentum, the y slope, and the y position of the Ξ. Each parameter was

binned in 100 bins for a total of one million weights. The ratio of the weighted proton and antiproton $\cos\theta$ distributions was then made. Any nonzero slope in that ratio is evidence of *CP* violation. The ratio was fit to the following form,

$$R = C\frac{1+\alpha_\Xi\alpha_\Lambda\cos\theta}{1+(\alpha_\Xi\alpha_\Lambda-\delta)\cos\theta}, \tag{5}$$

to extract the asymmetry $\delta \equiv \alpha_\Xi\alpha_\Lambda - \overline{\alpha}_\Xi\overline{\alpha}_\Lambda \cong 2\alpha_\Xi\alpha_\Lambda{\cdot}A_{\Xi\Lambda}$, where the known value of $\alpha_\Xi\alpha_\Lambda$ was used.

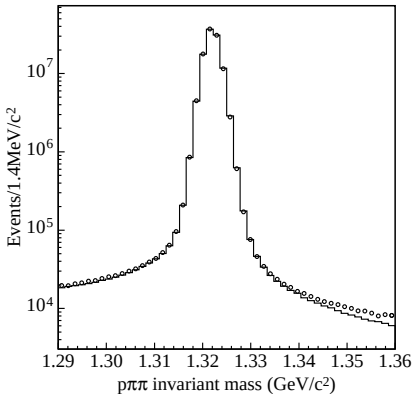

Figure 2: *The unweighted $p\pi^-\pi^-$ (histogram) and $\overline{p}\pi^+\pi^+$ (circles) invariant masses.*

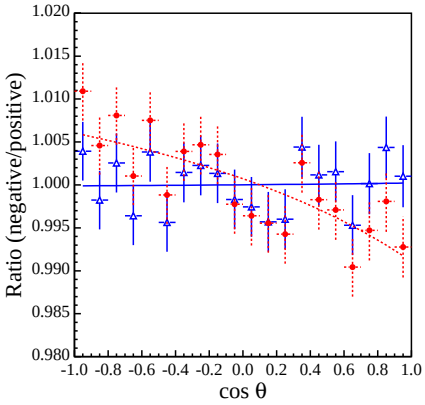

Figure 3: *Fits to the weighted (triangles) and unweighted (circles) p to $\overline{p}$ $\cos\theta$ ratios from Analysis Set 1.*

About 117 (41) million Ξ^- ($\overline{\Xi}^+$) decays selected from the end of the 1999 run were used — about 10% of the dataset. Fig. 2 shows the Ξ^- and $\overline{\Xi}^+$ masses after all cuts. The background under the peak is 0.42% for both. The data were divided into 18 parts (Analysis Sets) each of roughly equal size. Each Analysis Set was analyzed separately. Fig. 3 shows the $\cos\theta$ ratio for one of the Analysis Sets, before and after weighting. Fits to Eq. (5) were good: the average chi-squared per degree of freedom, for all 18 Analysis Sets, was 0.97.

The average asymmetry from all 18 Analysis Sets, after background subtraction and with no acceptance or efficiency corrections, was found to be zero: $A_{\Xi\Lambda} = [0.0\pm5.1(\text{stat})\pm4.4(\text{syst})]\times10^{-4}$, with $\chi^2 = 24$. This is a factor of twenty improvement in sensitivity over the best previous result [8].

Systematic errors were small for several reasons. First, taking the ratio of

$\cos\theta$ distributions reduced those common to the proton and antiproton. Second, the analysis locked in to the signal, in a manner analogous to a lock-in amplifier, by measuring the proton $\cos\theta$ distributions in the Lambda Helicity Frame, the polar axis of which changed from event to event. The largest systematic error (2.4×10^{-4}) is due to the uncertainties in the calibration of the Hall probes situated in the Analyzing Magnets. The next largest (2.1×10^{-4}) is the statistics-limited uncertainty due to differences in the calorimeter efficiencies between positive- and negative-polarity running. The only other significant systematic error is the uncertainty in the validation of the analysis code (1.9×10^{-4}), again a statistics-limited result. Wire chamber and hodoscope efficiency differences were so small that they were not corrected for, but rather added in as negligibly small systematic errors. No dependence of the asymmetry on Ξ momentum, secondary-beam intensity, or time was found.

The analysis of the entire 1999 *HyperCP* data set is well underway and it is hoped that within a year a result with an improvement in precision of at least two will be obtained, both in statistical and systematic errors.

4 Acknowledgments

I wish to thank the organizers of DAΦNE 2004 for a most enlightening and entertaining conference, and, as always, my *HyperCP* colleagues. This work was supported in part by the U.S. Department of Energy.

References

1. J.F. Donoghue, X.-G. He, and S. Pakvasa, Phys. Rev. D **34**, 833 (1986).
2. L.D. Roper, R.M. Wright, and B.T. Feld, Phys. Rev. **138**, B190 (1965).
3. M. Huang *et al.*, Phys. Rev. Lett. **93**, 011802 (2004).
4. J. Tandean and G. Valencia, Phys. Rev. D **67**, 056001 (2003).
5. J. Tandean, Phys. Rev. D **69**, 076008 (2004).
6. X.-G. He *et al.*, Phys. Rev. D **61**, 071701(R) (2000).
7. R. Burnstein *et al.*, hep-ex/0405034.
8. K.B. Luk *et al.*, Phys. Rev. Lett. **85**, 4860 (2000).

Frascati Physics Series Vol. XXXVI (2004), pp. 67–76
DAΦNE 2004: Physics at meson factories – Frascati, June 7-11, 2004
Invited Review Talk in Plenary Session

PROSPECTS ON CP VIOLATION IN THE B SECTOR AT HADRON COLLIDERS

Marta Calvi
Dipartimento di Fisica Università di Milano-Bicocca
and INFN Sezione di Milano

Abstract

Hadron Colliders are the most copious source of b hadrons. We present results on B Physics and CP violation from the running experiments CDF and DØ at the Tevatron Run II, and prospects for future measurements by the next generation of experiments: LHCb at LHC and BTeV at Tevatron.

1 Introduction

B decays offer great opportunities to test the Standard Model paradigm of quark mixing and CP violation, but also to discover signal of new couplings and measure their strength and phases. Several B decay modes can be used to measure the sides and the angles of the Unitarity Triangles making possible to over-constraint the Triangles and, comparing different results, eventually show the effects of New Physics.

B physics at Hadron Colliders have the great advantage of the high $b\bar{b}$ cross section, several order of magnitude higher than at e^+e^- Colliders at the $\Upsilon(4S)$, and of the production of all species of b-hadrons, including B_s, b-baryons and B_c. The challenge in the physics analysis is related to the high track multiplicity and to the high rate of background events. This demands to the experiments an excellent trigger capability, with good efficiency also on fully hadronic decay modes of b-hadrons, excellent tracking and vertexing capability, resulting in high mass resolution and proper time resolution, and excellent particle identification capability for separation of exclusive decays.

The feasibility and the good perspectives of this approach have already been demonstrated by the first results obtained at the Tevatron Collider Run II by the CDF and DØ experiments, this program will be further developed and completed in the coming years by the new generation of experiments: LHCb and BTeV.

2 Present and future Experiments

2.1 CDF and DØ

The Tevatron accelerator complex has undergone an extensive upgrade for the Run II phase. The instantaneous luminosity has been growing steadily up to the recent maximum of 7.3×10^{31} sec^{-1} cm^{-2}. Projection for the future are to accumulate from 4.4 to 8.5 fb^{-1} for the year 2009. A description of the major upgrades CDF and DØ Detectors can be found elsewhere [?]. It is relevant to mention here the installation in CDF of a new Silicon Vertex Trigger, selecting on tracks with high impact parameter and high p_T, which is pioneering the hadronic track triggers of the future experiments.

2.2 LHCb and BTeV

A comparison of the future LHC and Tevatron features is given in Table**??**. The higher energy at LHC, with respect to the Tevatron, will give a $b\bar{b}$ cross section about five times larger, with an inelastic cross section which is only a factor 1.6 higher.

The LHCb luminosity will be controlled during the high-luminosity LHC runs by locally de-tuning the beam focus, and will give an average of about 0.4 visible interaction per bunch crossing. Having a single primary vertex have

Table 1: *Expected features of the Tevatron and LHC Colliders*

	LHC (LHCb)	Tevatron (BTeV)
Energy/collision mode	14 TeV pp	2 TeV $p\bar{p}$
$b\bar{b}$ cross section	$\sim 500\mu$b	$\sim 100\mu$b
inelastic cross section	~ 50 mb	~ 80 mb
bunch spacing	25 ns	396 ns
Luminosity (cm^{-2} s^{-1})	2×10^{32}	2×10^{32}
$b\bar{b}$ events per 10^7 s	10^{12}	2×10^{11}
interactions per crossing	~ 0.4	~ 6
σ_z	5 cm	30 cm
expected year of startup	2007	2009

several advantages: reducing confusion to the trigger, reducing particle occupancy and hence improving pattern recognition in the detector components. Low luminosity also ensures less radiation damage.

At the Tevatron, in the present running scheme, the average number of interaction per bunch crossing will be about 6 at the luminosity foreseen for BTeV, however the interactions will be distributed on a long luminous region, and this will allow to reconstruct different interactions.

Both the LHCb and BTeV are single-arm forward detectors. The $b\bar{b}$ production cross section is sharply peaked in the forward (backward) direction, with a strong correlation between the direction of the b and the $\bar{b}$. Therefore the acceptance for the selected B decay and its companion b quark, which is used for tagging purposes, is high. B hadrons produced in the high pseudorapidity region have a larger boost than in the central region, therefore a longer decay length which is an advantage for signal separation. A schematic of the LHCb detector, presently under construction, is shown in Fig. **??**. A description of the detector and its performances can be found in [?]. The BTeV detector [?] has recently undergone first stages of approval and is planned to be installed at the Tevatron Collider during the 2009 summer shutdown. A schematic is shown in Fig. **??**.

3 B Flavour Tagging

The identification of the flavour of the B hadron at its production is necessary for oscillation measurements and most CP violation measurements. This

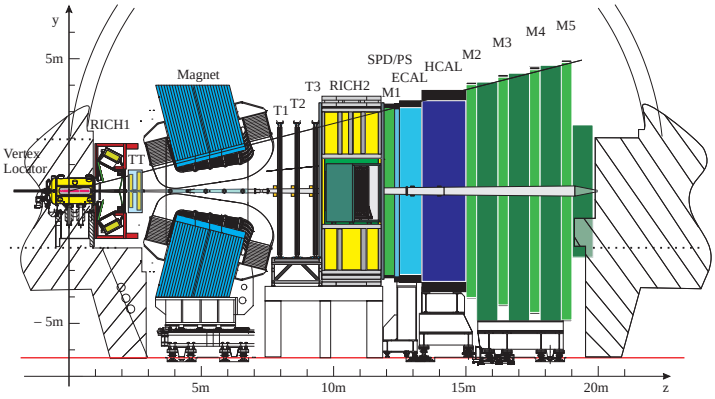

Figure 1: *A schematic of the LHCb detector.*

is usually obtained at the B-Factories by the exclusive reconstruction of the opposite B meson. At Hadron Colliders several inclusive tagging methods are used, which are designed either to identify directly the flavour of the $\bar{b}$ (b) quark in the signal B ($\bar{B}$) meson (same side tag) or that of its companion b ($\bar{b}$) (opposite side tag). Same side tags exploit the correlation between a B_d^0 and a positively charged pion originating in the fragmentation chain, or pions produced in the decay of an excited B^{**} state. The same correlation is present between B_s^0 and K^+ and can be exploited if kaon/pion identification is possible in the detector. Opposite side tags are based on the identification of leptons from the semileptonic decay of the b-hadrons, of kaons from the $b \to c \to s$ decay chain or on the reconstruction of the jet charge or of the charge of an inclusive secondary vertex. The flavour tagging optimization is still in progress in both CDF and DØ experiments, Table **??** shows preliminary results on the tagging power ϵD^2 obtained with different algorithms.

Expectation for LHCb and BTeV flavour tagging performance are also shown in Table **??**. They get substantial improvement from kaon tagging, due to the ID capability.

4 Perspectives on $B_s^0 - \bar{B}_s^0$ mixing measurements

4.1 Δm_s measurements

The $B_s^0 - \bar{B}_s^0$ oscillation frequency is too fast to be resolved at LEP and SLC, despite the relevant statistics of B_s^0 decays collected there. Tevatron is at

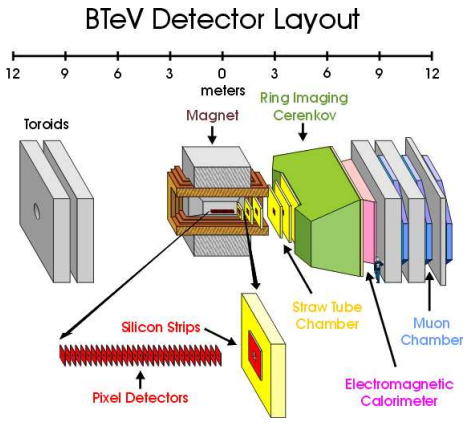

Figure 2: *A schematic of the BTeV detector.*

present the unique available source of B_s^0 mesons and CDF and DØ have the chance to find a mixing signal in the next coming years. The measurement requires best performances in the event reconstruction, purity, proper time resolution and flavour tagging.

If the true value of Δm_s is only slightly above the current world average limit ($\Delta m_s > 14.5$ ps^{-1} at 95% CL) it can be reached using semileptonic decays $B_s^0 \to D_s \ell \nu X$, ($D_s \to \phi\pi$, $\phi \to KK$) since the large statistics compensates the limited proper time resolution caused by the missing momentum of the neutrino. Thanks to the large acceptance on muons, DØ currently has a specific yield in the muon channel of about 31 pb, and expects to reach a 1.5 σ sensitivity up to $\Delta m_s = 15$ ps $^{-1}$ with 0.5 fb^{-1} of data. CDF has a lower efficiency in this channel, but is favored in the selection of exclusive hadronic decays with better purity and proper time resolution. Some improvements are expected in the event yield from the addition of other decay modes like $B_s^0 \to D_s \pi\pi\pi$ and $D_s \to K^*K, K_s^0 K$, in the proper time resolution up to $\sigma_\tau = 50$ fs and in the flavour tagging performances to reach ϵD^2=5%. In this condition CDF expects to reach a 5 σ sensitivity up to $\Delta m_s = 18$ ps^{-1} with 1.7 fb^{-1} and up to $\Delta m_s = 24$ ps^{-1} with 3.2 fb^{-1}.

But the definitive answer on $B_s^0 - \bar{B}_s^0$ mixing may come from the next generation of B experiments. Results of LHCb full simulation indicate a proper time resolution for $B_s^0 \to D_s \pi$ events of $\sigma_\tau = 33$ fs and an annual yield of 80.000 events with a background over signal ratio of 0.32. The expected proper time

Table 2: *Tagging powers ϵD^2 (in%) obtained by the CDF and DØ experiments (preliminary), and expected in the LHCb and BTeV experiments. In the last line combined results are shown, after removing the overlaps between different tagging algorithms.*

	CDF	DØ	LHCb		BTeV	
			B_d^0	B_s^0	B_d^0	B_s^0
Opposite μ	0.7 ± 0.1	1.6 ± 1.1	1.0	1.0	1.2	1.3
Opposite e	in progress	in progress	0.4	0.4	0.8	0.9
Opposite K	in progress	-	2.4	2.4	6.0	5.8
Jet charge	0.42 ± 0.02	3.3 ± 1.7	1.0	1.0	4.8	4.5
Same side π	2.4 ± 1.2	5.5 ± 2.0	0.7		1.8	
Same side K	in progress	-		2.1		5.7
Combined			4.7	6.0	10.0	13.0

distribution of tagged events is shown in Fig. **??** for two different values of Δm_s. In one year of data taking a 5 σ sensitivity up to $\Delta m_s = 68$ ps^{-1} is expected, and a precision on the measurement $\sigma(\Delta m_s) \sim 0.01$ ps^{-1}. Similar performances are expected in BTeV with a 5 σ observation of B_s^0 oscillations up to 51 ps^{-1} in one year.

4.2 ϕ_s and $\Delta\Gamma_s/\Gamma_s$ measurements

The phase ϕ_s of $B_s^0 \bar{B}_s^0$ mixing has high sensitivity to possible New Physics contributions in $b \to s$ transition because it is expected to be very small in the Standard Model $\phi_s = -2\chi = -2\lambda^2\eta \simeq -0.04$. Hint of New Physics could also be found in the measurement of the decay width difference between the two B_s CP eigenstates $\Delta\Gamma_s = \Gamma(B_L) - \Gamma(B_H)$ which is expected in the Standard Model to be of the order of 10%. Both quantities can be measured using $B_s^0 \to J/\psi\phi$ decays. CDF and DØ have observed the exclusive decays $B_s^0 \to J/\psi\phi$ ($J/\psi \to \mu\mu, \phi \to KK$). The mass distribution is shown in Fig. **??**.

Due to the fact that both J/ψ and ϕ are vector mesons, there are three distinct amplitudes contributing to this decay: two CP even and one CP odd. The two CP components can be disentangled on a statistical basis taking into account the distribution of the so-called transversity angle θ_{tr}, defined as the angle between the positive lepton and the ϕ decay plane, in the J/ψ rest frame.

LHCb in one year of data taking expects to collect 100.000 $J/\psi\phi$ decays

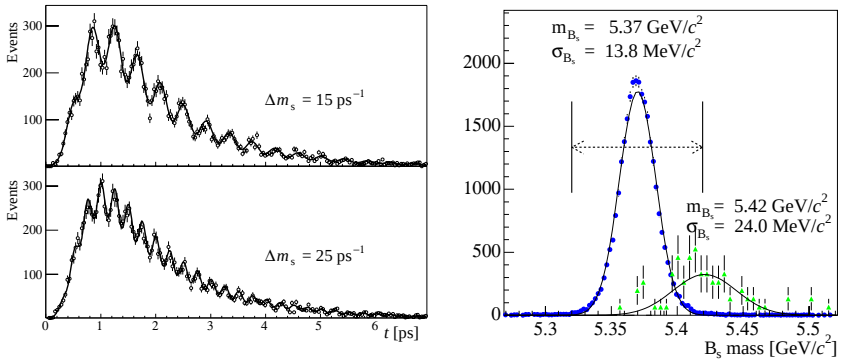

Figure 3: *Left: LHCb Expected proper time distribution of simulated* $B_s^0 \to D_s\pi$ *candidates that have been flavour tagged as having not oscillated, for two different values of* Δm_s*. The statistics corresponds to one year of data taking. Right: The* B_s^0 *mass distribution of* $B_s^0 \to D_sK$ *decays, as determined from the full LHCb MC. Also shown is the mass distribution of* $B_s^0 \to D_s\pi$ *decays that have been reconstructed as* $B_s^0 \to D_sK$ *decays. The histograms are correctly normalized to compensate for the different branching ratios.*

with $J/\psi \to \mu\mu$ and 20.000 decays with $J/\psi \to ee$, with proper time resolution of 38 fs. The values of the physics parameters can be extracted from a simultaneous fit to the proper time, $cos(\theta_{tr})$ and m_s distributions, reaching in one year a precision on the phase ϕ_s of about 3.6 degrees and precision on $\Delta\Gamma_s/\Gamma_s$ of about 0.018, if Δm_s=20 ps^{-1}.

BTeV intends to use $B_s^0 \to J/\psi\eta^{(')}$ events, which allow for the measurements of ϕ_s with a simpler analysis, since they are pure CP eigenstates. Thanks to the excellent resolution of BTeV calorimeter, the expected annual yield in these channels is of 10.000 for $J/\psi\eta$ and 3.000 events for $J/\psi\eta'$, with a B/S ratio of 0.07 and 0.03, respectively. The expected sensitivity on the phase ϕ_s is of about 2.8 degrees in one year.

5 Two body charmless B_d^0 and B_s^0 decays

Several strategies have been proposed **?)** to extract informations on the CKM angle γ from two body charmless decays of B mesons, some of them make use of assumptions on dynamics or on U-spin symmetry.

A first sample of $B_{d,s}^0 \to h^+h'^-$ events has been collected by the CDF ex-

periment, the invariant mass spectrum is shown in Fig. **??**. Different channels contribute to the mass peak: $B_d^0 \to \pi^+\pi^-, K^+\pi^-$; $B_s^0 \to K^+K^-, \pi^+K^-$. A statistical separation has been performed combining PID from specific ionization and kinematic variables. With a subsample of 65 pb^{-1} CDF gets the first evidence of $B_s^0 \to K^+K^-$ decays with a relative branching ratio $[f_s \times BR(B_s^0 \to K^+K^-)]/[f_d \times BR(B_d^0 \to K^+\pi^-)] = 0.74 \pm 0.20(stat) \pm 0.22(syst)$ and the direct CP asymmetry $A_{CP}(B_d^0 \to K^+\pi^-) = 0.02 \pm 0.15(stat) \pm 0.02(syst)$. The next step is the measurement of time dependent asymmetries in flavour tagged samples. In an integrated luminosity of 3.5 fb^{-1}, about 11.700 $B_d^0 \to K^+\pi^-$, 3.500 $B_d^0 \to \pi^+\pi^-$ and 7.100 $B_s^0 \to K^+K^-$ events are expected, with which the uncertainties on the time dependent asymmetries are of the order of 20-30%.

Future experiments will have RICH detectors to separate the K/π channels with high efficiency and purity. LHCb in one year of data taking expects to collect 135.000 $B_d^0 \to K^+\pi^-$, 26.000 $B_d^0 \to \pi^+\pi^-$ and 37.000 $B_s^0 \to K^+K^-$ decays, with mass resolution $\sigma(M_B) = 17$ MeV and a proper time resolution of $\sigma_\tau = 33$ fs. The two time dependent CP asymmetries:

$$A_{CP}(B_d^0 \to \pi^+\pi^-)(t) = A_{CP}^{dir,\pi\pi} cos(\Delta m_d t) + A_{CP}^{mix,\pi\pi} sin(\Delta m_d t)$$
$$A_{CP}(B_s^0 \to K^+K^-)(t) = A_{CP}^{dir,KK} cos(\Delta m_s t) + A_{CP}^{mix,KK} sin(\Delta m_s t)$$

will be used to fit for the four CP asymmetries, giving a precision of about 5-6%. Following the method suggested in **?)**, exploiting U-spin flavour symmetry and assuming the knowledge of the mixing phases ϕ_d and ϕ_s from previous measurements, the γ angle can be extracted with a precision of $\sigma_\gamma = 4 - 6$ degrees in one year.

BTeV in one year expect to collect 15.000 $B_d^0 \to \pi^+\pi^-$ and 62.000 $B_s^0 \to K^+\pi^-$ decays, with a precision of about 3% on the CP asymmetries.

6 γ measurements from $B \to DK$ decays

$B_s^0 \to D_s^\mp K^\pm$ decays can proceed through two tree diagrams which interference gives access to the phase $\gamma + \phi_s$. If ϕ_s has been determined otherwise, γ can be extracted, from the measurement of the time-dependent decay asymmetries, without theoretical uncertainties, and independently on New Physics.

Strong particle identification capabilities are required to separate the small $B_s^0 \to D_s K$ channel from the $\sim$12 times larger $B_s^0 \to D_s\pi$ one. The performances of the LHCb RICH detectors will be fully adequate, as it is shown in Fig. **??**. Montecarlo studies have shown that 5400 $D_s^\mp K^\pm$ events will

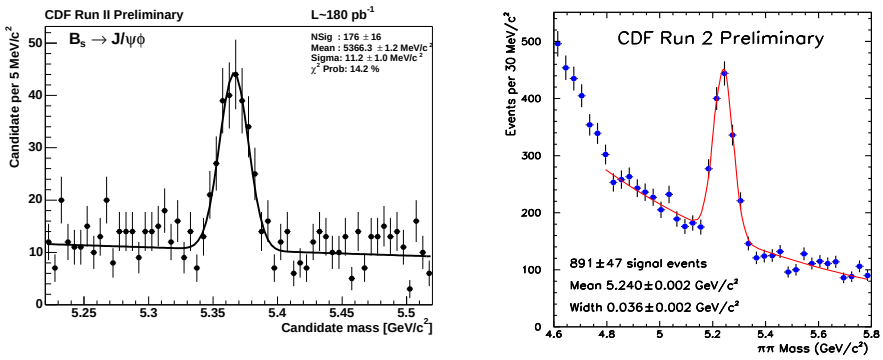

Figure 4: *Left: CDF. Mass distribution of* $B_s^0 \to J/\psi\phi(J/\psi \to \mu\mu, \phi \to KK)$ *decays. Right: CDF. Invariant mass distribution of* $B_{d,s}^0 \to h^+h'^-$ *candidates with* π *mass assumed for both tracks.*

be collected in one year of data taking and a sensitivity of $\sigma_\gamma = 14$ degrees can be obtained, if Δm_s=20 ps^{-1}. Similar performances are expected by the BTeV experiment.

Another theoretically clean determination of the angle γ can come from $B^0 \to D^0 K^{*0}$ decays. The method in [?] is similar to the analysis of $B^\pm \to D^0 K^\pm$ decays, currently under study at the B-Factories, but has the advantage of using B decay amplitudes of more comparable values. It is based on the measurement of six time-integrated decay rates: $B_d^0 \to D^0 K^{*0}, \bar{D}^0 K^{*0}, D_{CP} K^{*0}$ and CP conjugates. The $D^0 K^{*0}$ decays are self-tagged through $K^{*0} \to K^+\pi^-$, while the CP auto-states D_{CP} can be reconstructed in K^+K^- and $\pi^+\pi^-$ decays. LHCb in one year of data taking expects to collect a total of about 4.000 decays leading to a sensitivity on γ of $\sigma_\gamma = 7 - 8$ degrees.

7 $b \to s$ penguin dominated decays

The discrepancy between $sin(2\beta)$ measured in $B_d^0 \to J/\psi K_S$ and $B_d^0 \to \phi K_S$ channels at the B-Factories has still to be understood and points to a possible New Physics contribution. The $B_d^0 \to \phi K_S$ channel is dominated by a $b \to s$ penguin diagram and similar diagrams are involved in several other B meson decays which can be measured in Hadron Collider experiments. As an example CDF has a first signal of 12 $B_s^0 \to \phi\phi$ events, in a sample of 180 pb^{-1}, from

which a preliminary branching fraction of $BR = 1.4 \pm 0.6(stat) \pm 0.2(syst) \pm 0.5(BRs)) \times 10^{-5}$ is obtained.

LHCb will collect about 1200 $B_s^0 \to \phi\phi$ events in one year of data taking (B/S$<$ 0.4) and will also perform studies of channels like $B_d^0 \to \phi K_S, \phi K^{*0}$, $B^+ \to \phi K^+$ and $B_s^0 \to \phi\phi$, $\phi K, \phi\gamma$.

8 Conclusion

CP asymmetries will be measured at Hadron Colliders in the coming years in many channels of B_d^0, B_s^0 mesons and b-baryons decays. In particular, very rare decays will be studied, thanks to the high $b\bar{b}$ cross section available. This program is complementary to the B-Factories one and will allow to complete and improve their results.

9 Acknowledgments

I would like to thank the help of F.Bedeschi and G.Punzi in providing informations on Tevatron experiments.

References

1. R. Blair *et al*, CDF Collaboration; FERMILAB-PUB-96/360-E(1996); S. Abachi *et al*, DØ Collaboration; FERMILAB-PUB-96/357-E(1996).
2. R. Antunes *et al*, LHCb Collaboration; CERN/LHCC 2003-030 (2003).
3. G.Y. Drobychev*et al*, BTeV Collaboration; BTeV-doc-316-v3.
4. See for example M. Battaglia, A.J. Buras, P. Gambino and A. Stocchi, eds. CERN-2003-002 and referencies therein.
5. R. Fleisher, Phys.Lett. **B 459**, 306 (1999); R. Fleisher and J. Matias, Phys. Rev. **D 66**, 054009 (2002).
6. M. Gronau and D. Wyler, Phys.Lett. **B 265**, 172 (1991); I. Dunietz, Phys.Lett. **B 270**, 75 (1991).

Frascati Physics Series Vol. XXXVI (2004), pp. 77–82
DAΦNE 2004: Physics at meson factories – Frascati, June 7-11, 2004
Selected Contribution in Plenary Session

THE FINAL RESULT OF THE T-VIOLATION EXPERIMENT KEK-E246

C. Rangacharyulu *
Department of Physics, University of Saskatchewan,
Saskatoon, SK, Canada, S7N5E2

Abstract

We have been carrying out a measurement of transverse muon polarization in the $K^+ \to \pi^0 \mu^+ \nu(K^+_{\mu 3})$ to deduce the parameter $Im\xi$, a quantitative estimate of breakdown of Time reversal invariance in this decay. From a cumulative data sample of nearly 12 million events, we deduced $P_T = -0.0017 \pm 0.0023(stat) \pm 0.0011(syst)$ or the T-violation parameter $Im\xi = -0.0053 \pm 0.0071(stat) \pm 0.0036(syst)$ which correspond to upper limits of $|P_T| < 0.005$ and $Im\xi < 0.016$ (95% confidence limit).

*KEK-E246 Collaboration: *Japan - National High Energy Research Accelerator Organization (KEK), Tsukuba, Tsukuba University, Tokyo Institute of Technology, Osaka University; Russia - Institute for Nuclear Research, Moscow; Canada - University of Saskatchewan, Université de Montréal, TRIUMF, University of British Columbia; Korea - Yonsei University, Korea University; USA - Virginia Polytechnic Institute, Princeton University.*

1 Introduction

Though several dedicated investigations in different decays and reactions spreading over four decades have been carried out, the CP violation is found only in neutral mesons, specifically in neutral K and B mesons. Also, it is very disconcerting to note that one finds direct evidence of T-violation only in neutral K mesons. Our experiment was motivated to look for direct evidence of breakdown of Time reversal in a charged Kaon (K^+) system. The experiment was based on the physics principle suggested by J. J. Sakurai [1)] that the transverse muon polarization in the three-body decay of $K^+ \to \pi^0 \mu^+ \nu$ will be finite if the Time reversal invariance symmetry is broken. Earlier, groups at Brookhaven [2)] measured this channel with a negative result. In the meantime, there have been several model arguments in the frameworks of Multi Higgs and Supersymmetry etc., [3)] which gave reasons to consider that non-zero P_T may be just within reach of present-day experiments.

2 Experiment

This experiment was carried out at the 12 GeV proton synchrotron of the KEK-High Energy Accelerator Research Organization, Tsukuba, Japan. It was designed to take advantage of azimuthal symmetry of the 12-sector superconducting toroidal spectrometer. A large acceptance photon calorimeter of 768 CsI crystals, an active target of of 256 scintillators were built. Also built were 12 drift chamber tracking systems and muon polarimeters, one set for each of the toroidal magnet sectors were built. The system is thoroughly described in Macdonald et al. [4)] and a cross sectional diagram of the system is shown in Fig. 1.

Briefly, the low momentum K^+ beams were passed through energy degrader and stopped in the active scintillating fiber target. The momentum tracking of charged particles is done. The polarization of muons of $K^+_{\mu 3}$ are determined by the direction of decay positrons. For each gap in the spectrometer, a pair of paddles served to measure asymmetry in the positrons emitted in the clockwise and counter clockwise directions. Summation over the 12 sectors played an important role. Also, we note that the transverse polarization is written as $P_T = \vec{s}_\mu \cdot (\vec{p}_\pi \times \vec{p}_\mu)/|\vec{p}_\pi \times \vec{p}_\mu|$ and necessitates asymmetry measurements transverse to the decay plane. One recognizes that the transverse

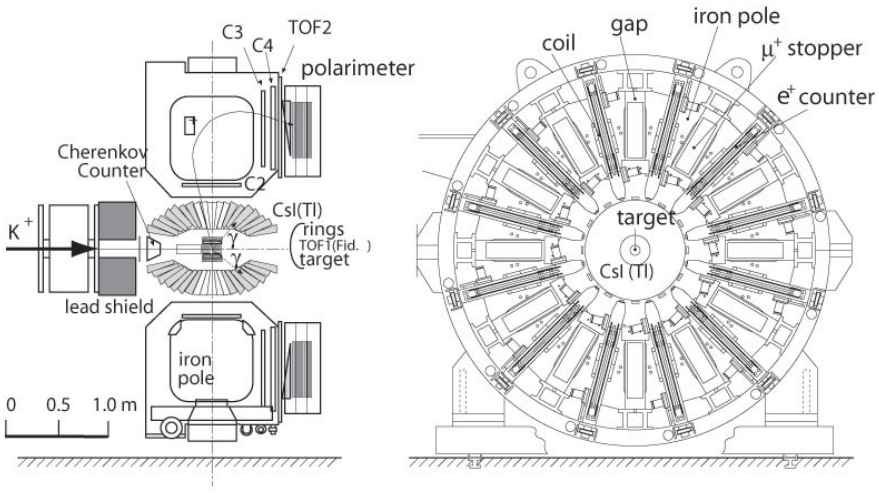

Figure 1: *Cross section side view and end view of the spectrometer. Kaon beams entering from the left.*

polarization is of opposite sign for the forward going pions to that of backward going pions. Thus the events of forward going pions and backward going pions have opposite sign for the asymmetry. We exploit this feature to double the signal. It also serves as a powerful means to cancel the systematic errors.

The experiment ran over about 4 years, and the data were grouped into three periods of (I) 1996-97, (II)1998 and (III) 1999-2000. The first result from the earliest runs were published in Abe et al [5] Since then, the data volume almost tripled and we also refined our analysis procedures as we better understood the system. The final results are in press. [6]

The data analysis was carried out by two independent teams, who set their own event selection criteria and off-line analysis apart from some basic principles. To make maximum use of the data set, π^0 identification relied on events where both the photons (2γ) were detected and also those with

a single photon (1γ) of energy $E_\gamma > 70MeV$ was detected. There was a small, but non-negligible amount of uncommon events in the two analysis due to slight differences in the cut criteria between the two analysis. We thus categorized them as common (A1.A2)events, and two sets of ($\overline{A1} \cdot A2$ and $A1 \cdot \overline{A2}$) uncommon events and separately for the 2γ and 1γ types. The time spectra integrated between 20 ns to 6 μs after subtraction of the constant background was used as a measure of the positron yields. The main background was due to the $K^+ \rightarrow \pi^+\pi^0$ and the subsequent decay of π^+ mesons. The estimated background contamination was included in the systematic error.

The P_T was calculated as the $P_T = A_T/(\alpha_{int} < \cos\theta_T >)$, where A_T is the asymmetry, α is analyzing power and $< cos\theta_T >$ is the angular attenuation factor. The analyzing power is not constant over the 'y' coordinate of the polarimeter. We could calibrate the y-dependence of the analyzing power using the positron asymmetry $A_N(y)$ associated with the normal polarization. The absolute value of the analyzing power was deduced from the Monte Carlo simulation result. We obtained an analyzing power of $\alpha_{int} = 0.271 \pm 0.027$. The $P_T(y)$ thus calculated was found to be nearly constant with slight but opposite-sign gradients for the 2γ and 1γ. We believe this dependence has its origins in the differences in kinematics of muon stopping distributions for the 2γ from that of 1γ types. We have checked the sector dependence of the measured asymmetries and found it to be insignificant.

3 Result

The T-violation parameter $Im\xi$ was obtained from the measured transverse polarization P_T using the conversion factors $\Phi = 0.327$ and 0.287 for the 2γ and 1γ events respectively. This value is what we have employed in our earlier analysis [5]. The left side of Fig. 2 shows an ideogram of the results of $Im\xi$ for the six sets of events as labeled in the figure. There is considerable overlap between the separate values; the average value is $< Im\xi > = 0.0053 \pm 0.0071$, consistent with zero.

Almost all the systematic errors cancel as we sum over the 12 sectors and double ratio of forward and backward going π^0 are used. However, a few errors remain. The principal sources are due to misalignment of $\vec{B}$ fields and the muon multiple scattering etc. Altogether, they amounted to less than 10^{-3} and thus the statistical uncertainty is the main contributing factor in our errors.

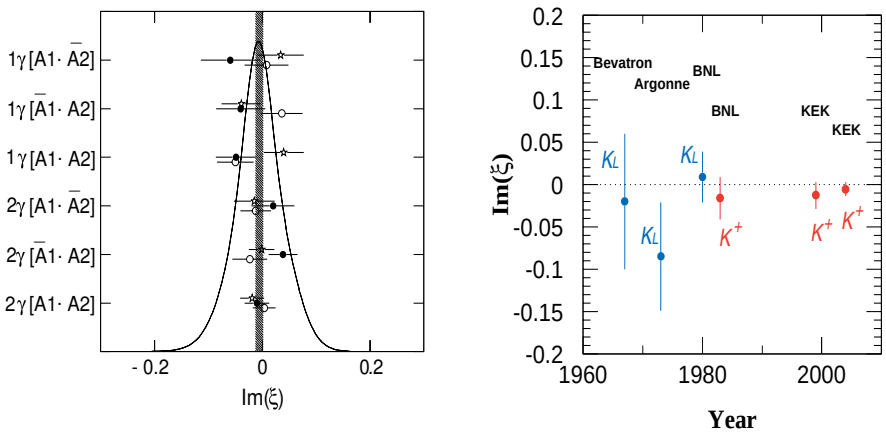

Figure 2: *The ideogram(left) shows the results of analysis six sets of data. Our present result(KEK-2004) is compared with earlier works(right).*

It is of interest to compare our result with earlier measurements. The right portion of Fig. 2 shows that we achieved about a factor of three improvement over the previous K^+ decay measurement. It is much more improved compared to the polarization measurements in the neutral kaon decays.

4 Summary and Conclusions

A dedicated experiment of the T-violation test by the KEK-PS-E246 collaboration in the $K^+_{\mu 3}$ has attained a higher precision than the experiments so far. The result does not warrant the occurrence of light Higgs ($M < 100GeV$). It revealed that in the model frame work of Garisto and Kane, [3] the d-quark contribution to the neutron electric dipole moment is about an order of magnitude smaller than the current experimental limit of $d_n < 6 * 10^{-26}$.

Our collaboration has plans to push this limit by another order of magnitude further at the new high intensity proton machine of 50 GeV under construction at J-PARC, Tokaimura, Japan. The motivations for this project are clear. The high intensity, high quality kaon beams at J-PARC in conjunction with an optimum detector system will allow us to push the experimental limit very close to the estimates of standard model incorporating the final state interactions. This improved precision will allow us to offer stringent constraints

of the extensions of standard model. There are plans to upgrade the current detector and/or build a more powerful detector to achieve this limit [7].

5 Acknowledgments

Several collaborators (both young and not-so-young) from different parts of the world contributed to this project. It was indeed an exhilarating experience to work with them and I thank them all.

References

1. J.J. Sakurai, Phys. Rev. **109**, 980 (1958).
2. S. R. Blatt *et al*, Phys. Rev. **D27** 1056(1983).
3. For example, R. Garisto and G. Kane, Phys. Rev. **D44** 2038 (1991); G. -H. Wu and J. N. Ng, Phys. Lett. **B392** 93 (1997).
4. J. A. Macdonald *et al*, Nucl. Instr. Method **A506**, 60 (2003).
5. M. Abe *et al*, Phys. Rev. Letters **83**,4253 (1999).
6. M. Abe *et al*, Phys. Rev. Letters *in press*.
7. J. Imazato, NP04 workshop at J-PARC, Tokaimura, Japan Aug 2-4, 2004 http://j-parc.jp/NP04

Frascati Physics Series Vol. XXXVI (2004), pp. 83–88
DAΦNE 2004: Physics at meson factories – Frascati, June 7-11, 2004
Selected Contribution in Plenary Session

STATUS OF ASYMMETRY MEASUREMENT AT NA48/2 EXPERIMENT

Luca Fiorini *
Scuola Normale Superiore and Istituto Nazionale Fisica Nucleare, Pisa, Italy

Abstract

NA48/2 is a high precision experiment of charged kaon decays using a novel design for simultaneous K^+/K^- beams and an upgraded NA48 set-up. The experiment is installed at the SPS site of CERN, where data taking is scheduled to end in August 2004.
The main goal is to search for CP-violation in $K^\pm \to \pi^+\pi^-\pi^\pm$ and $K^\pm \to \pi^0\pi^0\pi^\pm$ decays. The experiment is designed to reach a sensitivity, limited by statistics rather than systematics, of the order of 10^{-4} in the measurement of the direct CP-violating asymmetry in the linear slope of the Dalitz plot [1)].
Over $10^6 K_{e4}$ decays have been collected in order to measure a_0^0 scattering length and other Kaon rare decays are studied as well.

* On behalf of NA48/2 Collaboration: Cambridge, CERN, Chicago, Dubna, Edinburgh, Ferrara, Firenze, Mainz, Northwestern, Perugia, Pisa, Saclay, Siegen, Torino, Vienna

1 Introduction

After the measurement of the direct CP violation component in the decay of the neutral Kaons [2], the NA48 collaboration is actually engaged in the search of direct CP violation in the $K^{\pm} \to \pi^+\pi^-\pi^{\pm}$ decays, by measuring the asymmetry

$$A_g = (g^+ - g^-)/(g^+ + g^-), \tag{1}$$

where g^+ and g^- are the slope parameters describing, respectively, the linear dependence of the K^+ and K^- decay probabilities on the u kinematic variable of the Dalitz plots. The u variable is related to the energy (E^*_π) of the *odd* pion (the pion having the sign opposite to that of the decaying kaon) in the kaon centre of mass system as follows: $u = (2M_K/m^2) \cdot (M_K/3 - E^*_\pi)$, where M_K and m are the kaon and pion mass, respectively. Exploiting the high detection efficiency and precision in energy measurement for photons of the NA48 Liquid Krypton calorimeter (LKr), also the corresponding asymmetry A^0_g in $K^{\pm} \to \pi^0\pi^0\pi^{\pm}$ decays will be measured. High statistics ($\sim 10^6$) of K_{e4} can be analyzed allowing the $\pi - \pi$ scattering length parameter a^0_0 to be measured with an accuracy of better than $1 \cdot 10^{-2}$. This permits the size of the $q\bar{q}$ condensate of the QCD vacuum postulated in χPT to be measured.

2 Beam Lines

The beam line transports simultaneously positive and negative particles with average momentum of 60 GeV/c and 3.8% rms. The two beams originate at 0 angle relatively to the impinging primary protons and have $\pm 0.36 mrad$ opening angle on both planes (Fig.1). The fluxes at the end of the final collimator are of $3.8 \cdot 10^7$ positive ppp ($2.2 \cdot 10^6 K^+$) and $2.6 \cdot 10^7$ negative ppp ($1.3 \cdot 10^6 K^-$) in a 16.8 s cycle time and 4.8 s flat-top.

3 Detector Apparatus

The main device for $K^{\pm} \to \pi^+\pi^-\pi^{\pm}$ decays identification is the magnetic spectrometer [3]: it consists of a dipole magnet ($120 MeV/c$ kick) and 4 drift chamber, two before and two after the magnet. Spatial resolution is $\sim 100 \mu m$ per plane, providing a better than 1% momentum measurement.
The $K^{\pm} \to \pi^0\pi^0\pi^{\pm}$ decays identification relays on the liquid krypton calorimeter [4] divided in $2 \times 2 cm^2$ cells. Time resolution for showers above 20 GeV is

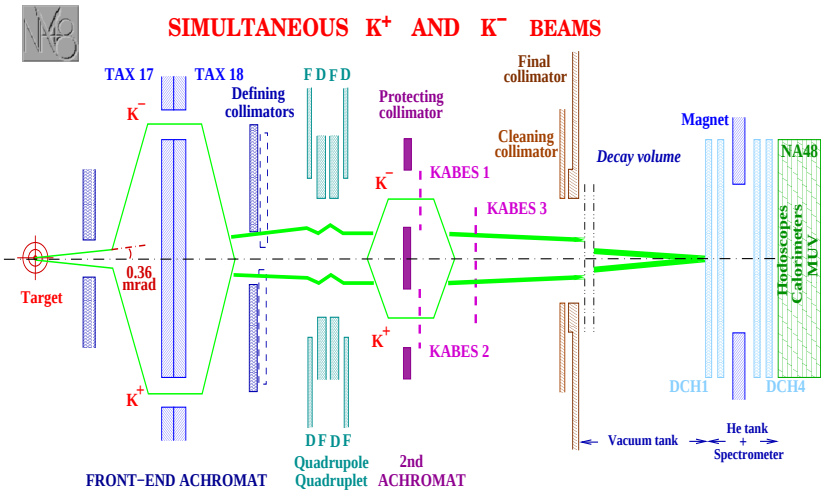

Figure 1: *Vertical section of the simultaneous K^+ and K^- beam line (not to scale).*

better than 300 ps, position resolution better than 1.3 mm and energy resolution better than 1%.
A new detector called KABES, built specifically for NA48/2 is installed $\sim 40m$ after the proton target. It is a TPC Micromega detector, providing particle by particle beam momentum measurement with a resolution better than 1%.

4 Data Taking

In order to minimize systematic uncertainties related to the apparatus asymmetry and beam structure, the magnetic fields in the spectrometer and beam line magnets were alternated regularly. The spectrometer magnet current was alternated on a daily basis, and all the beam line magnets were cycled and inverted once per week during the machine development pauses. The latter frequency was chosen to minimize losses of data, since the procedure is rather long and requires subsequent retuning of the beams, which in any case needed to be done after the MD.
Actual results are based on 2 self-complete data set, called *supersamples* and 1 partial supersample accumulated on the last month of 2003 data taking for

a total of 720 million $K^+_{3\pi}$ and 400 million $K^-_{3\pi}$. In addition $\sim$ 50 millions of $K^\pm \to \pi^\pm\pi^0\pi^0$ were reconstructed for the same *supersamples*.

5 Asymmetry Measurement

Given the parametrization of the $K^\pm \to 3\pi$ Daliz plot: $|M(u,v)|^2 \sim 1 + gu + hu^2 + kv^2$, if acceptance for K^+ with magnetic field up is equal to acceptance for K^- with magnetic field down, and in case of perfect time stability, A_g can be extracted by a linear fit:

$$R_S(u) = \frac{N(u, K^+, B_{up})}{N(u, K^-, B_{down})} \propto (1 + g_+u)/(1 + g_-u) \sim (1 + 2gA_gu) \qquad (2)$$

we have also the symmetrical ratio $R_J(u) = N(u, K^+, B_{down})/N(u, K^-, B_{up})$ where the subscripts S and J are chosen to indicate the direction of deflection of pions of the same charge as the kaon by the spectrometer magnet toward the *Saleve* and *Jura* sides. In order to study systematic effect, it is useful to define $R_+(u) = N(u, K^+, B_{up})/N(u, K^+, B_{down})$ and $R_-(u) = N(u, K^-, B_{up})/N(u, K^-, B_{down})$ as the sum $R_+(u) + R_-(u)$ is different from 0 only for apparatus induced asymmetries.

It can easily be proved that:

- any Right-Left acceptance asymmetry which is stable between successive runs with U and D polarities of the magnetic field does not affect either A_S or A_J;
- a Right-Left symmetric change in acceptance during or between successive runs could affect both A_S and A_J but would be canceled when averaging A_S and A_J.

Thus a deviation from zero in the average of these slopes:

$$A = 0.5 \cdot (A_S + A_J)$$

would signal the CP-violating asymmetry, as long as the set-up is either *stable in time* or *symmetric*.

At this preliminary stage of the analysis the Collaboration considers premature to show any number which could be ascribed to a real physics effect. Therefore, the above-mentioned slopes are shown with *offsets* applied to the scale. Preliminary results show that asymmetry value is stable with Kaon momentum (Fig.2) and that it is stable with time (Fig.3).

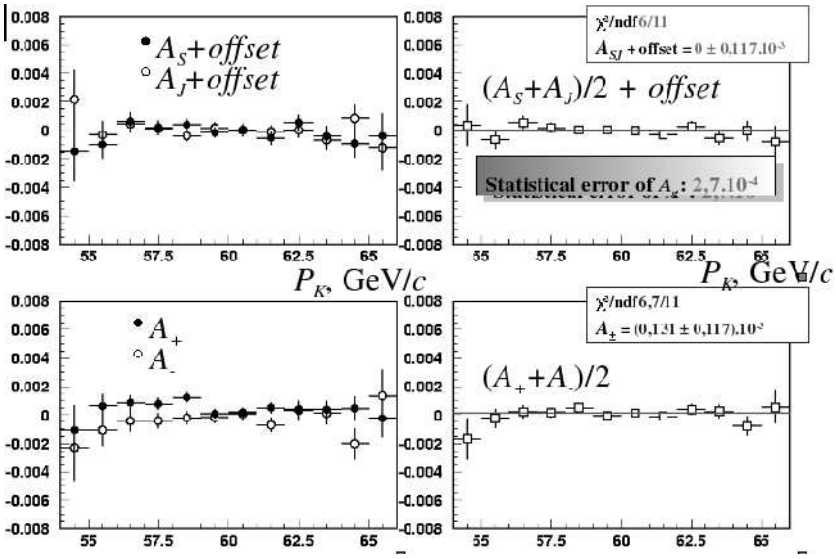

Figure 2: *The slopes A_S, A_J, A_+, A_- and their averages A integrated over all momenta and measured independently in each couple of day-samples with opposite orientation of magnetic field relative to the overall average value (an offset is introduced on the vertical scales).*

6 Summary

The experiment NA48/2 has been well prepared and the beam line, detector and triggers put into operation and tuned. The data accumulated in the 2003 run corresponds to only a part ($\sim 50\%$) of the planned statistics for the measurement of the direct CP-violating asymmetry in charged kaon decays.

A preliminary express analysis of a part of the 2003 run shows that the estimated statistical precision and systematic uncertainties of the measured asymmetry A_g are in agreement with those indicated in the proposal. The experiment will benefit fully from the complement of running time in 2004.

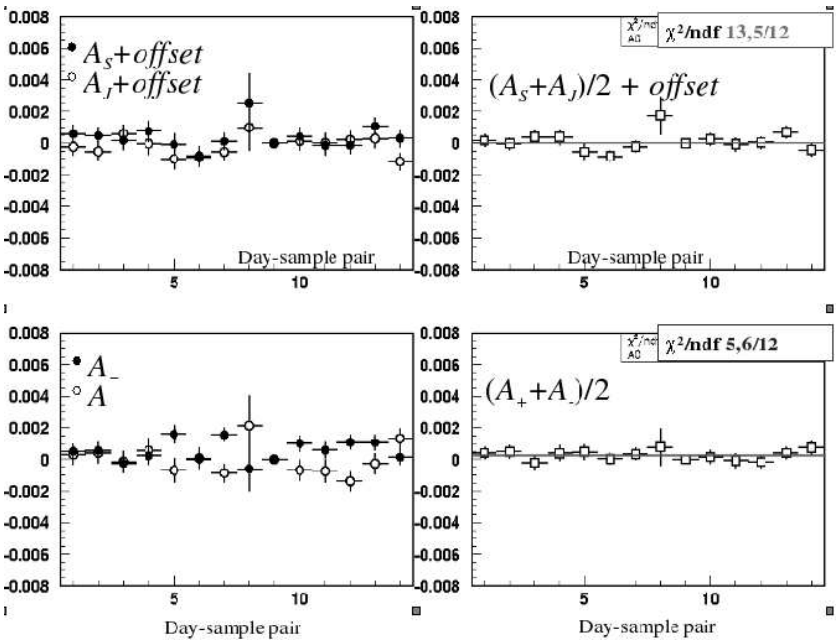

Figure 3: *The slopes A_S, A_J, A_+, A_- and their averages A integrated over all momenta and measured independently in each couple of day-samples with opposite orientation of magnetic field relative to the overall average value (an offset is introduced on the vertical scales).*

References

1. J.R. Batley *et al*, CERN/SPSC 2000-003, (2000);
   NA48/2 status report (2001);
   NA48 Status Report SPSC/M691, CERN/SPSC 2002-035 (3 November 2002).

2. J.R. Batley et al. Phys.Lett. B **544** (2002) 97.

3. G.D. Barr *et al.*, Nucl. Instrum. Methods A **370**, 413 (1993).

4. D. Bderde *et al.*, Nucl. Instrum. Methods A **367**, 88 (1995).

Frascati Physics Series Vol. XXXVI (2004), pp. 89–94
DAΦNE 2004: Physics at meson factories – Frascati, June 7-11, 2004
Selected Contribution in Plenary Session

ON EXPECTED VALUE OF CP EFFECTS IN DECAY OF CHARGED KAONS INTO 3 PIONS

E. Shabalin
Institute for Theoretical and Experimental Physics, Moscow, Russia

Abstract

The amplitudes of the $K^{\pm} \to 3\pi$ and $K \to 2\pi$ decays are expressed in terms of different combinations of one and the same set of CP-conserving and CP-odd parameters. Extracting the magnitudes of these parameters from the data on $K \to 2\pi$ decays, we estimate an expected CP-odd difference between the values of the slope parameters g^+ and g^- of the energy distributions of "odd" pions in $K^+ \to \pi^+\pi^+\pi^-$ and $K^- \to \pi^-\pi^-\pi^+$ decays.

1 Introduction

The observation of CP effects in $K^{\pm} \to 3\pi$ decays would allow to understand better how the mechanisms of CP violation work.

Now the Collaboration NA48/2 began a search for such effect with accuracy $\delta(\frac{g^+-g^-}{g^++g^-}) \leq 2 \times 10^{-4}$.

Contrary to the case of $K_L \to 2\pi$ decay, where CP violates both in $\Delta S = 2$ and $\Delta S = 1$ transitions, in the $K^\pm \to 3\pi$ decays, only the last (the so-called "direct") CP violation takes place. Experimentally, an existence of the direct CP violation in $K_L \to 2\pi$ decays, predicted by Standard Model (SM) and characterized by the parameter ε', is established: $\varepsilon'/\varepsilon = (1.66 \pm 0.16) \times 10^{-3}$.

What is expected for CP effects in $K^+ \to \pi^\pm\pi^\pm\pi^\mp$ decay? To give an answer, it is necessary to understand the role of the electroweak penguin (EWP) operators in both decays and get rid of the large uncertainties usual for the theoretical calculations. The real scale of these uncertainties is characterized by the following predictions obtained before the above experimental result:

$$\frac{\varepsilon'}{\varepsilon} = (17^{+14}_{-10}) \times 10^{-4} \quad ^{1)}, \qquad \frac{\varepsilon'}{\varepsilon} = (1.5 \div 31.6) \times 10^{-4} \quad ^{2)}.$$

To avoid the uncertainties arising in the theoretical calculation of the ingredients of the theory, we use the following procedure. We express the amplitudes of $K \to 2\pi$ and $K^\pm \to 3\pi$ decays in terms of one and the same set of parameters, and calculating $g^+ - g^-$, we use the magnitudes of these parameters extracted from data on $K \to 2\pi$ decays.

2 The scheme of calculation

A theory of $\Delta S = 1$ non-leptonic decays is based on the effective Lagrangian [3)]

$$L(\Delta S = 1) = \sqrt{2} G_{\rm F} \sin\theta_{\rm C} \cos\theta_{\rm C} \sum_i c_i O_i \,, \tag{1}$$

where O_{1-6} are the 4-quark operators represented in [3)] and O_{7-8} are the 4-quark operators generated by electroweak penguin (EWP) diagrams

$$O_7 = \frac{3}{2} \bar{s}\gamma_\mu(1+\gamma_5)d(\sum_{q=u,d,s} e_q \bar{q}\gamma_\mu(1-\gamma_5)q) \qquad (\Delta I = 1/2, 3/2); \tag{2}$$

$$O_8 = -12 \sum_{q=u,d,s} e_q (\bar{s}_L q_R)(\bar{q}_R d_L), \quad e_q = (\frac{2}{3}, -\frac{1}{3}, -\frac{1}{3}) \quad (\Delta I = 1/2, 3/2). \tag{3}$$

Representing $M(K \to 2\pi)$ in the form

$$M(K_1^0 \to \pi^+\pi^-) = A_0 e^{i\delta_0} - A_2 e^{i\delta_2}, \tag{4}$$

$$M(K_1^0 \to \pi^0\pi^0) = A_0 e^{i\delta_0} + 2A_2 e^{i\delta_2}, \tag{5}$$

$$M(K^+ \to \pi^+\pi^0) = -\frac{3}{2} A_2 e^{i\delta_2}, \tag{6}$$

and using the relations expressing the diquark operators in terms of pseudoscalar fields [4] we find

$$A_0 = G_{\rm F} F_\pi \sin\theta_{\rm C} \cos\theta_{\rm C} \frac{m_K^2 - m_\pi^2}{\sqrt{2}} [c_1 - c_2 - c_3 + \frac{32}{9}\beta({\rm Re}\tilde{c}_5 + i{\rm Im}\tilde{c}_5)]; \qquad (7)$$

$$A_2 = G_{\rm F} F_\pi \sin\theta_{\rm C} \cos\theta_{\rm C} \frac{m_K^2 - m_\pi^2}{\sqrt{2}} \cdot [c_4 + i\frac{2}{3}\beta\Lambda^2 {\rm Im}\tilde{c}_7 (m_K^2 - m_\pi^2)^{-1}] \qquad (8)$$

where

$$\tilde{c}_5 = c_5 + \frac{3}{16}c_6, \quad \tilde{c}_7 = c_7 + 3c_8, \quad \beta = \frac{2m_\pi^4}{\Lambda^2(m_u + m_d)^2}, \quad \Lambda \approx 1 \text{ GeV}$$

The contributions from $\tilde{c}_7 O_7$ into ${\rm Re}A_0$ and ${\rm Im}A_0$ are small because $\tilde{c}_7/\tilde{c}_5$ is proportional to the electromagnetic constant α and we neglected these corrections. From data on widths of $K \to 2\pi$ decays we obtain

$$c_4 = 0.328; \quad c_1 - c_2 - c_3 + \frac{32}{9}\beta{\rm Re}\tilde{c}_5 = -10.13. \qquad (9)$$

At $c_1 - c_2 - c_3 = -2.89$ [3, 5] we obtain

$$\frac{32}{9}\beta{\rm Re}\tilde{c}_5 = -7.24. \qquad (10)$$

Using the general relation

$$\varepsilon' = ie^{i(\delta_2 - \delta_0)} \left[-\frac{{\rm Im}A_0}{{\rm Re}A_0} + \frac{{\rm Im}A_2}{{\rm Re}A_2} \right] \cdot |\frac{A_2}{A_0}| \qquad (11)$$

and the experimental value $|\varepsilon'| = (3.78 \pm 0.38) \times 10^{-6}$, we come to the relation

$$-\frac{{\rm Im}\tilde{c}_5}{{\rm Re}\tilde{c}_5} \left(1 - \Omega_{\eta,\eta'} + 24.36 \frac{{\rm Im}\tilde{c}_7}{{\rm Im}\tilde{c}_5} \right) = (1.63 \pm 0.16) \times 10^{-4}, \qquad (12)$$

where $\Omega_{\eta,\eta'}$ takes into account the effects of $K^0 \to \pi^0\eta(\eta') \to \pi^0\pi^0$ transitions.

Introducing the notations

$$-\frac{{\rm Im}\tilde{c}_5}{{\rm Re}\tilde{c}_5} = x\frac{{\rm Im}\lambda_t}{s_1}, \qquad \frac{24.36}{1 - \Omega_{\eta,\eta'}} \cdot \frac{{\rm Im}\tilde{c}_7}{{\rm Im}\tilde{c}_5} = -y \qquad (13)$$

and using [6]

$$({\rm Im}\lambda_t)/s_1 \approx s_2 s_3 \sin\delta = \frac{(1.2 \pm 0.2) \times 10^{-4}}{0.223}, \qquad (14)$$

we can write Eq.(11) for $\Omega_{\eta,\eta'} = 0.25 \pm 0.08$ in the form

$$x(1-y) = 0.40 \times (1 \pm 0.22). \tag{15}$$

In the last two equations s_i and δ are the parameters of CKM matrix. The Eq.(15) depends on the variables x and y representing the contribution of QCD penguin and relative contribution of EWP, respectively. To move farther, we are enforced to apply to existing theoretical estimates of one of these variables.

In terms of notations in [7, 8, 9]

$$y = \frac{\Pi_2}{\omega}/\Pi_0(1-\Omega_{\eta,\eta'}). \tag{16}$$

According to [7], $y \approx 0.3$ and hence $x = 0.57 \pm 0.12$. But $\varepsilon'/\varepsilon = 2.2 \cdot 10^{-3}$ or by 30% is larger than the experimental value . In [9], the central value of y is $y \approx 0.5$ and, consequently, $x = 0.80 \pm 0.18$. From [10] $x = 0.71 \pm 0.27$; from [11] $x = 1.4 \pm 0.28$; from [12] $x = 2$; from [13] $x = 2.8$; from [14] $x = 5.5$. Such difference of the theoretical estimates of x makes very desirable an investigation of CP-effects in $K^\pm \to \pi^\pm\pi^\pm\pi^\mp$ decays, where, contrary to $K_L \to 2\pi$ decays, the EWP contributions increase CP effects .

3 Decay $K^\pm \to \pi^\pm\pi^\pm\pi^\mp$

The slope parameters g^+ and g^- are defined by the relation

$$|M(K^\pm(k) \to \pi^\pm(p_1)\pi^\pm(p_2)\pi^\mp(p_3))|^2 \sim [1 + g^\pm Y + ...], \qquad Y = (s_3 - s_0)/m_\pi^2, \tag{17}$$

where $s_3 = (k-p_3)^2$ and $s_0 = m_K^2/3 + m_\pi^2$. Our calculations give [15]:

$$R_g \equiv \frac{g^+ - g^-}{g^+ + g^-} = \frac{a(b_{KM} - a_{KM})}{1+ab} \tag{18}$$

where a_{KM} and b_{KM} are induced by the Kobayashi-Maskawa phase:

$$a_{KM} = \left[\frac{32}{9}\beta \mathrm{Im}\tilde{c}_5 + 4\beta \mathrm{Im}\tilde{c}_7\left(\frac{3\Lambda^2}{2m_K^2} + 2\right)\right]/c_0, \tag{19}$$

$$b_{KM} = \left[\frac{32}{9}\beta \mathrm{Im}\tilde{c}_5 + 8\beta \mathrm{Im}\tilde{c}_7\right]/(c_0 + 9c_4). \tag{20}$$

$$c_0 = c_1 - c_2 - c_3 - c_4 + \frac{32}{9}\beta \mathrm{Re}\tilde{c}_5 = -10.46. \tag{21}$$

The quantities a and b are the CP-even imaginary parts produced by rescattering of the pions (see [15]). To leading order $a = 0.121, \quad b = 0.714$. At the fixed above numerical values of the parameters and $\Omega_{\eta,\eta'} = 0.25$ we obtain to leading p^2 approximation

$$R_g = 0.030\frac{\mathrm{Im}\tilde{c}_5}{\mathrm{Re}\tilde{c}_5}(1-14.9\frac{\mathrm{Im}\tilde{c}_7}{\mathrm{Im}\tilde{c}_5}) = \ = -(2.44\pm0.44)\times10^{-5}x\left(1-\frac{0.13\pm0.03}{x}\right). \tag{22}$$

The higher-order corrections lead to 20% larger result

$$\begin{aligned}(R_g)_{corr} &= 0.039\frac{\mathrm{Im}\tilde{c}_5}{\mathrm{Re}\tilde{c}_5}\left(1-11.95\frac{\mathrm{Im}\tilde{c}_7}{\mathrm{Im}\tilde{c}_5}\right) = \\ &= -(3.0\pm0.5)\times10^{-5}x\left(1-\tfrac{0.11\pm0.025}{x}\right).\end{aligned} \tag{23}$$

Therefore, the corrections to the result obtained in the framework of conventional chiral theory to the leading approximation are not so large, as it was declared in [16].

4 Conclusion

From Eqs.(11), (15) and (23), it follows that EWP contributions diminish ε'/ε and increase R_g. The EWP corrections cancel one half of the QCD penguin contribution into ε'/ε at $x = 0.8$ and cancel 80% of QCD penguin contribution at $x = 2$. In both cases ε'/ε is the same.

In the case of $K^{\pm} \to 3\pi$ decays, the *direct* influence of EWP corrections themselves on CP effects is not so crucial as in $K_L \to 2\pi$ decays. But if a cancellation between the contribution of QCD and electroweak penguins in ε'/ε is large, the factor x in Eq.(23) is also larger than 1. So, for $x = 2$, the predicted R_g must be 2.5 times larger than at $x = 0.8$.

Therefore, measuring R_g, one obtains a possibility to determine the true relation between QCD and EWP contributions into CP violation in kaon decays.

References

1. S.Bertolini *et al.*, Nucl.Phys.B **514**, 93 (1998).
2. T.Hambye *et al.*, Nucl.Phys.B **564**, 391 (2000).
3. M.A.Shifman, A.I.Vainshtein and V.I.Zakharov, Zh.Eksp.i Teor.Fiz. **72**, 1277 (1977).
4. W.A.Bardeen, A.J.Buras and J.-M.Gerard, Nucl.Phys.B **293**, 787 (1987).
5. L.B.Okun, *Leptons and Quarks* (North-Holland Publ.Co. 1982) pp.315,323.
6. A.Ali and D.London , Eur.Phys.J. C **18**, 665 (2001).
7. S.Bertolini, J.O.Eeg and M.Fabbrichesi, Phys.Rev. D **63**, 056009 (2001).
8. A.J.Buras and J.-M.Gerard, Phys. Lett. B **517**, 129 (2001).
9. T.Hambye, S.Peris and E.de Rafael, hep-ph/0305104 v. 2.
10. J.F.Donoghue and E.Golovich, Phys.Lett. B **478**, 172 (2000).
11. M.B.Voloshin, preprint ITEP-22. (Moscow 1981).
12. S.Bertolini *et al.*, preprint SISSA 102/95/EP.
13. A.J.Buras, M.Jamin and M.Lautenbacher, Nucl.Phys.B **408**, 209 (1993).
14. S.Bertolini, J.O.Eeg and M.Fabbrichesi, Nucl.Phys. B **449**, 197 (1995).
15. E.P.Shabalin, hep-ph/040522x9 v.1
16. A.A.Bel'kov *et al.*, Phys.Lett.B **300**, 283, (1993).

Session II — Flavour Physics

(Chairpersons: U. Dosselli, G. Alexander)

H. Mahlke-Krüger	Puzzle Pieces: Results on $b\bar{b}$ and $c\bar{c}$ Spectroscopy and Decay
E. Barberio	Determination of $\lvert V_{cb} \rvert$
D. Côté	Semileptonic B Decays, B Mixing and Magnitudes of CKM Elements at Babar
XiaoHu Mo	Recent BES Results on ψ' Decay
M. Iori	Measurement of the Ω_c^0 Lifetime
M. Paulini	Results on Heavy Quark Physics at TeV Energies
E. Blucher	A New Determination of $\lvert V_{us} \rvert$ from KTeV
U. Moosbrugger	Semileptonic Decays of Neutral Kaons at NA48
C. Gatti	Kaon Semileptonic Decays at Kloe
V. Lubicz	Lattice QCD Calculation of the Vector Form Factor for $K_{\ell 3}$ Semileptonic Decays
S. Shimizu	Measurement of Direct Photon Emission in $K^+ \to \pi^+ \pi^0 \gamma$ Decay Using Stopped Positive Kaons
F. Mandl	Semileptonic Decay of $D^0 \to \pi l \nu$ and Form Factors for the Measurement of $\lvert V_{ub} \rvert$ at KEKB

Frascati Physics Series Vol. XXXVI (2004), pp. 97–104
DAΦNE 2004: Physics at meson factories – Frascati, June 7-11, 2004
Invited Review Talk in Plenary Session

PUZZLE PIECES: RESULTS ON $b\bar{b}$ AND $c\bar{c}$ SPECTROSCOPY AND DECAY

Hanna Mahlke-Krüger
Cornell University, Ithaca, NY 14853

Abstract

Recent results in the field of Heavy Quarkonia are reviewed, with results either providing new precision measurements or addressing key unanswered questions.

1 Introduction

Heavy quarkonia exhibit features similar to the positronium spectrum: a discrete system of states with the spacings and transition rates dictated by the binding force, which in this case is the strong interaction. Investigating heavy quarkonia therefore enables us to study important aspects of QCD. While heavy quarkonia parton level decay by annihilation is a perturbatively calculable process, transitions among them are not as they are soft due to the energy spread between the states, which is below 1 GeV.

Theory has made progress recently that indicates the need for experimental results at the few percent level in precision. On the other hand, there are important unanswered questions where experimental information is scant. The following results have been selected so as to address one or the other.

In view of the very limited space available for this report, no figures are shown, but references to publications where they can be found are given. More $\psi(2S)$ results from BES were presented in a separate talk by X.H. Mo at this conference.

2 Spectroscopy

2.1 Measurements of the η_c' Mass [1)]

After the first evidence for the η_c' more than twenty years ago, which established it from the direct M1 transition $\psi(2S) \to \gamma\eta_c'$, the experimental picture has consolidated in the past two years: In $B \to \eta_c' K$, $e^+e^- \to J/\psi\eta_c'$, and $\gamma\gamma \to \eta_c'$ studies, the η_c' mass is found to be around 3638 MeV, or 44 MeV higher than measured before. This means that the 2^3S_1-2^1S_0 mass splitting is reduced by a factor of two, and is now two times smaller than the hyperfine splitting at $n = 1$. Comparing these two is interesting because, due to the difference in $c\bar{c}$ distance, they sample different areas of the binding potential, which connects the confinement region with that of asymptotic freedom.

2.2 $X(3872)$ [2)]

Since the discovery of the "$X(3872)$" by Belle and subsequent confirmation by BaBar, CDF, and D0, several attempts to explain this narrow state have been made on the theory side. Among the plausible ones are that it could be a charmonium state, a $D\bar{D}$ molecule, or even an exotic state. Experimental efforts have focussed on studying decay or production modes that can clarify the nature of this state by virtue of establishing its quantum numbers. The decay mode $X \to \pi^+\pi^- J/\psi$, which gives rise to the state's characterization as "charmonium-like", remains the only one seen so far. The dipion mass distribution is of special interest as one hopes to answer the question whether or not the decay proceeds through an intermediate ρ. In this context, searching for $X(3872) \to \pi^0\pi^0 J/\psi$ is of special importance. CLEO has engaged in a search for X(3872) in two-photon fusion and ISR production, using 15 fb^{-1}

of data at $\sqrt{s} = 9.46 - 11.30\,\mathrm{GeV}$. This allows access to $J^{PC} = 1^{--}$ and $2n^{\pm+}$. Preliminary upper limits have been placed: $\Gamma_{ee} \times \mathcal{B}(X \to \pi^+\pi^- J/\psi) < 6.8\,\mathrm{eV}$ or 1% of the production rate of $\psi(2S)$ in ISR events (assuming a similar branching fraction $\mathcal{B}_{\pi^+\pi^- J/\psi}$), and $(2J+1)\Gamma_{\gamma\gamma} \times \mathcal{B}(X \to \pi^+\pi^- J/\psi) < 16.7\,\mathrm{eV}$, or one tenth of the η_c production rate in two-photon fusion. A similar ISR study has been done of BES data, using using $22.3\,\mathrm{pb}^{-1}$ at $\sqrt{s} = 4.03\,\mathrm{GeV}$, which arrived at an upper limit of $\Gamma_{ee} \times \mathcal{B}(X \to \pi^+\pi^- J/\psi) < 10\,\mathrm{eV}$.

2.3 Transitions [3)]

Transitions between states of heavy onia are by emission of photons or hadrons such charged pion pairs, neutral single pions or pion pairs, and etas. In bottomonium, also an ω transition has recently been observed as the first non-pionic hadronic transition in $\Upsilon(3S) \to \gamma\chi_{b1,2}(2S)$, $\chi_{b1,2} \to \omega\Upsilon(1S)$. The branching fractions are found to be substantial and also in compliance with a prediction for them to be about equal: $\mathcal{B}(\chi_{b1[2]} \to \omega\Upsilon(1S)) = (1.63^{+0.31+0.15}_{-0.32-0.11})$ $[(1.10^{+0.35+0.16}_{-0.28-0.10})]\%$. Radiative decays to Υs are, to date, the only other known exclusive decay mode of the χ_{bJ} states, and are only a factor 5-6 more common.

While η and single π^0 transitions have been seen in charmonium, with recent BES studies showing a much increased precision over previous results, a similar measurement in bottomonium is yet to be made.

Dipion transitions are the most common ones both in $c\bar{c}$ and $b\bar{b}$. Naively, one would expect that the ratio of branching fractions for neutral and charged modes would be, related by isospin, 1:2. A direct measurement of this quantity resulted in $\mathcal{B}(\psi(2S) \to \pi^0\pi^0 J/\psi)/\mathcal{B}(\psi(2S) \to \pi^+\pi^- J/\psi) = 0.570 \pm 0.009 \pm 0.026$; taking the most recent PDG values for the individual branching fractions yields 0.59 ± 0.04. An interesting new measurement has been made by BaBar, using radiative return events to the $\psi(2S)$ in $90\,\mathrm{fb}^{-1}$ of $\Upsilon(4S)$ data. They find $\mathcal{B}(\psi(2S) \to \pi^+\pi^- J/\psi) = 0.361 \pm 0.40$, which decreases the ratio by over 12%, thereby bringing it within reach of 0.5.

3 Decays

3.1 $\psi(3770) \to$ non-$D\bar{D}$? [4)]

The experimental indication for the existence of a significant $\psi(3770)$ non-$D\bar{D}$ hadronic decay width stems from the difference between early total hadronic

and the D pair production cross section measurements: $\sigma(\psi(3770) \to D\bar{D}) = 5.0 \pm 0.5\,\mathrm{nb}$, $\sigma(\psi(3770) \to hadrons) = 7.8 \pm 0.8\,\mathrm{nb}$. This invites the the following set of questions: Which non-$D\bar{D}$ channels are available to $\psi(3770)$ decay? Can the measurement of the total hadronic cross section be confirmed? Can the measurement of the D-pair production cross section be confirmed?

As to the last question, preliminary measurements seem to indicate a higher D-pair production cross section: $\sigma(\psi(3770) \to D\bar{D})^{CLEO} = (5.78 \pm 0.11 \pm 0.38)\,\mathrm{nb}$, $\sigma(\psi(3770) \to D\bar{D})^{BES} = (6.51 \pm 0.44 \pm 0.39)\,\mathrm{nb}$. The experimental techniques are somewhat different in that BES tags one of the D mesons, thereby gaining statistical advantage, while CLEO tags both D mesons, resulting in independence from external branching fractions. While there is an indication that the gap might not be as wide as previously thought, about 20% of the total width of $(23.6 \pm 2.7)\,\mathrm{MeV}$ [5] remain currently unaccounted for. Convincing unanimous evidence for what this gap is filled by has yet to be presented. The BES collaboration measured $\mathcal{B}(\psi(3770) \to \pi^+\pi^- J/\psi) = (0.34 \pm 0.14 \pm 0.08)\%$ or $\Gamma(\psi(3770) \to \pi^+\pi^- J/\psi) = (80 \pm 32 \pm 21)\,\mathrm{keV}$, which is to be compared with an upper limit set by CLEO of $\mathcal{B}(\psi(3770) \to \pi^+\pi^- J/\psi) < 0.26\%$ (90% CL). However, this channel, even if contributing of the order of 100 keV to the decay width, will not be able to account for the discrepancy previously observed. Radiative $\psi(3770)$ decays are estimated to amount to at most a few hundred keV. In addition, the question whether or not there are hadronic non-$D\bar{D}$ decays of the $\psi(3770)$ is interesting in the context of mixing scenarios. If mixing is at work, the modes expected from J/ψ that seem suppressed at the $\psi(2S)$ can give rise to a partial width at the $\psi(3770)$. An improved understanding of $\psi(2S)$ decays will aid in settling this question.

3.2 Decay into lepton pairs [6]

Studying bottomonium decay into lepton pairs provides access to the total width, which at some 10 keV for the narrow $\Upsilon(1,2,3S)$ resonances is below the typical beam energy spread of an e^+e^- collider of a few MeV, through $\Gamma_{tot} = \Gamma_{\ell\ell}/\mathcal{B}_{\ell\ell}$. In practice, the most precise measurement comes from employing lepton universality and using Γ_{ee} together with $\mathcal{B}_{\mu\mu}$. Measurements of dilepton branching fractions are interesting in their own right to confront LQCD predictions (the precision of which has reached the percent level now), to test lepton universality, and to compare $\Gamma_{\ell\ell}$ with the hadronic widths $\Gamma_{ggg,\gamma gg,q\bar{q}}$.

CLEO studied $\Upsilon(1/2/3S) \to \mu^+\mu^-$ production using $1.1/1.2/1.2\,\mathrm{fb}^{-1}$ on-resonance and $0.19/0.44/0.16\,\mathrm{fb}^{-1}$ off-resonance data. The CLEO results, corrected for interference with continuum, are: $\mathcal{B}(\Upsilon(1/2/3S) \to \mu^+\mu^-)^{CLEO} = (2.49 \pm 0.02 \pm 0.07)/(2.03 \pm 0.03 \pm 0.08)/(2.39 \pm 0.07 \pm 0.10)\%$, to be compared with the PDG values of [5] $(2.48 \pm 0.06)/(1.31 \pm 0.21)/(1.81 \pm 0.17)\%$. This illustrates that the desired precision to keep up with progress in Lattice QCD has been reached. Since the CLEO $\mathcal{B}(\Upsilon(2,3S))$ are found to be substantially higher, thereby reducing the total width by the same percentage, predictions for cascade decays such as $\Upsilon(3S) \to \gamma\chi_{bJ} \to \gamma\gamma\Upsilon(2S)$ are bound to change.

3.3 Baryon pair production in J/ψ and χ_{cJ} decays [7]

BES used their 58M J/ψ sample to measure $\mathcal{B}(J/\psi \to p\bar{p}) = (2.26 \pm 0.01 \pm 0.14)$. This is the single most precise measurement of this branching fraction to date. The angular distribution is fit with the expression $dN/d\cos\theta_p = 1 + \alpha_p \cos^2\theta_p$, where θ_p is the angle between the proton and the beam direction. Neglecting baryon and quark masses one would expect $\alpha = 1$ for all baryons; including masses yields $\alpha_p = 0.66$ and $\alpha_\Lambda = 0.51$. The experimental results are $\alpha_p^{exp} = 0.676 \pm 0.036 \pm 0.042$ and $\alpha_\Lambda^{exp} = 0.52 \pm 0.33 \pm 0.13$, in agreement with the prediction. Proton pairs are produced about twice as copiously in J/ψ decays as $\Lambda\bar{\Lambda}$ pairs. In $\psi(2S)$ decays, their branching fractions are comparable.

Baryon pairs from χ_{cJ} decay can be observed through $\psi(2S) \to \gamma\chi_{cJ} \to \gamma B\bar{B}$ and compared with the Color Octet Model prediction that one should expect half as many $\Lambda\bar{\Lambda}$ events as $p\bar{p}$ events. These have been made based on $\chi_{cJ} \to p\bar{p}$ measurements, which they describe well, and then generalized to other baryons. The BES $\chi_{cJ} \to \Lambda\bar{\Lambda}$ results from 14 M $\psi(2S)$ decays indicated an excess over this prediction by about a factor of two rather than a suppression, which has been confirmed as the branching fractions $\mathcal{B}(\chi_{cJ} \to p\bar{p})$ have been remeasured.

3.4 "Heavy to Heavy": Charmonium in $\Upsilon(1S)$ Decays

The Color Octet Mechanism (COM) $b\bar{b} \to gc\bar{c},\ ggc\bar{c}$ was employed to explain J/ψ production rates that could not be attributed to the thus far successful Color Singlet Model (CSM), which employs $b\bar{b} \to ggc\bar{c}c\bar{c}$. The two approaches predict different J/ψ momentum spectra as well as angular distributions and branching fractions for $\Upsilon(1S) \to J/\psi X$. A portion of the observed J/ψ signal

will be from $\Upsilon(1S) \to \psi(2S), \chi_{cJ} + X_1 \to J/\psi + X_2$ (not observed before). The magnitude of this feed-down contribution is also predicted by the two models.

A CLEO study of charmonium production in $\Upsilon(1S)$ data intends to shed additional light onto the question which mechanism is at work. Data taken on or near the $\Upsilon(4S)$ resonance is appropriately scaled and used to calculate the continuum background, which is small in comparison with the signal.

The inclusive branching fraction $\Upsilon(1S) \to J/\psi + X$ is measured to be $(6.4 \pm 0.4 \pm 0.6) \times 10^{-4}$, in compliance with both COM and CSM predictions, both at about 6×10^{-4}. The process $\Upsilon \to \gamma^* \to q\bar{q} \to J/\psi + X$ is linked with the continuum process $e^+e^- \to \gamma^* \to q\bar{q} \to J/\psi + X$ and can thus be estimated relative to the process $\Upsilon \to ggg, gg\gamma \to J/\psi + X$. The sum of the gluonic reactions dominates at a ratio of about 9:1. Also, the J/ψ momentum spectrum, scaled according to J/ψ momentum $x = p_{J/\psi}/p_{max}$ to eliminate beam energy dependence, has been measured. The COM predicts a peak at the highest x values, whereas the CSM shows an accumulation around $x = 0.5$. The measured spectrum peaks at $x = 0.3$. The situation is complicated by the fact that final state interactions, which could in principle soften the predicted spectra somewhat, have not been taken into account in the predictions.

Other results of this work include the first determination of the branching fractions of and feed-down from $\Upsilon(1S) \to \psi(2S), \chi_{cJ} + X, J = 1, 2$, which is found to be a factor of two above both the CSM and the COM predictions. (Since $\mathcal{B}(\chi_{c0} \to J/\psi\gamma)$ is an order of magnitude smaller than $\mathcal{B}(\chi_{c[1,2]} \to J/\psi\gamma)$, the absence of a signal for χ_{c0} is not surprising.)

3.5 "Heavy To Light" Charmonium Decays [9]

Decays of charmonia into light hadrons have often be studied in the light of the "12% rule". This is a scaling prescription connecting $\psi(2S)$ and J/ψ decays into hadronic final states. It allows one to compare the branching fraction ratio with that for decay into lepton pairs, which is measured to be 12% [5]. Modifications to this simple picture arise from non-relativistic corrections, form factor dependence on the two different center-of-mass energies, powers of $\alpha_s(m_{\psi(2S)})/\alpha_s(m_{J/\psi})$, and many more. Exact agreement with the prediction is therefore not to be expected. However, even with a more generous view some modes exhibit a substantial suppression, such as $\rho\pi$ and K^*K. It has been conjectured that the suppression is related to quantum numbers and that

vector pseudoscalar final states might be especially affected. Also, interference with continuum could play an important role as for tiny branching fractions the resonant and non-resonant cross section may be of comparable magnitude. Finally, it is possible that the prescription only holds for electromagnetic processes ($c\bar{c} \to \gamma^* \to q\bar{q}$), but not for those mediated by decay into gluons. This would imply that isospin violating modes, where the otherwise dominant gluonic process is absent, are of special importance to study. A consistent picture has thus far not emerged, partly due to lack of experimental data.

CLEO and BES have brought forward new $\psi(2S) \to VP$ measurements. The most prominent channel is $\psi(2S) \to \rho\pi$, which constitutes a big branching fraction on the J/ψ. It is not understood why it is so rare in $\psi(2S)$ decays. Another interesting feature is the different population of the Dalitz plane from what is seen in continuum and J/ψ. These two show clear ρ bands over some non-resonant background, whereas $\psi(2S)$ decays appear to proceed dominantly non-resonantly. To determine what mechanism is at work, a partial wave analysis would be helpful, which is not possible with the data at hand.

4 Summary and Acknowledgements

Experimental progress continues in the area of heavy quarkonia, thereby adding puzzle pieces to our understanding of many aspects of QCD. It is to be hoped that with future larger data samples more precision studies become feasible and that the remaining undiscovered states disclose themselves.

The author wishes to thank her many colleagues who provided analysis results, discussion, and guidance.

References

1. C. Edwards *et al.* (Crystal Ball), Phys. Rev. Lett. **48**, 70 (1982); S.K. Choi *et al.* (Belle), Phys. Rev. Lett. **89**, 102001 (2002); K. Abe *et al.* (Belle), Phys. Rev. Lett. **89**, 142001 (2002); D.M. Asner *et al.* (CLEO), Phys. Rev. Lett. **92**, 142001 (2004); B. Aubert *et al.* (BaBar), Phys. Rev. Lett. **92**, 142001 (2004).

2. $X(3872)$ Discoveries: S.K. Choi *et al.* (Belle), Phys. Rev. Lett. **91**, 262001 (2003); D. Acosta *et al.* (CDF), hep-ex/0312021; V.M. Abazov *et al.* (D0), hep-ex/0405004. $X(3872)$ Properties: S.K. Choi (Belle), hep-ex/0405014;

B. Aubert *et al.* (BaBar), Phys. Rev. Lett. **93**, 041801 (2004); C.Z. Yuan, X.H. Mo, P. Wang, Phys. Lett. **B579**, 74 (2004).

3. ω transitions in bottomonium: D. Cronin-Hennessy *et al.* (CLEO), hep-ex/0311043, accepted by PRL; M.B. Voloshin, Mod. Phys. Lett. A **18**, 1067 (2003). η, π^0 transitions in charmonium: J.Z. Bai *et al.* (BES), Phys. Rev. D **70**, 012006 (2004). Dipion transitions in charmonium: M. Ablikim *et al.* (BES), Phys. Rev. D **70**, 012003 (2004); M. Davier, hep-ex/0312063.

4. $\sigma(\psi(3770) \to hadrons)$: R.A. Partridge, Ph.D. thesis, CALT-68-1150 (1984); R.H. Schindler, Ph.D. thesis, SLAC-219, UC-34d (T/E) (1979). $\sigma(\psi(3770) \to D\bar{D})$: J. Adler *et al.* (Mark III), Phys. Rev. Lett. **60**, 89 (1988); G. Rong (BES), hep-ex/0406027; B. Sanghi (CLEO), Talk presented at 2004 Spring APS meeting, Denver, CO (unpublished), update: hep-ex/0408055. $\psi(3770) \to \pi\pi J/\psi$: J.Z. Bai *et al.* (BES), hep-ex/0307028; T. Skwarnicki, Int. J. Mod. Phys. **A 19**, 1030 (2004). $\psi(3770) \to \gamma\chi_{cJ}$: J.L. Rosner, hep-ph/0405196 (subm. to PRD).

5. S. Eidelman *et al.*, Phys. Lett. **B592**, 1 (2004).

6. G.S. Adams *et al.* (CLEO), hep-ex/0408010, intended for PRL.

7. $\alpha_{p,\Lambda}$: C. Carimalo, Int. J. Mod. Phys. **A 2**, 249 (1987). $J/\psi \to \Lambda\bar{\Lambda}$: J.Z. Bai *et al.* (BES), Phys. Lett. **B424**, 213 (1998), Erratum ibid. **B438**, 447 (1998). $\chi_{cJ} \to p\bar{p}$: J.Z. Bai *et al.* (BES), Phys. Rev. D **69**, 092001 (2004). COM: S.M.H. Wong, Eur. Phys. J. C **14**, 643 (2000). $\chi_{cJ} \to \Lambda\bar{\Lambda}$: J.Z. Bai *et al.* (BES), Phys. Rev. D **67**, 112001 (2003). $J/\psi \to p\bar{p}$: J.Z. Bai *et al.* (BES), Phys. Lett. **B591**, 42 (2004).

8. R.A. Briere *et al.* (CLEO), hep-ex/0407030 (subm. to PRD) and references therein.

9. Y.F. Gu, X.H. Li, Phys. Rev. D **63**, 114019 (2001). $J/\psi \to \pi^+\pi^-\pi^0$: J.Z. Bai *et al.* (BES), Phys. Rev. D **70**, 012005 (2004). $\psi(2S) \to 1^-0^-$: N.E. Adam *et al.* (CLEO), hep-ex/0407028 (subm. to PRL); M. Ablikim *et al.* (BES), hep-ex/0407037.

Frascati Physics Series Vol. XXXVI (2004), pp. 105–112
DAΦNE 2004: Physics at meson factories – Frascati, June 7-11, 2004
Invited Review Talk in Plenary Session

DETERMINATION OF $|V_{cb}|$

E. Barberio
University of Melbourne

Abstract

The present status of our knowledge of the magnitude of the quark mixing parameter V_{cb} is reviewed, with particular emphasis on the factors affecting experimental and theoretical errors and on prospects for a more precise determination.

1 Introduction

In the framework of the Standard Model, the quark sector is characterised by a rich pattern of flavour-changing transitions, described by the Cabibbo-Kobayashi-Maskawa (CKM) matrix. This report focuses on the quark mixing parameter $|V_{cb}|$.

Two different methods are used to extract this parameter from data: the **exclusive** measurement, where $|V_{cb}|$ is extracted by studying exclusive $B \rightarrow$

$D^\star \ell\nu$ and $B \to D\ell\nu$ decay processes; and the **inclusive** measurement, which uses the semileptonic width of b-hadron decays. Theoretical estimates play a crucial role in extracting $|V_{cb}|$, and an understanding of their uncertainties is very important.

2 Exclusive $|V_{cb}|$ determination

The exclusive $|V_{cb}|$ determination is obtained studying the $B \to D^\star \ell\nu$ and $B \to D\ell\nu$ decays, using Heavy Quark Effective Theory (HQET). HQET predicts that the differential partial decay width for $B \to D^\star \ell\nu$ process, $d\Gamma/dw$, is related to $|V_{cb}|$ through:

$$\frac{d\Gamma}{dw}(B \to D^\star \ell\nu) = \frac{G_F^2 |V_{cb}|^2}{48\pi^3} \mathcal{K}(w) \mathcal{F}(w)^2,$$

where w is the inner product of the B and $D^\star$ meson 4-velocities, $\mathcal{K}(w)$ is a known phase-space factor, and the form factor $\mathcal{F}(w)$ is generally expressed as the product of a normalisation constant, $\mathcal{F}(1)$, and a function, $g(w)$, constrained by dispersion relations [1].

The analytical expression of $\mathcal{F}(w)$ is not known a-priori. All recent published results use a non-linear shape for $\mathcal{F}(w)$, approximated with an expansion near $w = 1$ [2]. $\mathcal{F}(w)$ is parameterised in terms of the variable ρ^2, which is the slope of the form factor at zero recoil given in [2].

The decay $B \to D^\star \ell\nu$ has been studied in experiments performed at center-of-mass energies equal to the $\Upsilon(4S)$ mass and the Z^0 mass. At the $\Upsilon(4S)$, experiments have the advantage that the w resolution is quite good. However, they have more limited statistics near $w = 1$ in the decay $\overline{B}^o \to D^{\star +} \ell\nu$, because of the lower reconstruction efficiency of the slow pion, from the $D^{\star +} \to \pi^+ D^0$ decay. The decay $B^- \to D^{\star 0} \ell\overline{\nu}$ is not affected by this problem. In addition, kinematic constraints enable $\Upsilon(4S)$ experiments to identify the final state, including the $D^\star$, without a large contamination from the poorly known semileptonic decays including a hadronic system heavier than $D^\star$, commonly identified as $D^{\star\star}$. At LEP, B's are produced with a large momentum (about 30 GeV on average). This give a relatively poor w resolution and limited physics background rejection capabilities. By contrast, LEP experiments benefit from an efficiency that is only mildly dependent upon w.

Experiments determine the product $(\mathcal{F}(1) \cdot |V_{cb}|)^2$ by fitting the measured

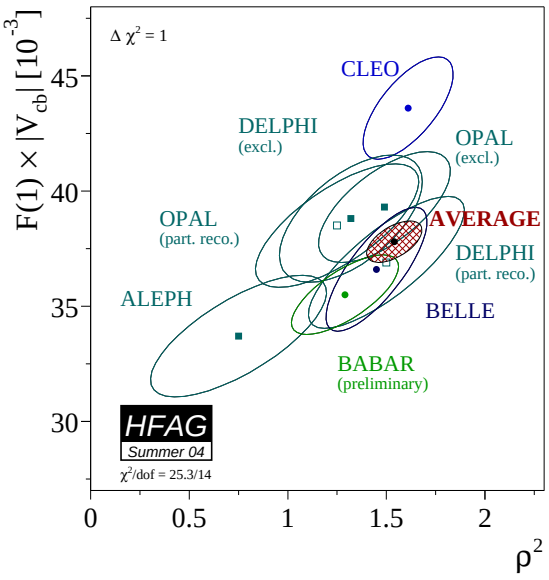

Figure 1: *The error ellipses for the corrected measurements and world average for* $\mathcal{F}(1)|V_{cb}|$ *vs* ρ^2*. The ellipses are the product between the 1* σ *error of* $\mathcal{F}(1)|V_{cb}|$*,* ρ^2*, and the correlation between the two.*

$d\Gamma/dw$ distribution. Averaging [3] all published results [4] we get:

$$\mathcal{F}(1)|V_{cb}| = (37.8 \pm 0.9) \times 10^{-3}$$

and

$$\rho^2 = 1.54 \pm 0.14$$

with a χ^2 per degree of freedom of 23.5/14. The error ellipses for the corrected measurements and for the world average are shown in Fig.1.

There are several different corrections to the infinite mass value $\mathcal{F}(1) = 1$ [5]. Estimates of these corrections have been performed with OPE sum rules [6], and with an HQET based lattice gauge calculation [7]. The central values obtained with both methods are similar. Consequently, we use $\mathcal{F}(1) = 0.91 \pm 0.04$ [8], from which we get $|V_{cb}| = (41.5 \pm 1.0_{\rm exp} \pm 1.8_{\rm theo}) \times 10^{-3}$, where the dominant error is theoretical.

The study of the decay $B \to D\ell\nu$ is challenging both from the theoretical and experimental point of view. The differential decay rate for $B \to D\ell\nu$ can be expressed as:

$$\frac{d\Gamma_D}{dw}(B \to D\ell\nu) = \frac{G_F^2|V_{cb}|^2}{48\pi^3}\mathcal{K}_{\mathcal{D}}(w)\mathcal{G}(w)^2,$$

where w is the inner product of the B and D meson 4-velocities, $\mathcal{K}_{\mathcal{D}}(w)$ is the phase space, and the form factor $\mathcal{G}(w)$ is generally expressed as the product of a normalisation factor, $\mathcal{G}(1)$, and a function, $g_D(w)$, constrained by dispersion relations [1].

The strategy to extract $\mathcal{G}(1)|V_{cb}|$ is identical to that used for the $B \to D^\star\ell\nu$ decay. However, $\mathcal{G}(1)$ is calculated with less accuracy than $\mathcal{F}(1)$ [9] [10], and $d\Gamma_D/dw$ is more heavily suppressed near $w = 1$ than $d\Gamma_{D^*}/dw$, due to the helicity mismatch between initial and final states. This channel is also hard to isolate from the dominant background $B \to D^\star\ell\nu$, as well as from fake D–ℓ combinations. Thus, the extraction of $|V_{cb}|$ from this channel is less precise than the one from the $B \to D^\star\ell\nu$ decay. Nevertheless, the $B \to D\ell\nu$ channel provides a consistency check.

Belle [11] and ALEPH [4] studied the $\overline{B}^0 \to D^+\ell^-\overline{\nu}$ channel. CLEO [12] studied both $B^+ \to D^0\ell^+\overline{\nu}$ and $\overline{B}^0 \to D^+\ell^-\overline{\nu}$ decays. Averaging all data [3], we get $\mathcal{G}(1)|V_{cb}| = (42.0 \pm 3.7) \times 10^{-3}$ and $\rho_D^2 = 1.15 \pm 0.16$, where ρ_D^2 is the slope of the form factor at zero recoil given in [2]. Using $\mathcal{G}(1) = 1.04 \pm 0.06$, we get $|V_{cb}| = (40.4 \pm 3.6_{\rm exp} \pm 2.3_{\rm theo}) \times 10^{-3}$, consistent with the value extracted from $B \to D^\star\ell\nu$ decay, but with a larger uncertainty.

3 $|V_{cb}|$ determination from inclusive B semileptonic decays

Alternatively, $|V_{cb}|$ can be extracted from the inclusive branching fraction for semileptonic b hadron decays $\mathrm{B}(B \to X_c\ell\nu)$ [13] [14]. Several studies have shown that the spectator model decay rate is the leading term in a well-defined expansion controlled by the parameter $\Lambda_{\rm QCD}/m_b$. Non-perturbative corrections to this leading approximation arise only to order $1/m_b^2$.

The coefficients of the $1/m_b$ power terms are expectations values of operators that include non-perturbative physics. There are two ways [15] [16] [13] [14] to handle the energy scale μ used to separate long-distance from short-distance physics. HQET is most commonly renormalised in a mass-independent scheme,

thus making the quark masses the pole masses of the underlying theory (QCD). The second group of authors prefer the definition of the non-perturbative operators using a mass scale $\mu \approx 1$ GeV.

The corresponding equations for the semileptonic width can be found in 13) 17) and 25).

4 HQE and moments in semileptonic decays

Experimental determinations of the HQE parameters are important in several respects. Non-calculable quantities are parametrised in terms of expectation values of hadronic matrix elements, which can be related to the shape (moments) of inclusive decay spectra. Furthermore, redundant determinations of these parameters may uncover inconsistencies.

CLEO 18) determines the parameter $\bar{\Lambda}$ from the first moment of the γ energy in the decay $b \to s\gamma$, which gives the average energy of the γ emitted in this transition, using the formalism of 17).

Babar, CLEO and DELPHI performed moments measurements the hadronic mass M_X^2 spectrum. Babar measures up to the fourth moment of this distribution, DELPHI up to the third moment.

Babar 21) and CLEO 26) explored the moments of the hadronic mass M_X^2 as a function of the lepton momentum cuts. CLEO performs a fit for the contributions of signal and backgrounds to the full three-dimensional differential decay rate distribution as a function of the reconstructed quantities q^2, M_X^2, $\cos\theta_{W\ell}$. BaBar uses a sample where the hadronic decay of one B is fully reconstructed and the charged lepton from the other B is identified. In this case the main sources of systematic errors are the uncertainties related to the detector modelling and reconstruction. Moments of the M_X distribution without an explicit lepton momentum cut have been extracted from DELPHI data 24) and give consistent results.

The shape of the lepton spectrum provides further constraints on OPE. Moments of the lepton momentum with a cut $p_\ell^{CM} \geq 1.5$ GeV/c have been measured by the CLEO collaboration 28). Babar 22) extract up to the third moment of this distribution, using a low momentum cut of $p_\ell^{CM} \geq 0.6$ GeV/c. Moments of the lepton momentum without an explicit lepton momentum cut have been extracted from DELPHI data 24) and give consistent results.

The results are compared with theory and they are consistent.

Babar [23] determine the non-perturbative parameters and $|V_{cb}|$ simultaneously from a fit to the moments of the hadronic-mass and electron-energy distributions from B($B \to X_c \ell\nu$) using the calculation in Ref. [25]. This fit yields significantly improved measurements of the inclusive branching fraction B($B \to X_c \ell\nu$) and $|V_{cb}|$. Using Babar only data, we get [23]:

$$|V_{cb}|_{\rm incl} = (41.4 \pm 0.4_{\rm exp} \pm 0.4_{\rm HQE} \pm 0.6_{\rm theo}) \times 10^{-3}$$

where the first error is experimental, and the second is from the measured value of the moments assumed to be universal up to higher orders. The third error is from $1/m_b^4$ corrections and from the ambiguity in the α_s scale definition. The error on the average b-hadron lifetime is assumed to be uncorrelated with the error on the semileptonic branching ratio.

5 Conclusions

The values of $|V_{cb}|$ obtained both from the inclusive and exclusive method agree within errors. The value of $|V_{cb}|$ obtained from the analysis of the $B \to D^\star \ell\nu$ decay is:

$$|V_{cb}|_{\rm exclusive} = (41.5 \pm 1.0_{\rm exp} \pm 1.8_{\rm theo}) \times 10^{-3} \ ,$$

where the first error is experimental and the second error is from the $1/m_Q^2$ corrections to $\mathcal{F}(1)$. The value of $|V_{cb}|$, obtained from inclusive semileptonic branching fractions is:

$$|V_{cb}|_{\rm incl} = (41.4 \pm 0.4_{\rm exp} \pm 0.4_{\rm HQE} \pm 0.6_{\rm theo}) \times 10^{-3},$$

where the first error is experimental, the second error is from the measured HQE values, and the last is from $1/m_b^4$ corrections and α_s.

References

1. C. Glenn Boyd, B. Grinstein, and R.F. Lebed,Physics Phys.Lett. B353,306(1995).
2. I. Caprini, L. Lellouch, and M. Neubert, Nucl. Phys. B530,153(1998), C.G. Boyd, B. Grinstein, R.F. Lebed, Phys.Rev. 56,6895(1997).
3. The Heavy Flavor Averaging Group (HFAG); http://www.slac.stanford.edu/xorg/hfag/semi/index.html LEP V_{cb} Working Group, Internal Note, `http://lepvcb.web.cern.ch/LEPVCB/`.
4. BaBar Collaboration, this conference Belle Collaboration, Phys.Lett.B526:247-,2002, CLEO Collaboration, Phys.Rev.Lett.89:081803,2002, ALEPH Collaboration, Phys.Lett.B395:373-,1997, DELPHI Collaboration,Phys.Lett.B510:55-,2001, DELPHI Collaboration,Eur.Phys.J.C33:213-,2004, OPAL Collaboration, Phys.Lett.B482:15-,2000.
5. P.F. Harrison and H.R. Quinn, editors *The BaBar Physics Book* (1998) and references therein.
6. M. Shifman, N.G. Uraltsev, and A. Vainshtein, Phys.Rev. D51,2217(1995).
7. J.N. Simone *et al*, Nucl. Phys. Proc. Suppl. **83**, 334 (2000); `hep-ph/0110253`.
8. Working Group 1 Summary, CKM Workshop, CERN, CH (2002); `http://ckm-workshop.web.cern.ch/ckm-workshop/`.
9. M. Neubert, Phys. Lett.B264,455(1991)
10. Z. Ligeti, Y. Nir, and M. Neubert, Phys. Rev. D49,1302(1994) Z. Ligeti, hep-ph/9908432.
11. K. Belle Collaboration, Phys.Lett.B526:258-268,2002.
12. CLEO Collaboration, Phys.Rev.Lett.82:3746-,1999.

13. I. Bigi, M. Shifman, and N. Uraltsev, Ann. Rev. Nuc. Part. Sci. **47**, 591 (1997).

14. A.V. Manohar and M.B. Wise, Phys.Rev. D49,110(1994).

15. M. Gremm and N. Kapustin, Phys.Rev.D55,6924(1997).

16. A. Falk, M. Luke, and M.J. Savage, Phys.Rev. D33,2491(1996).

17. A. Falk and M. Luke, Phys.Rev.D57,424(1998).

18. S. Chen *et al*, Phys.Rev.Lett. 87,251807(2001).

19. D. CLEO Collaboration, Phys.Rev.Lett. 87,251808(2001).

20. C. W. Bauer, Z. Ligeti, M. Luke and A. V. Manohar, Phys.Rev. D67, 054012 (2003).

21. BABAR Collaboration, Phys.Rev. D69,111103, 2004.

22. BABAR Collaboration, Phys.Rev. D69,111104, 2004.

23. BABAR Collaboration, Phys.Rev. Lett. 93 ,011803, 2004.

24. DELPHI Collaboration, ICHEP04 contribution.

25. P. Gambino and N.Uraltsev hep-ph/0401063 , hep-ph/0403166 N.Uraltsev, hep-ph/0302262.

26. CLEO Collaboration, arXiv:hep-ex/0307081.

27. C.S. Bauer and M. Trott, Phys.Rev.Lett 67,014021 (2003).

28. CLEO Collaboration, Phys.Rev.Lett D67, 072001, 2003.

Frascati Physics Series Vol. XXXVI (2004), pp. 113–118
DAΦNE 2004: Physics at meson factories – Frascati, June 7-11, 2004
Selected Contribution in Plenary Session

SEMILEPTONIC B DECAYS, B MIXING AND MAGNITUDES OF CKM ELEMENTS AT BABAR

David Côté
Université de Montréal

Abstract

The value of $|V_{cb}|$ has been measured recently from a simultaneous fit to moments of the hadronic-mass and lepton-energy distributions in inclusive semileptonic B-mesons decays with a precision of 2%. Both exclusive and inclusive measurements of $|V_{ub}|$ have also been carried out in $B \to X_u \ell \nu$ decays. Precision measurements of the mixing parameter, Δm_d, have been obtained. In addition, direct limits on the total decay-rate difference $\Delta\Gamma$ between the two B^0 mass eigenstates and on CP, T and CPT violation due exclusively to oscillations have recently been provided by BaBar.

1 Introduction

There are strong motivations for studying semileptonic B decays and $B^0\bar{B}^0$ mixing. First of all, these processes are related to some of the fundamental

parameters of the Standard Model. With input from theory, it is then possible to determine the values of $|V_{ub}|$ and $|V_{cb}|$ from measurements of inclusive and/or exclusive branching fractions of $B \to X_u \ell\nu$ and $B \to X_c \ell\nu$, respectively. The measurement of the $B^0\bar{B}^0$ oscillation frequency, Δm_d, constrains the value of $|V_{td}|$. From a fit of heavy quark expansion (HQE) relations to the data, the inclusive study of $B \to X_c \ell\nu$ also yields a relatively precise determination of the b and c quark masses. Secondly, the $B^0\bar{B}^0$ mixing and semileptonic B decay branching fractions have large effects on other measurements and thus need to be measured precisely. Indeed, Δm_d is used in all the time-dependent CP measurements while the semileptonic decays are an important source of background for many measurements. Finally, the semileptonic B decays are useful to test various QCD effective theories.

2 Inclusive $|V_{cb}|$ measurement [5)]

The first attempts to determine $|V_{cb}|$ suffered from large uncertainties due to poorly known theoretical parameters. For BaBar's latest inclusive $|V_{cb}|$ measurement, we aimed to measure simultaneously these parameters, $Br(B \to X_c \ell\nu)$ and $|V_{cb}|$, by using HQE relations calculated in the kinetic mass scheme to order $1/m_b^3$ and α_S [1)]. These HQE relations depend on the m_b and m_c quark masses and on the non-perturbative QCD parameters μ_G, μ_π, ρ_{LS} and ρ_D. All are poorly known but constraints on a large number of measurable quantities allow their experimental determination as well as $Br(B \to X_c \ell\nu)$ and $|V_{cb}|$. This was achieved with a global HQE fit to the measured first moments of the lepton energy and hadronic mass distribution as a function of different lepton energy cuts.

2.1 Electron energy moments [3)]

Taking $R_i(E_0, \mu) = \int_{E_0}^{\infty} (E_e - \mu)^i (\frac{d\Gamma}{dE_e}) dE_e$, the electron energy moments are then defined as: partial branching fraction (0^{th} moment): $Br(E_0) = \tau_B \cdot R_0(E_0, 0)$; first moment: $M_1(E_0) = \frac{R_1(E_0,0)}{R_0(E_0,0)}$; central moments: $M_n(E_0) = \frac{R_n(E_0, M_1(E_0))}{R_0(E_0,0)}$, $n = 2, 3$. These moments were extracted from $B \to X_c e\nu$ decays tagged with di-electron events containing one high momentum electron and one opposite charge electron as well as requiring a typical B-B event topology. The remaining backgrounds, determined mostly from data control sam-

ples, were then subtracted. Various corrections were applied to correct for the effect of Bremsstrahlung, electron ID efficiency, etc... Four hundred thousand signal events were kept from a sample of 47.4 fb^{-1}. The 0^{th} to 3^{rd} electron energy moments were then computed for various minimum electron energy cuts, varying from 0.6 GeV to 1.5 GeV in the $\Upsilon(4S)$ frame.

2.2 Hadronic mass moments [4)]

This measurement used events consisting of a fully reconstructed B meson - B_{reco} (via its hadronic decays). The other B meson decaying semileptonically was required to have exactly one energetic lepton and a missing energy, momentum and total charge consistent with a single neutrino. The hadronic mass, M_{Xc}, was then reconstructed with a kinematic fit to all the remaining particles of the event. The first four hadronic mass moments (as defined in Sect. 2.1) were then computed for minimum electron energy cuts varying between 0.9 GeV and 1.5 GeV in the $\Upsilon(4S)$ frame.

2.3 Fit results and comparison with other measurements

The global fit (Sect. 2) to the measured moments (Sect. 2.1 and 2.2) shows an impressive agreement between HQE predictions and experimental data. The results of fits to electron energy moments alone are consistent with those to hadronic mass moments alone. The results are:

$$|V_{cb}| = (41.4 \pm 0.4_{exp} \pm 0.4_{HQE} \pm 0.2_{\alpha_S} \pm 0.6_{\Gamma_{SL}}) \times 10^{-3};$$
$$Br(B \to X_c e\nu) = (10.61 \pm 0.16_{exp} \pm 0.06_{HQE})\ \%;$$
$$m_b(1GeV) = (4.61 \pm 0.05_{exp} \pm 0.04_{HQE} \pm 0.02_{\alpha_S})\ GeV;$$
$$m_c(1GeV) = (1.18 \pm 0.07_{exp} \pm 0.06_{HQE} \pm 0.02_{\alpha_S})\ GeV.$$

These values represent the best measurements to date of these parameters. It is interesting to note that the b and c quark masses are in excellent agreement with theoretical expectations. Results for the HQE parameters: μ_π^2, μ_G^2, ρ_D^3 and ρ_{LS}^3 are also presented in [5)].

3 Inclusive $|V_{ub}|$ measurement [7)]

The semileptonic B decays investigated for the inclusive measurement of $|V_{ub}|$ were identified by the same method as described in Sect.2.2. To isolate the relatively rare $B \to X_u \ell\nu$ decays out of the very abundant $B \to X_c \ell\nu$, we required

a small reconstructed m_X and no kaon on the semileptonic side of the events. $Br(B \to X_u \ell\nu)$ is determined from the measured ratio $R_u = \frac{Br(B\to X_u\ell\nu)}{Br(B\to X\ell\nu)}$, where $Br(B \to X\ell\nu)$ is taken from a previous BaBar measurement [2]. This method allows a cancellation of systematic errors due to B_{reco} on the tag side and lepton ID on the semileptonic side. Using [6]:

$$|V_{ub}| = 0.0045 \cdot \left(\frac{Br(B \to X_u \ell\nu)}{0.002} \frac{1.55ps}{\tau_B} \right)^{1/2} \times (1.0 \pm 0.020_{pert} \pm 0.052_{1/m_b^3}) \quad (1)$$

, we obtained: $|V_{ub}| = (4.62 \pm 0.28(stat) \pm 0.27(syst) \pm 0.48(theo)) \times 10^{-3}$ and $Br(B \to X_u \ell\nu) = (2.24 \pm 0.27(stat) \pm 0.26(syst) \pm 0.39(theo)) \times 10^{-3}$.

4 Exclusive $|V_{ub}|$ measurement [8]

BaBar's first attempt to measure $|V_{ub}|$ from an exclusive channel used a technique which consisted of selecting $B \to \rho e\nu$ events containing a very energetic electron and having missing energy and momentum consistent with a single neutrino. The exclusive reconstruction of the $B \to \rho e\nu$ decay is achieved by reconstructing a ρ and requiring $\Delta E = E_{beam} - E_\rho - E_\ell - E_{miss}$ to be compatible with zero. This analysis led to:
$Br(B \to \rho e\nu) = (3.29 \pm 0.42(stat) \pm 0.47(syst) \pm 0.60(theo)) \times 10{-}4$
and $|V_{ub}| = (3.64 \pm 0.22(stat) \pm 0.25(syst)^{+0.39}_{0.56}(theo)) \times 10{-}3$.

5 $B^0\bar{B}^0$ mixing

BaBar had previously [9] performed several precision measurements of the $B^0\bar{B}^0$ oscillation frequency, Δm_d, and of the B^0 lifetime, τ_B. In those analyses, the total decay-rate difference between B^0 and $\bar{B}^0$, CP violation in mixing and CPT violation were assumed to be negligible. Recently, a generalized $B^0\bar{B}^0$ mixing analysis was performed [10] which didn't made these assumptions. In all analyses, the experimental technique consisted of first fully reconstructing a B (as in Sect. 2.2) and of measuring the vertex position of this "B_{reco}". The vertex of the second "B_{tag}" was determined using the remaining charged tracks of the event. Its flavor was determined from the charge of lepton(s) and/or kaon(s) and/or soft pion(s) among the remaining tracks. The distance along the beam axis between the B_{reco} and B_{tag} vertices was then used to estimate the lifetime difference Δt between the two B mesons. The reconstructed B

pairs were classified in categories which depended on the flavor of B_{reco} and B_{tag}. A fit to the measured Δt distributions in the different categories was performed to extract the $B^0\bar{B}^0$ mixing parameters.

5.1 Previous $B^0\bar{B}^0$ mixing analyses

In these measurements, the $B^0\bar{B}^0$ pairs are classified as "mixed" or "unmixed", where the unmixed events correspond to $B^0\bar{B}^0 \to B^0\bar{B}^0$ events and the mixed ones to $B^0\bar{B}^0 \to B^0B^0/\bar{B}^0\bar{B}^0$ events. The mixed and unmixed samples are described by two different probability density functions (PDF):

$$N_{\pm}(\Delta t, \Delta m_d) = \frac{e^{-|\Delta t|/\tau}}{4\tau} \cdot (1 \pm \cos(\Delta t \Delta m_d)) \otimes (Reconstruction\ effects). \quad (2)$$

The parameter Δm_d is then extracted from the asymmetry A:

$$A(\Delta t) = \frac{N_+(\Delta t) - N_-(\Delta t)}{N_+(\Delta t) + N_-(\Delta t)} = \cos(\Delta m_d \Delta t). \quad (3)$$

From a sample of 23 millions B pairs, we obtained:
$\Delta m_d = 0.500 \pm 0.008 \pm 0.006 ps^{-1}$ and $\tau_{B^0} = 1.529 \pm 0.012 \pm 0.029 ps$.

5.2 "Generalized" $B^0\bar{B}^0$ mixing analysis

In this analysis, the $B^0\bar{B}^0$ pairs are classified in 6 different categories: B^0B^0, $B^0\bar{B}^0$, $\bar{B}^0B^0$, $\bar{B}^0\bar{B}^0$, B^0B_{CP}, $\bar{B}^0B_{CP}$, where the two Bs are B_{tag} and B_{reco}, respectively. Unlike the previous mixing analysis, the B_{reco} which are CP eigenstates are also used in this analysis leading to a more complex fit formula. From a sample of 82 fb^{-1}, we obtained:

$$\begin{aligned} sgn(Re\lambda_{CP})\Delta\Gamma_d/\Gamma_d &= -0.008 \pm 0.037(stat) \pm 0.018(syst); \\ |q/p| &= 1.029 \pm 0.013(stat) \pm 0.011(syst); \\ (Re\lambda_{CP}/|\lambda_{CP}|)Rez &= 0.014 \pm 0.035(stat) \pm 0.034(syst); \\ Imz &= 0.038 \pm 0.029(stat) \pm 0.025(syst). \end{aligned}$$

where $\lambda_{CP} \equiv (q/p)(\bar{A_{CP}}/A_{CP})$, A_{CP} ($\bar{A_{CP}}$) is the amplitude for $B^0 \to f_{CP}$ ($\bar{B}^0 \to f_{CP}$), and $z \equiv \frac{\delta m_d - (i/2)\delta\Gamma_d}{\Delta m_d - (i/2)\Delta\Gamma_d}$. Here, δ (Δ) means the difference between the B^0 flavor (mass) eigenstates and $sgn(Re\lambda_{CP})$ indicate that the sign of $Re\lambda_{CP}$is undetermined. More detailed explanations are given in Ref. [10] but we note here that $\Delta\Gamma_d/\Gamma_d$ is the lifetime difference between the B_{heavy} and B_{light} mass eigenstates, $z \neq (0,0)$ imply CPT violation and $|q/p| \neq 1$ imply $P(B^0 \to \bar{B}^0) \neq P(\bar{B}^0 \to B^0)$. All our present results confirmed the assumptions previously made in the $B^0\bar{B}^0$ mixing and CP analyses.

6 Summary

New BaBar precision measurements of $|V_{cb}|$, $Br(B \to X_c e\nu)$, m_b, m_c and 4 HQE parameters were obtained, improving significantly our knowledge of these quantities. Inclusive (exclusive) $|V_{ub}|$ measurements with a precision of 13% (18%) were also carried out at BaBar using $B \to X_u \ell\nu$ decays. These are currently dominated by theoretical errors, but much progress is expected soon. Finally, a new analysis with variable $\Delta\Gamma_d/\Gamma_d$, $|q/p|$ and z mixing parameters validate the assumptions made in previous BaBars mixing and CP measurements.

References

1. P. Gambino, N. Uraltsev, Eur. Phys. J. **C34**, 181-189 (2004), N. Uraltsev, hep-ph/0403166.
2. BaBar Collaboration (B. Aubert *et al.*), Phys. Rev. **D67**, 031101 (2003).
3. BaBar Collaboration (B. Aubert *et al.*), Phys. Rev.**D69**, 111104 (2004).
4. BaBar Collaboration (B. Aubert *et al.*), Phys. Rev. **D69**, 111103 (2004).
5. BaBar Collaboration (B. Aubert *et al.*), Phys. Rev. Lett. **93**, 011803 (2004).
6. M. Battaglia *et al*, The CKM matrix and the unitarity triangle (2002), e-print archive: hep-ph/0304132.
7. BaBar Collaboration (B. Aubert *et al.*), Phys. Rev. Lett. **92**, 071802 (2004).
8. BaBar Collaboration (B. Aubert *et al.*), Phys. Rev. Lett. **90**, 181801 (2003).
9. BaBar Collaboration (B. Aubert *et al.*), Phys. Rev. Lett. **88**, 221802 (2002), BaBar Collaboration (B. Aubert *et al.*), Phys. Rev. Lett. **88**, 221803 (2002), BaBar Collaboration (B. Aubert *et al.*), Phys. Rev. Lett. **89**, 011802 (2002), BaBar Collaboration (B. Aubert *et al.*), Phys. Rev. **D66**, 032003 (2002), BaBar Collaboration (B. Aubert *et al.*), Phys. Rev. **D67**, 072002 (2003).
10. BaBar Collaboration (B. Aubert *et al.*), Phys. Rev. Lett. **92**, 181801 (2004), BaBar Collaboration (B. Aubert *et al.*), Phys. Rev. **D70**, 012007 (2004).

Frascati Physics Series Vol. XXXVI (2004), pp. 119–124
DAΦNE 2004: Physics at meson factories – Frascati, June 7-11, 2004
Selected Contribution in Plenary Session

RECENT BES RESULTS ON ψ' DECAY

XiaoHu Mo *
Institution of High Energy Physics, CAS, Beijing 100039, China

Abstract

With 14 M ψ' events, many two-body decay channels are studied, which include VP, VT and PP channels. Based on systematical measurements for charmonium decay, 12% rule is tested, the phase between strong and EM amplitudes is studied. In addition, hadronic and radiative transition of charmonia are measured to improve experimental accuracy and test theoretical calculations.

1 Introduction

Charmonium decay continues to present itself as a challenge to our understanding of the strong interaction. Up to 2004, BES collaboration has collected 14 Million (M) ψ' events (luminosity is 19.72 pb^{-1}), 58 M J/ψ events, 27 pb^{-1}

* On behalf of BES collaboration

ψ'' data and 6.4 pb^{-1} data taken at 3.65 GeV for continuum study. With all these samples, studies have made systematically for charmonium decay. Herein the results of ψ' decay is the main content of this report, which contains the following topics: decays of ψ' to Vector Pseudoscalar (VP), Vector Tensor (VT), Pseudoscalar Pseudoscalar (PP) channels, and hadronic and radiative transition of ψ'.

As it is known, both J/ψ and ψ' decays are expected to be dominated by annihilation into three gluons, with widths that are proportional to the square of the $c\bar{c}$ wave function at the origin [1]. This yields the pQCD expectation (so-called "12 % " rule) that

$$Q_h = \frac{\mathcal{B}_{\psi' \to X_h}}{\mathcal{B}_{J/\psi \to X_h}} = \frac{\mathcal{B}_{\psi' \to e^+e^-}}{\mathcal{B}_{J/\psi \to e^+e^-}} = (12.3 \pm 0.7)\% \quad . \tag{1}$$

The observation of deviation from 12 % rule will provide some new clues concerning the dynamics of charmonium decay. Another study relevant to charmonium decay is the relative phase ϕ between strong and electromagnetic (EM) amplitudes. At J/ψ region, the nature of ϕ has been studied in many two-body decay modes: 1^-0^- [2, 3], 0^-0^- [4, 5, 6], 1^-1^- [6] and $N\overline{N}$ [7]; while at ψ' region, only two modes 0^-0^- [8] and 1^-0^- [9] have been discussed phenomenologically, more researches are needed.

Here it is necessary to stress a point. In e^+e^- experiment, the production of ψ' is accompanied by one photon continuum process

$$e^+e^- \to \gamma^* \to \text{hadrons} \ , \tag{2}$$

in which e^+e^- pair annihilates into a virtual photon without going through the intermediate resonance state. Taking the contribution from this process and its interference effect into consideration, it could determine not only the magnitude but also the sign of ϕ. Furthermore, the continuum contribution and its interference effect will exert obvious influence on the branching ratio measurement, which should be treated carefully in corresponding analyses.

2 Study of ψ' two-body decay

2.1 VP channel

As forementioned the continuum contribution need to be treated carefully, the data at both resonance and continuum are analyzed. Fig. 1 shows the invari-

ant mass distribution of ω, from which the numbers of events are fitted to be 7.4 ± 2.8 at $E_{cm} = 3.65$ GeV and 31.3 ± 7.4 at $E_{cm} = 3.686$ GeV, respectively. The rough estimation based on the present results shows that the continuum contribution is around 70%, which is consistent with 60%, the phenomenological calculation [11]. For $K^*\overline{K}$ channel, $K\pi K_S$ ($K_S \to \pi^+\pi^-$) final state is studied. From the invariant mass distributions of $K\pi$ and $K_S\pi$ at ψ' peak (continuum), the numbers of events are fitted to be 65.6 ± 9.0 (2.5 ± 1.9) and 9.6 ± 4.2 (0) for $K^*\overline{K}^0 + c.c.$ and $K^{*+}\overline{K}^- + c.c.$ respectively. With the luminosities, it is easy to transform the observed numbers of events into the corresponding cross sections. If the parameterization forms in reference [6] are adopted, and observed cross sections are used as inputs, the phase between strong and EM amplitudes can be fitted, at the same time, obtaining the branching ratios, which are 12.7×10^{-5} and 3.1×10^{-5} for $K^*\overline{K}^0 + c.c.$ and $K^{*+}\overline{K}^- + c.c.$, respectively. Comparing with the results listed in Table 1, from which the continuum contribution has not been subtracted, the largest difference is around 18%.

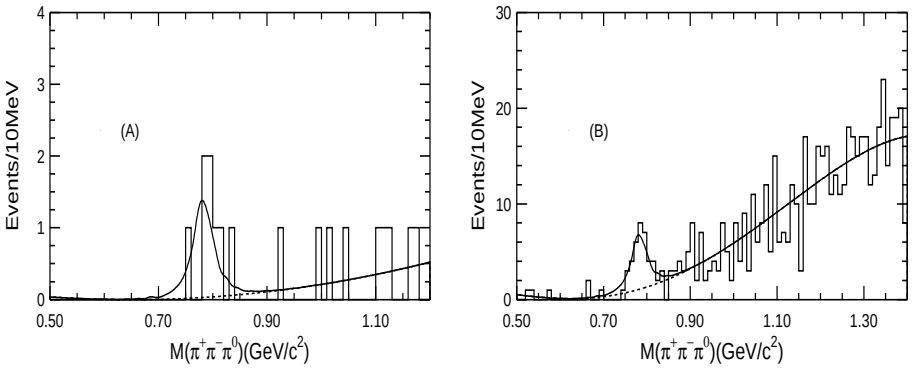

(a) At $E_{cm} = 3.65$ GeV (b) At $E_{cm} = 3.686$ GeV

Figure 1: *The invariant mass distribution of ω at (a) continuum and (b) resonance. The dashed line indicates the background while the solid line the synthetic fitting result.*

2.2 VT channel

The measured results for VT channel [10] are listed in Table 1, from which we notice that the Q-value for all VT channel are suppressed by a factor of 3 to 5

compared with the 12 % rule.

2.3 PP channel

For PP channel, the parameterization forms [12]

$$\begin{array}{rll} \pi^+\pi^- : & & E \ , \\ K^+K^- : & \sqrt{3/2}\, M & + E \ , \\ K_S^0K_L^0 : & \sqrt{3/2}\, M & \ , \end{array} \tag{3}$$

are adopted to determine the phase ϕ. So far as e^+e^- experiment is concerned, E must be replaced by $E + E_C$, where E_C denotes the continuum contribution. Fitting together the previous measurements [8] and the recently measured branching ratio for $\psi' \to K_S^0K_L^0$, we determine ϕ to be $(-82 \pm 29)^\circ$ or $(+121 \pm 27)^\circ$. The detailed analyses of $K_S^0K_L^0$ in J/ψ and ψ' decay can be found in references [13] and [14], the final results are summarized in Table 1.

Table 1: *The results of ψ' two-body decay.*

VP channel	$\mathcal{B}_{\psi'}$ (10^{-5}) (from BES)	$\mathcal{B}_{J/\psi}$ (10^{-4}) (from PDG2002)	Q_h
$K^*\overline{K}^0 + c.c.$	$15.0 \pm 2.1 \pm 1.7$	42 ± 4	3.6 ± 0.7
$K^{*+}\overline{K}^- + c.c.$	$2.9 \pm 1.3 \pm 0.4$	50 ± 4	0.58 ± 0.29
$\omega\pi^0$	< 3.27	4.2 ± 0.6	< 7.8
VT channel	$\mathcal{B}_{\psi'}$ (10^{-4}) (from BES)	$\mathcal{B}_{J/\psi}$ (10^{-3}) (from PDG2002)	Q_h
ωf_2	$2.05 \pm 0.41 \pm 0.38$	4.3 ± 0.6	4.8 ± 1.5
ρa_2	$2.55 \pm 0.73 \pm 0.47$	10.9 ± 2.2	2.3 ± 1.1
$K^*\overline{K_2^*} + c.c.$	$1.86 \pm 0.32 \pm 0.43$	6.7 ± 2.6	2.8 ± 1.3
$\phi f_2'$	$0.44 \pm 0.12 \pm 0.11$	1.23 ± 0.21	3.6 ± 1.5
PP channel	$\mathcal{B}_{\psi'}$ (10^{-5}) (from BES)	$\mathcal{B}_{J/\psi}$ (10^{-4}) (from BES)	Q_h
$K_S^0K_L^0$	$5.24 \pm 0.47 \pm 0.48$	$1.82 \pm 0.04 \pm 0.13$	28.8 ± 3.7

3 12% rule and mixing model

The Q-values for three kinds of two-body decay, VP, VT and PP, are listed in Table 1. It clearly shows that the Q-value is enhanced for some channels

while suppressed for others. Indeed, many theoretical efforts are made to settle the problems [15], however, none explains all the existing experimental data naturally. Here we only mention one point: some recent phenomenological studies indicate that S- and D-wave mixing model is a natural and calculable model. It probably give a unified explanation for all 12% rule deviated decays. Using this model, according to the measurement results at J/ψ and ψ', the corresponding decay at ψ'' can be predicted. So the measurement at ψ'' can be used to test the mixing model. One example is given in reference [16], according to which the branching ratio of $\psi'' \to K_S^0 K_L^0$ is estimated to be within a range from $(0.12 \pm 0.07) \times 10^{-5}$ to $(3.8 \pm 1.1) \times 10^{-5}$. With the data at ψ'', BES has detected an upper limit, which does not contradict the current prediction.

4 ψ' hadronic and radiative transition

Motivation for such study is to improve experimental accuracy and test theoretical calculations. Inclusive and exclusive methods are adopted to analyze the following channels extensively:

$XJ/\psi(J/\psi \to \mu^+\mu^-)$ final state	$\gamma\gamma J/\psi(J/\psi \to \ell^+\ell^-)$ final state
$Anything\ J/\psi$	$\pi^0 J/\psi$
$\pi^0\pi^0 J/\psi$	$\eta J/\psi$
$\eta J/\psi$	$\gamma\chi_{c1}, \chi_{c1} \to \gamma J/\psi$
$\gamma\chi_{c1}, \chi_{c1} \to \gamma J/\psi$	$\gamma\chi_{c2}, \chi_{c2} \to \gamma J/\psi$
$\gamma\chi_{c2}, \chi_{c2} \to \gamma J/\psi$	

(4)

For XJ/ψ final states, μ-pair is used to identify J/ψ particle, the invariant mass distributions of X with and without extra charged-track cases are fitted simultaneously with component shapes determined from Monte Carlo simulation [17]; for $\gamma\gamma J/\psi$ final states, lepton-pair is used to identify J/ψ particle, the various exclusive channels are fitted separately [18]. Based on BES results, some theoretical calculations are tested. Comparisons show that the calculation based on PCAC are smaller than BES measurement, while the Multipole expansion evaluations are consistent with BES present values [18].

5 Acknowledgments

Thanks my colleagues of BES collaboration who provide me so many good results which are reported here.

References

1. T. Appelquist and H. D. Politzer, Phys. Rev. Lett. **34**, 43 (1975); A. De Rújula and S. L. Glashow, Phys. Rev. Lett. **34**, 46 (1975).
2. J. Jousset *et al.*, Phys. Rev. **D41**, 1389 (1990).
3. D. Coffman *et al.*, Phys. Rev. **D38**, 2695 (1988).
4. M. Suzuki, Phys. Rev. **D60**, 051501. (1999).
5. G. López, J. L. Lucio M. and J. Pestieau, hep-ph/9902300.
6. L. Köpke and N. Wermes, Phys. Rep. **174**, 67 (1989).
7. R. Baldini *et al.*, Phys. Lett. **B444**, 111 (1998).
8. C. Z. Yuan, P. Wang and X. H. Mo, Phys. Lett. **B567**, 74 (2003).
9. P. Wang, C. Z. Yuan, and X. H. Mo, Phys. Rev. **D69**, 057502 (2004).
10. J. Z. Bai et al., Phys. Rev. **D69**, 072001 (2004).
11. P. Wang, X. H. Mo and C. Z. Yuan, Phys. Lett. **B557**, 192 (2003).
12. E. Haber and J. Perrier, Phys. Rev. **D69**, 2961 (2004).
13. J. Z. Bai et al., Phys. Rev. **D69**, 012003 (2004).
14. J. Z. Bai et al., Phys. Rev. Lett. **92**, 052001 (2004).
15. W. S. Hou and A. Soni, Phys. Rev. Lett. **50**, 569 (1983); S. J. Brodsky and M. Karliner, Phys. Rev. Lett. **78**, 4682 (1997); M. Chaichian and N. A. Törnqvist, Nucl. Phys. **B323**, 75 (1989); S. S. Pinsky, Phys. Lett. **B236**, 479 (1990); G. Karl and W. Roberts, Phys. Lett. **B144**, 243 (1984); X. Q. Li, D. V. Bugg and B. S. Zou, Phys. Rev. **D55**, 1421 (1997); J. M. Gérard and J. Weyers, Phys. Lett. **B462**, 324 (1999); T. Feldmann and P. Kroll, Phys. Rev. **D62**, 074006 (2000).
16. P. Wang, X. H. Mo and C. Z. Yuan, hep-ph/0402227.
17. J. Z. Bai et al., Phys. Rev. **D70**, 012006 (2004).
18. J. Z. Bai et al., Phys. Rev. **D70**, 012003 (2004).

Frascati Physics Series Vol. XXXVI (2004), pp. 125–131
DAΦNE 2004: Physics at meson factories – Frascati, June 7-11, 2004
Selected Contribution in Plenary Session

MEASUREMENT OF THE Ω_c^0 LIFETIME

M. Iori *
University of Rome "La Sapienza" and I.N.F.N
Rome Italy

Abstract

We report a precise measurement of the Ω_c^0 lifetime. The data were taken by the SELEX experiment (E781) spectrometer using 600 GeV/c Σ^-, π^- and p beams. The measurement has been done using 79 $\pm$ 16 reconstructed Ω_c^0 from a total sample of 107 $\pm$ 22. The lifetime of the Ω_c^0 is measured to be $(74 \pm 16(stat.))$ fs using $\Omega^-\pi^+\pi^-\pi^+$ and $\Omega^-\pi^+$ decay modes. The mass of the Ω_c^0 is measured to be $(2706.5 \pm 2.1 \pm 1.2)$ MeV/c^2.

1 Introduction

Several experiments [1, 2, 3, 4, 5] in the last years have detected the Ω_c^0 ground state. Recently at Fermilab the photoproduction experiment FOCUS (E831) reported an observation of a sample of 64 Ω_c^0 events and they measured its lifetime [6]. They report also, in an earlier publication [5] , the Ω_c^0 lifetime

* On behalf of SELEX Collaboration

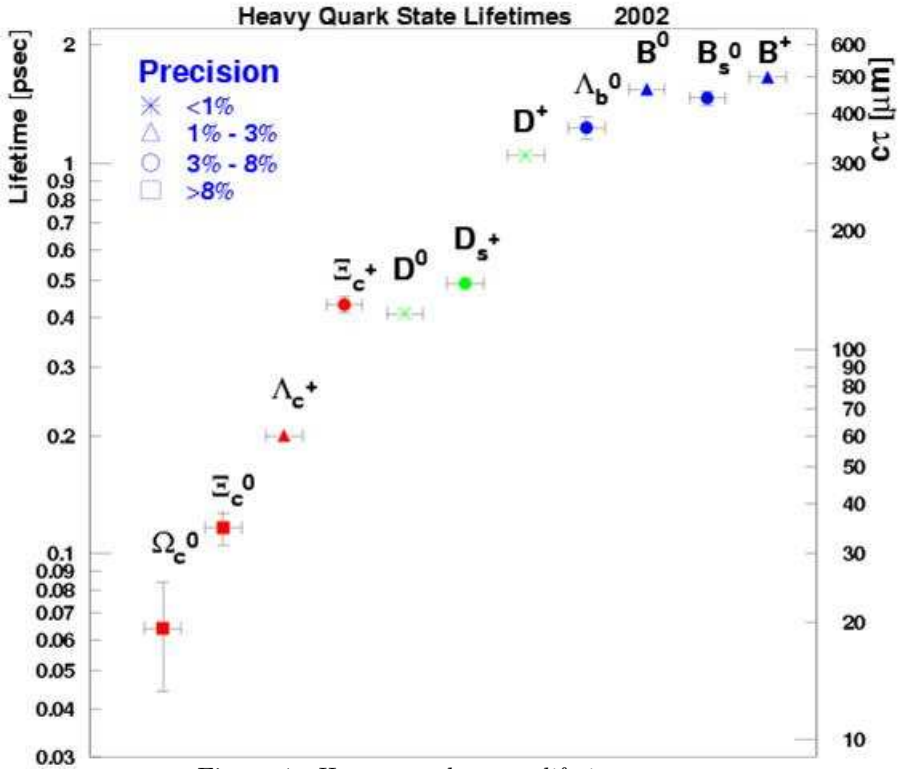

Figure 1: *Heavy quark states lifetimes.*

measurement. The experiment WA89 reported 200 Ω_c^0 events in several decays modes and a measurement of lifetime of $55^{+13}_{-11}\ ^{+18}_{-23}$ fs from two decays modes only [7]. A qualitative hierarchy of lifetime has been predicted [8]. Fig. 1 shows the charmed baryon and meson lifetime is spread in a range of 50-1000 fs in strong contrast with the B mesons. Clearly additional measurements of lifetime as well the branching ratios with more statistical accuracy are needed to test theoretical models [9]. In this talk we report the results of a new measurement of the lifetime based on data from the hadroproduction experiment SELEX (E781) at Fermilab (throughout this article, charge conjugate states are assumed). The measurement is based on a subsample of 79 $\pm$ 16 fully reconstructed Ω_c^0 from a sample of 15.2 $\times 10^9$ hadronic triggers.

The SELEX detector at Fermilab is a 3-stage magnetic spectrometer. The

negatively charged 600 GeV/c beam contains nearly equal fractions of Σ and π. The positive beam contains 92% protons. Beam particles are identified by a Transition Radiation detector. The spectrometer was designed to study charm production in the forward hemisphere with good mass and decay vertex resolution for charm momenta in the range 100-500 GeV/c. Five interaction targets (2 Cu and 3 C) had a total target thickness of 4.2% λ_{int} for protons. The targets are spaced by 1.5 cm. Downstream of the targets are 20 silicon planes with a strip pitch of 20-25 μm oriented in X, Y, U and V views. The scattered-particle spectrometers have momentum cutoffs of 2.5 GeV/c and 15 GeV/c respectively. A Ring-Imaging Cerenkov detector (RICH) [10], filled with Neon at room temperature and pressure, provides single track ring radius resolution of 1.4% and 2σ K/π separation up to about 165 GeV/c. A layout of the spectrometer can be found elsewhere [11, 12].

2 Data set and charm selection

The charm trigger is very loose. It requires a valid beam track, at least 4 charged secondaries in the forward 150 mrad cone, and two hodoscope hits after the second bending magnet from tracks of charge opposite to that of the beam. We triggered on about 1/3 of all inelastic interactions. A computational filter linked PWC tracks having momenta > 15 GeV/c to hits in the vertex silicon and made a full reconstruction of primary and secondary vertices in the event. An event was written to tape if it was inconsistent with having come from a single vertex. This filter passed 1/8 of all interaction triggers and had about 50% efficiency for otherwise accepted charm decays. The experiment recorded data from 15.2 $\times 10^9$ inelastic interactions and wrote about 10^9 events to tape using both positive and negative beams.

In the full analysis the vertex reconstruction was repeated with tracks of all momenta. Again, only events inconsistent with having a single primary vertex were considered. The RICH detector identified charged tracks above 25 GeV/c. Results reported here come from a second pass reconstruction through the data, using a production code optimized for speed and cascade Reconstruction. To separate the signal from the non charm background we require that: (i) the spatial separation L between the reconstructed production and decay vertices exceeds 6 times the combined error σ_L, each decay track, extrapolated to the primary vertex z position, must miss by a transverse distance length $t \geq$

Table 1: *Invariant mass results and signal yields for the two Ω_c^0 modes analyzed.*

Ω_c^0	$Mass(\mathrm{MeV}/c^2)$	Signal
$\Omega^-\pi^+\pi^+\pi^-$	2708.0 ± 4.5	44 ± 14
$\Omega^-\pi^+$	2707.1 ± 2.4	35 ± 12
$\Xi^-K^+\pi^-\pi^+$	2702.8 ± 8	28 ± 12
Average	$2706.5 \pm 2.1 \pm 1.2$	107 ± 22

2.5 times its error σ_t, (iii) each decay track, extrapolated to the *kink* vertex z position, must miss by a transverse distance length $t \geq 300$ μm ,(iv) decays must occur within a fiducial region and (v) the total transverse momentum of pions from $\Omega^-\pi^+\pi^-\pi^+$ decay must be greater than 0.35 GeV/c to the Ω_c^0 direction. These cuts optimize the ratio signal background. There are 107 ± 22 events Ω_c^0 candidates that pass these cuts and they are summarized in Table I and the mass spectrum is shown in Fig. 1. We divide them into three decay channels: , $\Omega^-\pi^+\pi^-\pi^+$, $\Omega^-\pi^+$, $\Xi^-K^-\pi^+\pi^+$. The invariant mass is measured to be $2706.5 \pm 2.1 \pm 1.2$ MeV/c^2, 2.7 σ above the PDG mass value [13]. No dependence of mass value on momentum is found. We know that our mass resolution is quite accurate because the previous charm invariant masses, D,D_s and Λ_c agree well with word average [14]. The systematic error was obtained by comparing the SELEX measured mass value to the current PDG average. It results an offset < 1 MeV/c^2. π/K misidentification causes a reflection of Ξ_c under the Ω_c^0 peak. The sample was selected requiring a minimum π momentum of 8 GeV/c to reduce misidentification in the RICH as well as the fake invariant mass combination. We formed the invariant mass distribution of these events when one pion is interpreted as a K meson and Ξ^- as Σ^-. At most one of the two possible reflections per event falls into the Ω_c^0 mass window. We count the misidentified Ξ_c in the Ω_c^0 sample by fitting the Ω_c^0 mass distribution within $\pm$ 20 MeV/c^2 interval around the Ω_c^0 mass . The resultant misidentified Ω_c^0 is less than 2 events.

3 Lifetime evaluation using a maximum likelihood fit

The average longitudinal error σ_z on the primary and secondary vertices is 270 μm and 500 μm, which gives a combined error of 570 μm. In the Ω_c^0 sample, the average momentum is 250 GeV/c, corresponding to a time resolution of

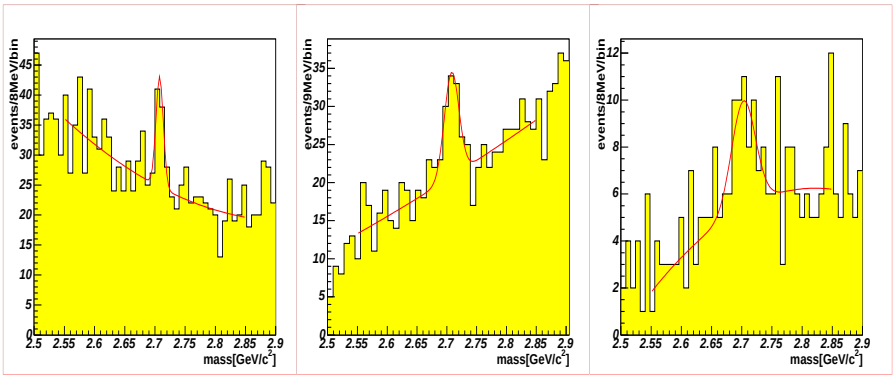

Figure 2: *From left to right: Invariant mass of* $\Omega^-\pi^+$, $\Omega^-\pi^+\pi^-\pi^+$ *and* $\Xi^-K^-\pi^+\pi^+$ *respectively. The yield is reported in Table 1.*

16 fs, about 22% of $\tau_{\Omega_c^0}$. Because bin-smearing effects are small, we used a binned maximum likelihood fitting technique to determine the Ω_c^0 lifetime. The fit was applied to a reduced proper time distribution, $t^* = M(L - L_{min})/pc$ where M is the known charm mass [13], p the reconstructed momentum, L the measured vertex separation and L_{min} the minimum L for each event to pass all the imposed selection cuts. L_{min} is determined event-by-event. We fitted all events with $t^* < 600$ fs in the mass range $2.630 < M(\Omega_c^0) < 2.760$ GeV/c^2, $\pm\ 2.5\sigma$ from the Ω_c^0 central mass value.

To evaluate the mean lifetime we used a maximum likelihood method. The probability density was performed by the function :

$$f(\tau_{\Omega_c^0},\ \tau_{Bck1},\ \tau_{Bck2},\ \alpha,\ \beta;\ t^*) = (1-\alpha)N_S\frac{e^{-t^*/\tau_{\Omega_c^0}}}{\epsilon(t^*)\tau_{\Omega_c^0}} + \alpha N_S B(t^*) \qquad (1)$$

where

$$B(t^*) = \beta\frac{e^{-t^*/\tau_{Bck1}}}{\tau_{Bck1}} + (1-\beta)\frac{e^{-t^*/\tau_{Bck2}}}{\tau_{Bck2}} \qquad (2)$$

The function is the sum of a term for the Ω_c^0 exponential decay corrected by the acceptance function $\epsilon(t^*)$ plus a background function $B(t^*)$ consisting of two exponentials to describe the strong decays and charm decays respectively. Its parameters were determined from the Ω_c^0 sideband t^* distribution. The mass range of the sideband background windows, $2.610 < M(\Omega_c^0) < 2.630$ GeV/c^2 and $2.760 < M(\Omega_c^0) < 2.780$ GeV/c^2 was twice the signal mass window.

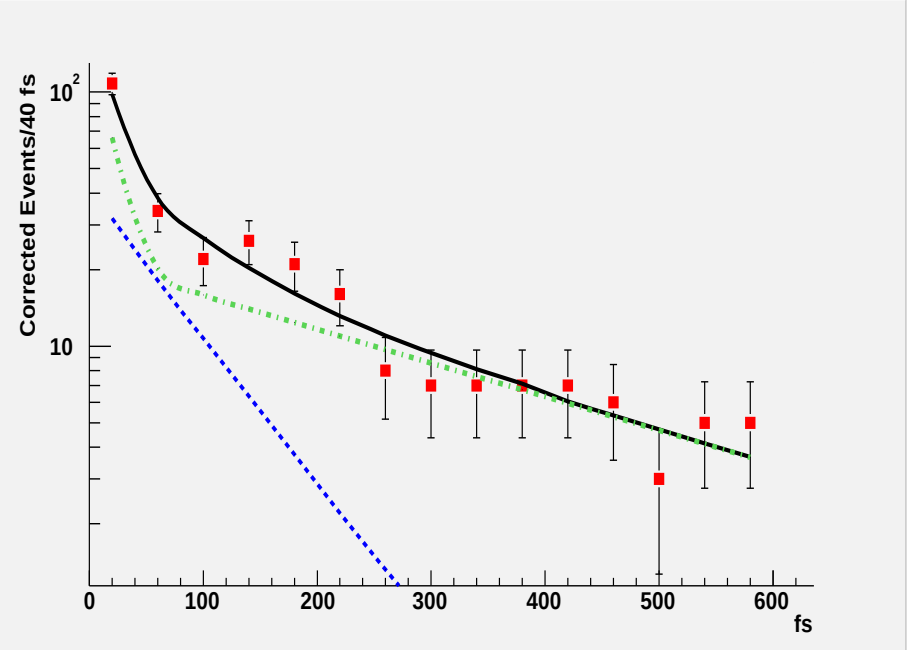

Figure 3: *Corrected reduced proper time distribution for* $\Omega^-\pi^+\pi^+\pi^-$ *and* $\Omega^-\pi^+$ *(squares) and result from the maximum likelihood fit (solid curve). The dashed dot curve shows the fitted background. The dashed curve shows the* $\Omega_c^{\,0}$ *lifetime.*

The fitted parameters are: $\tau_{\Omega_c^0}$ (Ω_c^0 lifetime), τ_{Bck1}, τ_{Bck2} (background lifetimes), α (background fraction in the signal region) and β (background splitting function). N_S is the total number of events in the signal region.

The proper-time-dependent acceptance $\epsilon(t^*)$ is independent of spectrometer features after the first magnet, e.g., RICH efficiency and tracking efficiency. These efficiencies affect only the overall number of events detected. The proper time distribution of these events depends crucially on vertex reconstruction. To evaluate $\epsilon(t^*)$ we generated $2{\times}10^6$ events by Monte Carlo simulation. The acceptance $\epsilon(t^*)$, does not differ significantly from unity and it is rather constant. Fig. 3 shows the overall fits to the data distributions as a function of reduced proper time for $\Omega^-\pi^+\pi^-\pi^+$ and $\Omega^-\pi^+$ decay modes.

We measure an average lifetime $\tau_{\Omega_c^0} = 74 \pm 16$ fs. The uncertainties are statistical only, evaluated where $-\ln\mathcal{L}$ increases by 0.5; the evaluation of systematic error is in progress.

References

1. J. Stiewe, Proc. 26th Int. Conf. in High Energy Physics, Dallas Vol. 1 1076.
2. P. L. Frabetti et al., Phys. Lett. B338 1994 106.
3. P. L. Frabetti et al., Phys. Lett. B300 1993 190.
4. D. Cronin-Hennessy et al., Phys. Rev. Lett. 86 2001 3730.
5. P. L. Frabetti et al., Phys. Lett. B357 1995 678.
6. J. M. Link et al., Phy. Lett. B561 41 2003.
7. M. I. Adamovich et a., Phys. Lett. B358 1995 151.
8. B. Guberina, R. Ruckl and j. Trampetic, Z. Phys. C**33** 297 (1986).
9. S. Bianco,F.L. Fabbri, D. Benson and I. Bigi Riv. Nuovo Cimento 26N7-8 2003.
10. J. Engelfried et al. (SELEX), Nucl. Instrum. Meth A433 149 1999.
11. M.E. Matton (SELEX) 2002 Fermilab-Thesis 2002-03.
12. J. Russ et al. (SELEX) 1998 hep-ex/9812031.
13. K. Hagiwara et al., Phys. Rev. D66 2002 010001.
14. A. Kushnirenko et al. (SELEX) Phys. Rev. Lett 86 5243 2001 hep-ex/00100114.

Frascati Physics Series Vol. XXXVI (2004), pp. 133–140
DAΦNE 2004: Physics at meson factories – Frascati, June 7-11, 2004
Invited Review Talk in Plenary Session

RESULTS ON HEAVY QUARK PHYSICS AT TEV ENERGIES

Manfred Paulini *
Carnegie Mellon University, Pittsburgh, PA 15213, U.S.A.

Abstract

We review recent result on heavy quark physics at TeV energies focusing on Run II measurements from the CDF and DØ experiments at the Tevatron.

1 Introduction

The CDF and DØ experiments can look back to an already successful heavy flavour physics program during the 1992-1996 Run I data taking period (for a review of B physics results from CDF in Run I see e.g. Ref. [1]). The Fermilab accelerator complex has undergone a major upgrade in preparation for Tevatron Run II. The centre-of-mass energy has been increased from 1.8 TeV to 1.96 TeV

* Representing the CDF and DØ Collaboration.

and the Main Injector, a new 150 GeV proton storage ring, has replaced the Main Ring as injector of protons and anti-protons into the Tevatron.

The initial Tevatron luminosity steadily increased throughout Run II. By the summer of 2004, the peak luminosity reached is $\sim 10 \times 10^{31}$ cm^{-2}s^{-1}. The total integrated luminosity delivered by the Tevatron to CDF and DØ by the time of this conference is ~ 400 pb^{-1}. More than 300 pb^{-1} were recorded to tape by each CDF and DØ. However, most results shown in this review use about 150-250 pb^{-1} of data. The CDF and DØ detectors have also undergone major upgrades for Run II which can be found elsewhere [2].

1.1 Triggering on Heavy Quark Decays

The total inelastic $p\bar{p}$ cross section at the Tevatron is about three orders of magnitude larger than the b production cross section. The CDF and DØ trigger system is therefore the most important tool for finding B decay products. B physics triggers at CDF and DØ are based on leptons including single and dilepton triggers. Identification of dimuon events down to very low momentum is possible, allowing for efficient $J/\psi \to \mu^+\mu^-$ triggers. Both experiments also use inclusive lepton triggers designed to accept semileptonic $B \to \ell\nu_\ell X$ decays. New to the CDF detector is the ability to select events based upon track impact parameter. The Silicon Vertex Trigger (SVT) gives CDF access to purely hadronic B decays and makes CDF's B physics program fully competitive with the one at the e^+e^- B factories.

2 Selected Heavy Quark Physics Results from the Tevatron

With the different B trigger strategies above, the Collider experiments are able to trigger and reconstruct large samples of heavy flavour hadrons. Due to the restricted page limit for these proceedings, we can only very briefly discuss a few selected heavy quark physics results from CDF and DØ in the following.

2.1 B Hadron Masses and Lifetimes

Measurements of B hadron masses and lifetimes are basic calibration measures to demonstrate the understanding of heavy flavour reconstruction. CDF and DØ use exclusive B decay modes into J/ψ mesons for precision measurements of B hadron masses reconstructing the decay modes $B^0 \to J/\psi K^{*0}$, $B^+ \to$

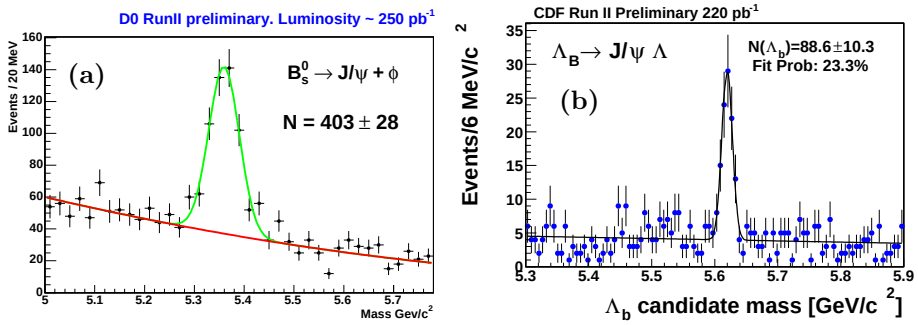

Figure 1: *Invariant mass distribution of (a) $J/\psi\phi$ (DØ) and (b) $J/\psi\Lambda$ (CDF).*

Table 1: *Summary of B hadron mass m_B and lifetime τ_B measurements from CDF and DØ.*

Mode	m_B (CDF) [MeV/c^2]	τ_B (CDF) [ps]	τ_B (DØ) [ps]
$B^0 \to J/\psi K^{*0}$	$5279.6 \pm 0.5 \pm 0.3$	$1.54 \pm 0.05 \pm 0.01$	$1.47 \pm 0.05 \pm 0.02$
$B^+ \to J/\psi K^+$	$5279.1 \pm 0.4 \pm 0.4$	$1.66 \pm 0.03 \pm 0.01$	$1.65 \pm 0.08^{+0.09}_{-0.12}$
$B_S^0 \to J/\psi\phi$	$5366.0 \pm 0.7 \pm 0.3$	$1.37 \pm 0.10 \pm 0.01$	$1.44 \pm 0.10 \pm 0.02$
$\Lambda_b \to J/\psi\Lambda$	$5619.7 \pm 1.2 \pm 1.2$	$1.25 \pm 0.26 \pm 0.10$	$1.22 \pm^{+0.22}_{-0.18} \pm 0.04$

$J/\psi K^+$, $B_S^0 \to J/\psi\phi$ and $\Lambda_b \to J/\psi\Lambda$ (see Fig. 1). These modes combine good signal statistics with little background. The results of the mass and corresponding B hadron lifetime measurements are summarized in Table 1. The B_S^0 and Λ_b masses and lifetimes are currently the world best results.

2.2 Measurement of Lifetime Ratio $\tau(B^+)/\tau(B^0)$

The study of heavy flavour lifetimes is intimately related with the understanding of the decay dynamics of these particles. The DØ experiment measured the lifetime ratio for neutral and charged B mesons using a novel technique. This result exploits the large semileptonic sample of $B \to \mu X$ decays reconstructed in about 250 pb^{-1} of $p\bar{p}$ data. Rather than measuring the individual B^0 and B^+ lifetimes and forming the ratio, this analysis makes use of the fact that $D^{*-}\mu^+$ events mainly originate from B^0 mesons ($\sim$ 86%) while $\bar{D}^0\mu^+$ indicate a B^+ signature ($\sim$ 82%). The construction of the B decay vertex

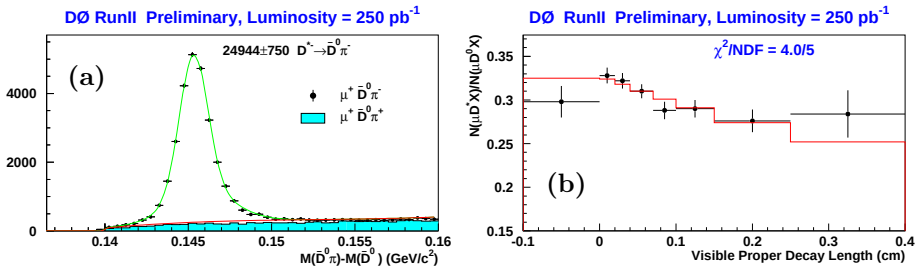

Figure 2: *(a) Mass difference $m(\bar{D}^0\pi) - m(\bar{D}^0)$ for $\bar{D}^0\mu$ events. (b) Ratio of events in D^{*-} (B^0) and $\bar{D}^0$ (B^+) samples as a function of proper decay length.*

uses only $\bar{D}^0\mu^-$ while the slow pion from the decay $D^{*-} \to \bar{D}^0\pi^-$ is only used to distinguish B^0 from B^+ (see Fig. 2(a)) drastically reducing the systematic uncertainty between both decay modes. The events are grouped into bins of proper decay length and the $\bar{D}^0$ event yield is extracted from the $K^+\pi^-$ mass distribution. Feed-down from D^{**} decays is accounted for using Monte Carlo studies. The ratio of events in the D^{*-} (B^0) and $\bar{D}^0$ (B^+) samples as a function of proper decay length, as shown in Fig. 2(b), is used to extract a lifetime ratio of $\tau^+/\tau^0 = 1.093 \pm 0.021 \pm 0.022$. This is one of the most precise measurements of the B^+/B^0 lifetime ratio.

2.3 Charmless B Decays

CDF has shown examples of fully reconstructed hadronic B decays from data using the displaced track trigger (see e.g. Ref. [3]). We report on a new search for charmless B decays mediated by gluonic $b \to s$ penguin decays. These decays are of interest in the light of a possible contribution other than the usual mixing induced phase in the time dependent CP violation asymmetry observed at the B factories. CDF uses 180 pb^{-1} of displaced track trigger data to search for $B^+ \to \phi K^+$ and $B_S^0 \to \phi\phi$. Figure 3(a) shows the ϕK^+ invariant mass distribution indicating a signal of (47.0 ± 8.4) B^+ signal events. From this yield, CDF determines the ratio of branching ratios $\mathcal{B}(B^+ \to K^+\phi)/\mathcal{B}(B^+ \to J/\psi K^+) = (7.2 \pm 1.3 \pm 0.7) \cdot 10^{-3}$ and the charge asymmetry $\mathcal{A}_{CP} = -0.07 \pm 0.17^{+0.06}_{-0.05}$. Both results are in good agreement with the B factories.

The search for the never observed mode $B_S^0 \to \phi\phi$ was performed in a blind fashion using kinematically similar decays such as $B^0 \to J/\psi K^{*0}$ plus MC

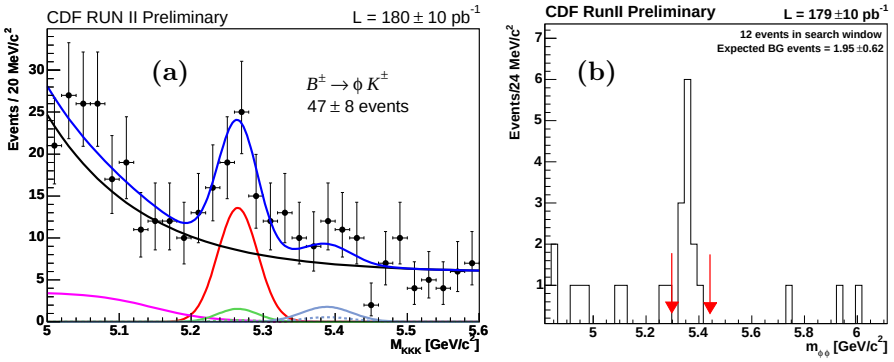

Figure 3: *Invariant mass distribution of (a) $B^+ \to \phi K^+$ and (b) $B_S^0 \to \phi\phi$.*

for cut optimization. Fig. 3(b) displays a signal of 12 events on an estimated background of about 2 events. CDF determines $\mathcal{B}(B_S^0 \to \phi\phi) = (1.4 \pm 0.6 \pm 0.2 \pm 0.5_{BR}) \cdot 10^{-5}$ where the error of $\pm 0.5_{BR}$ results from the uncertainty in $\mathcal{B}(B_S^0 \to J/\psi\phi)$ used as normalization mode.

2.4 Measurement of Hadronic Invariant Mass Moments

Using 180 pb^{-1} of data, CDF measured the first two moments of the hadronic invariant mass squared distribution in semileptonic B decays using lepton plus SVT trigger data. Combining a direct measurement of the D^{**} piece – see Fig. 4(a) for the fully corrected inv. mass distribution $m(D^{(*)+}\pi^-_{**})$ – with the D and D^* pieces taken from PDG, CDF finds $M_1 \equiv \langle s_H \rangle - m_D^2 = (0.459 \pm 0.037 \pm 0.019 \pm 0.062_{BR})$ GeV^2 and $M_2 \equiv \langle (s_H - \langle s_H \rangle)^2 \rangle = (1.04 \pm 0.25 \pm 0.07 \pm 0.10_{BR})$ GeV^4 where 0.062_{BR} and 0.10_{BR} refer to the uncertainties coming from the branching ratios needed for the combination of the D, D^* and D^{**} pieces. Fig. 4(b) shows good agreement between the CDF measurement of M_1 and previous determinations.

2.5 Observation of $X(3872)$

Recently, the Belle collaboration reported a new particle $X(3872)$ observed [4] in exclusive decays of B mesons at a mass of 3872 MeV/c^2 decaying into $J/\psi\pi^+\pi^-$. The observation of this narrow resonance has been confirmed by the CDF collaboration and recently also by the DØ experiment as shown in Fig. 5.

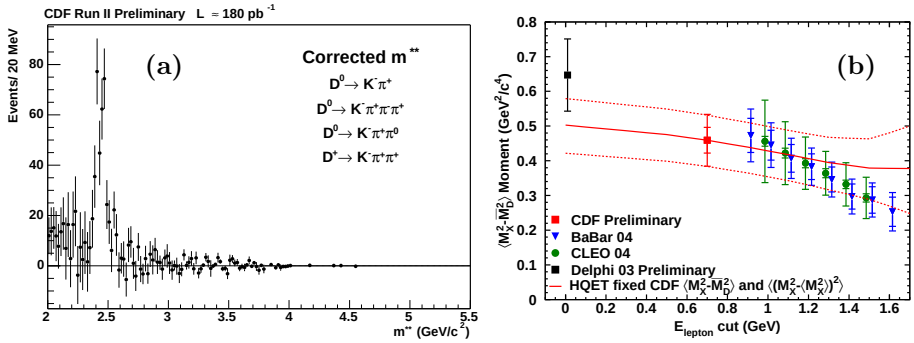

Figure 4: *(a) Fully corrected invariant mass distribution* $m(D^{(*)+}\pi^-_{**})$. *(b) Comparison between the CDF measurement of* M_1 *and previous determinations.*

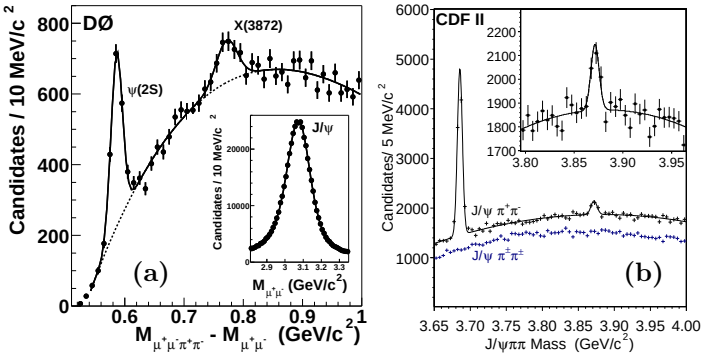

Figure 5: *Mass distribution of* $J/\psi\pi^+\pi^-$ *candidates from (a) DØ and (b) CDF.*

DØ observes 552 ± 100 $X(3872)$ candidates and measures the mass difference between the $X(3872)$ state and the J/ψ to be $(774.9 \pm 3.1 \pm 3.0)$ MeV/c^2. CDF observes 730 ± 90 events at a mass of $(3871 \pm 0.7 \pm 0.4)$ MeV/c^2 with a width consistent with the detector resolution.

2.6 Search for Pentaquark States

An exotic baryon, $\Theta^+(1540)$, with the quantum numbers of K^+n has recently been reported by several groups (for an overview, see e.g. Ref. [5]). Such a state has a minimal quark content of $|uudd\bar{s}\rangle$. Evidence for other pentaquark states such as an isospin 3/2 multiplet of Θ's with strangeness $S = -2$ [6] and

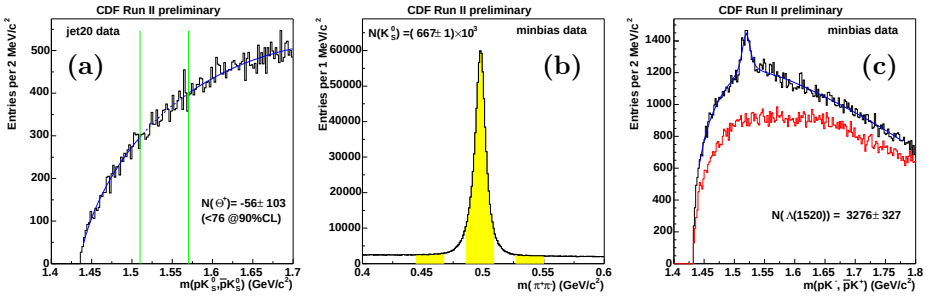

Figure 6: *(a) Search for pentaquark state* $\Theta^+(1540) \to pK^0_S$. *Reference states (b)* $K^0_S \to \pi\pi$ *and (c)* $\Lambda(1520) \to pK^-$.

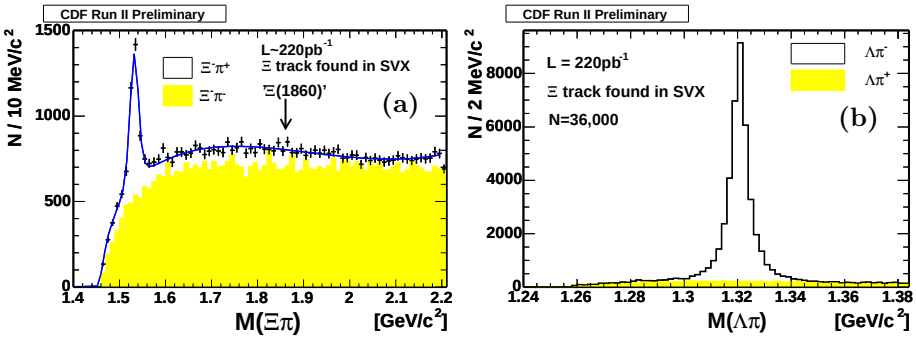

Figure 7: *(a) Search for pentaquark state* $\Xi^{--}_{3/2}/\Xi^0_{3/2} \to \Xi^-\pi^-/\pi^+$. *(b) Reference channel* $\Xi \to \Lambda\pi$.

charmed pentaquarks [7] has also been reported. CDF performed a search for the following pentaquark states: $\Theta^+(1540) \to pK^0_S$, $\Xi^{--}_{3/2}/\Xi^0_{3/2} \to \Xi^-\pi^-/\pi^+$ and $\Theta_c \to pD^{*-}$. In each case a reference state has been reconstructed. As shown in Figures 6, 7 and 8, no evidence for a narrow signal has been found.

3 Summary

We review recent result on heavy quark physics at TeV energies focusing on Run II measurements at the Tevatron. A wealth of new B physics measurements from CDF and DØ has been reported. In particular, DØ demonstrates a very competitive B physics program in Run II.

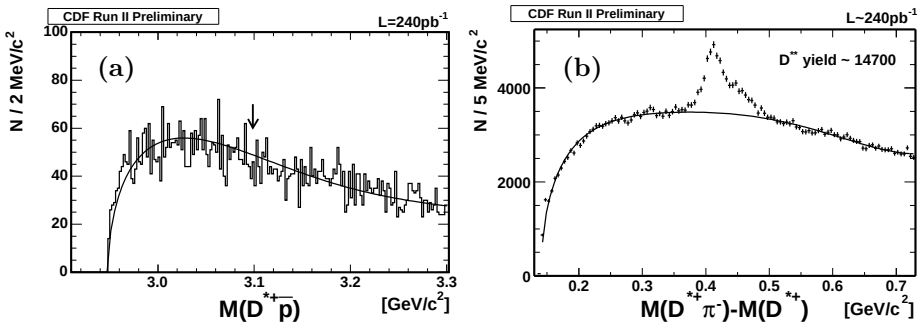

Figure 8: *(a) Search for pentaquark state* $\Theta_c \to pD^{*-}$. *(b) Reference channel* $D^{*-}\pi^+$.

Acknowledgments

I like to thank the organizers for a stimulating meeting. It was a pleasure to attend this great conference. I also would like to thank Ann, Emma and Helen, a constant source of inspiration and support, for their continuous understanding about the life of a physicist.

References

1. M. Paulini, Int. J. Mod. Phys. A **14** (1999) 2791 [hep-ex/9903002].
2. R. Blair *et al.* [CDF II Collaboration], FERMILAB-PUB-96-390-E (1996); S. Abachi *et al.* [DØ Collaboration], FERMILAB-PUB-96-357-E (1996).
3. M. Paulini, [hep-ex/0402020].
4. S. K. Choi *et al.* [Belle Collaboration], Phys. Rev. Lett. **91** (2003) 262001.
5. D. Diakonov, V. Petrov and M. V. Polyakov, Z. Phys. A **359** (1997) 305; R. L. Jaffe and F. Wilczek, Phys. Rev. Lett. **91** (2003) 232003.
6. C. Alt *et al.* [NA49 Collaboration], Phys. Rev. Lett. **92** (2004) 042003.
7. A. Aktas *et al.* [H1 Collaboration], [hep-ex/0403017].

Frascati Physics Series Vol. XXXVI (2004), pp. 141–146
DAΦNE 2004: Physics at meson factories – Frascati, June 7-11, 2004
Selected Contribution in Plenary Session

A NEW DETERMINATION OF $|V_{us}|$ FROM KTEV

E. Blucher
Department of Physics and The Enrico Fermi Institute
The University of Chicago, 5640 S. Ellis Ave., Chicago, IL 60637 USA

Abstract

We present a determination of the CKM parameter $|V_{us}|$ based on new measurements of the six largest K_L branching fractions and semileptonic form factors by the KTeV (E832) experiment at Fermilab. Our value of $|V_{us}|$ is consistent with unitarity of the CKM matrix.

1 Introduction

The first row of the Cabibbo-Kobayashi-Maskawa (CKM) matrix provides the most stringent test of the unitarity of the matrix. Current measurements [1)] deviate from unitarity at the 2.2 sigma level: $1 - (|V_{ud}|^2 + |V_{us}|^2 + |V_{ub}|^2) = 0.0043 \pm 0.0019$. $|V_{us}|$, which contributes an uncertainty of 0.0010 to this unitarity test, has been determined from charged and neutral kaon semileptonic

decay rates. This determination is based on the partial width for semileptonic K decay, $\Gamma_{K\ell 3}$:

$$\Gamma_{K\ell 3} = \frac{G_F^2 M_K^5}{192\pi^3} S_{EW}(1+\delta_K^\ell) C^2 \left|V_{us}\right|^2 f_+^2(0) I_K^\ell, \tag{1}$$

where ℓ refers to either e or μ, G_F is the Fermi constant, M_K is the kaon mass, S_{EW} is the short-distance radiative correction, δ_K^ℓ is the mode-dependent long-distance radiative correction, $f_+(0)$ is the calculated form factor at zero momentum transfer for the $\ell\nu$ system, and I_K^ℓ is the phase-space integral, which depends on measured semileptonic form factors. C^2 is 1 (1/2) for neutral (charged) kaon decays.

In this paper, we present a new determination of $|V_{us}|$ by the KTeV[1] (E832) experiment at Fermilab based on measurements of the $K_L \to \pi^\pm e^\mp \nu$ and $K_L \to \pi^\pm \mu^\mp \nu$ partial widths and form factors. These measurements are described in detail elsewhere [2, 3, 4]; a brief summary is given here.

2 Partial Width Measurements

To determine the $K_L \to \pi^\pm e^\mp \nu$ and $K_L \to \pi^\pm \mu^\mp \nu$ partial widths, we measure the following five ratios:

$$\Gamma_{K\mu 3}/\Gamma_{Ke3} \equiv \Gamma(K_L \to \pi^\pm \mu^\mp \nu)/\Gamma(K_L \to \pi^\pm e^\mp \nu) \tag{2}$$

$$\Gamma_{+-0}/\Gamma_{Ke3} \equiv \Gamma(K_L \to \pi^+ \pi^- \pi^0)/\Gamma(K_L \to \pi^\pm e^\mp \nu) \tag{3}$$

$$\Gamma_{000}/\Gamma_{Ke3} \equiv \Gamma(K_L \to \pi^0 \pi^0 \pi^0)/\Gamma(K_L \to \pi^\pm e^\mp \nu) \tag{4}$$

$$\Gamma_{+-}/\Gamma_{Ke3} \equiv \Gamma(K_L \to \pi^+ \pi^-)/\Gamma(K_L \to \pi^\pm e^\mp \nu) \tag{5}$$

$$\Gamma_{00}/\Gamma_{000} \equiv \Gamma(K_L \to \pi^0 \pi^0)/\Gamma(K_L \to \pi^0 \pi^0 \pi^0), \tag{6}$$

where internal bremsstrahlung contributions are included for all decay modes with charged particles. Since the six decay modes listed above account for more than 99.9% of the total decay rate, the five partial width ratios may be converted into measurements of the branching fractions for the six decay modes. The PDG average K_L lifetime [1] of $\tau_L = (5.15 \pm 0.04) \times 10^{-8}$ s is then used to convert these branching fractions into partial widths.

[1]The KTeV Collaboration includes Arizona, Chicago, Colorado, Elmhurst, Fermilab, Osaka, Rice, UCLA, UCSD, Virginia, and Wisconsin.

Table 1: *K_L branching fractions and partial widths (Γ_i).*

Decay Mode	Branching fraction	Γ_i $(10^7 s^{-1})$
$K_L \to \pi^\pm e^\mp \nu$	0.4067 ± 0.0011	0.7897 ± 0.0065
$K_L \to \pi^\pm \mu^\mp \nu$	0.2701 ± 0.0009	0.5244 ± 0.0044
$K_L \to \pi^+\pi^-\pi^0$	0.1252 ± 0.0007	0.2431 ± 0.0023
$K_L \to \pi^0\pi^0\pi^0$	0.1945 ± 0.0018	0.3777 ± 0.0045
$K_L \to \pi^+\pi^-$	$(1.975 \pm 0.012) \times 10^{-3}$	$(3.835 \pm 0.038) \times 10^{-3}$
$K_L \to \pi^0\pi^0$	$(0.865 \pm 0.010) \times 10^{-3}$	$(1.679 \pm 0.024) \times 10^{-3}$

Simple event reconstruction and selection may be used to distinguish different kaon decay modes from each other, and to reduce background to a negligible level for all decay modes. A Monte Carlo simulation is used to correct the ratios in Eqs. 2 - 6 for acceptance differences between numerator and denominator.

Table 1 summarizes the measured branching fractions and partial widths. Figure 1 shows a comparison of the KTeV and PDG values for the six branching fractions. The new KTeV measurements are on average a factor of two more precise than the current world average values, but are not in good agreement with these averages. Compared to the PDG fit [1)], the KTeV measurement of $B(K_L \to \pi^\pm e^\mp \nu)$ is higher by 5%, $B(K_L \to \pi^0\pi^0\pi^0)$ is lower by 8%, $B(K_L \to \pi^+\pi^-)$ is lower by 5%, and $B(K_L \to \pi^0\pi^0)$ is lower by 8%. Our measurements of $B(K_L \to \pi^\pm \mu^\mp \nu)$ and $B(K_L \to \pi^+\pi^-\pi^0)$ are consistent with the PDG fit.

3 Semileptonic Form Factor Measurements

The semileptonic form factors describe the distribution of t, the square of the momentum transfer to the $\ell\nu$ system. This t dependence increases the decay phase space integrals, I_K^e and I_K^μ, by about 10%. We use the following parametrization for the two independent semileptonic form factors:

$$f_+(t) = f_+(0)\left[1 + \lambda'_+ \frac{t}{M_\pi^2} + \frac{1}{2}\lambda''_+ \frac{t^2}{M_\pi^4}\right], \quad f_0(t) = f_+(0)\left[1 + \lambda_0 \frac{t}{M_\pi^2}\right], \qquad (7)$$

where $f_+(0)$ is obtained from theory, and we measure λ'_+, λ''_+, and λ_0.

The $f_+(t)$ form factor is measured in both semileptonic decay modes; the effect of $f_0(t)$ is proportional to the lepton mass, so it is only measured in

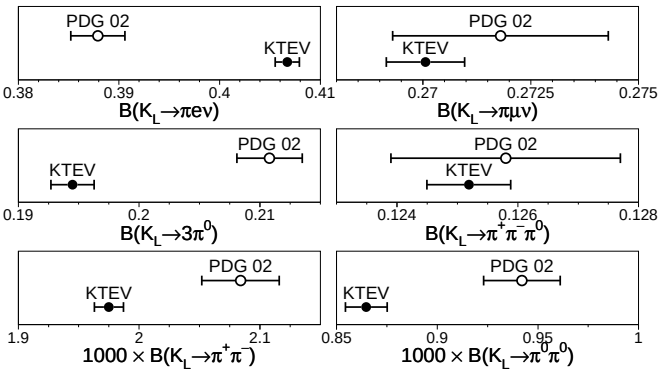

Figure 1: *K_L branching fractions measured by KTeV (dots) and from PDG fit (open circles).*

$K_L \to \pi^{\pm}\mu^{\mp}\nu$ decays. The measured parameters for the semileptonic form factors are $\lambda'_+ = (20.64 \pm 1.75) \times 10^{-3}$, $\lambda''_+ = (3.20 \pm 0.69) \times 10^{-3}$, and $\lambda_0 = (13.72 \pm 1.31) \times 10^{-3}$. The corresponding phase space integrals are $I_K^e = 0.15350 \pm 0.00105$ and $I_K^\mu = 0.10165 \pm 0.00080$, where the quoted errors include an additional uncertainty related to the form factor parameterization [4]. Compared to phase space integrals based on PDG form factors, KTeV's I_K^e and I_K^μ integrals are 1.7% and 4.2% lower, respectively. If we fit our data without the λ''_+ term, our I_K^e and I_K^μ integrals are increased by 1%, and are consistent with PDG averages that use only linear terms.

4 Consistency of Branching Fraction and Form Factor Measurements with Lepton Universality

To check the consistency of our branching fraction and form factor measurements with lepton universality, we compare G_F for the two decay modes by taking the ratio of Eq. 1 for $K_L \to \pi^{\pm}\mu^{\mp}\nu$ and $K_L \to \pi^{\pm}e^{\mp}\nu$:

$$\left(\frac{G_F^\mu}{G_F^e}\right)^2 = \left[\frac{\Gamma(K_L \to \pi^{\pm}\mu^{\mp}\nu)}{\Gamma(K_L \to \pi^{\pm}e^{\mp}\nu)}\right] \Big/ \left(\frac{1+\delta_K^\mu}{1+\delta_K^e} \cdot \frac{I_K^\mu}{I_K^e}\right). \tag{8}$$

Many common uncertainties cancel in this ratio. The ratio of radiative corrections is calculated to be [5] $(1+\delta_K^\mu)/(1+\delta_K^e) = 1.0058 \pm 0.0010$, the ratio

of the phase space integrals is $I_K^\mu/I_K^e = 0.6622 \pm 0.0018$, and $\Gamma_{K\mu3}/\Gamma_{Ke3} = 0.6640 \pm 0.0026$. The resulting ratio of couplings squared is $(G_F^\mu/G_F^e)^2 = 0.9969 \pm 0.0048$, consistent with lepton universality. The same ratio calculated from PDG widths and form factors is $(G_F^\mu/G_F^e)^2 = 1.0270 \pm 0.0182$. Note that the 0.5% uncertainty in our universality test is much smaller than the 5% difference between the KTeV and PDG values of $\Gamma_{K\mu3}/\Gamma_{Ke3}$.

5 Determination of $|V_{us}|$

The measured partial widths and phase space integrals for semileptonic decays can be combined with theoretical corrections to calculate $|V_{us}|$ using Eq. 1. The short-distance radiative correction, $S_{EW} = 1.022$, [6] is evaluated with a cutoff at the proton mass. The long-distance radiative corrections are taken from [5]: $\delta_K^e = 0.013 \pm 0.003$ and $\delta_K^\mu = 0.019 \pm 0.003$. For $f_+(0)$, we use the same value used in the PDG evaluation of $|V_{us}|$ [7]: $f_+(0) = 0.961 \pm 0.008$.

Assuming lepton universality, we average the results for $K_L \to \pi^\pm e^\mp \nu$ and $K_L \to \pi^\pm \mu^\mp \nu$ (accounting for correlations):

$$|V_{us}| = 0.2252 \pm 0.0008_{\rm KTeV} \pm 0.0021_{\rm ext}. \quad (9)$$

The KTeV error comes from uncertainties in the KTeV branching fraction and form factor measurements. The external error comes from $f_+(0)$, the K_L lifetime, and radiative corrections.

To compare our result with previous charged and neutral kaon measurements, we use the product of $|V_{us}|$ and $f_+(0)$ rather than $|V_{us}|$ to avoid significant common uncertainties from $f_+(0)$. Figure 2 shows a comparison of our measurement of

$$|V_{us}| f_+(0) = 0.2165 \pm 0.0012 \quad (10)$$

with values from the PDG and Brookhaven E865 [8]. Our value of $|V_{us}|f_+(0)$ is inconsistent with previous K_L determinations, but is consistent with K^+ results. The figure also shows $f_+(0)(1 - |V_{ud}|^2 - |V_{ub}|^2)^{1/2}$, the expectation for $f_+(0)|V_{us}|$ assuming unitarity, based on $|V_{ud}| = 0.9734 \pm 0.0008$, $|V_{ub}| = (3.6 \pm 0.7) \times 10^{-3}$, and several recent calculations of $f_+(0)$. Our value of $|V_{us}|$ (Eq. 9), based the Leutwyler and Roos calculation of $f_+(0)$, is consistent with unitarity: $1-(|V_{ud}|^2+|V_{us}|^2+|V_{ub}|^2) = 0.0018 \pm 0.0019$. For other calculations of $f_+(0)$, the consistency with unitarity ranges from 1 to 1.7 sigma, as shown in Fig. 2.

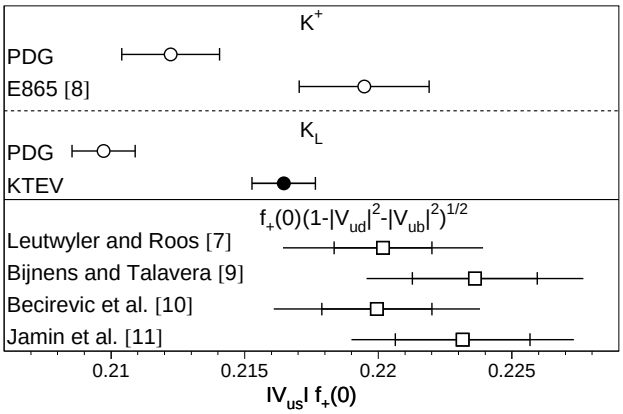

Figure 2: *Comparison of the KTeV measurement of* $|V_{us}|f_+(0)$ *with Brookhaven E865, PDG, and also with determinations of* $f_+(0)(1-|V_{ud}|^2-|V_{ub}|^2)^{1/2}$ *based on different theoretical calculations of* $f_+(0)$*. PDG refers to our evaluation based on PDG partial widths and form factors. For* $f_+(0)(1-|V_{ud}|^2-|V_{ub}|^2)^{1/2}$*, the inner error bars are from* $f_+(0)$ *uncertainty; the total uncertainties include the* $|V_{ud}|$ *and* $|V_{ub}|$ *errors.*

References

1. Particle Data Group, Phys. Rev. D **66**, 1 (2002).
2. T. Alexopoulos *et al.*, accepted in Phys. Rev. Lett., hep-ex/0406001 (2004).
3. T. Alexopoulos *et al.*, accepted in Phys. Rev. D, hep-ex/0406002 (2004).
4. T. Alexopoulos *et al.*, accepted in Phys. Rev. D, hep-ex/0406003 (2004).
5. T. Andre, submitted to Phys. Rev. D, hep-ph/0406006 (2004).
6. A. Sirlin, Nucl. Phys. **B196**, 83 (1982).
7. H. Leutwyler and M. Roos, Z. Phys. **C25**, 91 (1984).
8. A. Sher *et al.*, Phys. Rev. Lett. **91**, 261802 (2003).
9. J. Bijnens and P. Talavera, Nucl. Phys. **B669**, 341 (2003).
10. D. Becirevic *et al.*, hep-ph/00403217 (2004).
11. M. Jamin, J. A. Oller, and A. Pich, JHEP **02**, 047 (2004).

Frascati Physics Series Vol. XXXVI (2004), pp. 147–152
DAΦNE 2004: Physics at meson factories – Frascati, June 7-11, 2004
Selected Contribution in Plenary Session

SEMILEPTONIC DECAYS OF NEUTRAL KAONS AT NA48

Ulrich Moosbrugger *
University of Mainz, Institute of Physics
Staudingerweg 7, 55099 Mainz, Germany

Abstract

In 2001 the NA48 experiment at CERN has performed a new measurement of the branching ratio of the semileptonic neutral kaon decay mode $\mathrm{BR}(K_L \to \pi^+\pi^0 e^-\nu) = (5.21 \pm 0.07_{\mathrm{stat}} \pm 0.09_{\mathrm{syst}}) \cdot 10^{-5}$ $(Ke4)$. A fit of the Cabibbo-Maksymowicz variables for the Ke4 decay yielded new precise values for its form factors. For the decay $K_L \to \pi^\pm e^\mp \nu(\overline{\nu})$ the linear form factor q^2-dependency (λ_+) has been measured while observing no hint for *scalar* nor *tensor* couplings. In addition the relative branching ratio of the radiative K_{e3} decay was determined to $\mathrm{BR}(K_L \to \pi^\pm e^\mp \nu(\overline{\nu})\gamma / K_L \to \pi^\pm e^\mp \nu(\overline{\nu})) = (0.960 \pm 0.07^{+0.012}_{-0.011})\%$.

* On behalf of the NA48 Collaboration: Cagliari, Cambridge, CERN, Dubna, Edinburgh, Ferrara, Firenze, Mainz, Orsay, Perugia, Pisa, Saclay, Siegen, Torino, Warsaw, Vienna

1 The NA48 experiment at SPS (CERN)

The data samples used for the analysis presented here have been taken using the K_L beam of the two simultaneous kaon beams of the NA48 experiment dedicated to measure ϵ'. A detailed description of the experiment and the beam-line can be found elsewhere [1)].

2 $K_L \to \pi^+\pi^0 e^-\nu$

2.1 Branching ratio

The investigation of the decay $K_L \to \pi^+\pi^0 e^-\nu$ (K_{e4}) represents a good testing-ground to check *ChPT* predictions for long distance meson interactions. A previous measurement of that decay has been performed by the experiment *E731* at *Fermilab* with a data sample of 729 events. Using data collected during a run in 2001 by NA48, 5464 selected signal events with an estimated background of 62 events have been recorded [2)].

When measuring the branching ratio, the decay $K_L \to \pi^+\pi^-\pi^0$ ($K_{\pi 3}$), where one of the charged pions is mis-identified as an electron (positron), turns out to be the main source of background. To reject those events one requires a χ^2 variable, defined as

$$\chi^2_{3\pi} = \left(\frac{M_{3\pi} - M_K}{\sigma_M}\right)^2 + \left(\frac{p_t - p_{t_0}}{\sigma_p}\right)^2, \tag{1}$$

to be greater than 16, where $M_{3\pi}$ is the invariant mass of the visible particles under a 3π assumption, p_t is the transverse momentum, p_{t_0} is the maximum value of the p_t distribution, M_K is the kaon mass and σ is the corresponding resolution. In addition, a neural network which has been trained using well identified e and π from $K_{\pi 3}$ and K_{e3} events improved further the e/π distinction. Using the decay $K_L \to \pi^+\pi^-\pi^0$ with a branching fraction of $(12.58 \pm 0.19)\%$ as the normalization channel, the K_{e4} branching ratio has been determined to be:

$$\mathrm{BR}(K_{e4}) = (5.21 \pm 0.07_{\mathrm{stat}} \pm 0.09_{\mathrm{syst}}) \cdot 10^{-5}. \tag{2}$$

The systematic uncertainty of the result above is dominated by the error on the branching fraction of $K_{\pi 3}$ ($\pm 0.08 \cdot 10^{-5}$). The result measured by

NA48 is consistent with previous measurements [3) 4)] and more accurate by a factor of 2.5 (both statistically and systematically).

Since the neutral K_{e4} branching fraction is mainly sensitive to the chiral coupling parameter L_3 and very little to L_5 and L_9 one can deduce [5)]:

$$L_3 = (-4.1 \pm 0.2) \cdot 10^{-3}. \tag{3}$$

2.2 Form factors

The hadronic part of the matrix element ($V-A$ structure) can be parametrized by the relative (normalized to the g form factor) form factors $\overline{f}_s, \overline{f}_p$ for the vector part and $\overline{h}$ for the axial part. The $M_{\pi\pi}$ dependence of the g form factor is described by the parameter λ_g.

The form factor analysis has been performed by means of 5 kinematic variables, the so-called *Cabibbo-Maksymowicz* variables. A simultaneous fit of all one-dimensional projections was performed, yielding the following results:

$$\begin{array}{ll} \overline{f}_s & = 0.052 \pm 0.006_{\rm stat} \pm 0.002_{\rm syst}, \\ \overline{f}_p & = -0.051 \pm 0.011_{\rm stat} \pm 0.005_{\rm syst}, \\ \lambda_g & = 0.087 \pm 0.019_{\rm stat} \pm 0.006_{\rm syst}, \\ \overline{h} & = -0.32 \pm 0.12_{\rm stat} \pm 0.07_{\rm syst}. \end{array} \tag{4}$$

3 Relative branching ratio $K_L \to \pi^\pm e^\mp \nu(\overline{\nu})\gamma / K_L \to \pi^\pm e^\mp \nu(\overline{\nu})$ $(K_{e3\gamma}/K_{e3})$

The so far most precise measurement of the relative branching fraction $K_{e3\gamma}/K_{e3}$ was reported by the *KTeV* experiment at *Fermilab* to be [6)]

$$Br^{\rm exp}_{\rm KTeV}(K_L \to \pi^\pm e^\mp \nu\gamma / K_L \to \pi^\pm e^\mp \nu) = 0.908 \pm 0.008^{+0.013}_{-0.012}\% \tag{5}$$

which is in disagreement with the theoretical predictions of

$$Br^{\rm theo}(K_L \to \pi^\pm e^\mp \nu\gamma / K_L \to \pi^\pm e^\mp \nu) = (0.95 - 0.99)\%. \tag{6}$$

The NA48 experiment has performed a measurement of this relative branching fraction using a special 2 days run of the year 1999 dedicated to

collect K_{e3} and $K_{e3\gamma}$ decays, applying only a minimum bias trigger. It turned out that the Monte Carlo simulation using the *PHOTOS* [7] package and the model by *Fearing, Fischbach* and *Smith* [8] [9] could not reproduce the recorded data very well. Hence in this analysis, in addition to the *PHOTOS* package, the angular distribution between the outgoing e and γ in the CMS system has been weighted to fit the data. This procedure also cured some discrepancies in other observables, for instance in the γ spectrum between data and MC.

Basing on 19000 $K_{e3\gamma}$ and $5.6 \cdot 10^6$ K_{e3} reconstructed events the relative branching ratio has been deduced:

$$Br^{\mathrm{exp}}_{\mathrm{NA48}}(K_L \to \pi^{\pm} e^{\mp} \nu\gamma / K_L \to \pi^{\pm} e^{\mp} \nu) = 0.960 \pm 0.07^{+0.012}_{-0.011}\%. \tag{7}$$

This result is in a very good agreement with a recent calculation [10] predicting a theoretical value of:

$$Br^{\mathrm{theo}}_{\mathrm{Andre}}(K_L \to \pi^{\pm} e^{\mp} \nu\gamma / K_L \to \pi^{\pm} e^{\mp} \nu) = 0.956 \pm 0.01. \tag{8}$$

4 Form factor measurement of the decay $K_L \to \pi^{\pm} e^{\mp} \nu(\overline{\nu})$

Since in former experiments [11] [12] evidence for non-zero scalar and tensor form factors have been reported, this issue is still of big interest when dealing with semileptonic kaon decays, although recent experiments could not confirm those observations on charged kaon decays [13] [14]. For the extraction of the form factors in the decay $K_L \to \pi^{\pm} e^{\mp} \nu(\overline{\nu})$, the data sample from the minimum bias run in 1999 was used as well, resulting in a total amount of $5.6 \cdot 10^6$ reconstructed K_{e3} events. The form factors have been measured by fitting the *Dalitz plot density* allowing for all possible Lorentz-covariant couplings, i.e.

- vector interaction $f_+(q^2) = f_+(0)(1 + \lambda_+ q^2/m_\pi^2)$
- scalar interaction f_S
- tensor interaction f_T

Thereby the following results have been obtained:

$$\begin{aligned} \lambda_+ &= 0.0284 \pm 0.0007_{\rm stat} \pm 0.0013_{\rm syst}, \\ |f_S/f_+(0)| &= 0.015^{+0.007}_{-0.010} \pm 0.012_{\rm syst}, \\ |f_T/f_+(0)| &= 0.05^{+0.03}_{-0.04} \pm 0.03_{\rm syst}. \end{aligned} \tag{9}$$

In this analysis no hint for scalar nor tensor couplings could be observed. The correlation of the result between the scalar and tensor form factor is shown in Figure 1.

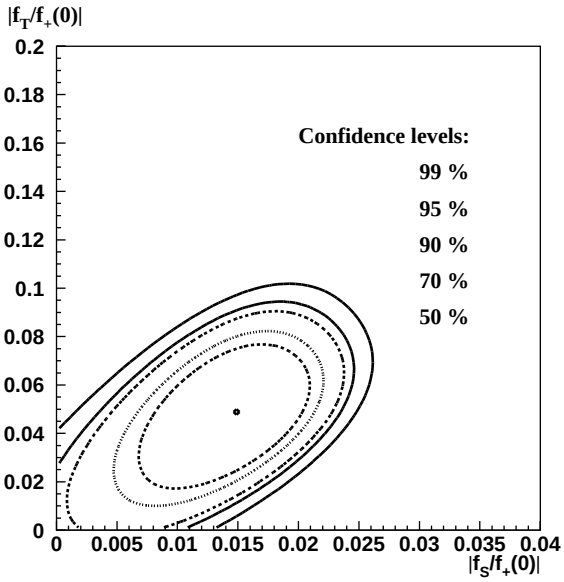

Figure 1: *Confidence levels contour plot in the* $|f_S/f_+(0)|, |f_T/f_+(0)|$ *plane.*

In addition to this general fitting procedure, a more constrained analysis, admitting only a vector form factor in accordance to pure *V-A* coupling, has been carried out. From this fit the following result for λ_+ has been obtained:

$$\lambda_+ = 0.0288 \pm 0.0005_{\rm stat} \pm 0.0011_{\rm syst}. \tag{10}$$

This is in a good agreement with the value calculated above. The form factor measurements presented here are the most precise obtained so far.

5 Outlook

In 2003 and 2004 new measurements on semileptonic charged kaon decays have been performed. Results for the form factors and branching ratios in the charged kaon sector are expected to be reported soon. Other analysis dealing with the form factors of the decay $K_L \to \pi^{\pm}\mu\mp\nu(\overline{\nu})$ are underway. Besides new determinations of V_{us} derived from charged and neutral kaon decays are presented this summer on other conferences.

References

1. V. Fanti *et al*, Phys. Lett. B **465**, 335 (1999).
2. J.R. Batley *et al*, Phys. Lett. B **595** 75 (2004)
3. A.S. Caroll *et al*, Phys. Lett. B **96**, 407 (1980).
4. G. Makoff *et al*, Phys. Rev. Lett. **70**, 1591 (1993).
5. L.M. Widhalm, Ph.D. Thesis, Technische Universität Wien (2001)
6. A. Alavi-Harati *et al*, Phys. Rev. D. **64**, (2001).
7. E. Barberio, Z. Was, Comput. Phys. Commun **79**, 291 (1994).
8. H. Fearing *et al*, Phys. Rev. Lett **24**, 189 (1970).
9. H. Fearing *et al*, Phys. Rev. D **2**, 542 (1970).
10. T.C. Andre, arXiv:hep-ph/0406006 (Submitted to Phys.Rev.D).
11. S.A. Akimenko *et al*, Phys. Lett. B **259**, 225 (1991).
12. H.J. Steiner *et al*, Phys. Lett. B **36**, 521 (1971).
13. I. Ajinenko *et al*, Phys. At. Nucl. **65**, 2064 (2002).
14. A.S. Levchenko *et al*, Phys. At. Nucl. **65**, 2232 (2002).

Frascati Physics Series Vol. XXXVI (2004), pp. 153–158
DAΦNE 2004: Physics at meson factories – Frascati, June 7-11, 2004
Selected Contribution in Plenary Session

KAON SEMILEPTONIC DECAYS AT KLOE

The KLOE Collaboration*
presented by Claudio Gatti
Università di Roma "La Sapienza" -INFN

Abstract

KLOE has collected $\sim 450\text{pb}^{-1}$ in the previous two years of data taking. The analyses on the semileptonic decays of charged and neutral kaons performed with this data is discussed in this paper. Preliminary results are shown on the branching ratio and charge asymmetry of the $K_S \to \pi e \nu$ decay.

* A. Aloisio, F. Ambrosino, A. Antonelli, M. Antonelli, C. Bacci, M. Barva, G. Bencivenni, S. Bertolucci, C. Bini, C. Bloise, V. Bocci, F. Bossi, P. Branchini, S. A. Bulychjov, R. Caloi, P. Campana, G. Capon, T. Capussela, G. Carboni, F. Ceradini, F. Cervelli, F. Cevenini, G. Chiefari, P. Ciambrone, S. Conetti, E. De Lucia, A. De Santis, P. De Simone, G. De Zorzi, S. Dell'Agnello, A. Denig, A. Di Domenico, C. Di Donato, S. Di Falco, B. Di Micco, A. Doria, M. Dreucci, O. Erriquez, A. Farilla, G. Felici, A. Ferrari, M. L. Ferrer, G. Finocchiaro, C. Forti, P. Franzini, C. Gatti, P. Gauzzi, S. Giovannella, E. Gorini, E. Graziani, M. Incagli, W. Kluge, V. Kulikov, F. Lacava, G. Lanfranchi, J. Lee-Franzini, D. Leone, F. Lu, M. Martemianov, M. Martini, M. Matsyuk, W. Mei, L. Merola, R. Messi, S. Miscetti, M. Moulson, S. Müller, F. Murtas , M. Napolitano, F. Nguyen, M. Palutan, E. Pasqualucci, L. Passalacqua, A. Passeri, V. Patera, F. Perfetto, E. Petrolo, L. Pontecorvo, M. Primavera, P. Santangelo, E. Santovetti, G. Saracino, R. D. Schamberger, B. Sciascia, A. Sciubba, F. Scuri, I. Sfiligoi, A. Sibidanov, T. Spadaro, E. Spiriti, M. Tabidze, M. Testa, L. Tortora, P. Valente, B. Valeriani, G. Venanzoni, S. Veneziano, A. Ventura, R. Versaci, I. Villella, G. Xu

1 Introduction

The measurement of semileptonic kaon decay widths provides several tests of fundamental aspects of the standard model. The matrix element V_{us} is extracted from semileptonic kaon decays, both charged and neutral. Its value is used to test the unitarity of CKM matrix at per-mil level.

The validity of the rule $\Delta S = \Delta Q$ can be tested through the quantity

$$\mathrm{Re}(\mathrm{x}_+) \equiv \frac{1}{2}\left[\frac{\langle \mathrm{e}^+\pi^-\nu|\,\mathrm{T}\,|\bar{\mathrm{K}}^0\rangle}{\langle \mathrm{e}^+\pi^-\nu|\,\mathrm{T}\,|\mathrm{K}^0\rangle} + \frac{\langle \mathrm{e}^-\pi^+\bar{\nu}|\,\mathrm{T}\,|\mathrm{K}^0\rangle^*}{\langle \mathrm{e}^-\pi^+\bar{\nu}|\,\mathrm{T}\,|\bar{\mathrm{K}}^0\rangle^*}\right], \tag{1}$$

which can be measured from the relative difference of K_S and K_L decay widths into $\pi e\nu$:

$$\mathrm{Re}(\mathrm{x}_+) = \frac{1}{2}\frac{\Gamma(\mathrm{K_S}\to\pi\mathrm{e}\nu) - \Gamma(\mathrm{K_L}\to\pi\mathrm{e}\nu)}{\Gamma(\mathrm{K_S}\to\pi\mathrm{e}\nu) + \Gamma(\mathrm{K_L}\to\pi\mathrm{e}\nu)}. \tag{2}$$

$\mathrm{Re}(\mathrm{x}_+)$ is expected to be of the order $G_F m_\pi^2 \sim 10^{-7}$ in the Standard Model.

Finally, discrete symmetries are tested through the measurement of the charge asymmetries

$$\mathrm{A_{L,S}} = \frac{\Gamma(\mathrm{K_{L,S}}\to\pi^-\mathrm{e}^+\nu) - \Gamma(\mathrm{K_{L,S}}\to\pi^+\mathrm{e}^-\overline{\nu})}{\Gamma(\mathrm{K_{L,S}}\to\pi^-\mathrm{e}^+\nu) + \Gamma(\mathrm{K_{L,S}}\to\pi^+\mathrm{e}^-\overline{\nu})}. \tag{3}$$

We took into account the presence of a photon in the final state of the decays into charged particles, by introducing a complete Monte Carlo (MC) simulation of the process for each decay [1)].

2 $K_S \to \pi^\mp e^\pm \nu(\overline{\nu})$

We select a pure K_S-beam by identifying the K_L interactions inside the calorimeter. The K_S decays close to the interaction point (IP) with a decay length of ~ 0.6 cm. We select events with two tracks forming a vertex close to the IP, and with two energy clusters associated. Pions and electrons are recognized using a time of flight technique. Using the K_S momentum estimated from the K_L-cluster position ($\sigma_p \sim 2$ MeV), and the particle momenta, we calculate the difference between missing energy and momentum $E_{miss} - p_{miss}$. The signal peaks at zero due to the missing neutrino as shown in Fig. 1. The background is due to $K_S \to \pi^+\pi^-$ decays where one of the pions decays before entering the drift chamber or where the tracks are not well reconstructed. We count

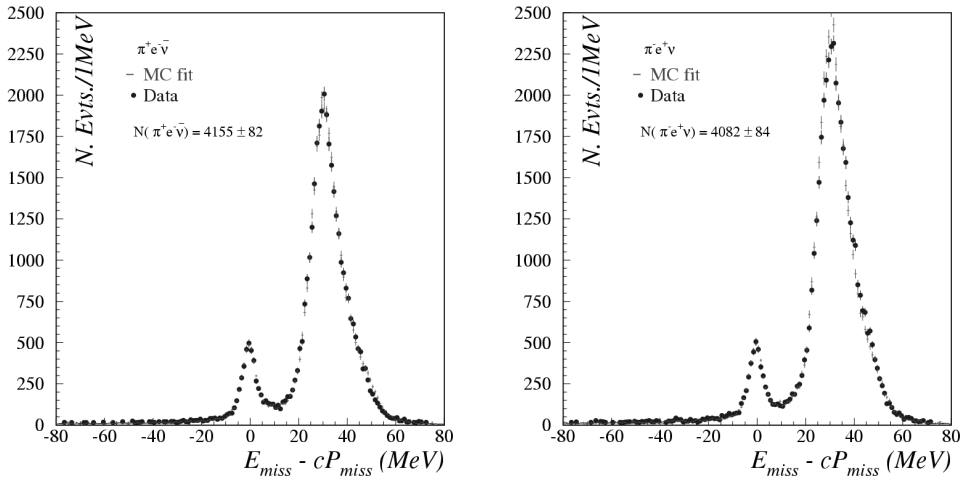

Figure 1: *Fit to the $E_{miss} - p_{miss}$ distributions for $K_S \to \pi^+ e^- \overline{\nu}$ (Left) and $K_S \to \pi^- e^+ \nu$ (Right) decays, for the data collected during the year 2001. The dots represent data while the crosses represent MC after the fit.*

the signal events by fitting the $E_{miss} - p_{miss}$ spectrum with the MC distributions for signal and background. The fit is performed independently for the two charge states $K_S \to \pi^+ e^- \overline{\nu}$ and $K_S \to \pi^- e^+ \nu$. We obtain $\sim 23\,000$ events in the whole data set. The $K_S \to \pi^\mp e^\pm \nu(\overline{\nu})$ branching ratio is obtained by normalizing the number of signal events to the number of $K_S \to \pi^+\pi^-$ decays collected in the same data set, correcting for the selection efficiencies, and using the present experimental value of $\mathrm{BR}(\mathrm{K_S} \to \pi^+\pi^-)$:

$$\mathrm{BR}(\pi \mathrm{e} \nu) = \frac{\mathrm{N}(\pi \mathrm{e} \nu)}{\mathrm{N}(\pi\pi)} \times \frac{\varepsilon^{\pi\pi}_{\mathrm{tot}}}{\varepsilon^{\pi \mathrm{e} \nu}_{\mathrm{tot}}} \times \mathrm{BR}(\pi\pi). \tag{4}$$

we obtain:

$$\begin{aligned} \mathrm{BR}(\mathrm{K_S} \to \pi^- \mathrm{e}^+ \nu) &= (3.54 \pm 0.05_{\mathrm{stat}} \pm 0.05_{\mathrm{syst}}), \\ \mathrm{BR}(\mathrm{K_S} \to \pi^+ \mathrm{e}^- \overline{\nu}) &= (3.54 \pm 0.05_{\mathrm{stat}} \pm 0.04_{\mathrm{syst}}), \\ \mathrm{BR}(\mathrm{K_S} \to \pi \mathrm{e} \nu) &= (7.09 \pm 0.07_{\mathrm{stat}} \pm 0.08_{\mathrm{syst}}). \end{aligned}$$

The charge asymmetry is equal to:

$$\mathrm{A_S} = (-2 \pm 9_{\mathrm{stat}} \pm 6_{\mathrm{syst}}). \tag{5}$$

We can extract the parameter $\mathrm{Re}(x_+)$, defined in Eq. 1, using the experimental values for the K_L branching ratio and lifetime. Using the PDG value for the branching ratio we obtain:

$$\mathrm{Re}(x_+) = (12.6 \pm 3.1_{\mathrm{stat}} \pm 2.9_{\mathrm{syst}}) \times 10^{-3}, \tag{6}$$

while using the recent value obtained from the KTeV Collaboration [2]:

$$\mathrm{Re}(x_+) = (0.9 \pm 2.9_{\mathrm{stat}} \pm 2.9_{\mathrm{syst}}) \times 10^{-3}. \tag{7}$$

The most precise published measurement of $\mathrm{Re}(x_+)$ is from the CPLEAR Collaboration [3]:

$$\mathrm{Re}(x_+) = (-1.8 \pm 4.1_{\mathrm{stat}} \pm 4.5_{\mathrm{syst}}) \times 10^{-3}. \tag{8}$$

Finally, following the prescription in [4] we extract the value of $f_+^{K^0\pi^-} \times V_{us}$

$$f_+^{K^0\pi^-} \times V_{us} = 0.2157 \pm 0.0018 \tag{9}$$

which is compatible with the unitarity of the CKM matrix.

3 Measurement of τ_L

The K_L lifetime has been measured in 1972. Its uncertainty dominates the error on the estimate of V_{us} from K_L decays. In KLOE we observe K_L decays for a large fraction ($\sim$ 50%) of its decay length ($\sim$ 340 cm). Furthermore, the momentum of the kaon is well known. We select $K_L \to \pi^0\pi^0\pi^0$ decays starting from an event with a $K_S \to \pi^+\pi^-$ decay. The decay vertex of the K_L is obtained through the measurement of the photon time of flight and position. The time scale calibration is checked at the per-mil level measuring the DAΦNE bunch crossing period with $\gamma\gamma$ events. The fit to the K_L proper time distribution is shown in Fig. 2 (Left panel). We reach a precision of $\sim 0.4\%$ with $\sim 15 \times 10^6$ K_L decays. The systematic is $\sim 0.6\%$, at present limited by the MC statistics.

4 Measurement of the dominant K_L branching ratios

$K_S \to \pi^+\pi^-$ decays are used as a tag for K_L decays. $K_L \to \pi^0\pi^0\pi^0$ are selected as described in the previous section, while all the events with a vertex reconstructed from two tracks in the drift chamber are retained as $K_L \to$ *charged*

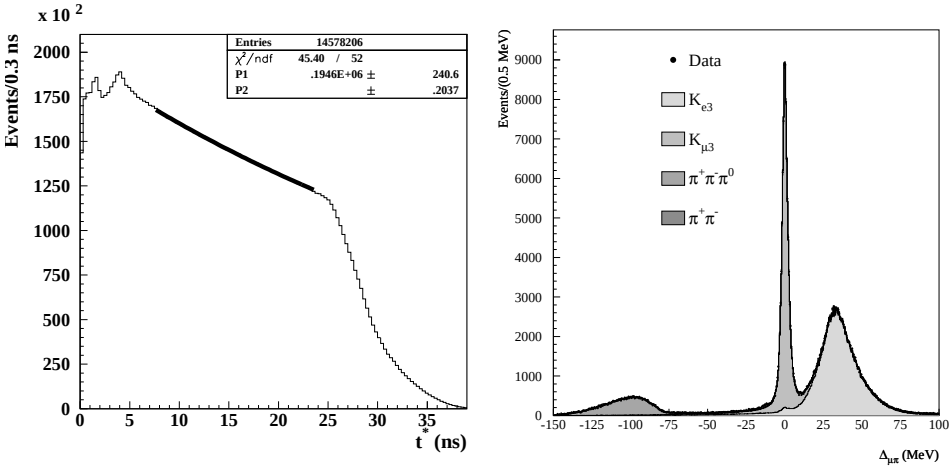

Figure 2: *Left: K_L proper time distribution. The fit is superimposed. Right: Fit to the $E_{miss} - p_{miss}$, in the $\pi\mu$ hypothesis, for charged decays of the K_L.*

events. For these events the distribution $E_{miss} - p_{miss}$, in the $\pi\mu$ hypothesis, is shown if Fig. 2 (Right panel). A fit to this distribution is performed using MC spectra for the different decays. With 2×10^7 selected events inside a fiducial volume, we reach a statistical precision of $\sim 0.1\%$.

5 $K^{\pm} \to \pi^0 e^{\pm} \nu$

$K^{\pm} \to \mu^{\pm}\nu$ decays are used as a tag for charged kaon events. Starting from these events, $K^{\pm} \to \pi^0 e^{\pm}\nu$ are selected with few kinematic cuts and by measuring the charged particle mass through the measurement of the time of flight, T_{tof}, and momentum, p:

$$m^2 = p^2 \times \left[\left(\frac{cT_{tof}}{L} \right)^2 - 1 \right], \tag{10}$$

where L is the track length. We count the number of semileptonic events by performing a fit using MC distributions, as shown in Fig. 3. With the data collected in the years 2001 and 2002 we find ~ 200000 $K^{\pm} \to \pi^0 e^{\pm}\nu$ events, reaching a statistical precision of $\sim 0.2\%$.

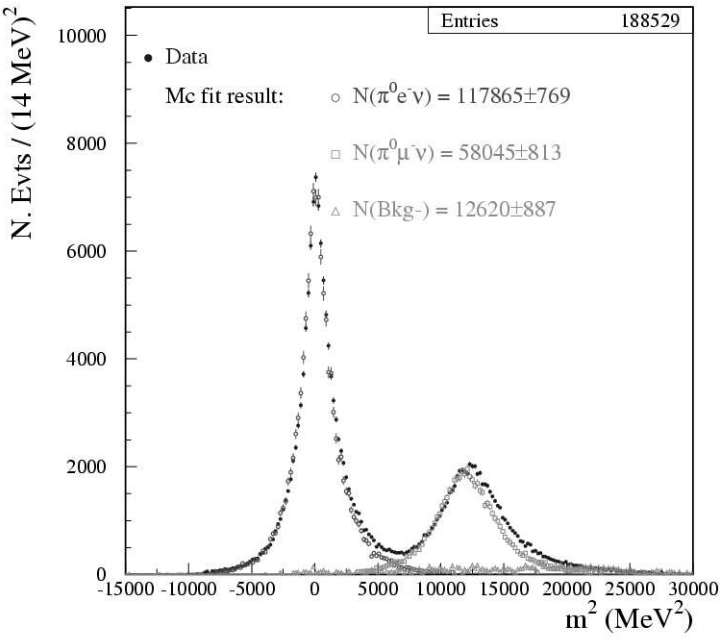

Figure 3: m^2 *spectrum (see text). The fit performed using MC distributions is superimposed.*

References

1. C. Gatti KLOE NOTE 194 (2004)
   http://www.lnf.infn.it/kloe/pub/knote/kn194.ps

2. Alexopulos et al. hep-ex/0406002 Submitted to Phys.Rev. D.

3. A. Angelopoulos et al. Phys.Lett. B444 (1998) 38.

4. "The CKM matrix and the unitarity triangle"
   CERN-2003-002-corr 10 October 2003, hep-ph/0304132.

Frascati Physics Series Vol. XXXVI (2004), pp. 159–166
DAΦNE 2004: Physics at meson factories – Frascati, June 7-11, 2004
Selected Contribution in Plenary Session

LATTICE QCD CALCULATION OF THE VECTOR FORM FACTOR FOR $K_{\ell 3}$ SEMILEPTONIC DECAYS

V. Lubicz[1,2], D. Bećirević[3], G. Isidori[4], G. Martinelli[5], F. Mescia[1,4], S. Simula[2], C. Tarantino[1,2], G. Villadoro[5]

[1] *Dip. di Fisica, Università di Roma Tre, Via della Vasca Navale 84, I-00146 Rome, Italy*
[2] *INFN, Sez. di Roma III, Via della Vasca Navale 84, I-00146, Rome, Italy*
[3] *LPT, Univ. Paris Sud, Centre d'Orsay, F-91405 Orsay-Cedex, France*
[4] *INFN, Lab. Naz. di Frascati, Via E. Fermi 40, I-00044 Frascati, Italy*
[5] *Dip. di Fisica, Università di Roma "La Sapienza" and INFN, Sezione di Roma, P.le A. Moro 2, I-00185 Rome, Italy*

Abstract

We present a quenched lattice calculation of the vector form factor at zero-momentum transfer, $f_+(0)$, relevant for the determination of $|V_{us}|$ from semileptonic $K \to \pi\ell\nu$ decays. Our final result is $f_+^{K^0\pi^-}(0) = 0.960 \pm 0.005_{\rm stat} \pm 0.007_{\rm syst}$, in good agreement with the old quark model estimate made by Leutwyler and Roos. The impact of our result on the extraction of $|V_{us}|$ is discussed by taking into account the new experimental determinations.

1 Introduction

The most precise determination of the CKM matrix element $|V_{us}|$ is presently obtained from the semileptonic weak decays of kaons. The analysis of the experimental data on $K \to \pi\ell\nu$ ($K_{\ell 3}$) decays gives access to the quantity $|V_{us}| \cdot f_+(0)$, where $f_+(0)$ is the vector form factor at zero-momentum transfer.

Vector current conservation guarantees that, in the SU(3)-symmetric limit, $f_+(0) = 1$. A good theoretical control on these transitions is obtained via the Ademollo-Gatto (AG) theorem, which states that $f_+(0)$ is renormalized only by terms of at least second order in the breaking of the SU(3)-flavor symmetry. The estimate of the difference of $f_+(0)$ from its SU(3)-symmetric value represents the main source of theoretical uncertainty and it presently dominates the error in the determination of $|V_{us}|$.

The amount of SU(3) breaking due to light quark masses can be investigated within Chiral Perturbation Theory (CHPT) by performing a systematic expansion of the type $f_+(0) = 1 + f_2 + f_4 + \ldots$, where $f_n = \mathcal{O}[M_{K,\pi}^n/(4\pi f_\pi)^n]$. Thanks to the AG theorem, the first non-trivial term in the chiral expansion, f_2, does not receive contributions of local operators appearing in the effective theory and can be computed unambiguously in terms of M_K, M_π and f_π ($f_2 = -0.023$ in the $K^0 \to \pi^-$ case [1]). The higher-order terms of the chiral expansion, instead, involve the coefficients of local chiral operators, that are difficult to estimate. The next-to-leading correction, f_4, has been evaluated many years ago by Leutwyler and Roos (LR) in the quark model framework [1], by using a general parameterization of the SU(3) breaking structure of the pseudoscalar meson wave functions. Their result is $f_4 = -(0.016 \pm 0.008)$ and this value still represents the estimate of reference [2].

The two-loop CHPT calculation of f_4 has been recently completed [3, 4]. The whole result is the sum of a loop contribution, expressed in terms of chiral logs and the $\mathcal{O}(p^4)$ low-energy constants, plus an analytic term that involves a single combination of the (unknown) $\mathcal{O}(p^6)$ chiral coefficients. Furthermore, the separation between non-local and local contribution quantitatively depends on the choice of the renormalization scale, only the whole result for f_4 being scale independent. An important observation by Bijnens and Talavera [3] is that, in principle, the combination of low-energy constants entering in f_4 could be constrained by experimental data on the slope and curvature of the scalar form factor; the required level of experimental precision, however, is far from the presently available one. Thus, one is left with the LR result, and the large scale dependence of the $\mathcal{O}(p^6)$ loop calculations seems to indicate that its 0.008 error might well be underestimated [5].

Very recently [6] the SU(3)-breaking effects on $f_+(0)$ have been computed with lattice QCD simulations. Within this non-perturbative approach, which

is only based on the fundamental theory, a new strategy has been proposed and successfully applied, in the quenched approximation, in order to reach the challenging goal of a $\approx 1\%$ error on $f_+(0)$. In this paper we present this result, we discuss its impact on the determination of $|V_{us}|$ and briefly explain the strategy of the lattice calculation.

2 Lattice result and phenomenological implications

The procedure developed in Ref. [6] to compute $f_+(0)$ on the lattice is described in the next section. Here we anticipate our final result for the form factor at zero momentum transfer and briefly discuss its phenomenological implications in the light, in particular, of the new experimental results on $K_{\ell 3}$ decays.

Our result is [6]

$$f_+^{K^0\pi^-}(0) = 0.960 \pm 0.005_{\rm stat} \pm 0.007_{\rm syst} \qquad (1)$$

where the systematic error does not include an estimate of quenched effects beyond $\mathcal{O}(p^4)$. The value (1) compares well with $f_+^{K^0\pi^-}(0) = 0.961 \pm 0.008$, quoted by the PDG [2] and based on the LR estimate of f_4 [1].

By averaging the old experimental results for $K_{\ell 3}$ decays with the recent measurement of the E865 experiment [7], and by using the LR determination of the vector form factor, the PDG quotes $|V_{us}| = 0.2200 \pm 0.0026$ [2]. This estimate, once combined with the accurate determination of $|V_{ud}|$ from nuclear $0^+ \to 0^+$ and nucleon beta decays, $|V_{ud}| = 0.9740 \pm 0.0005$ [8], implies a $\sim 2\,\sigma$ deviation from the CKM unitarity condition, $|V_{us}|^{\rm Unit.} \simeq \sqrt{1-|V_{ud}|^2} = 0.2265 \pm 0.0022$. In this respect, our lattice determination of the vector form factor, being in agreement with the LR estimate, does not modify the picture.

A significant novelty, however, is introduced by the new experimental results for both charged and neutral $K_{\ell 3}$ decays recently obtained by the E865 [7], KTeV [9], NA48 [10] and KLOE [11] collaborations. The corresponding determinations of $|V_{us}|\cdot f_+(0)$ are shown in Fig.1 [12], together with the averages of the old results quoted by the PDG.

Remarkably, the average of the new results, represented in the plot by the gray band, turns out to be in good agreement with the unitarity prediction, once either the LR or the lattice determination of the vector form factor is taken into account. The unitarity prediction is illustrated by the yellow band in Fig.1.

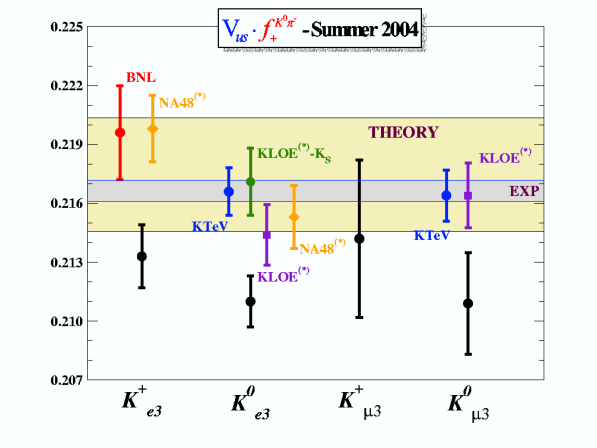

Figure 1: *Experimental results for* $|V_{us}| \cdot f_+(0)$. *The gray band indicates the average of the new experimental results, whereas the yellow band represents the unitarity prediction combined with our determination of the vector form factor.*

In terms of $|V_{us}|$, our determination of the vector form factor combined with the new experimental results implies $|V_{us}| = 0.2256 \pm 0.0022$.

We also note that the recent theoretical estimate [3] $f_+(0) = 0.976 \pm 0.010$, based on two loops CHPT and the LR quark model calculation, implies $|V_{us}| = 0.2219 \pm 0.0022$, which represent a $\sim 1.5\sigma$ deviation from the unitarity prediction.

3 Strategy of the lattice calculation

In this section we briefly illustrate the strategy to compute $f_+(0)$ with $\approx 1\%$ of accuracy, by referring to Ref. [6] for all details. This strategy is based on three main steps.

1) Precise evaluation of the scalar form factor $\mathbf{f_0}(q^2)$ at $\mathbf{q^2 = q^2_{max}}$.
By following a procedure originally proposed in Ref. [13] to study heavy-light form factors, the scalar form factor $f_0(q^2)$ can be calculated very efficiently at

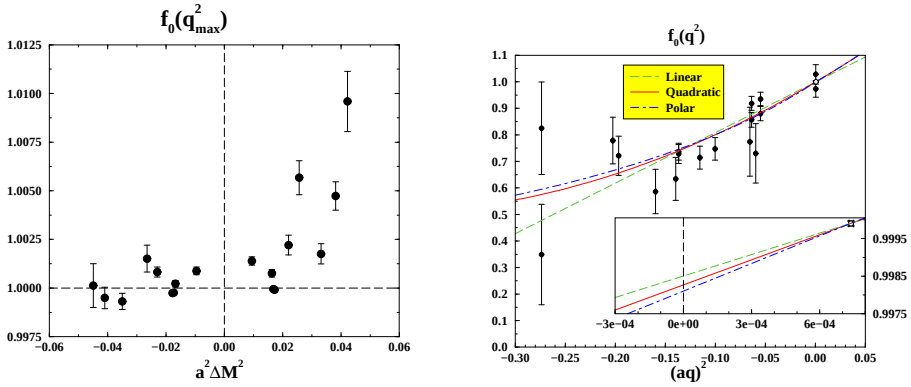

Figure 2: *Left: values of* $f_0(q^2_{\rm max})$ *versus the SU(3)-breaking parameter* $a^2\Delta M^2 \equiv a^2(M_K^2 - M_\pi^2)$. *Right: the form factor* $f_0(q^2)$ *as a function of* q^2 *for one of the quark mass combinations. The dot-dashed, dashed and solid lines correspond to the polar, linear and quadratic fits given in Eq. (3). The inset is an enlargement of the region around* $q^2 = 0$.

$q^2 = q^2_{\rm max} = (M_K - M_\pi)^2$ from the following double ratio of matrix elements:

$$\frac{\langle\pi|\bar{s}\gamma_0 u|K\rangle\,\langle K|\bar{u}\gamma_0 s|\pi\rangle}{\langle K|\bar{s}\gamma_0 s|K\rangle\,\langle\pi|\bar{u}\gamma_0 u|\pi\rangle} = [f_0(q^2_{\rm max})]^2\,\frac{(M_K+M_\pi)^2}{4M_K M_\pi}\,, \qquad (2)$$

where all the external particles are taken at rest. There are several crucial advantages in the use of the double ratio (2) which are described in Ref. [6]. From this ratio the values of $f_0(q^2_{\rm max})$ can be determined on the lattice with an uncertainty smaller than 0.1%, as it is illustrated in Fig.2-left.

2) Extrapolation of $\mathbf{f_0}(q^2_{\rm max})$ to $\mathbf{f_0}(0) = f_+(0)$.

For each set of quark masses, hadronic matrix elements can be calculated on the lattice for external mesons with various momenta, in order to extract the q^2 dependence of both $f_0(q^2)$ and $f_+(q^2)$. New suitable double ratios are introduced also in this step, which allows to improve the statistical uncertainties on $f_0(q^2)$. The quality of the results is shown in Fig.2-right for one of the combinations of quark masses used in Ref. [6].

In order to extrapolate the scalar form factor to $q^2 = 0$ three different functional forms have been considered, namely a polar, a linear and a quadratic

fit:

$$f_0(q^2) = f_0^{(pol.)}(0)/(1-\lambda_0^{(pol.)}\,q^2) \quad , \quad f_0(q^2) = f_0^{(lin.)}(0)\cdot(1+\lambda_0^{(lin.)}\,q^2)\,,$$
$$f_0(q^2) = f_0^{(quad.)}(0)\cdot(1+\lambda_0^{(quad.)}\,q^2 + c_0\,q^4)\,. \qquad (3)$$

These fits are shown in Fig.2-right and provide values of both $f_0(0)$ and the slope λ_0, which are consistent with each other within the statistical uncertainties. The differences of the results obtained from the various fit are taken into account in the estimate of the systematic error. Our results for the slope λ_0, given in units of $M_{\pi^+}^2$, are: $\lambda_0^{(pol.)} = 0.0122(22)$, $\lambda_0^{(lin.)} = 0.0089(11)$ and $\lambda_0^{(quad.)} = 0.0115(26)$. The "polar" value is consistent with the recent accurate determination from KTeV $\lambda_0^{(pol.)} = 0.01414 \pm 0.00095$ [14] and represents a true theoretical prediction, having been obtained before the KTeV result were published. We also mention that the result for the polar slope of the vector form factor, $\lambda_+ = 0.026 \pm 0.002$ in units of $M_{\pi^+}^2$, is in good agreement with the recent accurate measurement from KTeV, $\lambda_+ = 0.02502 \pm 0.00037$ [14], obtained using a pole parameterization.

3) Extrapolation of $\mathbf{f_+(0)}$ to the physical meson masses.

The physical value of $f_+(0)$ is finally determined by extrapolating the lattice results to the physical kaon and pion masses. The problem of the chiral extrapolation is substantially simplified if the AG theorem (holding also in the quenched approximation) is taken into account and if the leading (quenched) chiral logs are subtracted. Thus in [6] the following quantity is introduced

$$R(M_K, M_\pi) = \frac{1 + f_2^q(M_K, M_\pi) - f_+(0; M_K, M_\pi)}{(M_K^2 - M_\pi^2)^2} \qquad (4)$$

where f_2^q represents the leading chiral contribution calculated in quenched CHPT [6] and the quadratic dependence on $(M_K^2 - M_\pi^2)$, driven by the AG theorem, is factorized out. After the subtraction of f_2^q we expect that $R(M_K, M_\pi)$ is well suited for a smooth polynomial extrapolation in the meson masses. Indeed, we find that $R(M_K, M_\pi)$ is well described by a simple linear fit:

$$R^{(lin.)}(M_K, M_\pi) = c_{11} + c_{12}[(aM_K)^2 + (aM_\pi)^2]\,, \qquad (5)$$

whereas the dependence on $(M_K^2 - M_\pi^2)$ is found to be negligible. In order to check the stability of the results, quadratic and logarithmic fits have been also

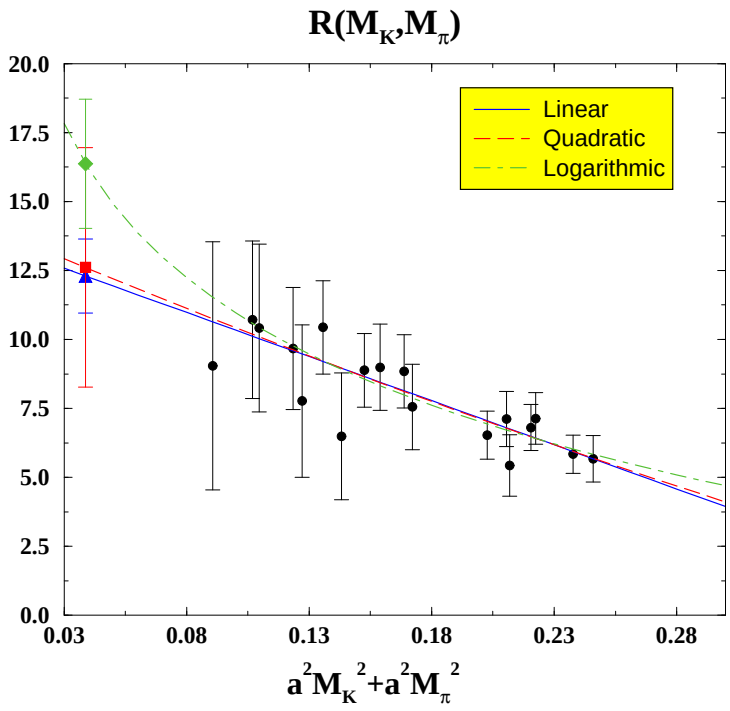

Figure 3: *Comparison among linear, quadratic and logarithmic fits of the ratio* $R(M_K, M_\pi)$ *as a function of* $[a^2 M_K^2 + a^2 M_\pi^2]$.

considered. In Fig.3 it is shown that all these functional forms provide equally good fits to the lattice data with consistent results also at the physical point.

Combining our estimate of $R(M_K, M_\pi)$ at the physical meson masses with the unquenched value of $f_2 = -0.023$ [1], we finally obtain the result quoted in Eq. (1). Note that the systematic error does not include an estimate of quenched effects beyond $\mathcal{O}(p^4)$.

4 Conclusions

We have presented a quenched lattice calculation of the $K_{\ell 3}$ vector form factor at zero-momentum transfer, $f_+(0)$. Our calculation is the first one obtained using a non-perturbative method based only on QCD, except for the quenched

approximation. The impact of our result on the determination of $|V_{us}|$ has been also addressed. We find that, once combined with the new experimental determinations, a very good agreement with CKM unitarity is obtained.

References

1. H. Leutwyler and M. Roos, Z. Phys. **C25**, 91 (1984).
2. PDG: S. Eidelmann *et al.*, Phys. Lett. **B592**, 1 (2004).
3. J. Bijnens and P. Talavera, Nucl. Phys. **B669**, 341 (2003).
4. P. Post and K. Schilcher, Eur. Phys. J. **C25**, 427 (2002).
5. V. Cirigliano, H. Neufeld and H. Pichl, Eur. Phys. J. **C35**, 53 (2004).
6. D. Becirevic *et al.*, hep-ph/0403217.
7. A. Sher *et al.* [E865 Coll.], Phys. Rev. Lett. **91**, 261802 (2003) and hep-ex/0307053.
8. A. Czarnecki, W. J. Marciano and A. Sirlin, hep-ph/0406324.
9. T. Alexopoulos *et al.* [KTeV Coll.], hep-ex/0406001.
10. L. Litov [NA48 Coll.], talk given at ICHEP'04, http://www.ihep.ac.cn/.
11. P. Franzini [Kloe Coll.], invited talk at PIC 2004, hep-ex/0408150. M. Antonelli [Kloe Coll.], talk given at ICHEP'04, http://www.ihep.ac.cn/.
12. F. Mescia, talk given at ICHEP'04, http://www.ihep.ac.cn/.
13. S. Hashimoto *et al.*, Phys. Rev. **D61**, 014502 (2000).
14. T. Alexopoulos *et al.* [KTeV Coll.], hep-ex/0406003.

Frascati Physics Series Vol. XXXVI (2004), pp. 167–170
DAΦNE 2004: Physics at meson factories – Frascati, June 7-11, 2004
Short Talk in Plenary Session

MEASUREMENT OF DIRECT PHOTON EMISSION IN $K^+ \to \pi^+\pi^0\gamma$ DECAY USING STOPPED POSITIVE KAONS

S .Shimizu *
Department of Physics, Osaka University, Osaka 560-0043, Japan

1 Motivation

Since the discovery of kaons, their decay properties have continued to provide testing grounds for interaction and structure physics. While various kaon decay channels have long histories as remarkable tools to test the weak and electromagnetic interactions, they also offer means to study strong interaction dynamics at low energy in terms of effective theories such as chiral perturbation theories (ChPT), which have been developing recently.

Since the $K^+ \to \pi^+\pi^0$ decay is hindered as it violates the ΔI=1/2 rule, the internal bremsstrahlung (IB) to the radiative $K^+ \to \pi^+\pi^0\gamma$ ($K_{\pi 2\gamma}$) decay is also suppressed. This feature, in turn, enhances the direct emission (DE) which is sensitive to the meson structure. It should be noted this is rather unusual, since most of the radiative decays of mesons are predominantly IB type. The current interest of the DE process is the sensitivity to the chiral anomaly which appears as the magnetic component of DE. In terms of ChPT, it enters the magnetic amplitude at $O(p^4)$ predominantly, while IB arises from $O(p^2)$ with suppression. Also, the electric amplitude of DE may arise from $O(p^4)$, which one can identify through the interference pattern (INT) with IB.

Four experiments [3, 4] have reported on the DE branching ratio in the

* On behalf of KEK-PS E470 collaboration

region of $55 < T_{\pi^+} < 90$ MeV, where T_{π^+} is the π^+ kinetic energy. Although the DE component is significantly enhanced with decreasing π^+ energy, these experiments restrict the π^+ energy region to remove backgrounds from $K^+ \to \pi^+\pi^0\pi^0$ ($K_{\pi 3}$). Here, we present a measurement of DE in the $K_{\pi 2\gamma}$ decay. The experiment used a stopped K^+ beam in conjunction with a superconducting toroidal spectrometer. We collected the $K_{\pi 2\gamma}$ events by extending the T_{π^+} region below the $K_{\pi 3}$ end-point energy $T_{\pi^+}^{\max} = 55$ MeV.

2 Experiment

The experiment (KEK-PS E470 experiment) was performed at the KEK 12 GeV proton synchrotron. The $K_{\pi 2\gamma}$ data were collected with the experimental apparatus based on the E246 experiment searching for T-violation in $K^+ \to \pi^0\mu^+\nu$ decay [5]. Beside the T-violation search, spectroscopic studies for various decay channels have been carried out using the same detector system [6]. For the E470 experiment, a Pb-plastic sandwich detector with 2.6 radiation length was newly installed at the outer radius of the magnet pole to monitor photons escape from the photon detector holes.

A separated 660 MeV/c K^+ beam ($\pi^+/K^+ \sim 7$) was used. The kaons were slowed down by a degrader and stopped in the active target located at the center of the detector system. The $K_{\pi 2\gamma}$ events were identified by analyzing the π^+ momentum with the spectrometer and detecting three photons in the CsI(Tl) calorimeter. Charged particles from the target were tracked and momentum-analyzed using MWPCs. The π^+ were discriminated from e^+ and μ^+ by measuring time-of-flight between counters.

The most important point to reconstruct $K_{\pi 2\gamma}$ was to determine which photons were a pair from a π^0, because there are three combinations to form the π^0. The pair which satisfies the $K_{\pi 2\gamma}$ kinematics was adopted as the correct π^0 pair. However, because of the finite kinematical resolution, the correct pairing probability was 85% for IB and 79% for DE. Since $K_{\pi 3}$ and $K_{\pi 2}$ decays do not satisfy the $K_{\pi 2\gamma}$ kinematics, these backgrounds can be rejected by this analysis.

3 Results

The number of good $K_{\pi 2\gamma}$ events is 4434. The solid lines in Fig. 1 show the experimental $K_{\pi 2\gamma}$ spectra. In order to obtain the detector acceptance and

response functions, a Monte Carlo simulation was performed using a GEANT-based Monte Carlo code. The background fraction of the $K_{\pi 3}$ decay was estimated to be 1.2% from the simulation.

The DE branching ratio was determined using the three observables, $\cos\theta_{\pi^+\gamma}$, $\cos\theta_{\pi^0\gamma}$, and E_γ which have characteristic spectra corresponding to the decay processes. The experimental distribution $\rho(\cos\theta_{\pi^+\gamma}, \cos\theta_{\pi^0\gamma}, E_\gamma)$ was fitted to the simulation spectrum of IB[1+α(DE/IB)+β(INT/IB)] with α and β being free parameters. The dotted and dashed lines in Fig. 1 show the fitted spectra and the sole DE components, respectively. The DE and INT components were obtained to be $\alpha = 0.92^{+0.44}_{-0.38}\%$ and $\beta = -0.58^{+0.91}_{-0.83}\%$, respectively [7]. The DE branching ratio in the region of $55 < T_{\pi^+} < 90$ MeV was then derived as $Br(\mathrm{DE}) = [3.2 \pm 1.3(\mathrm{stat.}) \pm 1.0(\mathrm{syst.}] \times 10^{-6}$ [7], which is consistent with the previous stopped experiment [4]. On the other hand, any significant effects due to the INT term were not observed [7].

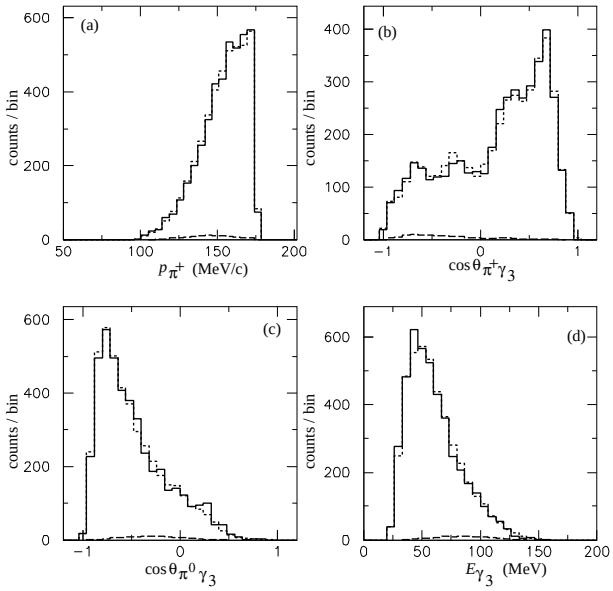

Figure 1: $K_{\pi 2\gamma}$ spectra: (a) π^+ momentum, (b) opening angle between π^+ and γ, (c) opening angle between π^0 and γ, (d) γ energy. The solid lines are the experimental data. The dotted and dashed lines show the fitted spectra and the sole DE components, respectively. The bump structure in (b) is due to the CsI(Tl) assembly structure with 12 holes.

4 Conclusion

We have performed a measurement of the $K^+ \to \pi^+\pi^0\gamma$ decay by extending the T_{π^+} region lower bound down to 35 MeV. The detector response and acceptance functions were evaluated by a Monte Carlo simulation based on GEANT. The $K_{\pi 3}$ background contamination in the $K_{\pi 2\gamma}$ data sample was estimated to be negligible by the simulation. The observed DE branching ratio is consistent with the previous stopped experiment. We did not observe any significant effect due to the interference component for IB and DE, indicating the pure magnetic nature of the direction photon emission in the $K_{\pi 2\gamma}$ decay.

References

1. S.L. Adler, Phys. Rev. **177** 2426 (1969); J.S. Bell and R. Jackiw, Nuovo Cimento **60A** 47 (1969); W.A. Bardeen, Phys. Rev. **184** 1848 (1969).
2. A. Buras, Theoretical review of K-physics, hep-ph/9609324; A. Pich, Rare kaon decays, hep-ph/9610243.
3. R.J. Abrams *et al.*, Phys. Rev. Lett. **29** 1119 (1972); K.M. Smith *et al.*, Nucl. Phys. **B109** 173 (1976); V.N. Bolotov *et al.*, Sov. J. Nucl. Phys. **45** 1023 (1987).
4. S. Adler *et al.*, Phys. Rev. Lett. **85** 4856 (2000).
5. M. Abe *et al.*, Phys. Rev. Lett. **83** 4253(1999) .
6. S. Shimizu *et al.*, Phys. Lett. **B495** 33 (2000); A.S. Levchenko *et al.*, hep-ex/0111048; Y.-H. Shin *et al.*, Eur. Phys. J. **C12** 627 (2000); K. Horie *et al.*, Phys. Lett. **B513** 311 (2001).
7. M.A. Aliev *et al.*, Phys. Lett. **B554** 7 (2003).

Frascati Physics Series Vol. XXXVI (2004), pp. 171–175
DAΦNE 2004: Physics at meson factories – Frascati, June 7-11, 2004
Short Talk in Plenary Session

SEMILEPTONIC DECAY OF $D^0 \to \pi l \nu$ AND FORM FACTORS FOR THE MEASUREMENT OF $|V_{ub}|$ AT KEKB

L. Widhalm, F. Mandl, G. Leder, J. MacNaughton
Institute for High Energy Physics, Austrian Academy of Sciences, Austria
Belle Collaboration

1 Introduction

The quark mixing parameters of the standard model are fundamental parameters of the weak interaction. Semi-leptonic decays have provided most of the information on these matrix elements, and the simplest way to take into account effects of the strong interactions has been to do so in terms of form factors, but even so the dominant uncertainties can come from the uncertainties in the form factors [1]. So, the form factors in semileptonic D decay itself are of great interest.

When V_{ub} is measured via $B \to \pi l \nu$, one has to use a form factor $f_B(q^2)$. The form factors f_B and f_D have both been calculated in the quenched approximation of lattice QCD, with the unquenched result to come soon [2].Using the ratio of these form factors cancels common theoretical errors and with good information available for the analogous form factor $f_D(q^2)$ from the de-

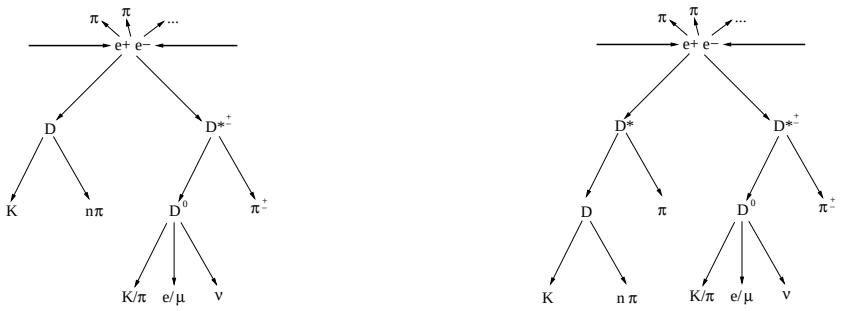

Figure 1: *Scheme of reconstructed event topology, DD^* events (left) and D^*D^* events (right).*

cay $D \to \pi l\nu$, the values of V_{ub} determined in this way will be improved.

Using the same method of reconstruction described below also form factors for $D \to Kl\nu$ can be evaluated. With some modification this method is also very powerful to study inclusive decays of D^0. All is preliminary.

2 Method of Reconstruction

The choice of the event topology used in this analysis is based on the observation of [3] that the cross sections for $e^+e^- \to D^*D^*$ and $e^+e^- \to DD^*$ are quite large. Instead of primary D^0 mesons, we use primary $D^{*\pm}$ mesons decaying to $D^0\pi^\pm$, a decay which has the very welcome property of a small phase space[1], resulting in a *slow pion* with well-defined momentum and a very good selection power for the D^0. This D^* is called *signal-side*; on the other *tag side*, both D and D^* are allowed to enhance statistics.

Since $c\bar{c}$ production threshold is well below the available energy at BELLE, the $D^{(*)}D^*$ pair is often accompanied by several π and/or K mesons. To achieve the best possible statistics, no restriction on this number of *additional mesons* is applied in the reconstruction.

As indicated in Fig.1 reconstruction starts with the tag-side $D^{(*)}$, looking for the decay channels $D \to K^\pm n\pi$ with $n = 1, 2, 3$ (total $\approx 25\%$ BR) and subsequently $D^* \to D\pi, D\gamma$; if no D^* can be reconstructed, a DD^* event is assumed. A combined mass- and vertex fit is applied to the D (and the D^* if applicable) to improve resolution. After this full reconstruction of tag-

[1] due to $m_{D^{*\pm}} - (m_{D^0} + m_{\pi^\pm}) = 5.8$ MeV

side, and allowing for an arbitrary number of additional primary π or K, the known beam momentum is used to deduce the momentum of the signal-side $D^{*\pm}$ via momentum conservation (so-called *recoil method*). Appropriate mass- and vertex fits are then made also on the signal side, identifying events where $D^{*\pm} \to D^0\pi^\pm$ on the signal side. The neutrino in $D^0 \to \pi\ell\nu$ or $D^0 \to K\ell\nu$ is similarly reconstructed using the recoil-method. Finally, the neutrino candidates are selected by requiring a successful fit and $m_\nu^2 < 0.05$ GeV^2.

3 Detector and data sets

The data sample used came from $152 fb^{-1}$ of data collected by the BELLE experiment. The BELLE detector at KEKB is described in [4].

4 Analytical procedure and first preliminary results

Applying the method described in Section 2 on the data (Section 3) candidates for semileptonic decays of D^0 have been found, shown in Fig. 2. The very good resolution $\sigma_{m_\nu^2} = 0.01\ GeV^2$ is achieved.

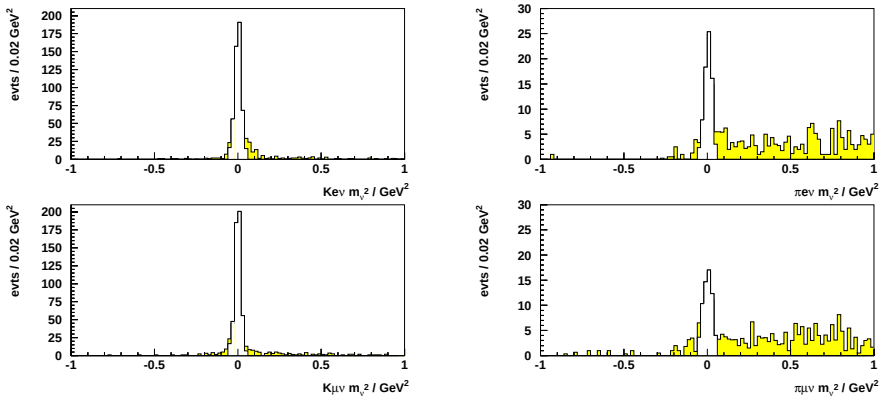

Figure 2: m_ν^2 *for four semileptonic modes (shaded: without neutrino cuts).*

Background can be subdivided into 3 main categories: Non D^0-events which fake a D^0 on the signal side: a side-band study yielded 0.7% for $D^0 \to K\ell\nu$ and 7% for $D^0 \to \pi\ell\nu$. Hadronic D^0-decays with fake lepton: a Monte Carlo study yielded 4.3% and 1.5%. Fake K/π in semileptonic decays: negligible and 10.6%

The preliminary numbers of events found for $D \to K/\pi\ell\nu$ *before* and *after* background subtraction are:

$D \to K/\pi\ell\nu - before$	K	π	$D \to K/\pi\ell\nu - after$	K	π
e	510	77	e	501	60.7
μ	529	62	μ	487	51.5
ℓ	1039	139	ℓ	988	112.2

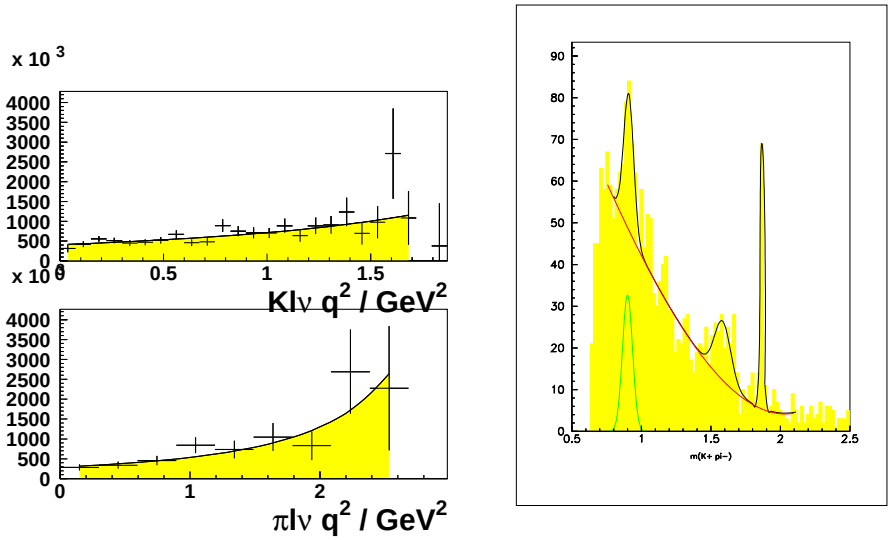

Figure 3: $f_+(q^2)$ *distributions for* $Kl\nu$ *and* $\pi l\nu$ *together with a pole fit (left),* $K\pi$ *mass distribution (in GeV-units) for particles constituting a* D^0 *(right).*

For a first "taste" preliminary $f_+(q^2)$ distributions (the resolution for q^2 is very good, σ_{q^2} around $0.01 GeV^2$) are given in Fig. 3 (left). A pole fit parametrises very well the distributions. The aim of $\Delta(f_D)/f_D < 10\%$ for $D \to \pi\ell\nu$ is within reach even with the currently available data.

Also branching ratio of $D^0 \to K^{*0}(892)X$ was investigated. In Fig.3 right the peak at the $K^{*0}(892)$ mass corresponds to the inclusive cross section; that at the D^0 mass to the exclusive decay $D^0 \to K\pi$. The broad peak is a reflection of $D^0 \to K\pi^+\pi^0$.

The suggestions of the theoreticians T.Onogi and S.Hashimoto, who provided the original motivation for this work, are appreciated. Constant support by Ch.Schwanda is acknowledged.

References

1. G. S. Huang et al. CLNS 04/1876, CLEO04-06.
2. A.El-Khadra et al, MILAB-PUB-00/346-T [hep-ph/0101023].
3. T. Uglov *et al* (Belle Collaboration), hep-ex/0401038.
4. A. Abashian *et al.* (Belle Collab.), Nucl. Instr. and Meth. A **479**, 117 (2002).

Session III — Hypernuclear Physics

(Chairpersons: L. Foà, D. Gill)

P. Gianotti	Prospects on Hypernuclear Physics
L. Benussi	First Results of FINUDA on Hypernuclear Spectroscopy
F. De Mori	First Observations of Hypernuclear non Mesonic Weak Decays with FINUDA
M. Palomba	Search for Neutron–Rich Hypernuclei in FINUDA: Preliminary Results
S. Piano	Examining Σ–Bound States with FINUDA
Y. Akaishi	Deeply Bound Mesonic Nuclear States
H. Outa	Search for Deeply–Bound Kaonic Nuclei at FINUDA
T. Fukuda	Present Status and Future Plans for Hypernuclear Physics in Japan
M.J. Kim	First Exclusive Measurement of the Non-Mesonic Weak Decay of the ${}^{12}_{\Lambda}\mathrm{C}$
H. Bhang	Non–Mesonic Weak Decay of ${}^{5}_{\Lambda}\mathrm{He}$ and ${}^{12}_{\Lambda}\mathrm{C}$ and the Effect of FSI on its Observables
G. Garbarino	Towards a Solution of the Γ_n/Γ_p Puzzle in the Weak Decay of Λ–Hypernuclei

Frascati Physics Series Vol. XXXVI (2004), pp. 179–188
DAΦNE 2004: Physics at meson factories – Frascati, June 7-11, 2004
Invited Review Talk in Plenary Session

PROSPECTS ON HYPERNUCLEAR PHYSICS

Paola Gianotti
INFN-Laboratori Nazionali di Frascati, P.O.Box 13, I-Frascati, Italy

Abstract

In spite of its age, hypernuclear physics is experiencing a renewed youth. Thanks to the high quality data coming form KEK, BNL and today also from LNF, some old standing problems are going to be solved. In this talk I present a review of the most recent results obtained in the last years and I'll show some prospects for the near future.

1 Hypernuclear physics: state of the art

Hypernuclear physics is an excellent environment to match nuclear and particle physics. The study of this field is extremely useful to make systematic studies in many sectors that cannot be addressed directly. Since 1953, when the first hypernucleus was observed into a stack of emulsions exposed to cosmic

radiation [1], different experimental techniques have been used to explore this field.

The earliest studies were carried out with the emulsion technique by using the (K^-_{stop},π^-) reaction. Light hypernuclei (A<16) were produced and the binding energies of the ground states were measured. From these pioneering measurements the well depth of the Λ-nucleus potential was established to be about 1/2 of that of the nucleon.

In the seventies, a new series of experiments with counter detectors started at CERN and at BNL with the intention of evaluating the spin-orbit contributions of the Λ-N interaction [2, 3, 4]. The production reaction more used was (K^-,π^-) in flight. The energy resolution available in those experiments was actually quite poor ($\sim$ 5 MeV), therefore only qualitative speculations could be hold. Nevertheless, the non-observation of spin-orbit splitting of the energy levels seemed to indicate a contribution of the spin terms to the ΛN potential smaller than that of ordinary nuclei, which amount to 3-5 MeV.

In the eighties the (π^+,K^+) reaction was proposed [5] as a better tool to perform spectroscopic studies. Here the Λ hyperon is produced with a large momentum ($\sim$ 350 MeV/c) allowing to populate many excited hypernuclear levels. This new technique was intensively used both at BNL and at KEK. In the last years, at KEK, it has been performed on target materials from A=10÷208 a complete survey, by using this production reaction and the SKS spectrometer [6, 7]. This systematic study has pointed out the independence of the Λ binding energy from the atomic mass number, revealing the single-particle nature of the Λ-nucleus interaction. This has been the arrival point of hypernuclear spectroscopy up to the introduction of the Ge detectors γ-ray spectroscopy technique. The measurement of the energy of the γ-rays emitted in the transitions among the different hypernuclear levels has pin down the energy resolution from the MeV to the keV level, allowing to attack the long standing puzzle of the ΛN spin-orbit interaction. Firstly tried at KEK, this new experimental technique was then exported to BNL, reveling new subjects for hypernuclear physics like the Λ "*glue-like role*" [9] and the study of the meson properties modification in the nuclear medium [10].

For what concerns the production mechanisms, presently two new techniques are starting to demonstrate their good possibilities: photo-production, and the use of (K^-_{stop},π^-) reaction employing the low energy kaons arising from

the ϕ-decay. Photo-production, in spite of its low cross-section, that nevertheless is fully compensated by the high intensity of the TJNAF electron beam, is characterized by a large momentum transfered to the Λ, and also by the possibility to induce spin-flip transitions. This allows to populate hypernuclear states with unnatural parity [11, 12]. On the other hand, the K^- of 127 MeV/c available at DAΦNE, the Frascati ϕ factory, may be stopped in very thin nuclear targets ($\sim$ mg/cm^2) reducing the energy degradation suffered by the pion emitted in the hypernucleus formation reaction. This feature, combined with the high momentum transfered to the Λ particle, is opening new possibilities for hypernuclear spectroscopy. The new production techniques, used in conjunction with modern spectrometers designed to achieve sub MeV energy resolutions, are producing a new high quality data set both for studying hypernuclear spectroscopy and hypernuclear decay modes. Figure 1 shows the preliminary $^{12}_{\Lambda}$C spectrum, obtained by the FINUDA Collaboration at DAΦNE [13], and the $^{12}_{\Lambda}$B one obtained with the photo-production technique [11].

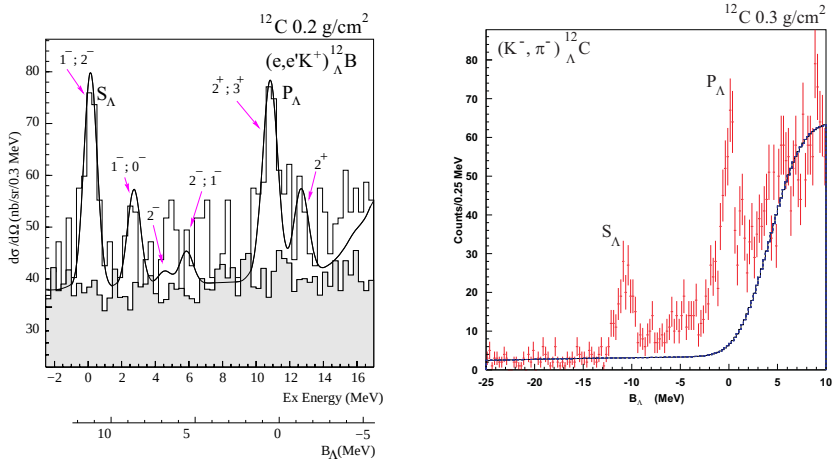

Figure 1: *Left: Spectrum of $^{12}_{\Lambda}B$ measured at JLAB (energy resolution 900 keV). Right: Spectrum of $^{12}_{\Lambda}C$ measured at DAΦNE (energy resolution 1.4 MeV).*

In the following sections I will review some of the most important results that are coming out from different experiments in this field.

2 Hypernuclear spectroscopy

The spectroscopic studies of hypernuclei are of paramount importance for constraining ΛN interaction models. In fact, direct measurements of hyperon-nucleon interaction [14, 15] are extremely difficult due to the low hyperon beam intensity and short lifetime ($c\tau \sim 10$ cm). Production and scattering in the same target is almost automatically required. Two classes of theoretical models of ΛN interaction are nowadays available: meson exchange models (where the exchange of one or sometimes two mesons is considered) [16], and quark-cluster models that introduce quark degrees of freedom to better describe short-range interaction [17]. To overcome the lack of scattering data both classes of models try to determine free parameters by fitting together NN and YN experimental data. Nevertheless, none of these theoretical approaches is completely satisfactory and discrepancies come out especially when the spin-terms of the interaction are considered. Since the quality of the YN scattering data cannot be improved, alternative information are extracted from hypernuclear spectroscopic studies. At present, experimental measurements of the spin-observable, performed mainly using Ge detectors, are the major source of data to discriminate among the different approaches.

The two-body ΛN effective interaction is normally expressed as the sum of five radial integrals associated with different contributions:

$$V_{\Lambda N}(r) = V_0(r) + V_\sigma(r)\vec{s}_\mathcal{N} \cdot \vec{s}_\Lambda + V_\Lambda(r)\vec{l}_{\Lambda N} \cdot \vec{s}_\Lambda + V_N(r)\vec{l}_{\Lambda N} \cdot \vec{s}_N + V_T(r)\mathbf{S_{12}} \quad (1)$$

where $\mathbf{S_{12}} = 3(\vec{\sigma}_N \cdot \vec{r})(\vec{\sigma}_\Lambda \cdot \vec{r} - \vec{\sigma}_N \cdot \vec{\sigma}_\Lambda)$

These five terms ($\bar{V},\ \Delta,\ S_\Lambda,\ S_N,\ T$) are taken to be constant throughout the shell. The average central interaction ($\bar{V}$) has been fixed to reproduce the measured Λ binding energies (B_Λ), and the spin dependent terms can be determined by observing γ ray transitions from p-shell hypernuclei. The spin-spin force (Δ), the Λ spin-orbit force (S_Λ), and the tensor force (T) are obtained from hypernuclear fine structure. The nucleon spin-orbit force (S_N) determines the difference between the nucleon excitation energy of the hypernucleus and its core nucleus.

Since 1998, when the Hyperball Ge-detector started its experimental activity, a big bulk of data have been collected on the energy of the gamma-ray transitions of many light hypernuclei both at KEK and at BNL.

The data collected up to now [18, 19, 20, 21] show the great potentialities of hypernuclear γ-spectroscopy, nevertheless, the contradictory results presently available do not allow to draw any firm conclusion. Probably, the picture will become more clear after the completion of the research program under way for the J-PARC future facility [22]. Furthermore, complementary information will come also form FINUDA2 [23] and from PANDA at GSI [24] where similar activities are foreseen.

2.1 $\Lambda\Lambda$-hypernuclei

The case of double Λ hypernuclei is quite peculiar: they were discovered in an emulsion experiment in 1963 [25], but after this first observation several counter experiment tried to detect them unsuccessfully. Finally, in the last years new experiments at KEK (E176 and E373) and at BNL (E906) have detected new events. The strong interest in this research is related to the fact that $\Lambda\Lambda$-hypernuclei could be the door to access the H-particle, a dybarionic S = -2 state ($uuddss$) [26] never seen up to now, and also because this is the unique possibility to get information on YY interaction. The new evidence of ${}^{6}_{\Lambda\Lambda}$He through the so called Nagara event [27] has provided an invaluable source of information on the strength of the $\Lambda\Lambda$ interaction. Before this discovery, relying on the old measurements giving a value for $\Delta B_{\Lambda\Lambda} \sim 4.3$ MeV, it was believed that the $\Lambda\Lambda$ force would be more attractive than the corresponding ΛN. Now it seems more reasonable that the $\Lambda\Lambda$ interaction should be weakly attractive. In fact, the $\Delta B_{\Lambda\Lambda}$ value deduced from the Nagara event is 1.01 ± 0.20 MeV [28, 29].

Double Λ hypernuclei could be abundantly produced at the new facilities JPARC and PANDA allowing a systematic study of the binding energies of ground and excited states. Therefore, more information on the effective strength of YY interaction will come in the near future. Furthermore, the encouraging results obtained analyzing the γ-ray spectra of Λ-hypernuclei led to the proposal of the PANDA experiment of using the same technique for getting more information on $\Lambda\Lambda$ interaction [24].

2.2 Neutron-rich hypernuclei

Nuclear matter with an extreme N/Z ratio is at present a hot topic of nuclear physics. It has been discovered that in such nuclear systems there is a so called "*halo phenomenon*": some of the nucleons extend far outside the region of the nuclear core. Following this line, Majiling [30] stressed that Λ-hypernuclei may be even better candidates to have larger values of N/Z and halo phenomena thanks to the "glue-like role" of the Λ particle [9]. The existence of neutron-rich hypernuclei, like ${}^{7}_{\Lambda}$H, with a value of N/Z = 5, and of halo hypernuclei like ${}^{7}_{\Lambda}$He and ${}^{9}_{\Lambda}$He, has been predicted by many theoreticians, but an experimental confirmation has not yet been found.

Present experiments, KEK E521 and FINUDA are looking for these systems, but up to now, only upper limits on the production rates have been given [31, 32, 33]. Nevertheless, with the facilities foreseen for the future [22, 34] it would be possible to study systematically the production of neutron rich hypernuclei, assessing their existence and determining their binding energies.

3 Hypernuclear decays

Hypernuclear decay studies may give access to experimental information not otherwise achievable, in particular non-mesonic decays (NMWD). They consist into a weak interaction of the Λ with a nucleon, producing in the final state a pair of nucleons: $\Lambda + n \rightarrow n + n + 176\mathrm{MeV}; \Lambda + p \rightarrow p + n + 176\mathrm{MeV}$. These processes $(\Gamma_n; \Gamma_p)$ are the only way to explore the four fermions, strangeness changing, baryon-baryon weak interaction. The ratio Γ_n/Γ_p is an important observable used to study the isospin contributions to the NMWD. During the last 40 years there has been a long standing puzzle concerning this ratio. In fact the experimental value (close to 1) was fairly in disagreement with the theoretical calculations, based on One Pion Exchange models (OPE), predicting a number close to zero. This large discrepancy stimulated many theoretical speculations while the experimental data still remain with large errors. Recently, the neutron and proton energy spectra from ${}^{5}_{\Lambda}$He and ${}^{12}_{\Lambda}$C have been measured with high statistics [35]. The value obtained for the ratio Γ_n/Γ_p is ~ 0.5. This result rules out the theoretical calculations based on the OPE and supports recent speculations based on short-range interactions including also multi-nucleon induced processes, and large final state interaction effects [36, 37]. Neverthe-

less, it remains unclear why the same calculations reproduce well hypernuclear total width. New data on different target materials are also coming out from the FINUDA experiment. Here again, protons and neutrons are both detected, and Γ_n and Γ_p are thus directly evaluated. Some preliminary results on this analysis are reported in these proceedings [38].

4 The FINUDA experiment at DAΦNE

KEK and BNL activities in the hypernuclear physics sector are no more going on. At present, the running hypernuclear factories are only DAΦNE at LNF and CEBAF at TJNAF. DAΦNE has a very wide and complete hypernuclear physics program that is carried out by the FINUDA international collaboration. FINUDA (FIsica NUcleare a DAΦNE) is the first hypernuclear physics experiment carried out at an e^+e^- collider. At DAΦNE Λ-hypernuclei are produced by means of the reaction: $K^-_{stop} +^A Z \rightarrow^A_\Lambda Z + \pi^-$ stopping the low energy negative kaons from the ϕ decay into a thin ($200 \div 300$ mg/cm^2) nuclear target. The positive kaons emitted on the other side are extremely useful to tag the reaction [39].

FINUDA is a non-focusing magnetic spectrometer designed to achieve a resolution Δp/p of 0.35% (*FWHM*) for the π^- emitted in hypernucleus formation. This translates into an energy resolution of 830 keV for the levels of the hypernucleus. Furthermore, it detects the charged particles and the neutrons emitted after the Λ decay, allowing to perform, at the same time, hypernuclear spectroscopy and studies on the hypernuclear decay modes. More details on the FINUDA detector could be find in ref. [40].

The first round of the FINUDA data taking has been performed from October 2003 up to March 2004. A first integrated luminosity of about 50 pb^{-1} has been collected both for machine and detector calibration purposes; further 200 pb^{-1} are being used for the scientific analyses. With the two ^{6}Li targets FINUDA may access light hypernuclear systems; $^6_\Lambda$Li is unstable for proton emission that makes it decaying into $^5_\Lambda$He + p or it may transform into $^4_\Lambda$He + p + n or into $^4_\Lambda$H + p + p via a Coulomb assisted mechanism. Furthermore, ^{6}Li data are used to look for neutron-rich hypernuclei. The ^{7}Li target has been chosen since $^7_\Lambda$Li is the most extensively studied hypernucleus with γ-ray spectroscopy: FINUDA intention is to provide the first data on its decay modes. Another aspect that may be addressed through the light targets data

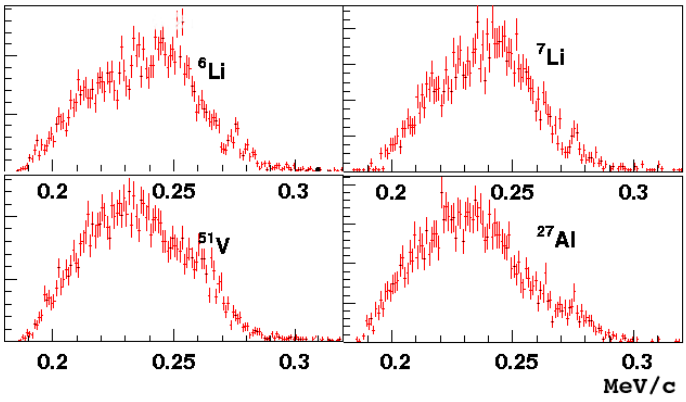

Figure 2: π^- *spectra measured by the FINUDA spectrometer on different nuclear targets.*

is the existence of the deeply-bound kaonic systems [41]. $^{12}_{\Lambda}$C is the best known hypernuclear system, therefore, the three targets of this material will help the calibration procedure of the apparatus and will provide enough statistics to perform non-mesonic decay studies. Finally, ^{27}Al, and ^{51}V are medium-heavy nuclei not well known. For $^{27}_{\Lambda}$Al there are old data taken using K^- in flight and a very coarse energy resolution (6 MeV *FWHM*). The excitation spectrum of $^{51}_{\Lambda}$V has been measured at KEK [42] with an energy resolution of 1.65 MeV (*FWHM*). The peaks corresponding to p and d orbits show possible splitting that might be better resolved with the FINUDA higher resolution. Figure 4 shows the raw spectra of π^- coming out from different nuclear targets measured by the FINUDA spectrometer. Hypernuclear peaks are clearly visible in all the histograms.

5 Conclusions

Hypernuclear physics has achieved nowadays the status of a mature science. Thanks to excellent facilities, first class detectors, and optimum theoretical contribution we can expect in the next future new high quality results.

References

1. M. Danysz and J. Pniewski, Philos. Mag. **44** (1953) 348.
2. G. C. Bonazzola *et al*, Phys. Rev. Lett. **34** (1975) 683.
3. W. Bückner *et al*, Phys. Lett. **62 B** (1976) 481. W. Bückner *et al*, Phys. Lett. **79 B** (1978) 157.
4. R. Bertini *et al*, Phys. Lett. **83 B** (1979) 306. R. Bertini *et al*, Nucl. Phys. **A 368** (1981) 365.
5. H. Thiessen, AGS proposal (1980) 758.
6. T. Hasegawa *et al*, Phys. Rev. Lett. **74** (1995) 224.
7. T. Hasegawa *et al*, Phys. Rev. **C 53** (1996) 1210.
8. C. Keil and H. Lenske, Phys. Rev. **C 66** (2002) 05437.
9. K. Tanida *et al*, Phys. Rev. Lett. **86** (2001) 1982.
10. Y. Miura *et al*, Act. Phys. Pol. B **35-3** (2004) 1019.
11. T. Miyoshi *et al*, Phys. Rev. Lett. **90** (2003) 232502.
12. F. Garibaldi, in press on Nucl. Phys. **A**.
13. L. Benussi for the FINUDA Collaboration, these proceedings.
14. G. Alexander *et al*, Phys. Rev. **173** (1968) 1452. B. Sechi-Zorn *et al*, Phys. Rev. **175** (1968) 1735. R. Engelmann *et al*, Phys. Lett. **21** (1966) 587.
15. J. A. Kadyk *et al*, Nucl. Phys. **B 27** (1971) 13.
16. T. Rijken, in press on Nucl. Phys. **A**.
17. Y. Fujiwara *et al*, Phys. Rew. **C 65** (2001) 014002.
18. H. Tamura *et al*, Phys. Rev. Lett. **84** (2000) 5963.
19. H. Akikawa *et al*, Phys. Rev. Lett. **88** (2002) 082501.
20. H. Kohri *et al*, Phys. Rew. **C 65** (2002) 034607.

21. E. Hiyama *et al*, Phys. Rev. Lett. **85** (2000) 270.

22. T. Fukuda, these proceedings.

23. A. Feliciello, *Proceeding of the workshop on e^+e^- in the 1-2 GeV range: Physics and Accelerator Prospects*, 10-13 Sept. 2003, Alghero (SS), Italy.

24. The PANDA collaboration, *Letter of Intent for Antiproton Physics at Darmstadt*, GSI-ESAC/Pbar 21 Jan. 2004.

25. M. Danysz *et al*, Nucl. Phys. **49** (1963) 121.

26. R. L. Jaffe, Phys. Rew. Lett. **38** (1977) 195.

27. H. Takahashi *et al*, Ohys. Rev. Lett. **87** (2001) 212502.

28. I. N. Filikhin *et al*, Phys. Rev. **C 68** (2004) 024002.

29. Y. Fujiwara *et al*, nicl-th/0405056, submitted to Phys. Rev. C.

30. L. Majiling, Nucl. Phys. **A585** (1995) 211c.

31. K. Kbota *et al*, Nucl. Phys. **A602** (1996) 327.

32. P. Saha *et al*, in press on Nucl. Phys. A.

33. M. Palomba for the FINUDA Collaboration, these proceedings.

34. V. Paticchio, *Proceeding of the workshop on e^+e^- in the 1-2 GeV range: Physics and Accelerator Prospects*, 10-13 Sept. 2003, Alghero (SS), Italy.

35. S. Okada *et al*, nucl-ex/0406020, submitted to Phys. Lett. B.

36. C. Garbarino *et al*, Phys. Rev. Lett. **91** (2003) 112501.

37. C. Garbarino *et al*, Phys. Rev. **C69** (2004) 054603.

38. F. De Mori for the FINUDA Collaboration, these proceedings.

39. C. Milardi *et al*, *Proceeding of the 9th EPAC*, 5-9 Jul. 2004, Lucerne.

40. M. Agnello *et al*, in press on Nucl. Phys. A., LNF-**03/23**(P) (2003).

41. H. Outa for the FINUDA Collaboration, these proceedings.

42. T. Nagae *et al*, Nucl Phys. **A691** (2001) 76c.

Frascati Physics Series Vol. XXXVI (2004), pp. 189–194
DAΦNE 2004: PHYSICS AT MESON FACTORIES – Frascati, June 7-11, 2004
Selected Contribution in Plenary Session

FIRST RESULTS OF FINUDA ON HYPERNUCLEAR SPECTROSCOPY

FINUDA Collaboration *

* M. Agnello[a], G. Beer[b], L. Benussi[c], M. Bertani[c], S. Bianco[c], E. Botta[d], T. Bressani[d], L. Busso[e], D. Calvo[f], P. Camerini[g], M. Caponero[t] P. Cerello[f], B. Dalena[h], F. De Mori[d], G. D'Erasmo[h], D. Di Santo[h], R. Donà[s], F.L. Fabbri[c], D. Faso[e], A. Feliciello[f], A. Filippi[f], V. Filippini[i], E.M. Fiore[h], H. Fujioka[j], P. Gianotti[c], N. Grion[k], A. Krasnoperov[l], V. Lucherini[c], S. Marcello[d], T. Maruta[j], N. Mirfakhrai[m], O. Morra[n], A. Olin[o], E. Pace[c], M. Pallotta[c] M. Palomba[h], A. Pantaleo[p], A. Panzarasa[i], V. Paticchio[p], S. Piano[g], F. Pompili[c], R. Rui[g], G. Simonetti[h], H. So[q], S. Tomassini[c], R. Wheadon[f], A. Zenoni[r].
[a] *Dipartimento di Fisica del Politecnico di Torino, and INFN, Sezione di Torino, Italy,* [b] *University of Victoria, Canada,* [c] *INFN, Laboratori Nazionali di Frascati, Frascati, Italy,* [d] *Dipartimento di Fisica Sperimentale, Università di Torino, and INFN Sezione di Torino, Italy,* [e] *Dipartimento di Fisica Generale, Università di Torino and INFN Sezione di Torino, Italy,* [f] *INFN Sezione di Torino, Italy,* [g] *Dipartimento di Fisica, Università di Trieste and INFN Sezione di Trieste, Italy,* [h] *Dipartimento di Fisica, Università di Bari and INFN Sezione di Bari, Italy,* [i] *INFN Sezione di Pavia, Italy,* [j] *Department of Physics, University of Tokyo, Japan,* [k] *INFN Sezione di Trieste, Italy,* [l] *Joint Institute for Nuclear Physics, Dubna, Moscow region,* [m] *Department of Physics, Shahid Beheshty University, Teheran, Iran,* [n] *CNR-IFSI Sezione di Torino and INFN Sezione di Torino, Italy,* [o] *TRIUMF, Vancouver, Canada,* [p] *INFN Sezione di Bari, Italy,* [q] *Department of Physics, Seoul National University, Seoul, Korea,* [r] *Dipartimento di Meccanica, Università di Brescia, Italy, and INFN Sezione di Pavia, Italy,* [s] *INFN Sezione di Bologna, Italy,* [t] *ENEA sezione di Frascati, Italy.*

Abstract

FINUDA is an experiment devoted to hypernuclear physics. The aim of FINUDA is to study simultaneously the formation and decay of hypernuclei produced by the strangeness exchange reaction induced by the stopped K^- coming from the decay of the $\phi(1020)$ mesons produced at the DAΦNE ϕ-factory. In this paper preliminary results concerning hypernuclear spectroscopy from the first FINUDA data set will be presented.

1 Introduction

An hypernucleus is a many-body system composed of conventional (non-strange) nucleons and one or more hyperons (Λ, Σ or Ξ). A Λ hyperon embedded in a nucleus is stable for mesonic decay and strong interaction; therefore it survives for a while, maintaining its own identity among other nucleons. In addition it can deeply penetrate inside the nucleus since the Pauli principle is not effective due to the strangeness degree of freedom. For these reasons hypernuclei can provide invaluable information concerning the behavior of a baryon deeply embedded in nuclear matter. Moreover a hypernucleus is an excellent tool to extract information on the Hyperon-Nucleon interaction and compare them with theoretical predictions, based either on meson-exchange mechanism or quark-gluon models. FINUDA is a non-focusing magnetic spectrometer with the typical, high-acceptance ($> 2\pi$sr), cylindrical geometry of collider experiments, providing high hypernuclear formation rates: 40 hypernuclei/hour at a luminosity of $5 \times 10^{31}\mathrm{cm}^{-2}\mathrm{s}^{-1}$ with a 10^{-3} capture rate. The apparatus, described in detail in [2, 3] and references therein, consists of an inner section surrounding the interaction-target region, an external tracker, an outer scintillator array and a superconducting solenoid providing a magnetic field of 1.0 T. The whole tracking volume (8 m^3) is immersed in a He atmosphere to minimize Multiple Coulombian Scattering. The geometry of the spectrometer, the position of the detectors and the value of the maximum magnetic field have been optimized for maximizing the momentum resolution and acceptance for the prompt π^- from hypernuclear formation $K^-_{stop} + {}^{A}Z \rightarrow {}^{A}_{\Lambda}Z + \pi^-$. For such π^- (250-280 MeV/c), the design momentum resolution is $\Delta p/p = 3.5 \times 10^{-3}\,(FWHM)$, corresponding to a resolution of 830 keV in the hypernuclear energy levels.

The first FINUDA data taking started on December 1^{st} 2003 up to March 22, 2004. DAΦNE [1] delivered in total an integrated luminosity of 250 pb^{-1},

of which 33 were used for machine tuning, 10 for FINUDA detector debug, the useful data correspond to 190 pb^{-1}. The maximum daily integrated luminosity delivered to FINUDA was 4.0 pb^{-1}, with a maximum peak instantaneous Luminosity of 6×10^{31} $cm^{-2}s^{-1}$. The first events triggered by FINUDA were Bhabha events, i.e. $e^+e^- \to e^+e^-$ and $e^+e^- \to e^+e^- + \gamma$, useful for in-beam calibration of the detectors and for luminosity evaluation. The e^+e^- invariant mass is shown in Fig.1 where the beam energy (1020 MeV) peak is clearly seen togheter with the peak due to $K_S \to \pi^+\pi^-$ (from $\phi \to K_S K_L$) (recorded in the Bhabha trigger) while small bump on the right of the K_S peak corresponds to the decay of the $\rho^0(770) \to \pi^+\pi^-$ coming from the $\phi \to \rho^0\pi^0$ decay. In Fig.1 is also shown the momentum distribution of positive tracks coming from the K^+ stopping points: the two peaks at 236 MeV/c and 205 MeV/c correspond respectively to the two-body decays $K^+ \to \mu^+\nu_\mu$ and $K^+ \to \pi^+\pi^o$. From the width of the μ^+ peak the momentum resolution of the apparatus can be estimated as $\Delta p/p = 0.8\%$ FWHM, about $\sim 4/3$ of the one for pions of 270 MeV as reported in next section. A typical candidate for a hypernucleus formation event is shown in Fig.2, with superimposed the reconstructed tracks emerging from the interaction region: the μ^+ from the K^+ decay and a 260 MeV/c negative pion from the hypernucleus formation on a ^6Li target.

2 First Preliminary Results on $^{12}_{\Lambda}C$ hypernuclear Spectroscopy

The whole sample of $\sim 3 \times 10^7$ collected events has been processed selecting hypernuclear candidate events for the formation of hypernuclei by means of the following requirements: 1) a negative track from a K^- (pion candidate), 2) a fitted track with 4 points in the spectrometer, 3) a forward track, i.e. not crossing back the interaction/vertex region, 4) the particle momentum reconstructed and corrected for the energy loss in the crossed materials, 5) quality cuts on track fitting. In Fig.3 the momentum distribution for the selected π^- in the eight targets is shown, where clean hypernuclear structures appear in the expected momentum range. All the cuts above mentioned have been chosen in order to optimize the signal-to noise-ratio. We start with the detailed study of the $^{12}_{\Lambda}C$ hypernucleus, which will be used as a reference. In the following we refer to only one ^{12}C target (about 20% of the available statistics on ^{12}C). Background reactions giving a π^- following K^-–Nucleus interactions have been simulated and the corresponding events have been reconstructed and

selected following the same selection criteria of the data hypernucleus formation candidates. The obtained spectra are then converted into Λ binding energy spectra.

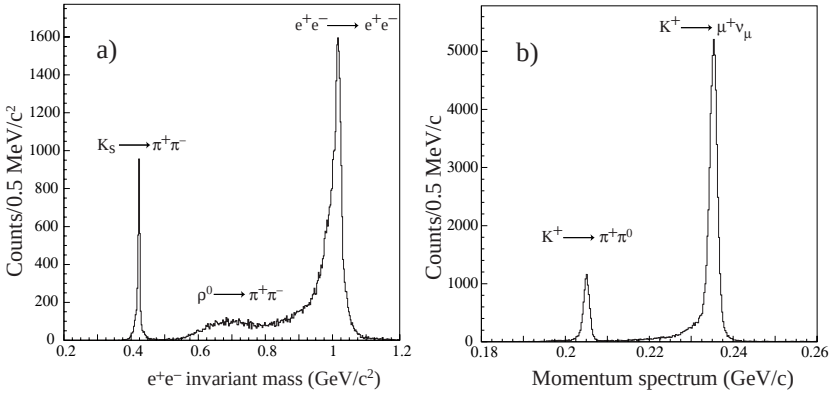

Figure 1: *a); reconstructed invariant mass of the e^+e^- system with the ϕ peak at 1020 MeV. b); reconstructed momentum distribution of the positive particles coming from the decay of positive kaons.*

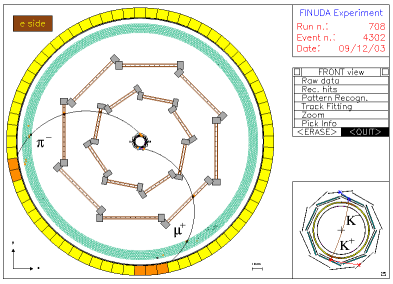

Figure 2: *Display of a typical hypernuclear formation event with reconstructed μ^+ and a π^- tracks. Enlarged view of the vertex region with the (K^+, K^-) trajectories are shown in the inset.*

Hence the shape background spectrum is parameterized and subtracted

from the experimental one; the results is shown in Fig.4(a): two prominent peaks at $B_\Lambda \simeq 11$ MeV and 0 MeV correspond to the ground state (s_Λ) configuration and to the excited state of the ${}^{12}_{\Lambda}C$ hypernucleus with the Λ in the p-shell (p_Λ). The FINUDA preliminary result on ${}^{12}_{\Lambda}C$ is compared (Fig.4(b)) with the result of experiment KEK-E369 [4] which used the (π^+, K^+) hypernuclear production mechanism: peaks #1 , #3 and #4 in Fig.4(a) are consistent with peaks #1, #5, #6 in Fig.4(b), while peak #2 does not appear in E369 data. The FINUDA spectrum has been fitted with four Gaussian after having excluded the region between the two main peaks due to the low statistical significance in this region. The energy resolution has been set at $\sigma_E = 600$ keV ($\Delta E = 1.45$ MeV, $\Delta p/p = 0.6\%$), given by the peak at $B_\Lambda = 0$. In the fit the Gaussian widths were constrained to be the same and equal to σ_E. The results of the fit are summarized in Table 1.

Peak number	Yield (events)	B_Λ (MeV)
1	185 ± 14	10.79 ± 0.04
2	131 ± 15	1.58 ± 0.09
3	338 ± 22	0.17 ± 0.06
4	131 ± 25	-1.99 ± 0.24

Table 1: *Preliminary results of the fitting for the ${}^{12}_{\Lambda}C$ spectrum. The quoted errors are statistical.*

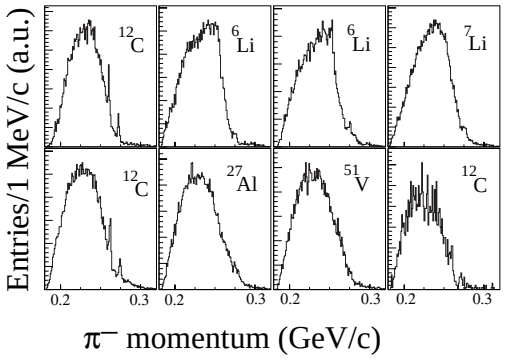

Figure 3: *Distribution of the momentum of the selected forward pions on the eight nuclear targets*

The capture rate for ${}^{12}_{\Lambda}C$ formation is estimated to be $\sim$ $1.8\times\ 10^{-3}/K^{-}_{stop}$ for the ground state and $3.3\times\ 10^{-3}/K^{-}_{stop}$ for the p_Λ state. The structure in the region between the two peaks will be investigated soon with the whole statistics on ${}^{12}C$.

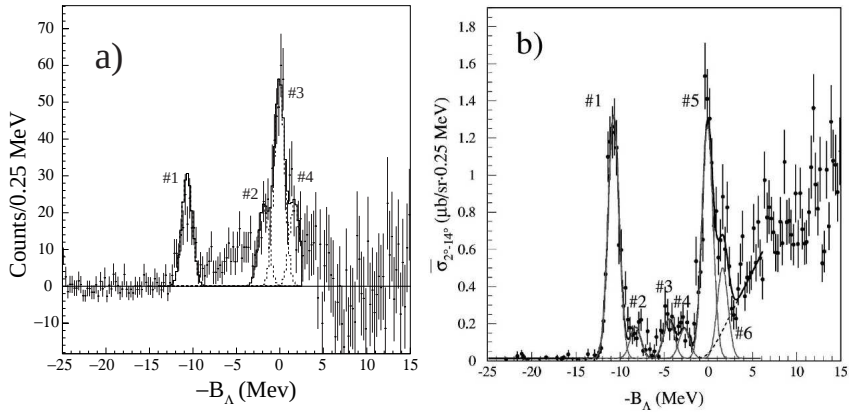

Figure 4: *a)* ${}^{12}C$ *hypernuclear mass spectrum after background subtraction with fitting curve described in the text and for comparison b) The* ${}^{12}C$ *hypernuclear mass spectrum obtained by E369* [4] *at KEK representing the previous world best result in hypernuclear spectroscopy.*

References

1. G. Vignola, The Dafne Project Team, *Proc. PAC'91* 68 (1991); C. Milardi *et al.*, *Proc. 9th EPAC'04* (2004) in publication.

2. The FINUDA Collaboration, M. Agnello *et al.*, "FINUDA, a detector for Nuclear Physics at DAΦNE" **LNF-93/021(IR)** (1993).

3. The FINUDA Collaboration, M. Agnello *et al.*, "FINUDA Technical Report" **LNF-95/024(IR)** (1995).

4. H. Hotchi, *et al.*, *Phys. Rev.* **C64**, 044302 (2001).

Frascati Physics Series Vol. XXXVI (2004), pp. 195–200
DAΦNE 2004: Physics at meson factories – Frascati, June 7-11, 2004
Selected Contribution in Plenary Session

FIRST OBSERVATIONS OF HYPERNUCLEAR NON MESONIC WEAK DECAYS WITH FINUDA

The FINUDA Collaboration *

*M. Agnello[a], G. Beer[b], L. Benussi[c], M. Bertani[c], S. Bianco[c], H.Bhang[q], E. Botta[d], T. Bressani[d], L. Busso[e], D. Calvo[f], P. Camerini[g], P. Cerello[f], B. Dalena[h], F. De Mori[d], G. D'Erasmo[h], D. Di Santo[h], F.L. Fabbri[c], D. Faso[e], A. Feliciello[f], A. Filippi[f], V. Filippini[i], E.M. Fiore[h],H. Fujioka[j],P. Gianotti[c], N. Grion[k], A. Krasnoperov[l], V. Lucherini[c], S. Marcello[d], T. Maruta[j], N. Mirfakhrai[m], O. Morra[n], A. Olin[o], E. Pace[c], M. Palomba[h], A. Pantaleo[p], A. Panzarasa[i], V. Paticchio[p], S. Piano[g], F. Pompili[c], R. Rui[g], G. Simonetti[h],H. So[q], S. Tomassini[c], R. Wheadon[f], A. Zenoni[r] [a] *Dipartimento di Fisica, Politecnico di Torino and INFN, Sezione di Torino, Italy* [b] *University of Victoria, Canada* [c] *INFN, LNF, Frascati,Italy* [d] *Dipartimento di Fisica Sperimentale, Università di Torino and INFN Sezione di Torino, Italy* [e] *Dipartimento di Fisica Generale, Università di Torino and INFN Sezione di Torino, Italy* [f] *INFN Sezione di Torino, Italy* [g] *Dipartimento di Fisica, Università di Trieste and INFN Sezione di Trieste, Italy* [h] *Dipartimento di Fisica, Università di Bari and INFN Sezione di Bari, Italy* [i] *INFN Sezione di Pavia, Italy* [j] *Department of Physics, University of Tokyo, Japan* [k] *INFN Sezione di Trieste, Italy* [l] *J.I.N.P., Dubna, Moscow region* [m] *Department of Physics, Shahid Beheshty University, Teheran, Iran* [n] *CNR-IFSI Sezione di Torino and INFN Sezione di Torino, Italy* [o] *TRIUMF , Vancouver, Canada* [p] *INFN Sezione di Bari, Italy* [q] *Department of Physics, Seoul National University, Seoul, Korea* [r] *Dipartimento di Meccanica, Università di Brescia and INFN Sezione di Pavia, Italy*

Abstract

The FINUDA experiment has successfully completed the first round of data taking at DAΦNE. The excellent detection capability for the hypernuclear decay products and the low momentum threshold on the proton spectra(20 MeV) will allow the measurement of the proton stimulated non-mesonic decay with an improved accuracy. Furthermore, for the first time, non mesonic decays such as ${}^{4}_{\Lambda}He \rightarrow d + d$ were observed.

1 First Observation of proton spectra from Non Mesonic Weak Decay

From the beginning the FINUDA detector [1)] was designed to measure the charged particles (pions, protons,deuterons) and the neutrons emitted in the Mesonic and Non-Mesonic(NM) decay of hypernuclei. It was clear that it was mandatory to perform measurements of the decay products in coincidence with the π^- emitted in the hypernucleus formation reaction $K^- + {}^{A}Z \rightarrow {}^{A}_{\Lambda}Z + \pi^-$. Thanks to the good energy resolution on the hypernuclear final states (better than 1 MeV) of FINUDA we can associate the detected particles to the decay of the ground state ${}^{A}_{\Lambda}Z$ or of an hypernucleus of lower mass. Due to the very small thickness of the stopping targets, the energy spectra of the charged particles should have quite a low energy acceptance cut, estimated around 20 MeV for protons-which is a nice figure of merit of FINUDA in comparison to the best SKS result [2)], whose cut is set to 40 MeV.

We present here some preliminary results of Weak Decays of hypernuclei, essentially on a qualitative level because a quantitative data analysis would require further development of the reconstruction code, presently in progress. The particle identification of the charged products, associated to the reconstructed vertex of the K^- stopped in a nuclear target, is performed by means of the $\Delta E/\Delta X$ measurement by the microstrip detectors facing the targets [3)]. Fig.1 shows the bidimensional plot of the $\Delta E/\Delta X$ as a function of particle momentum measured by the tracker. The plot refers to the charged positive particles emitted from the ${}^{6}Li$ targets(sec.2). Similar spectra were obtained from all the nuclear targets [1)] and all the $\Delta E/\Delta X$ plots were equalized by suitable software corrections [4)]. Fig.2 shows the proton spectrum measured in coincidence with the π^-, emitted in the three ${}^{12}C$ targets in the binding-energy

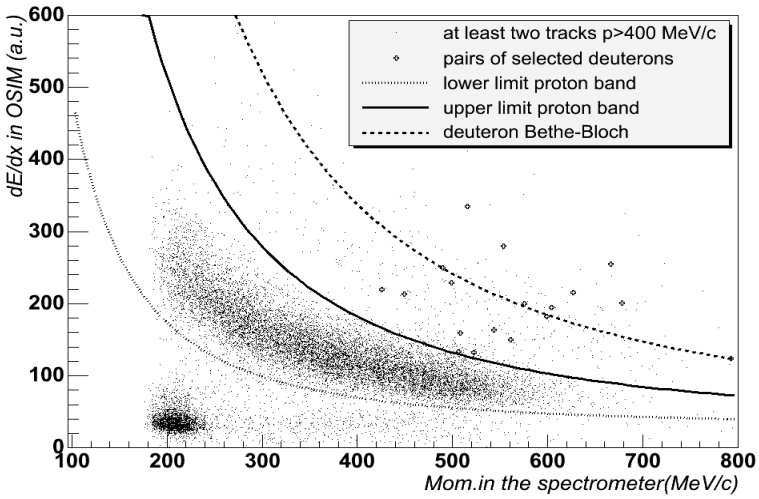

Figure 1: $\Delta E/\Delta X$ *(in arbitrary units) in* μ*strip detector vs measured momentum of the particle.*

range of the Λ bound states [1]. However, the spectrum is still contaminated by residual background contributions (e.g.Σ decay in flight): the background suppression analysis is under way.

2 First observation of the rare two body decay ${}^{4}_{\Lambda}He \rightarrow d + d$

The observation of Schumacher [5] of a possible violation of the $\Delta I = \frac{1}{2}$ rule in NM decays of hypernuclei induced an increased effort on the study of NM decays of hypernuclei (for a recent review see [6]). A convincing argument about a possible violation of the $\Delta I = \frac{1}{2}$ rule could only come from measurements of exclusive NM decays from selected hypernuclei, i.e. a measurement of :

$$ {}^{A}_{\Lambda}Z \rightarrow^{A-2} Z + n + p \qquad \text{and} \qquad {}^{\mathrm{A}}_{\Lambda}\mathrm{Z} \rightarrow^{\mathrm{A}-2} (\mathrm{Z}-1) + \mathrm{n} + \mathrm{n} \tag{1} $$

in which the nucleons are not only detected in coincidence with the signal of the formation of ${}^{A}_{\Lambda}Z$, but also their momenta are measured with the precision necessary to determine unambiguosly the state of the residual nucleus ${}^{A-2}Z$ or ${}^{A-2}(Z-1)$. This is unfortunately impossible in FINUDA, and also in previous experiments, because the neutrons are hardly spectroscopized with the required precision. An alternative way to obtain information about exclusive NM decays

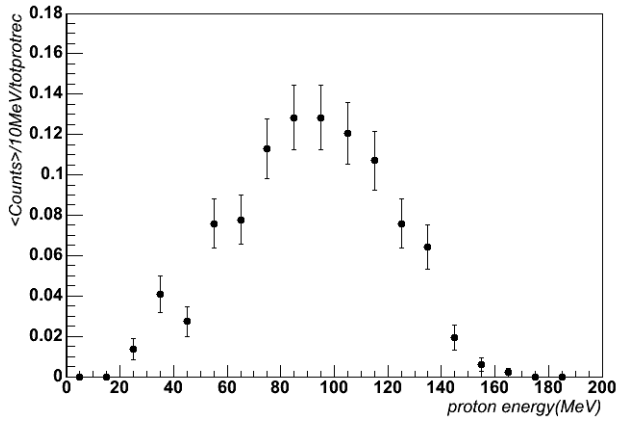

Figure 2: *Proton energy spectrum not acceptance-corrected, normalized to the number of protons reconstructed.*

could be to study rare two body decays of s-shell hypernuclei, like, e.g.:

$$ {}^{4}_{\Lambda}He \rightarrow d + d \; ; \; {}^{4}_{\Lambda}He \rightarrow {}^{3}H + p \; ; \; {}^{4}_{\Lambda}He \rightarrow {}^{3}He + n \qquad (2) $$

$$ {}^{5}_{\Lambda}He \rightarrow {}^{3}H + d \; ; \; {}^{5}_{\Lambda}He \rightarrow {}^{4}He + n \qquad (3) $$

and similar decays for heavier hypernuclei. The branching ratios for such decays are expected to be small (10^{-3} of the total decay rate) and they have never been observed up to now. Light hypernuclei like ${}^{4}_{\Lambda}He$ cannot be formed in two-body reactions in FINUDA for experimental reasons. Nevertheless they are produced abundantly as hyperfragments from heavier targets, like ${}^{6}Li$. Even though rare, the NM decays (Eq.2-3) show a very clean signature: a monochromatic charged particle, with high specific ionization. In some cases (first two channels (Eq.2) and the second one (Eq.3)) two of these particles are back-to-back emitted in the center of mass, with very peculiar and clean topologies. Reminding that the ${}^{6}_{\Lambda}Li$ is unstable for proton emission, we searched for the following chain of reactions:

$$ K^- + {}^{6}Li \rightarrow {}^{4}_{\Lambda}He + p + n + \pi^- \quad \text{and} \quad {}^{4}_{\Lambda}\mathrm{He} \rightarrow \mathrm{d} + \mathrm{d} \qquad (4) $$

$$ K^- + {}^{6}Li \rightarrow {}^{4}_{\Lambda}He + n + n + \pi^0 \quad \text{and} \quad {}^{4}_{\Lambda}\mathrm{He} \rightarrow \mathrm{d} + \mathrm{d} \qquad (5) $$

in order to find candidates for the rare decay (Eq.2). Its signature consists in two deuterons of 570 MeV/c, emitted back-to-back. The estimated momentum

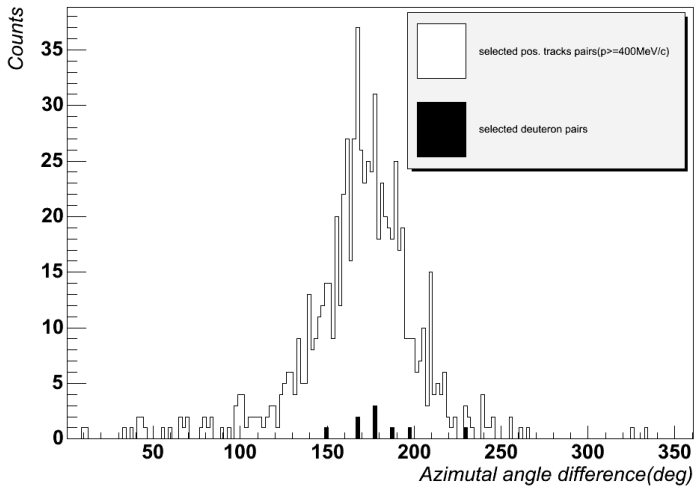

Figure 3: *The azimuthal angle between two positive tracks with momentum larger than 400* MeV/*c, emitted from* K^-*vertex. The selected deuteron pairs are shown in black.*

resolution for these deuterons is 2% FWHM and the angular acceptance about 32% [7].

We looked for events with: 1) at least two tracks corresponding to positive particles emitted from the K^- vertex in ^6Li targets, 2) with $\Delta E/\Delta X$ beyond the chosen upper limit of the proton band (Fig.1), 3) momentum larger than 400 MeV/c and 4) a loose back-to-back angular correlation. We chose these cuts since the exact geometrical description of the complex mechanical structure of the Lithium targets is still under way and we expect quite important corrections after this improvement on the evaluation of both the momenta and the angles of the deuterons emitted from ^6Li targets. Fig.3 shows the angular correlation observed for the tracks fullfilling 1) and 3): only nine events, black distribution in the figure, satisfy also 2) for both particles. The $\Delta E/\Delta X$ values of these particle pairs are marked with the crosses in Fig.1. This event topology is shown in Fig.4 ; the μ^+ track corresponding to the $K_{\mu 2}$ decay of the K^+ stopping in the opposite target is tracked too.

It is quite interesting to observe that also the events with two positive tracks and momenta larger than 400 MeV/c show a strong back-to-back correlation which can be an indication of different rare exclusive decays, like, e.g. ${}^4_\Lambda He \rightarrow d + p + n$.

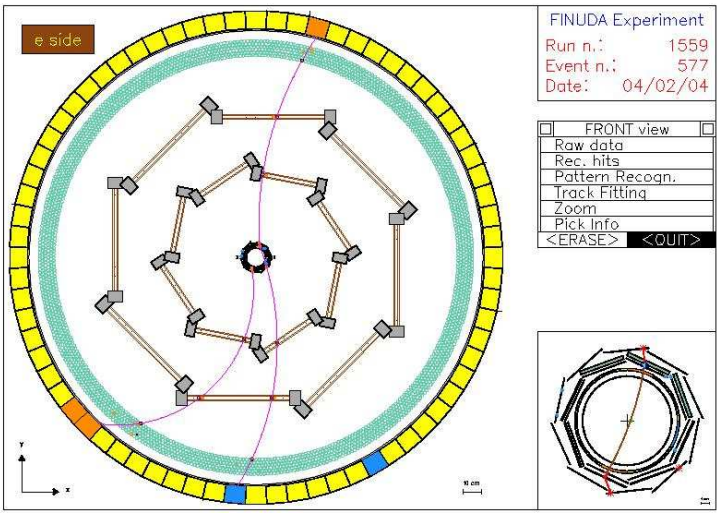

Figure 4: *Candidate event for the rare non mesonic decay* ${}^{4}_{\Lambda}He \rightarrow d + d$.

3 Conclusion

On the road of measuring with FINUDA Weak Decays of hypernuclei in several targets and in many channels, we have started with the observation of the rare two-body decay ${}^{4}_{\Lambda}He \rightarrow d + d$, never reported before. The cleanliness of the events promises us that we will be able to provide the branching ratios.

References

1. P. Gianotti, these proceedings.
2. H. Bhang, this proceedings.
3. P. Bottan et al., *Nucl. Instr. and Meth.* **A427**, 423-436 (1999). , P. Bottan et al., *Nucl. Instr. and Meth.* **A435**, 153-160 (1999).
4. S. Piano, these proceedings.
5. R. Schumacher, *Nucl. Phys.*, **A547** (1992),143c.
6. W. Alberico and G. Garbarino, *Phys. Rep.* **369** (2002), 1.
7. A.Feliciello, *Nucl. Phys.*, **A691**,(2001),170c.

Frascati Physics Series Vol. XXXVI (2004), pp. 201–207
DAΦNE 2004: Physics at meson factories – Frascati, June 7-11, 2004
Selected Contribution in Plenary Session

SEARCH FOR NEUTRON-RICH HYPERNUCLEI IN FINUDA: PRELIMINARY RESULTS

The FINUDA Collaboration *

* M. Agnello[a], G. Beer[b], L. Benussi[c], M. Bertani[c], S. Bianco[c], E. Botta[d], T. Bressani[d], L. Busso[e], D. Calvo[f], P. Camerini[g], P. Cerello[f], G. D'Erasmo[h], B. Dalena[h], F. De Mori[d], D. Di Santo[h], D. Elia[i], F.L. Fabbri[c], D. Faso[e], A. Feliciello[f], A. Filippi[f], V. Filippini[j], R. Fini[i], E.M. Fiore[h], H. Fujioka[k], P. Gianotti[c], N. Grion[l], A. Krasnoperov[m], V. Lenti[i], V. Lucherini[c], V. Manzari[i], S. Marcello[d], T. Maruta[k], N. Mirfakhrai[n], O. Morra[o], A. Olin[p], E. Pace[c], M. Palomba[h], A. Pantaleo[i], A. Panzarasa[j], V. Paticchio[i], S. Piano[g], F. Pompili[c], R. Rui[g], G. Simonetti[h], H. So[q], S. Tomassini[c], R. Wheadon[f], A. Zenoni[r]
[a] *Dipartimento di Fisica, Politecnico di Torino and INFN Sezione di Torino, Italy;* [b] *University of Victoria, Canada;* [c] *INFN, Laboratori Nazionali di Frascati, Frascati, Italy;* [d] *Dipartimento di Fisica Sperimentale, Università di Torino and INFN Sezione di Torino, Italy;* [e] *Dipartimento di Fisica Generale, Università di Torino and INFN Sezione di Torino, Italy;* [f] *INFN Sezione di Torino, Italy;* [g] *Dipartimento di Fisica, Università di Trieste and INFN Sezione di Trieste, Italy;* [h] *Dipartimento di Fisica, Università di Bari and INFN Sezione di Bari, Italy;* [i] *INFN Sezione di Bari, Italy;* [j] *INFN Sezione di Pavia, Italy;* [k] *Department of Physics, University of Tokyo, Japan;* [l] *INFN Sezione di Trieste, Italy;* [m] *J.I.N.P., Dubna, Moscow Region;* [n] *Department of Physics, Shahid Beheshty University of Teheran, Iran;* [o] *CNR-IFSI Sezione di Torino and INFN Sezione di Torino, Italy;* [p] *TRIUMF Laboratory, Vancouver, Canada;* [q] *Department of Physics, Seoul National University, Korea;* [r] *Dipartimento di Meccanica, Università di Brescia and INFN Sezione di Pavia, Italy.*

Abstract

The FINUDA experiment allows to investigate the existence of some rare hypernuclear states predicted by the theory and never observed up to now, the neutron-rich hypernuclei. These objects are produced in very rare events (predicted production rates $\sim 10^{-6} \div 10^{-5}/\mathrm{K}^-_{stop}$) and their formation is associated with a π^+ in the final state, whose momentum spectrum will provide information on their energy. The preliminary analysis of the π^+ spectra obtained for the employed targets (^{12}C, ^{6}Li, ^{7}Li) from the first data taking is presented; the results and the prospects for the future analysis will be discussed.

1 Introduction

The FINUDA experiment, performed at the e^+ e^- collider DAΦNE of the Laboratori Nazionali di Frascati, is mainly aimed at studying the spectroscopy and decays of Λ hypernuclei, produced by means of K^- from the reaction $e^+ + e^- \longrightarrow \phi(1020) \longrightarrow K^+ + K^-$ on different targets. A description of the FINUDA detector may be found in [1], [2] and references therein.

In the wide FINUDA physics program, the search for "neutron-rich" hypernuclei is foreseen. The existence of Λ-hypernuclei with a large neutron excess ($N/Z \gtrsim 2\ N/Z$[ordinary nuclei]) has been theoretically predicted [3] but not observed up to now. Their formation should be possible since the Λ hyperon does not undergo the Pauli principle costraints, providing an "extra-binding" energy to the nuclear structure and allowing a larger number of neutrons to be bound with respect to the ordinary nuclei.

The search of neutron-rich hypernuclei is a very relevant scientific task, in order to fill up the chart of nuclei in the strangeness = -1 sector and for its feedback with other fields of physics, for example in the study of phenomena related to the very high nuclear density of neutron stars [4] in astrophysics.

2 Neutron-rich hypernuclei production in FINUDA

FINUDA is an ideal laboratory to investigate the existence of hypernuclei with high N/Z ratios, that can be produced via the (K^-_{stop},π^+) reactions in the targets, according to two elementary reaction mechanisms:

1) *double charge exchange*:

$$K^- + p \longrightarrow \Lambda + \pi^0\ ; \qquad \pi^0 + p \longrightarrow n + \pi^+$$

2) *strangeness exchange* + $\Sigma - \Lambda$ *coupling*:

$$K^- + p \longrightarrow \Sigma^- + \pi^+\ ; \qquad \Sigma^- + p \longleftrightarrow \Lambda + n\ .$$

Both mechanisms produce in the final state a π^+ and a Λ hypernucleus with A and $Z-2$ (starting from a target nucleus with A and Z); the global production reactions on ^{12}C, ^{6}Li and ^{7}Li respectively are:

$$\begin{array}{lcll} \mathrm{K}^- + {}^{12}\mathrm{C} & \longrightarrow & {}^{12}_{\Lambda}\mathrm{Be} + \pi^+ & (N/Z = 1.75) \\ \mathrm{K}^- + {}^{6}\mathrm{Li} & \longrightarrow & {}^{6}_{\Lambda}\mathrm{H} + \pi^+ & (N/Z = 4) \\ \mathrm{K}^- + {}^{7}\mathrm{Li} & \longrightarrow & {}^{7}_{\Lambda}\mathrm{H} + \pi^+ & (N/Z = 5). \end{array} \quad (1)$$

The final π^+ momentum is directly related to the Λ binding energy B_Λ of ${}^{12}_{\Lambda}$Be, ${}^{6}_{\Lambda}$H, ${}^{7}_{\Lambda}$H by means of momentum and energy conservation, as for the π^- in the case of (K^-_{stop},π^-) reactions mainly studied in FINUDA [1].

At present, our knowledge about neutron-rich hypernuclei properties, such as binding energies and production rates for the reactions (1), is rather poor: the only available experimental datum is an upper limit for the ${}^{12}_{\Lambda}$Be production rate, measured at KEK in 1995 [5]. The whole set of known experimental and theoretical data is listed in Tab. 1.

Table 1: *Available experimental and theoretical data for the neutron-rich hypernuclei to be searched for in FINUDA:* ${}^{12}_{\Lambda}Be$, ${}^{6}_{\Lambda}H$ *and* ${}^{7}_{\Lambda}H$ *(EX = experimental value, TH = evaluated from theory, XT = extrapolated theoretical value).*

Hypernucleus	**Nuclear State**	**Λ Binding Energy B_Λ**	**π^+ momentum**	**Production rate per K^-_{stop}**
${}^{12}_{\Lambda}$Be	1^-	11.4 MeV (XT) [3]	261.8 MeV/c	$< 6.1 \cdot 10^{-5}$ (EX) [5] $1.8 \cdot 10^{-5}$ (TH) [6]
	0^+	-	-	$0.6 \cdot 10^{-5}$ (TH) [6]
${}^{6}_{\Lambda}$H	0^+	5.8 MeV (TH) [7] 4.2 MeV (XT) [3]	254.1 MeV/c 252.3 MeV/c	- -
${}^{7}_{\Lambda}$H	0^+	5.2 MeV (XT) [3]	245.3 MeV/c	-

3 Data analysis and preliminary results

From October 2003 to March 2004 FINUDA has successfully carried out its first round of data taking at DAΦNE, collecting about $\sim$ 220 pb^{-1} of integrated luminosity. The whole collected data have been analyzed, with a not yet refined analysis code, to extract first information about neutron-rich hypernuclei production.

The candidate events have been selected requesting a stopped K^- in the selected target and a successfully reconstructed positive charge track associated

to K^- itself. The positive charge track is identified as a π^+ by means of the energy loss $\Delta E/\Delta x$ in the outer silicon microstrip detector and the particle time of flight (TOF) as measured by the inner and outer scintillator barrels (see the detector description in [1), 2)]). An example of reconstructed candidate event is shown in Fig. 1.

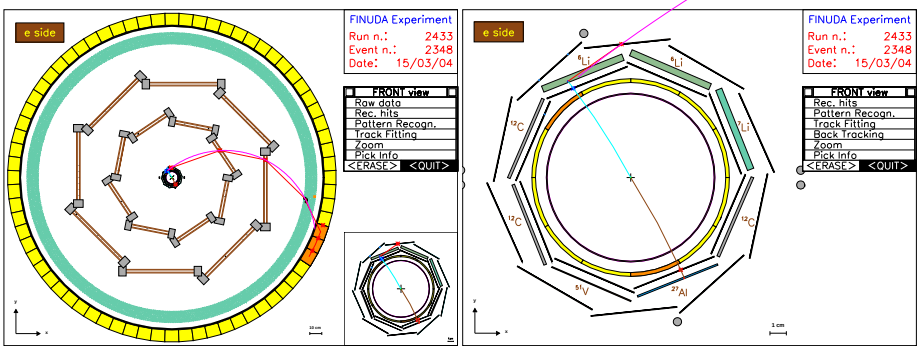

Figure 1: *Reconstructed candidate event for the neutron-rich hypernucleus formation: full detector view and enlarged view of the vertex zone. The fitted track of the π^+ coming out from the ^{6}Li target (where K^- has stopped) is also shown.*

Keeping in mind the production mechanisms (1), inclusive momentum spectra have been studied for the π^+ coming out from ^{12}C, ^{6}Li and ^{7}Li targets; the spectra have been observed in the region around $p \sim 250$ MeV/c (region of interest ROI), corresponding to the theoretical values of B_Λ in the ground state for the ${}^{12}_{\Lambda}$Be, ${}^{6}_{\Lambda}$H and ${}^{7}_{\Lambda}$H hypernuclei (see Tab. 1). The ROI width Δp has been set to $\pm$ 2 σ_p around the central value, where σ_p is the spectrometer momentum resolution. The resulting spectra are shown in Fig. 2, ordered by target nucleus; the shaded zones mark the selected ROI.

As it can be seen from the figure, at this preliminary stage there is no evidence of peaks to be ascribed to the formation of neutron-rich hypernuclei in the ROI yet; this is somewhat expected, since inclusive spectra would still include a large background due to other reactions producing a π^+.

Nevertheless, it is possible to extract from the data an upper limit for the neutron-rich hypernuclei ${}^{12}_{\Lambda}$Be, ${}^{6}_{\Lambda}$H, ${}^{7}_{\Lambda}$H production rates, in the following way. First, an evaluation of the π^+ count rate R_π in the ROI is possible, exploiting the FINUDA unique feature of working with opposite (K^+, K^-) pairs. In fact, about the same number of K^+ and K^- is expected to stop in a given target, and the μ^+ produced in the $K^+ \rightarrow \mu^+ + \nu_\mu$ decay with branching ratio $BR =$

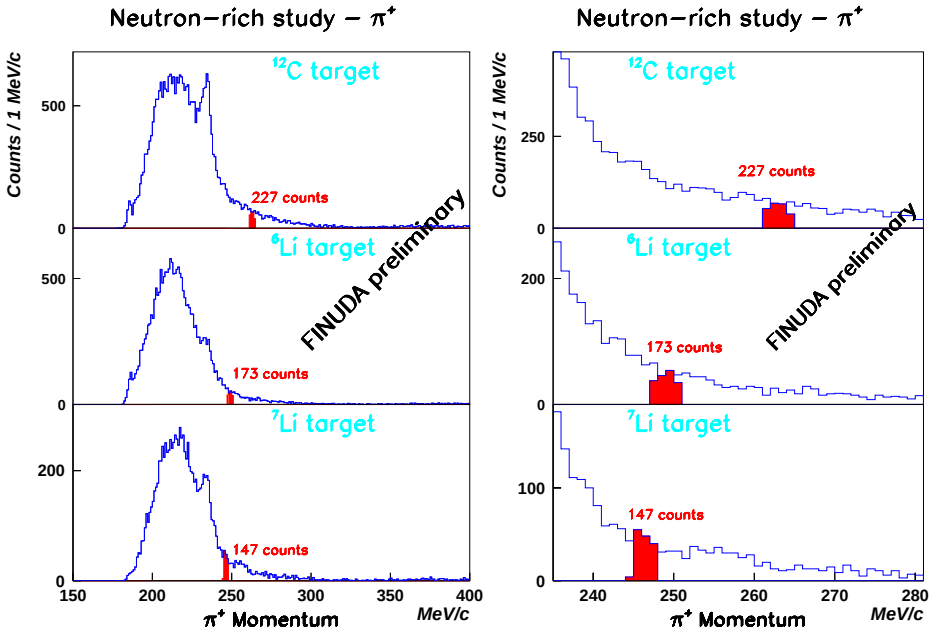

Figure 2: π^+ *momentum spectra obtained from* ^{12}C, ^{6}Li *and* ^{7}Li *targets (full view and enlarged view in the regions of interest ROI).*

0.63 may be used for normalization purposes. In this respect, the rate R_π can be written as [9]:

$$R_\pi \simeq \frac{N_\pi \cdot BR \cdot \varepsilon_\mu \cdot \alpha_{\mathrm{T}}}{N_\mu \cdot \varepsilon_\pi}\,, \tag{2}$$

where N_π is the number of reconstructed π^+ falling into the ROI shown in Fig. 2, N_μ is the μ^+ count number for the same target, ε_μ and ε_π are the total reconstruction efficiencies for μ^+ and π^+ respectively ($\varepsilon_\mu \approx \varepsilon_\pi$), and $\alpha_{\mathrm{T}} \approx 0.50 \pm 0.05$ is the μ^+ acceptance due to the trigger time gate.

On the other side, from statistical considerations, it can be shown that the absence of a neutron-rich "signal" in the spectra implies (at a confidence level of $k\sigma$) a signal-to-background ratio S/B satisfying the condition [9]:

$$(S+B) - k\sqrt{S+B} \leq B + k\sqrt{B} \quad \Longrightarrow \quad \frac{S}{B} \leq k \cdot \frac{2\sqrt{B}+k}{B}\,, \tag{3}$$

Assuming that the observed N_π counts are entirely due to background, we may set $B \simeq N_\pi$ and obtain from (2) and (3) the following relation, fixing

the upper limit U.L. for the hypernucleus production rate $(S/B) \cdot R_\pi$:

$$\frac{S}{B} \cdot R_\pi \lesssim k \cdot \frac{2\sqrt{N_\pi} + k}{N_\pi} \cdot R_\pi \simeq k \cdot \frac{2\sqrt{N_\pi} + k}{N_\mu} \cdot BR \cdot \alpha_{\rm T} = \text{U.L.} \qquad (4)$$

The U.L. values obtained from the (4) are shown in Tab. 2. The evaluation has been done for different confidence levels (90% or $k = 1.645$, 2σ, 3σ), different ROI widths (Δp corresponding to actual momentum resolution 0.9% FWHM and expected final momentum resolution 0.35% FWHM) and different π^+ PID methods. The estimated uncertainties are of the order of $\approx 10\%$.

Table 2: *Upper limits for the hypernucleus formation rate evaluated by eq. (4).*

U. L. value $(\cdot 10^{-5})$	**90% C.L.** $\Delta E/\Delta x$ **ONLY**	**90% C.L.** $\Delta E/\Delta x$ **+TOF**	**2 σ C.L.** $\Delta E/\Delta x$ **ONLY**	**2 σ C.L.** $\Delta E/\Delta x$ **+TOF**	**3 σ C.L.** $\Delta E/\Delta x$ **ONLY**	**3 σ C.L.** $\Delta E/\Delta x$ **+TOF**	
$^{12}_{\Lambda}$**Be**	2.6	2.1	3.2	2.6	4.9	4.0	**Actual**
$^{6}_{\Lambda}$**H**	3.5	2.9	4.3	3.6	6.6	5.6	p **resol.**
$^{7}_{\Lambda}$**H**	4.9	4.3	6.1	5.3	9.4	8.3	**(0.9%)**
$^{12}_{\Lambda}$**Be**	1.6	1.3	2.0	1.6	3.1	2.5	**Nominal**
$^{6}_{\Lambda}$**H**	2.1	1.8	2.6	2.2	4.1	3.5	p **resol.**
$^{7}_{\Lambda}$**H**	3.3	2.8	4.1	3.5	6.5	5.6	**(0.35%)**

The results are very encouraging, despite the fact that we are at a preliminary analysis stage, in which we are looking at the inclusive spectra only, before applying any coincidence technique. In fact, it is already possible to give, for the $^{12}_{\Lambda}$Be production rate, a preliminary U.L. value of $2.1 \cdot 10^{-5}$ at a 90% C.L. with the actual momentum resolution, that improves the KEK result $(6.1 \cdot 10^{-5}$ [5]$)$ of about a factor ~ 3; furthermore, it has to be stressed that the upper limits shown in Tab. 2 for the $^{6}_{\Lambda}$H and $^{7}_{\Lambda}$H production rates are measured for the first time for these hypernuclei.

4 Conclusions and prospects

The preliminary results reported in this paper are promising and demonstrate the potentiality of FINUDA in carrying out the search of neutron-rich hypernuclei. Some important improvements in the data analysis are foreseen, both from the events reconstruction and the coincidence-anticoincidence techniques in study, in order to reduce the background in the ROI of the π^+ momentum spectra.

Further refinements in the upper limit values are expected after the next data analysis and the possibility to evidence structures to be ascribed to neutron-rich hypernuclei in the π^+ spectra is expected.

References

1. M. Agnello *et al*, **LNF-03/23 (P)** (2003), to be published on Nucl. Phys. B (Proc. Supp.).
2. The FINUDA Collaboration, *First results of FINUDA on Hypernuclear Spectroscopy*, these proceedings.
3. L. Majling, Nucl. Phys. A **585**, 211c (1995).
4. Y. Yamamoto *et al*, Nucl. Phys. A **691**, 432c (2001).
5. K. Kubota *et al*, Nucl. Phys. A **602**, 327 (1996).
6. T. Tretyakova *et al*, Nucl. Phys. A **691**, 51c (2001).
7. Y. Akaishi *et al*, Frascati Phys. Ser. Vol. **XVI**, 59 (1999).
8. The FINUDA Collaboration, *Examining* Σ*-bound states with FINUDA*, these proceedings.
9. FINUDA note, in preparation.

Frascati Physics Series Vol. XXXVI (2004), pp. 209–215
DAΦNE 2004: PHYSICS AT MESON FACTORIES – Frascati, June 7-11, 2004
Selected Contribution in Plenary Session

EXAMINING Σ-BOUND STATES WITH FINUDA

The FINUDA Collaboration*

* M. Agnello[a], G. Beer[b], L. Benussi[c], M. Bertani[c], S. Bianco[c], E. Botta[d], M. Bregant[g], T. Bressani[d], L. Busso[e], D. Calvo[f], P. Camerini[g], P. Cerello[f], B. Dalena[h], F. De Mori[d], G. D'Erasmo[h], D. Di Santo[h], F.L. Fabbri[c], D. Faso[e], A. Feliciello[f], A. Filippi[f], V. Filippini[i], E.M. Fiore[h], H. Fujioka[j], P. Gianotti[c], N. Grion[k], A. Krasnoperov[l], V. Lucherini[c], S. Marcello[d], T. Maruta[j], N. Mirfakhrai[m], O. Morra[n], A. Olin[o], E. Pace[c], M. Palomba[h], A. Pantaleo[p], A. Panzarasa[i], V. Paticchio[p], S. Piano[g], F. Pompili[c], R. Rui[g], G. Simonetti[h], H. So[q], S. Tomassini[c], R. Wheadon[f], A. Zenoni[r]. [a] *Dipartimento di Fisica, Politecnico di Torino and INFN, Sezione di Torino, Italy;* [b] *University of Victoria, Canada;* [c] *INFN, Laboratori Nazionali di Frascati, Frascati, Italy;* [d] *Dipartimento di Fisica Sperimentale, Università di Torino and INFN Sezione di Torino, Italy;* [e] *Dipartimento di Fisica Generale, Università di Torino and INFN Sezione di Torino, Italy;* [f] *INFN Sezione di Torino, Italy;* [g] *Dipartimento di Fisica, Università di Trieste and INFN Sezione di Trieste, Italy;* [h] *Dipartimento di Fisica, Università di Bari and INFN Sezione di Bari, Italy;* [i] *INFN Sezione di Pavia, Italy;* [j] *Department of Physics, University of Tokyo, Japan;* [k] *INFN Sezione di Trieste, Italy;* [l] *J.I.N.P., Dubna, Moscow region;* [m] *Department of Physics, Shahid Beheshty University, Teheran, Iran;* [n] *CNR-IFSI Sezione di Torino and INFN Sezione di Torino, Italy;* [o] *TRIUMF, Vancouver, Canada;* [p] *INFN Sezione di Bari, Italy;* [q] *Department of Physics, Seoul National University, Seoul, Korea;* [r] *Dipartimento di Meccanica, Università di Brescia and INFN Sezione di Pavia, Italy.*

Abstract

A Σ-bound state can be formed when a Σ-hyperon substitutes a nucleon into a nucleus, the newly formed nuclear system acquires a unit of strangeness. In the case of Σ-hypernuclei only one bound state has been detected, ${}^{4}_{\Sigma}He$ [1) 2)], and there is no clear evidence of any other bound state with atomic number higher than four. Data analysis of a Σ-hypernuclear system is rather complex, and a comprehensive picture of the interaction has not been established yet. In the present paper, the preliminary results of a search of Σ-hypernuclei with FINUDA are discussed. Σ-hypernuclei are expected to form via the $K^- + {}^{A}Z \rightarrow {}^{A}_{\Sigma^{\pm},0}Z + \pi^{\pm}$ reactions, where ${}^{A}Z$ is a segmented target consisting of 5 different elements, ^{6}Li, ^{7}Li, ^{12}C, ^{27}Al, ^{51}V, and kaons are absorbed at rest. In order to suppress the overwhelming $\pi^{\pm}$ background due to quasi-free reactions, a tagging method is discussed, which is based on the tracking capabilities of FINUDA.

1 Introduction

FINUDA has recently concluded the first run of data taking by recording an integrated luminosity of about $\mathcal{L}$= 250 pb^{-1} [3)]. The spectrometer [4)] was designed for systematic studies of Λ-hypernuclei production and decay, with high momentum resolution and large detection acceptance. In the case of FINUDA, the hypernuclei are formed by stopping K^- mesons in a variety of targets: ${}^{6}Li$, ${}^{7}Li$, ${}^{12}C$, ${}^{27}Al$, ${}^{51}V$. Negative kaons are produced by ϕ decays, which in turn are originated by e^+e^- collisions at DAΦNE, Laboratori Nazionali di Frascati. For the Λ-hypernucleus studies, the magnetic field of the spectrometer was set at 1.0 T. With such a high field only a fraction of the Σ-hypernuclei produced could be examined; however, the collected statistics and the tracking capabilities of FINUDA makes the search for Σ-hypernucleus bound states possible.

2 Σ-hypernuclei in FINUDA

At the FINUDA interacting point the e^+e^- collisions produce $\phi(1020)$ mesons, which decay into pairs of charged kaons K^+ K^- at a rate of 49.1%. Negative kaons are brought to rest in a segmented target, which consists of $2 \times {}^{6}Li + 1 \times {}^{7}Li + 3 \times {}^{12}C + 1 \times {}^{27}Al + 1 \times {}^{51}V$ thin plates (200÷300 mg/cm^2). Negative kaons are initially caught by external atomic orbitals and finally absorbed at

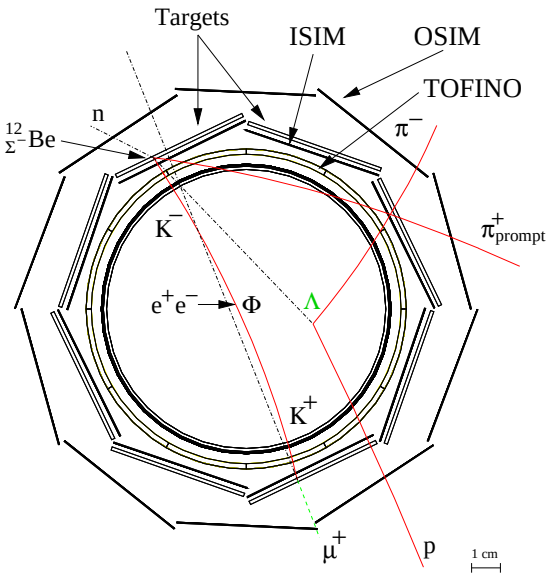

Figure 1: *Enlarged front view of the FINUDA vertex region with a simulated* Σ^-*-hypernuclear event at* $B = 1.0$ *T. The figure shows the prompt pion trajectory* (π^+_{prompt}) *from the* $K^-_{stop} + ^{12}C \rightarrow ^{12}_{\Sigma^-}Be + \pi^+_{prompt}$ *reaction. Two vertices corresponding to the* Σ*-hypernucleus formation* ($^{12}_{\Sigma^-}Be$) *and* $\Lambda \rightarrow \pi^- p$ *decay* (Λ) *are also shown.*

rest (K^-_{stop}) by a a nucleus (^AZ) such as to form a hyperon. The hypernucleus formation is promptly followed by the emission of a pion ($\pi^\pm_{prompt}$). A Σ bound state ($^A_\Sigma Z$) is originated by the reaction:

$$K^-_{stop} + \ ^AZ \rightarrow \ ^A_{\Sigma^{\pm,0}}Z + \ \pi^\pm_{prompt} \tag{1}$$

The Σ hyperon successively converts into a Λ hyperon through the *conversion reaction*:

$$\Sigma + N \rightarrow \Lambda + N \tag{2}$$

where N indicates a nucleon of $^A_\Sigma Z$. The Λ-hyperon acquires energy due to the Σ - Λ mass difference. This allows the Λ to move out of the nucleus and then to decay into the free space. A simulated Σ-hypernuclear event in FINUDA is displayed in Fig. 1. Two vertices can be distinguished: the first describes the topology of the $^{12}_{\Sigma^-}Be$ production and decay, while the second shows the $\Lambda \rightarrow \pi^- p$ decay following the $\Sigma \rightarrow \Lambda$ conversion reaction. The two vertices can be clearly separated one from the other since the vertex detector (see Sect.3) provides an high intrinsic spatial resolution ($\Delta r \sim 30\,\mu$m). The topology of the Σ-hypernucleus production and decay indicates a possible strategy for tagging

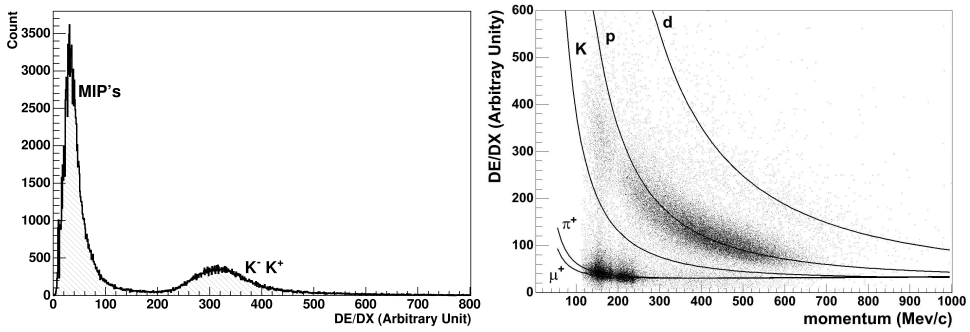

Figure 2: *Left panel: kaons are identified in FINUDA by the energy deposited in ISIM. Right panel: pions are discriminated from protons and from deuterons via the observed $\Delta E/\Delta x$ signal in OSIM versus the particle momentum, which is determined by the spectrometer.*

Σ events. This is based on the detection of π^+_{prompt}'s in coincidence with (π^-, p) pairs. In order to make sure that a coincidence (π^-, p) event originates from a Λ decay, the invariant mass of each event is reconstructed in combination with a $\Delta r > 30\,\mu$m requirement between the two vertices.

3 The FINUDA Silicon Vertex Detector

It is crucial for the Σ-hypernuclear search to discriminate positive pions from protons and from deuterons deriving from the K^--^AZ interaction. In the case of FINUDA, this is performed by the vertex detector, which was designed to mass-discriminate pions from protons (and from deuterons). The inner array of the FINUDA vertex detector consists of 8 double-sided silicon microstrip detectors (ISIM), whose geometry resembles that of an octagonal prism, see Fig. 1. The ISIM modules measure the particle's position with a resolution better than 30 μm; then the stopping position of a K^- can be determined with a precision better than 600 μm. The modules have an analogue readout with a dynamic range of 20 MIP's, so that particles crossing them can be identified according to their $\Delta E/\Delta x$ [5]. Kaons are identified by the energy deposited in ISIM (Fig. 2, left panel). The targets face the ISIM modules at an average distance of 2 mm. An outer layer of 10 silicon modules (OSIM) surrounds the octagonal target ladder, and is the first element of the FINUDA tracking system. In the case of OSIM, charged particles ($\pi^\pm$, p and d) are mass-identified by combining the observed energy loss in the modules with their momentum, the latter being measured by the tracking system of FINUDA (Fig. 2, right panel).

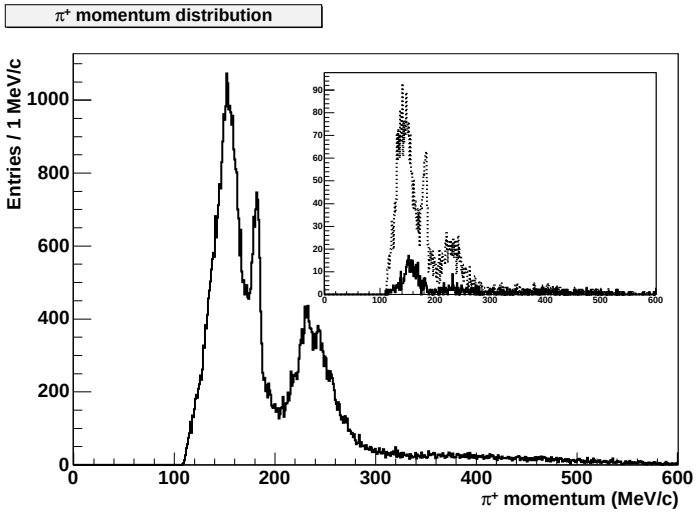

Figure 3: *Momentum distributions of π^+_{prompt}'s for the ^{12}C targets. The inset diagrams show the π^+_{prompt} distributions where the π^+_{prompt} is detected in coincidence with a negative pion (dotted line) and together with a proton (solid line) from reaction (3).*

4 Results

The present preliminary analysis relies on the reactions of Σ-hypernuclear formation and decay:

$$\begin{aligned} K^-_{stop} + {}^{12}C \quad &\rightarrow \quad {}^{12}_{\Sigma^-}Be + \pi^+_{prompt} \\ & \qquad {}^{12}_{\Sigma^-}Be \rightarrow {}^{10}Be + \Lambda + n \\ & \qquad\qquad\qquad \Lambda \rightarrow \pi^- + p \end{aligned} \tag{3}$$

The Σ-hypernuclear spectroscopy is based on the measurement of the π^+_{prompt} momentum distribution. Furthermore, FINUDA is designed to reconstruct the full Σ-hypernuclear event; therefore, it is possible to select exclusive events, which only involve particles of reaction (3). The inclusive momentum distribution of positive prompt pions is shown in Fig. 3 for ^{12}C (solid line). The diagrams in the inset depict the π^+_{prompt} momentum distribution in coincidence with a negative pion (dotted line) and a proton from reaction (3). This simple requirement drastically reduces the inclusive π^+_{prompt} yield, which is primary to select Σ events from the overwhelming quasi-free background. The momentum distribution of π^+_{prompt}'s detected in coincidence with (π^-, p) pairs is shown in Fig. 4. The two bumps appearing in the 150-200 MeV/c region have a width of about 6 Mev/c, which is mainly due to the $\Sigma \rightarrow \Lambda$ conversion reaction. The

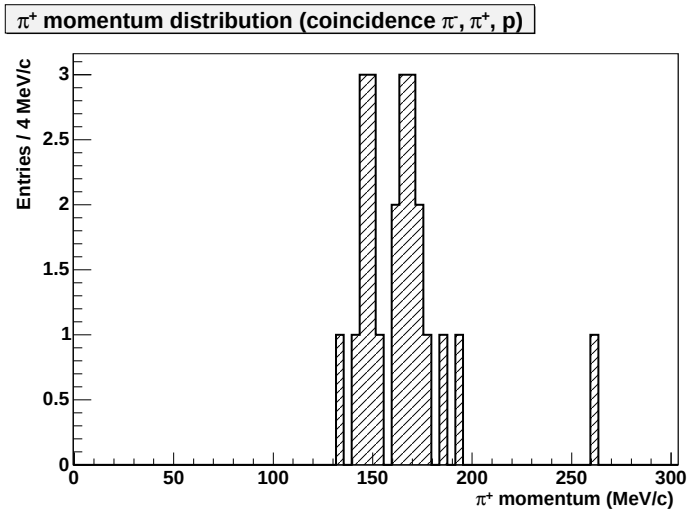

Figure 4: *The exclusive π^+_{prompt} momentum for ^{12}C. Positive pions are detected in coincidence with (π^-, p) pairs from reaction (3).*

existence of these bumps was earlier predicted by a work of [6], which yielded a Σ^- binding energy (width) of about 15 MeV (7 MeV) and 2 MeV (4 MeV) for the 1s and 1p orbitals, respectively.

In order to check whether the two peaks are due to Σ-bound states, one can examine the topology of events populating the two peaks. This approach exploits the tracking capabilities of FINUDA. A riconstructed event is displayed in Fig. 5. The reaction vertex of a hypernuclear formation (i.e., $K^-_{stop} \rightarrow \pi^+_{prompt}$) clearly happens inside the ^{12}C target. The secondary vertex accounting for the decay $\Lambda \rightarrow \pi^- p$ (i.e., $\Sigma N \rightarrow \Lambda N$ followed by the Λ decay) appears at about 1 cm from the primary vertex. This is a unique signature of a Σ-hypernuclear event (i.e., reaction (3)).

The dynamics of Σ-hypernuclear formation and decay is far from being understood. Some authors [6] predict the Σ-nucleus potential to be attractive, others [7] foresee a repulsive behavior, thus inhibiting the formation of Σ-hypernuclei. Although the FINUDA data analysis must be improved, the present results show that FINUDA is entitled to solve the controversial existence of bound Σ-hypernuclei.

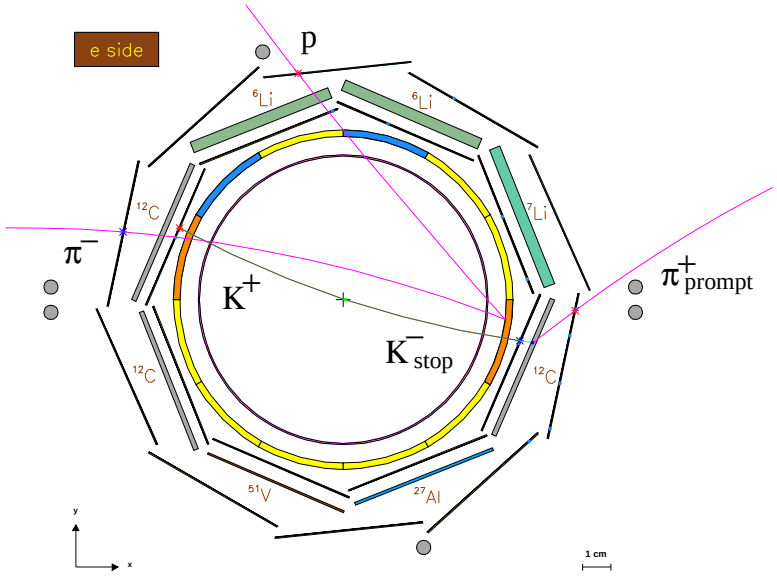

Figure 5: *Front view of a candidate* Σ*-hypernuclear event: two vertices are clearly visible, the former represents the hypernuclear formation in* ^{12}C*,* $K^-_{stop} \rightarrow \pi^+_{prompt}$ *(176 MeV/c), the latter describes the* Λ *decay to* π^- *p. The invariant mass of* (π^-, *p) system is 1116 MeV/*c^2.

References

1. R.S. Hayano *et al.*, Phys. Lett. B **231** (1989) 355.
2. T. Nagae *et al.*, Phys. Rev. Lett. **80** (1998) 1605.
3. M. Agnello *et al.* [FINUDA Collaboration], Preliminary results of the FINUDA experiment at DAΦNE, Ricerca Scientifica ed Educazione Permanente, Suppl.No.123,p.251(2004).
4. M. Agnello *et al.* [FINUDA Collaboration], First results on hypernuclear spectroscopy from the FINUDA experiment at DAΦNE, these proceedings.
5. P. Bottan *et al.*, Nucl. Instrum. Meth. A **427** (1999) 423.
6. E. Oset *et al.*, Phys. Rept. **188** (1990) 79.
7. J. Mares, E. Friedman, A. Gal and B. K. Jennings, Nucl. Phys. A **594** (1995) 311.

Frascati Physics Series Vol. XXXVI (2004), pp. 217–224
DAΦNE 2004: Physics at meson factories – Frascati, June 7-11, 2004
Invited Review Talk in Plenary Session

DEEPLY BOUND MESONIC NUCLEAR STATES

Yoshinori Akaishi
College of Science and Technology, Nihon University,
Funabashi 274-8501, Japan

Abstract

Strongly bound $\bar{\mathrm{K}}$ nuclear systems have been predicted, which are shown to have large binding energies about 100 MeV. The separation energies of a K^- in ^{2}He, ^{3}He and ^{4}He are calculated non-relativistically to be 48, 108 and 86 MeV with widths of 61, 20 and 34 MeV, respectively. A substantial contraction of the $\bar{\mathrm{K}}$ nuclei is induced due to the $I = 0$ $\bar{\mathrm{K}}$N strong attraction, thus forming an unusually dense nuclear object. Since these $\bar{\mathrm{K}}$ nuclei have large densities, *i.e.* several times the normal density, they provide a unique playground for studying possible QCD structure in dense and cold nuclear systems. We discuss implications of recent report on a strange tri-baryon $\mathrm{S}^1(3135)$ from ^{4}He(stopped K^-, n) experiment at KEK, which corresponds to the expected $T = 0$ ppnK^- state. The observed separation energy is substantially larger than the predicted non-relativistic value, which can be accounted for by introducing the relativistic effect and an in-medium $\bar{\mathrm{K}}$N interaction enhanced by 17%. A new paradigm is discussed, which would be deeply related to chiral symmetry restoration, kaon condensation and strange matter.

1 Introduction

In a series of publications [1, 2, 3, 4, 5, 6] we have predicted the possible existence of deeply bound $\bar{\mathrm{K}}$ nuclear states. The $\bar{\mathrm{K}}$N interaction used is derived from the available empirical data of $\bar{\mathrm{K}}$N scattering lengths [7] and kaonic hydrogen level shift [8] together with the supposition that $\Lambda(1405)$ is a bound state of $\bar{\mathrm{K}}$N. The existence of such exotic $\bar{\mathrm{K}}$ nuclear states results from the strongly attractive $\bar{\mathrm{K}}$N interaction in the two-body isospin $I = 0$ state. The interaction causes not only a large binding but also an enormous shrinkage of $\bar{\mathrm{K}}$ nuclei against the hard nuclear incompressibility. Thus, a $\bar{\mathrm{K}}$ produces a bound state with a "condensed nucleus". This extremely interesting possibility for studying dense and cold nuclei is worth pursuing theoretically and experimentally. An observation of such deeply bound states would confirm the underlying physics framework, providing profound information on in-medium modification of the $\bar{\mathrm{K}}$N interaction.

Very recently, experimental evidences have been reported by Iwasaki *et al.*'s E471 group. The first one was observed in the search for the predicted $T = 0$ ppnK$^-$ in the ^{4}He(stopped K$^-$, n) reaction at KEK [9]. A bump corresponding to a total mass of $M = 3137 \pm 4\ \mathrm{MeV}/c^2$ is seen, which is referred to as S^1(3135) and can be identified as $T = 0$ ppnK$^-$. The indicated separation energy, however, is much larger than the predicted value. The second one is a discovery of another species of $\bar{\mathrm{K}}$ nucleus, pnnK$^-$. A distinct peak appears at a mass of $M = 3117 \pm 5\ \mathrm{MeV}/c^2$, which is named S^0(3115) [10].

In this paper we survey works about various nuclear states of a $\bar{\mathrm{K}}$ in light nuclei done in collaboration with A. Doté and T. Yamazaki, and show that the recent experimental data can be understood within a framework of deeply bound $\bar{\mathrm{K}}$ states in condensed nuclei. Finally, future prospects are foreseen about physics of $\bar{\mathrm{K}}$ nuclear systems.

2 Deeply bound $\bar{\mathrm{K}}$ nuclei

2.1 ppK$^-$ and pppK$^-$

The ${}^{2}_{\bar{\mathrm{K}}}$H system is the lightest multi-baryon system, where the conventional nomenclature is employed, that is, ${}^{2}_{\bar{\mathrm{K}}}$H is the state of K$^-\otimes{}^2$He + $\bar{\mathrm{K}}^0\otimes{}^2$H ($T = 1/2$). Hereafter, we use ppK$^-$ as the abbreviation of ${}^{2}_{\bar{\mathrm{K}}}$H. This system is treated with a variational method named ATMS [11]. Although the pp

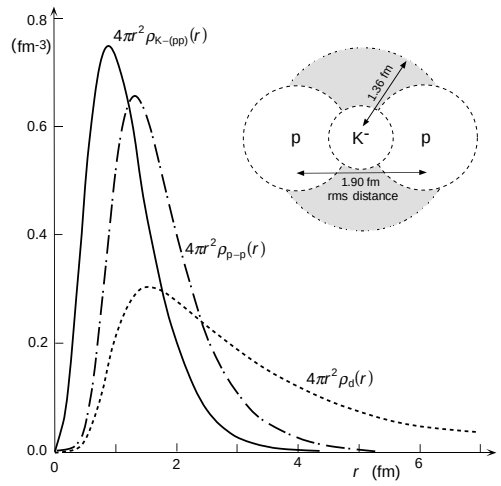

Figure 1: *K^- and proton density distributions in the ppK^- system. As a reference the p-n density distribution in the deuteron is also shown.*

system is unbound, the presence of a $\bar{\rm K}$ attracts two protons to form a bound state with $E_{\rm K} = -48$ MeV and $\Gamma = 61$ MeV. The density distributions of the $\rm K^-$ and the protons in the $\rm ppK^-$ system are shown in Fig. 1. The average distances of the $\rm K^-$ from the center of the pp and from the proton are 1.36 and 1.18 fm, respectively, while the r.m.s. radius between $\rm K^-$ and p is 1.31 fm for $\Lambda(1405)$. The average distance between the two protons is 1.90 fm, which is similar to that in ordinary nuclei. This distance, however, is much smaller than the p-n distance in the deuteron (3.90 fm).

The other $\rm NNK^-$ strange di-baryon systems, namely, $\rm nnK^-$ and $\rm dK^-$, are found to be unbound and less bound compared to $\rm ppK^-$, respectively. The reason is easily understood from the comparison of the weight of the strongly attractive $I = 0$ $\bar{\rm K}$N interaction:

$$2\ (v^{I=1}) \quad \text{for nnK}^-(T = 3/2), \tag{1}$$

$$2\ (\frac{1}{4}v^{I=0} + \frac{3}{4}v^{I=1}) \quad \text{for dK}^-(T = 1/2), \tag{2}$$

$$2\ (\frac{3}{4}v^{I=0} + \frac{1}{4}v^{I=1}) \quad \text{for ppK}^-(T = 1/2), \tag{3}$$

On the picture of $\rm pK^-$=Λ^*(=$\Lambda(1405)$) one may suppose that $\rm dK^-(T = 1/2)$=nΛ^*

and $ppK^-(T = 1/2)$=$p\Lambda^*$ have the same energy. This, however, is not true, because the $N\Lambda^*$ model contains a Pauli forbidden NN component. To remove the unphysical component one must consider the coupling of $N\Lambda^*$ with the isospin partner, $N\Sigma^*$. Thus, the proton-rich ppK^- is distinguished from the dK^- and is most deeply bound among all the NNK^-'s.

The proton-rich ${}^{3}_{\bar{K}}$He ($T = 1$) system ($pppK^-$) is a more exotic one, in which three protons (non-existing ^{3}Li) form a bound state with the aid of the strong attraction from a K^-, where a contraction of the nuclear core against the Pauli exclusion is again essential. A strange structure of "ppK^- plus a satellite p" is realized with a separation energy of 97 MeV from an *ab initio* calculation with the Antisymmetrized Molecular Dynamics (AMD) method [6].

2.2 $ppnK^-$ and $ppnnK^-$

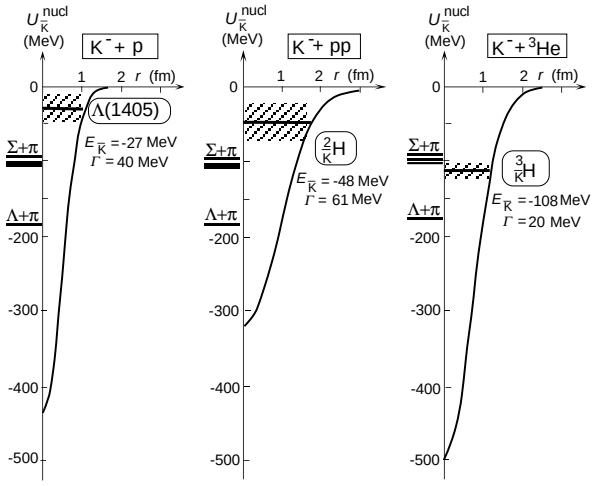

Figure 2: *Calculated $\bar{K}N$ and $\bar{K}$-nucleus potentials and bound levels:* $\Lambda(1405)$, ${}^{2}_{\bar{K}}H$ *and* ${}^{3}_{\bar{K}}H$ *for* pK^-, ppK^- *and* $ppnK^-$ *systems, respectively. The nuclear contraction effect is taken into account. The shaded zones indicate the widths. The* $\Sigma\pi$ *and* $\Lambda\pi$ *emission thresholds are also shown.*

Now, let's proceed to $\bar{K}$ bound states in ^{3}He and ^{4}He. Due to the strong $\bar{K}N$ attraction, a $\bar{K}$ acts as a *contractor* to combine all nucleons closer. Such a shrinkage induced by the $\bar{K}$ is counterbalanced by the hard incompressibility

of the core nucleus. The optimized r.m.s. radius of the core nucleus is 76 % of the free one (1.47 fm) for ppnnK$^-$($T = 1/2$) and, similarly, 60 % of the free one (1.61 fm) for ppnK$^-$($T = 0$).

Figure 2 depicts the bound states of ppK$^-$ and ppnK$^-$, which are extensions of the basic K$^-$+ p system with $\Lambda(1405)$ as its bound state, together with the optimized $\bar{\text{K}}$-nucleus potentials $U_{\bar{\text{K}}}$ of the K$^-$+ ^{2}He and K$^-$+ ^{3}He systems. The predicted bound states can be called *strange di-baryon* and *strange tri-baryon*, respectively. The system, ppnK$^-$($T = 0$), composed of K$^-\otimes{}^3$He + $\bar{\text{K}}^0\otimes{}^3$H, lies by 108 MeV below the ^{3}He + K$^-$ threshold, *i.e.* by 13 MeV below any threshold of the $\Sigma + \pi$ main decay channels: the level width is suppressed to 20 MeV which is only about 20 % of the separation energy. Thus, the deeply bound ppnK$^-$ nucleus, $^3_{\bar{\text{K}}}$H($T = 0$), has been predicted with a narrow width.

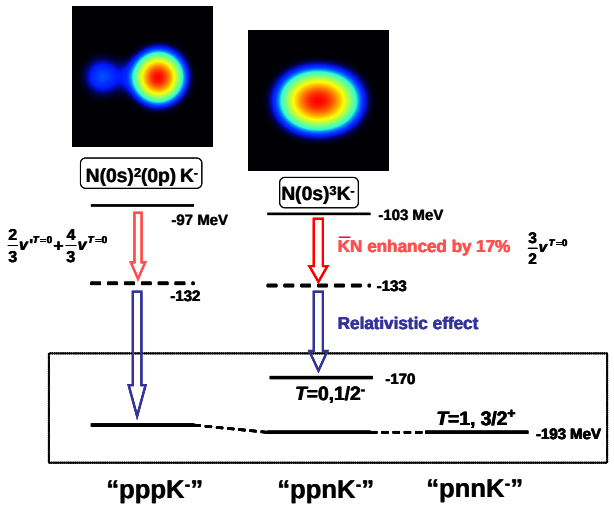

Figure 3: *Isospin-spin structure of strange tri-baryon systems. The relativistic corrections can explain about half of the discrepancy between theoretical values and experimental data of $S^1(3135)$ and $S^0(3115)$. The remaining parts are ascribed to a medium-modified $\bar{\text{K}}N$ interaction enhanced by 17%.*

3 Relativistic correction and enhanced $\bar{\mathrm{K}}$N interaction

The calculations made so far are based on the non-relativistic treatment of many-body systems. For deeply bound $\bar{\mathrm{K}}$, however, relativistic corrections are indispensable. The relativistic effect can be estimated by using a Klein-Gordon equation for $\bar{\mathrm{K}}$,

$$\left\{-\frac{\hbar^2}{2m_{\mathrm{K}}}\nabla^2 + U_{\mathrm{opt}}\right\}|\Phi\rangle = \left(\varepsilon_{\mathrm{K}} + \frac{\varepsilon_{\mathrm{K}}^2}{2m_{\mathrm{K}}c^2}\right)|\Phi\rangle, \tag{4}$$

where ε_{K} is the energy of $\bar{\mathrm{K}}$ without its rest mass. An optical potential, U_{opt}, is provided by *a shrunk nuclear core*. When we make a transformation of the KG energy as

$$\left(\varepsilon_{\mathrm{K}} + \frac{\varepsilon_{\mathrm{K}}^2}{2m_{\mathrm{K}}c^2}\right) \longrightarrow \varepsilon_{\mathrm{S}}, \tag{5}$$

Eq.(4) becomes equivalent to a Schrödinger equation with an energy solution of ε_{S}. Thus, the KG energy can be estimated from the Schrödinger solution as

$$\varepsilon_{\mathrm{K}} = m_{\mathrm{K}}c^2\left(\sqrt{1 + \frac{2\,\varepsilon_S}{m_{\mathrm{K}}c^2}} - 1\right) \tag{6}$$

In this treatment, we make consistent transformations on the threshold energies of decay channels and the complex energy of $\Lambda(1405)$, and obtain re-fitted $\bar{\mathrm{K}}$N interaction parameters (the ppnK^- energy changes from -108 MeV to -103 MeV). As the internal energy of the shrunk core is largely positive, the U_{opt} must be very deep. Thus, the relativistic treatment gives a substantial negative correction on the energy. Since the $T = 1$ state has a larger internal energy than the $T = 0$ state, the relativistic correction is larger for the former and is calculated to be $\Delta E_{\mathrm{rel}}(T = 1) = -61$ MeV and $\Delta E_{\mathrm{rel}}(T = 0) = -36$ MeV. Roughly speaking, the relativistic effect accounts for about a half of the discrepancies as shown in Fig. 3.

The remaining discrepancies between the non-relativistic predictions and the data of the tri-baryons [9, 10] may now be ascribed to a modification of $\bar{\mathrm{K}}$N interaction which could occur in the dense nuclear medium. In the case of ppnK^-, the average nucleon density attains to about 3 times the normal density, where a chiral-symmetry restoration [12, 13] is naturally expected. By considering such and other possibilities, we make phenomenologically a change in the bare $\bar{\mathrm{K}}$N interaction. An enhancement of the $\bar{\mathrm{K}}$N interaction by

17% is required so as to reproduce both the $S^1(3135)$ and $S^0(3115)$. If this enhancement is of other origin and also applicable to ppK^-, its separation energy changes from -48 MeV to -91 MeV with a width of 60 MeV. Thus, an experimental information on ppK^- would greatly help the understanding of the binding mechanism of $\bar{K}$ nuclear systems.

4 Concluding remarks

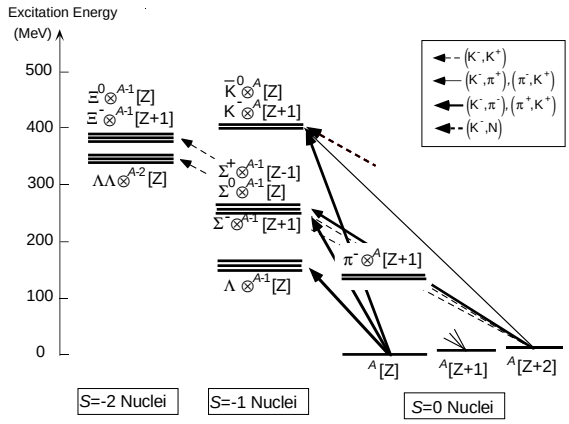

Figure 4: *Generalized diagram of nuclear excited states in the strangeness 0, -1 and -2 sectors. The possible exotic $\bar{K}$ states appear at 300∼400 MeV excitations. Some of possible connecting reactions are indicated.*

We predicted the possible existence of $\bar{K}$ nuclear states with narrow widths in ^{2}He, ^{3}He and ^{4}He. In the deeply bound $\bar{K}$ states the core nuclei are largely compressed due to the strong attraction from a $\bar{K}$, which plays a unique role as a *contractor* to bind nucleons tightly, and accommodates a nucleus of high density. The formation of deeply bound $\bar{K}$ nuclear states would provide a means to investigate properties of hadrons in a dense and cold nuclear medium. A search for the ${}^{3}_{\bar{K}}\mathrm{H}(T=0)$ state was conducted with the ^{4}He (stopped K^-, n) reaction, and an evidence of $S^1(3135)$ has been obtained [9]. Further experiments of missing-mass spectroscopies in formation channels and of invariant-mass spectroscopies in decay channels are planned in order to detect exotic $\bar{K}$ bound

states. It is vitally important to experimentally examine the simplest case of ppK^-, which can provide a gateway toward more complicated and more exotic systems.

Figure 4 shows a diagram of nuclear excited states generalized to the strangeness sectors. The $\bar{K}$ nucleus region is quite exotic: "bound-kaon nuclear spectroscopy" would create *a new paradigm* in nuclear physics. Many impacts are foreseen. *i)* Discrete structures of $\bar{K}$ nuclear systems would be formed at excitation energies of 300∼400 MeV. Nuclear dynamics under extreme conditions (nuclear compression, isovector deformation etc.) can be studied. *ii)* High-density cold nuclear matter would be locally formed around a K^-, which can provide information concerning a modification of the $\bar{K}N$ interaction in a nuclear medium and a transition from hadronic to quark structures. *iii)* Empirical information on the possibility for kaon condensation and for strange matter would be obtained.

References

1. Y. Akaishi and T. Yamazaki, Frascati Physics Series **XVI**, 59 (1999).
2. Y. Akaishi and T. Yamazaki, Phys. Rev. C **65**, 044005 (2002).
3. T. Yamazaki and Y. Akaishi, Phys. Lett. B **535**, 70 (2002).
4. T. Yamazaki and Y. Akaishi, Phys. Lett. B **587**, 167 (2004).
5. A. Doté, H. Horiuchi, Y. Akaishi, and T. Yamazaki, Phys. Lett. B **590**, 51 (2004).
6. A. Doté, H. Horiuchi, Y. Akaishi, and T. Yamazaki, Phys. Rev. C **70**, 1 (2004).
7. A.D. Martin, Nucl. Phys. B **179**, 33 (1981).
8. M. Iwasaki *et al.*, Phys. Rev. Lett. **78**, 3067 (1997).
9. M. Iwasaki *et al.*, nucl-ex/0310018 (2003).
10. T. Suzuki *et al.*, Phys. Lett. B **597**, 263 (2004).
11. Y. Akaishi, M. Sakai, J. Hiura and H. Tanaka, Prog. Theor. Phys. Suppl. **56**, 6 (1974).
12. T. Hatsuda and T. Kunihiro, Phys. Rep. **247**, 221 (1994).
13. W. Weise, Nucl. Phys. A **610**, 35c (1996) and references therein.

Frascati Physics Series Vol. XXXVI (2004), pp. 225–230
DAΦNE 2004: Physics at meson factories – Frascati, June 7-11, 2004
Selected Contribution in Plenary Session

SEARCH FOR DEEPLY-BOUND KAONIC NUCLEI AT FINUDA

The FINUDA Collaboration *

Abstract

By using the FINUDA detector, we carried out a search for deeply-bound kaonic nuclei. A preliminary result on the existence of the K^-pp bound system is reported.

* M. Agnello[a], G. Beer[b], L. Benussi[c], M. Bertani[c], S. Bianco[c], E. Botta[d], T. Bressani[d], L. Busso[e], D. Calvo[f], P. Camerini[g], P. Cerello[f], G. D'Erasmo[h], B. Dalena[h], F. De Mori[d], D. Di Santo[h], D. Elia[i], F. L. Fabbri[c], D. Faso[e], A. Feliciello[f], A. Filippi[f], V. Filippini[j], R. Fini[i], E.M. Fiore[h], H. Fujioka[k], P. Gianotti[c], N. Grion[l], A. Krasnoperov[m], V. Lenti[i], V. Lucherini[c], V. Manzari[i], S. Marcello[d], T. Maruta[k], N. Mirfakhrai[n], O. Morra[o], T. Nagae[p], H. Outa[q], A. Olin[r], E. Pace[c], M. Palomba[h], A. Pantaleo[i], A. Panzarasa[j], V. Paticchio[i], S. Piano[g], F. Pompili[c], R. Rui[g], G. Simonetti[h], H. So[s], S. Tomassini[c], A. Toyoda[p], R. Wheadon[f], A. Zenoni[t]. [a] *Dipartimento di Fisica, Politecnico di Torino and INFN Sezione di Torino, Italy;* [b] *University of Victoria, Canada;* [c] *INFN, Laboratori Nazionali di Frascati, Frascati, Italy;* [d] *Dipartimento di Fisica Sperimentale, Università di Torino and INFN Sezione di Torino, Italy;* [e] *Dipartimento di Fisica Generale, Università di Torino and INFN Sezione di Torino, Italy;* [f] *INFN Sezione di Torino, Italy;* [g] *Dipartimento di Fisica, Università di Trieste and INFN Sezione di Trieste, Italy;* [h] *Dipartimento di Fisica, Università di Bari and INFN Sezione di Bari, Italy;* [i] *INFN Sezione di Bari, Italy;* [j] *INFN Sezione di Pavia, Italy;* [k] *Department of Physics, University of Tokyo, Japan;* [l] *INFN Sezione di Trieste, Italy;* [m] *J.I.N.P., Dubna, Moscow Region;* [n] *Department of Physics, Shahid Beheshty University of Teheran, Iran;* [o] *CNR-IFSI Sezione di Torino and INFN Sezione di Torino, Italy;* [p] *KEK, Japan;* [q] *RIKEN, Japan;* [r] *TRIUMF, Vancouver, Canada;* [s] *Department of Physics, Seoul National University, Korea;* [t] *Dipartimento di Meccanica, Università di Brescia and INFN Sezione di Pavia, Italy.*

1 Introduction

Recently, Akaishi and Yamazaki suggested the existence of deeply bound states of a kaon in light systems [1, 2, 3]. Their predictions were based on the $\overline{\mathrm{K}}$N interaction which is introduced to explain three experimental data such as the $\overline{\mathrm{K}}$N scattering length, the kaonic hydrogen (K^--p) atomic shift, and the binding energy and width of $\Lambda(1405)$, which is regarded as an $I = 0$ quasi-bound state of $\overline{\mathrm{K}}$N. They calculated the binding energy and width for light systems and found that the strong attraction of $I = 0$ channel forbids the bound state decay via the main channel $\Sigma\pi$ energetically, and this fact results in its narrow width. Doté *et al.* also investigated the state with the method of antisymmetrized molecular dynamics and showed that its central density ρ becomes extremely high ($\rho > \rho_0$, where ρ_0 is the normal nuclear density) [4, 5]. While there still exist theoretical uncertainties whether the $\overline{K}$-nucleus potential is deep or shallow, it is important to experimentally investigate the possibility of producing such deeply bound states.

So far, two experimental groups have claimed the observation of the signatures for the deeply-bound states. Iwasaki *et al.* studied the $^4\mathrm{He}(K^-_{\mathrm{stop}},\ nX)$ reaction and observed K^-ppn state [6]. Further, they found a narrow peak in the proton spectrum in the $^4\mathrm{He}(K^-_{\mathrm{stop}},\ pX)$ reaction and assigned it to a strange tribaryon $^3S(3115)$ [7]. It is perhaps another kind of kaon bound state, K^-pnn. Kishimoto *et al.* found $^{15}\mathrm{O}K^-$ with the $^{16}\mathrm{O}(K^-,\ n)$ reaction at $P_{K^-} = 930\,\mathrm{MeV}/c$ [8].

Although the FINUDA detector was optimized for hypernuclear spectroscopy with $(K^-_{\mathrm{stop}},\ \pi^{\pm})$ reactions [9], it also has advantages for the search for the deeply-bound kaonic states. We can apply missing-mass spectroscopy in the $(K^-_{\mathrm{stop}},\ n$ or $p)$ reactions for various kinds of targets (^{6}Li, ^{7}Li, ^{12}C, ^{27}Al, ^{51}V) at the same time. One of the great advantages in the FINUDA detector is the ability to identify the hyperons through their decays. In particular, a Λ hyperon mass can be reconstructed from the decay mode $\Lambda \to p + \pi^-$. It enables us not only to tag the decay of deeply-bound states, but also to apply invariant-mass spectroscopy [10] to directly search them.

In this report, we will discuss preliminary results on the invariant-mass spectroscopy of the K^-pp system, decaying in non-mesonic channels as follows:

$$K^-pp \to \left\{ \begin{array}{l} \Lambda + p \\ \Sigma^0 + p \end{array} \right. , \tag{1}$$

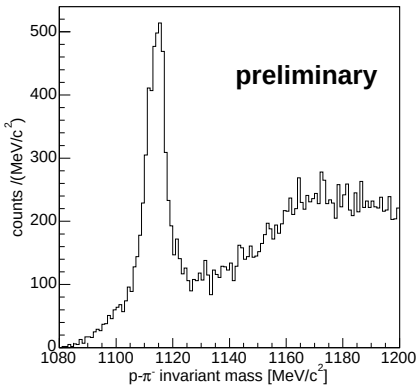

Figure 1: *Invariant mass of a proton and a π^- from K^- stopping point.*

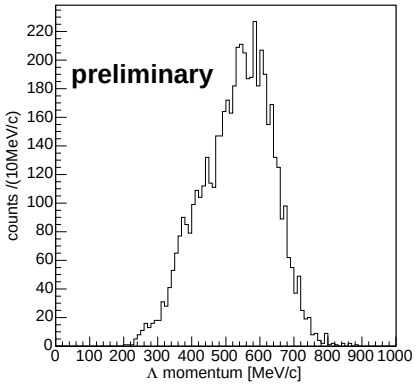

Figure 2: *Momentum distribution of Λ candidates.*

with the data obtained in the 2003–2004 data taking. The binding energy and width of the K^-pp system are calculated as $B = 48\,\mathrm{MeV}$ and $\Gamma = 61\,\mathrm{MeV}$ [11].

2 Identification of Λ

When a negative kaon stops at a nuclear target and is absorbed by the nucleus from its atomic orbit, it is known [12] that the two kinds of reactions predominantly occur, such as quasi-free hyperon production (K^-"N" $\rightarrow Y\pi$; $\sim 80\%$) and non-mesonic two-nucleon absorption (K^-"NN" $\rightarrow YN$; $\sim 20\%$), where Y represents a Λ or $\Sigma^{\pm/0}$ hyperon.

Here, we can identify the Λ by reconstructing the invariant mass $M(p\pi^-)$ of a proton and a negative pion with enough statistics and resolution, thanks to the good momentum resolution ($\Delta p/p \sim 0.3\%$[1] for $270\,\mathrm{MeV}/c$ π^-) and large acceptance ($\sim 70\%$) of FINUDA spectrometer. We used the sign of a track curvature and dE/dx in silicon microstrips for the particle identification. The invariant mass spectrum is shown in Fig. 1. The mass resolution of $8.6\,\mathrm{MeV}/c^2$ (FWHM) for the Λ peak is almost consistent with that estimated by a Monte Carlo simulation. The resolution is limited by the momentum resolution for the slow pions (100–200 MeV/c) emitted from the Λ decay, because less hit points

[1] At present, $\sim 0.6\%$ is achieved.

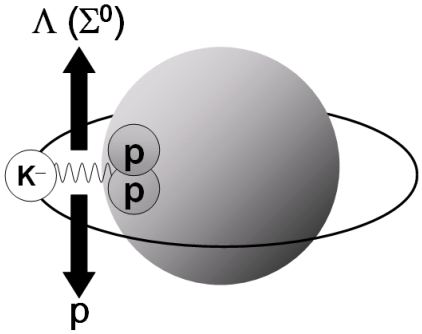

Figure 3: *An illustration of the K^-pp formation and the two-body decay mode, $\Lambda(\Sigma^0) + p$.*

are available for such curly tracks. Please note that the FINUDA detector has a good acceptance and momentum resolution for the tracks with the momenta larger than 200 MeV/c.

Applying the mass gate for this spectrum as $|M(p\pi^-) - m_\Lambda| < 10\,\mathrm{MeV}/c^2$, we obtain the momentum distribution of Λ candidates as shown in Fig. 2. There are little events below 300 MeV/c because of the acceptance, particularly of pions, so that most of Λ's ($p_\Lambda \lesssim 400\,\mathrm{MeV}/c$) from the quasi-free production are not observed.

3 Invariant mass spectroscopy of K^-pp

The two-nucleon absorption process takes place at $\sim 20\%$ for the stopped K^- reaction for a wide mass number range. For two-proton absorption K^-"pp" $\rightarrow$ $\Lambda + p$ or $\Sigma^0 + p$, we expect a hyperon and a nucleon are emitted in the final state almost back-to-back as shown in Fig. 3. Figure 4 is the angular distribution between a proton and a Λ observed in the present experiment. We can clearly find the back-to-back correlation ($\cos\theta < -0.8$). This correlation is observed for all of our targets (^{6}Li–^{51}V). Then, the invariant mass of the $\Lambda - p$ system should distribute around the sum of $K^- + p + p$ mass, assuming that the two protons are uncorrelated at nuclear surface with small binding energies. Figure 5 shows the invariant mass distribution of the $\Lambda - p$ system. We find a broad bump peaked at about 2270 MeV/c^2, which corresponds to the $\sim$ 100 MeV

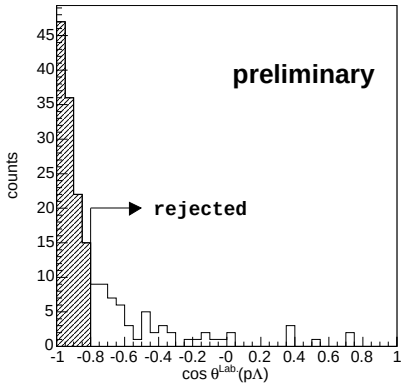

Figure 4: *Angular distribution between a proton and a* Λ *particle.*

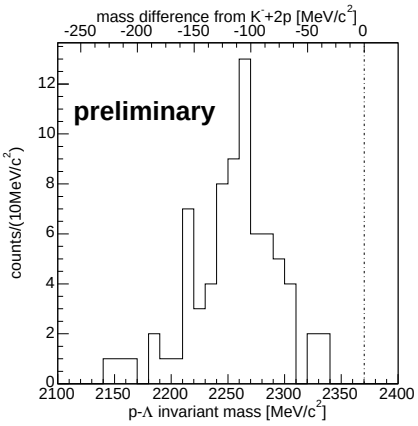

Figure 5: *Invariant mass of a proton and a* Λ *particle for* $\cos\theta^{\mathrm{Lab.}}(p\Lambda) < -0.8$. *The dotted line indicates the binding threshold of the* K^-pp *system.*

binding in the K^-pp system. We observed very few events in the unbound region, in fact. Even if the Λ we observed is all coming from the Σ^0 followed by the $\Lambda + \gamma$ decay, we expect the invariant mass would be shifted by only $\sim 74\,\mathrm{MeV}$ carried away with the γ-ray. It seems the current observation is far beyond this interpretation, and we know the Σ^0 contribution is only $\sim 20\%$ in ^{4}He [13]. Although the correction for the detector acceptance is still in progress, we think the present data strongly suggests the existence of the lightest kaon bound state K^-pp.

4 Summary

With the FINUDA spectrometer, we have succeeded to observe the reaction $K^-pp \to \Lambda + p$ (or $\Sigma^0 + p$) with explicitly observing a Λ and a proton in the back-to-back kinematics. The invariant mass distribution of the $\Lambda - p$ system strongly suggests a large amount of binding energy exists in the K^-pp system.

5 Acknowledgements

This work is supported in part by the Grant-In-Aid for Scientific Research (B) 15340087 of Ministry of Education, Culture, Sports, Science and Technology (MEXT).

References

1. Y. Akaishi and T. Yamazaki, Nucl. Phys. A **684** (2000) 409c.
2. Y. Akaishi and T. Yamazaki, Phys. Rev. C **65** (2002) 044005.
3. Y. Akaishi, in these proceedings.
4. A. Doté *et al.*, Phys. Lett. B **590** (2004) 51.
5. A. Doté *et al.*, nucl-th/0309062 (to be published in Phys. Rev. C).
6. M. Iwasaki *et al.*, nucl-ex/0310018.
7. T. Suzuki *et al.*, Phys. Lett. B **597** (2004) 263.
8. K. Kishimoto *et al.*, HYP2003 proceeding, to appear in Nucl. Phys. A.
9. M. Agnello *et al.* [FINUDA Collaboration], First Results of FINUDA on hypernuclear spectroscopy, these proceedings.
10. T. Yamazaki *et al.*, Phys. Lett. B **587** (2004) 167.
11. T. Yamazaki and Y. Akaishi, Phys. Lett. B **535** (2002) 70.
12. C. Vander Velde-Wilquet *et al.*, Nuovo Cimento **39A** (1977) 538.
13. P. A. Katz *et al.*, Phys. Rev. D **1** (1970) 1267.

Frascati Physics Series Vol. XXXVI (2004), pp. 231–236
DAΦNE 2004: Physics at meson factories – Frascati, June 7-11, 2004
Selected Contribution in Plenary Session

PRESENT STATUS AND FUTURE PLANS FOR HYPERNUCLEAR PHYSICS IN JAPAN

Tomokazu Fukuda
Osaka Electro-Communication University, Neyagawa, Osaka 572-8530, Japan

Abstract

A present status of the hypernuclear physics mainly performed at KEK was presented; a particular emphasis was made on the production of the neutron-rich hypernucleus. Future perspectives at J-PARC were also discussed.

1 Neutron-rich Λ hypernuclear production

1.1 Physics motivation and theoretical background

It has been discussed that the study of neutron-rich Λ hypernuclei would give new information of hypernuclear physics such as the coherent Λ-Σ coupling, which was first introduced to solve the long-standing "overbinding problem" of ${}^{5}_{\Lambda}$He [1]. This coherent coupling becomes more effective as the excess neutron number of the nucleus becomes larger and eventually will affect the baryon

interaction in high density nuclear matter like neutron stars [2, 3]. However, there have been few experimental efforts to produce neutron-rich Λ hypernuclei, which is difficult by the usual (K^-, π^-) or (π^+, K^+) reaction but is possible by using the double charge-exchange(DCX) mechanism like (π^-, K^+) or (K^-, π^+) reaction. In the past attempt by using (stopped-K^-, π^+) reaction [4], only the upper limits of the production cross section on ^{9}Be, ^{12}C and ^{16}O targets were given due to a limited statistics and a large background originating from Σ^+ decay. Recently FINUDA collaboration at DAPHNE is trying to observe neutron-rich hypernuclei by using (stopped-K^-, π^+) reaction with higher statistics than previous one, however, they also give an upper limit at present [5] because of an inherent background of Σ^+ decay in this reaction. In the present experiment, we used the in-flight (π^-, K^+) DCX reaction on a ^{10}B target in order to produce a $^{10}_{\Lambda}$Li hypernucleus for the first time with much less background.

A neutron-rich Λ hypernuclear production in the (π^-, K^+) reaction may proceed by the two-step mechanism of the meson charge-exchange, for example, $\pi^- p \to \pi^0 n$ followed by $\pi^0 p \to K^+\Lambda$, or $\pi^- p \to K^0\Lambda$ followed by $K^0 p \to K^+ n$. Another mechanism is the single-step process via a Σ^- admixture in the Λ hypernuclear state appearing due to the $\Sigma^- p \leftrightarrow \Lambda n$ coupling. Recently, there has been a theoretical calculation concerning both mechanisms on some light nuclear targets, where the two-step mechanism is found to be more dominant as compared to the single-step one [6]. The two-step transition with no angular momentum transfer ($\Delta l = 0$) in the charge-exchange process is found to favor for a maximum production cross section, which is possible for the target with a neutron orbit vacancy. As a result, the ground state cross section of the $^{10}_{\Lambda}$Li production in the (π^-, K^+) reaction on ^{10}B target is found as large as 70 nb/sr in the forward angle, which is significantly larger among others ($^{12}_{\Lambda}$Be or $^{16}_{\Lambda}$C) in the same calculation. The incident energy dependence of the cross section shows the maximum production at 1.05 GeV/c, same as the Λ hypernuclear production in the (π^+, K^+) reaction.

1.2 Experiment

The present experiment (KEK-PS-E521) [7] was performed in the K6 beam line of KEK 12-GeV proton synchrotron(PS) together with the superconducting kaon spectrometer(SKS) system [8]. The experimental target, ^{10}B, was 3.5

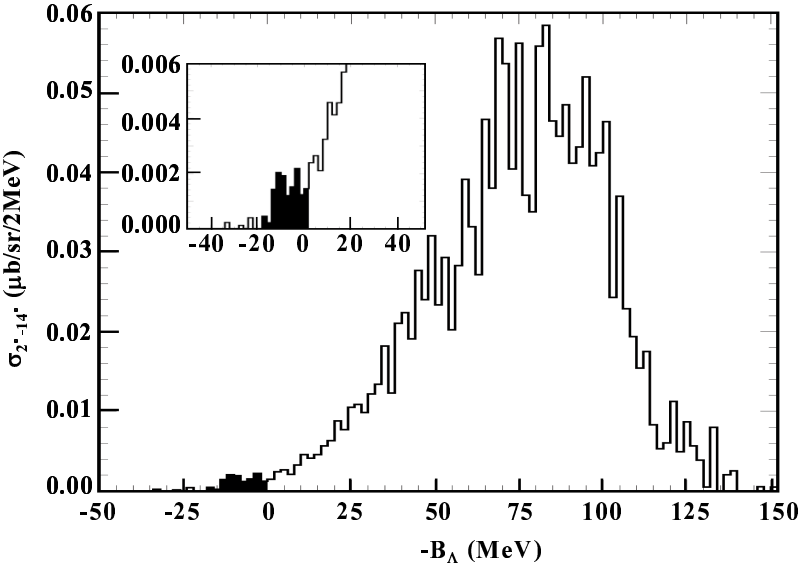

Figure 1: *Missing mass spectrum of the* (π^-, K^+) *reaction on* ^{10}B *target at 1.2 GeV/c. Horizontal axis shows the binding energy of a* Λ*, whereas vertical axis shows the cross section in terms of* $\mu b/sr/2$ *MeV.*

g/cm^2 in thickness and we started with the incident beam momentum of 1.05 GeV/c. The SKS was excited to 272A(2.2 Tesla), in which the central momentum was 720 MeV/c. The separated π^- beam intensity at the experimental target was typically 4×10^6/spill (4.0 sec). In the off-line analysis, incident π^- and outgoing K^+ momenta were obtained particle-by-particle by using the beam line and the SKS spectrometer, respectively. We clearly identified scattered kaons well separated from both pions and protons. Then, by selecting good kaons, the missing mass spectrum was obtained. The total number of π^- beam injection in this setting was about 440×10^9 but only 7 counts are found in the bound region and quasi-free(QF) events are also very small. The yield in the bound region is about one order of magnitude lower than expected from the theoretical calculation.

We then changed the beam momentum to 1.2 GeV/c, where the Σ^- production channel is open. In this case, the SKS was excited to 395A(2.6 Tesla), where the central momentum of SKS was 880 MeV/c. The total number

of π^- beam injection in this setting was about 1080×10^9. In total we got about 40 counts in the bound region. Figure 1 shows the missing mass spectrum on ^{10}B at 1.2 GeV/c. The vertical axis is the cross section in terms of μb/sr/2MeV, which was done by taking into account experimental and analysis efficiencies as well as the SKS acceptance, calculated by a Monte Carlo Simulation code, GEANT.

In order to calibrate the horizontal axis as well as to check the accuracy of the cross section in the present experiment, we measured the (π^+, K^+) reaction on ^{10}B and ^{12}C targets of the same thickness (3.5 g/cm^2). The (π^+, K^+) reaction on ^{12}C target was measured at both 1.05 and 1.2 GeV/c incident momenta. The calibration of the horizontal axis was checked by reproducing the known ground state (g.s.) energy of the $^{12}_{\Lambda}$C (-10.76 MeV). The precision of the horizontal axis was obtained to be $\pm$ 0.23 MeV. The experimental energy resolution was obtained by fitting the g.s. peak of the $^{12}_{\Lambda}$C, which was 2.5 MeV in FWHM. We found cross sections of the (π^+, K^+) reaction on both ^{10}B and ^{12}C targets at 1.05 GeV/c reproduced very well previous measurements done with SKS, whereas the cross section at 1.2 GeV/c on ^{12}C gives new experimental information.

1.3 Results and discussion

As seen in figure 1, there are significant yields below the $^{10}_{\Lambda}$Li production threshold($-B_{\Lambda}$=0), which can be seen more clearly in an expanded view. Backgrounds are very small and the tail from the quasi-free events will not much contribute to the yields because of a good energy resolution (2.5 MeV in FWHM), which is confirmed in the $^{12}_{\Lambda}$C spectrum. Hence almost all events in the bound region are expected to come from the signal of the produced hypernucleus, $^{10}_{\Lambda}$Li. Unfortunately, no significant discrete peaks were observed, which may be due to the limited statics, the experimental resolution and possible complicated nuclear structure. Note that Akaishi calculated the ground state energy to be around -12 MeV [9], which may not be inconsistent with the present data.

From the present experimental result, we obtained the Λ hypernuclear production rate in the (π^-, K^+) reaction at 1.2 GeV/c as compared to that in the (π^+, K^+) reaction on the same target(^{10}B). For simplicity, the total cross sections only in the bound region (-15.0$\leq -B_{\Lambda} \leq$0 MeV) for both cases are compared. The total cross section of the bound region for the ^{10}B$(\pi^+, K^+)^{10}_{\Lambda}$B

production was found to be 7.8 ± 0.3 μb/sr, whereas for the ^{10}B$(\pi^-, K^+)^{10}_{\Lambda}$Li production it was 0.012 ± 0.002 μb/sr, where the errors are only the statistical ones. Then we got the Λ hypernuclear production rate in the (π^-, K^+) reaction is 1.5×10^{-3} as compared to that in the (π^+, K^+) reaction. The production rate of $^{10}_{\Lambda}$Li at the beam momentum of 1.2 GeV/c is roughly twice higher than that at the beam momentum of 1.05 GeV/c.

We notice two important features of the reaction mechanism concerning the neutron-rich Λ hypernuclear production in contrast to the theoretical calculation based on a two-step mechanism with the meson charge-exchange. The production cross section is much smaller than expected in the calculation and the incident momentum dependence of the cross section shows opposite trend to that found in the calculation. Therefore the single-step process via a Σ^- admixture in the Λ hypernuclear state appearing due to the $\Sigma^- p \leftrightarrow \Lambda n$ coupling may contribute to the production. Further experimental as well as theoretical studies are necessary to understand the reaction mechanism.

2 Other hypernuclear experiments and future perspectives at J-PARC

I have also reported several experiments in hypernuclear physics at KEK and BNL including hypernuclear gamma-ray spectroscopy and double-Λ hypernuclear production. One of the main motivations of the hypernuclear gamma-ray spectroscopy is to observe γ transitions in several light Λ hypernuclear systems between the fine structures of Λ-hypernuclear states split by the ΛN spin-dependent interaction, such as the spin-orbit and spin-spin forces, and to extract the spin-dependent forces [10, 11]. One success is to determine a smaller spin-orbit interaction as compared to the nucleon case. Concerning the double-Λ hypernuclear production, we successfully observed a uniquely identified double-Λ hypernucleus $^{6}_{\Lambda\Lambda}$He by using the hybrid-emulsion technique, which gives an about four times smaller $\Lambda\Lambda$ interaction than previously believed [12]. In the BNL experiment E906 we are also claiming the production of the lightest double-Λ hypernucleus, $^{4}_{\Lambda\Lambda}$H, by using the Cylindrical Detector System [13].

All these hypernuclear physics will be more extensively pursued at J-PARC. We have already submitted six LOI's, which include the study of Ξ-

hypernucleus, double-Λ hypernucleus, hypernuclear gamma-ray spectroscopy and more exotic neutron-rich Λ hypernucleus, such as ${}^{6}_{\Lambda}$H. In the beginning we may have only one beam line with max. momentum of 1.8 GeV/c and reuse the present SKS with minor modifications, and would like to start the experiments around 2008. We want to have another beam line with max. momentum of 1.1 GeV/c and also a high-resolution, high-intensity beam line with a dispersion matching mode as early as possible, for which we may need additional budgets from all over the world.

References

1. Y. Akaishi *et al.*, Phys. Rev. Lett. **84**, 3539 (2000).
2. S. Shinmura *et al.*, J. Phys. G **28**, 1 (2002).
3. Y. Akaishi *et al.*, in: Proc. of the III Int. Workshop on Physics and Detectors For DAΦNE, Frascati Physics Series, Vol. XVI, 59 (2000).
4. K. Kubota *et al.*, Nucl. Phys. **A602**, 327 (1996).
5. M. Palomba *et al.*, in this Proceedings.
6. T. Yu. Tretyakova and D. E. Lanskoy, Phys. of Atomic Nuclei **66**, 1651 (2003).
7. T. Fukuda, *et al.*, KEK-PS-Proposal, (2002).
8. T. Fukuda *et al.*, Nucl. Inst. Meth. **A361**, 485 (1995).
9. Y. Akaishi, Nucl. Phys. **A738**, 80c (2004).
10. H. Tamura *et al.*, Phys. Rev. Lett. **84**, 5963 (2000).
11. H. Akikawa *et al.*, Phys. Rev. Lett. **88**, 082501 (2002).
12. H. Takahashi *et al.*, Phys. Rev. Lett. **87**, 212502 (2001).
13. J. K. Ahn *et al.*, Phys. Rev. Lett. **87**, 132504 (2001).

Frascati Physics Series Vol. XXXVI (2004), pp. 243–248
DAΦNE 2004: Physics at meson factories – Frascati, June 7-11, 2004
Selected Contribution in Plenary Session

NON-MESONIC WEAK DECAY OF ${}^{5}_{\Lambda}$He AND ${}^{12}_{\Lambda}$C AND THE EFFECT OF FSI ON ITS OBSERVABLES

H. Bhang *
School of Physics, Seoul National University, Seoul 151-747, Korea

Abstract

We have measured the emitted pair nucleons in the nonmesonic weak decay (NMWD) of ${}^{5}_{\Lambda}$He and ${}^{12}_{\Lambda}$C for the first time in coincidence method in the KEK-PS E462 and E508 experiments. We have clearly identified the prominent feature of back-to-back kinematics of NMWD and shown the Γ_n/Γ_p ratio close to 1/2. We still have to identify the contribution of two nucleon induced one in order to understand the NMWD. However, it is often mixed in with the effect of nuclear final state interaction (FSI). We have estimated the FSI effect on the singles nucleon number ratio and coincidence nucleon pair number ratio.

* On behalf of KEK-PS E462 and E508 Collaboration: S. Ajimura, K. Aoki, A. Banu, H. Bhang, T. Fukuda, O. Hashimoto, J.I. Hwang, S. Kameoka, B.H. Kang, E.H. Kim, J.H. Kim, M.J. Kim, T. Maruta, Y. Miura, Y. Miyake, T. Nagae, M. Nakamura, S.N. Nakamura, H. Noumi, S. Okada, Y. Okayasu, H. Outa, H. Park, P.K. Saha, Y. Sato, M. Sekimoto, T. Takahashi, H. Tamura, K. Tanida, A. Toyoda, K. Tsukada, T. Watanabe and H. Yim.

1 Introduction

The nonmesonic weak decay (NMWD) of Λ hypernuclei has attracted much attention during last couple of decades, since it provides an unique opportunity to study the strangeness changing baryonic weak interaction ΛN→NN, namely $\Lambda p \to np$ (Γ_p) and $\Lambda n \to nn$ (Γ_n). It also involves many important current issues, such as the long standing Γ_n/Γ_p ratio puzzle, the existence and the strength of the predicted two-nucleon ($2N$) induced NMWD components, ΛNN→nNN (Γ_{2N}), and the effect of nuclear final state interaction (FSI) on NMWD etc. All these are crucial issues in order to understand the weak decay mechanism of Λ hypernuclei and the strangeness changing baryonic weak interaction.

There has been a long standing concern on the Γ_n/Γ_p ratio of NMWD of Λ hypernuclei. Until a few years ago the experimental ratios have shown the ratio close to or greater than unity, implying the dominance of the neutron-induced channel while theoretical models for the ΔS=1 baryonic weak interaction predicted values much smaller than unity. We refer the details of the various models and their results on NMWD widths to the recent review article [1]. However more recently there has been an important developement finding the incorrect sign between pion and kaon exchange amplitude whose correction significantly increased the values of Γ_n/Γ_p [2]. Since then the direct quark interaction model calculation has produced the ratio for ${}^{5}_{\Lambda}$He up to 0.70. The heavy meson exchange model calculation of Jido *et al.* also reproduced the increased ratio of ${}^{12}_{\Lambda}$C reaching to 0.57 [1].

Important progresses have been made in the experimental studies of NMWD of Λ hypernuclei in a series of experiments at KEK. In the following sections, they will be introduced and discussed in terms of the effects of FSI on Γ_n/Γ_p ratio.

2 Experimental Progress

The accurate measurement of proton (E307) and neutron spectra (E369) of NMWD of ${}^{12}_{\Lambda}$C were reported [3, 4]. The quality of neutron spectrum of NMWD obtained in the experiment E369 was improved drastically both in the statistics and the signal to background (S/B) ratio over those of the previous one. With both proton and neutron spectra measured, Γ_n/Γ_p ratio was derived to

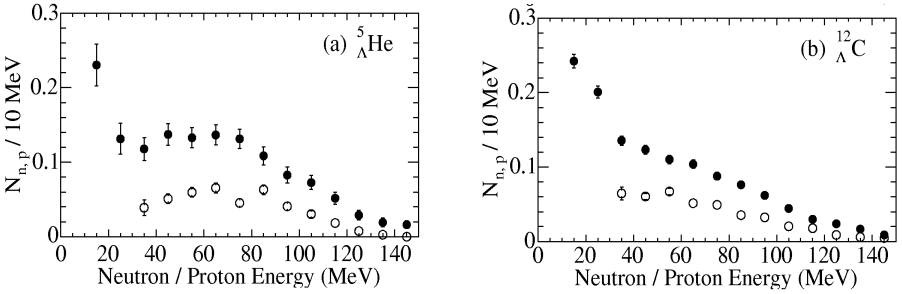

Figure 1: *Proton (open circle) and neutron (dark circle) spectra of the NMWD of* $^{5}_{\Lambda}$*He (a) and* $^{12}_{\Lambda}$*C(b) are shown* [5].

be about 0.5 directly from the measured neutron-to-proton number ratio cancelling out most of the FSI effect and considering NMWD 1N induced process. Recently we have reported the simultaneously measured spectra of neutrons and protons emitted in NMWD of $^{5}_{\Lambda}$He and $^{12}_{\Lambda}$C with much higher statistics than those of the previous experiments as shown in the fig.1 [5]. The neutron to proton yield ratios for both hypernuclei obtained with a much higher threshold energy (60 MeV) than that of the E307/E369 (40 MeV) were about two which suggests Γ_n/Γ_p ratios again about 0.5. However, the results still contained uncertainties due to the residual FSI effects and a possible large 2N induced NMWD contribution. Therefore, it was important and urgent to confirm the proton channel dominance and to establish the Γ_n/Γ_p ratio of NMWD unambiguously.

In order to remove such ambiguities, we have measured the emitted pair nucleons from the NMWD of $^{5}_{\Lambda}$He (E462) and $^{12}_{\Lambda}$C (E508) in coincidence method and determined the nucleon pair number ratio, N_{nn}/N_{np}, from the events of back-to-back opening angles which is the characteristics of two body kinematics of 1N NMWD [6, 7].

Fig.2 shows the normalized pair numbers, $N_{np(n)}(cos\theta)$, per NMWD in $cos\theta$ for $^{5}_{\Lambda}$He (left side) and $^{12}_{\Lambda}$C (right side). Upper figures show np pair distributions and lower ones nn pair distributions. Back to back peaking at $cos(\theta) = -1$ which is the signature of two body final state is clearly observed in both *np* and *nn* pair angular correlation. This is the first experimental observation of the Λp→np and Λn→nn 1N induced NMWD processes. N_{nn}/N_{np} ratios in the back-to-back kinematic region are shown in the tab.1 where N_{nn}

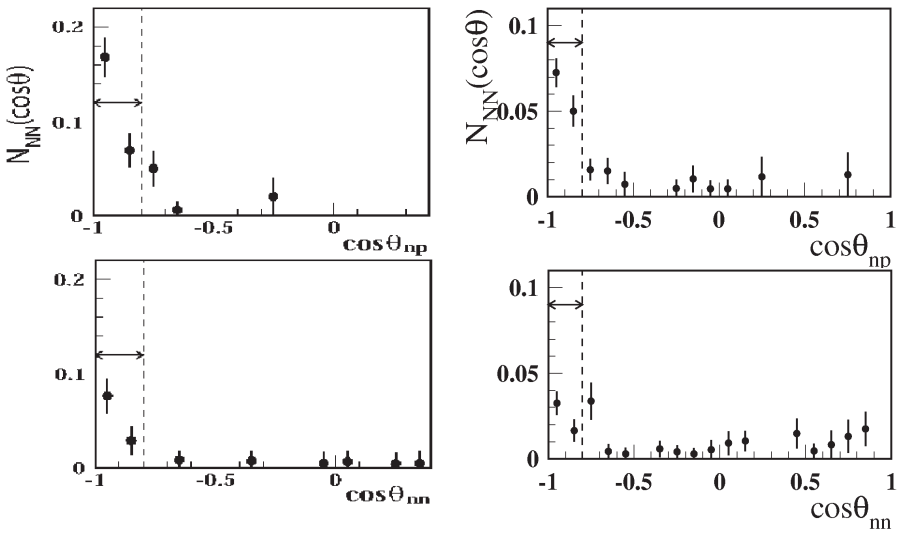

Figure 2: *Left side shows the Nnp(x)(above) and Nnn(x)(below) for* ${}^{5}_{\Lambda}He$ *and right side for those of* ${}^{12}_{\Lambda}C$*. x indicates cosθ.*

Table 1: N_n/N_p *and* N_{nn}/N_{np} *values from E462 and E508*

	Region	${}^{5}_{\Lambda}$He	${}^{12}_{\Lambda}$C
N_n/N_p	$E \geq 60MeV$	$2.17 \pm 0.15 \pm 0.16$	$2.00 \pm 0.09 \pm 0.14$
N_{nn}/N_{np}	$cos\theta \leq -0.9$	$0.45 \pm 0.11 \pm 0.04$	$0.45 \pm 0.11 \pm 0.04$
	$cos\theta \leq -0.8$		$0.40 \pm 0.09 \pm 0.04$
	$cos\theta \leq -0.7$		$0.60 \pm 0.12 \pm 0.04$

and N_{np} are the sum of $N_{NN}(cos\theta_i)$ over the back-to-back kinematic regions.

3 Effects of FSI on Γ_n/Γ_p

3.1 Inclusive nucleon number ratio of proton and neutron, N_n/N_p

Next we consider the effect of FSI on the Γ_n/Γ_p ratio. If we consider NMWD consisted of one nucleon induced ones only, namely proton- and neutron-induced channels, the normalized emitted neutron (proton) numbers per NMWD, $N_{n(p)}$, whose energies above a certain threshold energy can be written as

$$N_n \quad = \quad (2r_n + r_p)f_{nn} + r_p f_{pn}, \tag{1}$$

$$N_p \quad = \quad (2r_n + r_p)f_{np} + r_p f_{pp} \tag{2}$$

where r_p the branching ratio of the proton stimulated channel out of the NMWD so that r_n, that of neutron, is $1 - r_p$. f_{nn}(or f_{pp}) is the survival factor staying in the concerned range after the FSI with the residual nucleons while f_{np}(or f_{pn}) those due to the secondaries crossed over from the other channel. The crossed over contribution is not expected large in the high energy region. Considering the isospin independence of the strong interaction and the isospin symmetric propagating medium of carbon, we may assume $f_{nn} = f_{pp} = f$ and $f_{np} = f_{pn} = g$. Then the ratio of the neutron to proton number per NMWD can be expressed as

$$\frac{N_n}{N_p} = \frac{(2 - r_p) + r_p\beta}{(2 - r_p)\beta + r_p}. \tag{3}$$

When we apply $N_n/N_p = 0.69/0.4 = 1.73$ for the region of $E_N \geq 40$MeV from E307 and E369 spectra and β = g/f = (0.076, 0.11) extracted from the two currently available INC calculations, $\mathbf{\Gamma_n/\Gamma_p}(=r_n/r_p)$ becomes ($\mathbf{0.45}$, $\mathbf{0.51}$) for ${}^{12}_{\Lambda}$C. It is noted that these values are almost FSI model independent result and the first experimental result to show the proton channel dominance in the NMWD of Λ hypernuclei. Now this agrees very well with the recent theoretical predictions [1].

Similarly, we apply eq.3 to the N_n/N_p ratios shown in the tab.1 derived from the high statistics inclusive spectra of ${}^{5}_{\Lambda}$He (E462) and ${}^{12}_{\Lambda}$C (E508) shown in the fig.2 with a higher threshold energy, 60 MeV. Then we get $\mathbf{\Gamma_n/\Gamma_p}$ $\mathbf{0.61}(\mathbf{{}^{5}_{\Lambda}He})$ and $\mathbf{0.58}(\mathbf{{}^{12}_{\Lambda}C})$ when we use the β values of 60 MeV threshold energy 0.02 for ${}^{5}_{\Lambda}$He and 0.05 for ${}^{12}_{\Lambda}$C.

3.2 Coincidence nn and np nucleon pair number ratio, N_{nn}/N_{np}

In order to derive the Γ_n/Γ_p ratio from the N_n/N_p ratio of the singles spectra, we have made an assumption of 1N process of NMWD which cause the result some ambiguity due to 2N NMWD process. This ambiguity is removed when we measure both emitted nucleons, apply the back-to-back kinematics of 1N process and derive the Γ_n/Γ_p ratio from the pair number ratio, N_{nn}/N_{np}.

We can obtain the effect of FSI on the the nucleon pair number ratio similarly,

$$\frac{N_{nn}}{N_{np}} = \frac{r_n + r_p\beta'}{r_p + 2r_p\beta'}, \tag{4}$$

where N_{nn}/N_{np} values are shown in the tab.1 and β' is the reduced β due to the back-to-back opening angle selection. Here the assumption of $r_p + r_n = 1$ is removed. β' adopted for ${}^{12}_{\Lambda}$C were 0.059 ($cos\theta \leq$ -0.9), 0.066 ($cos\theta \leq$ -0.8) and 0.073 ($cos\theta \leq$ -0.7) while those for ${}^{5}_{\Lambda}$He $0.4{\cdot}\beta'({}^{12}_{\Lambda}$C). Then we get $\mathbf{\Gamma_n/\Gamma_p(= r_n/r_p)}$ $\mathbf{0.43}$ for $\mathbf{{}^{5}_{\Lambda}He}$ and $\mathbf{0.41}$ ($\mathbf{cos\theta \leq -0.9}$), $\mathbf{0.35}$ ($\mathbf{cos\theta \leq -0.8}$) and $\mathbf{0.59}$ ($\mathbf{cos\theta \leq -0.7}$) for $\mathbf{{}^{12}_{\Lambda}C}$.

Recent experimental results on NMWD at KEK-PS, of both singles and coincidence measurements, have shown the proton channel dominance with the Γ_n/Γ_p values close to 1/2. FSI effect have been estimated for N_n/N_p and N_{nn}/N_{np} ratio and Γ_n/Γ_p values are derived. The Γ_n/Γ_p from N_n/N_p tend to show about 20-30% bigger values than those from N_{nn}/N_{np}. We consider this difference due to the 2N NMWD contribution.

We are grateful to Prof. K.Nakamura and KEK-PS staff for the support of our experiment and stable operation of KEK-PS. Author H.B. acknowledges the support from the grants KOSEF (R01-2000-000-00019-0) and KRF (2003-070-C00015).

References

1. W. M. Alberico and G. Garbarino, Phys. Rep. **369**, 1 (2002), and references therein.
2. K. Sasaki, T. Inoue, and M. Oka, Nuc. Phys. A **669**, 331 (2000).
3. O. Hashimoto *et al.*, Phys. Rev. Lett. **88**, 042503 (2002), Y. Sato *et al.*, nucl-ex/0409007, submitted in Phys. Rev. C (2003).
4. J.H. Kim *et al*, Phys. Rev. C **68**, 065201 (2003).
5. S. Okada *et al.*, Phys. Lett. B **597**, 249 (2004).
6. B.H. Kang *et al.*, Ph.D. Dissertation, Seoul National University (2004).
7. M.J. Kim *et al.*, in this proceedings.

Frascati Physics Series Vol. XXXVI (2004), pp. 243–248
DAΦNE 2004: Physics at meson factories – Frascati, June 7-11, 2004
Selected Contribution in Plenary Session

NON-MESONIC WEAK DECAY OF ${}^{5}_{\Lambda}$He AND ${}^{12}_{\Lambda}$C AND THE EFFECT OF FSI ON ITS OBSERVABLES

H. Bhang *
School of Physics, Seoul National University, Seoul 151-747, Korea

Abstract

We have measured the emitted pair nucleons in the nonmesonic weak decay (NMWD) of ${}^{5}_{\Lambda}$He and ${}^{12}_{\Lambda}$C for the first time in coincidence method in the KEK-PS E462 and E508 experiments. We have clearly identified the prominent feature of back-to-back kinematics of NMWD and shown the Γ_n/Γ_p ratio close to 1/2. We still have to identify the contribution of two nucleon induced one in order to understand the NMWD. However, it is often mixed in with the effect of nuclear final state interaction (FSI). We have estimated the FSI effect on the singles nucleon number ratio and coincidence nucleon pair number ratio.

* On behalf of KEK-PS E462 and E508 Collaboration: S. Ajimura, K. Aoki, A. Banu, H. Bhang, T. Fukuda, O. Hashimoto, J.I. Hwang, S. Kameoka, B.H. Kang, E.H. Kim, J.H. Kim, M.J. Kim, T. Maruta, Y. Miura, Y. Miyake, T. Nagae, M. Nakamura, S.N. Nakamura, H. Noumi, S. Okada, Y. Okayasu, H. Outa, H. Park, P.K. Saha, Y. Sato, M. Sekimoto, T. Takahashi, H. Tamura, K. Tanida, A. Toyoda, K. Tsukada, T. Watanabe and H. Yim.

1 Introduction

The nonmesonic weak decay (NMWD) of Λ hypernuclei has attracted much attention during last couple of decades, since it provides an unique opportunity to study the strangeness changing baryonic weak interaction ΛN→NN, namely $\Lambda p \to np$ (Γ_p) and $\Lambda n \to nn$ (Γ_n). It also involves many important current issues, such as the long standing Γ_n/Γ_p ratio puzzle, the existence and the strength of the predicted two-nucleon ($2N$) induced NMWD components, ΛNN→nNN (Γ_{2N}), and the effect of nuclear final state interaction (FSI) on NMWD etc. All these are crucial issues in order to understand the weak decay mechanism of Λ hypernuclei and the strangeness changing baryonic weak interaction.

There has been a long standing concern on the Γ_n/Γ_p ratio of NMWD of Λ hypernuclei. Until a few years ago the experimental ratios have shown the ratio close to or greater than unity, implying the dominance of the neutron-induced channel while theoretical models for the ΔS=1 baryonic weak interaction predicted values much smaller than unity. We refer the details of the various models and their results on NMWD widths to the recent review article [1]. However more recently there has been an important developement finding the incorrect sign between pion and kaon exchange amplitude whose correction significantly increased the values of Γ_n/Γ_p [2]. Since then the direct quark interaction model calculation has produced the ratio for ${}^{5}_{\Lambda}$He up to 0.70. The heavy meson exchange model calculation of Jido *et al.* also reproduced the increased ratio of ${}^{12}_{\Lambda}$C reaching to 0.57 [1].

Important progresses have been made in the experimental studies of NMWD of Λ hypernuclei in a series of experiments at KEK. In the following sections, they will be introduced and discussed in terms of the effects of FSI on Γ_n/Γ_p ratio.

2 Experimental Progress

The accurate measurement of proton (E307) and neutron spectra (E369) of NMWD of ${}^{12}_{\Lambda}$C were reported [3, 4]. The quality of neutron spectrum of NMWD obtained in the experiment E369 was improved drastically both in the statistics and the signal to background (S/B) ratio over those of the previous one. With both proton and neutron spectra measured, Γ_n/Γ_p ratio was derived to

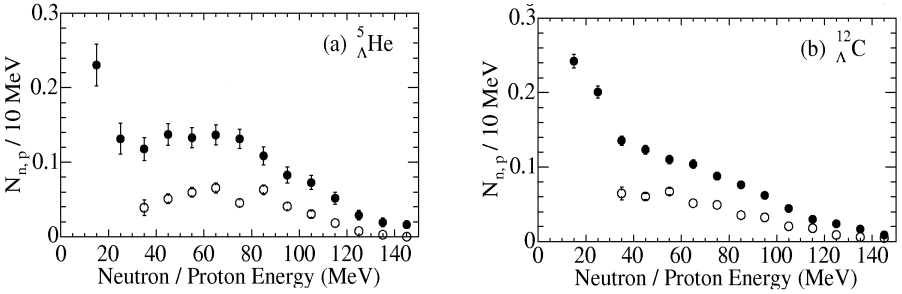

Figure 1: *Proton (open circle) and neutron (dark circle) spectra of the NMWD of* $^{5}_{\Lambda}$*He (a) and* $^{12}_{\Lambda}$*C(b) are shown* [5].

be about 0.5 directly from the measured neutron-to-proton number ratio cancelling out most of the FSI effect and considering NMWD 1N induced process. Recently we have reported the simultaneously measured spectra of neutrons and protons emitted in NMWD of $^{5}_{\Lambda}$He and $^{12}_{\Lambda}$C with much higher statistics than those of the previous experiments as shown in the fig.1 [5]. The neutron to proton yield ratios for both hypernuclei obtained with a much higher threshold energy (60 MeV) than that of the E307/E369 (40 MeV) were about two which suggests Γ_n/Γ_p ratios again about 0.5. However, the results still contained uncertainties due to the residual FSI effects and a possible large 2N induced NMWD contribution. Therefore, it was important and urgent to confirm the proton channel dominance and to establish the Γ_n/Γ_p ratio of NMWD unambiguously.

In order to remove such ambiguities, we have measured the emitted pair nucleons from the NMWD of $^{5}_{\Lambda}$He (E462) and $^{12}_{\Lambda}$C (E508) in coincidence method and determined the nucleon pair number ratio, N_{nn}/N_{np}, from the events of back-to-back opening angles which is the characteristics of two body kinematics of 1N NMWD [6, 7].

Fig.2 shows the normalized pair numbers, $N_{np(n)}(cos\theta)$, per NMWD in $cos\theta$ for $^{5}_{\Lambda}$He (left side) and $^{12}_{\Lambda}$C (right side). Upper figures show np pair distributions and lower ones nn pair distributions. Back to back peaking at $cos(\theta) = -1$ which is the signature of two body final state is clearly observed in both *np* and *nn* pair angular correlation. This is the first experimental observation of the Λp→np and Λn→nn 1N induced NMWD processes. N_{nn}/N_{np} ratios in the back-to-back kinematic region are shown in the tab.1 where N_{nn}

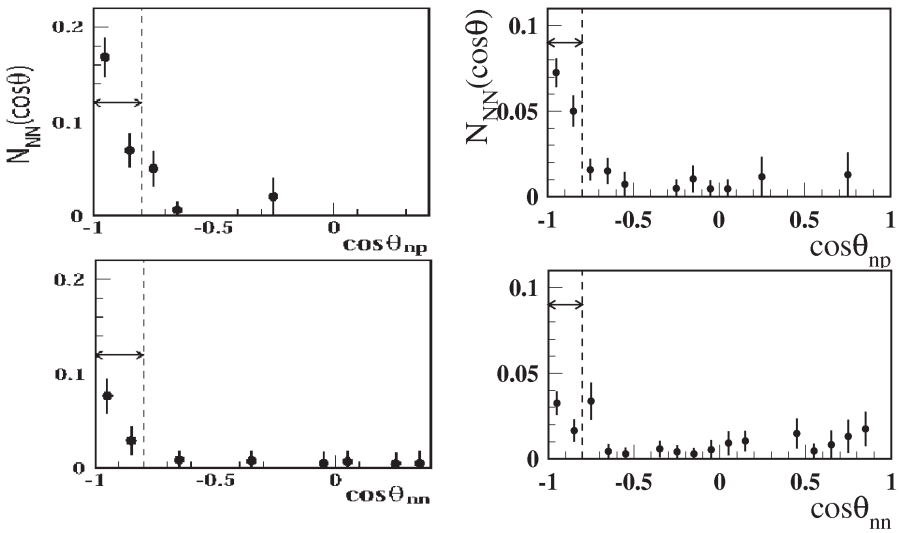

Figure 2: *Left side shows the Nnp(x)(above) and Nnn(x)(below) for* ${}^{5}_{\Lambda}He$ *and right side for those of* ${}^{12}_{\Lambda}C$*. x indicates cosθ.*

Table 1: N_n/N_p *and* N_{nn}/N_{np} *values from E462 and E508*

	Region	${}^{5}_{\Lambda}$He	${}^{12}_{\Lambda}$C
N_n/N_p	$E \geq 60MeV$	$2.17 \pm 0.15 \pm 0.16$	$2.00 \pm 0.09 \pm 0.14$
N_{nn}/N_{np}	$cos\theta \leq -0.9$	$0.45 \pm 0.11 \pm 0.04$	$0.45 \pm 0.11 \pm 0.04$
	$cos\theta \leq -0.8$		$0.40 \pm 0.09 \pm 0.04$
	$cos\theta \leq -0.7$		$0.60 \pm 0.12 \pm 0.04$

and N_{np} are the sum of $N_{NN}(cos\theta_i)$ over the back-to-back kinematic regions.

3 Effects of FSI on Γ_n/Γ_p

3.1 Inclusive nucleon number ratio of proton and neutron, N_n/N_p

Next we consider the effect of FSI on the Γ_n/Γ_p ratio. If we consider NMWD consisted of one nucleon induced ones only, namely proton- and neutron-induced channels, the normalized emitted neutron (proton) numbers per NMWD, $N_{n(p)}$, whose energies above a certain threshold energy can be written as

$$N_n \quad = \quad (2r_n + r_p)f_{nn} + r_p f_{pn}, \tag{1}$$

$$N_p \quad = \quad (2r_n + r_p)f_{np} + r_p f_{pp} \tag{2}$$

where r_p the branching ratio of the proton stimulated channel out of the NMWD so that r_n, that of neutron, is $1 - r_p$. f_{nn}(or f_{pp}) is the survival factor staying in the concerned range after the FSI with the residual nucleons while f_{np}(or f_{pn}) those due to the secondaries crossed over from the other channel. The crossed over contribution is not expected large in the high energy region. Considering the isospin independence of the strong interaction and the isospin symmetric propagating medium of carbon, we may assume $f_{nn} = f_{pp} = f$ and $f_{np} = f_{pn} = g$. Then the ratio of the neutron to proton number per NMWD can be expressed as

$$\frac{N_n}{N_p} = \frac{(2 - r_p) + r_p\beta}{(2 - r_p)\beta + r_p}. \tag{3}$$

When we apply $N_n/N_p = 0.69/0.4 = 1.73$ for the region of $E_N \geq 40$MeV from E307 and E369 spectra and β = g/f = (0.076, 0.11) extracted from the two currently available INC calculations, $\mathbf{\Gamma_n/\Gamma_p}(=r_n/r_p)$ becomes ($\mathbf{0.45}$, $\mathbf{0.51}$) for ${}^{12}_{\Lambda}$C. It is noted that these values are almost FSI model independent result and the first experimental result to show the proton channel dominance in the NMWD of Λ hypernuclei. Now this agrees very well with the recent theoretical predictions [1].

Similarly, we apply eq.3 to the N_n/N_p ratios shown in the tab.1 derived from the high statistics inclusive spectra of ${}^{5}_{\Lambda}$He (E462) and ${}^{12}_{\Lambda}$C (E508) shown in the fig.2 with a higher threshold energy, 60 MeV. Then we get $\mathbf{\Gamma_n/\Gamma_p}$ $\mathbf{0.61}(\mathbf{{}^{5}_{\Lambda}He})$ and $\mathbf{0.58}(\mathbf{{}^{12}_{\Lambda}C})$ when we use the β values of 60 MeV threshold energy 0.02 for ${}^{5}_{\Lambda}$He and 0.05 for ${}^{12}_{\Lambda}$C.

3.2 Coincidence nn and np nucleon pair number ratio, N_{nn}/N_{np}

In order to derive the Γ_n/Γ_p ratio from the N_n/N_p ratio of the singles spectra, we have made an assumption of 1N process of NMWD which cause the result some ambiguity due to 2N NMWD process. This ambiguity is removed when we measure both emitted nucleons, apply the back-to-back kinematics of 1N process and derive the Γ_n/Γ_p ratio from the pair number ratio, N_{nn}/N_{np}.

We can obtain the effect of FSI on the the nucleon pair number ratio similarly,

$$\frac{N_{nn}}{N_{np}} = \frac{r_n + r_p\beta'}{r_p + 2r_p\beta'}, \tag{4}$$

where N_{nn}/N_{np} values are shown in the tab.1 and β' is the reduced β due to the back-to-back opening angle selection. Here the assumption of $r_p + r_n = 1$ is removed. β' adopted for ${}^{12}_{\Lambda}$C were 0.059 ($cos\theta \leq$ -0.9), 0.066 ($cos\theta \leq$ -0.8) and 0.073 ($cos\theta \leq$ -0.7) while those for ${}^{5}_{\Lambda}$He $0.4{\cdot}\beta'({}^{12}_{\Lambda}$C). Then we get $\mathbf{\Gamma_n/\Gamma_p(= r_n/r_p)}$ $\mathbf{0.43}$ for $\mathbf{{}^{5}_{\Lambda}He}$ and $\mathbf{0.41}$ ($\mathbf{cos\theta \leq -0.9}$), $\mathbf{0.35}$ ($\mathbf{cos\theta \leq -0.8}$) and $\mathbf{0.59}$ ($\mathbf{cos\theta \leq -0.7}$) for $\mathbf{{}^{12}_{\Lambda}C}$.

Recent experimental results on NMWD at KEK-PS, of both singles and coincidence measurements, have shown the proton channel dominance with the Γ_n/Γ_p values close to 1/2. FSI effect have been estimated for N_n/N_p and N_{nn}/N_{np} ratio and Γ_n/Γ_p values are derived. The Γ_n/Γ_p from N_n/N_p tend to show about 20-30% bigger values than those from N_{nn}/N_{np}. We consider this difference due to the 2N NMWD contribution.

We are grateful to Prof. K.Nakamura and KEK-PS staff for the support of our experiment and stable operation of KEK-PS. Author H.B. acknowledges the support from the grants KOSEF (R01-2000-000-00019-0) and KRF (2003-070-C00015).

References

1. W. M. Alberico and G. Garbarino, Phys. Rep. **369**, 1 (2002), and references therein.
2. K. Sasaki, T. Inoue, and M. Oka, Nuc. Phys. A **669**, 331 (2000).
3. O. Hashimoto *et al.*, Phys. Rev. Lett. **88**, 042503 (2002), Y. Sato *et al.*, nucl-ex/0409007, submitted in Phys. Rev. C (2003).
4. J.H. Kim *et al*, Phys. Rev. C **68**, 065201 (2003).
5. S. Okada *et al.*, Phys. Lett. B **597**, 249 (2004).
6. B.H. Kang *et al.*, Ph.D. Dissertation, Seoul National University (2004).
7. M.J. Kim *et al.*, in this proceedings.

Frascati Physics Series Vol. XXXVI (2004), pp. 249–253
DAΦNE 2004: Physics at meson factories – Frascati, June 7-11, 2004
Short Talk in Plenary Session

TOWARDS A SOLUTION OF THE Γ_n/Γ_p PUZZLE IN THE WEAK DECAY OF Λ–HYPERNUCLEI

W. M. Alberico[1], G. Garbarino[1], A. Parrẽno[2] and A. Ramos[2]
presented by G. Garbarino[1]
[1] *Dipartimento di Fisica Teorica, Università di Torino and INFN, Sezione di Torino, I–10125 Torino, Italy*
[2] *Departament d'Estructura i Constituents de la Matèria, Universitat de Barcelona, E–08028 Barcelona, Spain*

1 Introduction

For many years, a theoretical explanation of the large experimental values of the ratio, Γ_n/Γ_p, between the neutron– and proton–induced non–mesonic decay widths, $\Gamma(\Lambda n \to nn)$ and $\Gamma(\Lambda p \to np)$, of Λ–hypernuclei has been missing [1)]. In this contribution we discuss some results of a calculation [2)] of nucleon–nucleon coincidence distributions for the hypernuclear non–mesonic weak decay (NMWD). The work is motivated by the fact that correlation observables are expected to allow a cleaner extraction of Γ_n/Γ_p from data than single–nucleon observables. Moreover, coincidence experiments have been performed recently at KEK [3)].

A one–meson–exchange model for the $\Lambda N \to nN$ processes in finite nuclei has been combined with an intranuclear cascade code, which takes into

account the nucleon final state interactions (FSI). The $\Lambda NN \to nNN$ process is included by treating the nuclear finite size effects via a local density approximation scheme. For details on the models employed see Ref. [2].

Preliminary results for the angular asymmetries in the NMWD of polarized Λ–hypernuclei are also presented.

2 Coincidence observables and determination of Γ_n/Γ_p

The ratio, $N_{nn}^{\rm wd}/N_{np}^{\rm wd}$, between the number of weak decay nn and np pairs equals Γ_n/Γ_p. Due to FSI and two–body induced decays, one predicts:

$$\frac{\Gamma_n}{\Gamma_p} \equiv \frac{N_{nn}^{\rm wd}}{N_{np}^{\rm wd}} \neq \frac{N_{nn}}{N_{np}} \equiv R_2\left[\Delta\theta_{12}, \Delta T_n, \Delta T_p\right], \tag{1}$$

when the observable numbers N_{nn} and N_{np} are determined by employing particular pair opening angle and nucleon kinetic energy intervals. The results of Ref. [2] clearly show the dependence of N_{nn}/N_{np} on $\Delta\theta_{12}$, ΔT_n and ΔT_p; N_{nn}/N_{np} turns out to be much less sensitive to FSI effects and variations of energy cuts and angular restrictions than N_{nn} and N_{np} separately.

The numbers of nucleon pairs N_{NN} —which we consider to be normalized per NMWD— are related to the corresponding quantities for the neutron ($N_{NN}^{\rm 1Bn}$) proton ($N_{NN}^{\rm 1Bp}$) and two–nucleon ($N_{NN}^{\rm 2B}$) induced processes by:

$$N_{NN} = \frac{N_{NN}^{\rm 1Bn}\,\Gamma_n + N_{NN}^{\rm 1Bp}\,\Gamma_p + N_{NN}^{\rm 2B}\,\Gamma_2}{\Gamma_n + \Gamma_p + \Gamma_2} \equiv N_{NN}^{\Lambda n\to nn} + N_{NN}^{\Lambda p\to np} + N_{NN}^{\Lambda np\to nnp}, \tag{2}$$

where $N_{NN}^{\rm 1Bn} \equiv N_{NN}^{\Lambda n\to nn}(\Gamma_n+\Gamma_p+\Gamma_2)/\Gamma_n$, etc.

In Table 1 the ratios N_{nn}/N_{np} predicted by the one–pion–exchange (OPE) and one–meson–exchange models (OMEa and OMEf, using NSC97a and NSC97f potentials, respectively) for ${}^{5}_{\Lambda}$He and ${}^{12}_{\Lambda}$C are given for the back–to–back kinematics ($\cos\theta_{NN} \leq -0.8$) and nucleon kinetic energies $T_n, T_p \geq 30$ MeV. The OMEa and OMEf results are in agreement with the preliminary KEK data: this comparison provides an indication for a ratio $\Gamma_n/\Gamma_p \simeq 0.3$ in both hypernuclei.

We have then performed a weak–decay–model independent analysis of KEK coincidence data. The 6 weak–decay–model independent quantities $N_{nn}^{\rm 1Bn}$,

Table 1: *Predictions for* $R_2 \equiv N_{nn}/N_{np}$ *in* ${}^{5}_{\Lambda}He$ *and* ${}^{12}_{\Lambda}C$*. The (preliminary) data are from KEK–E462 and KEK–E508* [3].

	${}^{5}_{\Lambda}$He		${}^{12}_{\Lambda}$C	
Model	N_{nn}/N_{np}	Γ_n/Γ_p	N_{nn}/N_{np}	Γ_n/Γ_p
OPE	0.25	0.09	0.24	0.08
OMEa	0.51	0.34	0.39	0.29
OMEf	0.61	0.46	0.43	0.34
EXP	0.44 ± 0.11		0.40 ± 0.09	

$N_{nn}^{1\mathrm{Bp}}$, $N_{nn}^{2\mathrm{B}}$, $N_{np}^{1\mathrm{Bn}}$, $N_{np}^{1\mathrm{Bp}}$ and $N_{np}^{2\mathrm{B}}$ of Eq. (2) are used to evaluate Γ_n/Γ_p as:

$$\frac{\Gamma_n}{\Gamma_p} = \frac{N_{nn}^{1\mathrm{Bp}} + N_{nn}^{2\mathrm{B}}\frac{\Gamma_2}{\Gamma_1} - \left(N_{np}^{1\mathrm{Bp}} + N_{np}^{2\mathrm{B}}\frac{\Gamma_2}{\Gamma_1}\right)\frac{N_{nn}}{N_{np}}}{\left(N_{np}^{1\mathrm{Bn}} + N_{np}^{2\mathrm{B}}\frac{\Gamma_2}{\Gamma_1}\right)\frac{N_{nn}}{N_{np}} - N_{nn}^{1\mathrm{Bn}} - N_{nn}^{2\mathrm{B}}\frac{\Gamma_2}{\Gamma_1}}, \tag{3}$$

from appropriate Γ_2/Γ_1 values. By using the KEK data of Table 1 we obtain:

$$\frac{\Gamma_n}{\Gamma_p}\left({}^{5}_{\Lambda}\mathrm{He}\right) = 0.39 \pm 0.11 \ \text{ if } \ \Gamma_2 = 0 \ , \frac{\Gamma_n}{\Gamma_p}\left({}^{5}_{\Lambda}\mathrm{He}\right) = 0.26 \pm 0.11 \ \text{ if } \ \frac{\Gamma_2}{\Gamma_1} = 0.2, \tag{4}$$

$$\frac{\Gamma_n}{\Gamma_p}\left({}^{12}_{\Lambda}\mathrm{C}\right) = 0.38 \pm 0.14 \ \text{ if } \ \Gamma_2 = 0 \ , \frac{\Gamma_n}{\Gamma_p}\left({}^{12}_{\Lambda}\mathrm{C}\right) = 0.29 \pm 0.14 \ \text{ if } \ \frac{\Gamma_2}{\Gamma_1} = 0.25. \tag{5}$$

These values are substantially smaller than those obtained from single–nucleon spectra analyses and are in agreement with pure theoretical predictions [4]. In our opinion, this represents an important progress towards the solution of the Γ_n/Γ_p puzzle.

Forthcoming data from KEK and FINUDA [5] could be directly compared with the results reported here and in Ref. [2]. This will permit to achieve better determinations of Γ_n/Γ_p and to establish the first constraints on Γ_2/Γ_1.

3 The asymmetry puzzle

An intriguing open problem concerns an angular asymmetry in the emission of NMWD protons from polarized hypernuclei. While theory predicts a negative intrinsic Λ asymmetry a_Λ, with a moderate dependence on the hypernucleus, the measurements seem to favor $a_\Lambda^{\mathrm{M}}({}^{5}_{\Lambda}\vec{\mathrm{He}}) > 0$ and $a_\Lambda^{\mathrm{M}}({}^{12}_{\Lambda}\vec{\mathrm{C}}) < 0$. However, while one predicts $a_\Lambda({}^{5}_{\Lambda}\vec{\mathrm{He}}) \simeq a_\Lambda({}^{12}_{\Lambda}\vec{\mathrm{C}})$, there is no known reason to expect

Table 2: *Results for the proton intensities from the NMWD of* ${}^{5}_{\Lambda}\vec{\rm He}$ *and* ${}^{12}_{\Lambda}\vec{\rm C}$.

Model	${}^{5}_{\Lambda}\vec{\rm He}$ $I_0^{\rm M}$	$a_\Lambda^{\rm M}$	${}^{12}_{\Lambda}\vec{\rm C}$ $I_0^{\rm M}$	$a_\Lambda^{\rm M}$
Without FSI	0.69	-0.68	0.75	-0.73
FSI and $T_p^{\rm th}=0$	1.27	-0.30	2.78	-0.16
FSI and $T_p^{\rm th}=30$ MeV	0.77	-0.46	1.05	-0.37
FSI and $T_p^{\rm th}=50$ MeV	0.59	-0.52	0.65	-0.51
FSI and $T_p^{\rm th}=70$ MeV	0.39	-0.55	0.38	-0.65
KEK [7]		0.07 ± 0.08		-0.44 ± 0.32

this approximate equality to be valid for the observable asymmetry, $a_\Lambda^{\rm M}$. To overcome this problem, we are evaluating [6] the effects of the nucleon FSI on the NMWD of polarized hypernuclei and performing the first calculation of $a_\Lambda^{\rm M}$.

In table 2 we show preliminary OMEf results for the weak decay and observable proton intensities, $I(\theta)=I_0(1+p_\Lambda\,a_\Lambda\cos\theta)$ and $I^{\rm M}(\theta)=I_0^{\rm M}(1+p_\Lambda\,a_\Lambda^{\rm M}\cos\theta)$, respectively, for ${}^{5}_{\Lambda}\vec{\rm He}$ and ${}^{12}_{\Lambda}\vec{\rm C}$. As a result of the nucleon FSI, $|a_\Lambda|\gtrsim|a_\Lambda^{\rm M}|$ for any value of the proton kinetic energy threshold: when $T_p^{\rm th}=0$, $a_\Lambda/a_\Lambda^{\rm M}\simeq 2$ for ${}^{5}_{\Lambda}\vec{\rm He}$ and $a_\Lambda/a_\Lambda^{\rm M}\simeq 4$ for ${}^{12}_{\Lambda}\vec{\rm C}$; $|a_\Lambda^{\rm M}|$ increases with $T_p^{\rm th}$ and $a_\Lambda/a_\Lambda^{\rm M}\simeq 1$ for $T_p^{\rm th}=70$ MeV in both cases. The KEK data quoted in the table correspond to a $T_p^{\rm th}$ varying between 30 and 50 MeV: our corresponding predictions agree (disagree) with the ${}^{12}_{\Lambda}\vec{\rm C}$ (${}^{5}_{\Lambda}\vec{\rm He}$) datum.

FSI turn out to be an important ingredient also when studying the NMWD of polarized hypernuclei, but they cannot explain the present asymmetry data. In our opinion, new and improved experiments more clearly establishing the sign and magnitude of $a_\Lambda^{\rm M}$ for s– and p–shell hypernuclei are necessary to disclose the origin of the asymmetry puzzle.

Acknowledgements

Work supported by EURIDICE HPRN–CT–2002–00311 and INFN. Discussions with H. Bhang, T. Maruta, T. Nagae and H. Outa are acknowledged.

References

1. W. M. Alberico and G. Garbarino, *Phys. Rep.* **369**, 1 (2002); E. Oset and A. Ramos, *Prog. Part. Nucl. Phys.* **41**, 191 (1998).

2. G. Garbarino, A. Parreño and A. Ramos, *Phys. Rev. Lett.* **91**, 112501 (2003); *Phys. Rev.* **C 69**, 054603 (2004).

3. H. Outa, *International School of Physics Enrico Fermi*, CLVIII Course, *Hadron Physics*, Varenna, Italy [IOS Press, Amsterdam (to be published)].

4. K. Sasaki, T. Inoue and M. Oka, *Nucl. Phys.* **A 669**, 331 (2000); **A 678**, 455(E) (2000); D. Jido, E. Oset and J. E. Palomar, *Nucl. Phys.* **A 694**, 525 (2001); A. Parreño and A. Ramos, *Phys. Rev.* **C 65**, 015204 (2002); K. Itonaga, T. Ueda and T. Motoba, *Phys. Rev.* **C 65**, 034617 (2002).

5. A. Feliciello, *Nucl. Phys.* **A 691**, 170c (2001).

6. W. M. Alberico, G. Garbarino, A. Parreño and A. Ramos, in preparation.

7. T. Maruta et al., *Eighth International Conference on Hypernuclear and Strange Particle Physics* (HYP2003), JLAB, Newport News, Virginia, nucl-ex/0402017 [*Nucl. Phys.* **A** (to be published)].

Session IV — Rare/Forbidden Decays Physics

(Chairpersons: Y. Akaishi, E. Blucher)

L.M. Sehgal	Rare Decays as Window to New Physics
V. Sharma	Rare B/D Decays
L. Mir	Rare Hadronic B Decays
G. Redlinger	Rare Kaon Decays: il Buono, il Brutto, il Cattivo
T. Sekiguchi	Recent Results on $K^+ \to \pi^+ \nu\bar{\nu}$
G. Ruggiero	NA48 Results on Kaon Rare Decays
N. Cabibbo	The a_0–a_2 Pion Scattering Lenght from $K^+ \to \pi^+\pi^0\pi^0$ Decays
M. Martini	A Direct Search for $K_s \to 3\,\pi^0$ Decay at Kloe
T. Komatsubara	Future Kaon Program at KEK/J–PARC
C. Smith	Recent Progress on the Rare Decay $K_L \to \pi^0\mu^+\mu^-$

Frascati Physics Series Vol. XXXVI (2004), pp. 257–264
DAΦNE 2004: Physics at meson factories – Frascati, June 7-11, 2004
Invited Review Talk in Plenary Session

RARE DECAYS AS WINDOW TO NEW PHYSICS

L. M. Sehgal
Institute for Theoretical Physics, RWTH Aachen
D-52056 Aachen, Germany

Abstract

Rare decays of K mesons are reviewed from the perspective of testing the "ones" and "zeros" of the standard model. Decays $K^+ \to \pi^+ \nu\overline{\nu}$ and $K_L \to \pi^0 \nu\overline{\nu}$ probe the one-loop effective Hamiltonian for $s \to d\nu\overline{\nu}$, and can constrain the ρ, η coordinates of the unitarity triangle. Decays such as $K_L \to \pi^0 l^+ l^-$, $K_L \to \mu^+\mu^-$, $K^+ \to \pi^+ l^+ l^-$ and $K_L \to \pi^+\pi^- e^+ e^-$ involve short-distance effects, as well as long-distance photon-induced contributions. Some comments are added on curious features of electroweak amplitudes in the "gaugeless" limit, and in the chiral electron limit $m_e \to 0$.

1 Ones and Zeros of the Standard Model

The study of rare decays may be regarded as a part of the endeavor to test the principles of symmetry and symmetry-breaking underlying the standard model

of weak interactions. In any theory based on symmetries, the most important numbers are the "ones" and "zeros", the intensity rules and selection rules. In the case of the standard model, the ones and zeros are associated with the unitarity of the quark-mixing matrix, e.g.

$$|V_{ud}|^2 + |V_{us}|^2 + |V_{ub}|^2 = 1 \text{ (ONE)} \quad (1)$$

$$V_{ud}V_{us}^* + V_{cd}V_{cs}^* + V_{td}V_{ts}^* = 0 \text{ (ZERO)} \quad (2)$$

Physically, Eq. (1) expresses the universality of the lepton and hadron charged current couplings. The present status of this relation may be judged from the empirical results [1] $|V_{ud}| = 0.9738(5)$, $|V_{us}| = 0.2200(26)$, and $|V_{ub}| = (3.67(47)) \times 10^{-3}$, which satisfy Eq. (1) to within a deficit $\Delta = 0.0033(21)$.

The zero in Eq. (2) represents a *unitarity triangle*, and is one of six that encode the structure of CP violation in the weak nonleptonic Hamiltonian. These triangles have diverse shapes, corresponding to the diversity of the elements V_{ij}. There is, however, a unity in this diversity: all unitarity triangles have the same area A_Δ, as a consequence of the fact that 3×3 unitary matrices have an invariant property given by the Jarlskog parameter

$$J = \mathrm{Im}(\lambda_t \lambda_u^*) = \mathrm{Im}(\lambda_u \lambda_c^*) \quad (3)$$

where $\lambda_u = V_{us}V_{ud}^*$, $\lambda_t = V_{ts}V_{td}^*$, $\lambda_c = V_{cs}V_{cd}^*$ with $\lambda_u + \lambda_c + \lambda_t = 0$, and $|J| = 2A_\Delta$. This invariant is a universal measure of CP violation in weak phenomena. In addition, the existence of unitarity triangles implies a unification of CP-violating and CP-conserving observables. The sides of a triangle are determined by the moduli $|V_{ij}|$, measurable in CP-conserving processes. Knowledge of the sides fixes the angles, which are measures of CP violation. This property, as well as the universal area of unitarity triangles, is a feature specific to a world with three generations.

The zero in Eq. (2) has ramifications for flavour-changing neutral currents (FCNC). To order G_F, the weak neutral current has the structure

$$J_\mu^{\mathrm{NC}} = (\overline{d},\, \overline{s},\, \overline{b})\gamma_\mu \frac{1-\gamma_5}{2} V^\dagger V (d,\, s,\, b)^{\mathrm{tr}} \quad (4)$$

and the unitarity of the matrix V ensures the absence of non-diagonal terms. However, the symmetries which lead to the FCNC zero are broken in the standard model by Yukawa couplings of the scalar doublet $(\varphi^+,\, \varphi^0)$ to fermions.

For a typical doublet $(t,\, b)$, the Yukawa interaction is

$$\mathcal{L}_{\rm Y} = y_b(\overline{t}_L,\, \overline{b}_L) \begin{pmatrix} \varphi^+ \\ \varphi^0 \end{pmatrix} b_R + y_t(\overline{t}_L,\, \overline{b}_L) \begin{pmatrix} \varphi^{0\dagger} \\ -\varphi^- \end{pmatrix} t_R \tag{5}$$

with $y_b = \sqrt{2}m_b/v$, $y_t = \sqrt{2}m_t/v$ (note that y_t is very nearly unity). These Yukawa couplings break chiral symmetry and give rise to a FCNC interaction like $(\overline{s}d)_{V-A}(\overline{\nu}\nu)_{V-A}$ at the level of one-loop (box and penguin) diagrams. Thus a typical FCNC amplitude has the form

$$A_{\rm FCNC} = G_F[0] + G_F\alpha \sum_{i=u,c,t} \lambda_i f(m_i). \tag{6}$$

2 Rare K Decays

2.1 Golden Modes: $K^+ \to \pi^+\nu\overline{\nu}$ and $K_L \to \pi^0\nu\overline{\nu}$

These two channels can be computed in an essentially model independent way from the effective Hamiltonian for $s \to d\nu\overline{\nu}$. The hadronic matrix element $\langle\pi^+|(\overline{d}s)_{V-A}|K^+\rangle$ can be related to the K_{l3} matrix element, and long-distance effects are negligible [2]. The effective Hamiltonian derived from the box and penguin diagrams is [3]

$$H_{\rm eff} = \frac{G_F}{\sqrt{2}} \frac{\alpha}{2\pi \sin^2\theta_W} \left[\lambda_c X_{NL} + \lambda_t X_t\right] (\overline{d}s)_{V-A}(\overline{\nu}\nu)_{V-A} \tag{7}$$

where X_{NL} is a small contribution due to c-quarks, and the dominant term is

$$X_t(x_t) = \frac{x_t}{8}\left[-\frac{2+x_t}{1-x_t} + \frac{3x_t-6}{(1-x_t)^2}\ln x_t\right] \tag{8}$$

with $x_t = m_t^2/m_W^2$. In a limited domain of m_t, X_t may be approximated as

$$X_t(x_t) = a + bx_t \tag{9}$$

The dominant term in the effective Hamiltonian Eq. (7) is then

$$H_{\rm eff} = \frac{G_F}{\sqrt{2}} \frac{\lambda_t}{4\pi^2}\left[\frac{1}{2}ag^2 + by_t^2\right] (\overline{d}s)_{V-A}(\overline{\nu}\nu)_{V-A} \tag{10}$$

This expression reveals the two types of forces that are at work in FCNC decays: gauge forces associated with the gauge coupling $g\,(= e/\sin\theta_W)$ and Yukawa forces associated with the top-quark Yukawa coupling y_t. The latter force is independent of the gauge coupling, and exists even when g is switched off. It is the subtle interplay of these forces that one is testing in the study of FCNC processes.

A thorough analysis of the decays $K^+ \to \pi^+ \nu\overline{\nu}$ and $K_L \to \pi^0 \nu\overline{\nu}$ has been carried out by Buras et al. [3]. The first reaction can be used to obtain $|V_{ts}V_{td}^*|$ and hence $[(1-\rho)^2+\eta^2]^{1/2}$, the second determines the CP-violating parameter $\mathrm{Im}(V_{ts}V_{td}^*) \sim \eta$. The two together can localise the ρ, η coordinates of the unitarity triangle, and provide a consistency check of the (ρ, η) domain delineated by B-decays. The predicted branching ratios are

$$Br(K^+ \to \pi^+ \nu\overline{\nu}) = (7.8 \pm 1.2) \times 10^{-11}, \tag{11}$$

(to be compared with the experimental result $(14.7^{+13}_{-8.9}) \times 10^{-11}$ based on 3 events from the E949 and E787 experiments [4]), and

$$Br(K_L \to \pi^0 \nu\overline{\nu}) = (3.0 \pm 0.6) \times 10^{-11}. \tag{12}$$

2.2 Decay Modes $K_L \to \pi^0 l^+ l^-$

These decays receive contributions from three sources: (a) a CP-violating short-distance interaction $s \to d l^+ l^-$, (b) a CP-conserving two-photon contribution associated with the decay $K_L \to \pi^0\gamma\gamma$, (c) an indirect CP-violating contribution associated with a one-photon transition $K_1 \to \pi^0 l^+ l^-$. Accordingly, the decay amplitude has the structure

$$A \;=\; \underbrace{\eta\lambda^5 A_{sd}}_{\text{Direct } \not{CP}} \;+\; \underbrace{\alpha^2 A_{2\gamma}}_{CP\text{–conserving}} \;+\; \underbrace{\alpha\epsilon A_{1\gamma}}_{\text{Indirect } \not{CP}} \tag{13}$$

The coefficients $\eta\lambda^5$, α^2, $\alpha\epsilon$ have similar order of magnitude ($\eta \sim 0.3$, $\lambda \sim 0.2$, $\alpha \sim 10^{-2}$, $\epsilon \sim 10^{-3}$). Data on the branching ratio and $\gamma\gamma$ spectrum of $K_L \to \pi^0\gamma\gamma$ enable an estimate of $A_{2\gamma}$. The fact that the 2γ state appears to be mainly $J = 0$ implies that $A_{2\gamma}$ is of importance mainly for the $K_L \to \pi^0\mu^+\mu^-$ channel. The indirect CP-violating amplitude $A_{1\gamma}$ is fixed (up to a model-dependent sign) by the observed branching ratio for $K_S \to \pi^0 l^+ l^-$ [5]. A recent analysis obtains the prediction [6]

$$\begin{aligned} Br(K_L \to \pi^0 e^+ e^-) &= (3.7 \pm 1.0) \times 10^{-11} \\ Br(K_L \to \pi^0 \mu^+ \mu^-) &= (1.5 \pm 0.3) \times 10^{-11} \end{aligned} \tag{14}$$

2.3 Decay $K_L \to \mu^+\mu^-$

The decay $K_L \to \mu^+\mu^-$ is subject to a unitarity bound associated with the 2γ intermediate state [7], given by

$$R^K = \frac{\Gamma(K_L \to \mu^+\mu^-)}{\Gamma(K_L \to \gamma\gamma)} \geq \frac{\alpha^2}{2\beta}\frac{m_\mu^2}{m_K^2}\left(\ln\frac{1+\beta}{1-\beta}\right)^2 = 1.2 \times 10^{-5} \qquad (15)$$

where $\beta = (1 - 4m_\mu^2/m_K^2)^{1/2}$. The measured value of R^K is just 4% above the unitarity limit:

$$R^K_{\rm exp} = (1.238 \pm 0.024) \times 10^{-5} \qquad (16)$$

This excess can be interpreted as an estimate of the quantity

$$|A_{\rm disp}(2\gamma) + A_{\rm s-d}|^2, \qquad (17)$$

where $A_{\rm disp}(2\gamma)$ is the dispersive part of the 2γ contribution, and $A_{\rm s-d}$ is the contribution of the short-distance interaction $(\overline{s}d)(\overline{l}l)$. Such an analysis requires a model for the form factor of the two-photon vertex $K_L \to \gamma^*\gamma^*$ [8]. In principle, access to the real and imaginary parts of the $K_L \to \mu\overline{\mu}$ amplitude is also possible by studying the decay $K_L \to \mu^+\mu^-\gamma$ in the soft-photon region where the bremsstrahlung and Dalitz pair amplitudes for this process interfere [9].

2.4 Decay $K_L \to \pi^+\pi^-e^+e^-$

The decay $K_L \to \pi^+\pi^-e^+e^-$ is calculable in terms of empirical knowledge of the radiative transition $K_L \to \pi^+\pi^-\gamma$. It reveals a remarkable CP-violating, T-odd asymmetry, which is triggered by the small ϵ impurity in the K_L wavefunction [10].

The $K_L \to \pi^+\pi^-\gamma$ amplitude is the sum of a bremsstrahlung component, proportional to the CP-violating parameter η_{+-}, and a direct $M1$ term obtained by a fit to the photon energy spectrum. The e^+e^- pair in $K_L \to \pi^+\pi^-e^+e^-$ is interpreted as an internal conversion of the photon in $K_L \to \pi^+\pi^-\gamma$. The theoretical analysis leads to the prediction

$$\frac{d\Gamma}{d\phi} = \Gamma_1 \cos^2\phi + \Gamma_2 \sin^2\phi + \Gamma_3 \sin\phi\cos\phi \qquad (18)$$

where ϕ is the angle between the $\pi^+\pi^-$ and e^+e^- planes. The last term is odd under CP as well as T, and gives rise to an asymmetry

$$A_\phi = \left(\int_0^{\pi/2} + \int_\pi^{3\pi/2} - \int_{\pi/2}^{\pi} - \int_{3\pi/2}^{2\pi}\right)\frac{d\Gamma}{d\phi}d\phi \Bigg/ \int_0^{2\pi}\frac{d\Gamma}{d\phi}d\phi \qquad (19)$$

The predicted value was 14% [10], and is in excellent agreement with the measured value [11]

$$A_\phi = \left\{ \begin{array}{cc} 13.7 \pm 1.4 \pm 1.5\% & (\mathrm{KTeV}) \\ 14.2 \pm 3.6\% & (\mathrm{NA48}) \end{array} \right. \tag{20}$$

In addition, the distribution of the $\pi^+\pi^-$ system in the final state confirms the presence of an s-wave amplitude, corresponding to a mean-square K^0 charge radius

$$\langle R^2 \rangle_{K^0} = \left\{ \begin{array}{cc} -0.077 \pm 0.014\, fm^2 & (\mathrm{KTeV}) \\ -0.09 \pm 0.02\, fm^2 & (\mathrm{NA48}) \end{array} \right. \tag{21}$$

in agreement with the theoretical expectation from vector meson dominance: $\langle R^2 \rangle_{K^0} = \frac{1}{2}\left[\frac{1}{m_\phi^2} - \frac{1}{m_\rho^2}\right] = -0.07\, fm^2$.

2.5 Decays $K^+ \to \pi^+ e^+ e^-$ and $K_S \to \pi^0 e^+ e^-$

These decays are determined mainly by the single photon intermediate state. The matrix elements have a similarity to that for the charged current decay $K^+ \to \pi^0 e^+ \nu$, and may be parametrized as

$$\begin{aligned} \mathcal{A}(K^+ \to \pi^0 e^+ \nu) &= \frac{G_F}{\sqrt{2}} \frac{f_+}{\sqrt{2}} \sin\theta_C (k+p)_\alpha \overline{\nu} \gamma^\alpha (1-\gamma_5) e \\ \mathcal{A}(K^+ \to \pi^+ e^+ e^-) &= a_+ \frac{G_F}{\sqrt{2}} \frac{\alpha}{\pi} f_+ \sin\theta_C (k+p)_\alpha \overline{e} \gamma^\alpha e \\ \mathcal{A}(K_S \to \pi^0 e^+ e^-) &= a_S \frac{G_F}{\sqrt{2}} \frac{\alpha}{\pi} f_+ \sin\theta_C (k+p)_\alpha \overline{e} \gamma^\alpha e \end{aligned} \tag{22}$$

An early analysis [12] yielded the prediction $a_+ = -0.7$, $a_S = 2.4$. A simple model of $K^+ \to \pi^+ e^+ e^-$ relates the matrix element to the weak two point vertex $K^+ - \pi^+$ and the charge radii of K^+ and π^+ [13]. A similar model was used a long time ago [14] to estimate the decay $K_S \to \pi^0 e^+ e^-$ in terms of the weak vertex $K_2 - \pi^0$ and the charge radius of the K^0 meson. The $K^+ - \pi^+$ and $K_2 - \pi^0$ vertices are given by current algebra and PCAC:

$$\langle \pi^0 | H_w | K_2 \rangle = -\langle \pi^+ | H_w | K^+ \rangle = 2 F_\pi g \tag{23}$$

where g is the coupling constant for $K_1 \to \pi\pi$, and $F_\pi = m_N g_A / g_{NN\pi} \approx 90\, MeV$. With these values, the measured branching ratios of $K^+ \to \pi^+ e^+ e^-$ and $K_S \to \pi^0 l^+ l^-$ are well reproduced.

3 Miscellaneous Remarks

As noted above, the standard model contains gauge couplings $\{g, g'\}$, which conserve chirality, and Yukawa couplings $\{y_f\}$ which are proportional to fer-

mion masses and violate chirality. It is the interplay of those couplings that determines the strength of the FCNC interaction responsible for decays like $K^+ \to \pi^+ \nu\overline{\nu}$.

The reality of the Yukawa interaction as a force independent of gauge interactions is revealed if one considers the "gaugeless" limit of the standard model, viz. $g \to 0$ with $v = (\sqrt{2}G_F)^{-1/2}$ fixed. In this limit, studied by Bjorken [15], one has the remarkable consequence that the electron is unstable, with decay width

$$\Gamma(e^- \to \nu_e W^-) = \frac{\sqrt{2}G_F m_e^3}{16\pi} = \frac{y_e^2}{32\pi} m_e = (10.3\, ns)^{-1}. \tag{24}$$

Note that in the limit $g \to 0$, $m_W = gv/2 \to 0$. The electron decays purely by virtue of its Yukawa coupling $y_e = \sqrt{2}m_e/v$, and the massless (longitudinal) W it decays into is nothing but the massless Goldstone boson φ^- of the scalar sector.

In a similar spirit, one can investigate the behaviour of amplitudes in the limit $y_e \to 0$ with v fixed. A remarkable feature that emerges is that the electron chirality is not conserved. This is evident already at the level of QED: the cross section of helicity-flip Compton scattering is

$$\lim_{m_e \to 0} \sigma(\gamma + e_L^- \to \gamma + e_R^-) = 2\pi \frac{\alpha^2}{s} \tag{25}$$

Likewise, helicity-flip bremsstrahlung $e_L^- + \mathcal{N} \to e_R^- + \mathcal{N} + \gamma$ has the characteristic angular distribution [16]

$$d\sigma_{hf} \sim \alpha \left(\frac{m_e}{E}\right)^2 \frac{d\theta^2}{\left(\theta^2 + \frac{m^2}{E^2}\right)^2} \tag{26}$$

which, integrated over angles, gives a finite non-zero result in the limit $m_e \to 0$.

As a further interesting consequence [17] electrons in radiative muon decay $\mu^- \to e^- \overline{\nu}_e \nu_\mu \gamma$ are not purely left-handed in the limit $m_e \to 0$. Despite the $V - A$ structure of the weak interaction, there is a significant probability for electrons in μ-decay to be right-handed. Such right-handed electrons are typically accompanied by hard collinear photons. The contribution of these wrong-helicity electrons to the muon decay width is $\Gamma_R = \frac{\alpha}{4\pi}(G_F^2 m_\mu^5/192\pi^3)$.

The above curiosities in the gaugeless limit or in the limit of a massless fermion may be of some relevance when one contemplates the interplay of gauge couplings and Yukawa couplings in electroweak amplitudes.

References

1. Particle Data Collaboration (S. Eidelman *et al.*), Phys. Lett. B **592**, 1 (2004).
2. D. Rein and L. M. Sehgal, Phys. Rev. D **39**, 3325 (1989).
3. A. Buras, F. Schwab and S. Uhlig, hep-ph/0405132.
4. G. Redlinger, these Proceedings.
5. J. Batley *et al.* (NA48/1 Collaboration), Phys. Lett. B **576**, 43 (2003).
6. G. Isidori, C. Smith and R. Unterdorfer, hep-ph/0404127; G. Buchalla, G. D′Ambrosio and G. Isidori, hep-ph/0308008.
7. L. M. Sehgal, Phys. Rev. **183**, 1511 (1969).
8. G. Isidori and R. Unterdorfer, hep-ph/0311184.
9. P. Poulose and L. M. Sehgal, Phys. Lett. B **554**, 141 (2003).
10. L. M. Sehgal and J. van Leusen, Phys. Rev. Lett. **83**, 4933 (1999); L. M. Sehgal and M. Wanninger, Phys. Rev. D **46**, 1035 (1992); **46**, 5209 (E) (1992); P. Heiliger and L. M. Sehgal, Phys. Rev. D **48**, 4146 (1993).
11. S. Ledovskoy (KTeV Collaboration), talk at XXXIX Rencontres de Moriond, 2004; A. Lai *et al.* (NA48 Collaboration), Eur. Phys. J. C **30**, 33 (2003).
12. A. Vainshtein *et al.*, Sov. J. Nucl. Phys. **24**, 427 (1976).
13. H. Burkhardt *et al.*, hep-ph/0011345.
14. L. M. Sehgal, Nucl. Phys. B **19**, 445 (1970).
15. J. D. Bjorken, Proc. Les Arcs Conference on New and Exotic Phenomena (Edition Frontieres, 1987) p. 1.
16. B. Falk and L. M. Sehgal, Phys. Lett. B **325**, 509 (1994).
17. L. M. Sehgal, Phys. Lett. B **569**, 25 (2003); V. Schulz and L. M. Sehgal, hep-ph/0404023.

Frascati Physics Series Vol. XXXVI (2004), pp. 265
DAΦNE 2004: Physics at meson factories – Frascati, June 7-11, 2004
Invited Review Talk in Plenary Session

RARE B/D DECAYS

Vivek Sharma
San Diego University 9500 Gilman Drive" La Jolla 92093-0319 USA

Written contribution not received

Frascati Physics Series Vol. XXXVI (2004), pp. 267–272
DAΦNE 2004: Physics at meson factories – Frascati, June 7-11, 2004
Selected Contribution in Plenary Session

RARE HADRONIC B DECAYS

Lluïsa-Maria Mir
Lawrence Berkeley National Laboratory

Abstract

The general methodology to search for rare hadronic B decays, including some examples from the *BABAR* experiment, is presented.

1 Introduction

The Standard Model (SM) has proven to be very healthy so far: the agreement between the theoretical predictions and the experimental results is really good. As a consequence, to find experimental deviations from the SM, we have to study processes that are expected to have small rates, like Cabibbo-Kobayashi-Maskawa (CKM) suppressed decays, or decays dominated by penguin loops. Rare hadronic B decays are well suited for this search because they have, in general, suppressed tree contributions and significant penguins. On the other hand, although rare, these decays are very abundant, and in the past few years

there have been many measurements of their branching ratios (BR), asymmetries, etc. In this note, I will describe the general tools used to perform this type of searches, and I will present three particular examples, especially interesting in the way to further test the SM and search for new physics.

2 Analysis method

For fully reconstructed events, the precise knowledge of the beam energy allows the energy and the mass of the reconstructed B to be constrained. The identification of signal events is based on two kinematic variables: the beam–energy substituted mass ($m_{\rm ES} = \sqrt{(s/2 + \mathbf{p}_i \cdot \mathbf{p}_{\rm B})^2/E_i^2 - \mathbf{p}_{\rm B}^2}$) (where the initial four–momentum $(E_i, \mathbf{p_i})$ and the B momentum $\mathbf{p_B}$ are defined in the laboratory frame), and the difference between the reconstructed B energy in the center–of–mass frame and its known value ($\Delta E = E_{\rm B}^{\rm CM} - \sqrt{s}/2$).

If the reconstruction was perfect, the difference between the beam and the B energies would be zero, and the reconstructed mass would be the B mass. Even with reconstruction uncertainties, these two variables provide good discrimination against the main background, which comes from continuum production. In B factories the B's are produced almost at rest, and consequently the topology of the events is spherical, whereas continuum events have a two–jet structure. Other typical discriminant variables are the masses of the intermediate resonances, the decay angles, and the decay time difference of the two B's. Some of these distributions are shown in fig. 1.

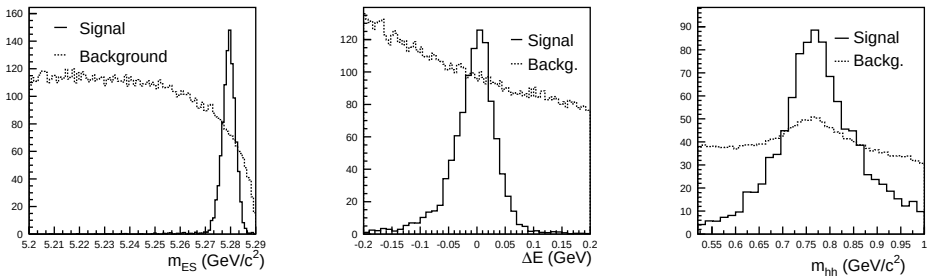

Figure 1: *From left to right: beam–energy substituted mass, energy difference, and resonance mass, for signal (solid) and continuum background (dashed).*

To measure BR's, these distributions are used to build probability density functions, and a likelihood fit is performed to determine signal yields. Differ-

ence of decay times and tagging information is included in time–dependent measurements.

3 Examples

3.1 Decays to pairs of isoscalars

We measure the BR's of all (η, η', $\omega\,\phi$) (η, η', $\omega\,\phi$) combinations except $\omega\omega$ and $\omega\phi$. The measured values for a sample of 82M B$\overline{\mathrm{B}}$ events are summarized in tab.1 [1)].

Table 1: *BR's of B decays to two isoscalars.*

Mode	S(σ)	$\mathcal{B}(10^{-6})$	UL (10^{-6})	UL (10^{-6}) (CLEO)
$\eta\eta$	0.0	$-0.9^{+1.6}_{-1.4} \pm 0.7$	2.8	18
$\eta\eta'$	0.3	$0.6^{+2.1}_{-1.7} \pm 1.1$	4.6	27
$\eta'\eta'$	0.4	$1.7^{+4.8}_{-3.7} \pm 0.6$	10	47
$\eta\omega$	4.3	$4.0^{+1.3}_{-1.2} \pm 0.4$	6.2	12
$\eta'\omega$	0.0	$-0.2^{+1.3}_{-0.9} \pm 0.4$	2.8	60
$\eta\phi$	0.0	$-1.4^{+0.7}_{-0.4} \pm 0.2$	1.0	9
$\eta'\phi$	0.8	$1.5^{+1.8}_{-1.5} \pm 0.4$	4.5	31
$\phi\phi$	0.3	$0.3^{+0.7}_{-0.4} \pm 0.1$	1.5	12

The upper limits on the BR's have been tightened considerably, and this translates into an improvement of a factor of 2 in the Grossman-Ligeti-Nir-Quinn bound [2)] on the difference of the S coefficient of the time–dependent asymmetry measured in $\mathrm{B} \to \mathrm{J}/\psi\mathrm{K}^0_\mathrm{S}$ and $\mathrm{B} \to \eta'\mathrm{K}^0_\mathrm{S}$ decays.

3.2 BR's and CP asymmetries in $\mathrm{B}^0 \to \mathrm{K}^+\mathrm{K}^-\mathrm{K}^0_\mathrm{S}$ and $\mathrm{B}^+ \to \mathrm{K}^+\mathrm{K}^0_\mathrm{S}\mathrm{K}^0_\mathrm{S}$

B decays to three kaons are interesting because there is a 2.7 σ discrepancy between the *BABAR* and Belle results in the measured S coefficient of the time–dependent asymmetry in the $\mathrm{B} \to \phi\mathrm{K}^0_\mathrm{S}$ decay. The measurement of the B decay to three kaons, integrated over all the phase–space, has the advantage over $\mathrm{B} \to \phi\mathrm{K}^0_\mathrm{S}$ of a better statistical precision due to the larger data sample. On the other hand, the CP–content of the final states is unknown and has to be measured. This is done using the isospin symmetry relation:

$$f_{\mathrm{even}} = \frac{N_{CP}}{N} = \frac{\Gamma(\mathrm{B}^+ \to \mathrm{K}^+\mathrm{K}^0_\mathrm{S}\mathrm{K}^0_\mathrm{S})}{\Gamma(\mathrm{B}^0 \to \mathrm{K}^+\mathrm{K}^-\mathrm{K}^0)} \qquad (1)$$

Figure 2 shows the Δt distributions for B^0 and $\overline{B^0}$ decays and the results of the fits for a sample of 124M $B\overline{B}$ events are listed in tab.2 [3]. Finally, tab.3 shows a comparison of the *BABAR* and Belle results on CP–asymmetries for ϕK^0 and KKK^0_S. The agreement in the three–kaon channel is good.

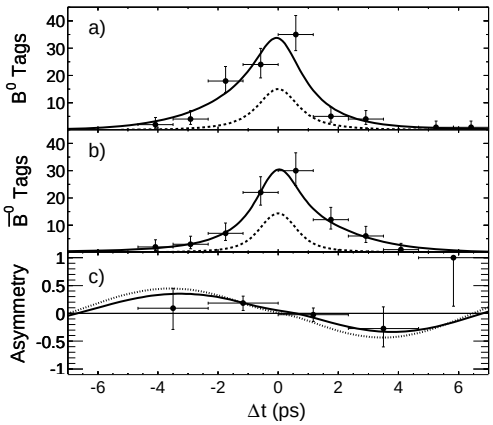

Figure 2: *Plots a) and b) show the Δt distributions of B^0– and $\overline{B^0}$–tagged $K^+K^-K^0_S$ events. Solid lines correspond to all events and dashed lines to background. Plot c) shows the raw asymmetry, where the solid line is obtained from the fit and the dotted line corresponds to the SM expectation.*

Table 2: *Summary of BR's ($\mathcal{B}$), time–dependent (S,C) and direct CP–asymmetry ($\mathcal{A}_{CP}$) results; f_{even} is the fraction of CP–even final states.*

	$(K^+K^-K^0)^{CP}$	$(K^+K^-K^0)^{all}$	$K^+K^0_SK^0_S$
$\mathcal{B}\,(10^{-6})$	$20.2 \pm 1.9 \pm 1.4$	$23.8 \pm 2.0 \pm 1.6$	$10.7 \pm 1.2 \pm 1.0$
f_{even}	$0.98 \pm 0.15 \pm 0.04$	$0.83 \pm 0.12 \pm 0.03$	–
S	$-0.56 \pm 0.25 \pm 0.04$	–	-0.16 ± 0.35
C	$-0.10 \pm 0.19 \pm 0.10$	–	-0.08 ± 0.22
$\mathcal{A}_{CP}$	–	–	$-0.04 \pm 0.11 \pm 0.02$

Table 3: *Comparison of BABAR and Belle measurements on time–dependent asymmetries for three kaon decays.*

$-\eta_f \times S_f$	ϕK^0	KKK^0_S
BABAR	$0.47 \pm 0.34^{+0.08}_{-0.06}$	$0.56 \pm 0.25 \pm 0.04^{+0.17}_{-0.00}$
Belle	$-0.96 \pm 0.50^{+0.09}_{-0.11}$	$0.51 \pm 0.26 \pm 0.05^{+0.18}_{-0.00}$
Average	0.02 ± 0.29 (0.28 stat only)	$0.54 \pm 0.18^{+0.17}_{-0.00}$ (0.18 stat only)

3.3 Angular analysis in ϕK^* decays

The angular distribution of the decay of a B meson to a vector pair is unknown a priori, but can be parameterized as a function of the decay angles and the helicity amplitudes as follows:

$$\frac{1}{\Gamma}\frac{d^3\Gamma}{d\cos\theta_1 d\cos\theta_2 d\Phi} = \frac{9}{8\pi}\frac{1}{|A_0|^2+|A_{+1}|^2+|A_{-1}|^2}\times$$
$$\left\{\frac{1}{4}\sin^2\theta_1\sin^2\theta_2\left(|A_{+1}|^2+|A_{-1}|^2\right)+\cos^2\theta_1\cos^2\theta_2|A_0|^2+\right.$$
$$\frac{1}{2}\sin^2\theta_1\sin^2\theta_2\left[\cos 2\Phi Re(A_{+1}A^*_{-1})-\sin 2\Phi Im(A_{+1}A^*_{-1})\right]-$$
$$\left.\frac{1}{4}\sin 2\theta_1\sin 2\theta_2\left[\cos\Phi Re\left(A_{+1}A^*_0+A_{-1}A^*_0\right)-\sin\Phi Im\left(A_{+1}A^*_0-A_{-1}A^*_0\right)\right]\right\} \quad (2)$$

The quantities that are obtained from the fit are the total number of events ($n_{\rm sig}$), the fractions of longitudinal ($f_{\rm L} = \frac{|A_0|^2}{\sum_m |A_m|^2}$), and transverse ($f_\perp = \frac{|A_\perp|^2}{\sum_m |A_m|^2}$) polarization, and the phases ($\phi_\parallel = arg(A_\parallel) - arg(A_0)$ and $\phi_\perp = arg(A_\perp) - arg(A_0)$). If differences between the B^0 and $\overline{B^0}$ decay amplitudes are allowed, we can define the following CP–violating asymmetries or differences: $\mathcal{A}_{\rm CP} = \frac{n^+_{\rm sig}-n^-_{\rm sig}}{n^+_{\rm sig}+n^-_{\rm sig}}$ (direct CP-asymmetry), $\mathcal{A}^0_{\rm CP} = \frac{f^+_{\rm L}-f^-_{\rm L}}{f^+_{\rm L}+f^-_{\rm L}}$ (longitudinal asymmetry), $\mathcal{A}^\perp_{\rm CP} = \frac{f^+_\perp-f^-_\perp}{f^+_\perp+f^-_\perp}$ (transverse asymmetry), $\Delta\phi_\parallel = \frac{1}{2}(\phi^+_\parallel - \phi^-_\parallel)$ (CP-even) and $\Delta\phi_\perp = \frac{1}{2}(\phi^+_\perp - \phi^-_\perp)$ (CP-odd).

The results of the fit for a sample of 124M $B\overline{B}$ events are summarized in tab.4 [4]. The surprising result is the fitted value of the longitudinal–polarization fraction, which is expected to be approximately 1 in the SM. We can visualize these results in the two–dimensional contours shown in fig.3.

Table 4: $B \to \phi K^{*0}$ *fit results.*

$n_{\rm sig}$	$f_{\rm L}$	$f_\perp$	$\phi_\parallel$
$129 \pm 14 \pm 9$	$0.52 \pm 0.07 \pm 0.02$	$0.27 \pm 0.07 \pm 0.02$	$2.63^{+0.24}_{-0.23} \pm 0.04$
$\phi_\perp$	$\mathcal{A}_{\rm CP}$	$\mathcal{A}^0_{\rm CP}$	$\mathcal{A}^\perp_{\rm CP}$
$2.71^{+0.22}_{-0.24} \pm 0.03$	$-0.12 \pm 0.10 \pm 0.03$	$-0.02 \pm 0.12 \pm 0.01$	$-0.10^{+0.25}_{-0.27} \pm 0.04$
$\Delta\phi_\parallel$		$\Delta\phi_\perp$	
$0.38^{+0.23}_{-0.24} \pm 0.04$		$0.30^{+0.24}_{-0.22} \pm 0.03$	

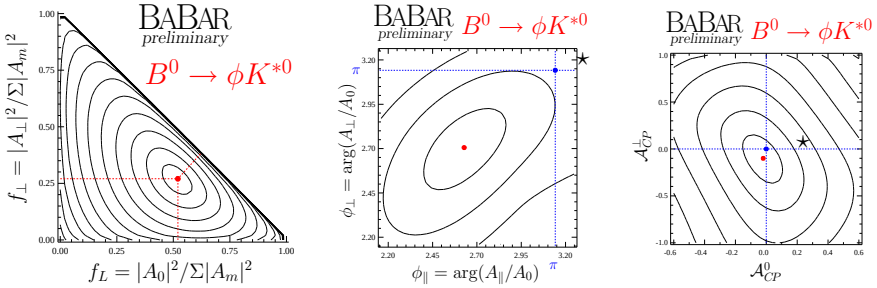

Figure 3: *From left to right: two–dimensional contour of longitudinal versus transverse polarization fraction, CP–odd versus CP–even phase, and transverse versus longitudinal asymmetry. The points correspond to the measured values and the stars to the SM expectations.*

References

1. B.Aubert *et al.* [*BABAR*] Sub. to Phys. Rev. Lett. (hep-ex/0403046).
2. Y.Grossman *et al.*, Phys. Rev. D **68**, 015004 (2003).
3. B.Aubert *et al.* [*BABAR*] Sub. to Phys. Rev. Lett. (hep-ex/0406005).
4. B.Aubert *et al.* [*BABAR*] Sub. to Phys. Rev. Lett. (hep-ex/0408017).

Frascati Physics Series Vol. XXXVI (2004), pp. 273–280
DAΦNE 2004: Physics at meson factories – Frascati, June 7-11, 2004
Invited Review Talk in Plenary Session

RARE KAON DECAYS: IL BUONO, IL BRUTTO, IL CATTIVO

G. Redlinger
Brookhaven National Laboratory, Upton, NY, USA 11973

Abstract

I briefly review recent progress in rare kaon decays, where I take "rare" to mean those with $\mathcal{B} < \mathcal{O}(10^{-7})$ [1].

1 Introduction

The title of this talk (which by the way borrows from the original title of the famous "spaghetti Western" "The Good, The Bad, and The Ugly") arose from the convergence of several trains of thought: first, that this conference was being held near Rome, where the filmmaker Sergio Leone was born and lived;

[1] I set the scale by the "classic" example of rare, the probability of getting killed by lightning in one year in the U.S. See for example http://mathforum.org/dr.math/faq.

second, various allusions to current world politics, which are best left to the coffee break; lastly, and most importantly, I was inspired by a writeup of a talk by Wilczek [?]:

> "Our current, working description of fundamental physics is based on three conceptual systems... it is not inappropriate to call them the Good, the Bad, and the Ugly"

For the purposes of this talk, we concentrate on the "Ugly" which is the flavor sector whose many parameters illustrate our lack of understanding of the Higgs Yukawa couplings. Experiment is a key driving force in making progress here; kaon decays have had a glorious history in elucidating this physics, and continue to serve as sensitive probes.

In the following, I cover rare kaon decay results[2] from approximately 2003 to the present. These can be grouped as follows:

- The Good. This includes the study of signatures explicitly beyond the Standard Model (BSM), of which the best known are the lepton flavor violating decays. Here we also include modes sensitive to quark-mixing parameters and CP violation (CPV) with small theoretical uncertainty, thus making them excellent candidates for searches for BSM physics.

- The Bad. This include studies of the low-energy behavior of the strong interactions. Obviously this is not "bad" in itself, but is not directly connected to studying the flavor sector.

- The Ugly. These are decay modes that potentially probe quark-mixing, CPV and BSM physics but which do not lend themselves to a clean extraction of the fundamental parameters.

I do not cover high-sensitivity experiments that require large numbers of kaons, but where the underlying branching ratios are relatively large, such as ϵ'/ϵ or the search for T violation in $K^+ \to \pi^0\mu^+\nu$. Needless to say, in the limited space available I can only give a cursory overview of the field; the interested reader should consult the many reviews available [?].

[2] All quoted limits are at 90% CL.

2 Lepton flavor violation

The state-of-the-art in lepton flavor violation (LFV) is set by the BNL experiments E871 and E865 which searched for the decays $K_L \to \mu^\pm e^\mp$ and $K^+ \to \pi^+\mu^+e^-$ respectively. The two decay modes are complementary in that the first probes parity odd couplings and the second parity even. The E871 result on $K_L \to \mu^\pm e^\mp$ actually predates the time frame of this review, but it is the best limit available: $\mathrm{BR}(K_L \to \mu^\pm e^\mp) < 4.7 \times 10^{-12}$ [?]. Limits on new physics are model dependent; it is typical to derive a limit in a "generic" sense for a heavy particle exchanged at tree level. For the same coupling strength as the electroweak couplings of the quarks, the limit on $K_L \to \mu^\pm e^\mp$ probes energy scales as high as 150 TeV [?]. E865 has completed analysis of its 1998 data set for $K^+ \to \pi^+\mu^+e^-$ [?]. The dominant background comes from the overlap of multiple K^+ decays, which are estimated from the time sidebands and extrapolated into the signal region from the region of high K^+ momentum. Eight events are observed in the signal region, consistent with background expectations; a likelihood analysis is used to obtain the branching ratio limit. Combining this with the E865 results from the 1995 and 1996 runs as well as with the result from the predecessor experiment BNL E777, yields the final E865 limit: $\mathrm{BR}(K^+ \to \pi^+\mu^+e^-) < 1.2 \times 10^{-11}$. New results from KTeV are also available on $K_L \to \pi^0\mu^\pm e^\mp$ [?] and $K_L \to e^\pm e^\pm \mu^\mp \mu^\mp$ [?].

3 Quark mixing and CP violation: $K \to \pi\nu\overline{\nu}$

The decays $K^+ \to \pi^+\nu\overline{\nu}$ and $K_L \to \pi^0\nu\overline{\nu}$ have attracted much attention for their potential (together with the decay $K^+ \to \pi^0 e^+\nu$) to completely determine the Unitarity Triangle from kaon decays alone. An inconsistency between the unitarity relation in kaon decays ($s \to d$ transitions) with that in B decays ($b \to d$ transitions) would provide clues to the flavor structure of physics beyond the SM. The clean theoretical nature of the $K \to \pi\nu\overline{\nu}$ decay modes was discussed at this conference by Sehgal; a detailed review can be found in [?].

First results from BNL E949 on the decay $K^+ \to \pi^+\nu\overline{\nu}$ have been published recently [?]. The signal region is analyzed with a signal-to-noise likelihood ratio technique. An event is seen in the 2002 dataset near the $K^+ \to \pi^+\nu\overline{\nu}$ kinematic endpoint, albeit with poorer signal-to-noise ratio compared to the previous two candidate events seen by E787; accordingly the new

event has an effective contribution to the branching ratio of about 0.5 events. The best estimate of the branching ratio, combining data from E787 and E949 is $\mathcal{B}(K^+ \to \pi^+\nu\overline{\nu}) = 1.47^{+1.30}_{-0.89} \times 10^{-10}$, consistent with the SM, although the central value remains about twice the SM value. Further details can be found in the presentation by Sekiguchi at this conference. A result from E787 on $K^+ \to \pi^+\nu\overline{\nu}$ from the 1997 dataset in the π^+ momentum region below 195 MeV/c has also been published recently [?].

A model-independent bound on the branching ratio for $K_L \to \pi^0\nu\overline{\nu}$ can be obtained from the $K^+ \to \pi^+\nu\overline{\nu}$ branching ratio [?]. Using the most recent result from E949, this so-called Grossman-Nir bound becomes $\mathcal{B}(K_L \to \pi^0\nu\overline{\nu}) < 1.4 \times 10^{-9}$, about 400 times lower than the best direct limit from KTeV [?]. As discussed at this conference by Komatsubara, the first experiment (KEK E391a) dedicated to studying this decay mode took its first data this year, hoping to cover the entire region between the KTeV and Grossman-Nir limits.

4 Quark mixing and CP violation: other decay modes

The decays $K_L \to \pi^0 l^+ l^-$ (where $l = e, \mu$) have also attracted interest for their potential to determine the Wolfenstein parameter η, responsible for CPV in the SM. However, while $K_L \to \pi^0\nu\overline{\nu}$ proceeds almost entirely due to "direct" CPV (sensitive to η), the $K_L \to \pi^0 l^+ l^-$ modes have large contributions to the branching ratio from "indirect" CPV ($K_L - K_S$ mixing, followed by CP conserving (CPC) K_S decay) and from the interference between direct and indirect CPV. In the case of $K_L \to \pi^0\mu^+\mu^-$, there is also a large contribution from the CP conserving amplitude. Much theoretical effort has gone into disentangling the various contributions as was covered briefly by Smith, and discussed in detail in [?, ?].

On the experimental side, KTeV has updated the search for $K_L \to \pi^0 e^+ e^-$, adding the results of their 1999 dataset [?]. One event is seen, consistent with expectations from background, dominated by $K_L \to e^+e^-\gamma\gamma$. Combining with the previous result from the 1997 dataset, yields the final KTeV limit: $\mathcal{B}(K_L \to \pi^0 e^+ e^-) < 2.8 \times 10^{-10}$. This is still about a factor of 10 above the SM prediction; to beat down the $K_L \to e^+e^-\gamma\gamma$ background further requires higher precision tracking and calorimetry, which may be difficult considering that KTeV is already state-of-the-art. An interference analysis might be a possible way out [?]. $K_L \to \pi^0\mu^+\mu^-$ has a less severe background prob-

lem from $K_L \to \mu^+\mu^-\gamma\gamma$, but the SM branching ratio is smaller by about a factor of two. Results from the 1999 dataset of KTeV are awaited; this data sample contains about a factor 1.3 more K decays compared to the 1997 data.

The measurements of $K_S \to \pi^0 l^+ l^-$ are important inputs to the computation of the contributions of indirect CPV (and hence also the magnitude of the interference term, but not the sign) to $K_L \to \pi^0 l^+ l^-$. As shown by Ruggiero, NA48/1 has made the first observation of both $K_S \to \pi^0 e^+ e^-$ and $K_S \to \pi^0 \mu^+ \mu^-$: $\mathcal{B}(K_S \to \pi^0 e^+ e^-) = (5.8^{+2.8}_{-2.3}(stat) \pm 0.8(sys)) \times 10^{-9}$ [?] and $\mathcal{B}(K_S \to \pi^0 \mu^+ \mu^-) = (2.9^{+1.4}_{-1.2} \pm 0.2) \times 10^{-9}$ [?]. The precision of these measurements currently set the uncertainty in the SM expectation for $K_L \to \pi^0 l^+ l^-$ to around 30%; it is thought that the ultimate theoretical precision could be brought below 10% [?, ?].

Much effort has also gone into extracting the Wolfenstein parameter ρ from $K_L \to \mu^+\mu^-$ decays. The decay itself is well-measured; the difficulty is that the branching ratio is almost saturated by the two-photon intermediate state, masking the short-distance contribution sensitive to ρ. The imaginary part of the two-photon amplitude can be obtained from $\mathcal{B}(K_L \to \gamma\gamma)$, as has been known for many years [?]. The real part can be constrained by studies of the form factor for K_L decays to virtual photons, with the final states $e^+e^-\gamma$, $e^+e^-e^+e^-$, $\mu^+\mu^-\gamma$, and $\mu^+\mu^-e^+e^-$. Studies of the $ee\gamma$, $eeee$ [?] and $ee\mu\mu$ [?] states have been updated by KTeV, now including their full dataset from the 1997 and 1999 runs. These KTeV form factor measurements are consistent with one another, but the more precise measurements ($ee\gamma$ and $\mu\mu\gamma$) are in disagreement with the previous NA48 measurement from $ee\gamma$ [?]. New results are expected from NA48 on $ee\gamma$ and $eeee$; a measurement of the $eeee$ branching ratio was shown at this conference by Ruggiero. Using the KTeV measurements as input, limits on ρ from $K_L \to \mu^+\mu^-$ have been derived [?]. While these limits are not competitive with other CKM constraints, and are not expected to improve significantly without new theoretical ideas, they do provide constraints on non-standard scenarios.

KLOE is starting to get into the rare decay regime with a new result on the CP-violating decay $K_S \to \pi^0\pi^0\pi^0$, as reported by Martini. The motivation for this decay mode is that the uncertainty on the $K_S \to \pi^0\pi^0\pi^0$ amplitude currently limits the precision on $Im(\delta)$, where δ parametrizes the CPT-violating part of the K_L, K_S wave-functions [?]. The result, $\mathcal{B}(K_S \to \pi^0\pi^0\pi^0)$

$< 2.1 \times 10^{-7}$, is about a factor 70 improvement over the current PDG limit, and improves the precision on $Im(\delta)$ by about a factor of 2.5. NA48/1 probes separately the real and imaginary parts of the $K_S \to \pi^0\pi^0\pi^0$ amplitude by looking at $K_L - K_S$ interference, with a similar sensitivity to $Im(\delta)$ [?].

5 Outlook and Conclusion

Concerning LFV, existing data on the most sensitive modes are now fully analyzed. There are no currently running or proposed LFV experiments in the kaon sector; current methods have been estimated to give perhaps another factor of 40 at best [?]. Attention has turned instead to the muon sector where sensitivity gains of 3-4 orders of magnitude are anticipated [?]. SUSY models generally put LFV far out of reach of kaon experiments while large parts of parameter space would be accessible by muon decays [?]. On the other hand, LFV K decays can probe interesting areas of parameter space in ETC models [?]. More generally, LFV K decays involve both quarks and leptons and could provide information complementary to that obtained in the muon sector.

Concerning precision tests of the CKM matrix, future efforts are concentrated on the "golden" modes: $K^+ \to \pi^+\nu\overline{\nu}$ and $K_L \to \pi^0\nu\overline{\nu}$. The current experimental situation on $K^+ \to \pi^+\nu\overline{\nu}$ cries out for completion of the BNL E949 program (only 20% of the proposed running has been completed), but the DOE has halted HEP operations at the AGS; a proposal to NSF to complete E949 has been submitted. In addition, experiments are under consideration at other labs to take the sensitivity one step further to the level of between 50 and 100 events with S/N=10. These include decay-in-flight experiments P940 at Fermilab [?], NA48/3 at CERN [?], and a stopped kaon experiment at J-PARC [?]. For $K_L \to \pi^0\nu\overline{\nu}$, KEK E391a may have another run in 2005, possibly going below the Grossman-Nir limit. The KOPIO experiment [?] expects to observe 40 events with S/N=2; the project was included in the FY05 President's Budget for a construction start in 2005. A 5-year construction is envisaged with test runs starting in 2008. There is also a letter of intent to use the E391a technique at J-PARC [?].

In conclusion, rare kaon decays continue to be an active area of study. LFV decays have reached single-event sensitivities at the $(2-5) \times 10^{-12}$ level, but further progress requires new measurement techniques. Heroic efforts have been made toward understanding the short distance components of

$K_L \to \pi^0 l^+ l^-$ and $K_L \to \mu^+ \mu^-$. Current experiments for $K_L \to \pi^0 l^+ l^-$ are within striking distance of the SM by a factor of about 10, but backgrounds are severe. Still, the potential exists for the discovery and study of BSM effects complementary to those in $K \to \pi\nu\overline{\nu}$; clever ideas for experiments are needed. The focus of the community is converging on the $K \to \pi\nu\overline{\nu}$ decays for precision CKM tests. There are many ideas for experiments at various labs; some even appear to be funded. Together with precision measurements at B factories, these could provide decisive tests of the flavor sector. It is worth recalling that at least in the movie, the "Good" was able to tease out the secret from the "Ugly" [3].

6 Acknowledgements

Thanks to S. Kettell for comments on the draft. This work was supported in part under US Department of Energy contract DE-AC02-98CH10886.

References

1. F. Wilczek, hep-ph/0401126.
2. Start with the review by L. Littenberg and G. Valencia in PDG04, Phys. Lett. **B592** (2004) 607.
3. D. Ambrose *et al*, Phys. Rev. Lett. **81** (1998) 5734.
4. J.L. Ritchie and S.G. Wojcicki, Rev. Mod. Phys. **65** (1993) 1149.
5. A. Sher, Ph.D. Dissertation, Universität Zürich (2004).
6. A. Bellavance, Ph.D Dissertation, Rice University (2002), available from http://kpasa.fnal.gov:8080/public/ktev_theses.html.
7. A. Alavi-Harati *et al*, Phys. Rev. Lett. **90** (2003) 141801.
8. A.J. Buras *et al*, hep-ph/0405132.
9. V.V.Anisimovsky *et al*, Phys. Rev. Lett. **93** (2004) 031801.
10. S. Adler *et al*, hep-ex/0403034. Accepted by Phys. Rev. D.

[3] But keep in mind the twist at the very end!

11. Y. Grossman and Y. Nir, Phys. Lett. **B398** (1997) 163.

12. A. Alavi-Harati *et al*, Phys. Rev. **D61** (2000) 072006.

13. G. Buchalla, G. D'Ambrosio and G. Isidori, Nucl. Phys. **B672** (2003) 387.

14. G. Isidori, C. Smith and R. Unterdorfer, Eur. Phys. J. **C36** (2004) 57.

15. A. Alavi-Harati *et al*, Phys. Rev. Lett. **93** (2004) 021805.

16. A. Lai *et al*, Phys. Lett. **B576** (2003) 43.

17. J.R. Batley *et al*, CERN PH-EP Preprint 2004-025. Accepted by Phys. Lett. B.

18. L.M. Sehgal, Phys. Rev. **183** (1969) 1511.

19. J. LaDue, Ph.D. Dissertation, Univ. of Colorado (2003). See **?)** for web location.

20. A. Ceccucci, presentation at Lepton-Photon 2003, writeup available at http://conferences.fnal.gov/lp2003/program/.

21. G. Isidori and R. Unterdorfer, J. High Energy Phys. 2004 **1** (2004) 9.

22. See the review by P. Bloch in PDG04, Phys. Lett. **B592** (2004) 623.

23. N. Cartiglia, hep-ph/0310152.

24. W. Molzon, in Kaon Physics (ed. J.L. Rosner and B.D. Winstein), p.377 (Univ. of Chicago Press, Chicago, 2001).

25. http://meg.psi.ch and http://meco.ps.uci.edu

26. A. Belyaev *et al* Eur. Phys. J. **C22** (2002) 715.

27. T. Applequist, M. Piai, and R. Shrock, Phys. Rev. **D69** (2004) 015002.

28. Follow the link to P940 from http://www.fnal.gov/faw/experimentsprojects/.

29. http://na48.web.cern.ch/NA48/NA48-3/.

30. http://kaon.kek.jp/∼kpwg.

31. http://pubweb.bnl.gov/users/e926/www.

32. http://www-ps.kek.jp/jhf-np/LOIlist/LOIlist.html.

Frascati Physics Series Vol. XXXVI (2004), pp. 281–286
DAΦNE 2004: Physics at meson factories – Frascati, June 7-11, 2004
Selected Contribution in Plenary Session

RECENT RESULTS ON $K^+ \to \pi^+ \nu\bar{\nu}$

Tetsuro Sekiguchi*
High Energy Accelerator Research Organization (KEK)
1-1 Oho, Tsukuba, Ibaraki, 305-0801 Japan

Abstract

Experiment 949 at Brookhaven National Laboratory (BNL) has observed, in its first data set from 2002, an additional $K^+ \to \pi^+ \nu\bar{\nu}$ candidate near the upper kinematic limit for this decay. Combining this data with previous E787 data, the branching ratio is $(1.47^{+1.30}_{-0.89}) \times 10^{-10}$ (68% CL) based on three events observed in the pion momentum region $211 < P < 229$ MeV/c.

1 Introduction

The rare decay $K^+ \to \pi^+ \nu\bar{\nu}$ is a flavor changing neutral current process involving up, charm and top quarks in loop diagrams. The top quark loops dominate and thus the decay is sensitive to the magnitude of the CKM matrix

* On behalf of the BNL-E949 Collaboration

element V_{td}. A precise measurement of $\mathcal{B}(K^+ \to \pi^+ \nu\bar{\nu})$ is a stringent test for the standard model (SM), since the uncertainty in extracting fundamental SM parameters is very small, and is also a probe of new physics.

E787 at BNL observed two candidate events, with a branching ratio $(1.57^{+1.75}_{-0.82}) \times 10^{-10}$ [1], whereas the SM prediction is $(0.80 \pm 0.11) \times 10^{-10}$ [2]. Collecting more events and enlarging the statistics are needed for understanding this decay process.

2 Experimental Overview

E949 at BNL [3] is a successor to E787. Beams and apparatus were similar to those of E787, but with several significant upgrades [4]. The signature of $K^+ \to \pi^+ \nu\bar{\nu}$ is a single π^+ and no other particle observed from the decay of a K^+ at rest. Side and end views of the upper half of the E949 detector are shown in fig.1. The K^+ beam entering the detector was identified by beam detectors (a Čerenkov counter, two wire chambers and a dE/dx counter), came to rest in a target of scintillating fibers and decayed after a suitable delay. The π^+ from the decay passed through a drift chamber, entered the cylindrical range stack (RS) of plastic scintillators, came to rest and decayed in the RS. The π^+ was identified by measuring its momentum, energy and range in scintillator, and by observing the $\pi^+ \to \mu^+ \to e^+$ decay sequence in the π^+ stopping counter. Photons from the K^+ decay were detected by a hermetic γ detector consisting of lead/scintillator sampling calorimeters (BV and BVL) surrounding the RS, undoped CsI calorimeters in End Caps (EC), and other detectors which covered the small solid angle around the beam line.

The new data was taken during the 12-week physics run in 2002. The number of kaons stopped in the target was $N_K = 1.8 \times 10^{12}$. Although the

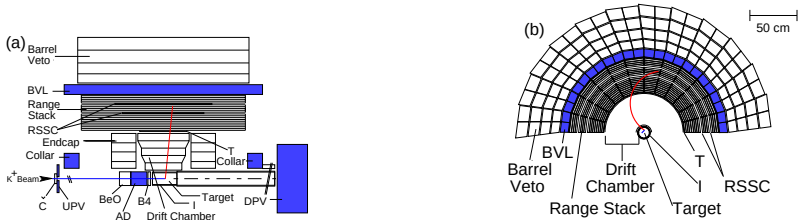

Figure 1: *Schematic views of the upper half of E949 detector from side (left) and end (right) views. The shaded detectors are the new γ detectors.*

instantaneous detector rate was twice that of E787, similar or even better kinematic measurement was achieved due to the detector upgrades (including, replacement of one third of the RS scintillators, installation of an RS gain monitor system, upgrades of electronics for the central drift chamber and replacement of electronics for the straw tube tracking chambers in the RS). Rejection of photons at the nominal acceptance increased by a factor of two compared to E787 because of the new γ detectors.

3 Analysis

The expected branching ratio is 10^{-10}, and large suppression of backgrounds is necessary. The reliable estimation of large rejection factors is challenging and required the development of a "bifurcated" method described below. A "blind" analysis was performed to avoid any bias due to small statistics. Background sources were identified a *priori* and a signal region was determined so that the sensitivity was optimized. The primary signal search is between the $K^+ \to \pi^+\pi^0$ ($K_{\pi 2}$) and $K^+ \to \mu^+\nu$ ($K_{\mu 2}$) momentum peaks, which is the cleanest search region. The main background sources are $K_{\pi 2}$, $K_{\mu 2}$, $K_{\mu m}$ (multibody decays with a muon, such as radiative $K_{\mu 2}$ and $K_{\mu 3}$) and scattered beam particles. The real data were used as much as possible for cut development and background estimation so that any unexpected bias or loophole could be suppressed. To reduce possible biases, a uniformly-sampled 1/3 portion of the whole data set was used for development of cuts and the remaining 2/3 portion for background estimation. The signal region was always masked out until the cut development and background estimation were finalized.

4 Likelihood Analysis

The backgrounds in the signal region were estimated with a "bifurcated" method. The method involved two uncorrelated cuts or group of cuts, which were independently inverted to enhance a particular background. That is, a background sample was created by selecting events which failed a specific cut. The rejection power of the complimentary cut was examined using the enhanced sample. Then a "background function" was developed by changing the severity of the cut. For example, the $K_{\mu 2}$ background was enhanced by selecting events which failed the requirement of the $\pi^+ \to \mu^+ \to e^+$ decay sequence in the RS

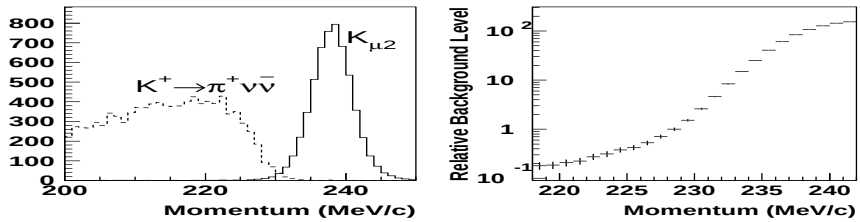

Figure 2: *The momentum distributions for $K_{\mu 2}$ (solid) and Monte Carlo $K^+ \to \pi^+ \nu\bar{\nu}$ (dashed) events (left) and the relative background level for $K_{\mu 2}$ as a function of momentum (right).*

stopping counter. The momentum distribution of this sample was examined to investigate how many events would be expected in the signal region, and the relative background level as a function of momentum was then obtained (see fig.2). All background functions were derived from the corresponding cuts used in the bifurcated method. Acceptance functions were also obtained in the same manner. Both acceptance and background functions gave the relative acceptance and background level at each cut position. The signal region was divided into small cells by binning all parameters of the functions and then the expected signal $S_i \equiv \mathcal{B}(K^+ \to \pi^+ \nu\bar{\nu}) N_K A_i$ and background b_i in each cell i were estimated, where A_i was the acceptance in cell i. The cells were characterized by the signal to background ratio S_i/b_i. Using a likelihood ratio technique [5], a confidence level (CL) and branching ratio were calculated from the S_i/b_i of the cells containing candidate events.

5 Sensitivity and Background Measurement

The acceptance and sensitivity are summarized in tab.1. With increased confidence in the likelihood technique the signal region was enlarged, increasing the background in the signal region (as summarized in tab.2), and increasing the acceptance by 30%. The total acceptance of E949 increased by about 10% (due to other losses) compared to that of E787.

Table 1: *Total acceptances and sensitivities for E787 and E949.*

	E787	E949
N_K (10^{12})	5.9	1.8
Acceptance (%)	0.20±0.02	0.22±0.02
Sensitivity (10^{-10})	0.83	2.6

Table 2: *Background levels in the signal region for E787 and E949.*

Sources	E787	E949
$K_{\pi 2}$	0.032	0.216
$K_{\mu 2}$	0.064	0.068
Beam	0.050	0.014
Total Backgrounds	0.146±0.005	0.298±0.026

6 Results

Examination of the signal region yielded one new event with $P = 227.3 \pm 2.7$ MeV/c, $R = 39.2 \pm 1.2$ cm (in equivalent cm of scintillator), and $E = 128.9 \pm 3.6$ MeV (see fig.3). This event has all the characteristics of the $K^+ \to \pi^+ \nu\bar{\nu}$ signal, although its momentum is near the upper kinematic limit for this decay and it has an early π^+ decay time of 6.2 ns, both of which increased the ambiguity in π^+ identification. The likelihood ratio technique gave $\mathcal{B}(K^+ \to \pi^+ \nu\bar{\nu}) = (0.96^{+4.09}_{-0.47}) \times 10^{-10}$ at 68% CL from the E949 data alone. The combined E787 and E949 result is $\mathcal{B}(K^+ \to \pi^+ \nu\bar{\nu}) = (1.47^{+1.30}_{-0.89}) \times 10^{-10}$ at 68% CL based on three candidate events. The signal to background ratio S/b and signal weight $W \equiv S/(S+b)$ based on the measured branching ratio are summarized in tab.3. The measured branching ratio is twice the SM prediction. This result is consistent with the SM and is consistent with more

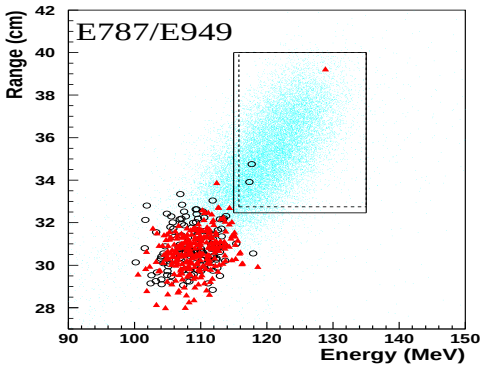

Figure 3: *Range and Energy of charged tracks for E787 (circles) and E949 (triangles) after all the other cuts are applied. Dots show the Monte Carlo $K^+ \to \pi^+ \nu\bar{\nu}$ events. Dashed and solid rectangles show the signal region for E787 and E949, respectively. A cluster near 110 MeV is due to $K_{\pi 2}$ events.*

Table 3: *Signal to background ratio and signal weight for E787 and E949.*

	E787		E949
Candidate	E787A	E787C	E949A
S/b	49	7	0.9
$W \equiv S/(S+b)$	0.98	0.88	0.48

than three times the SM and justifies the completion of the E949 experiment to increase the statistics and resolve the question.

7 Summary

BNL-E949 observed an additional $K^+ \to \pi^+\nu\bar{\nu}$ candidate in the new data and the measured branching ratio is $(1.47^{+1.30}_{-0.89}) \times 10^{-10}$ (68% CL) from the combined E787 and E949 data set.

Acknowledgments

This research was supported in part by the U.S. Department of Energy, the Ministry of Education, Culture, Sports, Science, and Technology of Japan, the Natural Sciences and Engineering Research Council and the National Research Council of Canada, the Russian Federation State Scientific Center Institute for High Energy Physics, and the Ministry of Industry, Science, and New Technologies of the Russian Federation.

References

1. S. Adler *et al*, Phys. Rev. Lett. **88**, 041803 (2002); S. Adler *et al*, Phys. Rev. Lett. **84**, 3768 (2000); S. Adler *et al*, Phys. Rev. Lett. **79**, 2204 (1997).
2. A.J. Buras *et al*, arXiv:hep-hp/0402112 (2004) and references therein.
3. V.V. Anisimovsky *et al*, Phys. Rev. Lett. **93** 031801 (2004); B. Bassalleck *et al*, E949 Proposal, BNL-67247, TRI-PP-00-06 (1999).
4. T. Yoshioka *et al*, IEEE Trans. Nucl. Sci, **51**, 199 (2004); O. Mineev *et al*, Nucl. Instr. Meth. **A494**, 362 (2002).
5. T. Junk, Nucl. Instr. Meth. **A434**, 435 (1999).

Frascati Physics Series Vol. XXXVI (2004), pp. 287–292
DAΦNE 2004: Physics at meson factories – Frascati, June 7-11, 2004
Selected Contribution in Plenary Session

NA48 RESULTS ON KAON RARE DECAYS

Giuseppe Ruggiero *
University of Firenze, Physics Department, via Sansone 1 Sesto Fiorentino

Abstract

The latest results of the NA48 experiment at CERN about rare K_L and K_S decays are reviewed. In particular the first observation of the decays $K_S \to \pi^0 e^+ e^-$ and $K_S \to \pi^0 \mu^+ \mu^-$ made by NA48 using the data collected during the 2002 K_S high intensity run are discussed. The measurement of the branching ratio of the $K_L \to e^+ e^- e^+ e^-$ decay using the 1998 and 1999 data is also presented.

1 Introduction

The NA48 experiment at CERN was designed to measure the direct CP violating parameter $Re(\epsilon'/\epsilon)$ using two simultaneous K_S and K_L beams. The

* On behalf of NA48 Collaboration

final result, based on the analysis of the data collected from 1998 to 2001, has been published [1]. Together with its main program, NA48 has also developed a research program on K_L and K_S rare decays. In 2002 the K_L beam was removed and decays from the K_S target only were collected with a proton intensity increased by about a factor 1000.

The NA48 detector revealed the products of the particles decaying in a 100 m long evacuated tube downstream to the K_S target. The detector, placed at the end of the decay tube, was composed by: a magnetic spectrometer consisting of 4 drift chambers separated by a dipole magnet, a quasi-homogeneous liquid krypton electromagnetic calorimeter, an iron scintillator hadronic calorimeter and a muon detector made by 3 scintillators planes separated by iron walls 80 cm thick [2].

2 The $K_S \to \pi^0 l^+ l^-$ decays

The parameter η of the Wolfenstein parametrization of the CKM matrix can be experimentally extracted from the measurement of the direct CP-violating component of the branching ratio of the $K_L \to \pi^0 l^+ l^-$ decay. However, also a CP conserving component and an indirect CP violating component contribute to the total branching ratio of this channel. The first component can be derived from the $K_L \to \pi^0 \gamma\gamma$ decay [3], while the second component from the $K_S \to \pi^0 l^+ l^-$ decays. Consequently the measurement of the branching ratio of the $K_S \to \pi^0 l^+ l^-$ decays allows η to be extracted from the $K_L \to \pi^0 l^+ l^-$ decay.

Because the predicted branching ratio for the $K_S \to \pi^0 l^+ l^-$ decay was about 10^{-9}, only few events were expected in the 2002 data taking period. We performed a blind analysis: a $2.5\sigma_{m_K} \times 2.5\sigma_{m_{\pi^0}}$ signal region and a $6.0\sigma_{m_K} \times 6.0\sigma_{m_{\pi^0}}$ control region were defined and kept masked until the selection cuts were fixed by using both data control samples and Monte Carlo simulations of signal and background.

2.1 The $K_S \to \pi^0 e^+ e^-$ decay

The $K_S \to \pi^0 e^+ e^-$ events were defined by two opposite charged tracks with momentum less than 40 GeV/c and at least 95% of their energy released in the electromagnetc calorimeter.

The backgrounds from final states with π^0 decaying in Dalitz mode ($\pi^0 \to \gamma e^+ e^-$) or with γ conversions in the detector were studied using Monte Carlo

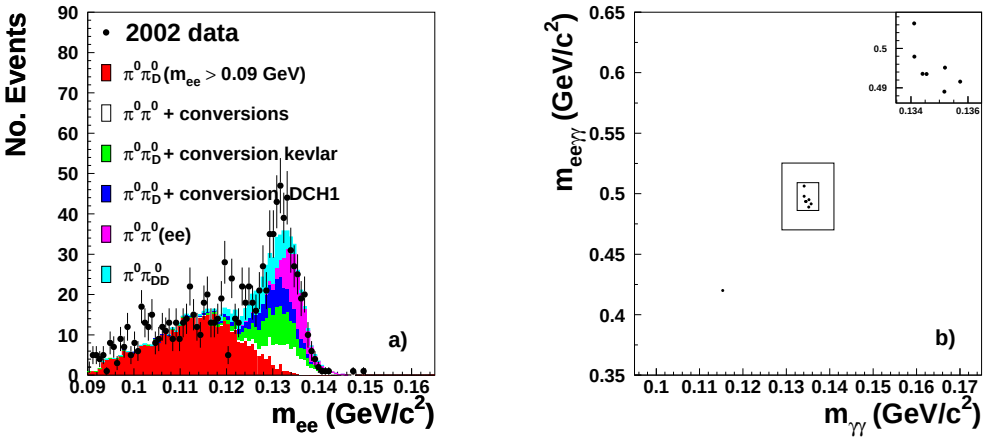

Figure 1: *(a) m_{ee} distribution of the Dalitz decays and γ conversions for data (dots) and Monte Carlo (curves). (b) Candidate events in m_K vs $m_{\gamma\gamma}$ mass plane. The boxes correspond to the control and signal region.*

simulations. An upper cut at 0.165 GeV/c^2 on m_{ee} was applied to reduce the expected contamination in signal region at a level of 0.01 event (see fig.1 (a)). The $K_L \to e^+e^-\gamma\gamma$ background was studied using 2001 K_L data and $0.08^{+0.03}_{-0.02}$ events were expected in signal region. The expected background from possible decays of the Ξ^0 in the beam was reduced at a negligible level by applying a cut on track momentum asymmetry. An accidental background due to the overlapping of different kaon decays was also taken into account by studying the data in extended time windows. About 0.07 events from accidental background were expected in signal region.

Seven events were found in signal region with an overall expected background of $0.15^{+0.10}_{-0.04}$. No events were found in control region, in agreement with the expectation (see fig.1 (b)). The signal acceptance was computed assuming an unit form factor in the $K_S \to \pi^0 e^+ e^-$ simulation. The final result is [4]:

$$BR(K_S \to \pi^0 e^+ e^-) = (5.8^{+2.8}_{-2.3}(stat) \pm 0.8(syst)) \times 10^{-9}. \qquad (1)$$

The main part of the systematic error comes from the extrapolation from the $m_{ee} > 0.165$ GeV/c^2 to the full m_{ee} region.

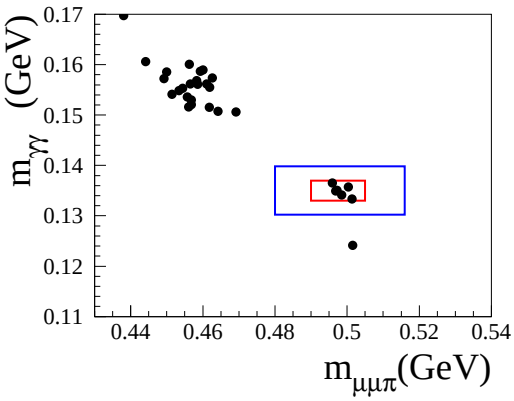

Figure 2: *The $K_S \to \pi^0\mu^+\mu^-$ candidates in the $m_{\gamma\gamma}$ vs m_K plane. The events at large $m_{\gamma\gamma}$ are consistent with $K_L \to \pi^+\pi^-\pi^0$ background, the event at low $m_{\gamma\gamma}$ with accidental background.*

2.2 The $K_S \to \pi^0\mu^+\mu^-$ decay

The $K_S \to \pi^0\mu^+\mu^-$ events were selected similarly to the $K_S \to \pi^0 e^+e^-$, but requiring the tracks to be associated to hits in the Moun Counters.

Suitable kinematical cuts allowed the expected background in the signal region from $K_L \to \pi^+\pi^-\pi^0$ events with two pions decaying in flight to be less than 0.02 events, as derived from Monte Carlo simulations. The background from Ξ^0 decays were rejected using a cut on track momentum asymmetry. Monte Carlo studies have shown an expected residual background in signal region from $K_L \to e^+e^-\mu^+\mu^-$ of 0.04 ± 0.04 events. The accidental background was taken into account as in the $K_S \to \pi^0 e^+e^-$ analysis. The accidental events expected in signal region were $0.18^{+0.18}_{-0.11}$.

Six events were found in signal region with an expected background of $0.22^{+0.19}_{-0.12}$. No events were found in control region in agreement with the expectation (see fig.2). As in the $K_S \to \pi^0 e^+e^-$ analysis, the signal acceptance was computed assuming an unit form factor in the $K_S \to \pi^0\mu^+\mu^-$ simulation. The final result is:

$$BR(K_S \to \pi^0\mu^+\mu^-) = (2.9^{+1.5}_{-1.2}(stat) \pm 0.2(syst)) \times 10^{-9}. \qquad (2)$$

2.3 Interpretation of the results

In the Chiral Perturbation Theory the branching ratio of the $K_S \to \pi^0 l^+ l^-$ depends on two parameters, a_S and b_S, that describe the $K_S \to \pi^0 l^+ l^-$ form factors [5]. The Vector Meson Dominance (VMD) model predicts $b_S/a_S = 0.4$. In this framework the parameter a_S, extracted independently from both the $K_S \to \pi^0 l^+ l^-$ branching ratio measurements, is:

$$|a_S|_{\pi^0 ee} = 1.06^{+0.26}_{-0.21} \pm 0.07 \tag{3}$$

$$|a_S|_{\pi^0 \mu\mu} = 1.55^{+0.38}_{-0.32} \pm 0.05 \tag{4}$$

These results agree each other within the errors. Moreover, the a_S and b_S extracted independently by a log-likelihood fit result compatible with the VMD.

2.4 Implications for $K_L \to \pi^0 l^+ l^-$

The CP violating component of the BR($K_L \to \pi^0 l^+ l^-$) can be written as:

$$BR(K_L \to \pi^0 l^+ l^-)_{CPV} \times 10^{12} = C_{MIX} \pm C_{INT} \left(\frac{\Im(\lambda_t)}{10^{-4}} \right) + C_{DIR} \left(\frac{\Im(\lambda_t)}{10^{-4}} \right)^2 . \tag{5}$$

C_{DIR} describes the direct CPV component, C_{MIX} and C_{INT} the indirect and interference CP violation part and depend on $|a_S|$. From the previous measurements of $|a_S|$, we can extract the overall dependence of $BR(K_L \to \pi^0 l^+ l^-)_{CPV}$ on $\Im(\lambda_t)$ within a sign ambiguity. Finally, taking $\Im(\lambda_t) = (1.36 \pm 0.12) \times 10^{-4}$ [6], we obtain:

$$BR(K_L \to \pi^0 e^+ e^-)_{CPV} \times 10^{12} = 17_{indirect} \pm 9_{interference} + 5_{direct} \tag{6}$$

$$BR(K_L \to \pi^0 \mu^+ \mu^-)_{CPV} \times 10^{12} = 9_{indirect} \pm 3_{interference} + 1_{direct} \tag{7}$$

3 The $K_L \to e^+ e^- e^+ e^-$ decay

The $K_L \to e^+ e^- e^+ e^-$ decay is expected to proceed mainly via the intermediate state $K_L \to \gamma^* \gamma^*$ [7, 8]. Therefore it depends on the structure of the $K_L \to \gamma^* \gamma^*$ vertex whose knowledge allows the CKM parameter ρ to be extracted from the $K_L \to \mu^+ \mu^-$ decay.

NA48 has measured the branching ratio of the $K_L \to e^+ e^- e^+ e^-$ decay using the data collected in 1998 and 1999. 4-Tracks events were identified as

candidate signal events if the tracks released in the electromagnetic calorimeter at least 93% of their energy. In the plane defined by the 4-tracks invariant mass, m_{eeee}, and the squared transverse momentum, p_t^2, the signal region was identified by the cuts 475MeV/c^2 < m_{eeee} <515MeV/c^2 and $p_t^2 < 0.0005$(GeV/c)^2.

200 Events were found in signal region with a background less than 1.0%. The background came from $K_L \to \pi^0\pi^0$ and $K_L \to \pi^0\pi^0\pi^0$ decays where at least two π^0 decayed in Dalitz mode or two γ's made conversion. The $K_L \to \pi^+\pi^-\pi^0$ decay was used as normalization channel and its acceptance, together with the signal acceptance, was computed using Monte Carlo simulations. The branching ratio was corrected for the electron identification efficiency measured both from data and Monte Carlo samples. The result is:

$$BR(K_L \to e^+e^-e^+e^-) = (3.30 \pm 0.24_{stat} \pm 0.14_{syst} \pm 0.10_{norm}) \times 10^{-8}. \quad (8)$$

4 Acknowledgments

It is a pleasure to thank the technical staff of the participating laboratories, universities and affiliated computing centers for their efforts in the construction of the NA48 detector apparatus, in the operation of the experiment, and in the processing of the data.

References

1. J.R. Batley *et al*, Phys. Lett. **B544**, 97 (2002).
2. A. Lai *et al*, Eur. Phys. J. **C22**, 231 (2001).
3. A. Lai *et al*, Phys. Lett. **B536**, 229 (2002).
4. A. Lai *et al*, Phys. Lett. **B576**, 43 (2003).
5. G. D'Ambrosio, G. Ecker, G. Isidori, J. Portoles, JHEP **9808**, 004 (1998).
6. M. Battaglia *et al*, "The CKM matrix and the unitarity triangle", hep-ph/0304132.
7. Z.E.S. Uy, Phys. Rev. **D43** 802 (1991) and Phys. Rev. **D43** 1572 (1991); T. Miyasaki, Nuovo Cimento **5** 125 (1972).
8. T. Miyasaki and E. Taksugi, Phys Rev. **D8** 2051 (1973).

Frascati Physics Series Vol. XXXVI (2004), pp. 293–298
DAΦNE 2004: Physics at meson factories – Frascati, June 7-11, 2004
Selected Contribution in Plenary Session

THE $a_0 - a_2$ PION SCATTERING LENGTH FROM $K^+ \to \pi^+\pi^0\pi^0$ DECAY

Nicola Cabibbo*
CERN, Physics Department CH-1211 Geneva 23, Switzerland

Abstract

I present a new method for determining the pion-pion scattering length combination $a_0 - a_2$ through the analysis of the Dalitz plot of the $K^+ \to \pi^+\pi^0\pi^0$ decay in the region where the invariant mass of the $\pi^0\pi^0$ pair is in the vicinity of the $\pi^+\pi^-$ threshold.

1 Pion-pion scattering lengths

An impressive development of the last few years is the emergence of technologies which allow for very high statistics experiments. The prime example of this trend is offered by BaBar and Belle which together have collected $\sim 10^8$ well

* On leave from Università di Roma 'La Sapienza' and INFN, Sezione di Roma

measured $B - \bar{B}$ pairs. High statistics means the possibility of studying subtle effects, such as the one I will discuss, which can lead to a precision measurement of the $\pi\pi$ scattering length combination $a_0 - a_2$, a measurement made possible by the availability in NA48 of $\sim 10^8$ well-analyzed $K^+ \to \pi^+\pi^0\pi^0$ events.

Weinberg's predictions of the S-wave $\pi\pi$ scattering lengths [1], or the modern improved computations, are justly considered as one of the principal results of Chiral Perturbation Theory in its purest form: that of a theory of low energy (soft) pions and their interactions. Pion-pion S-wave scattering lengths are now predicted in Chiral Perturbation Theory with a very small uncertainty [2, 3]:

$$\begin{aligned} a_0 m_{\pi^+} &= 0.220 \pm 0.005 \\ a_2 m_{\pi^+} &= -0.0444 \pm 0.0010 \\ (a_0 - a_2) m_{\pi^+} &= 0.265 \pm 0.004 \end{aligned} \tag{1}$$

Can the accuracy of these predictions be matched by experimental results? It was long recognized [4] that the angular distributions in $K^+ \to \pi^+\pi^- e^+\nu$ are sensitive to the $\pi\pi$ phase shifts, and can be used to obtain informations on the S-wave scattering lengths [5, 6]. The first results by the Geneva-Saclay experiment [7], leading to $a_0 m_{\pi^+} = 0.26 \pm 0.05$, were recently improved by the E865 collaboration at Brookhaven [8] that quotes a result: $a_0 m_{\pi^+} = 0.216 \pm 0.013$ (stat.)± 0.002 (syst.)± 0.002 (theor). Data on K_{e4}, with a large statistics, are currently being analyzed by the NA48 collaboration at CERN.

The K_{e4} decay yields values of the phase shift difference $\delta_0^0 - \delta_1^1$ as a function of the $\pi\pi$ invariant mass $M_{\pi\pi}$ in the range $2m_{\pi^+} < M_{\pi\pi} < M_K - m_{\pi^+}$, but the best data lies in the range > 310 MeV. The extraction of a value for a_0 requires an extrapolation to the threshold region and a substantial theoretical input, whence the interest in alternative methods which permit the determination of the scattering lengths through measurements that are directly sensitive to $\pi\pi$ scattering in the threshold region, $M_{\pi\pi} \sim 2m_{\pi^+}$. An example of this is the decay rate of the pionic atom $\pi^+\pi^-$. This decay is due to the $\pi^+\pi^- \to \pi^0\pi^0$ transition at an energy that essentially coincides with the $\pi^+\pi^-$ threshold, so that its rate is directly proportional to $(a_0 - a_2)^2$. The DIRAC experiment at CERN [9, 10] is now attempting a measurement of the pionic atom decay rate.

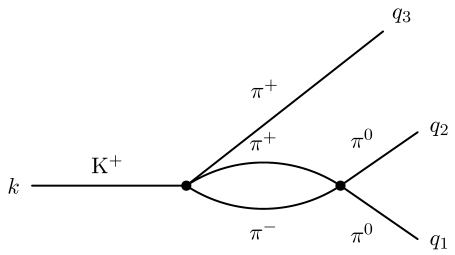

Figure 1: *Contribution of* $\pi^+\pi^- \to \pi^0\pi^0$ *to* $K^+ \to \pi^+\pi^0\pi^0$.

2 A new measurement of $a_0 - a_2$

An entirely new method [11)] for measuring the value of $a_0 - a_2$ is based on a subtle modification that $\pi\pi$ re-scattering introduces in the $K^+ \to \pi^+\pi^0\pi^0$ Dalitz plot when the $\pi^0\pi^0$ invariant mass is close to the $\pi^+\pi^-$ threshold. The new method can lead to a measurement of $a_0 - a_2$, and is also sensitive to the sign of this quantity.

The contribution of the $\pi^+\pi^- \to \pi^0\pi^0$ rescattering can be graphically represented by the diagram in fig. 1. The effect of this diagram can be directly computed in chiral perturbation theory, but the result is really independent from this theory, since in the vicinity of the $\pi^+\pi^-$ threshold the result can be directly derived from the unitarity of the **S**-matrix, $\mathbf{S}^\dagger\mathbf{S} = 1$, which determines the absorptive part of the amplitude above the threshold, and the analyticity of the **S**-matrix elements as a function of the external momenta, which determines their analytic continuation from the region above the threshold, where the amplitude of the diagram is absorptive, to the region below the threshold, where the amplitude is dispersive.

If we write the amplitude for the $K^+ \to \pi^+\pi^0\pi^0$ decay as

$$\mathcal{M} = \mathcal{M}(K^+ \to \pi^+\pi^0\pi^0) = \mathcal{M}_0 + \mathcal{M}_1 \tag{2}$$

with $\mathcal{M}_0$ the "unperturbed" amplitude, and $\mathcal{M}_1$ the contribution of the re-scattering graph, above the $\pi^+\pi^-$ threshold we obtain an imaginary value,

$$\mathcal{M}_1 = i2\frac{(a_0 - a_2)m_{\pi^+}}{3}\mathcal{M}_{+,\mathrm{thr}}\sqrt{(s_{\pi\pi} - 4m_{\pi^+}^2)/s_{\pi\pi}} \tag{3}$$

which turns into a real value below the threshold,

$$\mathcal{M}_1 = -2\frac{(a_0 - a_2)m_{\pi^+}}{3}\mathcal{M}_{+,\mathrm{thr}}\sqrt{(4m_{\pi^+}^2 - s_{\pi\pi})/s_{\pi\pi}} \tag{4}$$

where $\mathcal{M}_{+,\mathrm{thr}}$ is the amplitude of the $K^+ \to \pi^+\pi^+\pi^-$ decay evaluated at the $\pi^+\pi^-$ threshold. If now we look at the square of the amplitude in eq. (2), below threshold there is an interference term:

$$|\mathcal{M}|^2 = (\mathcal{M}_0)^2 + (\mathcal{M}_1)^2 + 2\mathcal{M}_0\mathcal{M}_1$$

which is absent above the threshold, where

$$|\mathcal{M}|^2 = (\mathcal{M}_0)^2 + |\mathcal{M}_1|^2$$

The interference term is proportional to $a_0 - a_2$. Taking the theoretical pre-

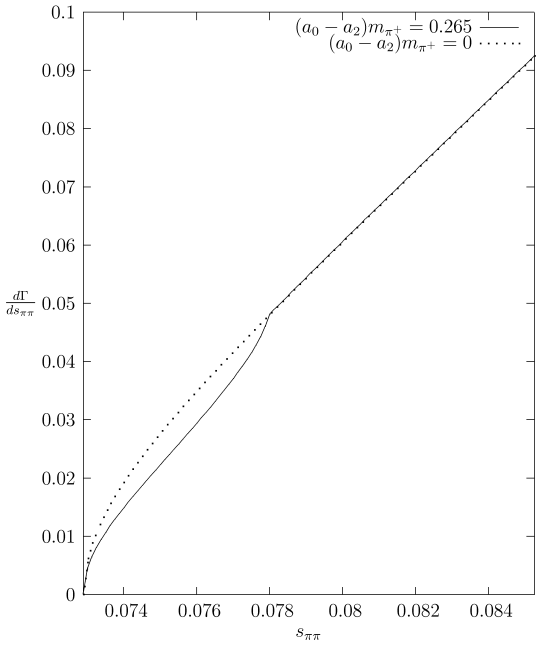

Figure 2: *The $s_{\pi\pi}$ invariant mass distribution with/without the re-scattering correction, in the threshold region, arbitrary units.*

dictions for $a_0 - a_2$, and the PDG values for the $K \to \pi\pi\pi$ decays one obtains

the $\pi^0\pi^0$ spectrum in fig. 2, which displays a $\sim$10% deviation below the $\pi^+\pi^-$ threshold. The region below the threshold contains only $\sim$ 3% of the events, but with $\sim 10^8$ $K^+ \to \pi^+\pi^0\pi^0$ events this 10% deviation can be determined with a $\sim$ 1.5% statistical error!

With such a small statistical error, the accuracy of the result will critically depend on a firm control of the systematics. From the theoretical side many aspects require more work. First of all we should include the effects of coulomb corrections, which may become significant close to the $\pi^+\pi^-$ threshold, and of radiative corrections. One would also like to revisit the derivation of the predictions in eq. (1) to take into account the fact that we are working in a region — between the $\pi^0\pi^0$ and the $\pi^+\pi^-$ thresholds — where in a sense isospin invariance is maximally broken. We should finally take into account the fact that both $\mathcal{M}_0$ and $\mathcal{M}_{+,\mathrm{thr}}$ receive small imaginary contributions from other rescattering diagrams [12]; these contributions, although not singular at the $\pi^+\pi^-$ threshold, modify the interference terms with $\mathcal{M}_1$ both above and below the $\pi^+\pi^-$ threshold.

References

1. S. Weinberg, Phys. Rev. Lett. **17** (1966) 616.
2. G. Colangelo, J. Gasser and H. Leutwyler, Phys. Lett. B **488** 261 (2000) [arXiv:hep-ph/0007112].
3. G. Colangelo, J. Gasser, and H. Leutwyler, Nucl. Phys. **B603**, 125 (2001).
4. E. P. Shabalin, Sov. Phys. (JETP) **17**, 517 (1963) (Zh. Eksp. Teor. Fiz. **44**, 765 (1963)).
5. N. Cabibbo, and A. Maksymowicz, Phys. Rev. **137**, B438 (1965).
6. A. Pais, and S.B. Treiman, Phys. Rev. **168**, 1858 (1968).
7. L. Rosselet *et al.*, Phys. Rev. D **15**, 574 (1977).
8. S. Pislak *et al.*, Phys. Rev. D **67** 072004 (2003) [arXiv:hep-ex/0301040]. For an independent analysis of the E865 data see: S. Descotes-Genon, N. H. Fuchs, L. Girlanda and J. Stern, Eur. Phys. J. C **24** (2002) 469 [arXiv:hep-ph/0112088].

9. F. Gomez *et al.*, DIRAC Coll., Proc. Int. Euroconf. on Quantum Chromodynamics: 15 Years of the QCD, Montpellier, France (July 2000), Nucl. Phys. Proc. Suppl. **96**, 259 (2001).

10. J. Gasser, V. E. Lyubovitskij and A. Rusetsky, Phys. Lett. B **471**, 244 (1999) [arXiv:hep-ph/9910438], and H. Sazdjian, Phys. Lett. B **490**, 203 (2000) [arXiv:hep-ph/0004226].

11. N. Cabibbo, to be published in Phys. Rev Lett. [arXiv:hep-ph/0405001].

12. G. D'Ambrosio, G. Isidori, A. Pugliese and N. Paver, Phys. Rev. D **50**, 5767 (1994) [Erratum-ibid. D **51**, 3975 (1995)] [arXiv:hep-ph/9403235].

Frascati Physics Series Vol. XXXVI (2004), pp. 299–304
DAΦNE 2004: Physics at meson factories – Frascati, June 7-11, 2004
Selected Contribution in Plenary Session

A DIRECT SEARCH FOR $K_S \to 3\pi^0$ DECAY AT KLOE

M. Martini *
Laboratori Nazionali di Frascati dell'INFN, Frascati, Italy.

*On behalf of the KLOE collaboration: A. Aloisio, F. Ambrosino, A. Antonelli, M. Antonelli, C. Bacci, G. Bencivenni, S. Bertolucci, C. Bini, C. Bloise, V. Bocci, F. Bossi, P. Branchini, S. A. Bulychjov, R. Caloi, P. Campana, G. Capon, T. Capussela, G. Carboni, F. Ceradini, F. Cervelli, F. Cevenini, G. Chiefari, P. Ciambrone, S. Conetti, E. De Lucia, P. De Simone, G. De Zorzi, S. Dell'Agnello, A. Denig, A. Di Domenico, C. Di Donato, S. Di Falco, B. Di Micco, A. Doria, M. Dreucci, O. Erriquez, A. Farilla, G. Felici, A. Ferrari, M. L. Ferrer, G. Finocchiaro, C. Forti, P. Franzini, C. Gatti, P. Gauzzi, S. Giovannella, E. Gorini, E. Graziani, M. Incagli, W. Kluge, V. Kulikov, F. Lacava, G. Lanfranchi, J. Lee-Franzini, D. Leone, F. Lu, M. Martemianov, M. Martini, M. Matsyuk, W. Mei, L. Merola, R. Messi, S. Miscetti, M. Moulson, S. Müller, F. Murtas, M. Napolitano, F. Nguyen, M. Palutan, E. Pasqualucci, L. Passalacqua, A. Passeri, V. Patera, F. Perfetto, E. Petrolo, L. Pontecorvo, M. Primavera, P. Santangelo, E. Santovetti, G. Saracino, R. D. Schamberger, B. Sciascia, A. Sciubba, F. Scuri, I. Sfiligoi, A. Sibidanov, T. Spadaro, E. Spiriti, M. Tabidze, M. Testa, L. Tortora, P. Valente, B. Valeriani, G. Venanzoni, S. Veneziano, A. Ventura, S. Ventura, R. Versaci, I. Villella, G. Xu

Abstract

We have searched for $K_S \to 3\pi^0$ decay in a sample of $\sim$450 pb^{-1} of electron-positron collisions collected at the Frascati ϕ-factory DAΦNE. A direct observation of this decay is a sign of CP violation and a stringent limit on its branching ratio, BR, helps on improving the accuracy on the CPT violation parameter of the mixing matrix δ. The most stringent limit on $BR(K_S \to 3\pi^0)$ is obtained.

1 The KLOE experiment

The data were collected with the KLOE [1, 4] detector at DAΦNE [5], the Frascati ϕ-factory. DAΦNE is an e^+e^- collider which operates at a center of mass energy W of $\sim$ 1020 MeV, the mass of the ϕ-meson [6]. ϕ mesons are produced, essentially at rest, with a visible cross section of $\sim$ 3.2 μb and decay into K^+K^- (K_SK_L) pairs with BR of $\sim$ 49% ($\sim$ 34%). All of the above implies that the detection of a K_L guarantees the presence of a K_S of given momentum and direction. We refer to this technique as K_S *tagging*.

The KLOE detector consists of a large cylindrical drift chamber, DC [1], surrounded by a lead-scintillating fiber electromagnetic calorimeter, EMC [2]. A superconducting coil around the EMC provides a 0.52 T field.

The drift chamber is 4 m in diameter and 3.3 m long. The position resolutions are σ_{xy} $\sim$150 μm and σ_z $\sim$ 2 mm. The momentum resolution is $\sigma(p_\perp)/p_\perp \approx 0.4\%$. Vertices are reconstructed with a spatial resolution of $\sim$3 mm.

The calorimeter is divided into a barrel and two endcaps and covers 98% of the solid angle. The arrival times of particles and the positions in three dimensions of the energy deposits are obtained from the signals collected at the two ends. Energy and time resolutions are $\sigma_E/E = 5.7\%/\sqrt{E\ (\mathrm{GeV})}$ and $\sigma_t = 57\ \mathrm{ps}/\sqrt{E\ (\mathrm{GeV})} \oplus 50$ ps, respectively.

During 2002 data taking, the maximum luminosity reached by DAΦNE was $7.5 \cdot 10^{31}$ cm^{-2} s^{-1} ($\sim$ 160 ϕ/s) and at the end of 2002, we collected $\sim$ 4.5 pb^{-1}/day. The entire collected sample (2001-2002) amounts to 450 pb^{-1}, equivalent to 1.4 billion (450 million) ϕ decays (K_S,K_L pairs).

The mean decay lengths of the K_S and K_L are $\lambda_S \sim 0.6$ cm and $\lambda_L \sim 340$ cm. The K_L interaction in the calorimeter (K_L-crash) is identified by requiring

a cluster of energy above 100 MeV, which is not associated to any track, and whose time corresponds to a velocity $\beta = R/cT$ compatible with that one of the K_L, $\beta_k \sim 0.2$. The K_L-crash provides a clean K_S tagging. Reconstruction of one kaon establishes the trajectory of the other one with an angular resolution of 1° and a momentum resolution of ~ 2 MeV.

2 Introduction

The decay $K_S \to 3\pi^0$ is a pure CP violating process. The related CP violation parameter is defined as the ratio of K_S to K_L decay amplitudes: $\eta_{000} = A(K_S \to 3\pi^0)/A(K_L \to 3\pi^0) = \varepsilon + \varepsilon'_{000}$ where ε describes the CP violation in the mixing matrix and ε'_{000} is a direct CP violating term. In the Standard Model we expect η_{000} to be similar to η_{00}. The expected branching ratio, BR, of this decay, is therefore $\sim 2 \cdot 10^{-9}$ The best upper limit on the BR has been set to $1.5 \cdot 10^{-5}$ by SND [7] The weighted average of the best published values [8, 9] gives: $\eta_{000} = (0.08 \pm 0.11) + i \cdot (0.07 \pm 0.16)$. Study this decay is also important because the uncertainty on η_{000} limits the precision on CPT test via the unitarity relation [10]. A neutral kaon state [6] can be expressed as: $K_{S,L} = K_{1,2} + (\varepsilon \pm \delta)K_{2,1}$ where K_1 and K_2 are the two CP eigenstates and δ is a CPT violation parameter in mixing. A possible form of the unitarity relation is:

$$(1 + i\tan(\phi_{sw}))(\Re(\varepsilon) - i\Im(\delta)) = \sum (A^*(K_S \to f)A(K_L \to f)/\Gamma_S) \qquad (1)$$

where the sum runs over all the possible decay channels f, and $\tan(\phi_{sw}) = 2\Delta m_{S,L}/(\Gamma_S - \Gamma_L)$. According to ref. [11], the value of $\Im(\delta) = (2.4 \pm 5.0) \cdot 10^{-5}$ is limited by the measurement on η_{000}. Neglecting this term, the same analysis yields $\Im(\delta) = (-0.5 \pm 2.0) \cdot 10^{-5}$; an improvement of around a factor 2.5 on the accuracy.

3 The direct search of $K_S \to 3\pi^0$

In this analysis we have used the whole sample of 450 pb^{-1}, and we expect 0.9 standard model $K_S \to 3\pi^0$ events produced.

Our selection starts by requiring a K_L-crash tag and six neutral clusters coming from the interaction point, IP. A tight constraint on β and moderate requirements on energy and angular acceptance are applied in order to have

a large control sample for the background, while retaining a large selection efficiency for the signal. Applying this selection we have an initial sample of ∼39000 events. To get the branching ratio we then normalize the final event counting to the rate of $K_S \to 2\pi^0$.

Since $K_S \to 3\pi^0$decay has 6 photons in the final state, the major expected background in this search is $K_S \to 2\pi^0$ +2 fake photons coming from shower fragments, machine background clusters in overlap with the events or both possibilities.

The first step to reduce the background is the application of a kinematic fit procedure which imposes K_S mass, K_L 4-momentum conservation and $\beta = 1$ for each γ. By cutting at reasonable χ^2_{fit} value (ndf=11, $\chi^2_{\rm fit}/{\rm ndf} < 3$) we retain 70% of the signal and reduce of a factor ~ 3 the background.

To further improve the rejection and disentangle $3\pi^0$ from $2\pi^0$ final states, we define 2 pseudo-χ^2, $\chi^2_{3\pi}$ and $\chi^2_{2\pi}$. The $\chi^2_{3\pi}$ is based only on the 3 best reconstructed pion masses, while the $\chi^2_{2\pi}$ selects 4 out of the 6 photons providing the best kinematic agreement with the $K_S \to 2\pi^0$ decay. By studying the correlation between $\chi^2_{3\pi}$ and $\chi^2_{2\pi}$ we define a signal box and five surrounding control boxes. To determine how well the data-MC normalization holds in different scatter-plot regions we have projected $\chi^2_{3\pi}$ in bands of $\chi^2_{2\pi}$. All bands show a reasonable data-MC agreement. Studying these comparison, we found a large peak near our signal box, due to fake K_L-crash tags given mostly by $K_S \to \pi^+\pi^-$, $K_L \to 3\pi^0$ events. For this background, the K_S charged pions interact on the quadrupoles creating late clusters which simulates the K_L-crash, while part of the K_L's decay close to the IP thus mimicking our signal. Our Monte Carlo simulates well the shapes of the fake K_L-crash background and we have calibrated its amount fitting data with a linear combination of MC with and without K_L-crash fakes.

Although by cutting on χ^2_{fit} we have a good handle on the fake K_L-crash background we reduce it to a negligible amount by vetoing events with tracks coming from the IP (see Fig. 1). Moreover, in order to enforce the $\chi^2_{2\pi}$ selection of photons we add a cut on the variable $\Delta E = M_\phi/2 - \sum E_i$, where the sum runs over the four γ's chosen by the $\chi^2_{2\pi}$ algorithm. For a $K_S \to 2\pi^0 + 2\gamma$ fake events $\Delta E \sim 0$ MeV, while for a signal event the missing π^0 mass reflects in a larger ΔE value (~ 135 MeV).

Before opening the signal-box we have optimized the limit [12] by varying

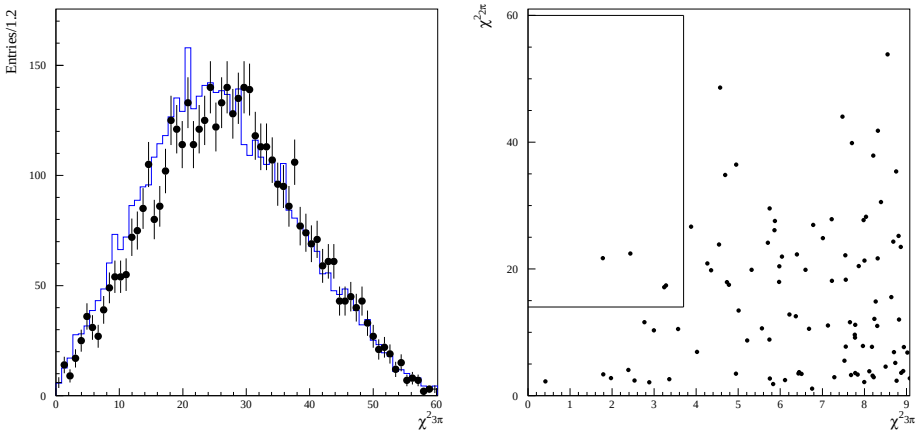

Figure 1: *(left)* $\chi 2_{3\pi}$ *distribution in the band of* $\chi 2_{2\pi}$ *which contain the signal box for DATA (●●) and Monte Carlo (–) after track veto; (right) candidates from data in the signal box, at the end of the analysis chain.*

the cuts on χ^2_{fit}, $\chi^2_{2\pi}$, $\chi^2_{3\pi}$ and ΔE on the MC samples. As a result of this procedure the final cuts have been set to: $\chi^2_{fit} < 31$, $\Delta E > 37$ MeV and we have defined the following signal box region ($14 < \chi^2_{2\pi} < 60$ and $\chi^2_{3\pi}$ <3.7).

With an efficiency, after tagging, of $\varepsilon_{3\pi} = (22.6 \pm 0.8)\%$, we count 4 events (See Fig. 1) for an expected background $N_b = 3.2 \pm 1.4_{MCstat} \pm 0.5_{syst}$. The systematic error on the background is evaluated by comparing, data and MC expectations, in the five control boxes while varying the analysis cuts. Folding a gaussian behavior to the background uncertainty, we quote the number of $K_S \to 3\pi^0$ decay to be below 5.8 at 90% C.L. In the same tagged sample, we count $3.8 \cdot 10^7$ $K_S \to 2\pi^0$ events to normalize the counting to the BR($K_S \to 2\pi^0$). By this normalization we finally derive BR($K_S \to 3\pi^0$) $\leq 2.1 \cdot 10^{-7}$ at 90% C.L. which improves of a factor ~ 70 the previous measurement.

4 Related physical results

Our result on the upper limit can be used to calculate other parameters directly related to CPT test. From relation:

$$|\eta_{000}| = \frac{A(K_S \to 3\pi^0)}{A(K_L \to 3\pi^0)} = \sqrt{\frac{\tau_S}{\tau_L} \frac{BR(K_S \to 3\pi^0)}{BR(K_L \to 3\pi^0)}} \qquad (2)$$

we obtain $|\eta_{000}| \leq 0.024$ at 90 % C.L. which reduces of a factor ~ 5 the

uncertainty on this parameter [7, 8, 9].

We can also set a conservative limit on the contribution of the $K_S \to 3\pi^0$decay to $\Im(\delta)$ ($\Im(\delta_{000})$). From eq. 1 we obtain:

$$\Im(\delta_{000}) = -\Im\left[\frac{1}{1+i\tan(\phi_{SW})}\alpha_{000}\right] \tag{3}$$

where $\alpha_{000} = \tau_S/\tau_L BR(K_L \to 3\pi^0)\eta_{000}$ [10]. We finally derive:

$$\Im(\delta_{000}) = BR(K_L \to 3\pi^0)\frac{\tau_S}{\tau_L}|\eta_{000}|cos(\phi_{SW})sin(\phi_{SW}-\phi_{000}) \tag{4}$$

where ϕ_{000} is the η_{000} complex-phase. For any possible value of ϕ_{000} our limit on $|\eta_{000}|$ bounds $|\Im(\delta_{000})| < 6.34 \cdot 10^{-6}$ at 90 % C.L.

Our measurement makes η_{000} comparable to the existing measurement of $\eta_{+-0} = [(-2 \pm 8) + i(-2 \pm 9)] \times 10^{-3}$. Hence, following the analysis of CPLEAR [11] we conclude that the accuracy on $\Im(\delta)$ is now reduced to $2.5{\cdot}10^{-5}$ without any further assumption.

References

1. KLOE collaboration, Nucl. Inst. Meth. A 488 (2002), 51.
2. KLOE collaboration, Nucl. Inst. Meth. A 482 (2002), 364.
3. KLOE collaboration, Nucl. Inst. Meth. A 483 (2002), 649.
4. KLOE collaboration, Nucl. Inst. Meth. A 492 (2002), 134.
5. S. Guiducci, in: P. Lucas, S. Weber (Eds.), Proceedings of the 2001 Particle Accelerator Conference, Chicago, Il., USA, 2001.
6. C.D. Buchanan *et al*, Phys. Rev. **D45**, 4088 (1992).
7. M.N. Achasov *et al*, SND collaboration, Phys. Lett. **B459**, 674 (1999).
8. V.V. Barmin *et al*, Phys. Lett. **B128**, 129 (1983).
9. CPLEAR collaboration, Phys. Lett. **B425**, 391 (1998).
10. G.B. Thomson and Y. Zou, Phys. Rev. **D51**, 1412 (1995).
11. CPLEAR collaboration, Phys. Lett. **B456**, 297 (1999).
12. J.F. Grivaz and F. Le Diberder, LAL **92-37**, (1992).

Frascati Physics Series Vol. XXXVI (2004), pp. 305–310
DAΦNE 2004: Physics at meson factories – Frascati, June 7-11, 2004
Selected Contribution in Plenary Session

FUTURE KAON PROGRAM AT KEK/J-PARC

Takeshi K. Komatsubara
High Energy Accelerator Research Organization (KEK),
Ibaraki 305-0801, Japan

Abstract

The current program of kaon-decay experiments at the KEK 12 GeV Proton Synchrotron (KEK-PS) and the prospects for the future kaon program at the new 50 GeV PS of J-PARC, being constructed in Japan, are reviewed.

1 Overview

Experiments at KEK-PS started in 1977, and distinguished kaon experiments in search of $K^+ \to \pi^+\nu\bar{\nu}$, heavy-neutrino emission in $K^+ \to \mu^+\nu$, right-handed currents in $K^+ \to \mu^+\nu$ and $K_L^0 \to \mu^\pm e^\mp$, respectively, were made in 1980's. After the Booster of BNL-AGS increased the proton intensity to be high, a measurement of $K_L^0 \to \pi^+\pi^- e^+ e^-$ and a search for T-violating transverse muon polarization in $K^+ \to \pi^0\mu^+\nu$, which were suitable for low-energy kaons and complementary to the experiments in other laboratories, were performed

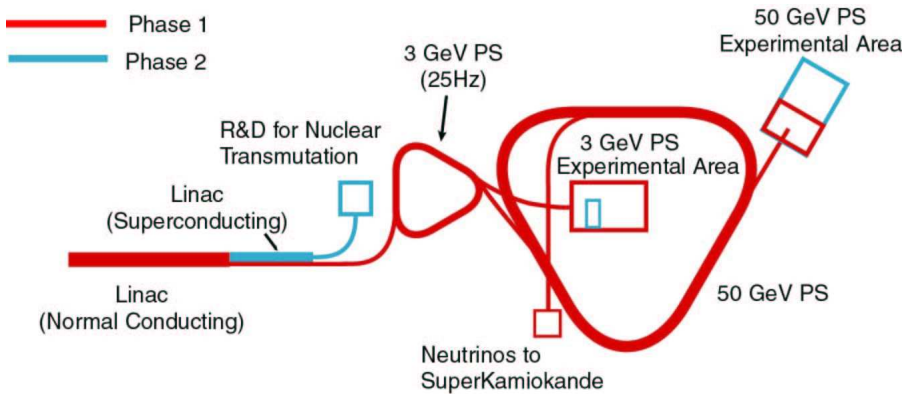

Figure 1: *J-PARC accelerators.*

at KEK-PS. Kaon physicists also participated in the E787/E949 experiments at BNL and the KTeV experiment at FNAL through the Japan-U.S. Cooperative Research Program.

To this day KEK-PS delivers fast-extracted beams to the K2K long-baseline neutrino experiment for 6 months per year and slow-extracted beams to the experiments in the East and North Counter Halls for 2 to 4 months per year [1]. A typical slow-extracted beam is $2.5 \cdot 10^{12}$ protons per 2.0-second spill in every 4.0 seconds. Experiment 391a [2], which is the first dedicated search for the $K_L^0 \to \pi^0 \nu\bar{\nu}$ decay, has carried out the first physics run successfully from February to June 2004.

J-PARC, which stands for Japan Proton Accelerator Research Complex [3], is the joint project of Japan Atomic Energy Research Institute (JAERI) and KEK. The accelerators (fig.1) are under construction at the Tokai site of JAERI located at 50km northeast of KEK. The construction will be finished in 2008 and, with very intense proton beams from the new 50 GeV PS, great opportunities for various researches in nuclear and particle physics, including kaon experiments with much higher sensitivities than ever, would be opened.

The rest of this article is devoted to a report of the status of the E391a

experiment and the future kaon experiments at J-PARC. The E246/E470 experiments on T-violation in $K^+ \to \pi^0\mu^+\nu$ and direct photon emission in $K^+ \to \pi^+\pi^0\gamma$ are reported elsewhere [4] [5].

2 E391a Experiment for $K_L^0 \to \pi^0\nu\bar{\nu}$

Observation of the rare decay $K_L^0 \to \pi^0\nu\bar{\nu}$ is a new evidence for CP violation in kaon decays. The branching ratio is represented within the Standard Model (SM) as [6]:

$$B(K_L^0 \to \pi^0\nu\bar{\nu}) = 2.12 \cdot 10^{-10} \times [\ \frac{\lambda}{0.224}\ ]^8 \times (\ \frac{Im\lambda_t}{\lambda^5} \cdot X(x_t)\ )^2 \qquad (1)$$

where $X(x_t)$ is the Inami-Lim loop function [7] with the QCD correction, x_t is the square of the ratio of the top to W masses, and

$$\lambda_t \equiv V_{ts}^* \cdot V_{td} = A^2\lambda^5 \cdot (1 - \rho - i\eta) \qquad (2)$$

in the Wolfenstein parametrization A, λ, ρ, and η. The SM prediction is $(3.0 \pm 0.6) \cdot 10^{-11}$, in which theoretical uncertainties are only a few %. A model-independent bound called the Grossman-Nir limit [8]:

$$B(K_L^0 \to \pi^0\nu\bar{\nu}) < 4.4 \times B(K^+ \to \pi^+\nu\bar{\nu}) < 1.4 \cdot 10^{-9} \qquad (3)$$

can be extracted from its isospin-relation to the $K^+ \to \pi^+\nu\bar{\nu}$ decay [9]. New physics beyond the SM could enhance the branching ratio by one order of magnitude: $(3.1 \pm 1.0) \cdot 10^{-10}$ [10]. The current upper limit on the branching ratio $< 5.9 \cdot 10^{-7}$ was set by the KTEV collaboration [11] using the Dalitz decay mode $\pi^0 \to e^+e^-\gamma$ of 1.2%.

The E391a experiment [1](fig.2) searches for the $K_L^0 \to \pi^0\nu\bar{\nu}$ decay with collimated "pencil" neutral beams. An endcap calorimeter with undoped CsI crystals detects two photons from $\pi^0 \to \gamma\gamma$ and measures their energy and position. The K_L^0-decay vertex position along the beam line is determined from the constraint of π^0 mass. Calorimeters that cover the decay region do hermetic photon detection and reject the background from $K_L^0 \to \pi^0\pi^0$. Charged particles are removed by their energy deposits in a plastic scintillator in front of each calorimeter.

[1]E391a is an international collaboration of KEK, Saga, Yamagata, RCNP, Osaka, NDA, JINR, Chicago, TNU, Pusan, and Kyoto.

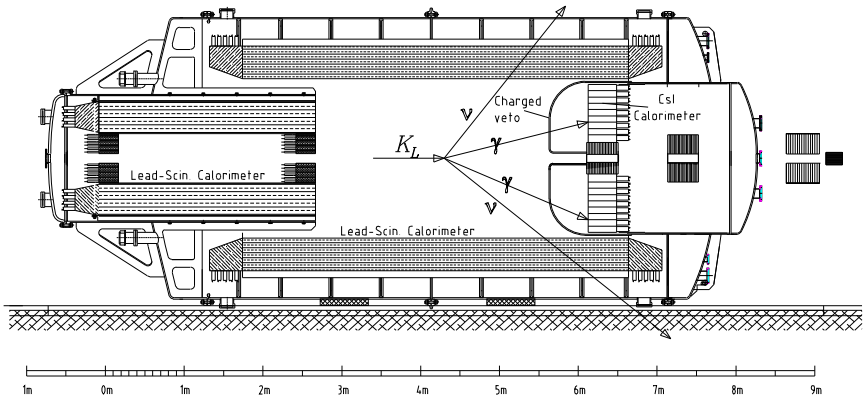

Figure 2: *Side-view of the E391a detector.*

Beam line survey and detector construction were performed from 2001 to 2003, and the first physics run was carried out in 2004. The beam line, which had been designed carefully, provided clean neutral beams; in the decay region a high vacuum of $1.21 \cdot 10^{-5}$ Pa was achieved. Fig.3 shows the $K_L^0 \to \pi^0\pi^0\pi^0$ decay reconstructed from the events with six clusters in the CsI calorimeter. These events were used online to monitor the beam line and detector during the data taking.

The goal of E391a is to achieve a sensitivity below the Grossman-Nir limit ($1.4 \cdot 10^{-9}$) and to reach the level predicted by new-physics ($3.1 \cdot 10^{-10}$). The analysis is in progress. They plan to continue the study at J-PARC.

3 Future Kaon Experiments at J-PARC

The J-PARC 50 GeV PS was designed to provide, in the slow extraction, $300 \cdot 10^{12}$ protons per 0.7-second spill in every 3.42 seconds to an experimental area named Hadron Experimental Hall. The beam energy at the initial operation phase (Phase-1) will be 30 GeV.

Call for Letters of Intent (LoI's) for nuclear and particle physics experiments at the J-PARC was issued in July 2002, and thirty LoI's [12] were

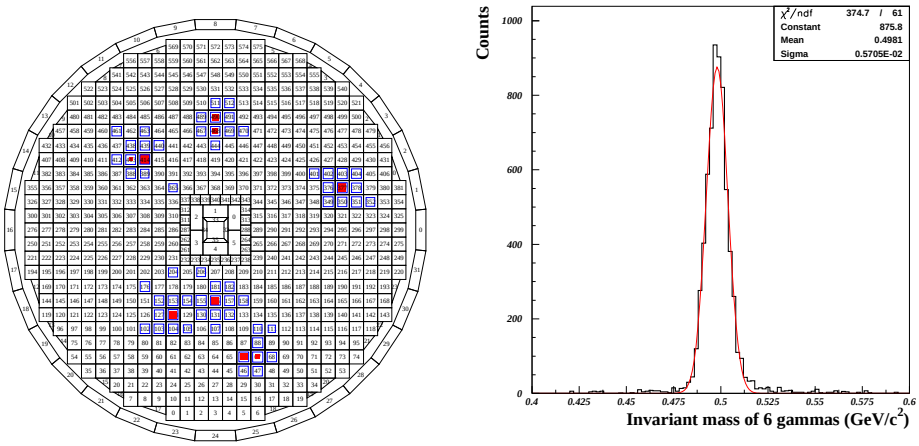

Figure 3: *Display of an event with six clusters in the E391a CsI calorimeter (left); invariant-mass distribution of the* $K_L^0 \to \pi^0\pi^0\pi^0$ *decay reconstructed from the six-cluster events (right).*

submitted. There were five LoI's for kaon experiments:

- measurement of the $K_L^0 \to \pi^0\nu\bar{\nu}$ branching ratio

with neutral beams and

- study of the $K^+ \to \pi^+\nu\bar{\nu}$ decay,
- search for T-violation in K^+ decay,
- study of the decay spectra of stopped kaons, and
- precise measurement of the $K^+ \to \pi^0 e^+\nu$ branching ratio

with K^+ beams of low momentum (0.6-0.8 GeV/c). These LoI's are regarded as a natural extension of the kaon program that has been worked out (E391a, BNL-E949 and E246/E470). In the beam-line layout plan of the Hadron Experimental Hall at Phase-1, reported in February 2004 [13], the hall has been designed so as to accommodate these experiments in the future. Call for full proposals is expected to be issued in the autumn of 2004; intensive discussions have been held in a series of workshops [14].

Acknowledgments

I would like to thank J. Imazato, T. Inagaki, G.Y. Lim, S. Sugimoto and T. Yamanaka for useful discussions. I would like to acknowledge support from Grant-in-Aid for Scientific Research in Priority Area: "Mass Origin and Supersymmetry Physics" by the MEXT Ministry of Japan.

References

1. `http://www-ps.kek.jp/kekps/` .
2. `http://www-ps.kek.jp/e391/` .
3. `http://j-parc.jp/` .
4. C. Rangacharyulu, in these Proceedings.
5. S. Shimizu, in these Proceedings.
6. A.J. Buras *et al*, hep-ph/0405132, and references therein.
7. T. Inami and C.S. Lim, Progr. Theor. Phys. **65**, 297 (1981); 1172(E) (1981).
8. Y. Grossman and Y. Nir, Phys. Lett. B **398**, 163 (1997).
9. V.V. Anisimovsky *et al* (E949 Collaboration), Phys. Rev. Lett. **93**, 031801 (2004); T. Sekiguchi, in these Proceedings.
10. A.J. Buras *et al*, Phys. Rev. Lett. **92**, 101804 (2004) and hep-ph/0402112.
11. A. Alavi-Harati *et al*, Phys. Rev. D **61**, 072006 (2000).
12. `http://www-ps.kek.jp/jhf-np/LOIlist/LOIlist.html` .
13. `http://www-ps.kek.jp/jhf-np/Layout/Layout.html` .
14. The international workshop on Nuclear and Particle Physics at J-PARC: see `http://j-parc.jp/NP04/` .

Frascati Physics Series Vol. XXXVI (2004), pp. 311–314
DAΦNE 2004: Physics at meson factories – Frascati, June 7-11, 2004
Short Talk in Plenary Session

RECENT PROGRESS ON THE RARE DECAY $K_L \to \pi^0\mu^+\mu^-$

C. Smith
INFN, Laboratory Nazionali di Frascati, I-00044 Frascati, Italy

1 Introduction

Studies of direct CP-violation are important to test the Standard Model, and possibly to discover New Physics effects. Here, we consider the following rare K_L modes, with CP-violating and CP-conserving contributions

	Direct-CPV	Indirect-CPV	CPC
$K_L \to \pi^0\nu\bar{\nu}$	$\sim 100\%$	$\sim 0\%$	$\sim 0\%$
$K_L \to \pi^0 e^+e^-$	$\sim 40\%$	$\sim 60\%$	$\sim 0\%$
$K_L \to \pi^0\mu^+\mu^-$	$\sim 30\%$	$\sim 35\%$	$\sim 35\%$

While the theoretical complexity increases, recent experimental results now permit reliable estimates for ICPV and CPC, making the $\ell^+\ell^-$ modes competitive with the $\nu\bar{\nu}$ one.

The CPC contribution proceeds through two photons, which can be in a scalar 0^{++} or tensor 2^{++} state. The former is helicity suppressed, hence contribute only for $\mu^+\mu^-$, while the later, much smaller, is the dominant one [1)] for e^+e^-. Our work was to estimate the 0^{++} CPC contribution [2)].

2 CP–conserving contribution

At leading order in Chiral Perturbation Theory, the process proceeds through a charged meson $(\pi; K)$ loop followed by a photon loop, see fig.1a. Provided one can parametrize the vertex $M\left(K_L \to \pi^0 P^+ P^-\right) = G_8 m_K^2 a\left(z\right)$, with $z = \left(p_{P^+} + p_{P^-}\right)^2 / m_K^2$ the invariant mass and $a\left(z\right)$ some function, the differential rate can be factorized

$$\Gamma_{\ell^+\ell^-} = \frac{G_8^2 m_K^5 \alpha^4}{512\pi^7} \int_{4r_\ell^2}^{\left(1-r_\pi\right)^2} dz \;\; \left|a\left(z\right)\right|^2 \lambda_\pi^{1/2} \left|\mathcal{J}\left(\frac{r_\pi^2}{z}, \frac{r_\ell^2}{z}\right)\right|^2 \frac{r_\ell^2}{z} \left(1 - \frac{4r_\ell^2}{z}\right)^{3/2}$$

where $\lambda_\pi = \lambda\left(1, r_\pi^2, z\right)$ is the standard two-body kinematical function for $\pi^0 \left(PP\right)_{0^{++}}$ in a $L = 0$ wave, r_ℓ^2/z is the helicity suppression factor and $\left(1 - 4r_\ell^2/z\right)^{3/2}$ stands for the lepton pair in a $L = 1$ wave. The two-loop function $\mathcal{J}$ describes the transitions $\left(PP\right)_{0^{++}} \to \ell^+\ell^-$ and is exactly the one occurring in $K_S \to \left(PP\right)_{0^{++}} \to \gamma\gamma \to \ell^+\ell^-$ [2, 3].

To proceed, we took the ratio $R_{\gamma\gamma} = \Gamma_{\ell^+\ell^-}/\Gamma_{\gamma\gamma}$, with $\Gamma_{\gamma\gamma}$ the $K_L \to \pi^0\gamma\gamma$ rate computed with the same $a\left(z\right)$ parametrization of the vertex $K_L \to \pi^0 P^+ P^-$ [4]. The crucial point is that for a large range of parametrization, $R_{\gamma\gamma}$ is stable. This means that both modes react similarly to modulations in the distribution of momentum entering the scalar subprocess. Given this observation, we infer the branching ratio of $\ell^+\ell^-$ from the experimental result for $\gamma\gamma$. In doing so, some higher order chiral corrections are included in our result. Taking $B\left(K_L \to \pi^0\gamma\gamma\right)^{\rm exp} = (1.42 \pm 0.13) \times 10^{-6}$ as the average of the KTeV and NA48 measurements [5], we find $B\left(K_L \to \pi^0\mu^+\mu^-\right)_{CPC}^{0^{++}} = (5.2 \pm 1.6) \times 10^{-12}$, with a conservative error estimate of 30%.

Finally, the differential rate is in fig.1b, and it shows that an appropriate kinematical cut can reduce the relative contamination of the CPC contribution to below 10%.

3 Phenomenological Analysis

The final parametrizations are ($\kappa = 10^4 \,{\rm Im}\,\lambda_t = 1.36 \pm 0.12$)

$$B\left(K_L \to \pi^0 e^+ e^-\right) \approx \left(2.4\kappa^2 \pm 6.2\left|a_S\right|\kappa + 15.7\left|a_S\right|^2\right) \times 10^{-12}$$
$$B\left(K_L \to \pi^0 \mu^+ \mu^-\right) \approx \left(1.0\kappa^2 \pm 1.6\left|a_S\right|\kappa + 3.7\left|a_S\right|^2 + 5.2\right) \times 10^{-12}$$

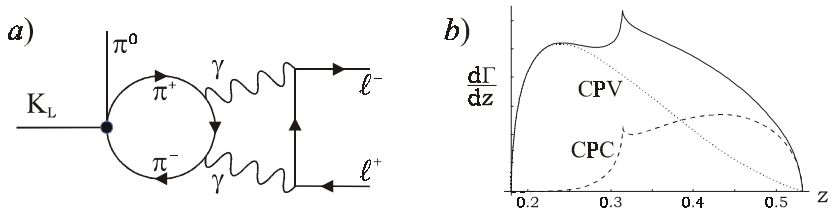

Figure 1: *a) Typical CPC pion loop contribution, b) Differential rate.*

The κ^2 terms are DCPV, the ICPV parameter a_S is the counterterm dominating $K_S \to \pi^0\ell^+\ell^-$, recently measured by NA48/1 [6] $|a_S^{\rm exp}| = 1.2 \pm 0.2$. The interference between DCPV and ICPV has been argued to lead to positive sign [1, 7]. In the same notation, $B\left(K_L \to \pi^0\nu\bar{\nu}\right) \approx \left(16\kappa^2\right) \times 10^{-12}$, see [8].

It is important to note that the muon mode DCPV term receives an additional helicity-suppressed axial-vector FCNC contribution, somewhat compensating the overall phase-space suppression. Due to this fact, the two modes have different sensitivities to the underlying weak physics, and the plot of the muon mode against the electron one for various $\mathrm{Im}\,\lambda_t$ is not a trivial straight line (see fig.2). This plot is then well-suited to study possible impacts of New Physics. Taking as an example the model of Buras et al. [9], we get the theoretical predictions for positive interference:

	S.M. $\left(\times 10^{-11}\right)$	EEWP $\left(\times 10^{-11}\right)$	Experiment [10]
$K_L \to \pi^0\nu\bar{\nu}$	3.0 ± 0.6	31 ± 10	$< 5.9 \times 10^{-7}$
$K_L \to \pi^0 e^+ e^-$	$3.7^{+1.1}_{-0.9}$	9.0 ± 1.6	$< 2.8 \times 10^{-10}$
$K_L \to \pi^0 \mu^+ \mu^-$	1.5 ± 0.3	4.3 ± 0.7	$< 3.8 \times 10^{-10}$

In conclusion, the set of decays $K_L \to \pi^0\nu\bar{\nu}$, $\pi^0 e^+ e^-$ and $\pi^0\mu^+\mu^-$ is now under theoretical control, and provides for a stringent test of the Standard Model. In addition, if a signal of New Physics is found, the observed pattern of branching ratios will give information on its nature. Experimentally, it is then clear that the $K_L \to \pi^0\mu^+\mu^-$ mode should be seriously considered. Also, additional measurements of $K_S \to \pi^0\ell^+\ell^-$ would be certainly very desirable since the main uncertainty on the theoretical prediction for the CPV parts, and thus the spreading of the confidence regions in Fig.2, comes from a_S.

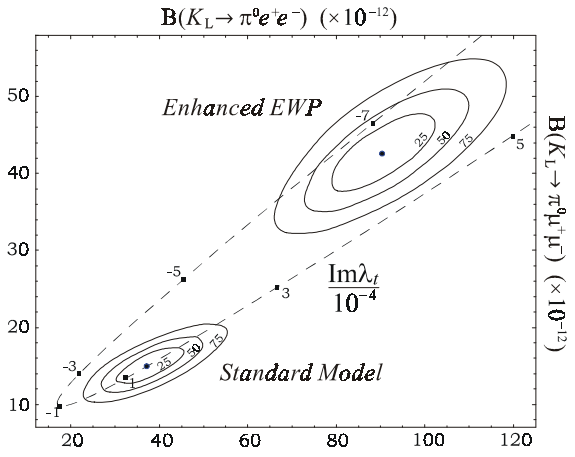

Figure 2: *SM and EEWP* [9] *theoretical predictions.*

4 Acknowledgements

This work has been supported by IHP-RTN, EC contract No. HPRN-CT-2002-00311 (EURIDICE).

References

1. G. Buchalla, G. D'Ambrosio and G. Isidori, Nucl. Phys. **B672**, 387 (2003).
2. G. Isidori, C. Smith and R. Unterdorfer, Eur. Phys. J. **C36**, 57 (2004).
3. G. Ecker and A. Pich, Nucl. Phys. **B366**, 189 (1991).
4. A. Cohen, G. Ecker and A. Pich, Phys. Lett. **B304**, 347 (1993).
5. A. Alavi-Harati *et al.* [KTeV], Phys. Rev. Lett. **83**, 917 (1999); A. Lai *et al.* [NA48], Phys. Lett. **B536**, 229 (2002).
6. J.R. Batley et al. [NA48/1], Phys. Lett. **B576**, 43 (2003).
7. S. Friot, D. Greynat, E. de Rafael, Phys. Lett. **B595**, 301 (2004).
8. A. J. Buras, F. Schwab and S. Uhlig, *hep-ph/0405132*.
9. A. J. Buras, R. Fleischer, S. Recksiegel and F. Schwab, *hep-ph/0402112*.
10. A. Alavi-Harati *et al.* [KTeV], Phys. Rev. **D61**, 072006 (2000); Phys. Rev. Lett. **84**, 5279 (2000); Phys. Rev. Lett. **93**, 021805 (2004).

Session V — Kaonic Atoms

(Chair: P. Ball)

J. Gasser	Kaonic Atoms in QCD
J. Zmeskal	First Measurement of Kaonic Hydrogen and Nitrogen X-Rays at DAΦNE
M. Iliescu	SIDDHARTA: The Future of Exotic Atoms Research at DAΦNE
M. Trassinelli	Precision Spectroscopy of Pionic Atoms: from Pion Mass Evaluation to Tests of Chiral Perturbation Theory
T. Jensen	Atomic Cascade in Kaonic Hydrogen and Deuterium

Frascati Physics Series Vol. XXXVI (2004), pp. 317–326
DAΦNE 2004: Physics at meson factories – Frascati, June 7-11, 2004
Invited Review Talk in Plenary Session

KAONIC ATOMS IN QCD

J. Gasser
Institute for Theoretical Physics, University of Bern,
CH-3012 Bern, Switzerland

Abstract

In this talk, I comment on the theoretical and experimental status of kaonic atoms, in particular $\bar{K}\pi$ and $\bar{K}p$ bound states.

1 Introduction

Kaonic atoms are particular examples of *hadronic atoms*. They are of the type $\bar{K}X$, with $X = \pi, K$; p; d; ^{3}He; ^{4}He ... . Kaonic atoms are by definition bound by electromagnetic interactions, so a more precise title of my talk would be *Kaonic atoms in QCD + QED*. On the other hand, deeply bound kaonic nuclear states are of a different variety - as far as I understand, they are predicted to exist already in the framework of QCD [1, 2], electromagnetic forces are not required for their formation. I do not consider these systems here (nor $\bar{K}K$ bound states [3]). The reason to investigate *hadronic atoms* in general is the

following: as just said, they are formed by electromagnetic forces, which are well known. Strong interactions - mediated by QCD - have two effects: they i) distort the spectrum, and ii) let the atoms decay. As we will see below, strong interactions may be considered a small perturbation in some cases, and it is then possible to calculate their effect. Indeed, as is known since fifty years [4], the energy shift and the lifetime of hadronic atoms are in general related to the pertinent T- matrix element in QCD at threshold. Therefore, measuring the spectra amounts to measure these amplitudes. Classic applications of this procedure to determine strong amplitudes are: *pionic hydrogen at PSI* [5] $\leftrightarrow$ $T_{\pi N}$*; pionium at DIRAC* [6] $\leftrightarrow$ $T_{\pi\pi}$*; kaonic Hydrogen at DEAR* [7] $\leftrightarrow$ $T_{\bar{K}N}$.

Data on hadronic atoms have therefore the potential to replace low energy experiments on $\pi N \to \pi N \leftrightarrow T_{\pi N}$; $\pi\pi \to \pi\pi \leftrightarrow T_{\pi\pi}$; $\bar{K}N \to \bar{K}N \leftrightarrow T_{\bar{K}N}$ that are difficult (or impossible) to perform. All in all, hadronic atoms allow one to confront high precision, low energy QCD predictions with data. As a now classic example I mention $\pi\pi$ scattering lengths, where the theoretical predictions are [8, 9]

$$a_0 = 0.220 \pm 0.005\,,\; a_0 - a_2 = 0.265 \pm 0.004\,, \tag{1}$$

to be confronted with e.g. data from K_{e4} decay [10],

$$a_0 = 0.216 \pm 0.013\,(\text{stat.}) \pm 0.002\,(\text{syst.}) \pm 0.002\,(\text{theor.})\;. \tag{2}$$

Data on $\pi\pi$ scattering from the DIRAC experiment are discussed in Tauscher's contribution to this conference [6]. Furthermore, a high statistics K_{e4} experiment is underway at NA48 [11]. As Cabibbo has pointed out at this conference, $K^\pm \to \pi^\pm\pi^0\pi^0$ decays may provide the possibility to determine the combination $a_0 - a_2$ with high precision [12, 13].

The procedure to confront QCD predictions with data on atomic spectra consists of two steps: First, one relates the spectra to QCD scattering amplitudes at threshold [4]. The precision of this calculation must match the accuracy of the data, which requires in many cases to go beyond the relation provided in [4]. Second, one calculates QCD amplitudes using effective field theories, lattice calculations ..., and compares with what one obtains from step one.

The experimental and theoretical situation for kaonic atoms is summarized in table 1.

Table 1: *Kaonic atoms: status of theory and experiment.*

	experiment	*theory*
$\bar{K}\pi$	Letter of Intent [14]	[15, 16]
$\bar{K}p$	DEAR [7]	[17, 18]
$\bar{K}d$	SIDDHARTA [19, 20]	[21]

The DEAR experiment is presently the only place where there is overlap between theory and data in *kaonic atoms*. Let us hope that the situation changes in the future.

2 $\bar{K}\pi$ atoms

$\bar{K}\pi$ atoms are interesting, because the hadronic effects in the spectrum are related to $SU(3) \times SU(3)$ chiral perturbation theory (ChPT) in the meson sector, which works, as far as is known today, very well. The modern way to interrelate the spectrum and QCD works as follows. First, one observes that the momenta of the constituents as well as of the decay products are small, of the order of 1 MeV or less. Therefore, it is advisable to use a non relativistic field theory framework for the calculation [22, 23] - for a relativistic approach see [24]. In order to verify that a perturbative calculation is reasonable, we note that the Coulomb binding energy of the ground state is $E_B \simeq 2.9$ keV, whereas the strong shift of the energy level is about -9 eV [15] - a tiny effect. Further, the lifetime of the ground state turns out to be about $4 \cdot 10^{-15}$ sec. An estimate of the number of orbits performed before decaying, $\tau \cdot E_B \simeq 1.8 \cdot 10^4$, reveals that the atom may be considered as nearly stable. I conclude that the calculation is self consistent - $\bar{K}\pi$ atoms belong to a class of systems where the perturbation of the QED spectrum by the strong interaction among the constituents is small. Next, we consider the decay channels allowed. The mass differences are

$$M_{K^-} + M_{\pi^+} = M_{K^0} + M_{\pi^0} + 0.60\text{MeV}\,, \tag{3}$$

as a result of which possible decay channels are

$$A_{K^-\pi^+} \to \bar{K}^0\pi^0, \bar{K}^0 + n\gamma, \ldots \tag{4}$$

One expands the decay width in powers of the isospin breaking parameters[1] α and $m_d - m_u$, that are counted as quantities of order δ. For the ground state, the leading and next-to-leading terms are due to the decay into $\bar{K}^0\pi^0$:

$$\Gamma_G = \underbrace{a\,\delta^{7/2} + b\,\delta^{9/2}}_{\bar{K}^0\pi^0} + \underbrace{\mathcal{O}(\delta^5)}_{\bar{K}^0\pi^0+\text{other channels}} \quad . \tag{5}$$

The formula for the decay width of the ground state at next-to-leading order has recently been worked out by Julia Schweizer [15],

$$\Gamma_G = 8\alpha^3\mu_c^2 p^*[a_0^-]^2(1+\epsilon) + \mathcal{O}(\delta^5)\,, \tag{6}$$

where a_0^- is the isospin odd S-wave scattering length in elastic πK scattering, p^* denotes the relative 3-momentum of the $\bar{K}^0\pi^0$ pair in the final state, and μ_c stands for the reduced mass of the charged mesons. Finally, the quantity ϵ is a correction due to isospin breaking, known at order δ [15]. Therefore, a measurement of the decay width of the ground state provides a_0^-,

$$\Gamma_G \quad \to \quad a_0^- \quad \leftrightarrow \quad \text{low energy QCD} \; . \tag{7}$$

We note that a_0^- is the scattering length in pure QCD, purified from electromagnetic corrections, evaluated at $m_u = m_d$, with $M_K = 493.7$ MeV. Using the value of a_0^- determined recently in a dispersive analysis [25] gives

$$\tau_G = (3.7 \pm 0.4) \cdot 10^{-15}\text{sec} \; . \tag{8}$$

The main open problem here concerns the experimental verification of this result, and an investigation of whether one may obtain in this manner more information on the LECs that occur in the chiral expansion of the scattering lengths [26].

For an exhaustive discussion of the various decay channels and energy shifts, I refer the interested reader to the work of Julia Schweizer [15]. I conclude with the observation that the theory of πK atoms very well understood. On the other hand, experiments are sadly missing.

3 Kaonic hydrogen

Here, I discuss properties of kaonic hydrogen, a system investigated in the last years at DEAR [7]. Let us first again discuss orders of magnitudes. The

[1] We denote the fine structure constant by $\alpha \simeq 1/137$.

Coulomb binding energy of the ground state is about 8.6 keV, the strong shift about .2 keV [7] - the perturbation is still small. The width is $\Gamma \simeq 250$ eV [7], such that the system performs about $\tau \cdot E_B \simeq 35$ orbits before decaying, considerably less than in the case of the πK atom, but still reasonably many. Note, however, that this number becomes $\simeq 10$ for the width found in [18] from unitarized ChPT - which is surprisingly small.

3.1 Theory

Some of the decay channels of kaonic hydrogen are

$$A_{\bar{K}p} \to \pi\Sigma, \Sigma\pi\gamma, \Sigma\pi e^+e^-, \Sigma\gamma, \ldots \tag{9}$$

Note that it cannot decay into an $\bar{K}^0 n$ pair for kinematic reasons: in our world, the value of the up and down quark masses are such that $M_{K^-} + M_p < M_{\bar{K}^0} + M_n$. This is in contrast to what happens in the $\bar{K}\pi$ atom, where the main decay channel is into the neutral pair $\bar{K}^0\pi^0$.

The necessary steps to get the pertinent formula for the energy shift and decay width have been performed recently by Meißner, Rusetsky and Raha [18] in a very nice piece of work in the framework of effective field theory, that accounts for a systematic expansion in isospin breaking effects. A different approach has been used in [17]. In order to illustrate the difficulties one is faced with in this system, I display in figure 1 the analytic properties of the forward $\bar{K}p \to \bar{K}p$ amplitude at $\alpha \neq 0, m_u \neq m_d$. The various branch points and cuts have to be taken into account properly in the derivation of the result, and this amplitude must then be related to the one in pure QCD, where e.g. the branch points at $\bar{K}p$ and $\bar{K}^0 n$ coincide, and where the $\Sigma\gamma$ cut is absent.

The main observation is the following [18]: there are large isospin breaking effects in the final formula, as large as the uncertainty in present DEAR data. Whereas this observation is not new [27, 28], the authors of [18] have shown how to sum up the most singular pieces, such that the remainder is of next order in isospin breaking and therefore expected to be small. The result for the energy shift and level widths of the S-states is similar in structure to the $\bar{K}\pi$ atom considered above, however considerably more complicated - I refer the interested reader to the original article [18] for the explicit formula. The main point is that the shift and width can be calculated, once the $I = 0, 1$ scattering lengths $a_{0,1}$ in $\bar{K}p \to \bar{K}p$ scattering are known in pure QCD, at $m_u = m_d$.

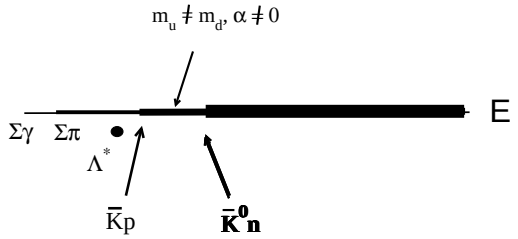

Figure 1: *The analytic properties of the forward amplitude for $\bar{K}p \to \bar{K}p$ scattering in the presence of isospin breaking interactions. Indicated are some of the branch points in the amplitude. The filled circle denotes the $\Lambda^*(1405)$ pole on the second Riemann sheet.*

Vice versa, if the shift and width is known, one may determine these scattering lengths.

3.2 Comparison with data

The scattering lengths $a_{0,1}$ have been calculated in [29] - see also [31, 32] - by use of unitarized ChPT. The comparison with the data from the DEAR collaboration is provided in Ref. [18], to which I refer the reader for details, see in particular their figure 3, that illustrates the large isospin breaking present in this system. The theoretical prediction [29] does not agree with the measurement performed at DEAR - although it must be said that the calculation of the scattering lengths in [29] does not include an error analysis of the final result. The reason for this disagreement has not yet been investigated [18, 30]. It is interesting to compare the scattering lengths in [29] with ChPT in the standard loop expansion. The relevant calculation had been performed by Kaiser [33]. It turns out that the one loop result for the isospin zero amplitude is completely off the correct answer, as a result of which the predicted energy shift in the ground state of kaonic hydrogen has the wrong sign. This shows that, due to the nearby resonance $\Lambda^*(1405)$, one has to go beyond a pure loop expansion. This is what has been done [31, 32, 29]. However, the procedure is not without pitfalls: the authors of e.g. Ref. [32] have provided scattering lengths that are in sharp conflict with the DEAR data. The reason for this failure is explained in [18].

Once data on kaonic hydrogen energy shift and width will be available at

the eV level, it will be even more dramatic to compare theoretical prediction with these data - I am rather curious to see whether unitarization procedures will pass this test. Needless to say that it would be comforting to have a precise prediction from theory, including uncertainties attached, before our experimental colleagues have done their job.

Finally, I shortly remind the reader that it would be, in my opinion, a theoretically tremendous effort to derive a precise relation between the scattering lengths determined through the measurement of kaonic hydrogen, and the kaon nucleon sigma terms [34].

4 More complicated systems

The are more complicated systems than the ones we have considered so far, e.g., kaonic deuterium. There are plans to investigate this system with SIDDHARTA, see the contributions by Iliescu and Jensen to this conference [19, 20]. The investigation of the relevant spectra can provide information on the $\bar{K}p, \bar{K}n$ scattering amplitude at threshold. Of course, one needs the corresponding formula, relating the scattering lengths to the spectrum. One may compare this with pionic deuterium, where first theoretical investigations using effective field theories are already available [35] or underway [36]. The $\bar{K}d$ system is even more complicated [21]. Whether a theoretically sound analysis in the framework of effective field theories is possible remains to be seen.

5 Conclusions

1. *Hadronic atoms* are a wonderful tool to measure QCD amplitudes at threshold.

2. $\bar{K}\pi$ *atoms* are theoretically well understood [15] [16]. The relevant $\bar{K}\pi$ scattering amplitude is now available to two loops in ChPT [26], and an analysis invoking Roy-Steiner equations has been performed as well [25]. On the other hand, the precise connection between the vacuum properties of QCD and $\bar{K}\pi$ scattering is still an open question, and experiments on the atom are absent.

3. The ground state of *kaonic hydrogen* has been investigated in a beautiful experiment at DEAR [7]. Data are available, the S-states state of the

atom are theoretically understood [18, 17].

4. On the other hand, the theory of $\bar{K}p$ scattering leaves many questions open. More precise data will reveal whether present techniques are able to describe the complicated situation properly.

5. Concerning *kaonic deuterium*, experiments are planned [19, 20]. Whether this systems allows for a theoretically sound analysis in the framework of effective field theory remains to be seen.

Acknowledgements

It is a pleasure to thank the organizers for the invitation to give this talk, and for the very stimulating atmosphere at the conference. Furthermore, I thank Ulf-G. Meißner and Akaki Rusetsky for illuminating discussions, Akaki Rusetsky for numerical values of scattering lengths evaluated in unitarized chiral perturbation theory, and Carlo Guaraldo and Akaki Rusetsky for useful comments concerning the manuscript. This work was supported in part by the Swiss National Science Foundation and by RTN, BBW-Contract No. 01.0357 and EC-Contract HPRN–CT2002–00311 (EURIDICE).

References

1. Y. Akaishi, contribution to this conference.

2. H. Outa, contribution to this conference.

3. S. Krewald, R. H. Lemmer and F. P. Sassen, Phys. Rev. D **69** (2004) 016003 [arXiv:hep-ph/0307288].

4. S. Deser, M. L. Goldberger, K. Baumann and W. Thirring, Phys. Rev. **96** (1954) 774; J.L. Uretsky and T.R. Palfrey Jr., Phys. Rev. **121** (1961) 1798; T.L. Trueman, Nucl. Phys. **26** (1961) 57; S.M. Bilenky, Van Kheu Nguyen, L.L. Nemenov and F.G. Tkebuchava, Sov. J. Nucl. Phys. **10** (1969) 469.

5. M. Trassinelli, contribution to this conference.

6. L. Tauscher, contribution to this conference.

7. T. Zmeskal, contribution to this conference.

8. G. Amoros, J. Bijnens and P. Talavera, Nucl. Phys. B **585** (2000) 293 [Erratum-ibid. B **598** (2001) 665] [arXiv:hep-ph/0003258].

9. G. Colangelo, J. Gasser and H. Leutwyler, Phys. Lett. B **488** (2000) 261 [arXiv:hep-ph/0007112].

10. S. Pislak *et al.*, Phys. Rev. D **67** (2003) 072004 [arXiv:hep-ex/0301040].

11. R. Wanke, *Status and Prospects of Rare K^+ and K_L decays from NA48*, talk given at the Kaon Miniworkshop, CERN, May 5, 2004.

12. N. Cabibbo, contribution to this conference.

13. N. Cabibbo, arXiv:hep-ph/0405001.

14. The DIRAC collaboration, Letter of Intent, CERN/SPSC-2000-032, SPSC/P284 Add. 2, 17 August 2000 [http://dirac.web.cern.ch/DIRAC].

15. J. Schweizer, Phys. Lett. B **587** (2004) 33 [arXiv:hep-ph/0401048]; [arXiv:hep-ph/0405034].

16. H. Sazdjian, private communication, and work in progress.

17. A. N. Ivanov, M. Cargnelli, M. Faber, J. Marton, N. I. Troitskaya and J. Zmeskal [arXiv:nucl-th/0310081].

18. U. G. Meissner, U. Raha and A. Rusetsky, Eur. Phys. J. C **35** (2004) 349 [arXiv:hep-ph/0402261].

19. M. Iliescu, contribution to this conference.

20. T. Jensen, contribution to this conference.

21. A. N. Ivanov *et al.*, Eur. Phys. J. A **21** (2004) 11 [arXiv:nucl-th/0406053].

22. W. E. Caswell and G. P. Lepage, Phys. Lett. B **167** (1986) 437.

23. P. Labelle and K. Buckley, arXiv:hep-ph/9804201; X. Kong and F. Ravndal, Phys. Rev. D **61** (2000) 077506 [arXiv:hep-ph/9905539]; X. Kong and F. Ravndal, Phys. Rev. D **59** (1999) 014031; D. Eiras and J. Soto, Phys. Rev. D **61** (2000) 114027 [arXiv:hep-ph/9905543]; J. Gasser, V. E. Lyubovitskij and A. Rusetsky, Phys. Lett. B **471** (1999) 244

[arXiv:hep-ph/9910438]; D. Eiras and J. Soto, Phys. Lett. B **491** (2000) 101 [arXiv:hep-ph/0005066]; V. Antonelli, A. Gall, J. Gasser and A. Rusetsky, Annals Phys. **286** (2001) 108 [arXiv:hep-ph/0003118]; J. Gasser, V. E. Lyubovitskij, A. Rusetsky and A. Gall, Phys. Rev. D **64** (2001) 016008 [arXiv:hep-ph/0103157].

24. H. Jallouli and H. Sazdjian, Phys. Rev. D **58** (1998) 014011 [Erratum-ibid. D **58** (1998) 099901] [arXiv:hep-ph/9706450]; H. Sazdjian, Phys. Lett. B **490** (2000) 203 [arXiv:hep-ph/0004226].

25. P. Buettiker, S. Descotes-Genon and B. Moussallam, Eur. Phys. J. C **33** (2004) 409 [arXiv:hep-ph/0310283].

26. J. Bijnens, P. Dhonte and P. Talavera, JHEP **0405** (2004) 036 [arXiv:hep-ph/0404150].

27. R.H. Dalitz and S.F. Tuan, Ann. Phys. 3 (1960) 307.

28. A. Deloff and J. Law, Phys. Rev. C **20** (1979) 1597.

29. J. A. Oller and U. G. Meissner, Phys. Lett. B **500** (2001) 263 [arXiv:hep-ph/0011146].

30. U. G. Meissner, arXiv:hep-ph/0408029.

31. N. Kaiser, P. B. Siegel and W. Weise, Nucl. Phys. A **594** (1995) 325 [arXiv:nucl-th/9505043].

32. E. Oset and A. Ramos, Nucl. Phys. A **635** (1998) 99 [arXiv:nucl-th/9711022].

33. N. Kaiser, Phys. Rev. C **64** (2001) 045204 [arXiv:nucl-th/0107006].

34. J. Gasser and M. E. Sainio, in: *Physics and detectors for DAPHNE 1999*, Frascati, p. 659 [arXiv:hep-ph/0002283].

35. B. F. Irgaziev and B. A. Fayzullaev, arXiv:hep-ph/0404203.

36. U.G. Meißner, U. Raha and A. Rusetsky, work in progress.

Frascati Physics Series Vol. XXXVI (2004), pp. 327–334
DAΦNE 2004: Physics at meson factories – Frascati, June 7-11, 2004
Selected Contribution in Plenary Session

FIRST MEASUREMENT OF KAONIC HYDROGEN AND NITROGEN X-RAYS AT DAΦNE

J. Zmeskal *
Institute for Medium Energy Physics, Austrian Academy of Sciences
Vienna, Austria

Abstract

The DEAR experiment (DAΦNE Exotic Atom Research) is a powerful effort to study low-energy kaon physics. DEAR uses the unique beam of almost monochromatic negative kaons produced by the Frascati Φ-Factory complex at LNF (Laboratori Nazionali di Frascati), to perform a precise measurement of the energies emitted in the transitions to the ground state of kaonic hydrogen. The shift and the width of the 1s state are sensitive quantities to test the current understanding of low-energy antikaon-nucleon interaction.

1 Introduction

The objective of DEAR is the precise determination of the isospin dependent antikaon-nucleon scattering lengths, through an eV-level measurement of the

* On behalf of the DEAR Collaboration

1s shift and width in kaonic hydrogen and kaonic deuterium [1]. DEAR investigates the characteristic properties of the strong interaction of antikaons with nucleons at almost zero energy, whereby the light quarks (u, d, s) are involved. The masses of the nucleons are considerable larger than the sum of their constituent quark masses. This phenomenon is proposed to originate from spontaneous breaking of chiral symmetry of massless quarks due to strong interaction [2]. In the world in which we live, quarks are massive and their masses are different: $m(s) \gg m(d) \sim m(u)$. Therefore, chiral symmetry must be broken and the SU(3) symmetry is not exact to the extent required to obtain the experimentally observed mass spectrum.

We do not know, at least on a fundamental level, the origin of the symmetry breaking, its nature, to what extent it is broken, which are the breaking mechanisms and therefore, which model must be used to describe it. In this work a measurement of energies and widths of the X-ray transitions to the ground state in kaonic hydrogen atoms, which will allow to extract the K^-p s-wave interaction at low-energy, is presented. Further on, this information will give an important contribution to the understanding of the chiral symmetry breaking scenario in the strangeness sector.

In contradiction to the analysis of the low-energy scattering experiments (extrapolated down to threshold, a negative energy shift was extracted) three out of four kaonic hydrogen X-ray experiments performed in the last twenty-five years claimed to observe a positive energy shift and therefore an attractive strong interaction between the kaon and the proton (only the KpX measurement gives also a negative shift) [3]. Our analysis of the kaonic hydrogen data gives a negative shift and therefore a repulsive contribution of the strong interaction, which confirms the result of the KpX experiment [4], but with a much better precision.

A repulsive contribution of the strong interaction can be traced back to the presence of the $\Lambda(1405)$ resonance, which leads to the possible existence of strongly bound kaonic states in light nuclei [5].

2 The DEAR experimental setup

DEAR makes use of low momentum negative kaons, produced by the decay of Φ-mesons at DAΦNE. The kaons are degraded in energy to a few MeV, enter a gaseous hydrogen target through a thin window and are finally stopped in

the gas. The kaon entrance window has a diameter of 100 mm and is made of Kapton with a thickness of 125 μm. The distance from the entrance window to the center of the beam pipe is approximately 110 mm.

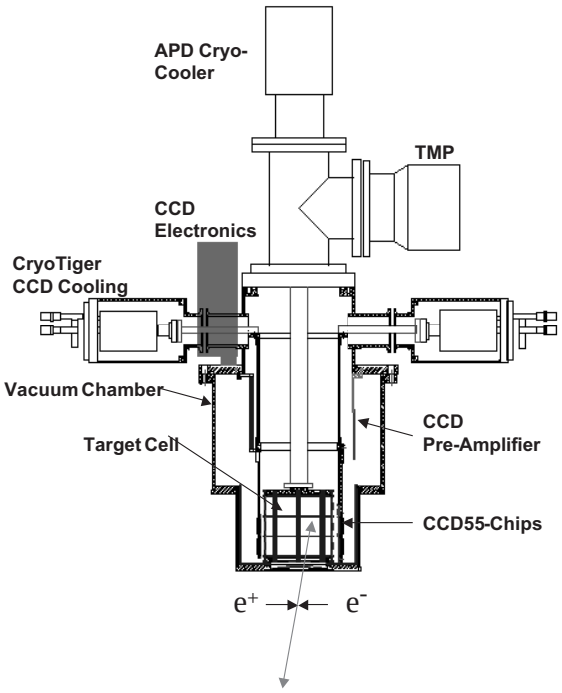

Figure 1: *The DEAR setup: A cryogenic lightweight target cell surrounded by a CCD-detector inside a common vacuum housing.*

The target cell, surrounded by the CCD mounting devices, is placed in the center of the vacuum chamber and is connected to the two-stage closed cycle helium refrigerator via a copper cylinder. The refrigerator system (APD Cryo-Cooler) provides a cooling power of about 10 W at 25 K. The insulation vacuum is maintained to better than 10^{-6} mbar using a wide-range turbo molecular pump (TMP), see also figure 1.

A light-weight target cell with a glass-fiber reinforced epoxy grid was constructed to avoid fluorescence X-rays in the region of interest and to minimize

the bremsstrahlung background. The cell has a diameter of 125 mm and a height of 140 mm. The hydrogen gas target cell (ultra pure hydrogen gas is used, which is cleaned through a palladium diffusion device) typically works at a gas pressure of 2 bar and has a temperature of 23 K, stabilized to better than 0.1 K. With these settings a gas density of 2.2 mg/cm^3 (3.1 % of liquid hydrogen density) is achieved, corresponding to a gas pressure at room temperature of about 30 bar.

16 CCD detector chips (CCD55-30) with a total area of 116 cm^2 were used. Each chip has 1242 x 1152 pixels with a pixel size of 22.5 μm x 22.5 μm and a depletion depth of 30 μm. To minimize thermal noise, and thus reduce the overall noise, the CCDs are operated at a temperature around 150 K, cooled by two one-stage closed-cycle refrigerators (APD CryoTiger), each with a refrigeration capacity of 20 W at 120 K. Thus, an energy resolution of 150 eV at 6 keV could be achieved.

A sophisticated shielding of the DEAR target and detector was developed through different test runs at DAΦNE. Finally, a graded shielding structure was used, starting with lead, followed by a copper and aluminum layer, with an inner layer of polycarbonate. With this setup the bremsstrahlung background could be reduced drastically, which was demonstrated using nitrogen as target gas.

3 Kaonic nitrogen results

The series of kaonic nitrogen measurements performed at DAΦNE had multiple tasks and deliverables: a first measurement of kaonic nitrogen transitions; the study of the machine background and the DEAR setup performance.

A refined analysis of the kaonic nitrogen spectrum taken in October 2002 was performed [6]. For the first time three lines of kaonic nitrogen transitions were clearly identified (fig. 2) and the corresponding X-ray yields could be determined (see table 1).

Using these experimental yields as input for a cascade calculation [7], in particular, the residual K-shell electron population could be extracted. A K-shell electron fraction of approximately 1-3% is found, using the present cascade approach [6]. Understanding the atomic cascade processes in kaonic nitrogen is especially important to prove the feasibility for a precision measurement to determine the charged kaon mass – still an open problem [8].

Table 1: *Kaonic nitrogen transition energies, measured events, and extracted yields*

transition	energy [keV]	events	yield [%]
$7 \rightarrow 6$	4.5773	3310 ± 690	$41.5 \pm 8.7 \pm 4.1$
$6 \rightarrow 5$	7.5957	5280 ± 380	$55.0 \pm 3.9 \pm 5.5$
$5 \rightarrow 4$	13.996	1210 ± 320	$57.4 \pm 15.2 \pm 5.7$

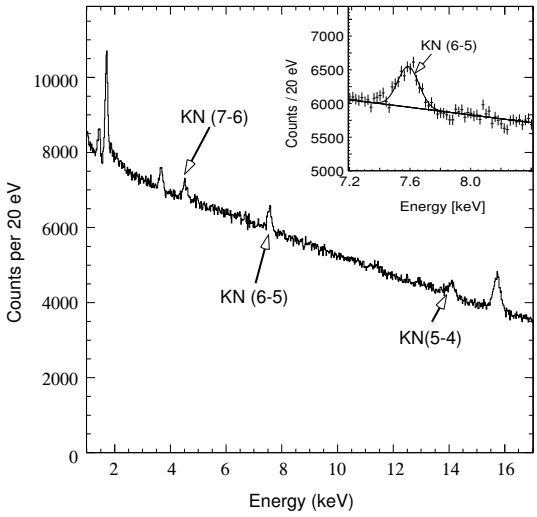

Figure 2: *Energy spectrum of kaonic nitrogen. The arrows indicate the position of the kaonic nitrogen X-ray lines. The peaks at 1.4, 1.7, 3.6 and 15.7 keV are the Al-Kα, Si-Kα, Ca-Kα, and Zr-Kα lines, respectively. The insert shows the fit of the 6→5 kaonic nitrogen transition.*

On the other hand the kaonic nitrogen measurement is essential to tune the machine and to optimize the apparatus for the kaonic hydrogen experiment. Improvements of the detector shielding (signal to background) as well as an optimization of the kaon stopping distribution in the gaseous target cell could be measured directly with kaonic nitrogen X-rays within a few days.

4 Kaonic hydrogen first (preliminary) results

The experimental challenge of DEAR is the extraction of a small signal in the presence of a large low-energy X-ray background mainly from electron gamma showers resulting from lost electrons and positrons due to either Touschek scattering or interaction with residual gas. The careful optimization of the shielding of our experimental setup and the improvements in the beam optics achieved by the machine crew made the goal of DEAR possible, namely, to perform a first measurement of kaonic hydrogen X-rays at DAΦNE in the last two months of 2002.

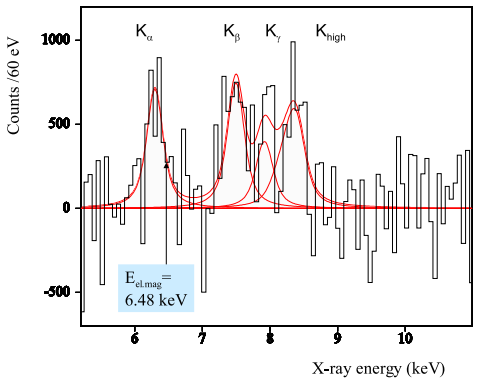

Figure 3: *Background subtracted kaonic hydrogen spectrum for an integrated luminosity of 60 pb^{-1}. Kaonic hydrogen lines $K\alpha$, $K\beta$ and $K\gamma$ are fitted.*

Although, all materials used for the target cell and the mounting devices for the CCDs were carefully checked, still it was not possible to avoid iron impurities completely. The iron fluorescence line coming from iron impurities overlaps partly with the kaonic hydrogen Kα-line. Due to background measurements with nitrogen gas in the target cell and with hydrogen, but without

collisions in the DAΦNE interaction zone (no kaons), the iron fluorescence line could be determined and therefore subtracted.

The linearity as well as the energy stability of the CCD detector were measured in-situ using titanium and zirconium lines (the foils were placed on top of the target cell). The CCD detector system was extremely stable (better than 0.1%) during beam time. Stability was checked by fixing the energy position of the Ti- and Zr-lines and then the position of the Ca-line (originating from the glass-fiber epoxy grid of the target cell) was fitted with an accuracy better than 1 eV. In addition the Ti Kα-line width for the sum of all CCDs was better than 150 eV for the whole beam time.

Two completely independent analyses starting from the set of raw-data were performed. The main differences were the treatment of the subtraction of the continuous background and the determination of the fluorescence X-ray lines. Figure 3 shows the resulting kaonic hydrogen spectrum with the continuous background as well as the fluorescence X-ray lines subtracted. The K_α-line together with the X-ray lines of the K-complex are clearly visible. Both analysis methods gave a compatible (preliminary) result:

$$\begin{aligned} \varepsilon &= -193 \pm 37\ (\text{stat.}) \pm 6\ (\text{syst.})\ \text{eV}, \\ \Gamma &= 249 \pm 111\ (\text{stat.}) \pm 30\ (\text{syst.})\ \text{eV}. \end{aligned}$$

In summary, the analysis of the first measurement of kaonic hydrogen at DAΦNE already leads to an improved accuracy in the determination of the shift and width of the ground state of kaonic hydrogen and confirms the repulsive contribution of the strong interaction found in the KpX experiment at KEK, Japan. For the first time the Kβ and Kγ lines could be disentangled.

Theoretical predictions based on chiral perturbation theory and quantum field theoretical approach are confronted with our new result [9) 10)].

5 Future program

DEAR has performed the most precise measurement on the kaonic hydrogen at present, disentangling the line of the K-complex for the first time. Essential for a future eV level measurement of the shift and width for kaonic hydrogen and for a first measurement of kaonic deuterium is an upgrade of the setup, which is in progress [11)]. A large area Silicon-Drift-Detector is under construction. A drastic improvement in the signal-to-background ratio is expected.

Studies of other light exotic atoms (mainly ^{4}He and ^{3}He) are in discussion. A high-precision experiment to determine the charged kaon mass [12] seems to be feasible in the future.

Acknowledgments

The DAΦNE group is thankfully acknowledged for the excellent cooperation and team-work. Part of the work was supported by "Transnational Access to Research Infrastructure" (TARI), Contract No. HPRI-CT-1999-00088.

References

1. S. Bianco et al., Rivista del Nuovo Cimento Vol. **22**, No. **11** (1999) 1-45.
2. Y. Nambu and G. Jona-Lasinio, Phys. Rev. **122** (1961) 345.
3. J. D. Davies et al., Phys. Lett. **B83** (1979) 55; M.Izycki et al., Z. Phys. **A297** (1980) 11; P.M.Bird et al., Nucl.Phys. **A404** (1983) 482.
4. T. M. Ito et al., Phys. Rev. **A58** (1998) 2366.
5. Y. Akaishi and T. Yamazaki Phys. Rev. **C65**, 44005 (2002).
6. T. Ishiwatari et al., Phys. Lett. **B593** (2004) 48.
7. T. Jensen, to be published.
8. Review of Particle Physics, Eur. Phys. J. **C3** (2000) 493.
9. N. Kaiser, P. B. Siegel and W. Weise, Nucl. Phys. **A594** (1995) 325; J. Gasser in Mini Proc. CD 2003, hep-ph/0311212.
10. A. Ivanov et al., Eur. Phys. J. A, nucl-th/0310081.
11. Contribution M. Iliescu this Workshop.
12. G. Beer et al., Phys. Lett. **B535** (2002) 52.

Frascati Physics Series Vol. XXXVI (2004), pp. 335–341
DAΦNE 2004: Physics at meson factories – Frascati, June 7-11, 2004
Selected Contribution in Plenary Session

SIDDHARTA: THE FUTURE OF EXOTIC ATOMS RESEARCH AT DAΦNE

Mihai Iliescu *
INFN, Laboratori Nazionali di Frascati, C. P. 13,
Via E. Fermi 40, I-00044 Frascati, Italy

Abstract

The SIDDHARTA (SIlicon Drift Detector for Hadronic Atom Research by Timing Application) experiment represents the scientific and technical development of the DEAR experiment, along the scientific line dedicated to exotic atoms at DAΦNE. The scientific program consists in a measurement of kaonic hydrogen K_α lines with eV precision and the first measurement of kaonic deuterium, in order to determine the kaon- nucleon sigma terms. The objective was only partially achieved by DEAR, who performed the best available measurement of kaonic hydrogen. SIDDHARTA collaboration is developing a new set of large area, triggerable X-ray Silicon Drift Detectors (SDD), which will improve by 2 orders of magnitude the background rejection, allowing accomplishing the proposed objectives. Results from the tests performed with two prototypes (7 x 5 mm^2 and 1 x 30 mm^2) on DAΦNE Beam Test Facility, will be presented.

* On behalf of SIDDHARTA Collaboration

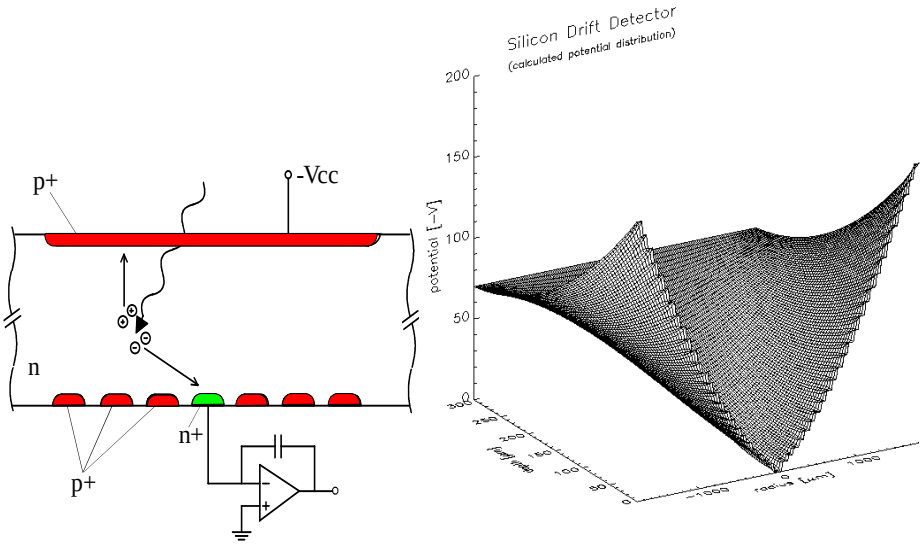

Figure 1: *SDD layout and potential model used in charge transport calculation.*

1 General description of SDD detectors

Silicon drift detectors were proposed by Gatti and Rehak in '83 [1)] as an alternative to conventional drift chambers. Radiation hardness resistance, spatial and time resolution, compactness, as well as the easiness to be interfaced to fast readout systems made them a leading detector in the field, presently used by most advanced experiments [2)]. Few years after, this kind of detector was developed as an X-ray spectroscopic tool, due to a series of characteristics that cannot be achieved (all together) by other X-ray detectors. Some of the most important ones are listed below.

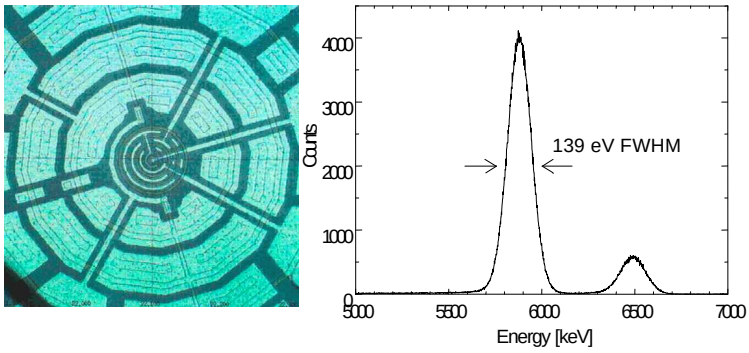

a. b.

Figure 2: *a) The SDD integrated JFET. b) Fe^{55} spectrum (Mn K lines) measured with a 30 mm^2 SDD at -40 C*

The high resolution of X-ray SDDs (near to Fano limit for silicon) is achieved by cooling and using a transport scheme which allows collecting the charges to a small anode. This last one has a low capacity and therefore, low noise level and high signal voltage (see Fig. 1). A key element for driving out a good signal from the collecting anode, is the integrated JFET amplifier. This one ensures a low sensitivity to electromagnetic interference and to parasitic capacitance. An image of the central part of the detector, containing the JFET structure, is presented in Fig. 2a.

In Fig. 2b, the Mn K_α fluorescence spectrum, measured with a large area SDD prototype (30 mm^2) is shown. The resolution obtained with a minimal cooling (139 eV FWHM at -40 Celsius) represents a very good result for a detector of this size.

The thickness of the SDD active layer represents another important characteristic. The commonly used values (300-500 microns) ensure at the same time a high quantum efficiency in the range of interest (near to unity, see Fig. 3) and a good energy separation between low-energy X-rays and minimum ionizing particles (peaked above 180 keV). In addition, the silicon layer is thin with respect to crystal detectors, and therefore, gives a low contribution to the electromagnetic cascade (low internal background).

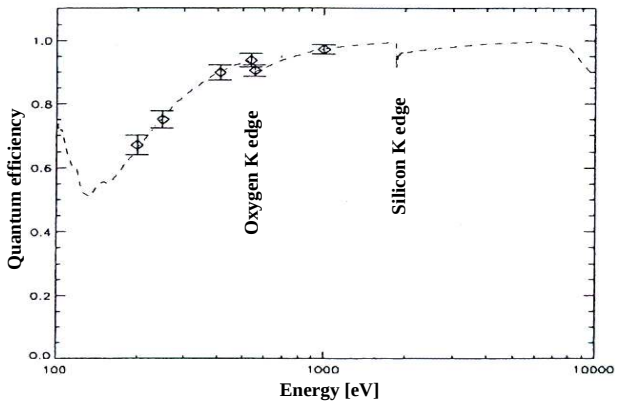

Figure 3: *The quantum efficiency of a 300 micron thick device.*

One of the most important features of the SDDs is the high speed of operation (10^4 to 10^6 particle/s, according to the requested precision and topology).

This characteristic, (together with the possibility of obtaining high energy resolutions for large active areas) represents the key element of the choice of this device as main detector of SIDDHARTA. A comparison between different X-ray detectors in terms of shaping time and resolution as a function of area is shown in Fig. 4.

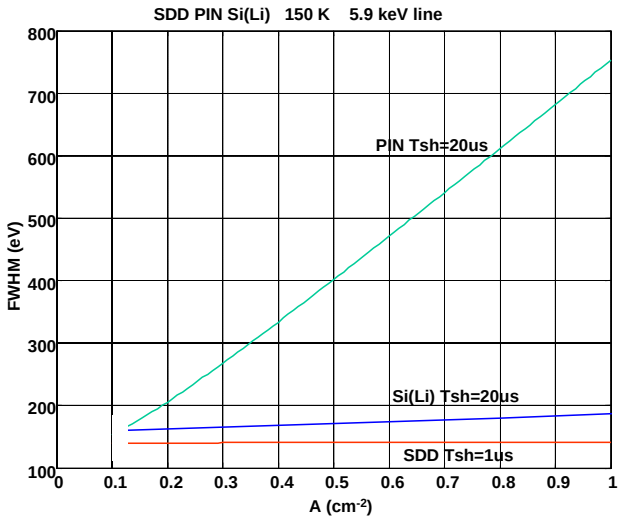

Figure 4: *Resolution and shaping time for different X-ray detectors.*

The relatively fast response of SDDs (few hundred nanoseconds) was poorly used in spectroscopic applications, until now. The only benefit taken was the high rate of acquisition. This is due to the fact that the timing of a drift chamber is usually given by another detector hit by the same particle. This technique could not be employed in the case of spectroscopic SDDs due to the high absorption of X-rays in a very thin layer of material. In the case of SIDDHARTA experiment, the exotic atom X-rays can be correlated with the kaon entrance in the target, which constitute the trigger. In consequence, our design is taking advantage of both energy and time resolution of spectroscopic SDDs, enlarging the area of usage of these detectors in triggered applications. This gives the possibility to detect and measure with accuracy very rare X-ray signals, in a high background environment.

The detection of rare events also requires a large active area. SID-

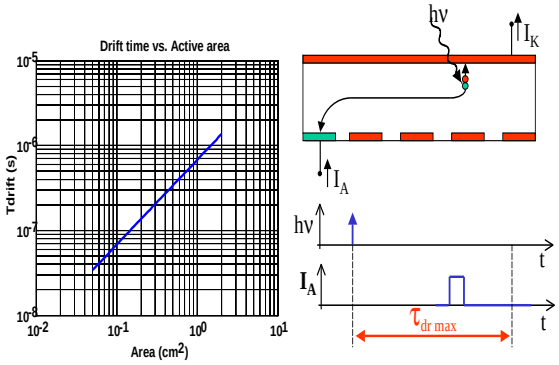

Figure 5: *SDD drift time as a function of area*

DHARTA group designed and start building a detection system with an active area of about 200 cm^2, a timing precision better than 1 microsecond and an energy resolution below 170 eV, at the level of Mn K_α line. The simulations show that both parameters (energy and time resolution) can be achieved by a multi-cell device, each cell having an active area of 1 cm^2. The system will operate under vacuum, at -125 Celsius.

The main parameter, which determines the trigger time window and therefore, the background rejection efficiency, is the drift time. This depends on detector size, high voltage used in transport and material characteristics (charge mobility). A calculation with parameters chosen according to experimental needs is presented in Fig. 5. This shows that maximum drift time expected in the case of 1 cm^2 device would not exceed 800 ns.

2 Signal and background expectations for SIDDHARTA

In the first phase of our scientific program, the best available data on kaonic Hydrogen was acquired by using the DEAR setup, based on X-ray CCDs. Despite the topological background rejection offered by CCDs and the effective shielding of the setup, a relatively low signal to background ratio was obtained (1/70). The main contribution to background came from machine lost electrons, via Touschek effect. This (asynchronous) part of background can be strongly suppressed by a triggered device with a time window of 1 microsecond, to a level of 1/20 of the signal (becomes negligible). The remaining part of background is produced by synchronous processes (hadronic background) and was estimated by Monte Carlo calculations. The expected signal to background

ratio is about 5/1 in the case of Kaonic Hydrogen and 1./4 in the case of kaonic Deuterium. A test of the trigger rejection power was done at DAΦNE Beam Test Facility. The result can be seen in Fig.6. The upper side represents a non-triggered acquisition with the BTF beam, a continuous background source (Sr 90), an Fe^{55} source and an excited material (Ni), while the lower part shows a spectrum, in the same background conditions, triggered with the BTF beam, which induces Cu excitation. A clean selection of Cu fluorescence events can be observed, impossible to distinguish in the first case due.

A version of the SIDDHARTA setup (optimal topology is presently under study), to be prepared and operative by 2006, is shown in Fig. 7, while expected Monte Carlo results for kaonic Hydrogen are shown in Fig. 8.

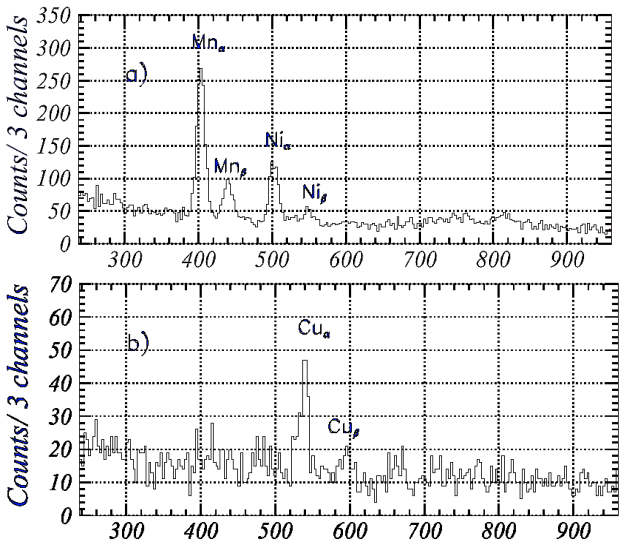

Figure 6: *SDD trigger test using 1 microsecond time window*

References

1. E. Gatti, P. Rehak, Nucl. Instr. and Meth. **225**(1984) 608.

2. E. Crescio *et al*, Nucl. Instr. and Meth. A **478** /1-2 321.

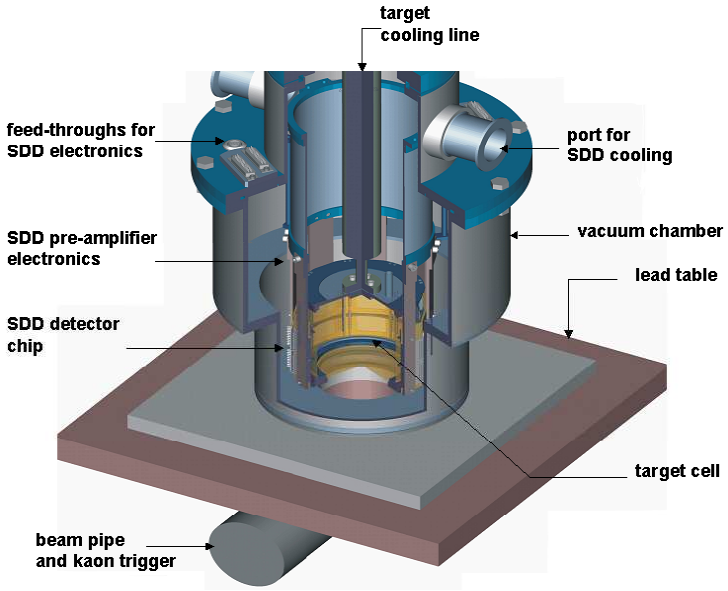

Figure 7: *SIDDHARTA setup (best shielding configuration)*

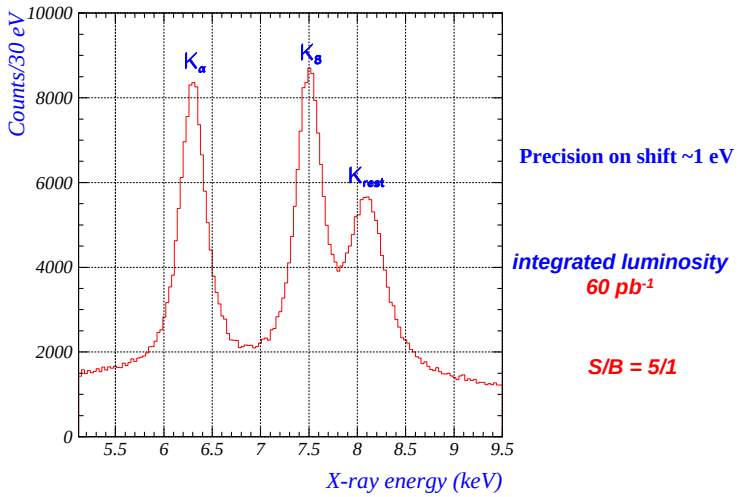

Figure 8: *Kaonic Hydrogen expected signal (Monte Carlo calculation).*

Frascati Physics Series Vol. XXXVI (2004), pp. 343–348
DAΦNE 2004: Physics at meson factories – Frascati, June 7-11, 2004
Selected Contribution in Plenary Session

PRECISION SPECTROSCOPY OF PIONIC ATOMS: FROM PION MASS EVALUATION TO TESTS OF CHIRAL PERTURBATION THEORY

Martino Trassinelli *
Laboratoire Kastler Brossel,Université P. et M. Curie, F-75252 Paris, France

Abstract

Preliminary results of the strong interaction shift and width in pionic hydrogen (πH) using an X-ray spectrometer with spherically bent crystals and CCDs as X-ray detector are presented. In the experiment at the Paul Scherrer Institute three different ($np \to 1s$) transitions in πH were measured. Moreover the pion mass measurement using the ($5 \to 4$) transitions in pionic nitrogen and muonic oxygen is presented

1 Introduction

Pionic hydrogen atoms are unique systems to study the strong interaction at low energies [2]. The influence of the strong interaction in pionic hydrogen can be extracted from the ($np \to 1s$) transitions. Compared to pure electromagnetic

*On behalf of the PIONIC HYDROGEN and PION MASS collaboration [1]

interaction, the 1s level is affected by an energy shift ϵ_{1s} and a line broadening Γ_{1s}. The shift and the broadening are related to the hadronic scattering lengths $a^h_{\pi^- \ p\to\pi^- \ p}$ and $a^h_{\pi^- \ p\to\pi^0 \ n}$, by the Deser-type formulae [3]:

$$\frac{\epsilon_{1s}}{E_{1s}} = -4\frac{1}{r_B}a^h_{(\pi^- \ p\to\pi^- \ p)}(1+\delta_\epsilon) \tag{1}$$

$$\frac{\Gamma_{1s}}{E_{1s}} = 8\frac{Q_0}{r_B}(1+\frac{1}{P})(a^h_{(\pi^- \ p\to\pi^0 \ n)}(1+\delta_\Gamma))^2 \tag{2}$$

where ϵ_{1s} is the strong interaction shift of the 1s level reflecting the $\pi\, p$ scattering process. Γ_{1s} is the width of the ground state caused by the reactions $\pi^- + p \to \pi^0 + n$ and $\pi^- + p \to \pi^0 + \gamma$. $Q_0 = 0.1421\ fm^{-1}$ is the kinetic center of mass momentum of the π^0 in $\pi^- + p \to \pi^0 + n$ reaction, and $P = 1.546 \pm 0.009$ [4] is the branching ratio of the charge exchange and radiative capture (Panofsky ratio). $\delta_{\epsilon,\Gamma}$ are corrections that permit to connect the pure hadronic scattering lengths to the measurable shift and width [7, 8, 9]. The hadronic scattering lengths can be related to the isospin-even and isospin-odd scattering length, a^+ and a^-:

$$a^h_{(\pi^- \ p\to\pi^- \ p)} = a^+ + a^- \qquad a^h_{(\pi^- \ p\to\pi^0 \ n)} = -\sqrt{2}\ a^- \tag{3}$$

The isospin scattering lengths can be related to ϵ_{1s} and Γ_{1s} in the framework of the Heavy Barion Chiral Perturbation Theory (χPT) [5]. Scattering experiments are restricted to energies above 10 MeV and have to rely on an extrapolation to zero energy to extract the scattering lengths. Pionic hydrogen spectroscopy permits to measure this scattering length at almost zero energy (in the same order as the binding energies, i.e., some keV) and verify with high accuracy the χPT calculations. Moreover, the measurement of Γ_{1s} allows an evaluation of the pion-nucleon coupling constant $f_{\pi N}$, which is related to a^- by the Goldberger-Miyazawa-Oehme sum rule (GMO) [6].

Pionic atom spectroscopy permits to measure another important quantity: the charged pion mass. Orbital energies of pionic atoms depend on the reduced mass of the system. These energies can be calculated with high accuracy using Quantum Electrodynamics. Measuring transition energies, not disturbed by strong interaction, allows to determine the reduced mass of the system and hence the mass of the pion. The accurate value of the pion mass is crucial to evaluate the upper bound of the mass of the muonic neutrino from a measurement of the pion decay [11].

2 Description of the setup

The pionic atoms are produced using the pion beam provided by the Paul Scherrer Institut [1]. The beam momentum is 110 MeV/c with an intensity of

10^8 s^{-1}. The pions are captured and slowed down using a cyclotron trap [12]. The target is made of a cylindrical cell with Kapton walls, positioned in the center of the trap. In the target cell the decelerated pions are captured in bound atomic states. During the de-excitation X-rays are emitted. As the muons from the pion decay in the beam are present as well, it is possible to produce muonic atoms and pionic atoms at the same time. The X-ray transition energies are measured using a bent crystal spectrometer and a position sensitive detector. The reflection angle Θ_B between the crystal planes and the X-rays is related to the photon wavelength $\lambda = hc/E$ by the Bragg formula:

$$n\ \lambda = 2\ d \sin \Theta_B \tag{4}$$

where n is the order of the reflection and d is the spacing of the crystal planes. The detector is formed by an array of 6 CCDs composed each by 600×600 pixels [11], the pixel size is 40 μm. The 3-4 keV X-rays excite mostly one or two pixels. Larger clusters are due to charged particle or high-energy gamma radiation and can be eliminated by cluster analysis. Transitions of different energies result in different reflection lines on the detector. By measuring the distance between these lines it is possible to determine the energy difference. The resolution of the spectrometer is of the order of 0.4 eV at 3 keV.

3 Extraction of the hadronic shift and width

The characteristics of the ground state of pionic hydrogen are evaluated measuring the X-ray transitions $np \rightarrow 1s$ (see fig.1). The line width is the result of the convolution of: the spectrometer resolution, the Doppler broadening effect from the non-zero atom velocity, the natural width of the ground state, and, of course, the hadronic broadening. A very accurate measurement of the response function of the crystal was performed using the $1s2s\,^3S_1 \rightarrow 1s^2\,^1S_0$ M1 transitions in He-like argon (with a natural line width less than 1 meV, Doppler broadening about 40 meV). For this measurement the cyclotron trap was converted into an Electron-Resonance Ion Trap (ECRIT) [13], with the crucial point that the geometry of the setup was preserved.
The Doppler broadening effect in the pionic transitions can be studied by working at different pressures and with different transitions. With the help of a cascade model we can predict the kinetic energy distribution of the atoms and the corresponding Doppler broadening [14].
A first series of measurements were completed in 2002. The hadronic broadening Γ_{1s} extracted from the experimental line width is:

$$\Gamma_{1s} = 0.80 \pm 0.03\ eV \tag{5}$$

By varying the target density, we were able to prove that the formation of complex systems $\pi p + H_2 \rightarrow [(\pi pp)p]ee$ [15], which can add an additional shift to the

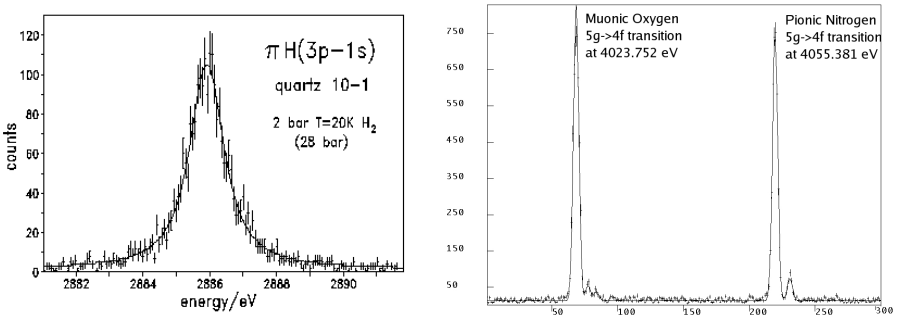

Figure 1: *Left:* $3p \rightarrow 1s$ *transition measurement of pionic hydrogen. Right:* $5g \rightarrow 4f$ *transition in pionic oxygen and muonic hydrogen.*

ground state, is negligible. Energy calibration for the $\pi H(3p \rightarrow 1s)$ transition is performed using the $6h \rightarrow 5g$ transition in pionic oxygen. Strong interaction and finite nucleus size effect are negligible for this transition. Orbital energies can be calculated with an accuracy of a few meV [16]. The result for the shift is:

$$\epsilon_{1s} = 7.120 \pm 0.017 \; eV \tag{6}$$

For the calculation of the shift a pure QED value of $E^{QED}_{3p-1s} = 2878.809 \; eV$ was used. The above given errors include statistical accuracy and systematic effects [17]. The value of ϵ_{1s} is in agreement with the result of a previous experiment, where the energy calibration was performed with $K\alpha$ fluorescence X-rays [18], but more precise by a factor of 3.

4 Pion mass measurement

The evaluation of the pion mass is obtained by the measurement of the transition energy of the $5g \rightarrow 4f$ transition in pionic nitrogen in 2000 (see fig.1). We used the analog transition in muonic oxygen as a reference line. The energy difference between the two lines depends on the ratio between the pion mass and the muon mass, which is known with 0.05 ppm accuracy. The expected accuracy for the pion mass is less than 2 ppm, to be compared with the actual value, which has an accuracy of 2.5 ppm. This value is the average of two measurements, obtained using two different techniques and which differ by 5.4 ppm [19]. To reach this precision, we need a perfect understanding of the crystal spectrometer aberrations and the exact distance between pixels in the

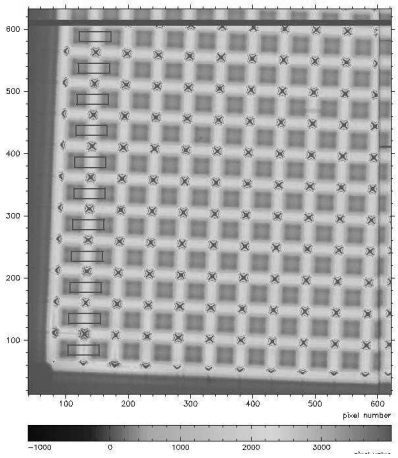

Figure 2: *Detail of the grid image on the CCD detector with the selected zones for the linear fit.*

detector. For the second task an experiment was set up in September 2003 to measure the pixel distance at the working temperature of $-100°$C. We used a nanometric grid composed by 21×14 lines, 20 μm thick, spaced by 2 mm with an accuracy of about 0.05 μm. The mask, at room temperature, was illuminated by a point-like source at a distance of 6426.7 mm, and positioned at 37 mm from the CCD detector (see fig.2). Applying linear fits to the lines of the grid in the CCD image it was possible to provide an accurate measurement of the average pixel distance:

$$pixel\ distance = 39.9943 \pm 0.0035\ \mu m \tag{7}$$

5 Conclusions and outlook

The strong interaction shift in pionic hydrogen has been determined with an accuracy of 0.2%. During spring-summer 2004 the crystals have been characterized with X-rays from the ECRIT. The measurement of the broadening in muonic hydrogen in November-December 2004, together with the cascade model, will allow us to reach an accuracy of 1% for Γ_{1s}.

6 Acknowledgments

We thank the PSI staff, in particular the nanotechnology group, which provided the nanometric mask for the pixel measurement.

References

1. PSI experiment R-97.02 and R-98.01: http://pihydrogen.web.psi.ch
2. D. Gotta, Prog. Part. Nucl. Phys. **52**, 133 (2004).
3. S. Deser *et al.*, Phys. Rev. **96**, 774 (1954),
   G. Rasche and W.S. Woolcock, Nucl. Phys. A **381**, 405 (1982).
4. J. Spuller *et al.*, Phys. Lett. A **67**, 479 (1977).
5. V. E. Lyubovitskij and A. Rusetsky, Phys. Lett. B **494**, 9 (2000).
6. M.L. Goldberger, H. Miyazawa, R. Oehme, Phys. Rev. **99**, 986 (1955).
7. J. Gasser *et al.*, Eur. Phys. J. C **26** , 13 (2002).
8. D. Sigg *et al.*, Nucl. Phys. A **609**, 310 (1996).
9. T.E. Ericson *et al.*, arXiv:hep-ph/0310134v1 (2003).
10. K. Assamagan *et al.*, Phys. Rev. D **53**, 6065 (1996).
11. N. Nelms *et al.*, Nuc. Instr. Meth. A **59**, 419 (2002).
12. L.M. Simons, Hyperfine Iteractions **81**, 253 (1993).
13. D.F. Anagnostopoulos *et al.*, Nucl. Instrum. Meth. B **205**, 9 (2003).
14. T.S. Jensen and V.E. Markushin, Eur. Phys. J. D **19**, 165 (2002).
15. S. Jonsell *et al.*, Phys. Rev. A **59**, 3440 (1999).
16. Paul Indelicato, private comunication.
17. M. Hennebach, thesis Universität zu Köln, 2003.
18. H.C. Schröder *et al.*, Eur. Phys. J. C **21**, 473 (2001).
19. Particle Data Group, Phys. Lett. B **592**, 1 (2004).

Frascati Physics Series Vol. XXXVI (2004), pp. 349–354
DAΦNE 2004: Physics at meson factories – Frascati, June 7-11, 2004
Selected Contribution in Plenary Session

ATOMIC CASCADE IN KAONIC HYDROGEN AND DEUTERIUM

T.S. Jensen
Laboratoire Kastler–Brossel, ENS et UPMC, Paris, France

Abstract

The atomic cascade in kaonic hydrogen and deuterium has been studied in the extended standard cascade model. We discuss predictions of K x–ray yields in relation to experimental data and the prospects for future experiments.

1 Introduction

Kaonic hydrogen and deuterium are initially formed in highly excited states. The formation is followed by the so–called atomic cascade where the exotic atoms deexcite to lower levels through various processes (radiative, Stark, Auger, and Coulomb transitions) until nuclear absorption or kaon decay takes place. The atomic cascade in kaonic hydrogen and deuterium was studied in refs. [1, 2]. In the present work, the K x–ray yields has been calculated in the

extended standard cascade model [3, 4] which is based on improved results for the collisional processes.

The predictions for the x–ray yields depend on the three (poorly known) strong interaction parameters: the $1s$ shift ($\Delta E_{1s}^{\rm had}$), the $1s$ width ($\Gamma_{1s}^{\rm had}$), and the $2p$ width ($\Gamma_{2p}^{\rm had}$).

2 Kaonic hydrogen

We have chosen the strong interaction parameters

$$\Delta E_{1s}^{\rm had} = 193\ {\rm eV\ (repulsive)}, \quad \Gamma_{\rm 1s}^{\rm had} = 249\ {\rm eV}, \quad \Gamma_{\rm 2p}^{\rm had} = 0.3\ {\rm meV} \qquad (1)$$

for the cascade calculations. For $\Delta E_{1s}^{\rm had}$ and $\Gamma_{1s}^{\rm had}$ this corresponds to the central values obtained recently by the DEAR Collaboration [5]. The value for the $2p$ width was chosen for the best agreement with the measured yields [6].

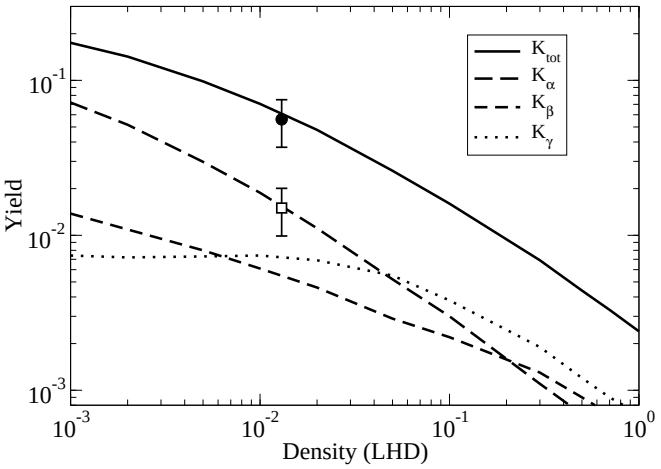

Figure 1: *The density dependence of the K x–ray yields in kaonic hydrogen. The experimental data for the* $K_{\rm tot}$ *and* K_α *yields are from ref.* [6].

Figure 1 shows the density dependence of the x–ray yields. The yields decrease strongly with the density as Stark transitions feed the s and p states, from which nuclear absorption takes place, faster.

The experimental data on x–ray yields suggest a $2p$ strong interaction width in the range $0.0 - 0.6$ meV. Besides the x–ray yields from KEK [6] at 0.013 LHD (liquid hydrogen density) shown in fig. 1, the DEAR Collaboration has presented preliminary results at 0.031 LHD [7]: $K_\alpha = 1 - 3\%$ and $K_\alpha \sim K_\beta \sim K_{>\gamma} > K_\gamma$. Table 1 and 2 shows the predicted K yields for $\Gamma_{2p}^{\rm had} = 0.0$, 0.3, 0.6 meV.

Table 1: *The predicted K x–ray yields (%) in kaonic hydrogen at 0.013 LHD for different values of the $2p$ strong interaction width.*

$\Gamma_{2p}^{\rm had}$	K_α	K_β	K_γ	$K_{>\gamma}$
0.0 meV	4.19	1.41	1.47	4.81
0.3 meV	1.61	0.59	0.69	3.64
0.6 meV	0.94	0.35	0.42	2.94

Table 2: *The predicted K x–ray yields (%) in kaonic hydrogen at 0.031 LHD for different values of the $2p$ strong interaction width.*

$\Gamma_{2p}^{\rm had}$	K_α	K_β	K_γ	$K_{>\gamma}$
0.0 meV	2.11	0.89	1.19	2.67
0.3 meV	0.81	0.36	0.66	2.10
0.6 meV	0.50	0.22	0.45	1.87

It would be interesting if the relatively high K_β yield observed by the DEAR Collaboration could be confirmed in future experiments because it could indicate that there is a large thermalized fraction of kaonic hydrogen atoms at $n = 3$. The reason is that the $3p - 3d$ energy difference of 0.18 eV makes Stark transitions irreversible at low energies as only $3d \rightarrow 3p$ is allowed energetically. This leads to an overpopulation of the $3p$ state and an increased K_β yield. A similar phenomenon is observed in pionic helium [8].

3 Kaonic deuterium

The SIDDHARTA Collaboration plans to measure the $1s$ strong interaction width in kaonic deuterium for the first time [9]. The feasibility of this experiment depends on the x–ray yields being high enough: a K yield of 1% or more

at 20 bar would be encouraging [10]. Cascade model predictions of the absolute x–ray yields are, therefore, important.

Though the strong interaction parameters have not been measured, predictions based on model estimates and phenomenological fits are possible. We will use the values

$$\Delta E_{1s} = 0.5 \text{ keV}, \quad \Gamma_{1s}^{\text{had}} = 1 \text{ keV}, \quad \Gamma_{2p}^{\text{had}} = 1 \text{ meV} \tag{2}$$

as a standard. The $1s$ parameters are based on a study of low–energy $(N\bar{K}, \Lambda\pi)$ and $(N\bar{K}, \Sigma\pi)$ data [11]. Predictions of the $2p$ width vary considerably: from 0.014 meV [11] to 25 meV [1]. Figure 2 shows the density dependence of the x–ray yields in kaonic deuterium. Compared to the yields in kaonic hydrogen they are lower but qualitatively similar.

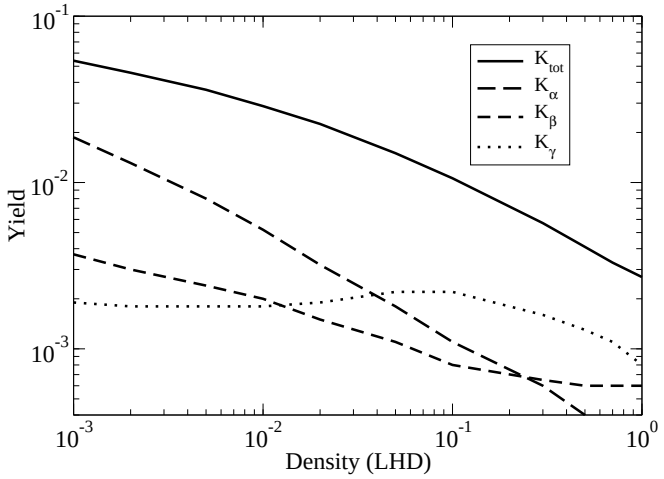

Figure 2: *The density dependence of the K x–ray yields in kaonic deuterium.*

Table 3, 4, and 5 show the dependence of the K_{tot} and K_α yields at 0.026 LHD on each of the three strong interaction parameters. The $2p$ width is the most important for the proposed measurement of the $1s$ strong interaction shift and width because it could reduce the K_α yield far below 1%. A possible scenario is that the K_α line is too weak for a precise determination of $\Delta E_{1s}^{\text{had}}$ and Γ_{1s}^{had} and that high statistics is obtained only for the K–complex (consisting of the overlapping lines of the higher transitions). In this case reliable

cascade model predictions of the relative yields are crucial for the analysis of the spectrum.

Table 3: *The predicted $K_{\rm tot}$ and K_α x–ray yields (%) in kaonic deuterium at 0.026 LHD for different values of the $1s$ shift (in keV).*

	ΔE_{1s}				
	0.1	0.2	0.5	1.0	1.5
$K_{\rm tot}$	1.61	1.66	2.00	2.91	3.70
K_α	0.23	0.23	0.26	0.41	0.52

Table 4: *The predicted $K_{\rm tot}$ and K_α x–ray yields (%) in kaonic deuterium at 0.026 LHD for different values of the $1s$ strong interaction width (in keV).*

	$\Gamma_{1s}^{\rm had}$					
	0.1	0.2	0.5	1.0	1.5	2.0
$K_{\rm tot}$	4.51	3.51	2.40	2.00	1.98	2.04
K_α	0.63	0.48	0.34	0.26	0.27	0.28

Table 5: *The predicted $K_{\rm tot}$ and K_α x–ray yields (%) in kaonic deuterium at 0.026 LHD for different values of the $2p$ strong interaction width (in meV).*

	$\Gamma_{2p}^{\rm had}$						
	0.0	0.2	0.5	1.0	2.0	5.0	10.0
$K_{\rm tot}$	6.05	3.95	2.76	2.00	1.28	0.69	0.45
K_α	1.91	0.98	0.50	0.26	0.12	0.04	0.02
$K_\alpha/K_{\rm tot}$	0.315	0.248	0.182	0.132	0.095	0.056	0.041

4 Conclusion

The x–ray yields in kaonic hydrogen and deuterium have been calculated in the extended standard cascade model. The predicted K yields depend strongly on the (poorly known) $2p$ strong interaction widths so measurements of x–ray spectra can be used to determine them.

A comparison of cascade model predictions in kaonic hydrogen with existing data from KEK [6] and preliminary data from the DEAR Collaboration [7]

restricts the $2p$ strong interaction width to the range $0.0 - 0.6$ meV.

For the proposed x–ray measurement by the SIDDHARTA Collaboration in kaonic deuterium, the poor knowledge of the strong interaction parameters makes three scenarios possible: (1) the K_α yield is high enough for a determination of the $1s$ shift and width. (2) The K_α yield is too low but the K–complex can be used in combination with reliable cascade model predictions. (3) If $\Gamma_{2p}^{\rm had} \gg 1$ meV the proposed experiment may not be feasible because the total K yield is too small.

5 Acknowledgments

This work was supported by the Swiss National Science Foundation.

References

1. T. Koike, T. Harada, and Y. Akaishi, Phys. Rev. C **53**, 79 (1996).
2. M.P. Faifman *et al.*, Frascati Phys. Series **XVI**, 637 (1999).
3. T.S. Jensen and V.E. Markushin, Eur. Phys. J. D **21**, 271 (2002).
4. T.S. Jensen and V.E. Markushin, in: Precision Physics of Simple Atomic Systems (Eds. S.G. Karshenboim; V.B. Smirnov), Springer Lecture Notes in Physics **627**, 37 (Springer, Berlin, 2003).
5. J. Zmeskal, these proceedings.
6. T.M. Ito *et al.*, Phys. Rev. C **58**, 2366 (1998).
7. M. Cargnelli, talk at HadAtom03, Workshop on Hadronic Atoms, 13-17 Oct. 2003, Trento, Italy.
8. J.E. Russell, Phys. Rev. A **18**, 521 (1978).
9. M. Iliescu, these proceedings.
10. C. Petrascu, private communication.
11. R.C. Barrett and A. Deloff, Phys. Rev. C **60**, 025201 (1999).

Session VI — CHPT and Low E Hadronic Physics

(Chairpersons: C. Guaraldo, M. Greco, T. Bressani)

S. Eidelman	$(g_\mu-2)/2$ and Adronic e^+e^- Cross Section
F. Nguyen	Measurement of the $e^+e^+ \rightarrow \pi^+\pi^- \gamma$ Cross Section Below 1 GeV with the Kloe Detector
N. Berger	Inclusive Hadron Results at BaBar: ISR and Pentaquark Searches
P. Lukin	Measurement of $e^+e^- \rightarrow \phi \rightarrow K^+K^-$ Cross Section with CMD-2 Detector at VEPP-2M Collider
D. Epifanov	New study of $\phi \rightarrow \pi^+\pi^-\pi^o$ Decay with CMD-2 Detector
M. Knecht	Chiral Perturbation Theory Confronted with Experiment
I. Bediaga	Open Problems on Light Meson Spectroscopy
L. Tauscher	Results from the DIRAC Experiment at CERN
B. Di Micco	Progress on Φ Radiative Decays with the Kloe Experiment
L. Edera	Dalitz Plot Analysis in FOCUS
D.R. Gill	TWIST: Triumf Weak Interaction Symmetry Test
L.A. Linden Levy	Flavor Decomposition of the Nucleon's Spin at HERMES
F. Borg	$K \rightarrow 3\pi$ Decays in Chiral Prturbation Theory
O. Shekhovtsova	Final–State Radiation in Electron–Positron Annihilation into Pion Pair
F. Ignatov	New Data on $e^+e^- \rightarrow \pi^+\pi^-$ Cross Section with CMD–2 in Energy Range $\sqrt{s} = 0.37 – 1.38$ GeV
E. Nowak	Nucleon Form Factors Measurements Via the Radiative Return at *B*–Meson Factories
M. Dreucci	Measurement of ϕ–Meson Leptonic Width in $e^+e^- \rightarrow e^+e^-, \mu^+\mu^-$ Processes
A. Zaytsev	Measurement of Neutral Kaon Mass with CMD-2 Detector

Frascati Physics Series Vol. XXXVI (2004), pp. 357– 366
DAΦNE 2004: Physics at meson factories – Frascati, June 7-11, 2004
Invited Review Talk in Plenary Session

$(g_\mu - 2)/2$ AND HADRONIC e^+e^- CROSS SECTIONS

Simon Eidelman
Budker Institute of Nuclear Physics,
Novosibirsk, 630090, Russia

Abstract

Recent measurements of the cross section of the process $e^+e^- \to$ *hadrons* are reviewed. Their implications for the calculation of the muon anomalous magnetic moment are discussed. e^+e^- based calculations are compared to those using τ data.

1 Introduction

Recently the E821 Collaboration at BNL published the final results on $a_\mu = (g-2)_\mu/2$, the muon anomalous magnetic moment (MAMM) [1]. The relative accuracy achieved in this experiment is $5 \cdot 10^{-7}$: $a_\mu = (11659208 \pm 6) \cdot 10^{-10}$. Although a_e is measured with a $4 \cdot 10^{-9}$ accuracy, a_μ is much more sensitive to new physics effects: the gain is usually $\sim (m_\mu/m_e)^2 \approx 4.3 \cdot 10^4$. Any significant

difference of $a_\mu^{\rm exp}$ from $a_\mu^{\rm th}$ indicates new physics beyond the Standard Model (SM). It is conventional to express the theoretical prediction as

$$a_\mu^{\rm th} = a_\mu^{\rm SM} + a_\mu^{\rm non-SM}, \qquad a_\mu^{\rm SM} = a_\mu^{\rm QED} + a_\mu^{\rm EW} + a_\mu^{\rm had}. \tag{1}$$

For the quantum electrodynamics (QED) term the analytical calculation of the α^3 terms, the numerical calculation of the α^4 terms and estimation of some of the α^5 terms gives after recent improvements [2, 3]: $a_\mu^{\rm QED} = (11658471.9 \pm 0.2) \cdot 10^{-10}$. For the electroweak (EW) term the most recent estimation including all one- and two-loop terms as well as part of three-loop terms gives [4]: $a_\mu^{\rm EW} = (15.4 \pm 0.1 \pm 0.2) \cdot 10^{-10}$. The hadronic contribution can also be written as a sum of three terms:

$$a_\mu^{\rm had} = a_\mu^{\rm had,LO} + a_\mu^{\rm had,HO} + a_\mu^{\rm had,LBL}. \tag{2}$$

The dominant contribution comes from the first, leading order term.

Although this term can't be calculated from first principles, one obtains from dispersion relations:

$$a_\mu^{\rm had,LO} = \left(\frac{\alpha m_\mu}{3\pi}\right)^2 \int_{4m_\pi^2}^{\infty} ds\, \frac{R(s)\, \hat{K}(s)}{s^2}, \tag{3}$$

where $R(s) = \sigma(e^+e^- \to hadrons)/\sigma(e^+e^- \to \mu^+\mu^-)$, and the kernel $\hat{K}(s)$ grows from 0.63 at $s = 4m_\pi^2$ to 1 at $s \to \infty$. The factor $1/s^2$ emphasizes the role of low energies, particularly important is the reaction $e^+e^- \to \pi^+\pi^-$ with a large cross section below 1 GeV. As a result, 73% of the central value comes from this channel and more than 92% comes from the energy region below 2 GeV.

Numerous attempts to estimate the leading order hadronic term exist in literature (see Ref. [5] and references therein), but most of them are model-dependent and do not take into account systematic uncertainties of the data. The authors of Ref. [5] were the first to perform a model-independent estimate based only on the data up to 40 GeV. Their result used the whole bulk of the experimental information existing before 1995 and gave: $a_\mu^{\rm had,LO} = (702 \pm 6 \pm 14) \cdot 10^{-10}$. Today, almost 10 years later, there are a lot of new precise measurements, mostly due to the experiments at the VEPP-2M collider in Novosibirsk and the BEPC collider in Beijing. We describe below a new evaluation based on new e^+e^- and τ lepton data.

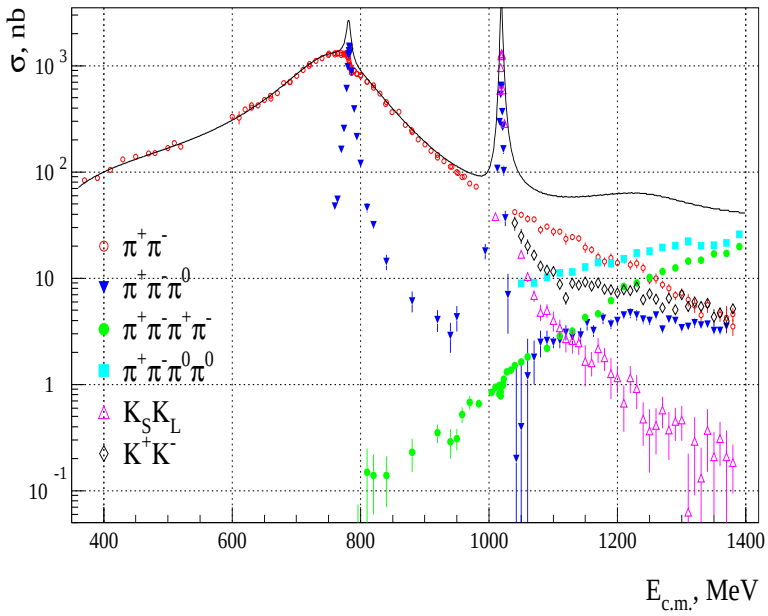

Figure 1: *Hadronic cross sections at CMD-2.*

2 New e^+e^- Based Evaluation of $a_\mu^{\rm had,LO}$

Two Novosibirsk groups (CMD-2 [6]) and SND [7]) studied a lot of exclusive modes at $\sqrt{s} < 1.4$ GeV ($\pi^+\pi^-, \pi^+\pi^-\pi^0, \ldots, K\bar{K}$) including the channels with a very small cross section ($\pi\pi\gamma, \pi^0\gamma, \eta\gamma, \ldots$) whereas BES studied the energy range from 2 to 5 GeV and measured the total cross section (R value) [8].

The VEPP-2M e^+e^- collider in Novosibirsk was running for experiment since 1974 and until 2000. It covered the c.m. energy range $0.36 < \sqrt{s} < 1.40$ GeV with the peak luminosity of $3 \cdot 10^{30}$ cm^{-2} s^{-1}. The integrated luminosity of ≈ 100 pb^{-1} was collected in Novosibirsk below 1.4 GeV compared to ≈ 6 pb^{-1} in Orsay and Frascati at $1.4 < \sqrt{s} < 3.0$ GeV!

As mentioned above, the contribution of the process $e^+e^- \to \pi^+\pi^-$ dominates $a_\mu^{\rm had,LO}$ ($\sim 73\%$). Therefore, its low systematics study is of paramount importance. CMD-2 reached the 0.6% systematic error in the crucial ρ meson region from 600 to 960 MeV using only a part of the full data sample [6]. Final analysis of the whole statistics will soon be completed.

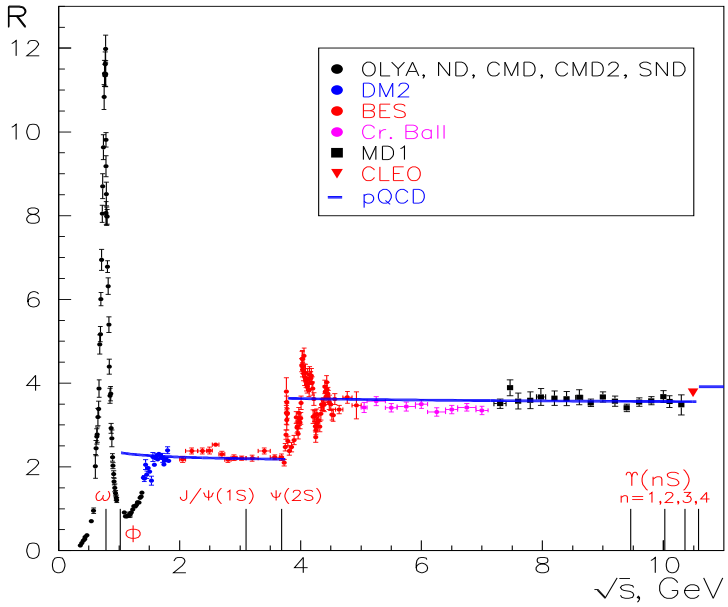

Figure 2: *R values below 10 GeV.*

Above 1 GeV another process - production of four pions dominates. Both possible final states have been studied: $e^+e^- \to \pi^+\pi^-\pi^+\pi^-$ and $e^+e^- \to \pi^+\pi^-\pi^0\pi^0$, and the cross sections are known with good accuracy below 1.4 GeV while a large data scatter is observed from 1.4 to 2 GeV.

In Fig. 1 we show various hadronic cross sections studied at CMD-2. One can see that the values of the cross section vary by three–four orders of magnitude, from more than one thousand nb for the processes $e^+e^- \to \pi^+\pi^-$ and $e^+e^- \to \pi^+\pi^-\pi^0$ at the peak of the ρ and ω mesons, respectively, to about 100 pb only for the process $e^+e^- \to \pi^+\pi^-\pi^+\pi^-$.

Another important feature of these studies is that for the first time cross sections of various purely neutral final states $\pi^0\gamma$, $\eta\gamma$, $\pi^0\pi^0\gamma$ and $\eta\pi^0\gamma$ were studied in a broad energy range with both detectors [9, 10], not only at the resonance peaks, but also at the energies between the resonances. The results of CMD-2 and SND are consistent with each other and show that the contributions

of the ρ, ω and ϕ mesons dominate the cross sections. From the upper limits on nonresonant cross sections CMD-2 set a 90% CL upper limit for the nonresonant contributions of such processes to the MAMM: $a_\mu^{\rm rad,LO} < 0.7 \cdot 10^{-10}$.

As we have already mentioned, measurements at 1.4 GeV $< \sqrt{s} <$ 2 GeV were performed long ago in Orsay and Frascati and their results have much worse accuracy. A detailed study of the energy range would be important not only for the MAMM problem, but also for the resonance spectroscopy. For example, even the basic properties of the five resonances in these energy range (2 ρ' mesons, 2 ω' mesons and the ϕ' meson) are rather badly known. There are indications for additional structures, e.g., the narrow one at 1.9 GeV in the 6π system [11]. There are also speculations that the spectroscopy of these states is even more complicated involving mixing with exotic states, e.g., hybrids [12].

A very important measurement of the total cross section $e^+e^- \to hadrons$ recently performed at the BES detector improved upon the accuracy of R in the energy range between 2 and 5 GeV at least by a factor of two [8].

In Fig. 2 we show the value of R obtained in the most precise experiments below 10 GeV. Good agreement is observed between the data and the theoretical predictions based on perturbative QCD. This justifies a possibility to use theory above 5 GeV for the calculations, particularly taking into account that this energy range gives less than a 1.5% contribution to the leading order hadronic term [13, 14]. As a result, our calculation gives $a_\mu^{\rm had,LO} = 696.3 \pm 6.2 \pm 3.6$. Note that a higher accuracy of e^+e^- data makes the error of $a_\mu^{\rm had,LO}$ two times smaller.

We should also mention the status of the higher order terms. The higher order hadronic contribution $a_\mu^{\rm had,HO}$ can also be calculated in terms of the $\int R(s)G(s)ds/s^{2(3)}$, where $G(s)$ is a smooth function of s, so that the low energy range again dominates the integral. Several calculations agree. The accepted value is [15]: $a_\mu^{\rm had,HO} = (-10.0 \pm 0.6) \cdot 10^{-10}$. Until recently the accepted value for a controversial light-by-light scattering term was $a_\mu^{\rm LBL} = (8.6 \pm 3.5) \cdot 10^{-10}$ based on the Refs. [16, 17]. In Ref. [18] this quantity was reevaluated to be $a_\mu^{\rm LBL} = (13.6 \pm 2.5) \cdot 10^{-10}$. Adding together all the contributions described above, we obtain for the theoretical prediction $a_\mu^{\rm th} = (11659180.9 \pm 8.0) \cdot 10^{-10}$ and $a_\mu^{\rm exp} - a_\mu^{\rm th} = (27.1 \pm 10.0) \cdot 10^{-10}$ or 2.7 standard deviations. If recent theory progress is taken into account, the difference becomes smaller, 2.1σ only.

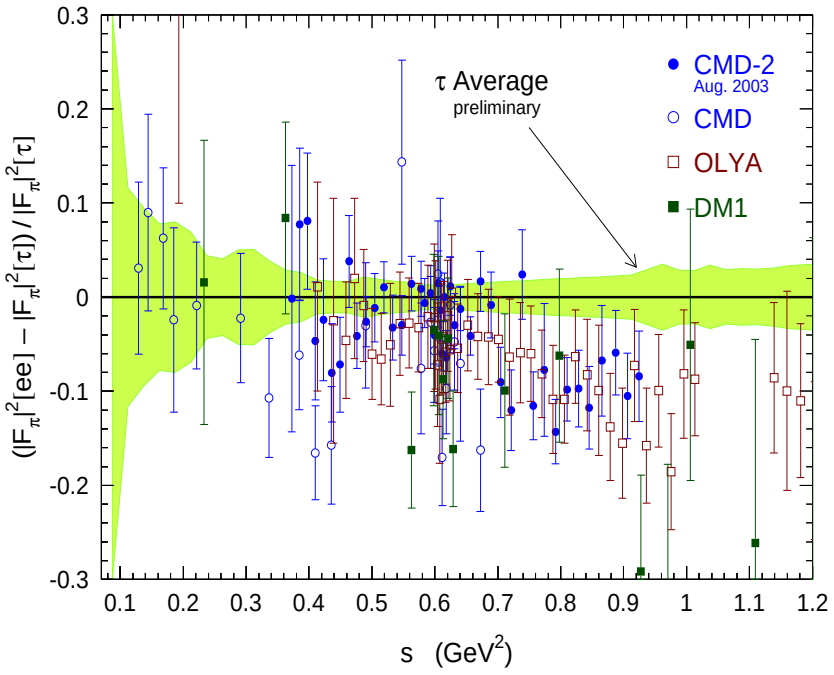

Figure 3: *Comparison of* 2π *spectral functions.*

3 Confronting e^+e^- and τ Lepton Based Evaluations

To improve on a theoretical error, it is very tempting to use the data on τ lepton decays into vector states 2π and 4π. It is known that from the conservation of vector current (CVC) and SU(2) symmetry the corresponding hadronic spectra in τ decays are related to the values of the e^+e^- cross sections [19]. Various CVC tests performed in 80-ies and the beginning of 90-ies showed that this relation was valid within the accuracy of the measurements available at that time [20]. Therefore, in Ref. [15] the authors assumed the CVC validity to use an independent τ lepton data set to perform a new τ lepton based estimate of $a_\mu^{\rm had,LO}$. Averaging their result with the e^+e^- based one they improved on the accuracy of $a_\mu^{\rm had,LO}$ by a factor of 1.5. With the increasing accuracy both in e^+e^- and τ sectors indications for some discrepancy appeared: the spectral functions in τ decays were higher than those in e^+e^- annihilation. A recent

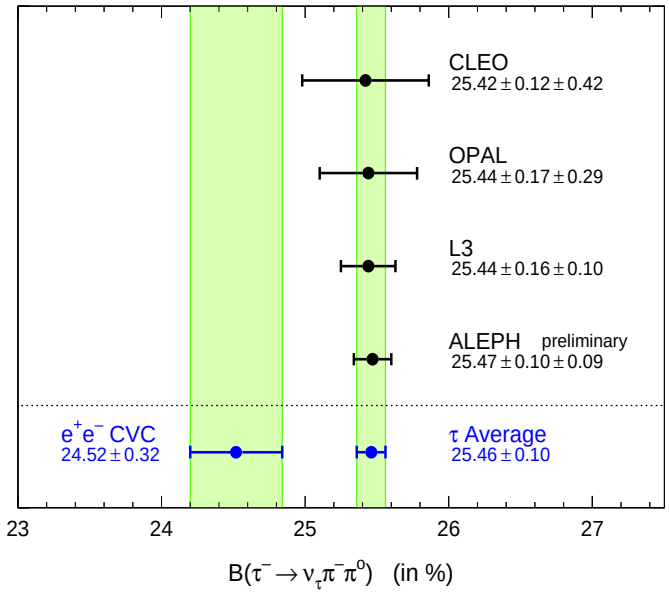

Figure 4: *$Br(\tau^- \to \pi^-\pi^0\nu_\tau)$ from CVC and τ decays.*

analysis, which used the latest data from both e^+e^- and τ sectors as well as a large set of corrections for SU(2) breaking [21, 22], confirmed the existence of such a discrepancy. It is illustrated for the 2π channel in Fig. 3, from which it is clear that above the ρ meson peak the τ spectral function is significantly higher than that in e^+e^- annihilation. Integrating the spectral function from e^+e^- one can obtain the prediction for the branching fraction $Br(\tau^- \to \pi^-\pi^0\nu_\tau)$ confronted in Fig. 4 to that measured in τ decays by different groups. It is clear that the value of the branching fraction from all groups is systematically higher than the CVC prediction. As a result, a possibility to use τ lepton data for MAMM becomes problematic. Indeed, the τ lepton based estimate of $a_\mu^{\rm had,LO}$ is $(711.0 \pm 5.8) \cdot 10^{-10}$, i.e., substantially higher than $(696.3 \pm 7.2) \cdot 10^{-10}$ from e^+e^- data [14]. Averaging of the two estimates becomes meaningless. The reasons of this discrepancy are not yet clear [23]. The current situation is summarized in Fig. 5.

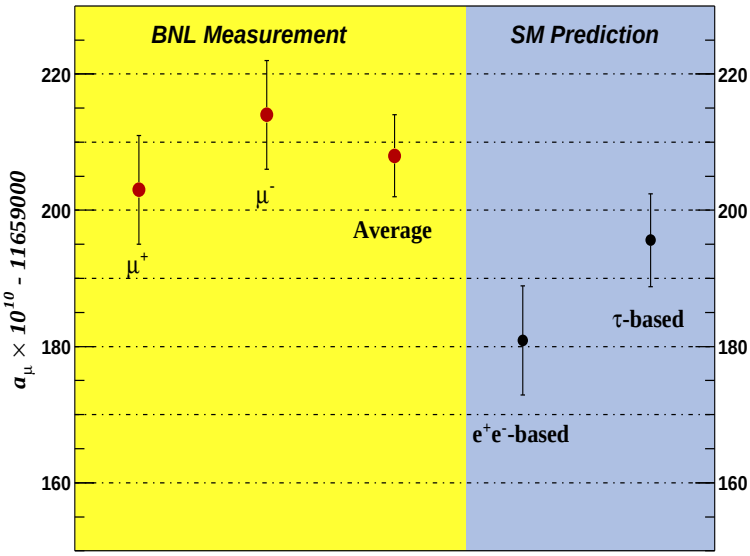

Figure 5: *Current status of* a_μ.

4 Prospects and Conclusions

We can conclude that the increased accuracy of e^+e^- data (VEPP-2M and BEPC) decreased an error of $a_\mu^{\rm had,LO}$ by a factor of 2, but the experimental accuracy of a_μ is still better. τ data could further improve upon the accuracy by a factor of 1.5 but e^+e^- and τ data differ. The experimental value of a_μ is higher than the theoretical prediction by (2.1–2.7) σ.

Future progress will be possible after experiments planned at the new machine VEPP-2000 (VEPP-2M upgrade) with 2 detectors (CMD-3 and SND) up to $\sqrt{s}$=2 GeV with $L_{\rm max} = 10^{32}$ cm^{-2}s^{-1} as well as other experiments at the CESRc and $(c-\tau)$ factory.

Also attractive is the idea to use for more precise R measurements the method of radiative return recently successfully employed in the KLOE experiment [24].

5 Acknowledgements

I'm indebted to the Organizing Committee for their help and support during this very interesting Conference. This work would be impossible without extraordinary efforts of my colleagues from the VEPP-2M collider, CMD-2 and SND Collaborations. I'm grateful to M. Davier, A. Höcker and F. Jegerlehner for the fruitful collaboration.

This work was supported in part by the grants RFBR-03-02-16843 and PST.CLG.980342.

References

1. G.W. Bennett *et al*, Phys. Rev. Lett. **92**, 161802 (2004).
2. V.W. Hughes and T. Kinoshita, Rev. Mod. Phys. **71**, 533 (1999).
3. T. Kinoshita and M. Nio, hep-ph/0402206.
4. A. Czarnecki, W.J. Marciano, A. Vainshtein, Phys. Rev. D **67**, 073006 (2003).
5. S. Eidelman and F. Jegerlehner, Z. Phys. C **67**, 585 (1995).
6. R.R. Akhmetshin *et al*, Phys. Lett. B **578**, 285 (2004).
7. S.I. Serednyakov, Nucl. Phys. B (Proc. Suppl.) **96**, 197 (2001).
8. J.Z. Bai *et al*, Phys. Rev. Lett. **88**, 101802 (2002).
9. M.N. Achasov *et al*, Phys. Lett. B **537**, 201 (2002).
10. R.R. Akhmetshin *et al*, Phys. Lett. B **562**, 173 (2003).
11. P.L. Frabetti *et al*, Phys. Lett. B **514**, 240 (2001).
12. T. Barnes *et al*, Phys. Rev. D **55**, 4157 (1997).
13. M. Davier *et al*, Eur. Phys. J. C **27**, 497 (2003).
14. M. Davier *et al*, Eur. Phys. J. C **31**, 503 (2003).
15. R. Alemany, M. Davier, A. Höcker, Eur. Phys. J. C **2**, 123 (1998).

16. J. Bijnens, E. Pallante, J. Prades, Nucl. Phys. B **626**, 410 (2002).

17. M. Hayakawa and T. Kinoshita, Phys. Rev. D **66**, 019902 (2002).

18. K. Melnikov and A. Vainshtein, hep-ph/0312226.

19. Y.S. Tsai, Phys. Rev. D **4**, 2821 (1971).

20. S.I. Eidelman and V.N. Ivanchenko, Phys. Lett. B **257**, 437 (1991).

21. V. Cirigliano, G. Ecker, H. Neufeld, Phys. Lett. B **513**, 361 (2001).

22. V. Cirigliano, G. Ecker, H. Neufeld, JHEP, **0208**, 002 (2002).

23. S. Ghozzi and F. Jegerlehner, Phys. Lett. B **583**, 222 (2004).

24. A. Aloisio *et al*, hep-ex/0708048.

Frascati Physics Series Vol. XXXVI (2004), pp. 367–372
DAΦNE 2004: Physics at meson factories – Frascati, June 7-11, 2004
Selected Contribution in Plenary Session

MEASUREMENT OF THE $e^+ e^- \to \pi^+ \pi^- \gamma$ CROSS SECTION BELOW 1 GEV WITH THE KLOE DETECTOR

The KLOE Collaboration *
Presented by Federico Nguyen
Institut für Experimentelle Kernphysik, Universität Karlsruhe, Germany

Abstract

The differential cross section for the process $e^+e^- \to \pi^+\pi^-\gamma$ has been measured with the KLOE detector at the e^+e^- collider DAΦNE, as a function of the $\pi\pi$ invariant mass. From this spectrum, the total cross section $\sigma_{e^+e^-\to\pi^+\pi^-}$ for the mass range $0.35\ \text{GeV}^2 < s < 0.95\ \text{GeV}^2$ is extracted and the hadronic contribution to the magnetic anomaly of the muon is evaluated.

*A. Aloisio, F. Ambrosino, A. Antonelli, M. Antonelli, C. Bacci, M. Barva, G. Bencivenni, S. Bertolucci, C. Bini, C. Bloise, V. Bocci, F. Bossi, P. Branchini, S. A. Bulychjov, R. Caloi, P. Campana, G. Capon, T. Capussela, G. Carboni, F. Ceradini, F. Cervelli, F. Cevenini, G. Chiefari, P. Ciambrone, S. Conetti, E. De Lucia, A. De Santis, P. De Simone, G. De Zorzi, S. Dell'Agnello, A. Denig, A. Di Domenico, C. Di Donato, S. Di Falco, B. Di Micco, A. Doria, M. Dreucci, O. Erriquez, A. Farilla, G. Felici, A. Ferrari, M. L. Ferrer, G. Finocchiaro, C. Forti, P. Franzini, C. Gatti, P. Gauzzi, S. Giovannella, E. Gorini, E. Graziani, M. Incagli, W. Kluge, V. Kulikov, F. Lacava, G. Lanfranchi, J. Lee-Franzini, D. Leone, F. Lu, M. Martemianov, M. Martini, M. Matsyuk, W. Mei, L. Merola, R. Messi, S. Miscetti, M. Moulson, S. Müller, F. Murtas, M. Napolitano, F. Nguyen, M. Palutan, E. Pasqualucci, L. Passalacqua, A. Passeri, V. Patera, F. Perfetto, E. Petrolo, L. Pontecorvo, M. Primavera, P. Santangelo, E. Santovetti, G. Saracino, R. D. Schamberger, B. Sciascia, A. Sciubba, F. Scuri, I. Sfiligoi, A. Sibidanov, T. Spadaro, E. Spiriti, M. Tabidze, M. Testa, L. Tortora, P. Valente, B. Valeriani, G. Venanzoni, S. Veneziano, A. Ventura, R. Versaci, I. Villella, G. Xu.

1 Introduction

The comparison of the recent precision measurement of the muon magnetic anomaly, a_μ, at the Brookhaven National Laboratory [1)] with the theoretical value is a fundamental test of the Electroweak Standard Model [2)]. Because of the nonperturbative regime of QCD, the hadronic contribution is evaluated from data of $\sigma_{e^+e^-\to hadrons}$ by a dispersion integral. In particular measurements of $\sigma_{e^+e^-\to\pi^+\pi^-} \equiv \sigma_{\pi\pi}$ below 1 GeV provide the 62%. The Standard Model a_μ value disagrees by 2.7 standard deviations from the measured value.

2 Radiative return

At DAΦNE $\sigma_{\pi\pi}$ is extracted from the measurement of the differential cross section in the $\pi\pi$ invariant mass, s_π, in the reaction $e^+e^- \to \pi^+\pi^-\gamma$, using [3)]:

$$s_\pi \frac{d\sigma_{\pi\pi\gamma}}{ds_\pi} = \sigma_{\pi\pi}(s_\pi)\ H(s_\pi)\ , \tag{1}$$

where the initial state radiation (ISR) of a photon is parameterized by the radiator function H. This approach allows studying $\sigma_{\pi\pi}$ as a function of s_π, for $s_\pi < M_\phi^2$, M_ϕ being the mass of the Φ meson. Final state radiation (FSR) events without any ISR photon are a background for our measurement and they are suppressed at a level lower than 1% by means of the geometrical acceptance of the photon. However events with at least one ISR and a FSR photon are considered as signal in order for $\sigma_{\pi\pi}$ to be inclusive with respect to final state radiative corrections. The signal process, $e^+e^- \to \pi^+\pi^-\gamma_{ISR}(\gamma_{FSR})$, is simulated by the Monte Carlo generator `Phokhara` [4)], used in this analysis for evaluating the acceptance corrections, the efficiency of the kinematic cuts and for estimating several systematic uncertainties.

3 Selection of $\pi^+\,\pi^-\,\gamma$ events

The KLOE detector consists of a high momentum and vertex resolution drift chamber, and a good energy resolution electromagnetic calorimeter providing very good time measurements. The data used for this measurement were taken from July to December 2001, yielding an integrated luminosity $\mathcal{L} = 141.4\ \mathrm{pb}^{-1}$. In the following, the main items of the analysis of the reaction $e^+e^- \to \pi^+\pi^-\gamma$ are briefly commented, further details can be found in ref. [5)].

3.1 Fiducial volume

We require the detection of two tracks with polar angles between 50° and 130°. The tracks must be connected to a vertex within a cylinder of radius $\sqrt{x^2+y^2} < 8$ cm and $|z| < 7$ cm. Additional cuts are applied on the transverse momentum, $p_T > 160$ MeV, or on the longitudinal component, $|p_z| > 90$ MeV, for rejecting spiralling tracks and ensuring good reconstruction conditions.

3.2 Photon geometrical acceptance

For enhancing ISR with respect to FSR, events with a photon emitted at small polar angle with respect the beam line are selected. Since the KLOE electromagnetic calorimeter does not cover angles smaller than 20°, *no photon detection is required*, but cuts on the polar angle of the $\pi\pi$ system are applied: $\theta_{\pi\pi} < 15°$ (or $\theta_{\pi\pi} > 165°$). With this configuration the collinear divergence of ISR events allows high statistics and the contamination from the resonant process $e^+e^- \to \phi \to \pi^+\pi^-\pi^0$ is reduced.

3.3 Pion identification

Discrimination of pions from electrons is performed using a function based on approximate likelihood estimators. They are based on the time of flight, and on the shape and quantity of the energy released along the calorimeter of the clusters associated to the tracks. Those observables have been modeled using control samples of $\phi \to \pi^+\pi^-\pi^0$ and $e^+e^- \to e^+e^-\gamma$ events in data, in order to obtain the calorimeter response for pions and electrons. An event is selected as signal if at least one of the two tracks is identified as a pion.

3.4 Kinematic cuts

Contaminations from the processes $e^+e^- \to \mu^+\mu^-\gamma$ and $\phi \to \pi^+\pi^-\pi^0$ are rejected by cuts on the track mass variable, m_{trk}. It is defined by the four-momentum conservation from the momenta of the two tracks and the centre of mass energy under the hypothesis of a final state consisting of two particles with the same mass and one photon.

4 The differential cross section $d\sigma_{\pi\pi\gamma}/ds_\pi$

After all selection cuts we find 1.55×10^6 events. From the observed spectrum, $\Delta N_{obs}/\Delta s_\pi$, we subtract the residual background events, $\Delta N_{bkg}/\Delta s_\pi$, we divide by the total efficiency of the selection, $\varepsilon_{sel}(s_\pi)$, and by the integrated luminosity, the mass resolution allows the bin width $\Delta s_\pi = 0.01$ GeV^2:

$$\frac{d\sigma_{\pi\pi\gamma}}{ds_\pi} = \frac{\Delta N_{obs} - \Delta N_{bkg}}{\Delta s_\pi} \frac{1}{\varepsilon_{sel}(s_\pi)\ \mathcal{L}} \ . \tag{2}$$

4.1 Background estimates

Residual background from $\mu^+\mu^-\gamma$ and $e^+e^-\gamma$ events is estimated fitting the m_{trk} spectrum of the selected data sample with a superposition of three distributions describing the signal and the two background sources. The distributions for signal and $\mu^+\mu^-\gamma$ events are obtained from Monte Carlo simulation, while for $e^+e^-\gamma$ events a dedicated data sample of 152 pb^{-1} is used. The only free parameters of these fits are the relative weights of signal and backgrounds in the data. Background from $\pi^+\pi^-\pi^0$ has been estimated fitting missing mass spectra in a similar way. This latter is the invariant mass of the X state for the process $e^+e^- \to \pi^+\pi^- X$. The contribution of the whole background is less than 2% for $s_\pi > 0.5$ GeV^2 and it increases up to 10% at $s_\pi = 0.35$ GeV^2.

4.2 Efficiencies of the selection

The overall efficiency of the selection is 60%, flat in s_π. During reconstruction an offline filter identifies and rejects background events using information from the calorimeter only. This procedure is related to the different conditions of the data taken during 2001 and it yields the major systematic error, 0.6%. The other sources of systematics are 0.3% or less. From the measured spectrum, $d\sigma_{\pi\pi\gamma}/ds_\pi$ as a function of the true value of s_π is retrieved. The resolution matrix is obtained from a Monte Carlo simulation corrected to reproduce the m_{trk} data histogram and it results nearly diagonal.

4.3 Integrated luminosity

The absolute normalization of the data sample is measured using very large angle Bhabha (VLAB) events, $55° < \theta < 125°$, with a cross section $\sigma \simeq 430$ nb. The integrated luminosity is provided dividing the observed number of VLAB

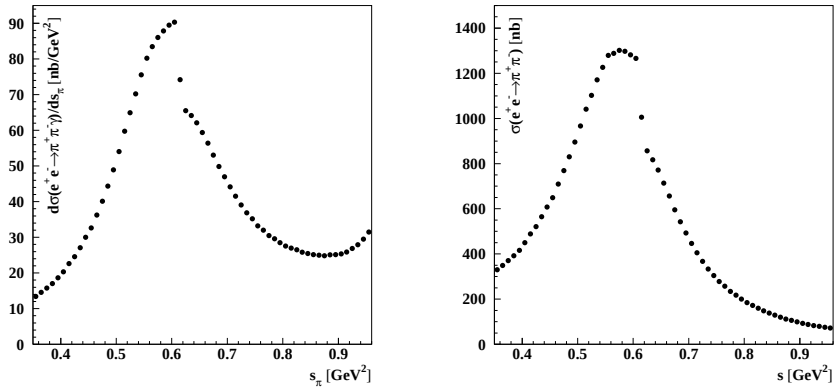

Figure 1: *Left:* $d\sigma_{\pi\pi\gamma}/ds_\pi$ *with* $\theta_{\pi\pi}<15^\circ$ *(*$\theta_{\pi\pi}>165^\circ$*). Right:* $\sigma_{e^+e^-\to\pi^+\pi^-}$.

events by the effective cross section evaluated by the Monte Carlo generator of Bhabha events `Babayaga` [6], including QED radiative corrections with the parton shower algorithm, inserted in the code simulating the KLOE detector. The quoted precision of `Babayaga` is 0.5%. The background, $\pi^+\pi^-(\gamma)$ and $\mu^+\mu^-(\gamma)$ events, is well below 1% and the main systematic effect is due to the angular acceptance: the overall systematic uncertainty of the measurement is 0.3%. Then, the relative precision is $\delta\mathcal{L}/\mathcal{L} = 0.6\%$.

5 Extraction of $\sigma_{\pi\pi}$

The radiator H needed for getting $\sigma_{\pi\pi}$ as in eq.(1), is provided by the code `Phokhara` after setting the pion form factor $F_\pi(s_\pi) = 1$. The assumption of eq.(1), *i.e.* the absence of interference terms between ISR and FSR, has been tested by an alternative procedure in which only genuine ISR events are considered as signal and FSR corrections to $e^+e^- \to \pi^+\pi^-$ are finally added to $\sigma_{\pi\pi}$. This latter result is compatible with that arising from the analysis within a relative difference of 0.2%, averaged in s_π. Then, $\sigma_{\pi\pi}$ is corrected for the running of the fine structure constant, due to lepton and quark loops [7], before computing the dispersion integral for a_μ.

6 Results and conclusions: a brief outlook

Fig. 1 shows $d\sigma_{\pi\pi\gamma}/ds_\pi$ (left) with $\theta_{\pi\pi} < 15^\circ$ ($\theta_{\pi\pi} > 165^\circ$) and $\sigma_{\pi\pi}$ (right), the ρ–ω interference pattern is clearly visible. The contribution to the muon magnetic anomaly due to the channel $e^+e^- \to \pi^+\pi^-$, measured in the range

$0.35\ \mathrm{GeV}^2 < s_\pi < 0.95\ \mathrm{GeV}^2$, is:

$$a_\mu^{\pi\pi} \;=\; (388.7 \;\pm\; 0.8_{stat} \;\pm\; 3.5_{syst} \;\pm\; 3.5_{th}) \;\times\; 10^{-10}\ .$$

The experimental systematic uncertainty is mainly due to the quality of the data taken in 2001, while the theoretical error takes account of the function H, the FSR corrections and the measurement of the luminosity. The presented value of $a_\mu^{\pi\pi}$, after summing all contributions, confirms the difference between theory and experiment. Future improvements are expected using data taken in 2002, where more stable data taking conditions and improved trigger logic will allow for a reduction of the experimental errors. Furthermore, improved Bhabha Monte Carlo codes are expected to be available in the near future, helping to reduce the theoretical uncertainty.

References

1. G. W. Bennett *et al.* [Muon g-2 Coll.], Phys. Rev. Lett. **92** (2004) 161802.
2. S. Eidelman, These Proceedings.
3. S. Binner, J. H. Kühn and K. Melnikov, Phys. Lett. B **459** (1999) 279.
4. H. Czyż, A. Grzelińska, J. H. Kühn and G. Rodrigo, Eur. Phys. J. C **33** (2004) 333, and references therein for the earlier versions of `Phokhara`.
5. A. Aloisio [KLOE Coll.], arXiv:hep-ex/0407048, and A. Denig *et al.*, KLOE Note 192 (2004), `http://www.lnf.infn.it/kloe/pub/knote/kn192.ps`
6. C. M. Carloni Calame *et al.*, Nucl. Phys. B **584** (2000) 459.
7. F. Jegerlehner, Nucl. Phys. Proc. Suppl. **126** (2004) 325.

Frascati Physics Series Vol. XXXVI (2004), pp. 373–380
DAΦNE 2004: Physics at meson factories – Frascati, June 7-11, 2004
Selected Contribution in Plenary Session

INCLUSIVE HADRONIC RESULTS AT BaBar: ISR AND PENTAQUARK SEARCHES

Nicolas Berger *
SLAC, Menlo Park, California, U.S.A.

Abstract

We present recent measurements of hadronic cross-sections from the BaBar experiment and report preliminary results on searches for pentaquark states.

1 Inclusive hadronic cross-section measurements using Initial State Radiation

1.1 Physics Motivation

The total cross-section $\sigma(e^+e^- \to \text{hadrons})$ for the production of hadrons in e^+e^- annihilation is a crucial ingredient for the calculation of hadronic corrections for the running of the QED coupling constant $\Delta\alpha^{Had}_{QED}$ and for the muon anomalous magnetic moment a_μ^{Had}. The hadronic contribution to the

* On behalf of the BaBar collaboration

running of α_{QED}, $\Delta\alpha^{Had}_{QED}$ is an input into the global standard model fits [1] which can provide an indirect measurement of the Higgs boson mass. In both cases, the hadronic contributions can be expressed as integrals of the ratio $R(s) = \sigma(e^+e^- \to \text{hadrons})/\sigma_0(e^+e^- \to \mu^+\mu^-)$, where σ_0 denotes the Born cross-section. We have

$$\Delta\alpha^{Had}_{QED} = -\frac{\alpha}{3\pi}\int_{4m_\pi^2}^{\infty}\frac{R(s)}{s}\left(\frac{m_Z^2}{s-m_Z^2}\right) \tag{1}$$

$$a_\mu^{Had} = \left(\frac{\alpha m_\mu}{3\pi}\right)^2\int_{4m_\pi^2}^{\infty}\frac{R(s)}{s}\left(\frac{K(s)}{s}\right), \tag{2}$$

where $K(s)$ is sharply peaked at $s = 0$. In the case of $\Delta\alpha^{Had}_{QED}$, the weight factor is almost independent of s for small values of s, so that the entire spectrum of $R(s)$ contributes to the integral. In the case of a_μ the integral is dominated by the low s region.

The error on $\Delta\alpha^{Had}_{QED}$ is dominated by the region $1\,\text{GeV} < \sqrt{s} < 7\,\text{GeV}$. Below 1 GeV, CMD-2 and KLOE have measured [2] $\sigma(e^+e^- \to \pi^+\pi^-)$ to $< 1\%$ accuracy. BES [3] has measured $R(s)$ in the range $2\,\text{GeV} < \sqrt{s} < 5\,\text{GeV}$ at 6% accuracy, but there are no recent measurements in the region $1\,\text{GeV} < \sqrt{s} < 2\,\text{GeV}$, leading to large uncertainties.

1.2 Initial-state Radiation at $\Upsilon(4S)$ Energies

The BaBar experiment operates at the PEP-II asymmetric e^+e^- collider. While PEP-II is a fixed-energy machine, initial-state radiation (ISR), can be used to vary of the center-of-mass energy of hadron production. The full spectrum of s', the reduced center-of-mass energy, is accessible. The range $0 < s' < 7\,\text{GeV}$ can be reached for ISR photon energies of $3-5.3\,\text{GeV}$ in the center-of-mass system. The photon can be detected by the BaBar electro-magnetic calorimeter (EMC) to provide a clear signature for the event. In particular, the presence of a hard photon can separate e^+e^- annihilation events from beam-gas processes which constitutes an important source of background for energy-scan experiments. The hadronic system is also collimated by its recoil against a hard photon and the spectrum of the observed particles is also hardened, improving detection efficiency and reducing the dependence on the hadronization model. Requiring the ISR photon in the sensitive part of the detector further improves

the fiducial containment of the hadronic system. Final-state radiation (FSR) effects are expected to be small and kinematically well-separated from ISR.

The cross-section for hadronic ISR events was evaluated using the Monte-Carlo generators. The total cross-section for $s' < 8\,\mathrm{GeV}$ in the fiducial region $15.3 < \theta_\gamma < 137.3^o$ is calculated to be 90 pb, corresponding to 18 million events in the current BaBar dataset of $200\,\mathrm{fb}^{-1}$. Of these we expect 5.7 million events for $2 < s' < 5\,\mathrm{GeV}$, to be compared with approximately 250,000 events used for the latest BES measurement in this energy range.

The main challenge of the method is the determination of the reduced center-of-mass energy $\sqrt{s'}$. This is addressed differently in the various analyses.

1.3 $e^+e^- \to h^+h^-h^+h^-\gamma$

BaBar performed a common analysis of the processes $e^+e^- \to \pi^+\pi^-\pi^+\pi^-\gamma$, $e^+e^- \to K^+K^-\pi^+\pi^-\gamma$ and $e^+e^- \to K^+K^-K^+K^-\gamma$. Events with at least 4 tracks and a neutral cluster are subjected to 1C kinematic fits with the constraint $m_\gamma = 0$. A kaon identification procedure is performed on the tracks, using ionization measurements in the tracking detectors and information from the Čerenkov detector. The cross-sections are normalized using the process $e^+e^- \to \mu^+\mu^-\gamma$. Results are shown in fig. 1.

The 4π and $2K2\pi$ results agree with existing results, but are considerably more precise and cover a larger energy range. The $4K$ result is the first measurement of this quantity. In all cases, the leading uncertainties are systematic, dominated by uncertainties on the luminosity, tracking efficiency and acceptance losses. The J/ψ resonance is clearly visible in all 3 cases, leading to branching fraction results of $\mathcal{B}(J/\psi \to \pi^+\pi^-\pi^+\pi^-) = (3.70\pm0.27\pm0.36)\times10^{-3}$, $\mathcal{B}(J/\psi \to K^+K^-\pi^+\pi^-) = (6.25\pm0.50\pm0.62)\times10^{-3}$, $\mathcal{B}(J/\psi \to K^+K^-K^+K^-) = (6.9 \pm 1.2 \pm 1.1) \times 10^{-3}$, assuming the PDG value for $\Gamma(J/\psi \to e^+e^-)$. These results agree with the PDG values but are significantly more precise. The 4π mode also provides a measurement of $\mathcal{B}(\psi(2S) \to J/\psi(\mu^+\mu^-)\pi^+\pi^-$ through the mis-identification of the muons as pions. Assuming the PDG values for $\Gamma(J/\psi \to \mu^+\mu^-)$, $\Gamma(\psi(2S) \to e^+e^-)$ and $\mathcal{B}(J/\psi \to \mu^+\mu^-)$, we get $\mathcal{B}(\psi(2S) \to J/\psi\pi^+\pi^-) = 36.1 \pm 1.5 \pm 3.7\%$.

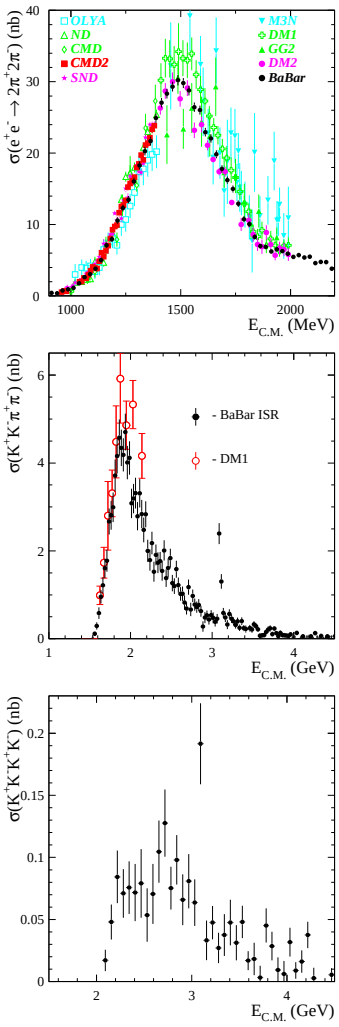

Figure 1: *Cross sections for* $e^+e^- \to \pi^+\pi^-\pi^+\pi^-$ *(top),* $K^+K^-\pi^+\pi^-$ *(center) and* $K^+K^-K^+K^-$ *(bottom) using* $89\,fb^{-1}$ *of data.*

1.4 $e^+e^- \to J/\psi(\mu^+\mu^-)\gamma$

The analysis of $e^+e^- \to J/\psi(\mu^+\mu^-)\gamma$ is done in similar fashion to that of the preceding section. We require energy and momentum conservation and perform a 1C kinematic fit with $m_\gamma = 0$. To reject ISR background, both tracks are required to be identified as muons.

The cross-section for J/ψ production is obtained from the ratio of peak to continuum production. Assuming PDG values for $B_{\mu\mu}$ and $\mathcal{B}(J/\psi \to e^+e^-)$, we obtain $\Gamma(J/\psi \to e^+e^-) = 5.61 \pm 0.20\,\text{keV}$ and the full width of the J/ψ to be $\Gamma_{J/\psi} = 94.7 \pm 4.4\,\text{keV}$.

1.5 Inclusive Analysis

Alongside the exclusive analyses presented above, a fully inclusive analysis of hadronic ISR processes is being performed, with the goal of extracting $\Delta\alpha^{Had}_{QED}$ with $3-4\%$ error. We select events with an ISR photon with center-of-mass energy greater than 3 GeV. The various efficiency terms can all be calibrated to 1% or below; we have a triggering efficiency of 98% and a fiducial photon detection efficiency of 90%. The s' integrated luminosity spectrum can be computed from the BaBar integrated luminosity, which is known to about 1%. The precision of this calculation is claimed to be less than 1%.

Leading background sources, such as radiative Bhabha, $e^+e^- \to \gamma\gamma$ and virtual Compton scattering processes can be vetoed with minimal signal losses and biases. Other modes such as $e^+e^- \to \mu^+\mu^-\gamma$ and $\tau^+\tau^-\gamma$ can be subtracted using theoretical predictions. Finally, $e^+e^- \to q\bar{q}$ events are a major source of background for $s' > 5\,\text{GeV}$, mainly due to production of high-momentum π^0 and η. Event shape variables of the hadronic system can be used to suppress this background.

For this inclusive measurement, s' is determined from the ISR photon energy. Due to the EMC energy resolution of about 3% for the energies considered here, the $R(s)/s$ spectrum is distorted, especially at low s'. However, since $\Delta\alpha^{Had}_{QED}$ is expressed as an integral in $R(s)/s$ with a weakly-varying weight factor, distortions in the spectrum do not affect the measured value for $\Delta\alpha^{Had}_{QED}$. The energy resolution therefore has minimal impact on the $\Delta\alpha^{Had}_{QED}$ measurement. The inclusive method cannot be applied to the measurement for a_μ^{Had} since the weight factor in this case is strongly peaked at $s' = 0$.

2 Searches for Pentaquark Resonances

Several experiments have recently claimed observations of exotic baryon resonances which seem to be composed of 5 constituent quarks. The LEPS [4] experiment has claimed observation of a resonance Θ^+ at a mass of about 1540 MeV. The NA49 experiment [5] reports two degenerate states, Ξ_5^0 and Ξ_5^{--} with masses of 1862 MeV. These resonances have been interpreted as members of a $\bar{10} + 8$ multiplet of flavor $SU(3)$, with the isospin-singlet Θ^+ associated with states denoted as N_5, Σ_5 and Xi_5 in analogy with the usual baryon multiplets.

BaBar is well suited to search for these states, with excellent kaon and proton identification and excellent tracking resulting in good mass resolutions. Searches for the Θ^+, Ξ_5^0, Ξ_5^- and Ξ_5^{--} states have been performed.

A search for Θ^+ was done for the decay mode $\Theta^+ \to pK_S^0$. We expect a resolution of about 2 MeV on the Θ^+ mass, which would be the most precise to date. However as shown in fig. 2, no peak is seen at the expected mass and only a large signal for $\Lambda_C \to pK_S^0$ is observed.

A search for the Ξ_5^0 and Ξ_5^{--} resonances was performed using the decay chain $\Xi_5^{0/--} \to \Xi^-\pi^\pm$, $\Xi^- \to \Lambda\pi^-$, $\Lambda \to p\pi^-$, with the proton identified as before. As shown in fig. 2, no peak is seen at the expected masses. In the $\Xi^+\pi^-$ spectrum, prominent peaks for the $\Xi^*(1530)$ and $\Xi_c^0(2250)$ are seen. No structure is observed in the exotic $\Xi^-\pi^-$ spectrum.

Searches for $\Xi_5^0 \to \Lambda K_S^0$, $N_5^0 \to \Lambda K_S^0$, $N_5^+ \to \Lambda K^+$ and $\Xi_5^- \to \Lambda K^-$, were also performed, using kaon identification and reconstructing $\Lambda \to p\pi^-$ and $K_S^0 \to \pi^+\pi^-$ as above. As shown in fig. 2 no exotic resonances were observed, while sharp peaks for $\Omega^- \to \Lambda K^-$, $\Lambda_c^+ \to \Lambda K^+$ and $\Xi_c^0 \to \Lambda K_S^0$ are clearly seen.

3 Conclusion

Studies of hadronic cross-sections using initial-state radiation offer promising prospects at BaBar. Many exclusive channels have already been measured, and more are in progress. A fully inclusive analysis should also offer a precise measurement of $\Delta\alpha_{QED}^{Had}$. Searches for pentaquark states have so far been negative, but they have served to highlight the potential for the study of charmed and non-charmed baryons at high-luminosity e^+e^- colliders.

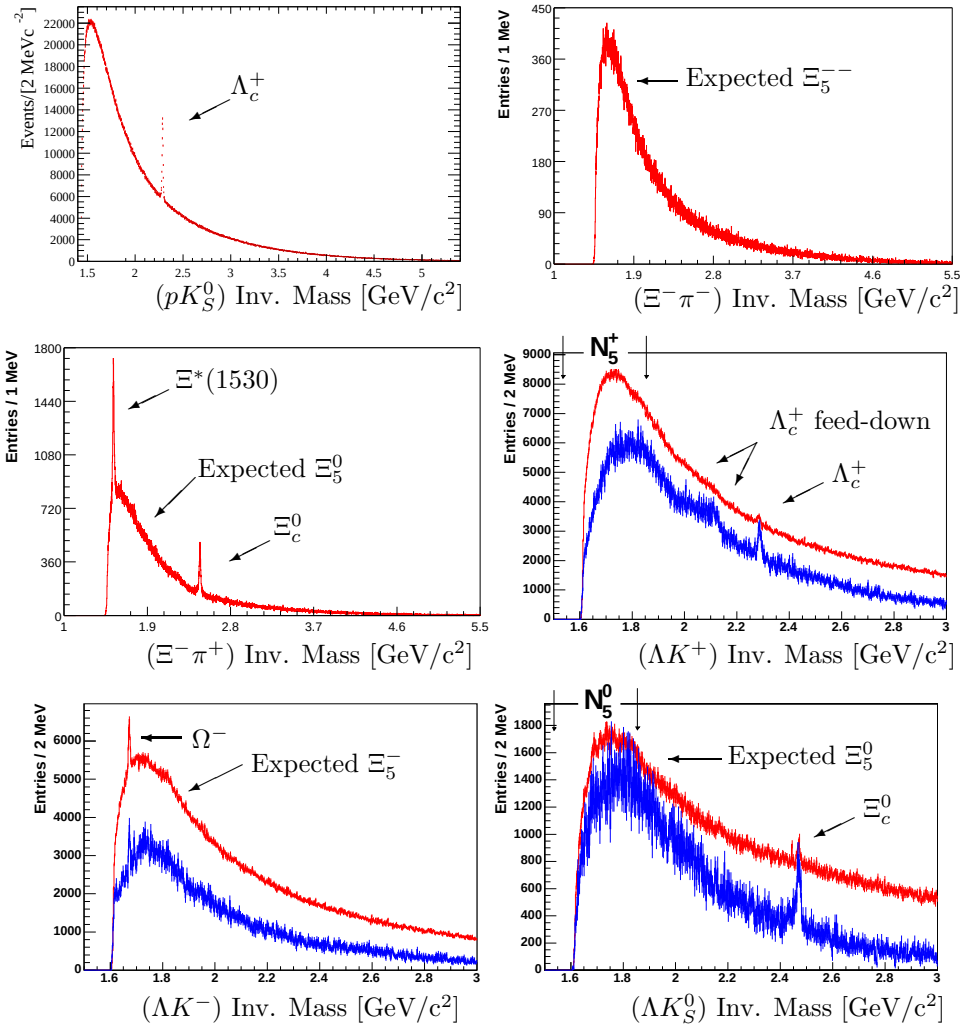

Figure 2: *Mass spectra for pK_S^0 and $\Xi^-\pi^-$ (top row), $\Xi^+\pi^-$ and ΛK^+ (middle row) and ΛK^- and ΛK_S^0 (bottom row) using $123\,fb^{-1}$ of data. For the three latter plots, the upper and lower histograms correspond to ΛK center-of-mass momenta respectively smaller than and greater than $3\,GeV$, with the lower histogram scaled up by a factor of 10 for lisibility. The positions of know resonances and expected Ξ_5 and N_5 pentaquarks are shown.*

References

1. LEP Collaborations, CERN-EP/2003-091 and hep-ex/0312023.

2. S.E. Muller *et al.*, Nucl. Phys. Proc. Suppl. **126**, 335-340 (2004),
   R.R. Akhmetshin *et al.*, Phys. Lett. **B527**, 161-172 (2002),
   R.R. Akhmetshin *et al.*, Phys. Lett. **B578**, 285-289 (2004).

3. J. Z. Bai *et al.*, Phys. Rev. Lett. **84**, 594 (2000),
   J. Z. Bai *et al.*, Phys. Rev. Lett. **88**, 101802 (2002).

4. T. Nakano *et al.*, Phys. Rev. Lett. **91**, 012002 (2003).

5. C. Alt *et al.*, Phys. Rev. Lett. **92**, 042003 (2004).

Frascati Physics Series Vol. XXXVI (2004), pp. 381–387
DAΦNE 2004: Physics at meson factories – Frascati, June 7-11, 2004
Selected Contribution in Plenary Session

MEASUREMENT OF $e^+e^- \to \phi \to K^+K^-$ CROSS SECTION WITH CMD-2 DETECTOR AT VEPP-2M COLLIDER

Peter A. Lukin*
Budker Institute of Nuclear Physics, Novosibirsk, Russia

Abstract

About 363 000 $e^+e^- \to \phi \to K^+K^-$ events in the center-of-mass energy range from 1010 to 1034 MeV were used for the measurement of the ϕ meson parameters. The following results have been obtained: $\sigma_0 = (2044 \pm 10 \pm 57)$ nb, $m_\phi = (1019.448 \pm 0.010 \pm 0.080)$ MeV/c^2, $\Gamma_\phi = (4.25 \pm 0.03 \pm 0.03)$ MeV, $B_{ee} \cdot B_{K^+K^-} = (14.46 \pm 0.07 \pm 0.40) \cdot 10^{-5}$.

1 Introduction

$\phi \to K^+K^-$ decay is the main ϕ meson decay mode (its branching ratio is about 50%), but until recently it was measured with relatively poor accuracy [1, 2]. A study of the K^+K^- production in the center-of-mass (CM) energy range around 1020 MeV also allows a determination of the ϕ meson parameters.

* On behalf of the CMD-2 Collaboration

In this paper we present the preliminary result of a study of the process $e^+e^- \to K^+K^-$ in the CM energy range 2E = 1010 – 1034 MeV, performed with the CMD-2 detector [3] at the VEPP-2M collider [4]. The analysis is based on 0.74 pb^{-1} of integrated luminosity collected in one scan of the ϕ meson region, corresponding to 6% of data taken at the ϕ resonance.

2 The CMD-2 Detector

The CMD-2 detector is described in more detail elsewhere [3]. Its tracking system consists of the cylindrical drift chamber (DC) surrounding the interaction point and providing precise particle momentum and dE/dx measurement, and proportional Z-chamber (ZC) for precise polar angle measurement, both also used for trigger. Both chambers are inside a thin (0.38 X_0) superconducting solenoid with a field of 1 T. The barrel electromagnetic calorimeter placed outside the solenoid consists of 892 CsI crystals of 6×6×15 cm^3 size. The muon-range system of the detector, also located outside the solenoid, is based on streamer tubes. The endcap electromagnetic calorimeter based on BGO crystals makes the detector almost hermetic for photons.

3 Selection Criteria

A candidate to a $e^+e^- \to K^+K^-$ event is an event with two low momentum tracks and high ionizing losses, originating from the interaction region. There is a number of effects, which lead to the loss of a charged kaon track: decays in flight, nuclear interactions, track reconstruction inefficiency etc. If one track is not reconstructed, the event can still be identified using second detected track. In our analysis we selected events with one or two "good kaons" found, where a "good kaon" is defined according to the following criteria:

- Track total momentum is $P_{tot} < 200$ MeV/c.
- Track ionization losses is $dE/dx > 4000.0$ (while minimal ionizing particle has $dE/dx_{MIP} = 2000.0$).
- Track impact parameter in $R - \phi$ plane is $\rho < 0.4$ cm.
- Polar angle of the track is $1.0 < \theta_K < \pi$ - 1.0.

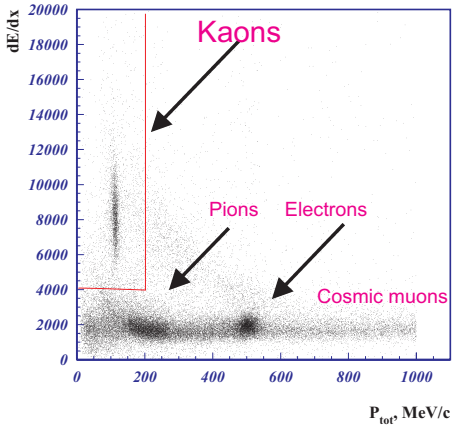

Figure 1: *Track ionization losses versus track momentum.*

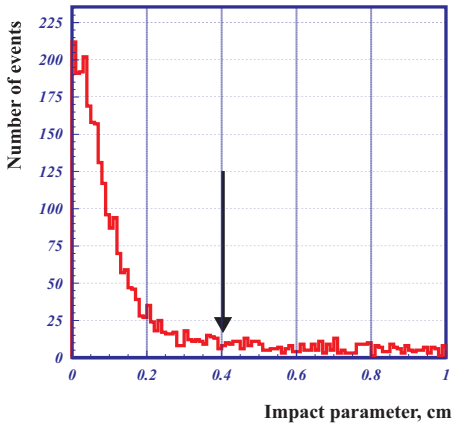

Figure 2: *Distribution of track impact parameter in the $R-\varphi$ plane.*

The selection criteria on the track total momentum and track ionization losses are shown (by lines) in Fig. 1. They allow to easily separate events with charged kaons from events with other particle types. Figure 2 demonstrates the event distribution over a track impact parameter in the $R-\phi$ plane. Our cut on this parameter is plotted by a vertical arrow.

The number of events with one or two "good" kaons found is determined from the distribution over a Z-coordinate of the point, closest to the interaction region along the beam axis. Figure 3 demonstrates the Z-distribution of events with one "good kaon" found. To determine the number of events, the distribution is fitted with the sum of a Gaussian, describing the effect, and smooth function, describing background. The shape of background was derived from the analysis of events, collected at the energy point below the thershold of charged kaon pair production. The background distribution is shown in Fig. 4. It was fitted with the sum of three Gaussians and all values of fitting parameters, but the number of background events, were then used for background description at each energy point.

After background subtraction we select about 1.21×10^5 events with one "good kaon" and about 2.42×10^5 events with two "good kaons".

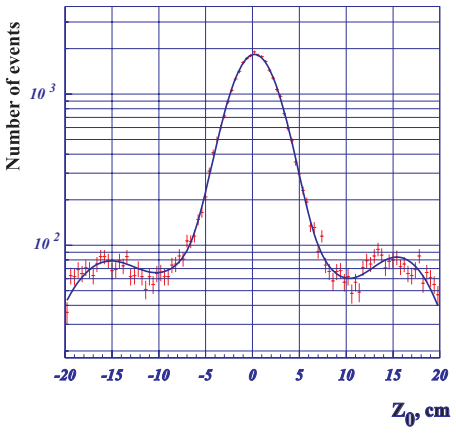

Figure 3: *Distribution over Z-coordinate of point closest to the interaction region for events with one "good" kaon found as well as the fitting function.*

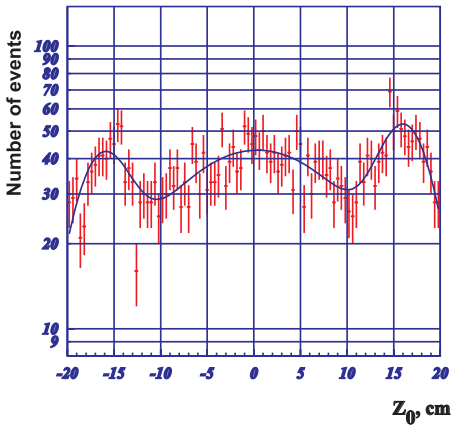

Figure 4: *Background events distribution over Z-coordinate of point closest to the interaction region as well as the fitting function.*

4 Analysis

At each energy point the $e^+e^- \to K^+K^-$ cross section is calculated according to formula:

$$\sigma = \frac{N_1 + N_2}{\varepsilon\mathcal{L} \cdot (1 + \delta_{rad})} \cdot \frac{1 + \Delta_{EXP}}{1 + \Delta_{SIM}}, \tag{1}$$

where N_1 – number of events with one "good" kaon, N_2 – number of events with two "good" kaons, ε – detection efficiency, $\mathcal{L}$ – the integrated luminosity, calculated using large angle scattering events according to procedure, described in [5], $(1 + \delta_{rad})$ – initial state radiative correction, determined according to Ref. [6]. Δ_{EXP} – probability to loose both charged kaons in an experimental event. Δ_{SIM} – probability to loose both charged kaon in a MC event.

Detection efficiency is determined using MC simulation events (50000 events of the process $e^+e^- \to K^+K^-(\gamma)$ at each energy point). It is a product of acceptance and trigger:

$$\varepsilon = \varepsilon_{geom} \cdot \varepsilon_{trig} \tag{2}$$

The typical values of the acceptance and trigger efficiency are the following: $\varepsilon_{geom} = 0.64$ and $\varepsilon_{trig} = 0.89$.

The probabality to loose both kaons in the event is determined for both experimental and MC events at each energy point, assuming that kaons are lost independently. For $E_{beam} = 510.0$ MeV this probability is $\Delta_{EXP} = 0.039$, $\Delta_{SIM} = 0.043$. These values are close to each other and the corrections are almost cancelled in the ratio.

The systematic error in the cross section value is estimated to be equal to 2.8% and its sources are listed in a Table 1.

Table 1: *Contributions to the systematic error of* $e^+e^- \to K^+K^-$ *cross section.*

Source	Contribution, %
Trigger efficiency	2
Selection criteria	1.4
Luminosity	1
Acceptance	0.7
Radiative correction	0.5
$\oplus$ Total	2.8

The experimental points were fit with a Breit-Wigner function [2], which includes the contributions of the ρ, ω and ϕ mesons. The following ϕ meson parameters were obtained from the fit:

$$\sigma_0(\phi \to K^+K^-) = 2043 \pm 10 \pm 56 \text{ nb} ,$$

$$m_\phi = 1019.448 \pm 0.010 \pm 0.080 \text{ MeV/c}^2,$$

$$\Gamma_\phi = 4.25 \pm 0.03 \pm 0.03 \text{ MeV},$$

$$B_{ee} \cdot B_{K^+K^-} = (14.46 \pm 0.07 \pm 0.40) \cdot 10^{-5},$$

where the first error is statistical and the second is systematic. Systematic error on ϕ-meson mass and total width is due to accuracy of beam energy determination. The parameters are in good agreemenet with their world average values from PDG [7] and are the most precise.

The experimental data together with the fitting curve are presented in Fig. 5 together with the results of the previous most precise experiments. The results of all experiments are in good agreement.

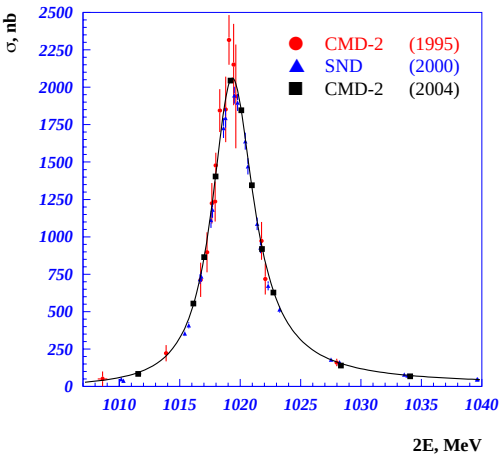

Figure 5: *Experimental cross section and ϕ meson excitation curve in the channel $e^+e^- \to \phi \to K^+K^-$, obtained in this analysis as well as in experiments* [1, 2].

5 Conclusion

Using the CMD-2 data sample of 3.63×10^5 $\phi \to K^+K^-$ events with one or two reconstructed charged kaons, the following preliminary ϕ-meson parameters have been obtained:

$$\sigma_0(\phi \to K^+K^-) = 2043 \pm 10 \pm 56 \text{ nb} ,$$

$$m_\phi = 1019.448 \pm 0.010 \pm 0.080 \text{ MeV/c}^2,$$

$$\Gamma_\phi = 4.25 \pm 0.03 \pm 0.03 \text{ MeV},$$

$$B_{ee} \cdot B_{K^+K^-} = (14.46 \pm 0.07 \pm 0.40) \cdot 10^{-5}.$$

These results are in agreement with the results of other experiments and are more precise than the corresponding measurements from any other e^+e^- experiment.

6 Acknowledgements

The authors are grateful to the staff of VEPP-2M for excellent performance of the collider, to all engineers and technicians who participated in the design, commissioning and operation of CMD-2.

This work was supported in part by Young Scientists Grant of SB RAS and by Grant RFBR 04-02-16223-a.

References

1. R.R. Akhmetshin *et al*, Phys. Lett. **B364**, 199 (1995).
2. M.N. Achasov *et al*, Phys. Rev. **D63**, 072002 (2001).
3. E.V. Anashkin *et al*, ICFA Instr. Bulletin **5**, 18 (1988).
4. A.N. Skrinsky, Proc. of the Workshop on Physics and Detectors for DAΦNE'95, Frascati, Vol. IV, 3 (1995).
5. R.R. Akhmetshin *et al*, Preprint Budker INP **99-11**, Novosibirsk, (1999).
6. E.A. Kuraev, V.S. Fadin, Sov. J. of Nucl. Phys. **41**, 466 (1985).
7. S. Eidelman *et al*, Phys. Lett. **B592**, 1 (2004).

Frascati Physics Series Vol. XXXVI (2004), pp. 389–395
DAΦNE 2004: Physics at meson factories – Frascati, June 7-11, 2004
Selected Contribution in Plenary Session

NEW STUDY OF $\phi \to \pi^+\pi^-\pi^0$ DECAY WITH CMD-2 DETECTOR

Denis A. Epifanov *
The Budker Institute of Nuclear Physics, Novosibirsk, Russia

Abstract

The analysis of a data sample of about 12 pb^{-1} collected with CMD-2 detector at the VEPP-2M collider was performed. The $e^+e^- \to \pi^+\pi^-\pi^0$ cross section in the ϕ-meson energy range was measured, and the value of Br($\phi \to \pi^+\pi^-\pi^0$)·Br($\phi \to e^+e^-$) was determined. The study of the decay dynamics was performed by analyzing the Dalitz plot distribution of 3π events, taking into account the $\rho\pi$ -mechanism as well as contact production.

1 Introduction

Although the $\phi \to \pi^+\pi^-\pi^0$ decay has been numerously studied starting from sixties, the interest to the process is not exhausted. It is one of the main

* On behalf of the CMD-2 collaboration

ϕ decays providing the substantial contribution to the total hadronic cross section. The detailed study of the composition of the 3π final state shed light on the mechanism of the light quark interaction. It was primarily proposed in [2] that $\phi \to \pi^+\pi^-\pi^0$ decay proceeds through the $\rho\pi$ intermediate state. First experimental evidence of $\rho\pi$ -dominance appeared in [3]. However, direct production of 3π is not excluded and some phenomenological models [4], [5] predict the value of the related contact amplitude in the wide range. More accurate analysis of 3π dynamics was done in Refs. [6], [7] where only upper limits on the value of the contact amplitude were set up. Recently the non-$\rho\pi$ amplitude was studied at KLOE [8] and the contact amplitude was measured with good accuracy.

In this work we study the process $e^+e^- \to \pi^+\pi^-\pi^0$ in the region of the $\phi-$ meson resonance with the CMD-2 detector. This detector is described elsewhere [9], see also the talk of P.A.Lukin in these proceedings. This analysis, based on 12 pb^{-1} of integrated luminosity, is aimed to measure the 3π cross section as well as to study its dynamics.

2 Selection of 3π events

The present analysis is based on completely reconstructed 3π events. At the initial stage events with one positive and one negative charged particle and two or more reconstructed photon clusters were selected. Then the following criteria were applied:

All charged particles and photons are required to hit detector within the solid angle limited by the polar angle $|\pi/2 - \theta| < 0.67$ radians to avoid edge effects for the detection efficiency. For charged particles:

- Tracks should be acollinear in the $(R-\varphi)$ projection $|\pi - |\varphi_2 - \varphi_1|| > 0.1$ to reject Bhabha events and a space angle between tracks should be $0.1 < \psi < 3.0$.
- The distance from each track to the beam axis should be $R_{min} < 0.2$ cm in the $(R-\varphi)$ projection and the distance from a track to the interaction point along the beam direction should be $|Z_{trk}| < 10$ cm.
- The momentum corresponding to each track is required to be 120 MeV/c $<$ P$_\pi$ $<$ 500 MeV/c.

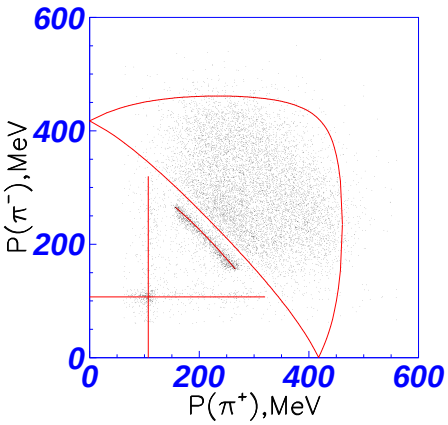

Figure 1: *Experimental 3π events in the 2D-plot $(|\vec{P_+}|, |\vec{P_-}|)$.*

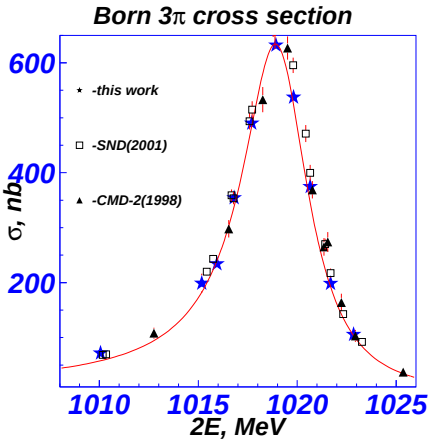

Figure 2: *Born cross section:this work, SND-2001, CMD-1998.*

- Energy losses in the DC for track should be $dE/dx < 4000$ (the dE/dx value for MIP particles is set to 2000) to suppress charged kaons.

For a neutral pion the invariant mass of two photons must be in the range 80 MeV/c^2 < M$_{\gamma\gamma}$ < 170 MeV/c^2. If more than two showers are detected we require only one π^0 candidate to be in the event $N_{\pi^0} = 1$.

With the above criteria, 114957 events were selected in total. In Fig.1 the 2D-plot of the selected experimental events (without cut on track momenta) at $E_{beam} = 509.5$ MeV is shown.

Clearly seen are events of three types: $\pi^+\pi^-\pi^0$ inside the allowed kinematic region; K_LK_S ,$K_S \to \pi^+\pi^-$ along calculated curve of $P_+(P_-)$ dependence; K^+K^- along two lines with P($K^\pm$)=107 MeV.

The background for this decay mode can originate from true e^+e^- interactions or from cosmic particles and beam interact –ions with the residual gas. The main processes which can imitate 3π events are: $e^+e^- \to \pi^+\pi^-\pi^0\pi^0$; $e^+e^- \to \phi \to \eta\gamma$, $\eta \to \pi^+\pi^-\pi^0$ or $\pi^+\pi^-\gamma$; $e^+e^- \to \phi \to K_LK_S$ or K^+K^-; $e^+e^- \to e^+e^-\gamma\gamma$, $e^+e^- \to \pi^+\pi^-\gamma\gamma$, $e^+e^- \to \pi^+\pi^-\gamma$; cosmic particles and beam interaction with the residual gas. The admixture of some background processes

was evaluated from experimental data and for the remaining channels relied on luminosity, their cross sections and detection efficiencies taken from MC simulation. We found in total $\simeq$ 1500 background events($\simeq$1.3% of the selected sample).

3 Measurement of cross section

For the cross section measurement 3π events are selected at 10 energy points from 2E=1010 to 1023 MeV. For each energy point the Born cross section is calculated according to the formula:

$$\sigma_B = \frac{N_{3\pi}}{L\varepsilon_{det}\varepsilon_{trig}(1+\delta_{wid})(1+\delta_{rad})(1-\delta_{MC})}, \quad (1)$$

where $N_{3\pi}$ is the number of 3π events, L is the integrated luminosity, ε_{det} is the detection efficiency calculated from Monte Carlo simulation, ε_{trig} is a trigger efficiency, δ_{wid} is a correction for the beam spread, δ_{MC} is a correction to the detection efficiency (it takes into account the difference between experimental and simulated reconstruction efficiencies for $\pi^{\pm}$ and π^0), δ_{rad} is a radiative correction, taking into account the difference between visible and Born cross sections due to the photons radiation by initial e^- and e^+. The calculation of δ_{rad} was done according to Ref. [10].

The Born cross section is approximated by a function incorporating contributions of ω,ϕ mesons and a constant term σ_{BG}:

$$\sigma_{3\pi}(s) = \frac{F_{3\pi}(s)}{s} \cdot |A_\omega + A_\phi e^{i\varphi_{\phi-\omega}}|^2 + \sigma_{BG}, \quad (2)$$

The detailed description of the parametrization can be found in [11]. Fig.2 demonstrates measured Born cross section with an optimal resonance curve. Free parameters of the fit are: peak 3π cross section $\sigma_{3\pi}$, $\omega-\phi$ mixing phase $\varphi_{\phi-\omega}$, mass of the ϕ-meson M_ϕ, total ϕ-meson width Γ_ϕ and constant term σ_{BG}. Parameters of the ω-meson are taken from [1]. The optimal parameters are:

$$\sigma_{\phi 3\pi} = 624 \pm 33\ nb,\ \varphi_{\phi-\omega} = 160 \pm 17^o$$
$$M_\phi = 1019.3 \pm 0.1\ MeV,\ \Gamma_\phi = 4.14 \pm 0.13\ MeV$$
$$\sigma_{bg} = 12 \pm 6\ nb,\ \chi^2/N = 8.6/5$$

The parameters of the ϕ-meson agree with world average results. Only statistical errors of the fit parameters are presented, systematics studies are in progress.

4 Analysis of $\phi \to \pi^+\pi^-\pi^0$ dynamics

We study $\phi \to \pi^+\pi^-\pi^0$ dynamics analyzing the 3π events distribution over the Dalitz plot with $X = (E_{\pi^-} - E_{\pi^+})/\sqrt{3}$ and $Y = 2E - E_{\pi^-} - E_{\pi^+} - m_{\pi^0}$ as coordinates. For this purpose about 80000 experimental 3π events were selected with CMS energies $2E = 1017 \div 1021$ MeV. After described selections, a kinematic reconstruction was applied using the maximum likelihood method with the constraints of 4-momentum conservation.

The differential cross section of the process can be presented as:

$$d\sigma = C(s)|\vec{p}_+ \times \vec{p}_-|^2 |A_n a e^{i\varphi} + A_{\rho\pi}|^2 dE_+ dE_-, \tag{3}$$

$$A_{\rho\pi} = \frac{1}{D_{\rho^+}(Q_+^2)} + \frac{1}{D_{\rho^-}(Q_-^2)} + \frac{1}{D_{\rho^0}(Q_0^2)}, \tag{4}$$

where $1/D_{\rho^i}(Q_i^2)$ is a propagator of the ρ-meson; $A_n a e^{i\varphi}$ is the contact term amplitude ($A_n = 7.52$). The case of $a = 1$ corresponds to the equal contributions from $\rho\pi$ and direct 3π final states.

For further analysis the plot was divided into 198 square 20×20 MeV bins as it is shown in Fig.3. Bins near the kinematic boundary were excluded from the analysis. The calculated number of 3π events is given by the expression:

$$N_i^{calc} = \varepsilon_{ij} \varepsilon_{jk}^{rad} N_k^{theory}, \tag{5}$$

where N_k^{theory} is the number of events in bin number "k", calculated according to Eq.3; ε_{jk}^{rad} is a 198×198 matrix taking into account the distortion of the Dalitz distribution due to initial state radiation; ε_{ij} is a 198×198 matrix of the detector apparatus function taken from full 3π Monte Carlo simulation. The graphical example of the ε_{ij} table for one bin is shown in Fig.3. The distribution of experimental 3π events is shown in Fig.4. To approximate it we minimize the χ^2 functional. Free parameters of the fit are: the total number of produced 3π events-N_0, absolute value of a contact amplitude - "a" and phase of the contact amplitude-φ. Obtained optimal parameters are given in tab.1. Also shown are the results on the contact term found by KLOE [8], SND [7],CMD-2 [6] groups.

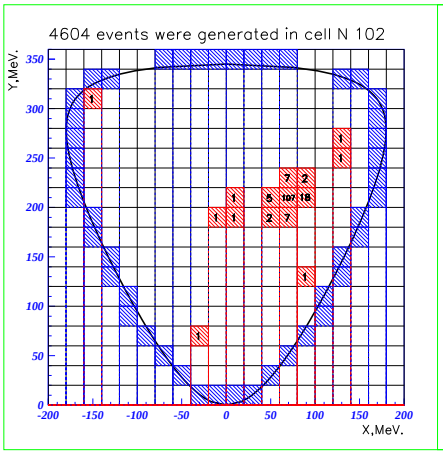

Figure 3: *The spread of events initially simulated in the bin (70,210).*

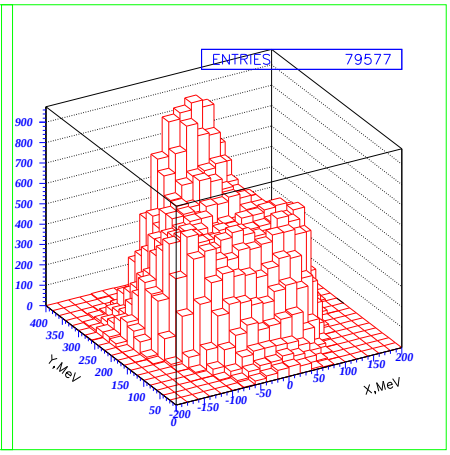

Figure 4: *Dalitz distribution of experimental events.*

Our preliminary result is in good agreement with the previous analysis of 3π dynamics at CMD-2, we also agree with KLOE in absolute value of contact amplitude, however the phase is different.

5 Summary

The Born cross section of the $e^+e^- \to \pi^+\pi^-\pi^0$ reaction was measured with a data sample of about 1.15×10^5 3π events in the energy range $2E = 1010 \div 1023$ MeV. Our preliminary result on the 3π peak cross section:

$$\sigma_{3\pi} = 624 \pm 33 \text{ nb}$$
$$Br(\phi \to \pi^+\pi^-\pi^0)Br(\phi \to e^+e^-) = (4.42 \pm 0.23) \times 10^{-5}$$

is in good agreement with previous measurements made by SND and CMD-2 groups.

Analysis of $\phi \to \pi^+\pi^-\pi^0$ dynamics is based on 80000 experimental events. The preliminary result on the absolute value and phase of the contact amplitude:

$$a = 0.103 \pm 0.028,\ \varphi = -2.0 \pm 0.3$$

Table 1: *Results on absolute value and phase of the contact amplitude.*

CMD-2	$a = 0.103 \pm 0.028$
this work	$\varphi = -2.0 \pm 0.3$; $P(\chi^2) = 81\%$
KLOE	$a = 0.104 \pm 0.01 \pm 0.02$
(2003)	$\varphi = 2.47 \pm 0.08 \pm 0.08$; $P(\chi^2) = 12\%$
SND	$-0.06 < a < 0.06$
(2002)	$\varphi = 0$-fixed; 90% CL
CMD-2	$-0.15 < a < 0.10$
(1998)	$\varphi = 0$-fixed; 90% CL

is in good agreement with the previous CMD-2 measurement.

6 Acknowledgements

The authors are grateful to the staff of VEPP-2M for the excellent performance of the collider, and to all engineers and technicians who participated in the design, commissioning and operation of CMD-2.

References

1. S. Eidelman *et al*, Phys. Lett. **B592**, 1 (2004).
2. M. Gell-Mann, D. Sharp, W.G. Wagner, Phys. Rev. Lett. **8**, 261 (1962).
3. G. Parrour, G. Cosme, A. Courau *et al*, Phys. Lett. **63B**, 362 (1976).
4. Y. Brihaye, N.K. Pak, P.Rossi, Nucl. Phys. **B254**, 71 (1985).
5. T. Fujiwara *et al*, Progress of Theoretical Physics **73**, 926 (1985).
6. R.R. Akhmetshin *et al*, Phys. Lett. **B434**, 426 (1998).
7. M.N. Achasov *et al*, Phys. Rev. **D65**, 032002 (2002).
8. A. Aloisio *et al*, Phys. Lett. **B561**, 55 (2003).
9. E.V. Anashkin *et al*, ICFA Instr. Bulletin **5**, 18 (1988).
10. E.A. Kuraev, V.S. Fadin, Sov.J.of Nucl. Phys. **41**, 466 (1985).
11. M.N. Achasov *et al*, Phys. Rev. **D63**, 072002 (2001).

Frascati Physics Series Vol. XXXVI (2004), pp. 397–404
DAΦNE 2004: Physics at meson factories – Frascati, June 7-11, 2004
Invited Review Talk in Plenary Session

CHIRAL PERTURBATION THEORY CONFRONTED WITH EXPERIMENT

Marc Knecht
Centre de Physique Théorique, CNRS Luminy, Case 907, F-13288 Marseille

Abstract

The general framework and the present status of the low energy theory of the standard model are briefly reviewed. Recent applications to a few topics of interest for the determinations of $|V_{ud}|$ and of $|V_{us}|$ are discussed.

1 Low energy theory of the standard model

At low energies, the standard model can be described in terms of an effective theory, involving only the lightest states as explicit degrees of freedom. In order that such an effective description becomes possible, two requirements need to be met. First, one must have a clear separation of scales (mass gap) between, on the one side, the light states, and, on the other side, the heavy states, which appear only indirectly in the effective theory, through their contribution to the infinite number of couplings, the low energy constants (LECs) describing

the local interactions of the light states. The second requirement is that the masses of the light degrees of freedom are protected by some symmetry, in order that their lightness appears as natural, in the very precise sense defined by 't Hooft [1] some time ago. In practice, this means that light spin 0 states have to correspond to Goldstone bosons produced by the spontaneous breaking of some continuous global symmetry. The masses of light fermion will be protected by chiral symmetry, whereas gauge invariance will ensure that spin 1 gauge fields remain massless (or massive but light, in t he presence of a Higgs mechanism).

In the case of the standard model, the light degrees of freedom that can be identified in this way comprise: i) the pseudoscalar meson octet, π, K and η, which, in the limit of massless quarks, become the Goldstone bosons associated with the spontaneous breaking of the chiral symmetry of QCD, ii) the light leptons, $e^{\pm}$, $\mu^{\pm}$ and their neutrinos (in principle, one might add the τ neutrino to this list, although the τ lepton itself belongs to the heavy states in the context of the present discussion), and iii) the photon. The range of applicability of this effective theory is limited by the typical mass scale $\Lambda_H \sim 1$ GeV provided by the non Goldstone mesonic bound states. Notice that according to the criteria adopted above, other effective theories could be considered, for instance the one involving only the electron, the three neutrinos, and the photon, with the limiting mass scale set by $m_\mu \sim M_\pi$, etc.

Chiral perturbation theory [2, 3, 4] (ChPT) organizes the low energy effective theory in a systematic expansion in powers of momenta and of light masses. The most convenient tool to materialize this expansion is to construct

Table 1: *The low energy constants corresponding to some of the parts of $\mathcal{L}_{eff}$ that have been constructed. They allow for a description of meson scattering amplitude and meson form factors up to two loops, anf for the inclusion of $\mathcal{O}(\alpha)$ radiative corrections up to one loop.*

	2 flavours	3 flavours
$\mathcal{O}(p^2)$	F, B	F_0, B_0
$\mathcal{O}(p^4)$	h_1,h_2, h_3, l_i, $i = 1 \ldots 7$ [3]	H_1,H_2, L_i, $i = 1 \ldots 10$ [4]
$\mathcal{O}(p^6)$	c_i, $i = 1 \ldots 57$ [5]	C_i, $i = 1 \ldots 94$ [5]
$\mathcal{O}(\alpha p^0)$	Z [6, 7]	Z [6]
$\mathcal{O}(\alpha p^2)$	k_i, $i = 1 \ldots 11$ [7]	K_i, $i = 1 \ldots 14$ [8], X_i, $i = 1 \ldots 8$ [11]

an effective lagrangian $\mathcal{L}_{\rm eff} = \mathcal{L}_2 + \mathcal{L}_4 + \cdots$,where $\mathcal{L}_n$ contains all the terms of order δ^n, with $\delta \sim p/\Lambda_H \sim M_P/\Lambda_H \sim m_\ell/\Lambda_H \sim e$, for instance, modulated by LECs whose values depend on the dynamical properties of the heavy degrees of freedom that have been integrated out. At lowest order, one only needs to compute tree graphs generated by $\mathcal{L}_2$, whereas the NLO involves both tree graphs from $\mathcal{L}_4$ and one loop graphs, and so on. It is essential to include the loop graphs, with increasing number of loops at each new order, in order to correctly account for all the singularities (poles, cuts) coming from the light degrees of freedom. Computing higher orders in the effective theory potentially increases the theoretical precision. However, the number of LECs also increases, as shown in Table 1. Predictions can thus only be made if some knowledge about their values is available. How this problem can be adressed in practice will be illustrated in the case of the few examples discussed below.

2 Radiative corrections to $\pi_{\ell 2}$, $K_{\ell 2}$, and $K_{\ell 3}$ decay modes

As a first application, let us consider the $\mathcal{O}(\alpha)$ electromagnetic contributions to the semileptonic decays of the pion and the kaon. The general structure of the $\pi_{\ell 2}$ and $K_{\ell 2}$ decay rates with radiative corrections included is known [9]

$$\Gamma_{P_{\ell 2}(\gamma)} = \frac{G_\mu^2}{8\pi}|V_{CKM}|^2 F_P^2 m_\ell^2 \left(1 - \frac{m_\ell^2}{M_P^2}\right)^2 \times \left[1 + \frac{\alpha}{\pi} C_P + \mathcal{O}(\alpha^2)\right] \qquad (1)$$

with $(P, V_{CKM}) = (\pi, V_{ud})$ or (K, V_{us}). ChPT reproduces this structure, with $C_P = C_P^{(0)} + C_P^{(2)} + \ldots$. The expressions [10, 11] for the $\mathcal{O}(p^0)$ contributions $C_{\pi,K}^{(0)}$ involve a (common) short distance logarithm [9], chiral logarithms, and the low energy constants K_i and X_i, while $C_{\pi,K}^{(2)}$ and higher represent SU(3) breaking quark mass corrections. Interestingly, the contributions of the low energy constants drop out [11] in the $\mathcal{O}(\alpha)$ correction to $\Gamma_{K_{\ell 2}(\gamma)}/\Gamma_{\pi_{\ell 2}(\gamma)}$,

$$C_\pi - C_K = \frac{Z}{4} \ln \frac{M_K^2}{M_\pi^2} + \mathcal{O}(M_K^2/\Lambda_H^2) = 0.50 \pm 0.15\,, \qquad (2)$$

with Z given by $M_{\pi^\pm}^2 - M_{\pi^0}^2 = 2e^2 F_\pi^2 Z$, and the error is a conservative estimate for SU(3) breaking corrections. This then leads to

$$\left|\frac{V_{us}}{V_{ud}}\right|^2 \frac{F_K^2}{F_\pi^2} = (7558 \pm 23 \pm 3) \times 10^{-5}\,, \qquad (3)$$

where the first error comes from the experimental uncertainties on the decay rates, and the second error comes from Eq. (2).

Turning now to $K_{\ell 3}$, the general structure of the amplitudes reads

$$\mathcal{M}^{(0)}(K_{\ell 3}) = G_\mu V_{us}^* C_{CG} L^\mu \left[f_+(t)(p_K + p_\pi)_\mu + f_-(t)(p_K - p_\pi)_\mu \right] . \quad (4)$$

For the K_{e3} modes, only $f_+(t)$ needs to be considered, whereas for the $K_{\mu 3}$ modes $f_-(t)$ has to be included as well. The chiral expansions of these form factors read $f_+ = 1 + f_+^{(2)} + f_+^{(4)} + \ldots$ and $f_- = f_-^{(2)} + f_-^{(4)} + \ldots$ The one loop corrections $f_\pm^{(2)}(t)$ arising from mesonic intermediate states, including isospin breaking effects induced by $m_u \neq m_d$, are known [12, 13] for quite some time. Including $\mathcal{O}(\alpha)$ radiative corrections [14, 15] amounts to replacing $f_\pm(t)$ by

$$F_\pm(t,v) = \left[1 + \frac{\alpha}{\pi} \Gamma(v, m_\gamma) \right] \times \left(\widetilde{f}_\pm(t) + \widehat{f}_\pm(t) \right) . \quad (5)$$

In this expression, $\widetilde{f}_\pm(t)$ contains corrections from the loops and from $\pi^0 - \eta$ mixing, while $\widehat{f}_\pm(t)$ collects the remaining counterterm contributions. Finally, $\Gamma(v, m_\gamma)$, with $v = (p_K - p_\pi)^2$ for $K^\pm_{\ell 3}$, and $v = (p_K - p_\pi)^2$ for $K^0_{\ell 3}$, contains the long distance components of the loops with a virtual photon. The IR divergence, materialized by the dependence on the photon mass m_γ, is cancelled upon considering the differential rates with the emission of a real soft photon. Corrections at order $\mathcal{O}(\alpha p^2)$ were computed [14, 15] and the corresponding numerical estimates read

$$\widetilde{f}_\pm(0) = 1.0002 \pm 0.0022 \,, \;\; \widehat{f}_\pm(0) = 0.0032 \pm 0.0016 \quad [K^\pm] \quad (6)$$

$$\widetilde{f}_\pm(0) = 0.097699 \pm 0.00002 \,, \;\; \widehat{f}_\pm(0) = 0.0046 \pm 0.0008 \quad [K^0] \quad (7)$$

The expressions of the two loop corrections $f_\pm^{(4)}(t)$ were worked out [16] in the isospin limit, and will be discussed below.

3 The pion beta decay $\pi^+ \to \pi^0 e^+ \nu_e$ and $|V_{ud}|$

The beta decay of the charged pion ($\pi\beta$) in principle provides a determination of $|V_{ud}|$ which combines the advantages of the superallowed nuclear Fermi transitions (pure vector transition, no axial vector admixture), and of the neutron beta decay (no nuclear structure dependent radiative corrections). There is however a serious drawback, the tiny branching ratio, $\mathrm{Br}(\pi\beta) \sim 1 \times 10^{-8}$. In

the absence of radiative corrections, the amplitude has the structure given in Eq. (4), with V_{us} replaced by V_{ud}, and $f_\pm(t)$ replaced by $f_\pm^{\pi\beta}(t)$. Contribution from $f_-^{\pi\beta}(t)$ are suppressed by m_e^2/M_π^2 and can be neglected. Furthermore, $f_+^{\pi\beta}(t) = 1 + f_{\pi\beta}^{(2)}(t) + \ldots$, where the one loop corrections [17] to the CVC result are small, $f_{\pi\beta}^{(2)}(0) = -7 \times 10^{-6}$. As a consequence, higher order corrections, $f_{\pi\beta}^{(4)}(0)$, etc., can be safely neglected. On the other hand, radiative corrections then become relevant. Including $\mathcal{O}(\alpha p^2)$ effects gives [17]

$$|V_{ud}| \cdot |f_+^{\pi\beta}(0)| = 9600.8 \sqrt{\mathrm{Br}(\pi^+ \to \pi^0 e^+ \nu_e(\gamma))},\ f_+^{\pi\beta}(0) = 1.0046 \pm 0.0005. \quad (8)$$

Radiative corrections enhance the branching ratio by (3.34 ± 0.10) % . The (very small) uncertainties come from the counterterm contributions. It is thus possible to give a very accurate prediction for $|f_+^{\pi\beta}(0)|$ in ChPT. With the latest result [18] of the PIBETA experiment, the relative precision on $|V_{ud}|$ obtained this way is still limited by the experimental precision

$$\delta|V_{ud}|/|V_{ud}| = (\pm 3.2_{\,\mathrm{exp}} \pm 0.5_{\,\mathrm{th}}) \times 10^{-3}\,. \quad (9)$$

4 Two loop $K_{\ell 3}$ form factors and strategies to extract $|V_{us}|$

The situation is somewhat less ideal for the $K_{\ell 3}$ decays, since the corrections are larger, and the one loop result is not sufficient for an accurate determination [13] of $|V_{us}|$. The NNLO expressions for the $K_{\ell 3}$ form factors $f_\pm(t)$ decompose into a two loop part, which depends only on the masses and on F_π, a one loop part involving the L_i's, and a tree level contribution depending on some of the $\mathcal{O}(p^6)$ LECs C_i. It should be stressed that the estimate of $f_+^{(4)}(0)$ given in Ref. [13] is neither a two loop calculation, nor an estimate of the LECs that enter the two loop expression. While the LECs giving the $\mathcal{O}(t)$ and the $\mathcal{O}(t^2)$ terms of $f_+(t)$ can in principle be obtained from the experimental measurements of the slope λ_+ and the curvature c_+, there remain two unknown LECs in $f_+(0)$, C_{12} and C_{34}. The important observation [16] here is that these same two LECs also appear in a combination of the scalar form factor $f_0(t)$ and of F_K/F_π. For instance,

$$\lambda_0 = 8\frac{M_\pi^2(M_K^2 + M_\pi^2)}{F_\pi^4}(2C_{12} + C_{34}) + \frac{M_\pi^2}{M_K^2 - M_\pi^2}\left(\frac{F_K}{F_\pi} - 1\right) + \Delta'(0)\,, \quad (10)$$

$$c_0 = -8\frac{M_\pi^4}{F_\pi^4}C_{12} + \Delta''(0)/2\,. \tag{11}$$

In the kinematical region of interest, the known function $\Delta(t)$ is well approximated by a polynomial [16], $\Delta(t) = \alpha t + \beta t^2 + \gamma t^3$. Thus, one may extract C_{12} from the knowledge of the curvature c_0 of $f_0(t)$, and then get C_{34} from its slope λ_0 *provided* F_K/F_π *is known*. The reason for the emphasis [19] here comes from the fact that the value usually quoted, $F_K/F_\pi = 1.22 \pm 0.01$, actually results from the analysis of Ref. [13], and thus cannot be used *a priori*. The effect of a variation in F_K/F_π on $f_+(0)$ reads,

$$\delta f_+(0)|_{F_K/F_\pi} = \frac{M_K^2 - M_\pi^2}{M_K^2 + M_\pi^2}\,\delta\left(\frac{F_K}{F_\pi}\right)\,, \tag{12}$$

and even a variation of F_K/F_π as small as a few percents directly affects the value of $f_+(0)$, and thus the determination of $|V_{us}|$, by about the same relative amount. This assumes that all the dependence on F_K/F_π is explicitly shown in Eqs. (10) and (11). The situation is however more complicated, since the values of the coefficients α, β, γ depend on the values of the L_i's, which are obtained from a fit [20] to various input observables, *including the fixed value* $F_K/F_\pi = 1.22 \pm 0.01$. A more accurate description of the dependence on F_K/F_π therefore requires to perform this fit for different values of this ratio, in the range, say, from 1.17 to 1.27, expressing, for instance, the numerical coefficients α, β, γ in the form $\alpha = \alpha_0 + \alpha_1(F_K/F_\pi - 1.22) + \alpha_2(F_K/F_\pi - 1.22)^2 + \ldots$, etc. The situation is thus similar to the one encountered previously in a different, but not unrelated, context [19], and the strategies to extract $|V_{us}|$ discussed there may be easily adapted. From Eq. (3), one can obtain F_K/F_π in terms of $|V_{us}/V_{ud}|$, thus expressing $f_+(0)$ as $1 + \mathcal{F}(\lambda_0, c_0, |V_{ud}|, |V_{us}|)$. Given a value of $|V_{ud}|$ and sufficiently accurate experimental determinations of λ_0 and of c_0 from the $K_{\mu 3}$ data (see the discussion in Ref. [16]

for the accuracy that is required), this would then allow to extract $|V_{us}|$ from the values of the $K_{\ell 3}$ branching ratios, and then to obtain F_K/F_π from Eq. (3). Independent information on F_K/F_π can of course modify the situation. For instance, there exists now a rather accurate determination of F_K/F_π from partially quenched lattice data with staggered fermions [21]. Using this imput allows to extract $|V_{us}|$ directly from Eq. (3) [22], given a value of $|V_{ud}|$. On the other hand, there exists also a direct, although quenched, lattice calculation [23] of $f_+(0)$. These new developments offer possibilities for cross checks.

In particular, one would like to have a determination of both F_K/F_π and $f_+(0)$ from the same lattice simulation with dynamical (domain wall ?) fermions, in order to check whether they satisfy the correlation implied by the above analysis of the two loop ChPT expression. As far as the latter is concerned, the inclusion of isospin breaking corrections would be welcome.

5 Acknowledgements

I wish to thank the organizers for the invitation to this very informative workshop, as well as J. Bijnens and J. Gasser for interesting discussions. Centre de Physique Théorique is Unité Mixte de Recherche (UMR 6207) of CNRS, and of the universities Aix-Marseille I, Aix-Marseille II, Sud Toulon-Var, and is affiliated to the FRUMAM (FR 2291). This work was supported in part by TMR, EC-Contract No. HPRN-CT-2002-00311 (EURIDICE).

References

1. G. 't Hooft, *Naturalness, Chiral Symmetry, And Spontaneous Chiral Symmetry Breaking*, in G. t'Hooft et al., editors, Proceedings of the NATO Advanced Study Institute, Cargèse, France, Aug. 26 - Sept. 8, 1979, Plenum Press (1980).

2. S. Weinberg, Physica A **96**, 327 (1979).

3. J. Gasser and H. Leutwyler, Ann. Phys. **158**, 142 (1984).

4. J. Gasser and H. Leutwyler, Nucl. Phys. B **250**, 465 (1985).

5. J. Bijnens, G. Colangelo and G. Ecker, JHEP **9902**, 020 (1999) [arXiv:hep-ph/9902437]; Ann. Phys. **280**, 100 (2000) [arXiv:hep-ph/9907333].

6. G. Ecker, J. Gasser, A. Pich and E. de Rafael, Nucl. Phys. B **321**, 311 (1989).

7. M. Knecht and R. Urech, Nucl. Phys. B **519**, 329 (1998) [arXiv:hep-ph/9709348]; U.-G. Meißner, G. Müller and S. Steininger, Phys. Lett. B **406**, 154 (1997) [Erratum-ibid. B **407**, 454 (1997)] [arXiv:hep-ph/9704377].

8. R. Urech, Nucl. Phys. B **443**, 234 (1995) [arXiv:hep-ph/9405341].

9. W. J. Marciano and A. Sirlin, Phys. Rev. Lett. **71**, 3629 (1993), and references therein.

10. H. Neufeld and H. Rupertsberger, Z. Phys. C **71**, 131 (1996) [arXiv:hep-ph/9506448].

11. M. Knecht, H. Neufeld, H. Rupertsberger and P. Talavera, Eur. Phys. J. C **12**, 469 (2000) [arXiv:hep-ph/9909284].

12. J. Gasser and H. Leutwyler, Nucl. Phys. B **250**, 517 (1985).

13. H. Leutwyler and M. Roos, Z. Phys. C **25**, 91 (1984).

14. V. Cirigliano, M. Knecht, H. Neufeld, H. Rupertsberger and P. Talavera, Eur. Phys. J. C **23**, 121 (2002) [arXiv:hep-ph/0110153].

15. V. Cirigliano, H. Neufeld and H. Pichl, Eur. Phys. J. C **35**, 53 (2004) [arXiv:hep-ph/0401173].

16. J. Bijnens and P. Talavera, Nucl. Phys. B **669**, 341 (2003) [arXiv:hep-ph/0303103].

17. V. Cirigliano, M. Knecht, H. Neufeld and H. Pichl, Eur. Phys. J. C **27**, 255 (2003) [arXiv:hep-ph/0209226].

18. D. Počanić et al. [PIBETA Collaboration], ArXiv:hep-ex/0312030.

19. N. H. Fuchs, M. Knecht and J. Stern, Phys. Rev. D **62**, 033003 (2000) [arXiv:hep-ph/0001188].

20. G. Amoros, J. Bijnens and P. Talavera, Nucl. Phys. B **602**, 87 (2001).

21. C. Aubin et al. [MILC Collaboration], ArXiv:hep-lat/0402030.

22. W. J. Marciano, ArXiv:hep-ph/0402299.

23. D. Bećirević et al., ArXiv:hep-ph/0403217; V. Lubicz, these proceedings.

Frascati Physics Series Vol. XXXVI (2004), pp. 405
DAΦNE 2004: Physics at meson factories – Frascati, June 7-11, 2004
Invited Review Talk in Plenary Session

OPEN PROBLEMS ON LIGHT MESON SPETTROSCOPY

Ignacio Bediaga
CBPF
Rua Xavier Sigaud 150, 22290-180 Rio de Janeiro, Brazil

Written contribution not received

Frascati Physics Series Vol. XXXVI (2004), pp. 407–413
DAΦNE 2004: Physics at meson factories – Frascati, June 7-11, 2004
Selected Contribution in Plenary Session

RESULTS FROM THE DIRAC EXPERIMENT AT CERN

L. Tauscher *
Basel University

Abstract

The goal of the DIRAC experiment is to measure the lifetime of the $\pi^+\pi^-$ atom and thus to determine the $\pi\pi$ s-wave scattering lengths $|a_2 - a_0|$. We describe the experimental methods and present first results from a subsample of data taken so far.

1 Introduction

The lifetime of a $\pi^+\pi^-$ atom ($A_{2\pi}$) is due to the reaction $\pi^+\pi^- \to \pi^0\pi^0$, whose amplitude is proportional to the difference of the s-wave $\pi\pi$ scattering lengths

* for the DIRAC collaboration at CERN

for isospins 0 and 2. Measuring the lifetime thus provides a measure of $|a_0 - a_2|^2$. The lifetime is about 3 femtoseconds and can be predicted theoretically [1, 2] with high precision. Measuring the lifetime thus provides a test of theory.

The method of measuring the lifetime has been developed by Nemenov [3]. Atoms produced in a high energy proton nucleus collision propagate until they annihilate. In a target of finite thickness the relativistic atom ($\gamma \approx 17$) collides with target atoms and becomes excited and/or broken-up. Cross sections and transport dynamics can be calculated accurately and a relation between break-up probability and lifetime can be established as a function of target material, target thickness and momentum of the $A_{2\pi}$ [4].

Pion pairs from break-up can be detected through their specific feature of very low relative momentum Q. In Figure 1 the distributions are shown for Q and its longitudinal component Q_L, at break-up and at the exit of the target.

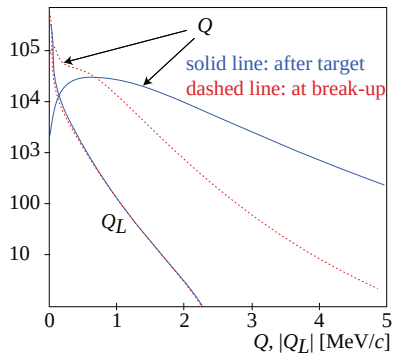

Figure 1: *Q and Q_L distributions of π^+ - π^- pairs from atomic break-up, at break-up (dashed) and at target exit (solid line). Remark the broadening of the Q distribution due to multiple scattering.*

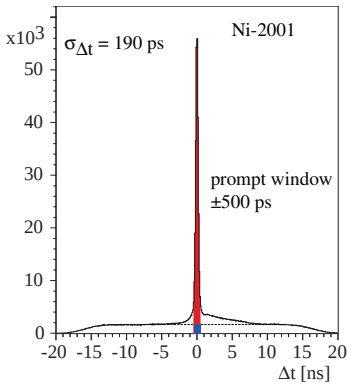

Figure 2: Time difference between positive and negative vertical hodoscope slabs associated with the selected tracks. The asymmetry for positive differences is due to protons.

Experimentally the measurement of a signal of $\pi^+\pi^-$ pairs from atom break-up n_A leads to the break-up probability $P_{br} = n_A/N_A$ where the number of produced atoms N_A has to be determined separately. DIRAC uses the background as a normalization for N_A, but has also introduced a method of lifetime determination free of normalization by using two targets.

The DIRAC experiment was proposed in 1995 [5] and has started data production in 1999. Here we report on the results from data taken on Ni targets in the years 2001 and 2002.

2 The Experiment

The DIRAC experiment uses a double arm spectrometer designed for detecting track pairs from pions of opposite charge with low relative momentum Q. Figure 3 shows the set-up of DIRAC. The resolutions are: $\sigma_p/p = 0.3\%$ and $\sigma_{Q_L} = \sigma_{Q_x} = \sigma_{Q_y} = 0.5$ MeV/c. Details may be found in [6, 7, 8, 9, 10].

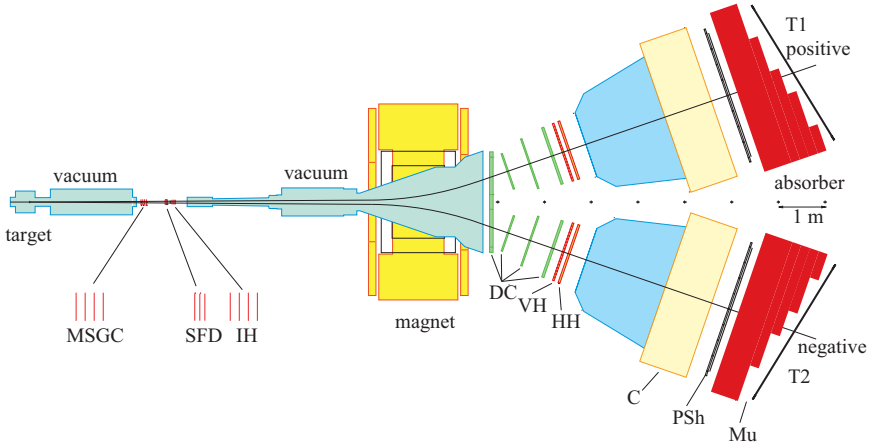

Figure 3: *Schematic top view of the DIRAC spectrometer. Upstream of the magnet: target, microstrip gas chambers (MSGC), scintillating fiber detectors (SFD), ionization hodoscopes (IH) and iron shielding. Downstream of the magnet: drift chambers (DC), vertical and horizontal scintillation hodoscopes (VH, HH), gas Cherenkov counter (Ch), preshower detectors (PSh) and, behind the iron absorber, muon detectors (Mu).*

3 Event selection, reconstruction.

We have analysed data taken in 2001 on Ni targets of 94 μm and 98μm thickness. Two event classes are used: "prompt" events, defined by a time difference

(corrected for the flight path assuming pions) in the VH's between the positive and the negative arm, $|\Delta t| \leq 0.5$ ns, and "accidental" events, defined by $-15 \leq \Delta t \leq -5ns$ and $7 \leq \Delta t \leq 15ns$ (cf. Fig. 2). $e^{\pm}$ and $\mu^{\pm}$ are rejected (Cherenkovs, Preshower and the Muon counters). Cuts are applied on $\sqrt{Q_x^2 + Q_y^2} = Q_T \leq 4\,\mathrm{MeV}/c$ and $|Q_L| < 22\,\mathrm{MeV}/c$. Reconstruction uses standard methods including Kalman filtering.

4 Background

Prompt pion pair background is produced by pions from hadronization or decay of short lived secondaries (e.g. ρ mesons), and decay of long lived particles (e.g. η mesons). Pions from the former background undergo final state Coulomb interaction, which results in an enhancement at low Q (Coulomb correlated (CC) background), while the second type of background is not affected (nC-background). Accidental background originates from two different proton interactions and is also present in the prompt time window (cf. Fig. 2).

5 Simulations.

The backgrounds and the break-up signal were simulated using appropriate generators (phase space for nC and accidental background, additional Coulomb enhancement for CC background [11]), and atomic break-up). The spectrometer was simulated with GEANT4. Detectors, triggers and digitalization were fully simulated. Thus Monte Carlo data could be treated as real data.

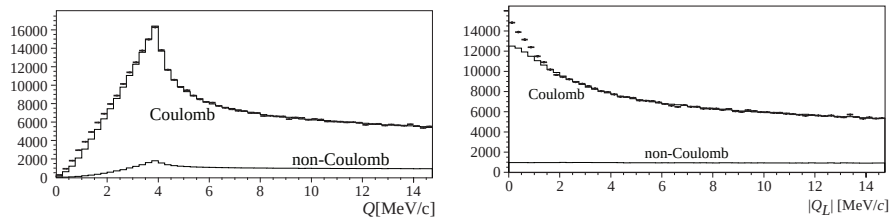

Figure 4: Measured prompt distributions in Q qnd Q_L. The fitted Monte Carlo backgrounds are also displayed [12]).

6 Signal extraction.

The signal (number of detected broken-up atoms n_A^{exp}) was obtained by approximating the prompt experimental Q and Q_L distributions with the Monte Carlo background distributions and with the (fixed) accidental distribution obtained from an extrapolation from the accidental window into the prompt window (cf. Fig. 2). The properly normalized backgrounds were fitted outside the signal region (see Fig. 4) and then subtracted from the experimental distributions (see Fig. 5).

7 Normalization and Break-up probability.

The break-up probability is $P_{br} = n_A/N_A$ with n_A the number of broken-up atoms and N_A the number of produced atoms. N_A may be obtained from the CC background since atom formation and Coulomb correlation are the same physics processes. Thus, theory provides $N_A = 0.615 N_{CC}^{norm}$ with $N_{CC}^{norm} = \int_{0\ MeV/c}^{2\ MeV/c} N_{CC}(Q)dQ$. Monte Carlo provides the fraction κ of N_{CC}^{norm} of the total reconstructed CC-background below a cut limit to be chosen, $N_{C\bar{C}}^{Q\leq Q_{cut}} = \int_{0\ MeV/c}^{Q\leq Q_{cut}} N_{C\bar{C}}^{exp}(Q)dQ$. Then $N_A = 0.615 \times \kappa \times N_{C\bar{C}}^{Q\leq Q_{cut}}$. The fraction ϵ of detected pairs from break-up whithin the same cut limits of total broken-up atoms is also obtained by Monte Carlo. The break-up probability thus becomes $P_{br} = n_A^{exp}/(0.615\ \kappa\ \epsilon\ N_{C\bar{C}}^{Q\leq Q_{cut}})$. With the number of events obtained from the fit [12], $n_A^{exp} = 6560 \pm 295$, $N_{C\bar{C}}^{Q\leq 4MeV/c} = 106114 \pm 1010$, and $0.615\ \kappa\ \epsilon = 0.1383$ we obtain $P_{br} = 0.447 \pm 0.023_{stat}$.

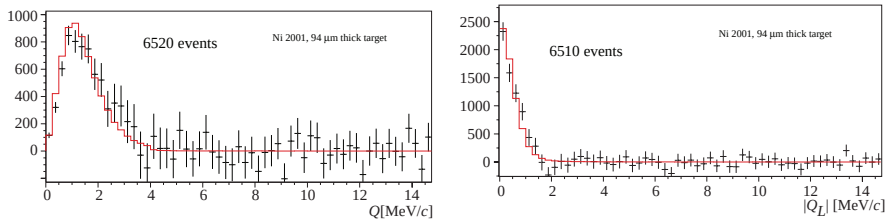

Figure 5: Measured prompt distributions in Q qnd Q_L after background subtraction. The Monte Carlo simulated atomic pair shapes are also displayed. [12]

8 Systematic errors.

We have investigated a large number of systematic errors, the most important ones being linked to differences in results obtained from Q and Q_L separately, to the CC background determination, to the line shape and to multiple scattering. We found a slight dependence of the CC background on the upper end of the fit range. We also found a dependence of the break-up probability on the line shape, but with diminishing importance when taking the whole signal ($Q_{cut} = 4MeV/c$). Variations in multiple scattering ($\pm$ 5% in scattering angle) yield small deviations. The total systematic error [12)] of the break-up probability is estimated to be $\pm$ 0.009.

9 Lifetime.

With $P_{br} = 0.447 \pm 0.023_{stat} \pm 0.009_{syst} = 0.447 \pm 0.025_{tot}$ we deduce a lifetime of $\tau = 2.85\ ^{+0.48}_{-0.41}$ [fs].

10 Conclusions.

The analysis presented here is obtained with only ≈ 30 % of all data collected so far by DIRAC. All the above results can be found in [12)] and are preliminary[1]. However, the systematic errors seem to be under control and are smaller than the statistical ones. This is also true if all the data of DIRAC will be used. In this case the total error on the lifetime will be around 10%.

References

1. G. Colangelo, J. Gasser and H. Leutwyler, Nucl. Phys. B603 (2001) 125.
2. G. Colangelo, J. Gasser and H. Leutwyler, Phys. Rev. Lett. 86 (2001) 5008.
3. L. L. Nemenov, Yad. Fiz. 41 (1985) 980; (Sov. J. Nucl. Phys. 41 (1985) 629).
4. T. A. Heim et al., J. Phys. B33 (2000) 3583;
   T. A. Heim et al., J. Phys. B34 (2001) 3763;
   M. Schumann et al., J. Phys. B35 (2002) 2683.

[1] In the sense that independent cross checks have still to be done.

5. B. Adeva et al., DIRAC proposal, CERN/SPSLC 95-1, SPSLC/P 284 (1995).

6. B. Adeva et al., Nucl. Instr. Meth. A515 (2003) 467.

7. L. Afanasyev et al. Nucl. Instr. Meth. A491 (2002) 376.

8. L. Afanasyev, M. Gallas, V. Karpukhin, A. Kulikov, Nucl. Instr. Meth. A479 (2002) 407.

9. M. Gallas, Nucl. Instr. Meth. A481 (2002) 222.

10. P. Kokkas, M. Steinacher, L. Tauscher, S. Vlachos, Nucl. Instr. Meth. A471 (2001) 358.

11. A. D. Sakharov, Zh. Eksp. Teor. Fiz. 18 (1948) 631.

12. Ch. P. Schuetz, Thesis, Basel University, March 2004. http://cdsweb.cern.ch/search.py?recid=732756

Frascati Physics Series Vol. XXXVI (2004), pp. 415–420
DAΦNE 2004: Physics at meson factories – Frascati, June 7-11, 2004
Selected Contribution in Plenary Session

PROGRESS ON Φ RADIATIVE DECAYS WITH THE KLOE EXPERIMENT

The KLOE collaboration*
presented by Biagio Di Micco
Università degli Studi di Roma Tre
I.N.F.N. sezione di Roma III

Abstract

We describe the status of the analyses in progress on light meson spectroscopy in the KLOE experiment. We present the analyses of ϕ decays into $f_0(980)\gamma$, the Dalitz plot analysis of the $\eta \to \pi^+\pi^-\pi^0$ decay, the branching ratio measurement of $\eta \to \pi^0\gamma\gamma$, the upper limits on $Br(\eta \to 3\gamma)$ and $Br(\eta \to \pi^+\pi^-)$, the measurement of the ratio $Br(\phi \to \eta'\gamma)/Br(\phi \to \eta\gamma)$.

* A.Aloisio, F.Ambrosino, A.Antonelli, M.Antonelli, C.Bacci, M.Barva, G.Bencivenni, S.Bertolucci, C.Bini, C.Bloise, V.Bocci, F.Bossi, P.Branchini, S.A.Bulychjov, R.Caloi, P.Campana, G.Capon, T.Capussela, G.Carboni, F.Ceradini, F.Cervelli, F.Cevenini, G.Chiefari, P.Ciambrone, S.Conetti, E.De Lucia, A.De Santis, P.De Simone, G.De Zorzi, S.Dell'Agnello, A.Denig, A.Di Domenico, C.Di Donato, S.Di Falco, B.Di Micco, A.Doria, M.Dreucci, O.Erriquez, A.Farilla, G.Felici, A.Ferrari, M.L.Ferrer, G.Finocchiaro, C.Forti, P.Franzini, C.Gatti, P.Gauzzi, S.Giovannella, E.Gorini, E.Graziani, M.Incagli, W.Kluge, V.Kulikov, F.Lacava, G.Lanfranchi, J.Lee-Franzini, D.Leone, F.Lu, M.Martemianov, M.Martini, M.Matsyuk, W.Mei, L.Merola, R.Messi, S.Miscetti, M.Moulson, S.Müller, F.Murtas, M.Napolitano, F.Nguyen, M.Palutan, E.Pasqualucci, L.Passalacqua, A.Passeri, V.Patera, F.Perfetto, E.Petrolo, L.Pontecorvo, M.Primavera, P.Santangelo, E.Santovetti, G.Saracino, R.D.Schamberger, B.Sciascia, A.Sciubba, F.Scuri, I.Sfiligoi, A.Sibidanov, T.Spadaro, E.Spiriti, M.Testa, L.Tortora, P.Valente, B.Valeriani, G.Venanzoni, S.Veneziano, A.Ventura, R.Versaci, I.Villella, G.Xu.

1 Introduction

The KLOE detector [1], operates at the Frascati e^+e^- collider DAΦNE [2], which runs at a CM energy W equal to the ϕ-meson mass, $W\sim$1019.5 MeV. The analyses presented here are based on data collected in the years 2001 and 2002 for an integrated luminosity of $\sim 450\ pb^{-1}$ corresponding to 20 millions of η mesons [Br($\phi \to \eta\gamma$) $\sim 1.3\%$ [3]]. This means that KLOE can study η physics in a clean environment with high statistic.

2 Search for $\phi \to f_0\gamma$ in $\pi^+\pi^-\gamma$ events.

The ϕ radiative decays to scalar mesons, $\phi \to S\gamma$, give significant insight in the assessment of the nature of lower mass scalar mesons [4]. An overall fit of these data is in progress, with the aim of extracting the f_0 parameters taking into account all the possible interferences of the f_0 term with the other amplitudes.

The search for $\phi \to f_0(\to \pi^+\pi^-)\gamma$ is characterized by the presence of irreducible backgrounds due to the initial state radiation (ISR), to $e^+e^- \to \pi^+\pi^-\gamma$ (FSR) and $\phi \to \rho^\pm(\to \pi^\pm\gamma)\pi^\pm$. The f_0 events are searched for in the large photon angle region $45^o < \theta < 135^o$ to reduce ISR background. The f_0 signal appears as a bump in the $\pi^+\pi^-$ invariant mass $M_{\pi\pi}$ spectrum around 980 MeV. Fig.1 (left) shows the spectrum obtained at $\sqrt{s} = M_\phi$.
An overall fit to the spectrum has been done applying the following formula:

$$\frac{dN}{dM_{\pi\pi}} = \left[(\frac{d\sigma}{dM_{\pi\pi}})_{ISR} + (\frac{d\sigma}{dM_{\pi\pi}})_{FSR+f_0} + (\frac{d\sigma}{dM_{\pi\pi}})_{\rho\pi} \right] \times L \times \epsilon(M_{\pi\pi})$$

with L the integrated luminosity and $\epsilon(M_{\pi\pi})$ the selection efficiency as a function of $M_{\pi\pi}$. The f_0 amplitude is taken from the kaon-loop approach [4]. A forward-backward asymmetry $A = \frac{N^+(\theta>90^o) - N^+(\theta<90^o)}{N^+(\theta>90^o) + N^+(\theta<90^o)}$ is expected, due to the interference between FSR and ISR [5]. Fig.1 (right) shows the asymmetry as a function of $M_{\pi\pi}$ compared to the prediction based on the ISR-FSR interference alone. A significant deviation from the prediction is observed in the high mass region clearly due to the f_0 contribution.

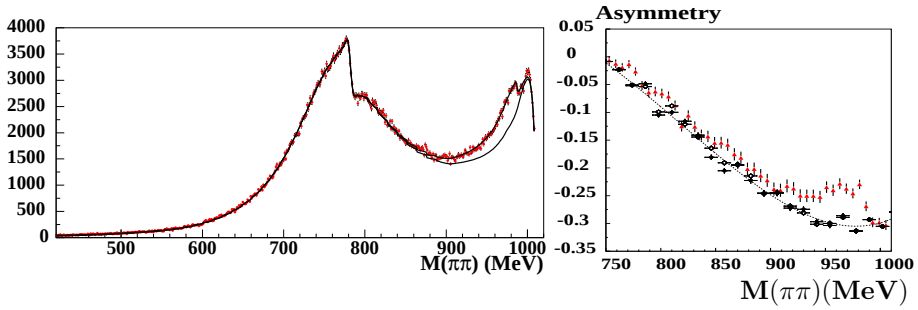

Figure 1: *(left) $M_{\pi\pi}$ spectrum of $\pi^+\pi^-\gamma$. The upper (lower) curves are the result of the fit and the estimated background due to ISR, FSR and $\rho\pi$. (right) Forward-Backward asymmetry A as a function of $M_{\pi\pi}$. The curve and the black points are the Montecarlo expectations based on the interference between FSR and ISR only. The experimental data are reported as triangles.*

3 Dynamics of $\eta \to \pi^+\,\pi^-\,\pi^0$

The dynamics of the $\eta \to \pi^+\,\pi^-\,\pi^0$ decay has been studied with a Dalitz plot analysis. The conventional variables X and Y are defined as: $X = \sqrt{3}\frac{T_+ - T_-}{Q_\eta}$,$Y = \frac{3T_0}{Q_\eta} - 1$, where $Q_\eta = m_\eta - 2m_{\pi^+} - m_{\pi^0}$ and T_+, T_- and T_0 are the kinetic energies of the particles. The measured distribution has been fitted as: $|A(X,Y)|^2 \simeq (1 + aY + bY^2 + cX + dX^2 + eXY + ...)$. C-parity conservation prevents odd powers in X being present in the expansion: thus parameters c and e should be zero as confirmed by our fit. The results of the fit are shown in table 3 Efficiency is ~ 36 % over the whole Dalitz plot. The

Table 1: *Fitted parameters $P(\chi^2) = 52$ od $\eta \to 3\pi$ Dalitz plot.*

a	b	c
$-1.075 \pm .008$	$.118 \pm .009$	$-.0005 \pm .004$
d	e	f
$.049 \pm .008$	$-.004 \pm .01$	$.13 \pm .02$

evaluation of systematic effects is under completion.

4 Rare and forbidden η decays ($\eta \to \pi^0\gamma\gamma$,$\eta \to \pi^+\pi^-$,$\eta \to \gamma\gamma\gamma$)

The $\eta \to \pi^0\gamma\gamma$ decay is interesting to test the Chiral Perturbation Theory prediction for the branching ratio and $m_{\gamma\gamma}$ spectrum. [6]. The most accurate measurement for the branching ratio [7] is, infact, far from any theoretical prediction for this decay based on ChPT. Recently a new measurement has been performed [8] giving a much lower value than the previous one, with a larger error. All previous experiments were done at hadron machines, using mainly $\pi^- p \to \eta n$, and are largely dominated by $\pi^0\pi^0$ background and geometrical acceptance. KLOE can perform a measurement of competitive precision in a cleaner environment. Furthermore, it has different background topologies and experimental systematics. The signal is searched looking for a $\pi^0\gamma\gamma\gamma$ topology, where the further γ comes from $\phi \to \eta\gamma$. Five prompt clusters are required and an overall kinematic fit requiring π^0 mass is performed. The clusters energy must be > 30 MeV and azimutal angle $> 21^\circ$ to reject fake clusters coming from machine background. The dominant background channel is $\eta \to 3\pi^0$ that has been reduced with several topological cut. With this selection we obtain an efficiency of 5.7 %. To give an idea of the sensitivity, in fig.2 we compare our data together with MC prediction based on the $Br(\eta \to \pi^0\gamma\gamma)$ measured by [7] and [8]. It is evident that our data are incompatible with [7] and are marginally in agreement with [8]. The background simulation and the efficiency for the signal is still under study.

$\eta \to 3\gamma$ decay is C violating. It is a sensitive test of C violation in the strong and electromagnetic interactions. For the details of this analysis see [9]. The KLOE result for the branching ratio is: $Br(\eta \to \gamma\gamma\gamma) \leq 1.6 \times 10^{-5}$ @90 % C.L. This limit is the experimental best limit for this decay. The expected branching ratio from the Standard Model is $\leq 10^{-12}$ [10], so any discovery of a larger decay rate would be a clear signal of Standard Model deviation.

$\eta \to \pi^+\pi^-$ decay is P and CP violating. This decay is allowed as a weak direct CP violating decay with a very low branching ratio: BR($\eta \to \pi^+\pi^-$)$\sim 10^{-27}$ [11]. Therefore the detection of this decay at an accessible level would be a signal of P and CP violation not explainable in the Standard Model framework. The latest published [12] direct search of this decay has given the following 90% C.L. upper limit: $BR(\eta \to \pi^+\pi^-) < 3.3 \times 10^{-4}$. In KLOE the

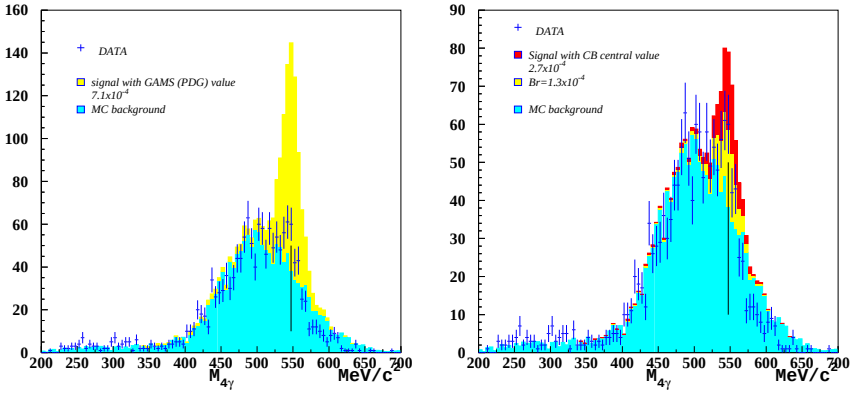

Figure 2: *M(4γ), the spectra expected from the GAMS* [7] *and Crystall Ball* [8] *measurement are shown. In the right plot we show also the expected spectrum for a Br* $\sim 1/2$ *of C.B. result.*

signal is searched in the M(η) region of the $\pi^+\pi^-$ invariant mass spectrum of $\pi^+\pi^-\gamma$ events selected according to the $f_0(980) \to \pi^+\pi^-$ analysis described before (see fig. 1). The signal efficiency is: ϵ_s=16.6%. The expected signal has a Gaussian shape with a mass resolution of 1.33 MeV. No signal is observed. The background is determined by fitting the theoretical model for $\pi^+\pi^-\gamma$ sample to the full spectrum. In order to determine an upper limit, we have added to this background a Gaussian function representing the signal multiplied by a constant N_s. We obtain: $N_s = -8 \pm 24$. The 90% confidence level upper limit on the number of events is obtained using the tables in [13]: $N_s < 32$. The branching ratio is $BR(\eta \to \pi^+\pi^-) = \frac{N_s}{\epsilon_s N_\eta}$ with N_η the number of η in the sample (1.43×10^7). The 90% C.L. upper limit is: $BR(\eta \to \pi^+\pi^-) < 1.3 \times 10^{-5}$. It improves by a factor ~ 30 the present best limit.

5 η- η' mixing

Here we present the $R = \frac{\Gamma(\phi \to \eta'\gamma)}{\Gamma(\phi \to \eta\gamma)}$ measurement. The η' is identified via the decays: $\phi \to \eta'\gamma$; $\eta' \to \pi^+\pi^-\eta$; $\eta \to \pi^0\pi^0\pi^0$ and the decays $\phi \to \eta'\gamma$; $\eta' \to \pi^0\pi^0\eta$; $\eta \to \pi^+\pi^-\pi^0$. The final state is thus charachterized by two charged pions and seven photons, and has no physics background with the same

topology in KLOE. After background subtraction we observe $3405 \pm 61 \pm 31$ $\phi \to \eta'\gamma$ events. We normalize to the number of observed $\eta \to \pi^0\,\pi^0\,\pi^0$ decays in the same runs to obtain a preliminary measurement of the ratio of BR's:$R = (4.9 \pm 0.1_{stat} \pm 0.2_{syst}) \times 10^{-3}$. This result compare favourably with our previous estimate [14)] (which already dominates the world average [3)]) but with considerably improved accuracy.

References

1. KLOE Coll., M. Adinolfi *et al.*, Nucl. Instrum. Meth. **A488**, 51 (2002).
2. S. Guiducci, in: Proc. 2001 Particle Accelerator Conf. (ed. P. Lucas, S. Webber, Chicago, 2001).
3. K. Hagiwara *et al.,* Phys. Rev. **D66** (2002).
4. N.N.Achasov, V.N.Ivanchenko, Nucl.Phys. **B315**, 465 (1989); F.Close, A.Kirk, Phys. Lett. **B515**, 13 (2001).
5. N.N.Achasov, V.V.Gubin, Phys. Rev. **D57**, 1987 (1998).
6. J. Bijnens and J. Gasser, in: Proc. Workshop on Production, Interaction and Decay of the η Meson (ed. J. Bijnen, G. Fäldt, B. M. K. Nefkens, Uppsala, October 2001), **T99**, 34 (Phys. Scripta, Stockholm, 2002).
7. Alde *et al.*, Z. Phys. **C25**, 225 (1984).
8. N. Knecht *et al.*, Phys. Lett. **B589**, 14 (2004).
9. KLOE Coll., A. Aloisio *et al.*, Phys. Lett. **B591**, 49 (2004).
10. P. Herczeg, in: Proc. Int. Workshop on Production and Decay of Light Mesons (ed. P. Fleury, Paris) 16 (World Scientific, 1988).
11. E.Shabalin, in: Second Dafne physics Handbook (ed. Rome, 1995) 445.
12. R.R. Akhmetshin *et al.*, Phys.Lett. **B462**, 371 (1999).
13. G.J. Feldman, R.D. Cousins, Phys. Rev. **D57**, 3873 (1998).
14. KLOE Coll.,A. Aloisio *et al.* Phys. Lett. **B541**, 45 (2002).

Frascati Physics Series Vol. XXXVI (2004), pp. 421–426
DAΦNE 2004: Physics at meson factories – Frascati, June 7-11, 2004
Selected Contribution in Plenary Session

DALITZ PLOT ANALYSIS IN FOCUS

Laura Edera *
Università degli Studi di Milano - INFN Sezione di Milano

Abstract

Proper tools of analysis are by now required to fully exploit the high statistics in the charm sector; Dalitz plot analysis has revealed to be one of the most powerful investigation methods to study charm phenomenology. FOCUS has performed a pioneering Dalitz plot analysis through the first application of the *K-matrix* formalism to the D^+ and $D_s^+ \to \pi^+\pi^-\pi^+$ final states, with a statistics of about 1500 events for each decay. The first Dalitz plot analysis of $D_s^+ \to K^+\pi^-\pi^+$ is also presented ($\sim$ 500 events) along with the $D^+ \to K^+\pi^-\pi^+$ one ($\sim$ 200 events).

1 Introduction

The analysis of the three-body final state by fitting Dalitz plots has proved to be a unique tool for investigating effects of resonant substructure, inter-

* On behalf of FOCUS collaboration

ference patterns, and final-state-interactions in the charm sector. The isobar formalism, which has been traditionally applied to charm amplitude analyses, provides an effective description valid for many decay channels. Nevertheless many amplitude analyses require detailed knowledge of the light-meson sector; in particular, the need to model intermediate scalar particles contributing to the charm meson in their decays has caused us to question the validity of the Breit-Wigner approximation for the description of the relevant scalar resonances. A formalism for studying overlapping and many channel resonances has been proposed long ago and is based on the *K-matrix* parametrization. This formalism, originating in the context of two-body scattering, can be generalized to cover the case of production of resonances in more complex reactions, with the assumption that the two-body system in the final state is an isolated one and that the two particles do not simultaneously interact with the rest of the final state in the production process. The *K-matrix* approach allows us to incorporate directly the results from spectroscopy experiments. In addition, the *K-matrix* formalism provides a direct way of respecting the two-body unitarity constraint which is not explicitly guaranteed in the simple isobar model. FOCUS has performed a pioneering analysis through the first application of the *K-matrix* formalism to the D_s^+ and $D^+ \to \pi^+\pi^-\pi^+$ final states [1].

The excellent quality of FOCUS data allows also for investigation of suppressed modes, such as D^+ and $D_s^+ \to K^+\pi^-\pi^+$, which are, respectively, doubly and singly Cabibbo suppressed decays. The simultaneous presence of both $\pi^+\pi^-$ and $K^+\pi^-$ resonances, along with the limited statistics of these samples, makes a *K-matrix* analysis for these decays not viable; thus we applied the traditional isobar model to fit these channels [2].

2 Amplitude parametrization

2.1 Isobar model

A resonant amplitude for a quasi-two-body channel, of the type

$$\begin{array}{rl} D \to & r + c \\ & \hookrightarrow a + b\,, \end{array} \tag{1}$$

is described, in the contest of the traditional isobar model, as:

$$A = F_D F_r \times |\bar{c}|^J |\bar{a}|^J P_J(\cos\Theta_{ac}^r) \times BW(m_{ab}) \tag{2}$$

i.e. as the product of two vertex form factors (Blatt–Weisskopf momentum-dependent factors), a Legendre polynomial of order J representing the angular decay wave function, and a relativistic Breit–Wigner (BW) representing the propagator. In this approach the total amplitude is assumed to consist of a constant term describing the direct non-resonant three-body decay and a coherent sum of functions (Eq. 2) representing intermediate two-body resonances.

2.2 *K-matrix* model

For a well-defined wave of specific isospin and spin IJ, characterized by narrow and isolated resonances the propagator is of the simple BW form. In contrast, when the specific wave IJ is characterized by large and heavily overlapping resonances, just as the scalars, the propagation is no longer dominated by a single resonance, but is the result of complicated interplay among the various resonances. In this case, it can be demonstrated on very general grounds that the propagator may be written in the context of the *K-matrix* approach as $(I - iK \cdot \rho)^{-1}$ where K is the matrix for the scattering of particle a and b of Eq.1 and ρ is the phase-space matrix. For a more detailed formalism description we refer to [1]. In the *K-matrix* approach, the production process is viewed as consisting of an initial preparation of several states, which then propagate via the term $(I - iK\rho)^{-1}$ into the final state. In order to write down the propagator, we need the scattering matrix and to perform a meaningful fit to D mesons to three-pion data, we need a full description of the scalar resonances in the relevant energy range. At the present time the only self-consistent description of S-wave isoscalar scattering is that given in the *K-matrix* representation by Anisovich and Sarantsev through a global fit of the available scattering data from the $\pi\pi$ threshold up to 1900 MeV. In the fit to our FOCUS data, the *K-matrix* parameters are fixed to the values of [3]; the free parameters are only those peculiar to the D decay process.

3 Dalitz plot analysis of D^+ and $D_s^+ \to \pi^+\pi^-\pi^+$ with the *K-matrix* formalism

The Dalitz plots of D^+ and D_s^+ in $\pi^+\pi^-\pi^+$ are represented in Fig. 1(a) and 1(b), respectively. The results of the fits of these decays, using the *K-matrix* formalism, are reported in table 1. The confidence levels of the fits are 7.7% for D^+ and 3% for D_s^+. It is interesting to point out that, in the $D^+ \to \pi^+\pi^-\pi^+$

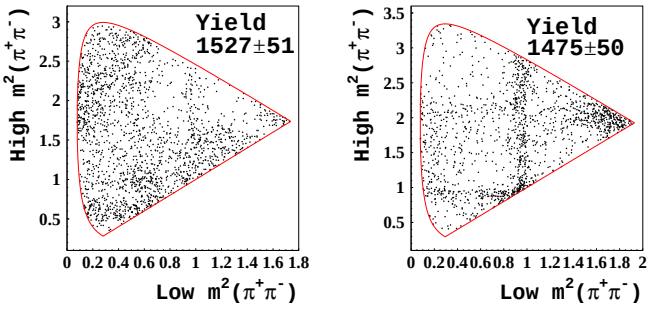

(a) $D^+ \to \pi^+\pi^-\pi^+$ (b) $D_s^+ \to \pi^+\pi^-\pi^+$

Figure 1: *Dalitz plots of* D^+ *and* $D_s^+ \to \pi^+\pi^-\pi^+$.

Table 1: *Fit results for* D^+ *and* $D_s^+ \to \pi^+\pi^-\pi^+$ *with the K-matrix formalism.*

Decay channel	Fit fraction (%)	Phase ϕ_j (degrees)	Amplitude coefficient
$D^+ \to \pi^+\pi^-\pi^+$			
$(S-wave)\,\pi^+$	$56.00 \pm 3.24 \pm 2.08$	0 (fixed)	1 (fixed)
$f_2(1270)\,\pi^+$	$11.74 \pm 1.90 \pm 0.23$	$-47.5 \pm 18.7 \pm 11.7$	$1.147 \pm 0.291 \pm 0.047$
$\rho(770)\,\pi^+$	$30.82 \pm 3.14 \pm 2.29$	$-139.4 \pm 16.5 \pm 9.9$	$1.858 \pm 0.505 \pm 0.033$
$D_s^+ \to \pi^+\pi^-\pi^+$			
$(S-wave)\,\pi^+$	$87.04 \pm 5.60 \pm 4.17$	0(fixed)	1(fixed)
$f_2(1270)\,\pi^+$	$9.74 \pm 4.49 \pm 2.63$	$168.0 \pm 18.7 \pm 2.5$	$0.165 \pm 0.033 \pm 0.032$
$\rho(1450)\,\pi^+$	$6.56 \pm 3.43 \pm 3.31$	$234.9 \pm 19.5 \pm 13.3$	$0.136 \pm 0.030 \pm 0.035$

analysis, no new resonance is necessary not present in the scattering to describe the decay dynamics. In contrast, the simple isobar model would require the presence of an "ad hoc" scalar resonance ($\sigma(600)$) to fit the data with a decent confidence level [4].

The $D_s^+ \to \pi^+\pi^-\pi^+$ decay is one of the best candidate for quantifying the role of the annihilation process in the charm hadronic decays through the evaluation of the non-resonant and $\rho(770)\pi^+$ components. It is interesting to note that our *K-matrix* results (table 1(b)) require neither of them. A high

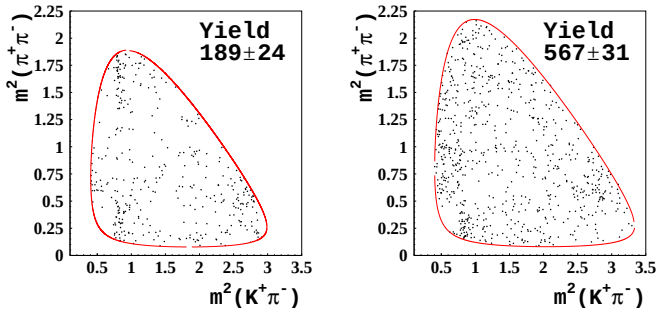

(a) $D^+ \to K^+\pi^-\pi^+$ (b) $D_s^+ \to K^+\pi^-\pi^+$

Figure 2: *Dalitz plots of* D^+ *and* $D_s^+ \to K^+\pi^-\pi^+$.

non-resonant component, about 25%, is otherwise necessary to get a decent fit to the data [5] through the isobar model. This flat contribution across the Dalitz plot seems to compensate for the model inadequateness to describe broad and overlapping resonances, thus weaking the potentiality of the Dalitz plot analysis to gauge the level of the annihilation contribution in the charm hadronic decays.

4 Dalitz plot analysis of D^+ and $D_s^+ \to K^+\pi^-\pi^+$ with the isobar model

The D^+ and $D_s^+ \to K^+\pi^-\pi^+$ Dalitz plots are fitted with the traditional isobar model. As already stated the simultaneous presence of both $\pi^+\pi^-$ and $K^+\pi^-$ resonances and the low statistics of these decays make not conceivable a *K-matrix* analysis. The Dalitz plots and the results of the fits are shown in Fig. 2 and in table 2, respectively. The confidence levels of the fits are 9.2% for D^+ and 5.5% for D_s^+. In both the decays the dominant contributions are $\rho(770)$ and $K^*(892)$ with a phase configuration almost real, suggesting a marginal role of final state interactions in these channels.

Table 2: *Fit results for* D^+ *and* $D_s^+ \to K^+\pi^-\pi^+$ *with the isobar formalism.*

Decay channel	Fit fraction (%)	Phase ϕ_j (degrees)	Amplitude coefficient
$D^+ \to K^+\pi^+\pi^-$			
$\rho(770)K^+$	$39.43 \pm 7.87 \pm 8.15$	0 (fixed)	1 (fixed)
$K^*(892)\pi^+$	$52.20 \pm 6.84 \pm 6.38$	$-167.1 \pm 14.4 \pm 23.0$	$1.151 \pm 0.173 \pm 0.161$
$f_0(980)K^+$	$8.92 \pm 3.33 \pm 4.12$	$-134.5 \pm 31.4 \pm 41.9$	$0.476 \pm 0.111 \pm 0.143$
$K_2^*(1430)\pi^+$	$8.03 \pm 3.72 \pm 3.91$	$54.4 \pm 38.3 \pm 20.9$	$0.451 \pm 0.125 \pm 0.129$
$D_s^+ \to K^+\pi^+\pi^-$			
$\rho(770)K^+$	$38.83 \pm 5.31 \pm 2.61$	0 (fixed)	1 (fixed)
$K^*(892)\pi^+$	$21.64 \pm 3.21 \pm 1.14$	$161.7 \pm 8.6 \pm 2.2$	$0.747 \pm 0.080 \pm 0.031$
NR	$15.88 \pm 4.92 \pm 1.53$	$43.1 \pm 10.4 \pm 4.4$	$0.640 \pm 0.118 \pm 0.026$
$K^*(1410)\pi^+$	$18.82 \pm 4.03 \pm 1.22$	$-34.8 \pm 12.1 \pm 4.3$	$0.696 \pm 0.097 \pm 0.025$
$K_0^*(1430)\pi^+$	$7.65 \pm 5.0 \pm 1.70$	$59.3 \pm 19.5 \pm 13.2$	$0.444 \pm 0.141 \pm 0.060$
$\rho(1450)K^+$	$10.62 \pm 3.51 \pm 1.04$	$-151.7 \pm 11.1 \pm 4.4$	$0.523 \pm 0.091 \pm 0.020$

5 Conclusions

Dalitz plot analysis is giving interesting and promising results. FOCUS has carried out a pioneering work through the first application of the *K-matrix* approach to charm sector in the D^+ and $D_s^+ \to \pi^+\pi^-\pi^+$ decays. The results are extremely encouraging since the same parametrization of both two-body $\pi\pi$ resonances, coming from light-quark experiments, works for charm decay too. The Dalitz plot analysis of the doubly and singly Cabibbo suppressed decays D^+ and $D_s^+ \to K^+\pi^-\pi^+$ has been performed as well; the $D_s^+ \to K^+\pi^-\pi^+$ represents the first amplitude analysis for this channel.

References

1. J. Link *et al.*, Phys. Lett. **B585**, 200 (2004).
2. J. M. Link *et al.*, hep-ex/0407014.
3. V. V. Anisovich and A. V. Sarantsev, Eur. Phys. J. **A16**, 229 (2003).
4. E. M. Aitala *et al.*, Phys. Rev. Lett. **86**, 770 (2001).
5. S. Malvezzi, Nucl. Phys. Proc. Suppl. **126**, 220 (2004).

Frascati Physics Series Vol. XXXVI (2004), pp. 427–432
DAΦNE 2004: Physics at meson factories – Frascati, June 7-11, 2004
Selected Contribution in Plenary Session

TWIST: TRIUMF WEAK INTERACTION SYMMETRY TEST

David R. Gill *
TRIUMF, 4004 Wesbrook Mall, Vancouver BC Canada V6T 2A3

Abstract

TWIST, the TRIUMF Weak Interaction Symmetry Test, has taken data in the first simultaneous precision measurement of the muon decay parameters ρ, δ, and $P_\mu\xi$. The ultimate goal of the experiment is to determine each of these parameters to a few parts in 10^4. With this precision TWIST will confront several proposed extensions to the Standard Model. For example, TWIST will be sensitive to right-handed W bosons with masses up to 800 GeV without needing to make assumptions about the form of the right-handed CKM matrix.

1 Physics of TWIST

The Standard Model(SM) of the strong, weak and electromagnetic interactions, based on the gauge group $SU(3)_C \times SU(2)_L \times U(1)_Y$, has proved to be remarkably successful in describing the existing experimental observations. Despite this success the SM is universally believed to be an incomplete theory of nature.

* for TWIST collaboration

Normal muon decay $\mu \rightarrow e\nu\overline{\nu}$ is an ideal system with which to investigate the space-time structure of the weak interaction because the purely leptonic nature of this decay eliminates any uncertainties due to the internal structure of the particles or contributions from other interactions. A model independent description [1) 2)] of the energy and angular distributions of the $e^{\pm}$ emitted in the decay of polarized $\mu^{\pm}$ is provided in terms of four parameters, ρ, δ, η, and ξ. In the limit where the electron mass, neutrino mass and radiative corrections are neglected this spectrum is given by:

$$\frac{d\Gamma}{x^2 dx d(\cos\theta)} \propto 3(1-x) + \frac{2}{3}\rho(4x-3) \pm P_\mu \xi \cos\theta[1 - x + \frac{2}{3}\delta(4x-3)] \quad (1)$$

where θ is the angle between the muon polarization and the outgoing electron direction, $x = E_e/E_{max}$, and P_μ is the muon polarization. The fourth parameter, η, appears in this equation when the electron mass is included in the analysis.

Table 1 presents the current experimental results [3)] for the Michel parameters and the precision to which TWIST aims to determine them. In the Standard Model with pure (V-A) coupling, the four spectrum shape parameters take the specific values presented in this table, the current results are consistent with these values.

If one or more of the measured parameters differs from its expected value it will constitute an observation of physics outside the Standard Model. For example, in left-right symmetric models [4)], a deviation in ρ from $\frac{3}{4}$ would imply that the mixing angle, ζ, between the W_R and W_L bosons of these models is non zero. A deviation of ξ from 1 provides a measure of the ratio of the squares of the W_R and W_L boson masses, the ultimate TWIST precision yielding a lower limit for the W_R mass of

$$M_R > 800 \ \ \mathrm{GeV}/c^2$$

When comparing such a limit to those from other experiments it must be recalled that most experimental tests of left-right symmetric theories are sensitive to the form assumed for the right-handed CKM matrix. Equations 2, 3 and 4 display the sensitivity for β decay, $p\overline{p}$ collider and μ decay experiments respectively.

$$[\frac{g_R}{g_L}]^4 [\frac{V_{ud}^R}{V_{ud}^L}]^2 [\frac{M_L}{M_R}]^4 \quad (2)$$

Table 1: *The accepted values of the Michel parameters* [3] *along with the TWIST final precision and the Standard Model values.*

	Accepted Value	TWIST Final	SM Value
ρ	0.7518 ± 0.0026	±0.0002	$\frac{3}{4}$
δ	0.7486 ± 0.0026 ± 0.0028	±0.0003	$\frac{3}{4}$
$P_\mu\xi$	1.0027 ± 0.0079 ± 0.0030	±0.0004	1
η	-0.007 ± 0.013	±0.01	0

$$[\frac{g_R}{g_L}]^2[\frac{V_{ud}^R}{V_{ud}^L}]^2 Function[\frac{M_L}{M_R}] \tag{3}$$

$$[\frac{g_R}{g_L}]^4[1+[\frac{V_{ud}^R}{V_{ud}^L}]^2][\frac{M_L}{M_R}]^4 \tag{4}$$

These formula display that there is a complementarity of results from such experiments, for example if TWIST results were to indicate a W_R mass in a range where the collider searches see nothing it would mean that V_{ud}^R may be very small.

The discussion thus far has assumed that the right-handed neutrinos are light, so they are not kinematically suppressed in muon decay. In models with general V, A interactions, deviations from pure $V-A$ can be described by three parameters, g_{LR}^V, g_{RL}^V, and g_{RR}^V, that specify the coupling strengths for right-handed electrons and muons. In the limit of light right-handed neutrinos lepton universality requires $|g_{LR}^V| = |g_{RL}^V|$, so δ retains its Standard Model value of 0.75. Alternative patterns for the three vector coupling constants appear in left-right symmetric models if one or both of the right-handed neutrinos are heavy. For example, if the right-handed muon neutrino is light, while the right-handed electron neutrino is heavy, g_{RR}^V and g_{RL}^V must both remain zero, while g_{LR}^V can be non-zero. This changes the relationships between ξ and ρ and ζ

and M_R, and permits δ to deviate from its Standard Model value. A similar situation arises if only the right-handed electron neutrino is light. In fact, in this case, Herczeg noted [4] that $P_\mu \xi\delta/\rho$, the quantity measured by Strovink *et al.* [5], must remain identically equal to its Standard Model value of 1, while ξ, δ, and ρ may separately deviate from their respective Standard Model values. *This emphasizes the importance of a comprehensive investigation of all of the Michel parameters over a broad energy range, as is provided by TWIST.* If both of the right-handed neutrinos are heavy, g^V_{LR}, g^V_{RL} and g^V_{RR} must all remain zero.

TWIST will also provide information on the more general extensions of the SM that include scalar and tensor interactions. For example, the linear combination

$$Q^\mu_R = \frac{1}{2}[1 + \frac{1}{3}\xi - \frac{16}{9}\xi\delta] \tag{5}$$

provides a model independent measure of the total right-handed contributions to muon decay.

The above discussion, while limited, indicates that an improved measurement of the Michel parameters of muon decay will have a significant impact on our understanding of the space time structure of the electroweak interactions and in the absence of non SM results will impose strict limits on new particles and proposed extensions of the Standard Model.

2 Experiment

The TWIST detector, which is shown Side-View in Figure 1, consists of 44 high precision drift chamber planes [6] and 12 MWPC planes.

It is centered in a solenoid magnet that provides a uniform 2T field. The surface muon beam, which is highly polarized, enters from the left as shown and the detector components are thick enough to bring these μ's to rest in the stopping target at the center. The drift chamber planes shown here are at right angles to the magnetic field and each consists of 80 wires at 4mm spacing. The positions of the 5000 wires are known in longitudinal and transverse positions to better than 5 parts in 10^5. The decay positrons spiral, either to the left or right in this figure, through the drift chambers producing hits on the wires that are recorded by TDCs. These helical tracks are later analyzed to precisely determine the positron energy and angle.

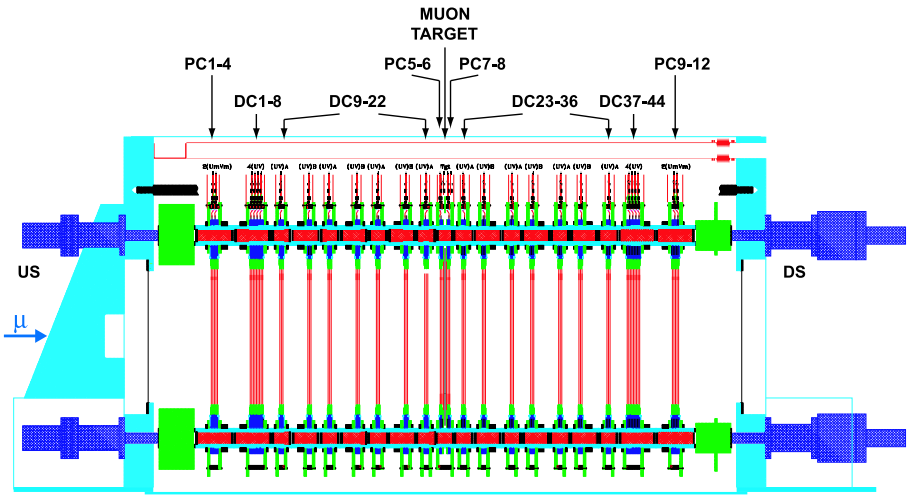

Figure 1: *Schematic of TWIST detector showing longitudinal arrangement of chamber planes. The stopped μ decays in the target at the center.*

The linearity of the decay spectrum in the shape parameters, as shown in Eq. 1, allows the employment of a blind analysis technique. The measured energy-angle spectrum is fit to the sum of a Monte Carlo generated spectrum for which the shape parameters are hidden, together with additional Monte Carlo distributions that describe the dependence on $\Delta\rho$, $\Delta\eta$, $\Delta\delta$, and $\Delta P_\mu \xi$. The Monte Carlo spectra are generated including the effects of the electron mass, plus the first- and many second-order radiative corrections not shown in Eq. 1.

3 Status

TWIST took data in the 2002 and 2003 with the goal of determining ρ and δ to 10^{-3}. TWIST is a systematics dominated experiment. Thus most of the beam time was used to collect data related to possible systematic effects with each effect amplified as much as practical. A total of 6×10^9 events were recorded to tape in sets of 3×10^8 events, each set being sufficient to determine ρ and δ to $\approx 6 \times 10^{-4}$. These independent sets explored the TWIST sensitivity to several categories of effects due to the beam properties, the detector performance, the magnetic field, the upstream-downstream symmetry of the system and overall system stability. Additional sets were taken to provide data to validate the quality of the GEANT-based Monte Carlo simulation.

The data analysis is now approaching completion and the results are very encouraging for a determination of ρ and δ to $\approx 10^{-3}$ level. The expectation

is that the box containing the hidden values of the shape parameters will be opened shortly and that the first physics results from TWIST will be published in the fall of 2004.

4 Acknowledgments

This work was supported in part by the Natural Sciences and Engineering Research Council and the National Research Council of Canada and by the U.S. Department of Energy.

References

1. L. Michel, Proc. Phys. Soc. **A63**, 514 (1950); C. Bouchiat and L. Michel, Phys. Rev. **106**, 170(1957).
2. T. Kinoshita and A. Sirlin, Phys. Rev. **108**, 844(1957).
3. K.Hagiwara *et al.*, Phys. Rev. **D66**, 010001(2002).
4. P. Herczeg, Phys. Rev. D34, 3449 (1986).
5. A.Jodidio *et al.*, Phys.Rev. D34(1986)1967-1990, ibid. D37(1988)237-238.
6. Yu. Davydov *et al.*, Nucl. Instrum. Methods **A461**, 68(2001).

Frascati Physics Series Vol. XXXVI (2004), pp. 433–438
DAΦNE 2004: Physics at meson factories – Frascati, June 7-11, 2004
Selected Contribution in Plenary Session

FLAVOR DECOMPOSITION OF THE NUCLEON'S SPIN AT HERMES

L. A. Linden Levy *
University of Illinois, 1110 W. Green Street, Urbana, IL 61801 USA

Abstract

Since 1995, the HERMES collaboration has measured inclusive and semi-inclusive double-spin asymmetries on polarized ^{3}He, hydrogen and deuterium targets in the kinematic range $0.023 < x < 0.6$ and 1 GeV^2< Q^2 < 10 GeV^2. With the installation of a ring imaging Čerenkov detector in 1998, the asymmetries of charged pions and kaons could be determined for the first time. Using the measured asymmetries, the polarized quark densities are extracted for all flavors separately in a leading order QCD analysis. This includes a determination of the difference of the *u-sea* and *d-sea* quark distributions as well as the first measurement of the strange *sea* polarization.

*On behalf of the HERMES collaboration

1 Introduction

Since the discovery of deep inelastic scattering (DIS) in the late 1960s at SLAC [1)], the technique has proven to be one of the most fruitful methods for studying the partonic structure of the nucleon. DIS interactions occur when a highly virtual photon interacts electro-magnetically with a nucleon so violently that it breaks up the nucleon. When this occurs the interaction can be approximated as the photon interacting with an individual constituent quark. Polarized DIS, in particular, allows one to study the partonic spin structure of the target. The first polarized DIS measurements, made by the EMC collaboration [2)], showed that only a small fraction of the total spin of the proton comes from the quarks. Experiments that followed at SMC, E143, E142, etc. [3)] found the contribution to be $20\% - 30\%$ rather than the $\simeq 60\%$ that is expected from relativistic quark model calculations [4)]. This interesting puzzle was dubbed the "spin crisis" and has launched many experimental and theoretical efforts to understand how the spin and orbital momentum of the partons (quarks and gluons) sum to yield the spin of the proton.

In DIS the measured kinematic quantities are the momenta of the beam lepton $k = (k^0, \vec{k})$, the scattered lepton $k' = (k'^0, \vec{k'})$, and, in the case of semi-inclusive (SI) DIS, the measured hadron $p' = (p'^0, \vec{p'})$ (see fig. 1). In the lab frame, the four momentum of the target nucleon collapses to $p = (M, \vec{0})$ for a fixed target. The common kinematic quantities used to characterize SIDIS interactions are: $Q^2 = -(k - k')^2$, the negative four momentum transfer of the virtual photon; $W^2 = M^2 + M\nu - Q^2$, the invariant mass of the final state; $x = Q^2/(2M\nu)$, the Bjorken scaling variable, where $\nu = (k^0 - k'^0)$; and $z = p'^0/\nu$, the fraction of the photon energy carried by the measured hadron.

In the SIDIS case, the measured hadron provides a *flavor tag*, thereby conveying some information about the flavor of the struck quark to the experimenter. The HERMES experiment uses the polarized 27.5 GeV positron (or electron) beam of the HERA accelerator and pure polarized gaseous targets of hydrogen and deuterium to measure inclusive and SI lepton-nucleon double spin asymmetries ($A_\parallel$, $A_\parallel^h$). The lepton-nucleon asymmetry is defined as the relative difference, in scattering cross section, for the beam and target helicity being aligned and anti-aligned. This can be related to the photon-quark

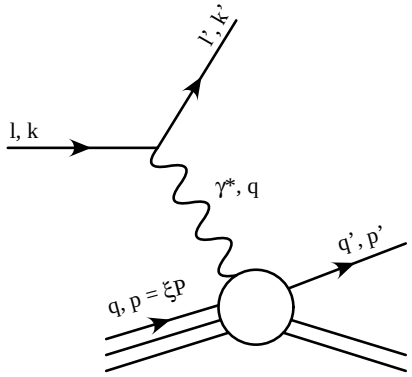

Figure 1: *Schematic depiction of DIS. In this process the virtual photon ($\gamma*$) breaks apart the nucleon and probes the interior quark structure.*

asymmetry and the structure function g_1 as follows:

$$A_1(x,Q^2) \simeq \frac{A_\parallel}{D(1+\eta\gamma)} \overset{g_2=0}{\simeq} \frac{g_1}{F_1} \tag{1}$$

where D represents the depolarization at the photon lepton vertex and η, γ are (small) kinematic factors. In the parton model of DIS the structure functions of the polarized (unpolarized) cross sections can, in LO QCD, be represented by a charge-weighted sum of the polarized (unpolarized) parton distribution functions (PDFs):

$$g_1 = \frac{1}{2}\Sigma_q e_q^2 \Delta q(x,Q^2) \quad (\ F_1 = \frac{1}{2}\Sigma_q e_q^2 q(x,Q^2)\ ) \tag{2}$$

where the sum runs over all quark and anti-quark flavors and the polarized (unpolarized) PDFs are given by the difference (sum) $\Delta q = q^+ - q^-$ ($q = q^+ + q^-$) between the density of quarks with spin along the direction of the nucleon spin and those with opposite helicity. In the SIDIS case the asymmetry can be written as:

$$A_1^h \sim \frac{\Sigma_q e_q^2 \Delta q(x,Q^2) \int_{z_{min}}^{z_{max}} D_q^h(z,Q^2)}{\Sigma_{q'} e_{q'}^2 \Delta q'(x,Q^2) \int_{z_{min}}^{z_{max}} D_{q'}^h(z,Q^2)} = \Sigma_q P_q^h(x) \frac{\Delta q(x)}{q(x)} \tag{3}$$

where $D_q^h(z)$ is the fragmentation function which parameterizes our ignorance of the dynamics involved in re-hadronization of the struck quark. It gives us the probability that when a quark q, is struck it will end up in a hadron of type h with fractional energy z. Additionally, the last equality sign has introduced the notion of a purity $P_q^h(x)$, which represents the probability that a measured hadron h came from a struck quark of flavor q. The suppression of the Q^2

dependence in this expression is the result of integrating each quantity over the available range of Q^2 in any x bin. In the HERMES analysis, these purities are calculated using a JETSET [5] based monte-carlo simulation, which is tuned to reproduce unpolarized data [6]. The only inputs to the simulation are unpolarized parton distribution functions from inclusive fits and the Lund string model of fragmentation. For the hydrogen data set, only pions could be identified with a threshold Čerenkov detector, but with the addition of a ring imaging Čerenkov detector in 1998, both pions and kaons could be identified for the deuterium target.

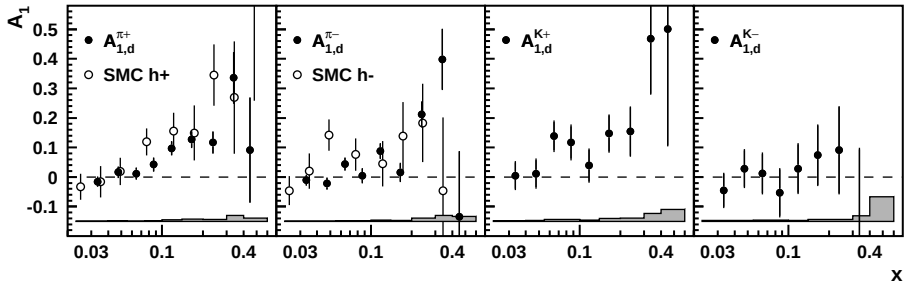

Figure 2: *HERMES results for SI pion and kaon double-spin asymmetries (A_1^h) on the deuteron. The positive and negative hadron asymmetries from the SMC measurement are also shown. The error band (bar) represents the systematic (statistical) uncertainty.*

2 Inclusive and Semi-Inclusive Asymmetries

The published HERMES data [7] on semi-inclusive asymmetries for the proton (not shown here) and the deuteron (fig. 2) targets is based on 1.8 and 6.5 million DIS respectively. In order to increase the probability that a measured final state hadron originated from a DIS event, the kinematic cuts $Q^2 > 1.0$ GeV^2 and $W^2 > 10$ GeV^2 are made. Semi-inclusive hadrons were selected by requiring $0.2 < z < 0.8$ and $x_F \simeq 2p'_L/W > 0.1$, where p'_L is the fraction of the hadron's momentum that lies along the virtual photon direction in the photon-nucleon center-of-mass frame. Setting a lower bound on z and x_F suppresses hadrons from the target region, while the upper limit on z eliminates exclusive events.

The quark polarizations are extracted by combining the inclusive and semi-inclusive asymmetries from both targets to over-constrain a multidimen-

sional χ^2 calculation (eq. 4) which arises from eq. 1.

$$\chi^2 = (\vec{A} - \mathbf{P}\vec{Q})^T \nu_A^{-1} (\vec{A} - \mathbf{P}\vec{Q}) \tag{4}$$

where the vector of PDFs is given by:

$$\vec{Q} = (\vec{q}_1, \vec{q}_2, ...\vec{q}_9) \quad \vec{q}_i = (\frac{\Delta u(x_i)}{u(x_i)}, \frac{\Delta d(x_i)}{d(x_i)}, \frac{\Delta \bar{u}(x_i)}{\bar{u}(x_i)}, \frac{\Delta \bar{d}(x_i)}{\bar{d}(x_i)}, \frac{\Delta s(x_i)}{s(x_i)}) \tag{5}$$

In eq. 4 the χ^2 is calculated for nine x bins and every asymmetry simultaneously, which leads to 45 free parameters for the minimization. Six out of 45 free parameters are lost by fixing the sea distributions to zero for $x > 0.3$. In contrast to LO QCD fits to inclusive data, this technique does not assume a symmetric sea, except for $\Delta s = \Delta \bar{s}$.

The x-weighted polarized parton distributions are shown in fig. 3. For this figure, the ratios $\Delta q/q$ were multiplied by the CTEQ5L unpolarized PDFs at a common $Q^2 = 2.5$ GeV^2 in order to isolate the polarized PDFs. The u distribution is positive and large above $x = 0.1$, while the d polarization is smaller and negative over the entire x range. All of the sea distributions are compatible with zero, which is particularly interesting in the strange sector where a small negative polarization is found from inclusive LO QCD fits.

In addition to the standard extraction, an attempt was made to extract the polarized light sea asymmetry which is predicted by the chiral quark soliton model and may be expected in light of its unpolarized counterpart. The result is shown in fig. 3 as compared to the theoretical prediction. Unfortunately, the uncertainty in the result does not prove the existence or lack of a polarized light sea asymmetry.

References

1. M. Breidenbach *et al*, Phys. Rev. Lett. **23**, 935 (1969).
2. J. Ashman *et al*, Phys. Lett. **B 206**, 364 (1988).
3. P. L. Anthony *et al*, Phys. Lett. **B 493**, 19 (2000).
4. J. Ellis and R. Jaffe, Phys. Rev. **D 9**, 14444 (1974).
5. T. Sjöstrand *et al*, Comp. Phys. Comm. **135**, 238 (2001).

6. A. Hillenbrand, Tuning of the Lund model for fragmentation functions and purities, in: Proc. DIS 2003 (St. Petersburg, Apr 2003).

7. A. Airapetian *et al*, Phys. Rev. Lett. **92** 012005 (2004).

8. B. Dressler *et al*, Eur. Phys. J. **C 14**, 147 (2000).

9. M. Glück *et al*, Phys. Rev. **D 063**, 094005 (2001).

10. J. Blümlein and H Böttcher, Nucl. Phys. **B 636**, 225 (2002).

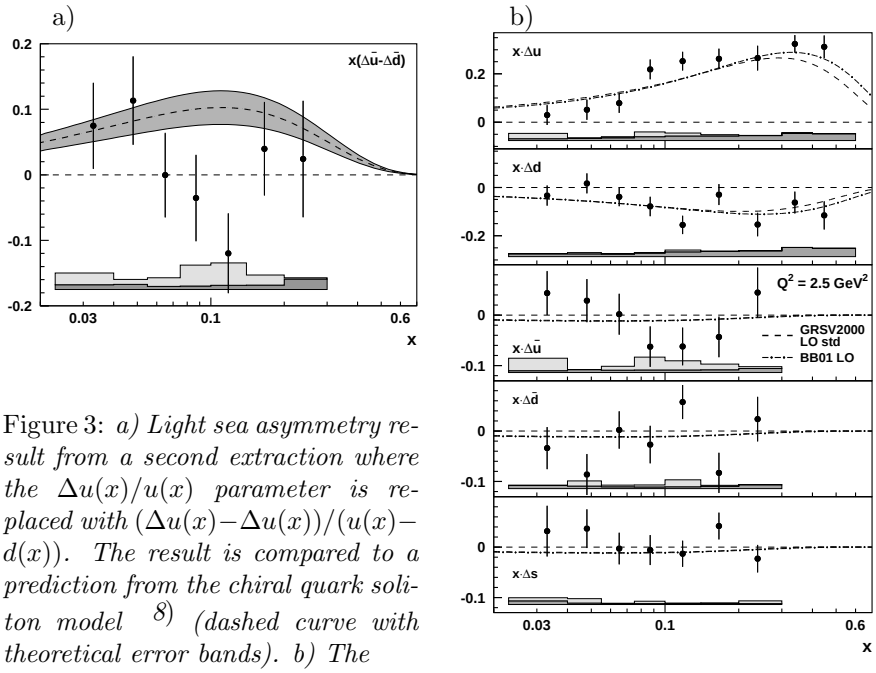

Figure 3: *a) Light sea asymmetry result from a second extraction where the* $\Delta u(x)/u(x)$ *parameter is replaced with* $(\Delta u(x)-\Delta u(x))/(u(x)-d(x))$*. The result is compared to a prediction from the chiral quark soliton model* [8] *(dashed curve with theoretical error bands). b) The x-weighted polarized PDFs* $x\Delta q(x)$ *extracted from the HERMES inclusive and semi-inclusive asymmetries on polarized hydrogen and deuterium targets at a common* $Q^2 = 2.5\ GeV^2$*. The curves represent LO QCD fits to inclusive data from* [9] *(dashed) and* [10] *(dot-dashed).The light error bands represent the systematic error arising from uncertainties in the fragmentation model and the dark band represents experimental uncertainties.*

Frascati Physics Series Vol. XXXVI (2004), pp. 439–443
DAΦNE 2004: Physics at meson factories – Frascati, June 7-11, 2004
Short Talk in Plenary Session

$K \to 3\pi$ DECAYS IN CHIRAL PERTURBATION THEORY

Fredrik Borg
Department of Theoretical Physics, Lund University,
Sölvegatan 14A, SE - 223 62 Lund, Sweden

1 Introduction

A kaon decaying into three pions is an example of a weak process. However, since the quarks are confined into mesons, the strong interaction also plays an important part. The reaction is a low-energy one, meaning that it takes place in the non-perturbative region of QCD. In that region perturbative QCD doesn't give you any answers and other methods have to be used. The one we use is called Chiral Perturbation Theory.

2 Chiral Perturbation Theory

ChPT is an effective field theory describing the low-energy interactions of the kaons, the pions and the eta. It can be used for strong as well as non-leptonic weak interactions. The Chiral Lagrangian is based on the spontaneous breaking of chiral symmetry.

Chiral symmetry is the separate symmetry between the left- and right-handed quarks. In the theory only the u, d and s quarks are included which means that the symmetry group is $SU(3)_L \times SU(3)_R$. This symmetry is spon-

$$
\begin{aligned}
K_L &\rightarrow \pi^0\,\pi^0\,\pi^0 \\
K_L &\rightarrow \pi^+\,\pi^-\,\pi^0 \\
K_S &\rightarrow \pi^+\,\pi^-\,\pi^0 \\
K^+ &\rightarrow \pi^0\,\pi^0\,\pi^+ \\
K^+ &\rightarrow \pi^+\,\pi^+\,\pi^-
\end{aligned}
$$

taneously broken by the vacuum condensate into $SU(3)$. Since the symmetry is only *approximate* (exact if $m_u = m_d = m_s = 0$), this generates 8 *light* (not massless) Goldstone particles, identified as the kaons, pions and eta. From the knowledge of interactions between Goldstone particles one then constructs the Chiral Lagrangian.

The Chiral Lagrangian is organized in terms of importance. However, since it deals with low-energy processes, α_S can not be used for this purpose. Instead it is written as an expansion in p and m, the momenta and the masses of the pseudoscalars (K, π, η). Properly normalized these quantities are small and can be used as perturbation expansion parameters. Lowest order then means p^2 and m^2 and next-to-leading order p^4, m^4, p^2m^2 and so on. If one includes also isospin breaking, the unit charge, e, is also considered an expansion parameter.

3 Isospin Symmetry

Calculations are often performed in the isospin limit, where the u and d quarks are treated as being identical. In practice this means setting $m_u = m_d$ and neglecting electromagnetism.

In our first paper [1)] the calculation was made in the isospin limit. In the second paper [2)] we took into account strong isospin breaking, ie. the quark mass difference $m_u - m_d$ as well as the local electromagnetic effects. Work is in progress to evaluate the other electromagnetic corrections as well.

4 Results

There are five different CP-conserving decays of the type $K \rightarrow 3\pi$. The K^- decays are not treated since they are counterparts to the K^+ decays.

A full isospin limit fit was made in [1)] taking into account all data pub-

lished before May 2002. One of the reasons for the further investigation of isospin breaking effects is to see whether isospin violation can solve the discrepancies in the quadratic slope parameters found there. A new full fit will be done after all the electromagnetic contributions have been included in the amplitudes (work in progress).

4.1 Results with and without strong isospin breaking

Our main result up to now is the comparison between the amplitudes in the isospin limit and including first order strong isospin breaking. In Fig. 1 we show the phase space boundaries for the five different decays and the three curves along which we compared the squared amplitudes with and without first order strong isospin breaking

In general the differences are of the size to be expected from this type of isospin breaking. For $K_L \to \pi^0\pi^0\pi^0$ the central value of the amplitude squared increases by about 3% when strong isospin breaking is included. The change in the quadratic slope is similar but the total variation over the Dalitz plot is small so the total decay rate increases by about 3% as well. The squared amplitude $K_L \to \pi^+\pi^-\pi^0$ increases by about 2.5%. The decay rate and the changes in the Dalitz plot slopes are of similar size. For the decay $K_S \to \pi^+\pi^-\pi^0$ the amplitude in the center of the Dalitz plot vanishes because of CP-asymmetry. The amplitude and the slopes increase by about 3%, see Fig. 2. The decay $K^+ \to \pi^0\pi^0\pi^+$ has the largest increase. The squared amplitude in the center changes by about 11%. The linear slopes decrease somewhat leading to an increase of about 8% to the total decay rate when compared with the isospin conserved case. The decay $K^+ \to \pi^+\pi^+\pi^-$ has a change of about 7.5% upwards in the center of the Dalitz plot and a similar change in the decay rate. The slopes decrease somewhat. For more figures and detailed results, see [2].

5 Conclusions

We have calculated the $K \to 3\pi$ amplitudes to next-to-leading order in ChPT. A first calculation was done in [1] in the isospin limit, but we have now also included effects from $m_u \neq m_d$ and local electromagnetic isospin breaking in [2]. This was done partly because it is interesting in general to see the possible importance of isospin breaking in this process, but also to investigate whether

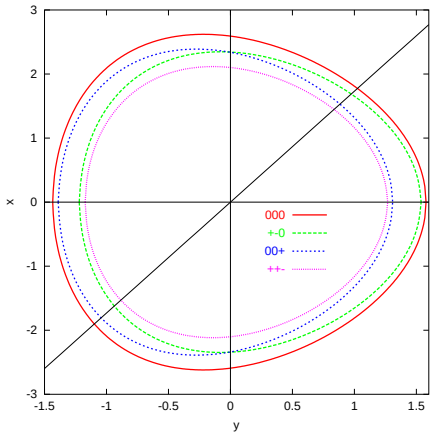

Figure 1: em The phase space boundaries for the five different decays and the curves along which we will compare the amplitudes.

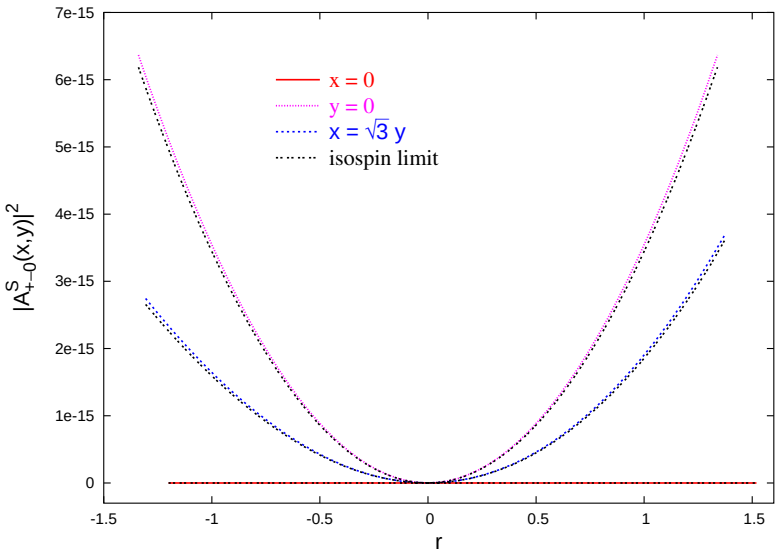

Figure 2: $K_S \to \pi^+\pi^-\pi^0$ *with and without strong isospin breaking.*

isospin violation will improve the fit to experimental data made in [1]. We have tried to estimate the effects of the breaking by comparing the squared amplitudes with and without isospin violation. The effect seems to be at a few percent level, and probably not quite enough to solve the dicrepancies. However, to really investigate this a new full fit has to be done, including the explicit photon diagrams and the new data published after [1] as well. This is work in progress and will be presented in future papers.

6 Acknowledgements

The program FORM 3.0 has been used extensively in these calculations. This work is supported in part by the Swedish Research Council and European Union TMR network, Contract No. HPRN-CT-2002-00311 (EURIDICE).

References

1. J. Bijnens, P. Dhonte and F. Persson, Nucl. Phys. B 648 (2003) 317, [hep-ph/0205341].

2. J. Bijnens and F. Borg, to be published in Nucl. Phys. B, [hep-ph/0405025].

Frascati Physics Series Vol. XXXVI (2004), pp. 445–449
DAΦNE 2004: Physics at meson factories – Frascati, June 7-11, 2004
Short Talk in Plenary Session

FINAL–STATE RADIATION IN ELECTRON–POSITRON ANNIHILATION INTO PION PAIR

O . Shekhovtsova *
NCS KIPT, Akademicheskaya 1, Kharkov 61108, Ukraine
shekhovtsova@kipt.kharkov.ua

1 Introduction

In this article the final-state radiation (FSR) of the hard photon in $e^-(p_1) + e^+(p_2) \to \gamma^*(Q) \to \pi^+(p_+) + \pi^-(p_-) + \gamma(k)$ reaction is considered in the framework of ChPT with vector ρ and axial–vector a_1 mesons [1)] (the FSR diagrams are shown in Fig.1).

Our consideration of FSR is motivated by the necessity to study model dependence of the next-to-leading order hadronic contribution $a_\mu^{had,\gamma}$ to anomalous magnetic moment (AMM) of the muon ($a_\mu^{had,\gamma}$ is the hadronic contribution, where additional photon is attached to hadrons). Also FSR is a main unre-

* co–autors: S. Dubinsky, A. Korchin and N. Merenkov – *NCS KIPT, Ukraine;* G. Pancheri– *INFN Labaroratori Nazionale di Frascati, Italy*

stricted background to scan the hadronic cross–section at meson factories by the radiative return method [2]. In this method only ISR (initial-state radiation) events have to be chosen and the FSR processes have to be rejected. Different methods have been suggested to separate ISR and FSR contributions for the dominant hadronic channel at low energies – the pion-pair production. One of them is to choose kinematics, where photon is radiated outside the narrow cones along the momenta of the pions. In these conditions the FSR contribution is suppressed. If the FSR background can be reliably calculated in some theoretical model then it can be subtracted from experimental cross section of $e^+e^- \to \pi^+\pi^-\gamma$ or incorporated in the Monte Carlo event generator used in analysis. Finally, the theoretical predictions for FSR can be tested by studying the C–odd interference of ISR and FSR [3].

The FSR cross section has been calculated [3] in framework of the scalar QED (sQED), in which the pions are treated as point-like particles, and the resulting amplitude is multiplied by the pion electromagnetic form factor $F_\pi(s)$ evaluated in VMD model (s is the total e^+e^- energy squared) to account for the pion structure. Although sQED in some cases works well [2, 3], it is clear that sQED is a simplified model of a complicated process, which may include excitation of resonances, loop contributions, etc. In view of the high requirements for the accuracy of theoretical predictions for AMM, further studies of the FSR contribution are necessary.

2 Results of calculation

In view of the restricted space of this contribution only the results of calculations are presented (for details see Ref. [4]).

First, the charge asymmetry [3] proportional to the interference of ISR and FSR is calculated for the so-called collinear kinematics in which the hard photon is radiated inside a narrow cone with the opening angle $2\theta_0$ ($\theta_0 \ll 1$) along the direction of initial electron. In Fig.1 we show the asymmetry dependence on pion polar angle at fixed two–pion invariant mass q^2. It follows that the asymmetry changes sign at about $q^2 = 0.5$ GeV^2. At all pion angles the difference between sQED and ChPT shows up only at small values of q^2 or, equivalently, at high photon energies. Thus only at high photon energies the contribution from a_1 intermediate meson (see diagrams with a_1–meson in Fig.2) is sizable. For large values of q^2 the difference between predictions of

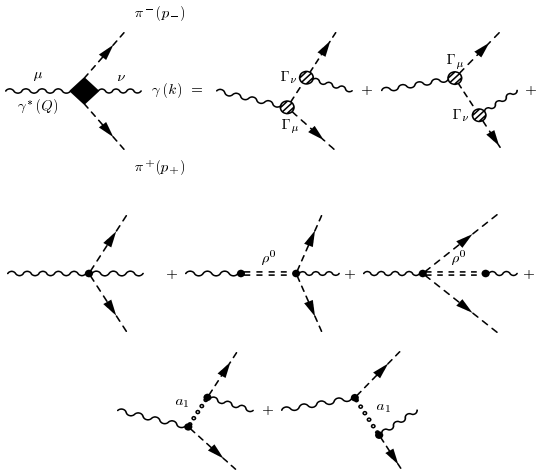

Figure 1: *Diagrams for FSR in the framework of ChPT.*

sQED and full calculation in ChPT is small: for $q^2 \geq 0.6$ GeV^2 it is less than 1% (the dashed and solid lines almost coincide in Fig.1). Taking into account that the asymmetry itself is less than 10^{-2}, the experimental observation of such deviations in the energy region $q^2 \geq 0.6$ GeV^2 is problematic.

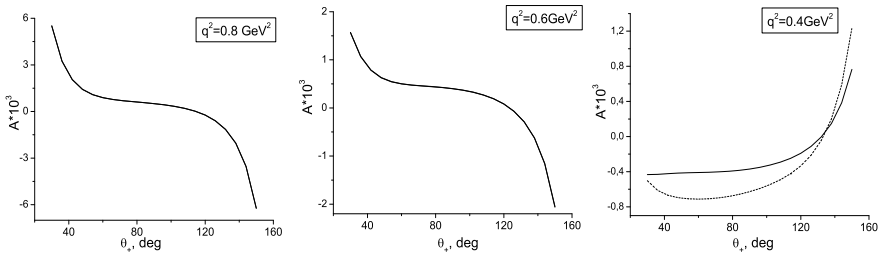

Figure 2: *Charge asymmetry as a function of pion polar angle at fixed q^2 for $s = 1$ GeV^2. The solid line corresponds to sQED, the dashed line – the full result in ChPT.*

Second, we apply the result of Ref. [4] to evaluation of $a_\mu^{\pi\pi,\gamma}$. It appears that the additional contributions to $a_\mu^{\pi\pi,\gamma}$ arising in ChPT are very small compared with sQED result (here only the radiation from hard photon ($\omega \geq E_{cut}$) is taken into account). Even for $E_{cut} = 200$ MeV the ChPT result differs from

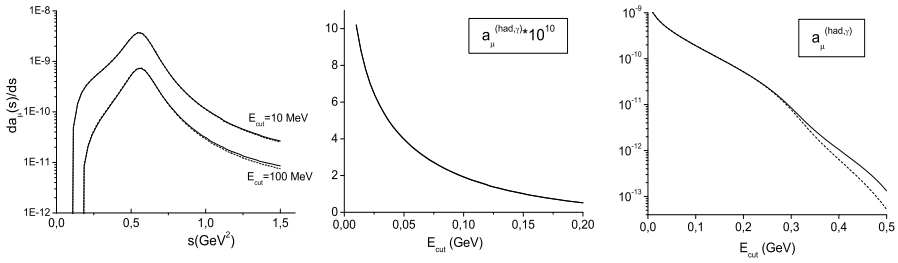

Figure 3: *Differential contribution $a_\mu^{\pi\pi,\gamma}$ (left panel). Integrated contribution to $a_\mu^{\pi\pi,\gamma}$ as a function of E_{cut} (central and right panels). Here $s_{max} = 1.5$ GeV^2. Notations for the curves are the same as in Fig.2.*

the sQED one by only 3.5%(see the solid and dashed lines in Fig.3 which almost coincide). These small deviations are not surprising. First, at fixed value of s the low–energy photon region, which is described in a similar way by both models, dominates in $a_\mu^{\pi\pi,\gamma}$. Second, the main contribution to $a_\mu^{\pi\pi,\gamma}$ comes from the region of the ρ–resonance, which is treated in the same manner in sQED and ChPT via VMD model.

At the same time, with increasing the photon energy sQED losses its predictive power. This is demonstrated in Figs.2 and 3 (right panel). In this region the contribution from a_1–meson is considerable and has to be taken into account. For example, at the photon energy about 500 MeV the deviation from sQED reaches 60%. However, this deviations (which are of the order of 10^{-12}) are beyond the accuracy of the present measurements of the muon AMM.

3 Conclusions

We demonstrated that the model dependence of the two–pion contribution to $a_\mu^{had,\gamma}$ is weak, and the value of $a_\mu^{had,\gamma}$ is not sensitive to chiral dynamics beyond the ρ–meson dominance. As for the charge asymmetry, its model dependence can be observed experimentally only for q^2 near the two-pion threshold region: $4m_\pi^2 \leq q^2 < 0.4$ GeV^2.

Therefore, in the bulk of energies up to 1 GeV, sQED is sufficient to describe the FSR contribution to both $a_\mu^{had,\gamma}$ and C–odd asymmetry. To observe deviations from sQED the existing experimental error bars for $a_\mu^{had,\gamma}$ have to

be reduced by at least one order of magnitude. Possibly, the more complicated many–particle channels in e^+e^- annihilation are more sensitive to the chiral dynamics.

References

1. G. Ecker *et al*, Nucl. Phys. **B321**, 311 (1989); G. Ecker *et al*, Phys. Lett. **B223**, 311 (1989).
2. A.Aloisio et al., The KLOE Collaboration, arXiv:hep-ex/0312056.
3. H. Czyz *et al*, Eur. Phys. J **C33**, 333 (2004).
4. S. Dubinsky *et al*, in preparation.

Frascati Physics Series Vol. XXXVI (2004), pp. 451–455
DAΦNE 2004: Physics at meson factories – Frascati, June 7-11, 2004
Short Talk in Plenary Session

NEW DATA ON $e^+e^- \to \pi^+\pi^-$ CROSS SECTION WITH CMD-2 IN ENERGY RANGE $\sqrt{s}$=0.37 - 1.38 GeV

F. Ignatov *
The Budker Institute of Nuclear Physics, Novosibirsk, Russia

1 Introduction

The measurement of the $e^+e^- \to \pi^+\pi^-$ cross section is important for a number of physical problems. Along with the most straightforward usage for determination of the parameters of the $\rho(770)$ meson and its radial excitations, this process gives the dominant contribution to the hadronic part of the muon anomalous magnetic moment (a_μ). In our previous papers [1, 2] we reported results of the determination of the $e^+e^- \to \pi^+\pi^-$ cross section in the energy region $\sqrt{s} = 0.6 \div 0.96$ GeV. In this publication we present preliminary results based on integrated luminosity of 30 pb^{-1} collected in the whole energy range covered by VEPP-2M.

*On behalf of the CMD-2 Collaboration

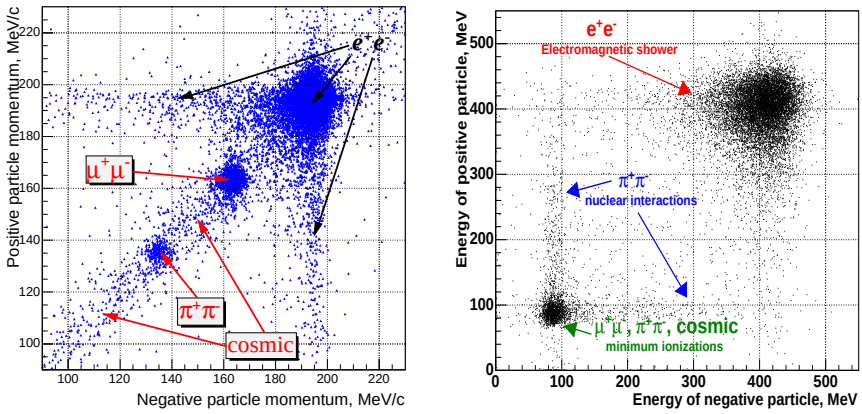

Figure 1: *Left: Particle momenta distribution at* $\sqrt{s} = 0.39$ *GeV. Right: Energy deposition distribution at* $\sqrt{s} = 0.98$ *GeV.*

The $\pi^+\pi^-$ cross section was studied at the VEPP-2M [3] electron-positron collider with the beam energy from 180 to 700 MeV and maximum luminosity $3 \cdot 10^{30}\text{cm}^{-2}\text{sec}^{-1}$. The pion form factor measurement was one of the major goals of the CMD-2 experiment which is described in some detail in works [4, 5]. 670 thousands $\pi^+\pi^-$ events were detected in 118 energy points.

2 Selection

The main selection criteria are based on particle parameters measured in the drift chamber allowing efficient rejection of non-collinear events. For particle separation either energy deposition in the calorimeter (at c.m. energies above 0.6 GeV) or particle momenta measured in the drift chamber (at c.m. energies below 0.6 GeV) were used (Fig. 1). Above 0.6 GeV the number of cosmic events was determined from the spatial distribution of vertex, while the number of muon events was fixed relative to the number of e^+e^- events according to QED. In both energy ranges the separation was based on the minimization of unbinned likelihood function. The number of selected events is shown in Table 1. The pion form factor is presented in Fig. 2. The fit was performed according to the Gounaris-Sakurai parametrization with the $\rho(770)$, ω, $\phi(1020)$, $\rho(1450)$ and $\rho(1700)$ mesons included.

Table 1: *Number of events.*

e^+e^-	$\mu^+\mu^-$	$\pi^+\pi^-$	cosmic	number of points	energy range,$\sqrt{s}$	
number of events, 10^3						
164	16	114	17	43	610 ÷ 960 MeV	94-95 scan [1)]
96	9	4	5	10	370 ÷ 520 MeV	96 scan
710	65	520	19	29	600 ÷ 960 MeV	98 scan
840	81	33	14	36	980 ÷ 1380 MeV	97 scan

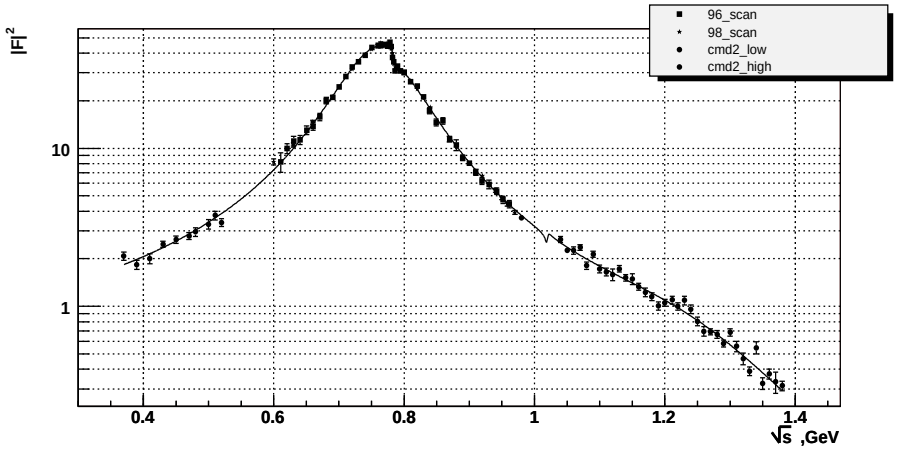

Figure 2: *Pion Form Factor.*

3 Systematic

The overall systematic error is estimated to be 0.6% for ρ-meson region in 96'scan and 1.1% in 98'scan, 1.2% at energies below 0.6 GeV due to a more complicated separation procedure, and 1.3÷5.0% for energies above 1 GeV because the uncertainty in the number of muon events gives a direct contribution to a systematic error of the pion form factor (N_μ/N_π ratio changed from 1 to 7 at $\sqrt{s} = 1 \div 1.4$ GeV). The contributions to systematic error are shown in Table 2.

The fiducial volume is determined by a measurement of polar angle Θ in the drift chamber. Calibration of the drift chamber along the beam axis is based on the Z-chamber which has a systematic error of z-coordinate measurement

about 0.1 mm, that corresponds to a systematic error in the form factor near ρ-meson about 0.2%.

The reconstruction efficiency was measured using the experimental data themselves. It was found to be within the 98-100% range at all energies and, within the statistical accuracy, is the same for all types of collinear events. Therefore, it cancels in the form factor calculation. The systematic error of the cancellation for different type of particles was estimated to be better than 0.2%. In 98'scan the degradation of the drift chamber was observed and preliminary conservative estimation of the systematic error is about 0.9%.

Pions could be lost by decays in flight and by nuclear interactions with the detector material. The correction for pion losses was calculated by full detector simulation using FLUKA [6] package for simulation of nuclear interaction. The value of nuclear interaction correction varies from 1.7% to 0.6%. The systematic error of the correction was estimated from uncertainty of experimental data on nuclear cross-sections used in FLUKA.

Radiative corrections were calculated according to Ref. [7] with a declared accuracy of 0.2%.

The increase of systematic error due to background events above the ϕ-meson is related to a decrease of the $N_{\pi\pi}/N_{cosmic}$ ratio.

The absolute beam energy in the ρ-scan in 96'scan was measured with the help of the resonance depolarization method, providing the accuracy better than $\delta E/E \ll 10^{-4}$. It gives a systematic error due to the beam energy measurement of 0.1% near the ρ-meson. In other experemental scans, the collider energy was set by dipole magnets with accuracy $\delta E/E < 10^{-3}$.

4 Conclusion

The preliminary results of the pion form factor measurement in the energy range $\sqrt{s}$=0.37 - 1.38 GeV are presented. They are based on a full experimental data set collected in the CMD-2 experiment. New data in the ρ-meson region have 2 times better statistical precision, and are in a good agreement with our previously published result.

Table 2: *Systematic error.*

Source	Value			
$\sqrt{s}=$	0.37÷0.52	0.6÷0.96		1.04÷1.38 GeV
		95scan	98scan	
Fiducial volume	0.2%	0.2%		0.2÷0.5%
Detection efficiency	0.3%	0.2%	0.9%	0.5÷2.0%
Correction for pion loses	0.2%	0.2%		0.2%
Radiative corrections	0.3%	0.4%		0.5÷2.0%
Background events	$< 0.1\%$	$< 0.1\%$		0.6÷1.6%
Energy calibration of collider	0.3%	0.1%	0.3%	0.7÷1.1%
Full event separation	1.0%	0.2%		0.5÷3.5%
	1.2%	0.6%	1.1%	1.3÷5.0%
statistic error in point	6%	4%	1.5%	5÷13%

5 Acknowledgments

This work is supported in part by grants RFBR-03-02-16280, RFBR-03-02-16477, RFBR-03-02-16843, RFBR-04-02-16217 and RFBR-04-02-16223.

References

1. R. R. Akhmetshin *et al.*, Phys. Lett. B **578**, 285 (2004).
2. R. R. Akhmetshin *et al.*, Phys. Lett. B **527**, 161 (2002).
3. V.V.Anashin *et al.*, Preprint Budker INP 84-114, Novosibirsk, 1984.
4. G.A.Aksenov *et al.*, Preprint Budker INP 85-118, Novosibirsk, 1985.
5. E.V.Anashkin *et al.*, ICFA Inst. Bull. **5**, 18 (1988).
6. A. Fasso *et al.*, eConf **C0303241**, MOMT005 (2003).
7. A.B. Arbuzov *et al*, JHEP **9710**, 006 (1997).

Frascati Physics Series Vol. XXXVI (2004), pp. 457–461
DAΦNE 2004: Physics at meson factories – Frascati, June 7-11, 2004
Short Talk in Plenary Session

NUCLEON FORM FACTORS MEASUREMENTS VIA THE RADIATIVE RETURN AT B-MESON FACTORIES *

E. Nowak
Institute of Physics, University of Silesia, Katowice, POLAND

1 Introduction

The present-day experimental situation concerning nucleon form factors in the space-like region shows a substantial discrepancy between measurements via the Rosenbluth method and the recoil polarization technique (see Ref. [1]) for a review). It was shown recently [2], that the difference can be partly explained by two-photon mediated processes, that were not taken into account in the original analysis. More information about nucleon form factors in the time-like region will not only improve poor experimental knowledge there, but it will also shed light on the situation in the space-like region. The radiative return method [3] is a powerful tool to provide that information using data of B-meson factories [4], as we shall advocate also here.

* Supported in part by EC 5th Framework Programme under contract HPRN-CT-2002-00311 (EURIDICE network).

2 The radiative return and nucleon form factors measurements

To profit fully from the radiative return method, a Monte Carlo event generator is needed. For that purpose an upgraded version of PHOKHARA [5] (PHOKHARA 4.0) was developed [4]. It allows for a simulation of the reaction $e^+e^- \to N\bar{N}\gamma(\gamma)$, where $N\bar{N}$ is a nucleon-antinucleon pair. It includes initial state radiation (ISR) at next-to-leading order (NLO). Basing on [6], we expect that the leading order (LO) final state radiation (FSR) is negligible at B-factories, but NLO FSR (not included yet in the program) will be important for a measurement aiming for a few percent accuracy.

2.1 The nucleon current

The matrix element of the electromagnetic nucleon current is given by

$$J_\mu = -ie \cdot \bar{u}(q_2) \left(F_1^N(Q^2)\gamma_\mu - \frac{F_2^N(Q^2)}{4m_N} [\gamma_\mu, \not{Q}] \right) v(q_1) \ , \qquad (1)$$

where F_1 and F_2 are the Dirac and Pauli form factors and m_N is the nucleon mass. The antinucleon and nucleon momenta are denoted by q_1 and q_2 respectively, and $Q = q_1 + q_2$. They are related to the magnetic and electric Sachs form factors by

$$G_M^N = F_1^N + F_2^N \ , \qquad G_E^N = F_1^N + \tau F_2^N \ , \quad \text{with} \ \ \tau = Q^2/4m_N^2 \ .$$

The parametrization of the form factors used in PHOKHARA follows from [7, 8] and is in agreement [4] with the ratio of the form factors measured with the recoil polarization method [9].

Available experimental data in the time-like region consist only of total cross section measurements, and give practically no information about the form factors. Predictions for $\sigma(e^+e^- \to p\bar{p})$, $\sigma(e^+e^- \to n\bar{n})$ and $\sigma(p\bar{p} \to e^+e^-)$, obtained with the form factors used in PHOKHARA, are in good agreement with the data, as shown in Fig. 1 for the reaction $e^+e^- \to p\bar{p}$. Other cross sections can be found in Ref. [4].

2.2 The method for the measurement of the nucleon form factors

The idea of the nucleon form factors measurements in the time-like region via the radiative return is based on studies of angular distributions. The hadronic tensor of the process $e^+e^- \to N\bar{N}\gamma$ depends only on $|G_M^N|^2$ and $|G_E^N|^2$ for non-polarized nucleons [4] and thus it is not possible to measure the relative phase between G_M^N and G_E^N, without measuring the nucleon polarization. Distributions in the the $\mathbf{q} = (\mathbf{q}_2 - \mathbf{q}_1)/2$ polar angle, for unpolarized nucleons, are

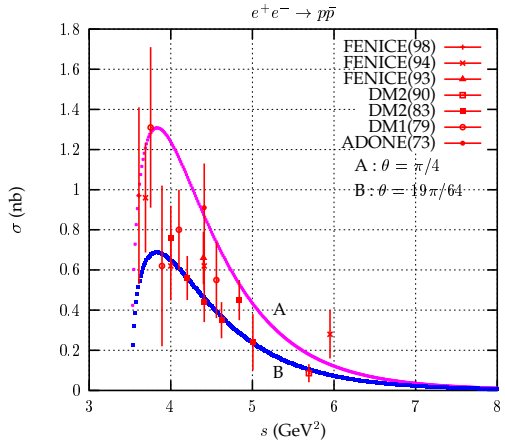

Figure 1: *Comparison of the measured* [10] $e^+e^- \to p\bar{p}$ *cross section with the model from Ref.* [7]. *Predictions are given for two different values* ($\pi/4$ *- curve A and* $19\pi/64$ *- curve B) of the parameter* θ.

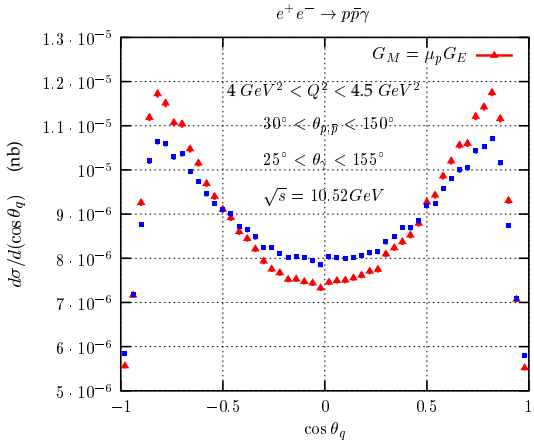

Figure 2: *Angular distribution in the polar angle of vector* $\mathbf{q} = (\mathbf{q}_2 - \mathbf{q}_1)/2$ *in the CMS of the* e^+e^- *pair.*

shown in Figs. 2 and 3. To show how sensitive are the angular distributions to the form factors ratio, two predictions are presented: differential cross sections obtained for the model described above, and differential cross section with the assumption that $G_M^p = \mu_p G_E^p$ and the constraint that the $\sigma(e^+e^- \to p\bar{p})$ remains unchanged. The predicted number of events, for BaBar energy and 4 GeV^2 < Q^2 < 4.5 GeV^2, is about 3500 with an accumulated luminosity of 200 fb^{-1}. It means, that a two parameter fit ($|G_M^N|$ and $|G_E^N|$) to the experimental angular distributions, preferably in the **Q**-rest frame (compare Fig. 2 and Fig. 3), with relatively small Q^2 spacing, is possible, and it will not be limited statistically.

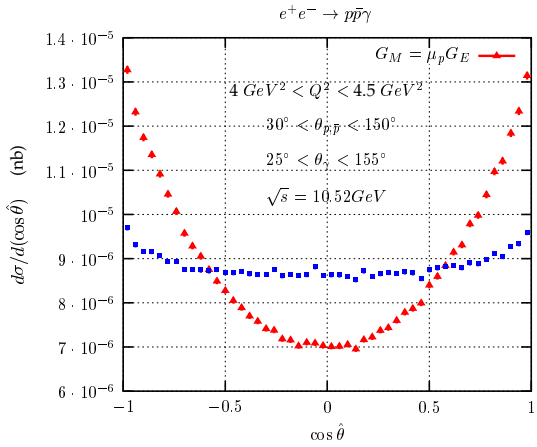

Figure 3: *Angular distribution in the polar angle of vector* $\mathbf{q} = (\mathbf{q}_2 - \mathbf{q}_1)/2$ *in the* **Q***-rest frame* ($\mathbf{q} = \mathbf{q}_2$ *in this frame).*

3 Summary

The Monte Carlo simulations with PHOKHARA 4.0 show that it is possible to measure separately the electric and magnetic nucleon form factors in time-like region at B-meson factories by studying nucleon angular distributions of events with emission of photons. The radiative return is well suited for this measurement over a wide kinematic range.

4 Acknowledgements

The author would like to thank H. Czyż and G. Rodrigo for careful reading the manuscript.

References

1. J. Arrington, Phys. Rev. **C 68** (2003) 034325 [nucl-ex/0305009].
2. Y. C. Chen, A. Afanasev, S. J. Brodsky, C. E. Carlson, M. Vanderhaeghen, hep-ph/0403058.
3. S. Binner, J. H. Kühn and K. Melnikov, Phys. Lett. B **459** (1999) 279 [hep-ph/9902399].
4. H. Czyż, J. H. Kühn, E. Nowak, G. Rodrigo, Eur. Phys. J. C **35** (2004) 527 [hep-ph/0403062].
5. G. Rodrigo, H. Czyż, J.H. Kühn and M. Szopa, Eur. Phys. J. C **24** (2002) 71 [hep-ph/0112184].
6. H. Czyż, A. Grzelińska, J. H. Kühn and G. Rodrigo, Eur. Phys. J. C **33** (2004) 333 [hep-ph/0308312]; hep-ph/0404078.
7. F. Iachello, A. D. Jackson, A. Lande, Phys. Lett. **B 43** (1973) 191
8. F. Iachello, eConf C0309101:FRWP003, 2003 [nucl-th/0312074].
9. O. Gayou *et al.* Phys. Rev. Lett. **88** (2002) 092301 [nucl-ex/0111010]; Phys. Rev. **C 64** (2001) 038202; M. K. Jones *et al.* Phys. Rev. Lett. **84** (2000) 1398 [nucl-ex/9910005].
10. A. Antonelli *et al.* (FENICE collaboration), Nucl. Phys. **B517** (1998) 3; Phys. Lett. **B 334** (1994) 431; Phys. Lett. **B 313** (1993) 283; D. Bisello *et al.* (DM2 collaboration), Z. Phys. **C48** (1990) 23; Nucl. Phys. **B224** (1983) 379; B. Delcourt *et al.* (DM1 collaboration), Phys. Lett. **B 86** (1979) 395; M. Castellano *et al.* (ADONE collaboration), Nouvo Cim. **14A** (1973) 1.

Frascati Physics Series Vol. XXXVI (2004), pp. 463–466
DAΦNE 2004: Physics at meson factories – Frascati, June 7-11, 2004
Short Talk in Plenary Session

MEASUREMENT OF ϕ-MESON LEPTONIC WIDTH IN $e^+e^- \to e^+e^-,\ \mu^+\mu^-$ PROCESSES

M. Dreucci
Laboratori Nazionali di Frascati

Abstract

The ϕ-meson leptonic widths, Γ_{ee} and $\Gamma_{\mu\mu}$, are obtained from the $e^+e^- \to e^+e^-$ forward-backward asymmetry and the $e^+e^- \to \mu^+\mu^-$ cross section around the ϕ-mass energy. We find $\Gamma_{ee} = 1.32\pm\ 0.05\pm\ 0.03$ keV and $\sqrt{\Gamma_{ee}\Gamma_{\mu\mu}}$ $= 1.320\pm\ 0.018\pm\ 0.017$ keV. These results, compatible with Γ_{ee}=$\Gamma_{\mu\mu}$, provide a most precise test of lepton universality. Combining the two results gives $\Gamma_{\ell\ell}(\phi) = 1.320 \pm 0.023$ keV.

1 Motivations

The ϕ-meson leptonic width:
- determines the total ϕ production cross section in e^+e^- annihilation and the ϕ-decay BRs [1, 3];
- in VMD model provides photon-ϕ coupling constant $g_{\phi\gamma}$;
- plays an important role for hadronic contribution to photon vacuum polarization [2];
- provides test for universality of leptonic coupling constant and for quark charge assignment in ϕ meson.

2 Observables

In $e^+e^- \to e^+e^-$process (Fig. 1) the observable is the forward-backward asymmetry A_{FB} :

$$A_{FB} = \frac{\sigma_F - \sigma_B}{\sigma_F + \sigma_B}. \tag{1}$$

In $e^+e^- \to \mu^+\mu^-$ process (Fig. 1) the observable is directly the cross section. In both cases we have an interference term depending on $\Gamma_{\ell\ell}$:

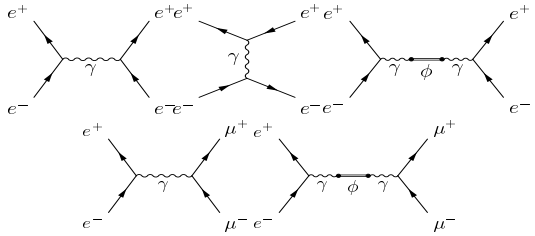

Figure 1: *Left: Amplitude for* $e^+e^- \to e^+e^-$ *process. Right: Amplitude for* $e^+e^- \to \mu^+\mu^-$ *process.*

$$\sigma_{\rm int} = \frac{3\alpha\Gamma_{\ell\ell}}{M_\phi} \frac{s - M_\phi^2}{(s - M_\phi^2)^2 + s\Gamma_\phi^2} \int_{\cos\theta_2}^{\cos\theta_1} {\rm d}\cos\theta f(\theta)_{\ell\ell} \tag{2}$$

where $\Gamma_{\ell\ell} = \Gamma_{ee}$ for $e^+e^- \to e^+e^-$, $\Gamma_{\ell\ell} = \sqrt{\Gamma_{ee}\Gamma_{\mu\mu}}$ for $e^+e^- \to \mu^+\mu^-$ and where θ_1 and θ_2 define our geometrical acceptance. Note that σ_{int} changes sign when s goes through M_ϕ^2. For this reason our analysis uses only 3 energy points: $\sim M_\phi, \sim M_\phi \pm \Gamma_\phi/2$

3 Detector and Data Sample

The KLOE detector [7)] consists of a large drift chamber (DC) and an electromagnetic calorimeter (ECAL) surrounded by a superconducting coil with B=0.52T. The DC, a cylinder of about 4m radius and 3.3m length, filled with a $90\%He - 10\%iC_4H_{10}$ gas mixture and having ∼13000 stereo sense wire, has a momentum resolution $\delta p/p \sim 0.4\%$, a hit resolution of $150\mu m$ (xy) and 2 mm(z) and a vertex resolution of ∼1 mm. The calorimeter, a sample of alternate lead/scintillating fibers, consisting of a barrel covering $45^o < \theta < 135^o$ and two end caps, measures energy with a resolution $\sigma(E)/E = 5.7\%/\sqrt{E({\rm GeV})}$

and arrival times with a resolution $\sigma(t) = [54/\sqrt{E(\mathrm{GeV})} \oplus 50]$ ps. Luminosity and energy are obtained from Bhabha scattering. The CM energies and luminosities for the collected data are summarized in Table 1.

Table 1: 2002 ϕ-scan statistics.

CM energy (mev)	integr.lum.(nb^{-1})
1017.17 ± 0.01	6966 ± 42
1019.72 ± 0.02	4533 ± 27
1022.17 ± 0.01	5912 ± 35

4 Analysis

Bhabha events are selected using DC and ECAL informations and, to enhance sensitivity, we measure forward-backward asymmetry (1). For $e^+e^- \to \mu^+\mu^-$ process we can measure directly cross section. While in Bhabha events background is almost negligible, in $\mu\mu$ production we have a strong contamination of $e^+e^- \to \pi^+\pi^-$ events. Initial state radiation (ISR), where one or both the initial colliding particles radiate a photon before interacting, changes the collision energy. ISR photons are mostly collinear to the beam, and therefore not detectable. The effective center-of-mass energy is so reduced from the nominal value, W, to a lower value, W'. Final state radiation (FSR), by interference with ISR, introduces an asymmetry in the angle distribution mainly in $e^+e^- \to \mu^+\mu^-$process. To enhance the ϕ-meson contribution, a lower cut on W'/W is imposed for both processes. All efficiencies are evaluated using the GEANFI Monte Carlo [6]. As fit function to our observables we use in both cases a Breit-Wigner cross section corrected for ISR [4, 5], FSR, and beam energy spread (BES) [8]. The fit parameters are $\Gamma_{ee}, M_\phi, A_{FB}(M_\phi)$ for $e^+e^- \to e^+e^-$ process and $\Gamma_{\mu\mu}, M_\phi, \sigma(M_\phi)$ for $e^+e^- \to \mu^+\mu^-$process. For bhabha the main systematic uncertainties on A_{FB} are the fiducial cuts on W'/W and polar angle ($\sim 80\%$) and the theoretical uncertainty on Γ_ϕ ($\sim 20\%$). For $e^+e^- \to \mu^+\mu^-$ process the main systematic contributions on $\sigma_{\mu\mu}$ come out from the fiducial cuts on W'/W and polar angle ($\sim 42\%$), from the theoretical uncertainty on Γ_ϕ ($\sim 50\%$) and from the event counting ($\sim 8\%$)(the number of

signal counts comes out by fitting data to a linear combination of MC spectra for signal ($\mu\mu$) and background ($\pi\pi$)).

5 Results

Our results are: $\Gamma_{ee} = 1.32 \pm 0.05 \pm 0.03$ keV and $\sqrt{\Gamma_{ee}\Gamma_{\mu\mu}} = 1.320 \pm 0.018 \pm 0.017$ keV. They are consistent with lepton universality within our errors. Combining the two results we find for the leptonic width of the ϕ-meson $\Gamma_{\ell\ell} = 1.320 \pm 0.017 \pm 0.015$ keV, with a total uncertainty of less than 2%.

References

1. S. Eidelman, F. Jegerlehner. *Z.Phys.* **C67** (1995), 585.
2. C. Quigg, J.L. Rosner. *Z.Phys.* **C67** (1995), 585; H. Gross, A. Martin *Phys.Rept.***60** (1980), 341; R. Van Royen; V.F. Weisskopf; *Nuovo Cimento* **A50** (1967), 617 and err. ibid. **A51**; E.C. Poggio, H.J. Schnitzer *Phys.Rev.* **D20** (1979), 1175 and err. ibid. **D21**; H. Krasemann *Phys.Lett.* **B96** (1980), 397; T.D. Newton, E.P. Wigner *Rev.Mod.Phys.* **21** (1949), 400.
3. M.N. Achasov et al.; *Direct measurement of the ϕ(1020) leptonic branching ratio. Budker INP 2000-71, preprint*
4. M. Greco, G. Montagna, O. Nicosini, F. Piccinini. QED radiative corrections and radiative Bhabha scattering at DaΦne *"The second DAϕNE physics handbook"*, 629.
5. E.A. Kuraev, V.S. Fadin. *On radiative corrections to the cross section for single-photon annihilation of an e+e- pair at high energy* Sov.J.Phys. **41** (1985), 466.
6. A. Antonelli, C. Bloise; *The Kloe Monte Carlo GEANFI* Kloe memo **128**.
7. S. Dell'Agnello *The KLOE detector* Proc. of the III Int. Work. on Phys. and Det. for DAFNE, Frascati, eds. S.Bianco et al., (S.I.S.) (1999), 381.
8. C. Gatti, T. Spadaro; *Kloe Memo in preparation.*

Frascati Physics Series Vol. XXXVI (2004), pp. 467–471
DAΦNE 2004: Physics at meson factories – Frascati, June 7-11, 2004
Short Talk in Plenary Session

MEASUREMENT OF NEUTRAL KAON MASS WITH CMD-2 DETECTOR

Alexander S. Zaytsev *
Budker Institute of Nuclear Physics, Novosibirsk, Russia

1 Introduction

A preliminary result of the K^0_S mass measurement performed recently with the CMD-2 detector based on the precision of beam energy calibration at VEPP-2M collider and $K^0_S \to \pi^+\pi^-$ decay reconstruction technique is presented.

2 VEPP-2M collider and CMD-2 detector

The electron-positron collider VEPP-2M [1)] has been running at Novosibirsk since 1974 up to 2000 carrying out experiments with the CMD-2 and SND detectors in the c.m. energy range $\sqrt{s} = 0.36 \div 1.4$ GeV.

* On behalf of CMD-2 Collaboration

The CMD-2 detector is described in more detail elsewhere [2]. Its tracking system consists of the cylindrical drift chamber (DC) surrounding the interaction point and providing precise particle momentum and dE/dx measurement and proportional Z-chamber (ZC) for precise polar angle measurement, both also used for trigger. Both chambers are inside a thin (0.38 X_0) superconducting solenoid with a field of 1 T. The barrel electromagnetic calorimeter placed outside the solenoid consists of 892 CsI crystals. The muon-range system of the detector, also located outside the solenoid, is based on streamer tubes. The endcap electromagnetic calorimeter based on BGO crystals makes the detector almost hermetic for photons.

3 Full two-body decay reconstruction technique

The measurement of neutral kaon mass performed with the CMD-2 detector is based on the full $K^0_S \to \pi^+\pi^-$ decay reconstruction. A kaon mass value can be determined for each decay event using the following equation, derived from energy-momentum conservation:

$$\beta^2_{K^0_S} = \frac{1}{\eta^2}\left(1+\cos\psi\sqrt{1-\eta^2}\right)\left[1-\sqrt{1-\beta^2_m\eta^2}\right], \qquad (1)$$

where $\eta \equiv \frac{1-Y^2}{1+Y^2}$, $Y = p_+/p_-$, $p_\pm \equiv |\overrightarrow{p_\pm}|$, $\overrightarrow{p_\pm}$ are charged pion momenta,

$$\beta^2_{K^0_S} \equiv 1-(M_{K^0_S}/E_{K^0_S})^2, \;\; \beta^2_m \equiv 1-(2M_{\pi^\pm}/E_{K^0_S})^2, \qquad (2)$$

$E_{K^0_S}$ is kaon energy and ψ is opening angle between pions in the c.m. frame. The main features of the technique are strong suppression of pion momentum measurement systematics and a requirement of precise beam energy calibration.

4 VEPP-2M collider beam energy calibration

In case of measuring $M_{K^0_S}$ via reconstruction of $K^0_S \to \pi^+\pi^-$ decay in the process of kaon pair production $e^+e^- \to \phi(1020) \to K^0_S K^0_L$ one needs to measure an average $\sqrt{s}$ value of the electron-positron system and then take into account beam energy spread and initial state radiation (ISR) effects.

The average beam energy of the VEPP-2M collider for a 355 nb^{-1} data set used for kaon mass measurement was determined by the resonant depolarization technique [3]. It was shown that the precision of single beam energy

measurement was $\sigma_E/E \approx 10^{-5}$ corresponding to $\sigma_E \approx 5$ keV for the c.m. energy near the $\phi(1020)$ meson peak. The typical duration of the CMD-2 experimental run was $T_{run} \approx 2$ hours so we had to study long term instabilities of beam energy.

The most significant instability was found to be the temperature drift due to variations of a collider ring perimeter caused by changing day/night temperature. Each bending magnet of VEPP-2M ring had a temperature probe and the data collected by these probes during the data taking allowed us to establish clear correlation between beam energy and average collider ring temperature. Recently the correlation was also studied via a technique based on measuring an average momentum of charged kaons in $e^+e^- \to K^+K^-$ process and full CMD-2 detector simulation. Combining both methods we managed to obtain average mean beam energy values for the data taking runs with $\sigma_E = 13 \div 19$ keV accuracy [4]. The total number of $e^+e^- \to K^0_S K^0_L$, $K^0_S \to \pi^+\pi^-$ events selected for further analysis is ≈ 45000 for the entire calibrated data set.

5 Event selection and visible mass values determination

Visible kaon mass values were obtained for each experimental run and then ISR radiative corrections (RC) and detector smearing corrections (NC) were applied. Pion charge dependent systematic effects of momentum measurements were taken into account for each run as well. In order to study the influence of pion energy losses (DE) in the CMD-2 drift chamber and vacuum tube material and effects of uniformity of detector magnetic field (MF) we separate all the experimental events into two "topological" classes. DE and MF corrections were applied event-by-event and it was found that these corrections do compensate all the experimentally observed systematic differences between average mass values measured for different event types.

6 Preliminary neutral kaon mass result

Performing the final fit over the K^0_S mass values for all runs, we obtained

$$M_{K^0_S} = 497.634 \pm 0.016 \pm 0.019 \text{ MeV/c}^2, \tag{3}$$

where the first contribution to the uncertainty is the sum of beam energy dependent systematics and statistical error with a scale factor 1.7 included and

Table 1: $M_{K_S^0}$ *systematic error budget.*

Source of systematic	Correction, keV/c^2	Error, keV/c^2
Beam energy measurement		$13 \div 19$
Beam energy temperature drift		3
Radiative corrections to initial state	$-(80 \div 630)$	$2 \div 12$
Beam energy spread correction	$+3$	0.3
Radiative corrections to final state	-6	6
Detector smearing corrections	$+(60 \div 140)$	$6 \div 15$
Correction for pion decay in flight	$+4$	3
Background		4
Z-chamber thermal expansion		3
Selection criteria variation		6
Fit bounds variation		8
Charged pion mass uncertainty		0.04

the second is the sum of energy independent systematics (all the contributions are listed in Table 1). Our preliminary result is in good agreement with all previous measurements and has a total error of 24 keV/c^2 which is close to the uncertainty of the PDG2004 neutral kaon mass fit [5].

7 Conclusion

The mass of K_S^0 meson was measured with the CMD-2 detector at the VEPP-2M electron-positron collider by using total $K_S^0 \to \pi^+\pi^-$ decay reconstruction technique. The preliminary result obtained has the accuracy almost the same as the world average value at the moment, so an updated world average $M_{K_S^0}$ value can be used for precision beam energy calibration of ϕ-factories.

The mass measurement techniques developed could be easily adopted to other experimental conditions (e.g., KLOE at DAΦNE) in order to measure the $M_{K_S^0} - M_{K^\pm}$ value and CPT-violating quantity $M_{K^+} - M_{K^-}$ even without precision collider energy calibration technique available.

8 Acknowledgments

The authors are grateful to the staff of VEPP-2M for excellent performance of the collider, to all engineers and technicians who participated in the design, commissioning and operation of CMD-2.

This work was supported in part by the Young Scientists Grant of SB RAS and RFBR 04-02-16223-a grant.

References

1. A.N. Skrinsky, Proc. of the Workshop on Physics and Detectors for DAΦNE'95, Frascati, Vol. IV, 3 (1995).
2. E.V. Anashkin *et al*, ICFA Instr. Bulletin **5**, 18 (1988).
3. A.P. Lysenko, I.A. Koop *et al.*, Nucl. Instr. and Meth., **A359**, 419 (1995).
4. K.Yu. Mikhailov *et al*, Preprint BINP **2003-39**, Novosibirsk (2003).
5. S. Eidelman *et al*, Phys. Lett. **B592**, 1 (2004).

Session VII — DAΦNE Upgrade

(Chair: I. Bigi)

Frascati Physics Series Vol. XXXVI (2004) pp. 475–484
DAΦNE 2004: PHYSICS AT MESON FACTORIES – Frascati, 7–11 June, 2004
Invited Review Talk in Plenary Session

DESIGN CONSIDERATIONS FOR FUTURE DAΦNE UPGRADES

A. Gallo*

INFN – Laboratori Nazionali di Frascati, P.O.Box 13, I–Frascati, Italy

Abstract

The Frascati Φ-Factory DAΦNE has been delivering luminosity to the KLOE, DEAR and FINUDA experiments since year 2000. Since April 2004 the KLOE run has been resumed and recently peak luminosity of $1.0 \cdot 10^{32} cm^{-2} s^{-1}$ and integrated luminosity of $6.2\ pb^{-1}/day$ have been achieved. The scientific program of the three high-energy experiments sharing DAΦNE operation will be completed approximately by the end of year 2006. A scientific program for DAΦNE beyond that date has not been defined yet and it is matter of discussion in the high-energy physics and accelerator physics communities.
In this paper we present some future scenarios for DAΦNE, discussing the expected ultimate performances of the machine as it is now and addressing the design for an energy and/or luminosity upgrade. The options presented in the following are not exhaustive and they are intended to give a glance of what is doable using the existing infrastructures.

1. Expected ultimate performances of DAΦNE with the present hardware

The histories of the achieved peak and daily integrated luminosities at DAΦNE since, respectively, years 2000 and 2002 are shown in Fig. 1. Even though the progress over the years has been continuous and substantial, we believe that a significant further improvement in terms of peak and integrated luminosities is still possible.

---

* Co-Authors: D. Alesini, G. Benedetti, M.E. Biagini, C. Biscari, R. Boni, M. Boscolo, A. Clozza, G. Delle Monache, G. Di Pirro, A. Drago, A. Ghigo, S. Guiducci, M. Incurvati, C. Ligi, F. Marcellini, G. Mazzitelli, C. Milardi, L. Pellegrino, M.A. Preger, P. Raimondi, R. Ricci, U. Rotundo, C. Sanelli, M. Serio, F. Sgamma, B. Spataro, A. Stecchi, A. Stella, F. Tazzioli, C. Vaccarezza, M. Vescovi, M. Zobov (LNF-INFN), E. Levichev, P. Piminov (BINP–Novosibirsk).

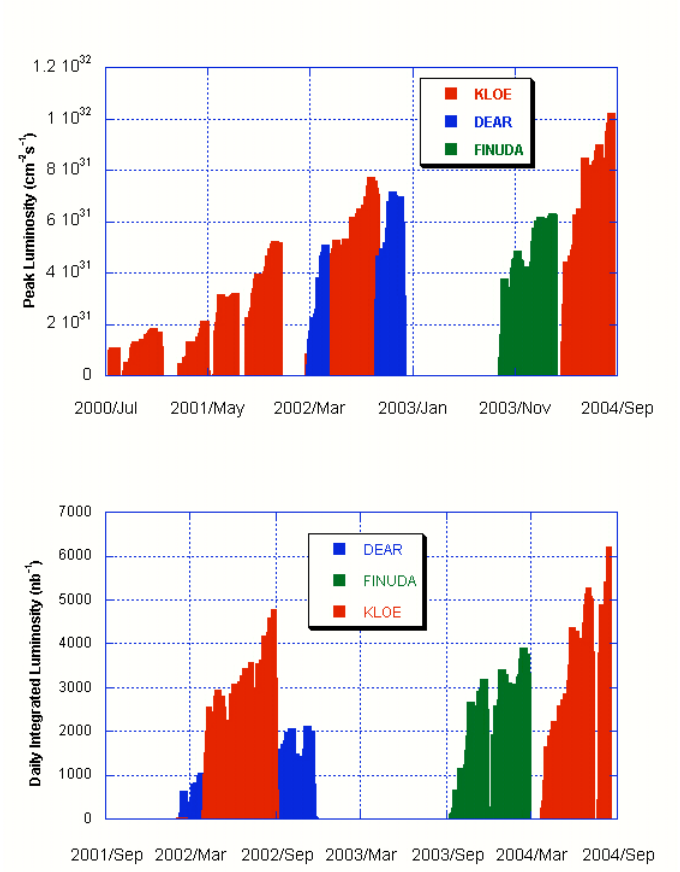

Fig. 1: History of peak and daily integrated luminosities at DAΦNE.

The improvement expectations mainly rely on:

- Implementing of a lattice providing negative momentum compaction factor α_c to shorten the bunch and decrease the vertical beta-function β_y^* at the Interaction Point (IP);
- Moving the betatron tunes $\nu_{x,y}$ towards the integer to reduce the beam-beam induced blow-up of the bunches;
- Increasing the beam currents by improving the beam dynamics and the performances of the active feedback systems.

Decreasing the β_y^*, i.e. the value of the vertical beta-function at the IP, is beneficial to the luminosity because it results in a reduction of the vertical size of the bunch σ_y^* and of the linear tune shift parameter ξ_y which is an indicator of the strength of the beam-beam effect. However, the beta-function has a parabolic shape around the IP, and the parabola is such that the length of the region where the beta-function remains small is comparable to the β_y^* value itself. Accordingly, the β_y^* value can not be reduced much

below the bunch length value σ_z to avoid a geometrical reduction of the luminosity known as "hourglass effect" [1].

The measured bunch length σ_z as a function of the bunch current I_b for both DAΦNE rings is shown in Fig. 2. The bunch lengthens with the current because its interaction with the surrounding vacuum chamber generates a self-induced e.m. field which is opposite in phase with respect to the longitudinal focusing RF field provided by the RF system. The bunch lengthens more in the electron ring because of the presence of some extra discontinuities (the ion clearing electrodes) in the vacuum chamber. Presently DAΦNE is operating with $\beta_y^* \approx 1.9\ cm$ and $I_b \approx 10\ mA$, at the threshold of the hourglass effect.

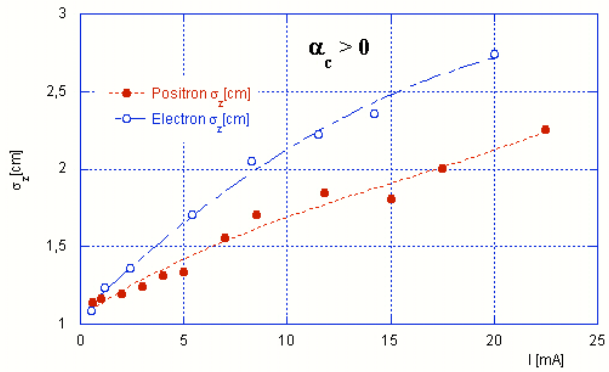

Fig. 2: Bunch length for positive α_c.

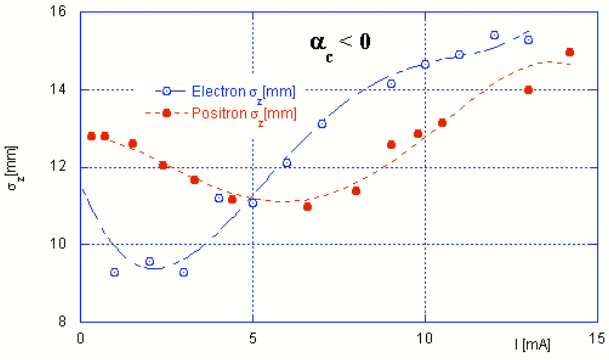

Fig. 3: Bunch length for negative α_c.

A very effective way to shorten the bunch is to implement a lattice with negative momentum compaction factor α_c [2]. The momentum compaction is the ratio between the relative closed orbit elongation and the relative energy deviation of a particle in a storage ring. In a standard ring ($\alpha_c > 0$) the most energetic particles travel a longer

closed orbit. However, if $\alpha_c < 0$ the bunch self induced field is typically in-phase with the external RF field, and the bunch tends to shorten with increasing current. Due to other effects, such as the increase of the bunch energy spread with the current, after reaching a minimum the bunch starts increasing again. Negative momentum compaction lattices have been tested in DAΦNE during machine study shifts. The measured bunch length as a function of the current for the two rings is reported in Fig. 3. Again, the different behavior of the two rings can be explained in terms of different wake-fields, but the bunch lengths remain below 1.5 cm up to bunch current of 15 mA. The potentiality of this kind of lattice is evident, but retuning the machine and all the feedback systems to optimize the luminosity in this configuration will require many machine development shifts. The expected luminosity gain after a complete machine retuning is in the 25÷50 % range.

The beam-beam effect, which is especially severe in the low-energy colliders, is also limiting the luminosity performances of DAΦNE. The primary effect induced by the beam-beam interaction is the blow-up of the transverse (in particular the vertical) size of the bunches of one beam as function of the current in the bunches of the other one.

From beam-beam simulations as well as from experimental data from other colliders we know that a way to limit the beam-beam induced blow-up is to work with betatron tunes close to the integer. According to numerical simulation of a tune scan, this is true also in the DAΦNE case [3)]. Presently we are running the machine with tune fractional parts around $\nu_x \approx 0.10$, $\nu_y \approx 0.18$ with a small asymmetry between the two beams. Since any storage ring is unstable at integer betatron tunes, working close to the integer is critical and requires a very fine tune-up of the machine linear and non linear corrections.

The reduction of the DAΦNE betatron tunes towards lower values has already started as a slow, adiabatic process requiring a machine re-optimization at every new small step. We believe that pushing this process further in this direction is worthwhile.

In the present DAΦNE operation the typical multibunch currents in collision after injection are $I^+ \approx 1.0\ A$ and $I^- \approx 1.2\ A$ in ≈ 100 bunches. Presently the main limitation is in the positron current and it is due to a horizontal multibunch instability causing saturation in the injection, high beam-induced background in the detector and spoiling the uniformity of the bunch train. The origin of this instability is not well understood, but the threshold is slowly increasing with time because of continuous improvements in the setting-up of the bunch-to-bunch feedback systems and non linear correction adjustments. Machine study shifts dedicated to the beam dynamics are needed to better understand and cure these effects in order to increase the current in collision. The progress in this field has been continuous and the colliding currents achieved, in spite of

the intrinsic sensitivity of the beam dynamics at low energy, are already comparable with those obtained at the B-factories.
If all the tasks indicated in this paragraph will be pursued during the next two years of operation, the goal of putting in collision multibunch currents in the *1.5÷2.0 A* range to double the present peak and daily integrated luminosities seems realistic. We believe that these numbers represent the DAΦNE potentiality with the present hardware.

2. Minimal changes for Energy upgrade from the Φ resonance to the n-nbar threshold

The minimal DAΦNE upgrade to operate the machine at energies from the Φ resonance (0.51 GeV/beam) to the threshold of the n-nbar production (1.1 GeV/beam) requires essentially new dipole magnets fitting the existing vacuum chamber and providing up to 2.4 T magnetic field in the gap [4)]. In this way the layout of the machine is preserved. Furthermore, new superconducting quadrupoles housed in the experimental detector to be powered for variable beam energies have to be designed for the low beta insertion. The other existing quadrupoles and their power supplies are basically compatible with 1.1 GeV operation, while only an optimization of the lattice to prevent their saturation is needed. The other existing machine subsystems (such as the vacuum system, the RF, the bunch-to-bunch feedbacks, …) are basically compatible with this option.
A 2D model of a C-shaped dipole for the DAΦNE energy upgrade has been designed. In this special design the magnetic pole tips are made of a special high saturation iron alloy named Hyperco® to reach the required B-field in the gap. The obtained preliminary results show that in principle the required dipoles are feasible, but more work is needed to get a reliable design providing the required field and field quality at any energy in the specified range.
The main machine parameters at the Φ and n-nbar threshold energies are reported in Table 1, columns 2 and 3. Since the luminosity naturally increases with the energy, a peak value $L_{pk} = 1 \cdot 10^{32}\ cm^{-2}s^{-1}$ at the energy of the n-nbar threshold can be obtained with only $\approx 0.5\ A$ of total current in 30 bunches, and with a Touschek lifetime larger than 4 hours. No significant differences are expected for the operation at the Φ energy since the hardware and the machine layout basically remain the same.
Concerning injection, there are two main options: upgrade the DAΦNE linac for full energy injection (without damping ring) [5)] or preserve the present injection system (including the damping ring) implementing an energy ramping scheme in the main rings [6)]. The energy ramping option requires a synchronized control of the magnet power supplies that is allowed by the existing hardware. This option does not allow topping-up

injection in the high energy operation. On the other side, the linac upgrade option surely allows a faster and more flexible injection procedure, but it is far more expensive and requires the upgrade also of the kickers and septum magnets in the ring.

3. A new flexible collider for both Energy (up to the n-nbar threshold and beyond) and Luminosity (up to 10^{33} $cm^{-2}s^{-1}$ at the Φ resonance) upgrade

If a significant increase of the luminosity at the Φ energy is required together with the capability of running at higher energies, the collider has to be completely redesigned and rebuilt. The basic guidelines of a design matching these requirements are drawn in this paragraph.

Table 1: upgraded DAΦNE and flexible collider parameters at Φ and n-nbar threshold energies.

	Minimal DAΦNE upgrade		New flexible collider	
Energy [GeV]	0.51	1.1	0.51	1.1
B-field central pole [T]	1.1	2.4	2.67	2.92
B-field lateral poles [T]	---	---	-1.48	1.64
Total Current [A]	1 - 2	0.5	3	0.5
Luminosity [$10^{32}cm^{-2}s^{-1}$]	2	1	10	1
N bunches	100	30	100	30
Current/bunch [mA]	10-20	17	>20	17
Synchrotron integral I_2 [m^{-1}]	9.7	5.9	17.5	4.5
Radiation damp. rate [s^{-1}]	25	160	45	115
Energy loss/turn Uo [keV]	9.3	125	17	110

Any upgrade design of DAΦNE as a Φ-factory has to start from an increase of the machine radiation damping rate. In fact, the physics of the beam-beam effect, extensively investigated both theoretically and experimentally, shows that fast radiation damping rates are essential to limit the beam-beam induced vertical blow-up and increase the achievable luminosity. The qualitative explanation of this result is quite intuitive: the faster the damping rate, the shorter the time needed by a particle to loose the "memory" of any experienced perturbation including those coming from beam-beam interaction.

In a storage ring the horizontal damping rate α_x and the energy loss per turn U_0 grow respectively with the 3rd and the 4th power of the beam energy E through the synchrotron integral I_2 defined as the integral of $1/\rho^2(s)$ over the ring, where $\rho(s)$ is the

local bending radius. Increasing I_2 is particularly important at low energies, where the damping rate is smaller. A possible way to do that is to divide a bending magnet in 3 pieces, as shown in Fig. 4. The solution is such that a total 30° bending angle is obtained at both 0.5 GeV and 1.1 GeV energies by inverting the polarity in the 2 lateral parts of the magnet and retuning the B-field by a small amount. As shown in Table 1, where a summary of the machine parameters at 0.51 GeV and 1.10 GeV is presented in columns 4 and 5, I_2 is ≈ 4 times larger at low energy giving a damping rate only a factor 2.5 smaller with respect to the high energy case. The damping rate at low energy is also almost doubled with respect to the DAΦNE present value, which is very promising for the luminosity performances.

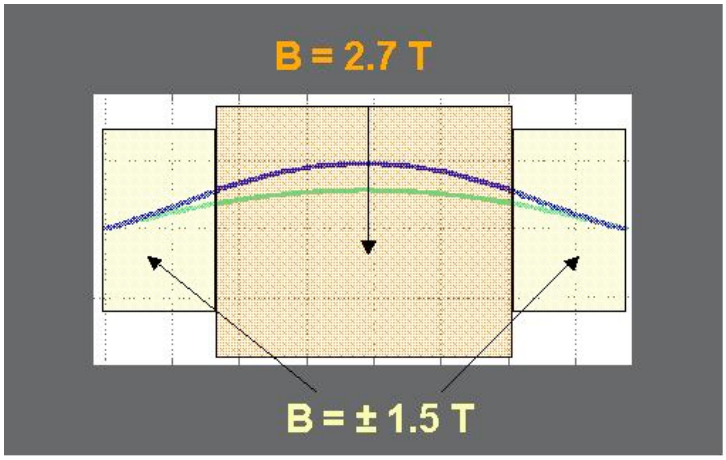

Fig. 4: 3-pieces dipole cell.

A total of 12 bending magnets, each made of 3 pieces, are needed for each ring. Due to the high B-field values assumed, the dipoles must be of superconducting type. Energies higher than 1.1 GeV are also accessible (up to the J/ψ or even the τ) provided the B-field in the dipoles and in all other magnets can be increased proportionally.

4. A super Φ-factory for Luminosities exceeding 10^{34} cm^{-2}s^{-1}

In this paragraph we summarize the study of a new Φ-factory fitting the existing DAΦNE buildings and pushing the design luminosity at the limit of the accelerator physics state of the art [7]. The ultra-high luminosity design is based on a mix of standard and new concepts, the most important ones being:

- Strong radiation emission to increase radiation damping;
- Large and negative momentum compaction lattice;
- Strong RF Focusing scheme to get bunch length in the mm scale.

The importance of enhancing the radiation emission and the potentiality of the negative momentum compaction factor have been already illustrated in the previous paragraphs.

The basic "wiggling" cell shown in Fig. 5 made of a sequence of inward and outward bending dipoles provides both large radiation damping and negative momentum compaction. Due to partial compensation of positive and negative dipoles, the total bending angle of one cell is small, and a large number of cells (i.e. a large number of dipoles) can be used to close the machine.

The momentum compaction α_c is given by the integral of the dispersion function *D(s)* divided by the local bending radius $\rho(s)$. Being the signs of *D(s)* and $\rho(s)$ opposite in the cell, α_c is naturally negative and large in this structure. A large α_c is necessary to keep the bunch short by implementing the strong RF focusing scheme.

To make a substantial step in the luminosity is necessary to decrease by about one order of magnitude the vertical beta-function at the IP β_y^* passing from cm to the mm scale. To do this, as discussed in paragraph 1, the bunch length must be reduced to about the same value to avoid the hourglass effect. Recently, a novel technique called Strong RF Focusing (SRFF) has been proposed to meet this requirement [8]. By combining a very large RF gradient with a large momentum compaction factor, the bunch length can be modulated along the ring. The bunch length has its maximum in the RF section, and the lattice can be tuned in such a way that the bunch length is minimum at the IP. This condition requires that the two portions of the ring delimited by the RF and the IP contribute equally to the total momentum compaction of the ring.

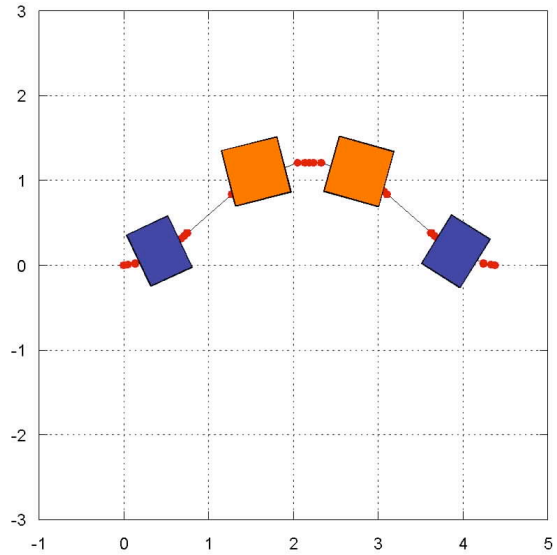

Fig. 5: Wiggling cell.

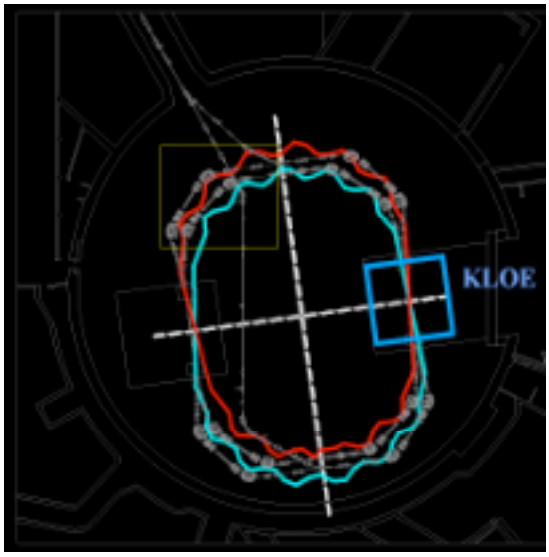

Fig. 6: Layout of the super Φ-factory.

It may be seen that even with large α_c values (of the order of 10^{-1}), the voltage needed to produce sizeable variations of the bunch length along the ring are of the order of

10 MV, a very large value for a 100 m long ring which surely requires a very efficient superconducting RF system.
The main advantage of the SRFF scheme is that the bunch is not short everywhere in the ring. This gives the possibility of placing the impedance generating elements (such as injection and correction kickers, bellows, beam position monitors, …) as much as possible close to the RF section where the bunch is longest. The amplitude of the generated wakefields can be minimized and the bunch can be kept short at the IP up to the nominal operating current (of the order of 15 mA/bunch). Numerical simulations based on the short range wake model of DAΦNE show that this result is achievable.
The new machine layout superimposed to the present one in the DAΦNE hall is shown in Fig. 6, while the main parameters are summarized in Table 2.

Table 2: super Φ-factory parameters.

Total length L [m]	105
Energy [MeV]	510
RF frequency f_{RF} [MHz]	497
RF voltage V_{RF} [MV]	10
Horiz. emittance ε_x [μ rad]	0.26
Vert. emittance ε_y [μ rad]	0.002
Momentum compaction α_c	- 0.165
Horiz. beta @ IP βx^* [m]	0.5
Vert. beta @ IP βy^* [mm]	2.0
N of particle / bunch	$5\ 10^{10}$
Harmonic number h	180
Lum./bunch [$cm^{-2}\ sec^{-1}$]	$9\ 10^{31}$
Lum. Tot. [$cm^{-2}\ sec^{-1}$]	$\sim 10^{34}$

The SRFF principle, which is essential to reach the highest luminosities, has never been demonstrated and studied experimentally. Many aspects of beam physics (such as Touschek lifetime, dynamic aperture, beam-beam, coherent synchrotron radiation emission, …) need to be investigated in more detail to establish whether or not a collider may efficiently work in this regime. In order to add reliability to a design based on this scheme, an SRFF experiment to be carried out at DAΦNE has been proposed [9]. A high momentum compaction lattice for DAΦNE has been designed, while an extra SC RF cavity to be temporarily installed in the FINUDA interaction

region is under design. Bunch lengths varying from 1.5 to 3 mm along the ring will be obtained. To reduce size and cost, the cavity design has been based on the existing 1.3 GHz, 9-cells TESLA cavities. According to this proposal, the experiment will be completed by the end of 2006 and will give the first SRFF experimental observation, together with other useful experimental results on the impact of this regime on the beam dynamics and on the bunch-by-bunch feedback systems. The experiment cost estimate is ≈1 M€ mainly for the construction of the new SC cavity and cryostat, and to the upgrade of the DAΦNE cryoplant to produce 2 K liquid Helium. The experiment has not been funded yet.

5. Conclusions

DAΦNE is running regularly for the KLOE, FINUDA and DEAR/SIDDARTHA experiments, with a continuous improvement of its performances and reliability. The scientific program of the experiments should be completed by the end of 2006 and a new high-energy scientific program beyond that date has not been yet defined. Different upgrade options of the collider fitting the existing infrastructures have been presented: energy upgrade to reach the n-nbar threshold with minimal changes, energy and luminosity upgrade with a new flexible machine, a new super Φ-factory to increase the luminosity by 2 orders of magnitude.

The LNF high-energy physics and the accelerator communities are working together to refine these proposals and converge to a new common enterprise renewing the well-established tradition of these laboratories.

References

[1] G. E. Fisher, SPEAR Note 154, SLAC, Dec. 1972.

[2] S.X. Fang et al., KEK Preprint 94-190, February 1995.

[3] M. Zobov, private communication.

[4] G. Benedetti et al., proc. of the PAC 2003, Portland (Oregon), May 12-16, p. 2279.

[5] R. Boni, e-Print Archive: physics/0402081.

[6] C. Milardi, e-Print Archive: physics/0403044.

[7] C. Biscari et al., proc. of the EPAC 2004, Luzern (CH), July 5-9, MOPLT056.

[8] A. Gallo et al., e-Print Archive: physics/0404020.

[9] A. Gallo et al., proc. of the EPAC 2004, Luzern (CH), July 5-9, MOPLT057.

Frascati Physics Series Vol. XXXVI (2004), pp. 485–494
DAΦNE 2004: Physics at meson factories – Frascati, June 7-11, 2004
Invited Review Talk in Plenary Session

THE PHYSICS CASE FOR A DAΦNE UPGRADE

Gino Isidori*
INFN, Laboratori Nazionali di Frascati, I-00044 Frascati, Italy

Abstract

Possible physics programs relevant for an upgrade of the Frascati Φ Factory are briefly discussed. Particular attention is devoted to the kaon-physics program of a realistic high-luminosity option, yielding up to 100 fb^{-1} at the Φ peak.

1 Introduction: low-energy physics in the LHC era

An upgrade of the DAΦNE complex is likely to produce physics results in a time period where most of the attention of the particle-physics community will be focused on the first (hopefully exciting!) results of LHC. It is therefore natural to address the general question of which type of low-energy experiments could

* Work partially supported by IHP-RTN, EC contract No. HPRN-CT-2002-00311 (EURIDICE).

still be relevant/attractive in such time period. On general grounds, we can identify three basic categories:

I. *Search/measurements of forbidden/rare processes* sensitive to short-distance dynamics, such as rare K decays, $(g-2)_\mu$, CPT tests, etc... The ultimate goal of such measurements is similar to the one of LHC, namely searching/understanding physics beyond the SM. But the two programs are not in competition. On the contrary, there is full complementary between the high-energy and the high-intensity frontiers: one would benefit from the progress of the other. Improving the understanding of theoretically clean rare processes is therefore very useful also in the LHC era.

II. *Precision measurements of fundamental SM parameters*, such as CKM angles, quark masses and gauge couplings. Also in this case there is a some complementarity with the LHC program. Several parameters of the SM Lagrangian (particularly in the Yukawa sector) are likely to be determined (in terms of fewer couplings) by some unknown high-energy dynamics. Their precise knowledge, which can be obtained only at low energies, could help to shed slight on physics beyond the SM.

III. *Deeper understanding of QCD in the non-perturbative regime* by means of precise measurements of exotic hadronic systems, such as hadronic atoms, hypernuclei, multiquark states, etc... To a large extent, this physics program is orthogonal to the one of LHC and will not be influenced by the developments at the high-energy frontier.

The present set-up of the DAΦNE complex, with an accelerator running at the Φ peak and three different type of experiments (KLOE, FINUDA and DEAR) has allowed (and is still allowing) to make significant advancements in all the three directions.

It is quite clear that a change of the c.o.m. energy of the accelerator, reaching the 2–2.5 GeV region, would bring a significant benefit to the last category. By this upgrade it would be possible to study with high precision nucleon form factors and to address spectroscopy issues which are not accessible at the Φ peak –a detailed discussion about the interest of this physics program can be found in the talk by F. Iachello [2]– However, it is also quite clear that leaving the Φ peak, there is no hope to make significant progress concerning the first two categories. Less obvious is the question if there is still room to make

significant progress in the first two categories, with a substantial but realistic increase of the luminosity at the Φ peak. In the rest of this talk we shall try to address this last question.

2 Dreams vs. realistic possibilities: the Alghero heritage

The possible upgrades of DAΦNE and their related physics program has been the subject of an entire workshop, held in Alghero in September 2003. [1] A few important conclusions of this workshop can be summarized as follows:

- Kaon physics offer an outstanding physics case belonging to the first category: the search and the measurement of the very rare decays $K \to \pi\nu\bar{\nu}$ [3] and $K_L \to \pi^0\ell^+\ell^-$. [4] Indeed, most of the future kaon programs at fixed-target colliders are focused on these rare decays modes. From the experimental point of view, a Φ factory would be an ideal environment to search for these rare decays. However, the tiny branching ratios (in the 10^{-10}–10^{-11} range) and the difficult experimental signature, calls for peak luminosities at the Φ peak around or above 10^{35} cm^{-2} s^{-1} (or integrated luminosities of at least 10^3 fb^{-1}). Such scenario does not appear to be feasible, at least in the short term.

- A realistic upgrade of the luminosity could yield at most 100 fb^{-1} at the Φ peak, or the production of $\approx 10^{11}$ $K\bar{K}$ pairs. Although the *golden* short-distance channels are not accessible with such statistics, the clean environment of the Φ factory would still allow a series of unique and fundamental measurements (categories I & II) in the kaon sector. [5] These includes CPT tests, neutral kaon interferometry, rare K_S decays, improved measurements of the Cabibbo angle and deeper studies of CHPT.

Similarly to the present set up, the Φ-peak option would also allow an intense hadron-physics program with hypernuclei, kaonic atoms, $\gamma\gamma$ spectroscopy, radiative Φ decays and hadronic cross-sections via radiative return. The possibility to perform these measurements without a serious conflict with the kaon program is certainly a positive aspect of the Φ-peak option. To our knowledge, the maximal luminosity is a less crucial issue for the hadronic of program. For this reason, in the following we shall discuss only a few kaon measurements which provide good motivations to reach luminosities above 10^{33} cm^{-2} s^{-1}.

3 The kaon-physics program with 10–100 fb^{-1}

3.1 CPT tests and interferometry

As is well known, the neutral kaon system offers a unique opportunity to search for possible violations of CPT invariance. Just to mention a famous example, CPT invariance predict equal masses and decay widths for particles and antiparticles: this prediction is currently probed at the 10^{-18} level of relative precision in the neutral kaon system.

CPT invariance necessary holds in any local Lorentz-invariant quantum field theory. Testing its validity is equivalent to probe some of the most fundamental hypothesis on which the present description of particle physics is based. Interestingly enough, these hypotheses are likely to be violated at scales where the quantum effects of gravitational interactions cannot be ignored. Unfortunately, since we still miss a consistent theory of quantum gravity, it is hard to predict at which level CPT-violating effects could become visible at low energies: the field is totally driven by experiments, with the most significant bounds setting the reference scale for future improvements.

A Φ factory could probe CPT in the neutral kaon system in several ways; an extensive discussion can be found in the *Second DAΦNE Physics Handbook*. [6] One of the cleanest probes is the comparison of the charge asymmetries ($\delta_{L,S}$) of K_L and K_S semileptonic decays ($K_{\ell 3}$). These two observables are *necessarily* equal in the limit of exact CPT invariance; assuming that CPT is violated only in the mass matrix, we can relate their difference to the K^0–$\bar{K}^0$ mass difference:

$$\frac{|m_{K^0} - m_{\bar{K}^0}|}{m_K} \approx 5 \times 10^{-15} \times |\delta_L - \delta_S| \; + \; O(\not{\text{CPT}} \text{ in } \Delta S = 1) \qquad (1)$$

The limiting factor of this CPT test is the error on δ_S, whose present best measurement is obtained by KLOE:

$$\delta_S = (-2 \pm 9 \pm 6) \times 10^{-3} \qquad (2)$$

(δ_L is known with an absolute error below 10^{-4}). With ≈ 100 fb^{-1} it should be possible to reach an absolute error on δ_S of $O(10^{-4})$ i.e. to probe the K^0–$\bar{K}^0$ mass difference below the 10^{-18} level.

The most powerful test of CPT invariance in the neutral kaon system is presently obtained by means of the Bell-Steinberger relation. [7] This relation

make use of unitarity (or the conservation of probability) to connect a possible violation of CPT in the neutral kaon system to the CP-violating interference of K_L and K_S decays into the same final state f. Unitarity implies that K^0 and $\bar{K}^0$ decay widths can be expressed as

$$\begin{array}{rcl} \Gamma_{K^0} & = & \sum_f \mathcal{A}(K^0 \to f)\mathcal{A}(K^0 \to f)^* \\ \Gamma_{\bar{K}^0} & = & \sum_f \mathcal{A}(\bar{K}^0 \to f)\mathcal{A}(\bar{K}^0 \to f)^* \end{array} \tag{3}$$

In the limit of exact CPT invariance, these two expressions should coincide. More in general, parameterizing the amount of CPT violation in the K^0–$\bar{K}^0$ system as

$$\Delta = \frac{i(m_{K^0} - m_{\bar{K}^0}) + \frac{1}{2}(\Gamma_{K^0} - \Gamma_{\bar{K}^0})}{\Gamma_S - \Gamma_L} \cos\phi_{SW} e^{i\phi_{SW}} \tag{4}$$

where $\phi_{SW} = \arctan[2(m_L - m_S)/(\Gamma_L - \Gamma_S)]$, the unitarity decomposition implies

$$\begin{aligned} \left[\frac{\Gamma_L + \Gamma_S}{\Gamma_S - \Gamma_L}\right] \frac{\mathrm{Re}(\epsilon_M)}{1 + |\epsilon_M^2|} + \tan\phi_{SW}\mathrm{Im}(\Delta) &= \frac{1}{\Gamma_S - \Gamma_L} \sum_f \mathcal{A}_L(f)\mathcal{A}_S(f)^* \\ &= \frac{\Gamma_S}{\Gamma_S - \Gamma_L} \sum_f B(K_S \to f)\eta_f \end{aligned} \tag{5}$$

This relation is exact in the limit of CPT invariance: only the CPT-violating term $\mathrm{Im}(\Delta)$ has been treated as a small parameter and expanded to first non-trivial order. In Eq. (5) everything but the CPT-violating term is measurable [$\epsilon_M = (\epsilon_L + \epsilon_S)/2$], and one can use data on $B(K_S \to f)$ and η_f to extract stringent bounds $\mathrm{Im}(\Delta)$. A non-vanishing result could only be attributed to one of the following non-standard scenarios: i) violation of CPT; ii) violation of unitarity; iii) existence of exotic invisible final states which escape detection. Needless to say that each of this scenarios would imply major breakthrough in fundamental physics.

A Φ factory is an ideal machine to study the Bell-Steinberg relation for two main reasons: i) the perfectly tagged K_S sample can be used to measure/bounds the poorly known K_S branching ratios; ii) it is possible to have direct access to the K_L–K_S interference terms. The first advantage has already been exploited by KLOE to control the contribution of the $3\pi^0$ final state in the r.h.s. of Eq. (5). Till few years ago the $3\pi^0$ final state was the dominant source of uncertainty in the bounds on $\mathrm{Im}(\Delta)$; thanks to the recent KLOE [8]

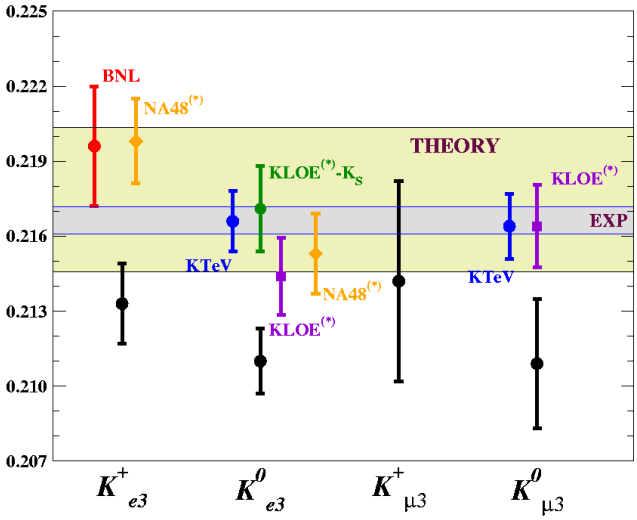

Figure 1: *Experimental results on* $|V_{us}| \cdot f_+(0)$. [12] *The gray band indicates the average of the new experimental results* ($|V_{us}| \cdot f_+(0) = 0.2166 \pm 0.0005$)*, as reported at the ICHEP '04 conference (the '*' indicates results which are still preliminary); the black points are the old PDG values; the yellow band represents the unitarity prediction combined with the recent Lattice* [11] *determination of the vector form factor* $[(1 - |V_{ud}|^2 - |V_{ub}|^2)^{1/2} \cdot f_+(0) = 0.2175 \pm 0.0029]$.

and NA48 [9] limits on $B(K_S \to 3\pi^0)$, this channel has become subleading in the final error, contributing only at $O(10^{-6})$ to $\sigma[\mathrm{Im}(\Delta)]$. Certainly much more could be done with higher statistics. In particular, with few$\times 10$ fb^{-1} the interference measurements in the leading $2\pi(\gamma)$ channels should bring the *total error* on $\mathrm{Im}(\Delta)$, from the present level of few$\times 10^{-5}$ down to few$\times 10^{-6}$. Such a sensitivity is equivalent to a relative precision on the K^0–$\bar{K}^0$ mass difference below 10^{-19}.

3.2 V_{us}

The improved determination of V_{us} from $K \to \pi\ell\nu$ decays is one of the highlights of this conference. The new data [10] from BNL-E865, KTeV, NA48 and KLOE leads to a consistent picture, substantially different from the old results quoted in the PDG. When combined with the Leutwyler–Ross estimate

of the $K \to \pi$ vector from factor at $q^2 = 0$ [$f_+(0)$] –whose validity has recently been reinforced by Lattice results [11]– these new data leads to an extraction $|V_{us}|$ (or the Cabibbo angle) in perfect agreement with the expectation of CKM unitarity (see Fig. 1).

Despite this important recent development, the field if far from being exhausted and there is still substantial room for improvements in the extraction of V_{us}. For instance, useful informations could still be extracted by precise measurements of the two $K_{\ell 3}$ form factors: their slopes provides important benchmarks to test and improve any method used in the (theoretical) evaluation of $f_+(0)$. Indeed, chiral perturbation theory let us to correlate unambiguously up to $\mathrm{O}(p^6)$ the amount of $SU(3)$-breaking in $f_+(0)$ to slope and curvature of the scalar form factor $f_0(t)$. [14] To reduce the theoretical error on $f_+(0)$ below 1% requires a measurement of the slopes λ_0 and λ_0', defined by

$$f_0(t) = f_+(0)\left[1 + \lambda_0 \frac{t}{m_\pi^2} + \lambda_0' \frac{t^2}{m_\pi^4}\right] , \qquad t = (p_K - p_\pi)^2,$$

with absolute errors of 10^{-3} (λ_0) and 10^{-4} (λ_0'). This goal is well within the reach of a Φ factory with few$\times 10$ fb^{-1}.

3.3 Rare K_S decays

As anticipated, the very rare K^+ and K_L short-distance dominated channels are not accessible with integrated luminosity below 10^4 fb^{-1}. Nonetheless, a Φ factory with ≈ 100 fb^{-1} could still play a significant role in this field: it would allow to perform a series of *auxiliary measurements*, which would help to reduce the theoretical uncertainties of some of the golden channels. The most representative examples of this type of measurements are the rates of the two $K_S \to \pi^0\ell^+\ell^-$ modes. These transitions, dominated by long-distance dynamics, contribute to a sizable $(30-50\%)$ fraction of the total $K_L \to \pi^0\ell^+\ell^-$ rate via K_L–K_S mixing. The size of this indirect-CP-violating pollution of the K_L channels (which have a sizable short-distance amplitude) can be computed with good accuracy in terms of the corresponding K_S rates. As a result, the knowledge of $B(K_S \to \pi^0\ell^+\ell^-)$ determines the precision on which we are able to extract the interesting short-distance info from $B(K_L \to \pi^0\ell^+\ell^-)$.

The two $K_S \to \pi^0\ell^+\ell^-$ transitions have recently been observed by the

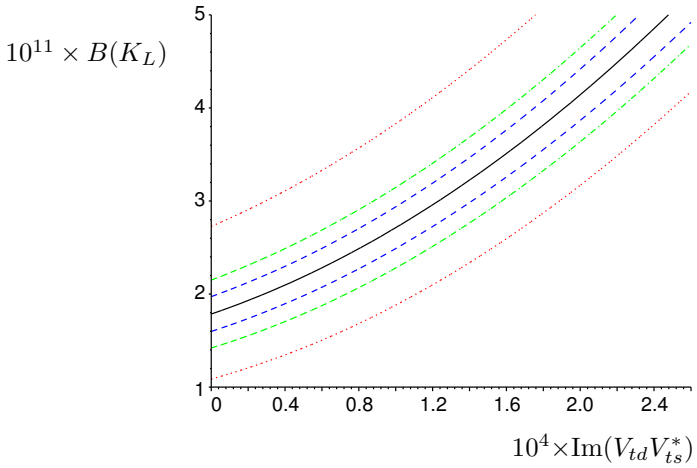

Figure 2: *SM Prediction for* $B(K_L \to \pi^0 e^+ e^-)$ *as a function of the CKM combination* $Im(V_{td}V_{ts}^*)$*, which rules the strength of the short-distance amplitude within the SM.* [4] *The three bands correspond to an error on* $B(K_S \to \pi^0 e^+ e^-)$ *of* 10% *(dashed blue lines);* 20% *(dashed green lines); present experimental uncertainty* [15] *(red dotted lines).*

NA48/1 experiment, but the present errors are still very large [15]

$$B(K_S \to \pi^0 e^+ e^-)_{m_{ee}>165 \text{ MeV}} = \left(3.0^{+1.5}_{-1.2} \pm 0.2\right) \times 10^{-9} , \quad (6)$$

$$B(K_S \to \pi^0 \mu^+ \mu^-) = \left(2.9^{+1.4}_{-1.2} \pm 0.2\right) \times 10^{-9} . \quad (7)$$

As shown in Fig. 2, with these large errors, the corresponding uncertainty on the K_L modes is $\approx 100\%$. A high-luminosity Φ factory is the ideal machine to improve these measurements: with ≈ 100 fb^{-1} we could reach $\sigma[B(K_S \to \pi^0 \ell^+ \ell^-)] \approx 10\%$. At this level of precision, the corresponding uncertainty on the K_L mode would also drop at the 10% level, allowing to perform a new very significant test of short-distance dynamics. [4] It is worth to stress that this test is unique and, in particular, is *not equivalent* to the one which could be performed in the $K \to \pi\nu\bar{\nu}$ system.

4 Conclusions

We concluded the Introduction with the following question: *is there is still room to make significant progress in fundamental physics* (searches of new phenomena and measurements of basic SM couplings) *with a substantial but realistic increase of the luminosity at the* Φ *peak*? We believe that the few examples of key measurements we have discussed (CPT tests & interferometry, $|V_{us}|$ and rare K_S decays) already provides a positive answer to this question. But of course this is only the top of the iceberg. As mentioned in the Introduction (and as discussed in more detail in Ref. 1), there are several other interesting measurements (both within and beyond the kaon sector) which could enlarge the physics program of this option.

References

1. Proceedings of the *Workshop on* e^+e^- *in the* 1–2 *GeV range: Physics and Accelerator prospect*, **eConf C0309101** (2004), eds. C. Biscari, F. Bossi, and G. Isidori.
2. F. Iachello, these proceedings.
3. See e.g.: A. J. Buras, F. Schwab and S. Uhlig, hep-ph/0405132
4. See e.g.: G. Buchalla *et al.* Nucl. Phys. B **672** (2003) 387; G. Isidori *et al.* Eur. Phys. J. C **36** (2004) 57.
5. P. Franzini, eConf **C0309101** (2003) SAPL003 [hep-ex/0401031].
6. G. D'Ambrosio, G. Isidori, and G. Pugliese, in *The Second DA*Φ*NE Physics Handbook*, eds. L. Maiani, G. Pancheri and N. Paver (Frascati, 1995).
7. J. S. Bell and J. Steinberger, in *Weak Interactions of Kaons* (1965), eds. R.G Moorhouse *et al.*
8. M. Martini [KLOE], these proceedings.
9. A. Lai *et al.* [NA48], hep-ex/0408053.

10. A. Sher *et al.* [BNL-E865] Phys. Rev. Lett. **91** (2003) 261802 [hep-ex/0305042]; T. Alexopoulos *et al.* [KTeV], hep-ex/0406001, hep-ex/0406002, hep-ex/0406003; U. Moosbroogger [NA48], these proceedings; C. Gatti [KLOE], these proceedings.

11. D. Becirevic *et al.*, hep-ph/0403217; V. Lubicz, these proceedings.

12. F. Mescia, talk presented at ICHEP '04 (Beijing, China, August 2004).

13. H. Leutwyler and M. Roos, Z. Phys. C **25** (1984) 91.

14. J. Bijnens and P. Talavera, Nucl. Phys. B **669** (2003) 341 [hep-ph/0303103].

15. J.R. Batley *et al.* [NA48/1], *Phys. Lett.* **B 576** (2003) 43 [hep-ex/0309075].

Frascati Physics Series Vol. XXXVI (2004), pp. 495–504
DAΦNE 2004: PHYSICS AT MESON FACTORIES – Frascati, June 7-11, 2004
Invited Review Talk in Plenary Session

STRUCTURE OF HADRONS FROM ELECTROMAGNETIC FORM FACTORS

F. Iachello
Center for Theoretical Physics, Sloane Physics Laboratory,
Yale University, New Haven, CT 06520-8120, USA

Abstract

It is suggested that *all* hadronic electromagnetic form factors be described in terms of a two-component model, in which the photon couples to both an intrinsic structure, q^3 for baryons and $q\bar{q}$ for mesons, and a cloud of $q\bar{q}$ pairs. The time-like form factors of this model can be tested at meson factories, especially DAΦNE-2.

1 Review of nucleon space-like form factors

1.1 Space-like proton

The study of the structure of the nucleon with electromagnetic probes has been the subject of many investigations since the pioneering work of Hofstadter *et al.* in the early 1960's. By 1995 a comprehensive experiment performed at SLAC [1)] using the Rosenbluth method to separate electric from magnetic form factors appeared to

indicate that the large Q^2 behavior of both the electric and magnetic form factor of the proton was $\propto 1/Q^4$ and in fact given by the empirical scaling law $G_D(Q^2) = 1/(1+\frac{Q^2}{0.71})^2$. This result was consistent with perturbative QCD and dimensional scaling [2]. However, in a series of experiments performed at TJNAF in 2000-2002 [3, 4] using the recoil polarization method which measures the ratio G_E/G_M directly, without Rosenbluth separation, an astounding result was found, namely that the proton electric form factor decreases dramatically with Q^2. This result is inconsistent with scaling and p-QCD but in agreement with an old calculation, performed in 1973, in terms of a two-component model [5]. This has reopen the question of what is the actually structure of the nucleon.

1.2 Space-like neutron

In other SLAC experiments in the 1990's [6] it appeared that the magnetic form factor of the neutron was also following the empirical scaling law, consistent with p-QCD, and that the electric form factor was consistent with zero. However, again in experiments performed at TJNAF in 2003 using the recoil polarization method [7], it was found that the electric form factor of the neutron is definitely different from zero and in fact increases dramatically with Q^2. This result is inconsistent with the 1973 parametrization.

1.3 Models of the nucleon

The TJNAF results have spurred a considerable amount of theoretical papers. Leaving aside the question of why the SLAC results are inconsistent with TJNAF, perhaps due to two-photon contributions, there remains the basic question of what is the structure of the nucleon.

Form factors can in principle be calculated on the lattice. Unfortunately these calculations are still far from being realized. For this reason one must resort to models. Different models of the nucleon correspond to different assumptions for the Dirac and Pauli form factors that appear in the nucleon electromagnetic current

$$J^\mu = F_1(Q^2)\gamma^\mu + \frac{\kappa}{2M_N}F_2(Q^2)i\sigma^{\mu\nu}q_\nu. \qquad (1)$$

Many lines of thought have been recently followed. Three of these are: (1) Two-component model [8], where the two components are the intrinsic valence quark structure, q^3 for baryons, and the meson $q\bar{q}$ cloud. (2) Relativistic constituent quark model

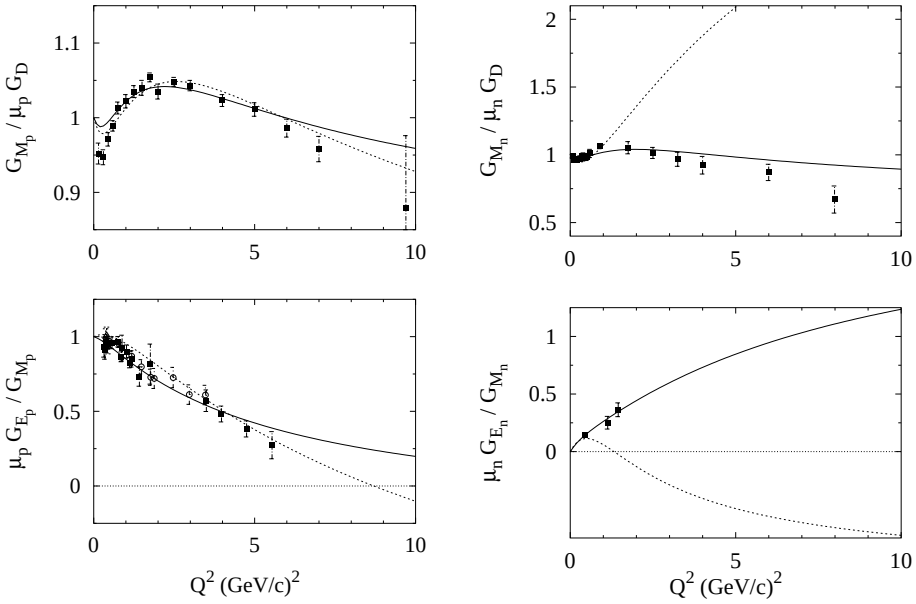

Figure 1: *(Left) Comparison between experimental and theoretical space-like proton form factors. Top panel: the magnetic form factor $G_{M_p}/\mu_p G_D$. Bottom panel: the ratio $\mu_p G_{E_p}/G_{M_p}$. The solid lines are from the 2004 parametrization [8], the dashed lines are from the 1973 parametrization [16]. (Right) Comparison between experimental and theoretical space-like neutron form factors. Top panel: the magnetic form factor $G_{M_n}/\mu_n G_D$. Bottom panel: the ratio $\mu_n G_{E_n}/G_{M_n}$. The solid lines are from the 2004 parametrization [8], the dashed lines are from the 1973 parametrization [16]. Adapted from [8].*

in the light-front approach with quark form factors [9, 10]. (3) Soliton model [11]. The results of the most recent analysis in terms of the two-component model are shown in Fig. 1. The conclusions drawn from the analysis of space-like form factors are: (i) The nucleon appears to be rather complex ($q\bar{q}$ pairs, or quark form factors, needed). (ii) p-QCD does not set in until large Q^2 (conservative estimate ≥ 10 (GeV/c)^2; more likely ≥ 30 (GeV/c)^2). (iii) None of the present models is fully consistent with all data (other components, gluons?, needed).

2 Nucleon time-like form factors

The first successful measurement of $e^+e^- \to p\overline{p}$ was performed in 1973 by Castellano *et al.* at Frascati [12]. In the 1970's many experiments were performed. In 1993 Armstrong *et al.* [13] performed the first successful measurement of $p\overline{p} \to e^+e^-$. Finally, Antonelli *et al.* [14] performed at Frascati in 1998 the only available measurement of $e^+e^- \to n\overline{n}$.

The analysis of time-like form factors makes use of the fact that time-like and space-like form factors are related by analytic continuation $q^2 = -Q^2$. For time-like form factors of the nucleon, the physical region is $q^2 \geq 4M_N^2$. Time-like form factors are usually analyzed by means of dispersion relations [15]. However, by an appropriate analytic continuation, they can also be analyzed in terms of models. Very recently, an analytic continuation of the two-component model has been suggested [16, 8]. Analytic continuation of the relativistic constituent quark model with quark form factors [10] can also be done, although it has not been implemented yet. The results for the two-component model are shown in Fig. 2. Conclusions drawn from presently available data are: (i) $\mid G_{M_n} \mid$ time-like is inconsistent with $\mid G_{M_n} \mid$ space-like. (ii) $\mid G_{M_p} \mid$ time-like is in good agreement with the two-component model. (iii) No information is available on the electric form factors $\mid G_{E_n} \mid$ and $\mid G_{E_p} \mid$.

In view of this situation, it appears that remeasurements of time-like form factors are of crucial importance for understanding the structure of the nucleon. An upgrade of DAΦNE provides an unique opportunity to solve one of the most important questions in Physics, namely what is the structure of the nucleon. In this respect, it is important to note that polarization measurements could be used to distinguish between different models as pointed out recently by Brodsky *et al.* [17].

Another important aspect that could be investigated with the DAΦNE upgrade is the question of whether or not there are subthreshold resonances in the $p\bar{p}$ and $n\bar{n}$ channel. From both proton and neutron data there are indications of subthreshold resonances. Adding [16] a subthreshold isoscalar resonance at $m_X \simeq 1870$ MeV [14] and negligible width to the two-component parametrization of F_2^S

$$\begin{aligned} F_2^S(q^2) &= \frac{1}{2}g(q^2)[(-0.120-\alpha_\varphi-\alpha_X)\frac{m_\omega^2}{m_\omega^2-q^2} \\ &\quad +\alpha_\varphi\frac{m_\varphi^2}{m_\varphi^2-q^2}+\alpha_X\frac{m_X^2}{m_X^2-q^2}] \end{aligned} \tag{2}$$

produces good agreement with experiment, Fig. 3. The resonance is weakly coupled,

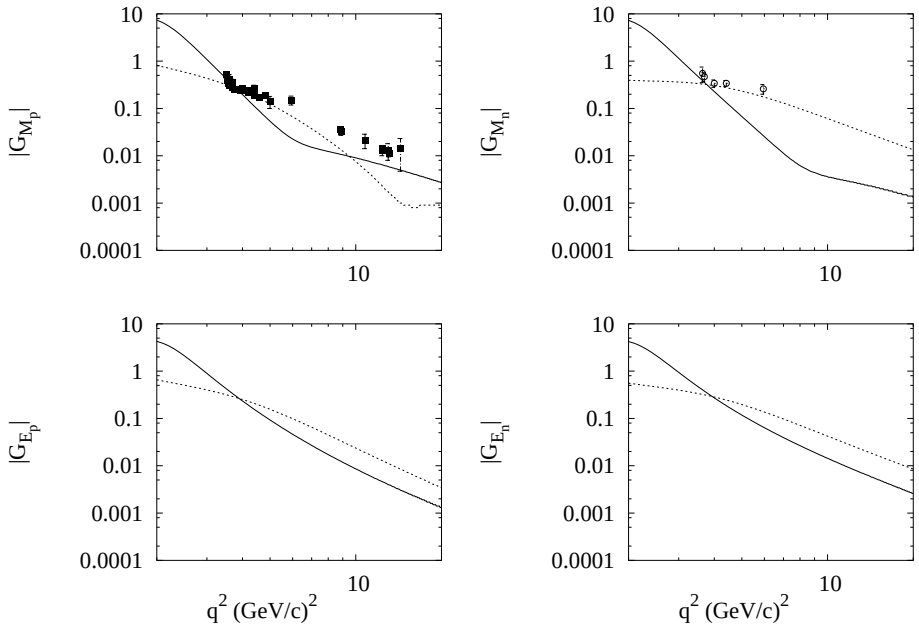

Figure 2: *(Left) Comparison between experimental and theoretical time-like proton form factors. Top panel: the magnetic form factor* $|\, G_{M_p} \,|$*. Bottom panel: the electric form factor* $|\, G_{E_p} \,|$*. The solid lines are from the 2004 parametrization [8] and the dashed lines are the analytic continuation of the 1973 parametrization [16]. (Right) Comparison between experimental and theoretical time-like neutron form factors. Top panel: the magnetic form factor* $|\, G_{M_n} \,|$*. Bottom panel: the electric form factor* $|\, G_{E_n} \,|$*. The solid lines are from the 2004 parametrization [8] and the dashed lines are the analytic continuation of the 1973 parametrization [16]. Adapted from [8].*

$\alpha_X = 0.001$. An isovector resonance would produce similar results except for the interchange of peaks in the neutron form factors. A careful remeasurement of G_{M_n} close to threshold at DAΦNE-2 can determine whether the resonance is isoscalar or isovector.

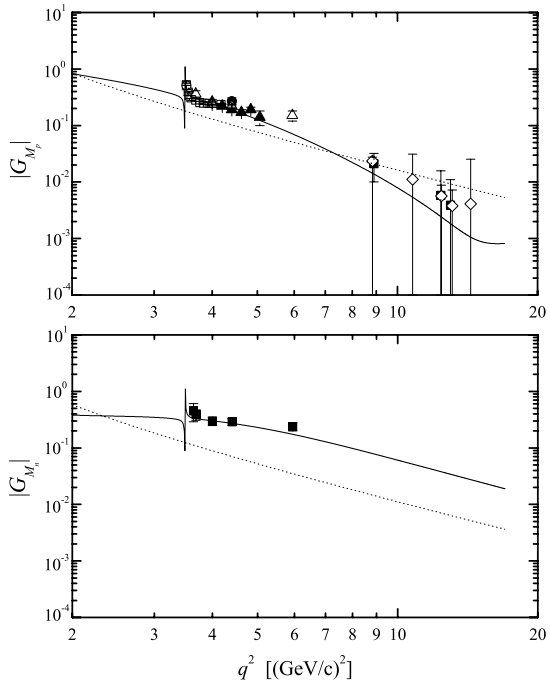

Figure 3: *Effects of an isoscalar subthreshold resonance on the time-like form factors* $|G_{M_p}|$ *(top panel) and* $|G_{M_n}|$ *(bottom panel). The dotted lines are the dipole form factors* $\mu_p G_D$ *and* $\mu_n G_D$*. From [16].*

3 Other hadronic form factors

3.1 Form factors of baryons

Model calculations provide predictions for all hadronic form factors. The two-component model complemented with $SU_f(3)$ flavor symmetry, provides predictions for the form factors of baryon belonging to the $\underline{8}$ and $\underline{10}$ representations of $SU_f(3)$, in particular for the time-like form factors in $e^+e^- \to \Sigma^+\Sigma^-$. These could be measured at DAΦNE-2.

3.2 Form factors of pseudoscalar mesons

It has been assumed for some time that form factors of pseudoscalar mesons in the time-like region were well described by the large Q^2 behavior predicted by p-QCD,

$\propto 1/Q^2$. Recent measurements at TJNAF [18] in the space-like region have shown that p-QCD fails to describe the observed behavior. On the other side, a two-component model appears to describe the data well [19]. In this model, the pion form factor is parametrized as

$$\begin{aligned} F_\pi(Q^2) &= g_{PS}(Q^2)\left[(1-\beta_\rho)+\beta_\rho\frac{m_\rho^2}{m_\rho^2+Q^2}\right] \\ g_{PS}(Q^2) &= \frac{1}{(1+\gamma_{PS}Q^2)}. \end{aligned} \tag{3}$$

An analytic continuation, similar to that for the nucleon, gives the pion form factor in the time-like region. The pion form factor in the time-like region could be measured at DAΦNE-2 by $e^+e^- \to \pi^+\pi^-$. A calculation of the pion form factor both in the space-like and time-like region is in the process of being completed and will be presented soon [20].

4 Inelastic form factors

4.1 The N-$\Delta(1232)$ form factors

These are the most extensively studied inelastic form factors. The first measurement was performed by Bartel *et al.* [21] at DESY in 1968. Many experiments were performed in the 1970's. In the 1990's it was found that the magnetic form factor drops faster than empirical scaling law, in disagreement with p-QCD that predict a fall-off as $1/Q^4$. Finally, in 2002 measurements at TJNAF have shown non-zero electric and longitudinal components.

The analysis of N-Δ form factors is by far more complex than that of the elastic form factors. I begin here with a brief reminder of some basic formulas. There are three form factors. These form factors can be written in terms of helicity amplitudes, as

A. Magnetic form factor

$$G_M^{Ash} = K\left[A_{1/2}+\sqrt{3}A_{3/2}\right], \tag{4}$$

where K is a kinematical factor.

B. Electric form factor. It is customary to quote the ratio of electric to magnetic form factor

$$R_{EM} = \frac{A_{1/2}-\frac{1}{\sqrt{3}}A_{3/2}}{A_{1/2}+\sqrt{3}A_{3/2}}. \tag{5}$$

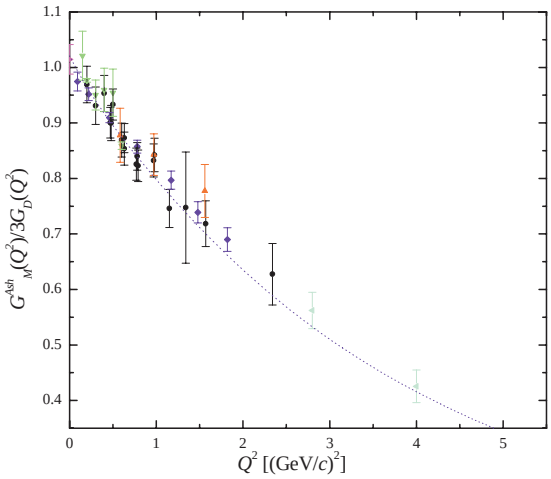

Figure 4: *The N-$\Delta(1232)$ magnetic form factor $G_M^{Ash}/3G_D$. The dashed line is the two-component calculation. From [20].*

C. Longitudinal form factor. It is customary to quote the ratio of longitudinal to magnetic form factor

$$R_{SM} = \frac{S_{1/2}}{A_{1/2} + \sqrt{3}A_{3/2}}. \tag{6}$$

Here $A_{1/2}$,$A_{3/2}$ are the transverse helicity amplitudes and $S_{1/2}$ is the longitudinal amplitude.

Inelastic form factors can be analyzed in terms of models. Two have been used: a two-component model [20] and a relativistic quark model [10]. Fig. 4 shows the comparison of the measured form factor with the calculation in the two-component model. Results of the analysis are: (i) N-Δ form factors appear to be dominated by coupling to ρ. (ii) p-QCD does not set in until large $Q^2 \geq 4$ (GeV/c)^2. (iii) R_{EM} and R_{SM} are very sensitive to models. The measured ratio R_{EM} favors the two-component model.

5 Conclusions

(i) In 1960 Hofstadter demonstrated that the nucleon is not point-like. In 2000-2002 experiments at JLab have shown that the nucleon has a complex structure.

(ii) A two-component model with an intrinsic (valence quarks) plus meson cloud

($q\bar{q}$ pairs) appears to describe all hadronic data well. The Fock state representation for baryons is

$$|N\rangle = a_0 \,|\, q^3\rangle + a_1 \,|\, q^3 q\bar{q}\rangle + ... \tag{7}$$

and for mesons

$$|\pi\rangle = b_0 \,|\, q\bar{q}\rangle + b_1 \,|\, q\bar{q}q\bar{q}\rangle + ... \tag{8}$$

(iii) The size of the intrinsic structure appears to be r.m.s.$\sim 0.34 - 0.49$ fm while the size of the cloud appears to be r.m.s. ~ 0.86 fm.

(iv) p-QCD is not reached at 10 (GeV/c)^2. Physics up to this scale is dominated by a mixture of hadronic and quark components.

The DAΦNE upgrade could contribute considerably to our understanding of the structure of hadrons, and hence of QCD in the non-perturbative regime. Possible projects are: $e^+e^- \to n\bar{n}$ (unique to DAΦNE); $e^+e^- \to p\bar{p}$; $e^+e^- \to \Sigma^+\Sigma^-$; $e^+e^- \to \pi^+\pi^-$.

6 Aknowledgements

This work was performed in part under DOE Contract No. DE-FG-02-91ER40608.

I wish to thank Gianni Salme' for many discussions on the relativistic quark model, Rinaldo Baldini for bringing to my attention the problem of time-like form factors, Richard Madey for discussions on the neutron form factors, Roelof Bijker and Qian Wan for performing the calculations and Mark Caprio for helping me preparing the manuscript.

References

1. L. Andivahis *et al.*, Phys. Rev. D **50**, 5491 (1994).
2. G.P. Lepage and S.J. Brodsky, Phys. Rev. Lett. **43**, 545 (1979); Phys. Rev. D **22**, 2157 (1980).
3. M.K. Jones *et al.*, Phys. Rev. Lett. **84**, 1398 (2000).
4. O. Gayou *et al.*, Phys. Rev. Lett. **88**, 092301 (2002).
5. F. Iachello, A.D. Jackson, and A. Lande, Phys. Lett. **43B**, 191 (1973).
6. A. Lung *et al.*, Phys. Rev. Lett. **70**, 718 (1993).

7. R. Madey *et al.*, Phys. Rev. Lett. **91**, 122002 (2003).
8. R. Bijker and F. Iachello, Phys. Rev. C **69**, 068201 (2004).
9. M. R. Frank, B.J. Jennings, and G.A. Miller, Phys. Rev. C **54**, 920 (1996).
10. E. Pace, G. Salme', F. Cardarelli and S. Simula, Nucl. Phys. A **666**, 33c (2000).
11. G. Holzwarth, Z. Phys. A **356**, 339 (1996).
12. M. Castellano *et al.*, Nuovo Cimento A **14**, 1 (1973).
13. T.A. Armstrong *et al.*, Phys. Rev. Lett. **70**, 1212 (1993).
14. A. Antonelli *et al.*, Phys. Lett. B **334**, 431 (1994).
15. H.-W. Hammer, Ulf-G. Meissner, and D. Drechsel, Phys. Lett. B **385**, 343 (1996).
16. F. Iachello and Q. Wan, Phys. Rev. C **69**, 055204 (2004).
17. S.J. Brodsky, C.E. Carlson, J.R. Hiller, and D.S. Hwang, Phys. Rev. D **69**, 054022 (2004).
18. J. Volmer *et al.*, Phys. Rev. Lett. **86**, 1713 (2001).
19. F. Iachello, Eur. Phys. J A **19**, s01, 29 (2004).
20. F. Iachello and Q. Wan (in preparation).
21. W. Bartel *et al.*, Phys. Lett. **B28**, 148 (1968).

Session VIII — Hot Topics

(Chair: G. Capon)

Frascati Physics Series Vol. XXXVI (2004), pp. 507–516
DAΦNE 2004: Physics at meson factories – Frascati, June 7-11, 2004
Invited Review Talk in Plenary Session

COSMOLOGICAL STANDARD MODEL

A.D. Dolgov
ICTP, Trieste, 34014, Italy, INFN, Ferrara, 40100, Italy,
ITEP, Moscow, 117218, Russia

Abstract

A review of the contemporary state of the cosmological standard model is presented. The bulk properties of the model seems to be solid and firmly established but unsolved and possibly serious problems exist. The cosmological data demanding new physics beyond the particle standard model are outlined.

1 Introduction

During the last 2-3 decades of the previous century a symbiotic development of cosmology and elementary particle physics has led to a striking success in both fields. Two standard models have been established: the (minimal) standard model of particle physics, (M)SMPP, and the cosmological standard model, CSM. Though both these models are called "standard", there is an important difference between them. (M)SMPP well agrees with all existing experimental

data in particle physics and could last without new physics. On the contrary, the CSM contains many unusual effects and phenomena which do not fit the framework of the MSMPP (and even of the SMPP) and surely demand new, not yet discovered physics.

In what follows the CSM and its relation to the SMPP are discussed. In sec. 2 matter-energy content of the universe is inventoried. Next, in sec 3 brief cosmological history is presented, as we understand it now, and a necessity of new physics is advocated. In sec. 4 basic facts about large scale structure (LSS) of the universe (observations and theory) are presented. A proper list of references would make this paper to go beyond the allocated volume limit and thus only references to reviews are made. In particular, all values of basic cosmological parameters presented below can be found in the new issue of the Particle Data Group [1)].

2 Matter-energy inventory.

The contribution of a certain form of matter into cosmological matter-energy density is usually expressed by dimensionless parameter $\Omega_a = \rho_a/\rho_c$, where

$$\rho_c = \frac{3H^2 m_{Pl}^2}{8\pi} = 1.88 \cdot 10^{-29} h^2 \frac{\mathrm{g}}{\mathrm{cm}^3} = 10.5\, h^2 \frac{\mathrm{keV}}{\mathrm{cm}^3} = 3 \cdot 10^{-47} h^2 \mathrm{GeV}^4 \qquad (1)$$

is the critical or closure energy density and $h = 0.72 \pm 0.05$. The position of the first acoustic peak in the angular spectrum of CMBR, combined with other astronomical observations, accurately confirms predicted by inflation flatness of the universe, $\Omega_{tot} = 1.02 \pm 0.02$. The usual baryonic matter makes only a tiny fraction of total mass density, $\Omega_b = 0.05 \pm 0.01$ This result is obtained from two *independent* pieces of data: from analysis of cosmological abundances of light elements produced during BBN and from the positions and heights of acoustic peaks of CMBR [1)]. Only 10% of all cosmic baryons are observed directly in the form of luminous or light-absorbing matter. It is an intriguing problem where are the remaining 90% of baryons [2)].

The total amount of clustered matter, the so called dark matter, observed by its gravitational action, is about 6 times larger than that of baryons: $\Omega_{DM} = 0.30 \pm 0.07$, where Ω_{DM} includes all kinds of non-relativistic gravitating matter with equation of state $p = 0$. Out of these 0.3 approximately 1/6 are normal baryons, while the dominant 0.25-part consists of some unknown

new form of matter. It is important that this serious conclusion is based on different independent pieces of astronomical data [3]:

1. Rotational velocities of gas clouds surrounding galaxies show that the amount of gravitating matter is much larger than that of the luminous one with the bulk of dark matter far outside the luminous part of the galaxy. Still the amount of dark matter is not enough to make $\Omega_m = 1$.

2. Peculiar velocities of galaxies superimposed on the cosmological Hubble flow are supposed to be induced by the surrounding matter. Measurements of these velocities are consistent with $\Omega_m \approx 0.3$.

3. Analysis of the equilibrium of hot gas in rich galactic clusters shows that the ratio of baryonic mass to the total mass is about 0.2.

4. Theory of cluster evolution predicts that in the universe with high matter content, $\Omega_m \approx 1$, the number of galactic clusters at $z = 1$ should be several, 3-5 times smaller, than at $z = 0$. Observations show that they are approximately the same, as is predicted by low Ω_m cosmology.

5. Gravitational lensing: light deflection from distant objects shows that the total clustered mass along the path of propagation is consistent with $\Omega_m = 0.3$.

One more argument in favor of non-baryonic dark matter comes from the theory of LSS formation. Small angular fluctuations of CMBR show that the density fluctuations at hydrogen recombination epoch, $z \approx 10^3$, were also small, $\delta\rho/\rho \sim 10^{-4}$. They could rise, due to gravitational instability, at most, as cosmological scale factor. Hence at the present time $\delta\rho/\rho$ might reach only 0.1, while it should be of the order of unity. This conclusion is true for the so called adiabatic density perturbations, in contrast to the isocurvature ones. According to CMBR data [4], the latter are small.

It is unknown at the present time what makes the dark matter. There are many possible candidates, we will mention only a few [5]:

1. The lightest supersymmetric particle, which would be stable if R-parity is conserved. The mass of such particles in natural model is about $10^2 - 10^3$ GeV.

2. Axion, its mass should be very small, about 10^{-5} eV, but since cosmological axions might be produced at QCD phase transition at rest, they would be non-relativistic and good for structure formation.

3. Primordial black holes or early formed star-like objects. They should be formed before BBN, otherwise successful predictions for light element abundances would be destroyed.

4. Mirror matter, a new world of particles which are connected to ours only through gravity and, possibly, through some other weak interaction. In contrast to mentioned above forms of DM mirror matter could be self-interacting and its cosmological evolution and cooling would be different.

Whatever dark matter particles could be, they, at least, have normal gravitational (inter)action by which their existence is detected. Really astonishing fact is that the bulk of matter in the universe, about 70%, anti-gravitates creating accelerated cosmological expansion. This unknown form of cosmological energy density is called *dark energy*. It is normally assumed that the energy density is positive, $\rho > 0$, and, to drive gravitational repulsion the pressure density should be negative and larger by absolute value than $\rho/3$. One should bear in mind, however, that with positive ρ gravitational repulsion (anti-gravity) may be created only in infinitely large systems; any finite object always gravitates. According to the combined astronomical data [1)] the fraction of dark energy in the universe is $\Omega_{DE} \approx 0.7$ with equation of state determined by $w_{DE} = -0.98 \pm 0.12$. Thus cosmological dark energy can be just vacuum energy with $w = -1$ or something quite close to it. Several sets of astronomical data support these results:

1. Direct observations of cosmological acceleration [6, 7)]. To do that one needs to measure the universe expansion law at high red-shifts. This is done with type Ia supernovae which are possibly the standard candles, i.e. astronomical objects with known luminosity. Their observations at $z \sim 1$ show that they are systematically dimmer than would be expected for normal decelerated expansion and a possible conclusion is that the universe expands with acceleration. Dimness of supernovae at large distances cold be explained by additional light absorption on the way by the so called gray dust. However, the effect of accelerated expansion must have maximum around $z = 0.7$; for larger z the normal matter should dominate and supernovae would be brighter. This is exactly what was observed [7)] and it is a very strong argument in favor of "accelerated" interpretation of the data.

2. Angular spectrum of CMBR shows a prominent acoustic peak at $l = 200$. This corresponds to geometrically flat universe i.e. $\Omega_{tot} = 1$. Since $\Omega_m = 0.3$, this result implies that there is 0.7 in unknown form of energy. Moreover, a slight decrease of multipoles from l=5 to l=20 is in agreement with evolution of perturbations in a universe with non-zero vacuum energy.

3. LSS is well described in the theory with $\Omega_{vac} = 0.7$ and $\Omega_m = 0.3$. This is the best fit model at the present time.
4. If $\Omega_{vac} = 0$ and $\Omega_m = 1$ then the universe age would be too short to be compatible with the age of globular clusters and nuclear chronology. However, if $\Omega_{vac} = 0.7$ the universe age is in a perfect agreement with the data.

Probably the most natural assumption about dark energy is that it is simply vacuum energy. The energy momentum tensor of the latter is proportional to the metric tensor, $T_{\mu\nu}^{(vac)} = g_{\mu\nu}\rho_{vac}$ and, evidently, $p = -\rho$. Quantum field theory claims many contributions into vacuum energy, thus a non-zero result is quite natural. The only problem is that these contributions are huge in comparison with the observed value. For example, the well known QCD vacuum energy created by quark or gluon condensates is about 10^{-2} GeV^2 which overshoots cosmological energy density by 45 orders of magnitude. Other estimated contribution into ρ_{vac} are much larger, up to 120 orders of magnitude. How these almost infinitely large contributions are tuned or adjusted down to the observed value is one of the most serious problems of fundamental physics [8].

Except for vacuum energy, the dark energy could be either created by a new very light or even massless field or might be mimicked by modification of gravity at large distances. Neither of these two approaches addresses a problem of mismatch of theoretical expectations and the observed value of cosmological energy density by 50-100 orders of magnitude. In principle both problems could be solved by adjustment mechanism, when a new field did both jobs: compensate vacuum energy down to the terms of the order of critical energy density, m_{Pl}^2/t^2, with non-compensated remnant being the dark energy. Unfortunately at the moment there is no realistic model of adjustment.

There is one more strange fact about cosmological matter. Mass density of baryons is determined by the process of baryogenesis which, to the best of our knowledge, is unrelated to the creation of most popular forms of dark matter. Hence the energy densities of these two could be easily different by several (many) orders of magnitude. In reality they differ only by factor 5. This probably means that the two processes are physically connected and this is yet to be discovered.

The coincidence becomes more impressive if one takes into account that the density of dark energy is almost the same as that of dark matter (they differ by factor 2 only). Moreover, vacuum (or vacuum-like) energy remains

constant (or almost constant, if $w \approx -1$), while the energy density of dark matter scales as $1/a^3$. These coincidences are so striking that one may even call them "cosmic conspiracy". The cosmic conspiracy would be much more profound if other forms of DM (e.g. WDM) exist with comparable contributions into Ω (see sec 4).

There are two more known, though sub-dominant, contributions into cosmological matter, CMBR and cosmic neutrino background (CNB). The properties of the former is very accurately studied. The photons have perfect equilibrium thermal spectrum, with $T = 2.725$K and with vanishing chemical potential, $\mu/T < 10^{-4}$. Their number density is $410/\text{cm}^3$. The radiation is almost isotropic with the precision of about 10^{-5}, except for rather large dipole component, $\delta T/T \approx 2 \cdot 10^{-3}$. The latter is believed to be induced by our motion with respect to cosmological rest frame and corresponds to about 600 km/sec. This velocity is probably too fast to be explained by the gravitational action of neighboring clusters of galaxies. If this is true, then some other explanation for a large dipole asymmetry would be necessary (intrinsic dipole?). Some concern creates also a too low value of the quadrupole asymmetry.

As usually in physics, small imperfections are much more interesting than an exact symmetry and the observed small angular fluctuations of CMBR are now one of the most powerful tools for studying universe. Spectrum of angular fluctuations of CMBR, which is now measured up to the multipole number $l = 1000$ allows to determine basis cosmological parameters; Ω_{tot}, Ω_b, Ω_{vac}, h, and the spectrum of primordial density fluctuations. The latter is assumed to have a power law form with $n = 0.97 \pm 0.03$ in good agreement with inflationary prediction. One should keep in mind, however, the problem of degeneracy, i.e. the same spectrum of $\delta T/T$ could be created with different values of cosmological parameters in certain combinations. To resolve the degeneracy other astronomical measurements, especially of the power spectrum at smaller scales, found from distribution of matter at galaxy cluster scales and around, is of primary importance. CMBR measures the spectrum of fluctuations at the scales between the present day horizon size (a few Gpc) down to 10 Mpc, while the study of matter distribution (galaxies, clusters, and superclusters) measures spectrum of fluctuations from galactic scales up to tens Mpc. The fact that the measurements made from different ends agree in the coinciding region is a strong argument in favor of the consistency of the CSM.

After photons of CMBR, neutrinos are the second most abundant particles in the universe (among known ones, since e.g. the number density of cosmic axions might be higher). In the standard model, the number density of neutrinos is $55/\mathrm{cm}^3$ for any type of neutrino and anti-neutrino. If neutrinos were massless they would have practically equilibrium Fermi-Dirac distribution with the present-day temperature $T_\nu \approx 1.95$ K. The observations of neutrino oscillations leads to conclusion that they must be massive with the mass of at least one of them being bigger than 0.05 eV. On the other hand, combined CMBR and LSS data put a stringent upper bound on neutrino mass [4], $\sum_a m_{\nu_a} < 0.7$ eV, where summation is made over all neutrino mass eigenstates. Correspondingly the relative contribution from CNB into total cosmological energy density is bounded by $10^{-3} < \Omega_\nu < 0.15$. Thus, a possible role of neutrinos in LSS formation is rather weak. Neutrinos might play a significant role there only if they do not obey Fermi statistics. In this case they even could form all dark matter in the universe - a thermal part of them would make hot dark matter, while a possible neutrino condensate would make cold dark matter.

3 Brief cosmological history

Observing universe today one can extrapolate this knowledge into the past and reconstruct main events in the universe history. Still it is not known what happened before time-zero or, in other words, how the universe started to evolve or if it existed for ever. There are several hypothesis: creation from nothing, eternal chaotic inflation, oscillating universe, string-motivated pre-big-bang cosmology, and possibly many more. None of them is either confirmed or rejected.

The earliest known period is *inflationary epoch* [9] when the universe expanded exponentially, $a \sim \exp(H_I t)$ with constant H_I. Inflation is practically an experimental fact. Of course one cannot rigorously exclude (unknown) alternatives but inflationary scenario is capable to solve by one blow the long standing problems of horizon, homogeneity and isotropy, to explain the origin of expansion and density perturbations on astronomically large scales. The generic predictions of inflation: $\Omega_{tot} = 1$, (almost) flat spectrum of density perturbations, Gaussian fluctuations of $\delta T/T$ are in a very good agreement with the data. Inflation cannot be realized in the framework of (M)SMPP and demands a new weakly interacting field, inflaton.

Next important step in the universe history was *baryogenesis* [10]. Inflation ended up with vanishingly small values of all conserved charges and to create the observed today excess of particles over antiparticles baryonic and leptonic charges must be non-conserved. Two other Sakharov's conditions of baryogenesis: breaking of C and CP and deviations from thermal equilibrium can be easily realized in big bang cosmology, allowing generation of the observed asymmetry, $\beta = (n_B - n_{\bar{B}})/n_\gamma = 6 \cdot 10^{-10}$. All three baryogenesis ingredients are present in electroweak interactions of MSMPP, but the magnitude of effect is much smaller than the necessary value. Thus an extension of MSMPP seems necessary. There are many possible scenarios of baryogenesis but we do not yet know which one was realized. It is a difficult problem to choose the correct scenario knowing only one observed number, β. In some models of baryogenesis a noticeable amount of antimatter could be produced in the form of antimatter domains, clouds of dispersed antimatter, or anti-stars and anti-planets. If search for cosmic antimatter is successful we will have a chance to find more about physics of baryogenesis.

Big bang nucleosynthesis (BBN) is already in "terrae cognitae". The underlying physics is low energy weak interactions and nuclear physics. The accuracy of theoretical predictions is a fraction of per cent for ^4He, and about 10% for ^7Li. The main part of theoretical uncertainty comes from the cross-sections of nuclear reactions. Much bigger errors arise in the process of extrapolation of the abundances of light elements produced in the early universe to the contemporary old universe when these elements are observed. Observational determinations of light element abundances are subject to rather large systematic errors and different corrections applied to raw data. Still despite all these uncertainties, there seems to be an inconsistency between measurements of deuterium and helium-4, and, even more, between different measurements of abundances of the same element in different astronomical systems. It is premature to conclude that the standard BBN is in trouble and some non-standard corrections are necessary but still the cloud exists and a resolution of the discrepancies is much needed [11].

At red-shifts about or below 10^4 initially small density perturbations started to rise making seeds for LSS formation, then at $z \approx 10^3$ hydrogen recombined and cosmic matter became practically neutral allowing for formation of baryonic structures and liberation of CMBR which from that moment

propagated freely and brought to us information about that period. In more detail LSS formation is discussed in a separate section below.

4 Large scale structure formation

According to the theory, cosmological density perturbations remained frozen (with logarithmic accuracy) till universe became dominated by non-relativistic matter. It happened at approximately $z = 10^4$. After that moment gravitational instability became operative and density contrast begun to rise as cosmological scale factor, $\delta\rho/\rho = (z+1)\,(\delta\rho/\rho)_{in}$. This is the so called linear regime when density perturbations remains small. When $\delta\rho/\rho$ reaches unity, non-linear and much faster rise comes into effect. It is relatively easy to determine the law of evolution of density perturbations in the linear stage, while at non-linear regime numerical simulation methods are used.

The necessary input for the calculations includes an assumption about the spectrum of initial density perturbations. It is usually assumed to be of the power law form and, in particular, flat Harrison-Zeldovich spectrum (supported by inflation). Second important piece of information is the type of perturbations. The latter can be decomposed into two "orthogonal" ones, adiabatic with the same $(\delta\rho/\rho)$ for all types of matter or isocurvature with $\delta\rho = 0$ but varying chemical content. These two types of perturbations evolve independently at initial stage but begin to interact when isocurvature perturbations generate non-zero $\delta\rho$ due to different equations of state in different space points. In the standard model density perturbations are assumed to be adiabatic, in accordance with inflation and in agreement with CMBR data.

One needs also to specify the properties of dark matter particles. From astronomical point of view the latter could either cold (decoupled from cosmic plasma being non-relativistic), warm (semi-relativistic), or hot (relativistic). Correspondingly the characteristic scale of structures formed with WDM is about galactic size and much larger than that for HDM. The dark matter particles have negligible interactions with photons and baryons and between themselves. The last property is not always assumed to be true, as e.g. in scenarios with mirror matter. The standard (reference) model is based on dissipation-less cold dark matter particles (30%) plus uniformly distributed vacuum energy (70%). This model rather well describes general features of the observed structure but there are several troubling signs [12]:

1. Theory predicts cusps in galactic centers which are not observed.
2. The predicted number of galactic satellites is much larger than observed.
3. The calculated angular momenta of galaxies is too small in comparison with the observed ones.

It is unclear if these discrepancies are the results of oversimplified numerical simulations with important physical effects neglected, or some new input is necessary as e.g. warm dark matter.

References

1. Particle Data Group, http://pdg.lbl.gov/pdg.html .
2. M. Fukugita, P.J.E. Peebles, astro-ph/0406095.
3. L. Van Waerbeke *et al*, astro-ph/0212150; R.H. Sanders, astro-ph/0402065; M. Trodden, S.M. Carroll, astro-ph/0401547.
4. D.N. Spergel *et al*, Astrophys. J. Suppl. **148**, 175 (2003).
5. G. Bertone, D. Hooper, J. Silk, hep-ph/0404175, submitted to Physics Reports; P. Gondolo, astro-ph/0403064.
6. A. G. Riess *et al.*, Astron. J. **116**, 1009 (1998); S. Perlmutter *et al.*, Astrophys. J. **517**, 565 (1999).
7. J. L. Tonry *et al.*, Astrophys. J. **594**, 1 (2003); A. G. Riess, *et al.*, astro-ph/0402512.
8. T. Padmanabhan, Phys. Repts. **380**, 235 (2003); A.D. Dolgov, hep-ph/0405089.
9. A. Guth, astro-ph/0404546; A. Linde, hep-th/0402051; D Langlois, hep-th/0405053; J. Garcia-Bellido, hep-ph/0406191.
10. A.D. Dolgov, hep-ph/0211260; F.W. Stecker, hep-ph/0207323.
11. K.A. Olive, E.D. Skillman astro-ph/0405588
12. J. Sommer-Larsen, astro-ph/0002231; J.R. Primack, astro-ph/0408359.

Frascati Physics Series Vol. XXXVI (2004), pp. 517
DAΦNE 2004: Physics at meson factories – Frascati, June 7-11, 2004
Invited Review Talk in Plenary Session

CP VIOLATION IN THE LEPTON SECTOR

Gabriela Barenboim
Valencia University, Av Moliner 50, 46100 Burjassot, Spain

Written contribution not received

Frascati Physics Series Vol. XXXVI (2004), pp. 519
DAΦNE 2004: Physics at meson factories – Frascati, June 7-11, 2004
Invited Review Talk in Plenary Session

CONFERENCE HIGHLIGHTS

Mario Calvetti
Firenze University, Via G.Sansone 1, I–50019 Sesto Fiorentino (FI) Italia

Written contribution not received

Participants

Akaishi Y.	Nihon Univ.	akaishi@post.kek.jp
Alesini D.	LNF INFN	david.alesini@lnf.infn.it
Alexander G.	Tel-Aviv Univ.	alex@lep1.tau.ac.il
Anulli F.	LNF INFN	fabio.anulli@lnf.infn.it
Ball P.	Durham Univ.	patricia.ball@durham.ac.uk
Barberio E.	Melbourne Univ.	elisabetta.barberio@cern.ch
Barenboim G.	Valencia Univ.	gabriela.barenboim@uv.es
Bediaga I.	CBPF	bediaga@cbpf.br
Beltrame P.	INFN - LNF	paolo.beltrame@lnf.infn.it
Benussi L.	LNF INFN	benussi@lnf.infn.it
Berger N.	SLAC	nberger@slac.stanford.edu
Bertani M.	LNF INFN	monica.bertani@lnf.infn.it
Bertolucci S.	LNF INFN	sergio.bertolucci@lnf.infn.it
Bhang H.	Seoul National Univ.	bhang@phya.snu.ac.kr
Bianco S.	LNF INFN	stefano.bianco@lnf.infn.it
Bigi I.	Notre Dame U. c/o INFN - LNF	ibigi@nd.edu
Blucher E.	Chicago Univ.	e-blucher@uchicago.edu
Bondar A.	Budker Institute	bondar@inp.nsk.su
Borg F.	Lund University	fredrik.borg@thep.lu.se
Bossi F.	LNF INFN	fabio.bossi@lnf.infn.it
Bressani T.	INFN Torino	tullio.bressani@to.infn.it
Cabibbo N.	University of Roma La Sapienza	nicola.cabibbo@roma1.infn.it
Calvetti M.	Firenze Univ.	calvetti@fi.infn.it
Calvi M.	Milano Bicocca Univ. e INFN	marta.calvi@mib.infn.it
Capon G.	LNF INFN	giorgio.capon@lnf.infn.it
Capussela T.	INFN - Napoli	capussela@na.infn.it
Cenci P.	INFN-Sezione di Perugia	cenci@pg.infn.it
Cooper P.	FERMILAB	pcooper@fnal.gov
Côté D.	Montréal Univ.	cote@slac.stanford.edu
Curatolo M.	INFN LNF	maria.curatolo@lnf.infn.it
Currie D. G.	Maryland Univ.	currie@ing.umd.edu

Dalena B.	INFN Bari	barbara.dalena@ba.infn.it
De Mori F.	Torino Univ.	demori@to.infn.it
Depommier	Montreal Univ.	pom@lps.umontreal.ca
Di Domenico A.	LNF INFN	antonio.didomenico@lnf.infn.it
Di Micco B.	Univ.Roma Tre	dimicco@fis.uniroma3.it
Dolgov A.	ICTP/ITEP, INFN, Ferrara	dolgov@itep.ru; adolgov@icto.trieste.it
Dosselli U.	INFN Padova	umberto.dosselli@pd.infn.it
Dreucci M.	LNF INFN	marco.dreucci@lnf.infn.it
Dukes E.	Virginia Univ.	craigdukes@virginia.edu
Edera L.	Milano Univ.	laura.edera@mi.infn.it
Eidelman S.	Budker Institute of Nuclear Physics	simon.eidelman@cern.ch
Epifanov D.	BINP	epifanov@inp.nsk.su
Escribano R.	Barcelona Univ.	rafel.escribano@ifae.es
Fabbri F.L.	LNF INFN	franco.fabbri@lnf.infn.it
Feliciello A.	INFN - Sezione di Torino	alessandro.feliciello@to.infn.it
Filippi A.	INFN Torino	filippi@to.infn.it
Fiorini L.	SNS Pisa	luca.fiorini@pi.infn.it
Foa` L.	INFN Pisa	foa@pi.infn.it
Fukuda T.	Osaka Univ.	fukuda@isc.osakac.ac.jp
Gambino P.	INFN Torino	gambino@to.infn.it
Garbarino G.	Torino Univ.	garbarin@to.infn.it
Gasser J.	Bern Univ.	gasser@itp.unibe.ch
Gastaldi U.	INFN LNL	gastaldi@lnl.infn.it
Gatti C.	LNF INFN	claudio.gatti@lnf.infn.it
Gershon T.	KEK	gershon@bmail.kek.jp
Gianotti P.	LNF INFN	paola.gianotti@lnf.infn.it
Gill D.	TRIUMF	drgill@triumf.ca
Giovannella S.	INFN LNF	simona.giovannella@lnf.infn.it
Greco M.	INFN Roma III	mario.greco@lnf.infn.it
Guaraldo C.	INFN LNF	carlo.guaraldo@lnf.infn.it
Iachello F.	Yale Univ.	francesco.iachello@yale.edu
Ignatov F.	BINP	ignatov@inp.nsk.su

Iliescu Mihail A.	INFN LNF	mihai.iliescu@lnf.infn.it
Iori M.	Roma Univ.	maurizio.iori@roma1.infn.it
Isidori G.	INFN LNF	gino.isidori@lnf.infn.it
Jensen T.	Lab. Kastler-Brossel	thomas.jensen@spectro.jussieu.fr
Kim M.	Seoul National Univ.	mijung@ieplab.snu.ac.kr
Kluge W.	Karlsruhe Univ.	wolfgang.kluge@phys.uni-karlsruhe.de
Knecht M.	Cen. de Phys. Theo.	knecht@cpt.univ-mrs.fr
Komatsubara T.	KEK	takeshi.komatsubara@kek.jp
Lanfranchi G.	LNF INFN	gaia.lanfranchi@lnf.infn.it
Lee-Franzini J.	INFN LNF	juliet@lnf.infn.it
Legendre M.	CEA/DAPNIA/ SPPSaclay	mlegendr@cea.fr
Linden Levy L.	Illinois Univ.	lindenle@uiuc.edu
Lubicz V.	Roma Tre Univ.	lubicz@fis.uniroma3.it
Lucherini V.	LNF INFN	vincenzo.lucherini@lnf.infn.it
Lukin P.	BINP	p.a.lukin@inp.nsk.su
Mahlke H.	Cornell	mahlke@mail.lns.cornell.edu
Mandl F.	F. Hochenergiephy. Inst.	mandl@hephy.oeaw.ac.at
Marcello S.	Torino Univ.	marcello@ph.unito.it
Martini M.	LNF INFN	matteo.martini@lnf.infn.it
Mihalyi A.	Wisconsin-Madison	attila@slac.stanford.edu
Mir L.-M.	LB National Lab.	lmmir@lbl.gov
Miscetti S.	LNF INFN	stefano.miscetti@lnf.infn.it
Mo X.	IHEP	moxh@mail.ihep.ac.cn
Moosbrugger U.	Mainz Univ.	ulrich.moosbrugger@uni-mainz.de
Morra P.	LNF INFN	morra@to.infn.it
Murtas F.	INFN LNF	fabrizio.murtas@lnf.infn.it
Nguyen F.	IEKP Karlsruhe U.	nguyen@fis.uniroma3.it
Nowak E.	Silesia Univ.	ela@higgs.phys.us.edu.pl
Outa H.	RIKEN	outa@riken.jp
Pacetti S.	LNF INFN	simone.pacetti@lnf.infn.it
Palomba M.	INFN Bari	maurizio.palomba@ba.infn.it
Pancheri G.	LNF INFN	giulia.pancheri@lnf.infn.it

Paulini M.	Carnegie Mellon U.	paulini@cmu.edu
Perfetto F.	INFN - Napoli	francesco.perfetto@na.infn.it
Petrascu C.	LNF INFN	catalina.petrascu@lnf.infn.it
Piano .	Trieste Univ.	stefano.piano@ts.infn.it
Poli Lener M.	INFN - LNF	marco.polilener@lnf.infn.it
Pompili F.	LNF INFN	fulvio.pompili@lnf.infn.it
Raimondi P.	LNF INFN	pantaleo.raimondi@lnf.infn.it
Rangacharyulu C.	Saskatchewan Univ.	chary@sask.usask.ca
Redlinger G.	Brookhaven N. Lab.	redlinger@bnl.gov
Ronchetti F.	LNF INFN	federico.ronchetti@lnf.infn.it
Ruggiero G.	Firenze Univ.	ruggiero@fi.infn.it
Sehgal L.	Inst. RWTH Aachen	sehgal@physik.rwth-aachen.de
Sekiguchi T.	KEK Tokyo Univ.	sekiguti@post.kek.jp
Shabalin E.P.	ITEP	shabalin@heron.itep.ru
Sharma V.	San Diego Univ.	vsharma@ucsd.edu
Shekhovtsova O.	NSC Kharkov Inst.	shekhovtsova@kipt.kharkov.ua
Shimizu S.	Osaka Univ.	suguru@phys.wani.osaka-u.ac.jp
Simonetti G.	Univ. Bari	giuseppe.simonetti@ba.infn.it
Smith C.	LNF INFN	christopher.smith@lnf.infn.it
So H.	Seoul Univ.	alphard@ieplab.snu.ac.kr
Sperandio L.	LNF INFN	laura.sperandio@lnf.infn.it
Tauscher L.	Basel Univ.	ludwig.tauscher@cern.ch
Tomassini S.	LNF INFN	sandro.tomassini@lnf.infn.it
Trassinelli M.	Ecole Normale Supérieure	martino.trassinelli@spectro.jussieu.fr
Venanzoni G.	INFN LNF	graziano.venanzoni@pi.infn.it
Zaytsev A.	Budker Institute	azaitsev@dx1cmd.inp.nsk.su
Zmeskal J.	IMEP	johann.zmeskal@oeaw.ac.at

Frascati Physics Series Volumes

Volume I
Heavy Quarks at Fixed Target
Eds. S. Bianco and F.L. Fabbri
Frascati, May 31-June 2, 1993
ISBN 88-86409-00-1

Volume II – Special Issue
Les Rencontres de Physique de la Vallée d'Aoste - Results and Perspectives in Particle Physics
Ed. M. Greco
La Thuile, Aosta Valley, March 5 -11, 1995
ISBN 88-86409-03-6

Volume III
Heavy Quarks at Fixed Target
Ed. B. Cox
University of Virginia, Charlottesville
October 7-10, 1994,
ISBN 88-86409-04-4

Volume IV
Workshop on Physics and Detectors for DAΦNE
Eds. R. Baldini, F. Bossi, G. Capon, G. Pancheri
Frascati, April 4-7, 1995
ISBN 88-86409-05-2

Volume V – Special Issue
Les Rencontres de Physique de la Vallée d'Aoste – Results and Perspectives in Particle Physics
Ed. M. Greco
La Thuile, Aosta Valley, March 3-9, 1996
ISBN 88-86409-07-9

Volume VI
Calorimetry in High Energy Physics
Eds. A. Antonelli, S. Bianco, A. Calcaterra, F.L. Fabbri
Frascati, June 8-14, 1996
ISBN 88-86409-10-9

Volume VII
Heavy Quarks at Fixed Target
Ed. L. Köpke
Rhinefels Castle, St. Goar, October 3-6, 1996
ISBN 88-86409-11-7

Volume VIII
ADONE a milestone on the particle way
Ed. V. Valente –1997
ISBN 88-86409-12-5

Volume IX – Special Issue
Les Rencontres de Physique de la Vallée d'Aoste –
Results and Perspectives in Particle Physics
Ed. M. Greco
La Thuile, Aosta Valley, March 2-8, 1997
ISBN-88-86409-13-3

Volume X
Advanced ICFA Beam Dynamics
Workshop on Beam Dynamics Issue for e^+e^- Factories
Eds. L. Palumbo, G. Vignola
Frascati, October 20-25, 1997
ISBN 88-86409-14-1

Volume XI
Proceedings of the XVIII International Conference on Physics in Collision
Eds. S. Bianco, A. Calcaterra, P. De Simone, F. L. Fabbri
Frascati, June 17-19, 1998
ISBN 88-86409-15-X

Volume XII –Special Issue
Les Rencontres de Physique de la Vallée d'Aoste –
Results and Perspectives in Particle Physics
Ed. M. Greco
La Thuile, Aosta Valley, March 1-7, 1998
ISBN 88-86409-16-8

Volume XIII
Bruno Touschek and the Birth of the e^+e^-
Ed. G. Isidori
Frascati, 16 November, 1998
ISBN 88-86409-17-6

Volume XIV – Special Issue
Les Rencontres de Physique de la Vallée d'Aoste –
Results and Perspectives in Particle Physics
Ed. M. Greco
La Thuile, Aosta Valley, February 28-March 6, 1999
ISBN 88-86409-18-4

Volume XV
Workshop on Hadron Spectroscopy
Eds. T. Bressani, A. Feliciello, A. Filippi
Frascati, March 8 –2 1999
ISBN 88-86409-19-2

Volume XVI
Physics and Detectors for DAΦNE
Eds. S. Bianco, F. Bossi, G. Capon, F.L. Fabbri, P. Gianotti, G. Isidori, F. Murtas
Frascati, November 16 -19, 1999
ISBN 88-86409-21-4

Volume XVII – Special Issue
Les Rencontres de Physique de la Vallée d'Aoste –
Results and Perspectives in Particle Physics
Ed. M. Greco
La Thuile, Aosta Valley, February 27 –March 4, 2000
ISBN 88-86409-23-0

Volume XVIII
LNF Spring School
Ed. G. Pancheri
Frascati 15-20 May, 2000
ISBN 88-86409-24-9

Volume XIX
XX Physics in Collision
Ed. G. Barreira
Lisbon June 29-July1st. 2000
ISBN 88-86409-25-7

Volume XX
Heavy Quarks at Fixed Target
Eds. I. Bediaga, J. Miranda, A. Reis
Rio de Janeiro, Brasil, October 9-12, 2000
ISBN 88-86409-26-5

Volume XXI
IX International Conference on Calorimetry in High Energy Physics
Eds. B. Aubert, J. Colas, P. Nédélec, L. Poggioli
Annecy Le Vieux Cedex, France, October 9-14, 2000
ISBN 88-86409-27-3

Volume XXII –Special Issue
Les Rencontres de Physique de la Vallée d'Aoste –-
Results and Perspectives in Particle Physics
Ed. M. Greco
La Thuile, Aosta Valley, March 4-10 , 2001
ISBN 88-86409-28-1

Volume XXIII
XXI Physics in Collision
Ed. Soo-Bong Kim
Seoul, Korea, June 28 –30, 2001
ISBN 88-86409-30-3

Volume XXIV
International School of Space Science –2001 Course on:
Astroparticle and Gamma-ray Physics in Space
Eds. A. Morselli, P. Picozza
L'Aquila, Italy, August 30 –September 7, 2000
ISBN 88-86409-31-1

Volume XXV
TRDs for the 3rd Millennium Workshop on
Advanced Transition Radiation Detectors for Accelerator and Space Applications
Eds. N. Giglietto, P. Spinelli
Bari, Italy, September 20-23, 2001
ISBN 88-86409-32-X

Volume XXVI
KAON 2001
International Conference on CP Violation
Eds. F. Costantini, G. Isidori, M. Sozzi
Pisa Italy, June 12th –17th, 2001
ISBN 88-86409-33-8

Volume XXVII – Special Issue
Les Rencontres de Physique de la Vallée d'Aoste –
Results and Perspectives in Particle Physics
Ed. M. Greco
La Thuile, Aosta Valley, March 3-9, 2002
ISBN 88-86409-34-6

Volume XXVIII
Heavy Quarks at Leptons 2002
Eds. G. Cataldi, F. Grancagnolo, R. Perrino, S. Spagnolo
Vietri sul mare (Italy), May 27th – June 1st, 2002
ISBN 88-86409-35-4

Volume XXIX
Workshop on Radiation Dosimetry: Basic Technologies, Medical Applications, Environmental Applications
Ed. A. Zanini
Rome (Italy), February 5–6, 2002
ISBN 88-86409-36-2

Volume XXIX – Suppl.
Workshop on Radiation Dosimetry: Basic Technologies, Medical Applications, Environmental Applications
Ed. A. Zanini
Rome (Italy), February 5–6, 2002
ISBN 88-86409-36-2

Volume XXX Special Issue
Les Rencontres de Physique de la Vallée d'Aoste – Results and Perspectives in Particle Physics
M. Greco
La Thuile, Aosta Valley, March 9-15, 2003
ISBN 88-86409-39-9

Volume XXXI
Frontier Science 2002 - Charm, Beauty and CP, First International Workshop on Frontier Science
L. Benussi, R. de Sangro, F.L. Fabbri, P. Valente
Frascati, October 6-11 2002
ISBN 88-86409-37-0

Volume XXXII
19th International Conference on x-ray and Inner-Shell Processes
A. Bianconi, A. Marcelli, N.L. Saini
Università di Roma "La Sapienza" June 24-28, 2002
ISBN 88-86409-39-07

Volume XXXIII
Bruno Touschek Memorial Lectures
M. Greco, G. Pancheri
Frascati, May 11, 1987
ISBN 88-86409-40-0

Volume XXXIV
Les Rencontres de Physique de la Vallée d'Aoste – Results and Perspectives in Particle Physics
M. Greco
La Thuile, Aosta Valley, February 29 – March 6, 2004
ISBN — 88-86409-42-7

Volume XXXV
Heavy Quarks And Leptons 2004
A. López
San Juan, Puerto Rico, 1-5 June 2004
In progress